Synthesis and Structure Determination of Molecular Cocrystals

By

Laura Thompson

A thesis submitted to

The University of Birmingham

For the examination of

DOCTOR OF PHILOSOPHY

This thesis and the work described in it are entirely my own, except where I have acknowledged either help from a named person or a reference is given to a published source or a thesis. Text taken from another source will be enclosed in quotation marks and a reference will be given.

24th February 2013

Abstract

Research into cocrystals is just a small field within crystallography, though the significant rise of investigation into cocrystals has made it an exciting area of research. This thesis initially introduces the phenomenon of cocrystals, including the design, formation, structure solution and the properties of cocrystals.

This thesis presents a number of new multi-component crystalline adducts that have been synthesised using dicarboxylic acids as coformers with isonicotinamide, nicotinamide or adenine. The first results chapter discusses a number of molecular adducts that contain distinct hydrogen bonding networks and includes the discovery of a new polymorph and the potential of adenine to tautomerise. The following two results chapters focus on molecular structures of nicotinamide and isonicotinamide with the dicarboxylic acids in which trends in crystal packing, cocrystal property studies and twisting of the acid backbone are discussed in detail.

In conjunction with the crystal structure and property studies, several powder X-ray diffraction datasets were collected from a synchrotron source. The final results chapter shows that a cocrystal structure, such as nicotinamide : succinic acid, can be solved without the need of single crystal X-ray diffraction data.

Acknowledgements

There are so many people who I need to thank for making this project not only possible but enjoyable. Firstly I must thank Dr Maryjane Tremayne, who gave me the chance to carry out such an exciting project to offered guidance and support from beginning to end. I must also thank Drs Louise Male and Adam Cowell who have been instrumental in the success of this project. Louise not only gave up a lot of time to teach me how to both collect and analyse single crystal data but was always being willing to help and Ad taught me all of the experimental techniques and software required to complete this research. The Tremayne group both past and present also deserve recognition for their knowledge, help and advice,

I would like to thank the post-grads, post-docs and academics of floor 2, namely Charlotte, Sarah, Nicola, Ad, Simon, Jan, Gareth and many more who I'm sure I've missed for all of the fun, gossip and tea breaks!

Finally I would like to thank all my friends and family for their support, in particular Matt and Helen and not forgetting my Mum and Dad whose financial support in particular I have been most grateful for!

Contents

List of figures

List of tables

List of equations

1.1 Bragg's law

1.2 $I_{hkl} \propto |Fhkl|^2$

1.3 $$\rho(xyz) = \frac{1}{V} \sum_{h,k,l} F(hkl) \times \exp[-2\pi i(hx + ky + lz)]$$

2.1 $$\% R_{wp} = 100x \sqrt{\frac{\sum_i w_i (y_{iobs} - y_{icalc})^2}{\sum_i w_i (y_{iobs})^2}}$$

2.2 Offspring = Parent + K (Random$_1$ – Parent) + F (Random$_2$ – Random$_3$)

1. Introduction

1.1 Introduction

The work presented and discussed within this thesis is focussed on small molecule crystallography and the design of new crystalline molecular materials. Some chapters are based on crystal engineering in which crystal structures and their bulk properties are tuned and predicted whilst other chapters focus on the ability to solve crystal structures from powder X-ray diffraction. The aim of this chapter is to introduce the fundamentals of crystallography (from reference 1) and to give a background into molecular cocrystals, their properties, synthon design and discuss the advantages of using powder X-ray diffraction in the structural analysis of these materials.

1.2 Cocrystals; what are they?

Both the word 'cocrystal' and the definition of this term have been the subject of much debate; should the word cocrystal be hyphenated? What is the difference between a cocrystal and a solvate? I will not delve any further into this as the potential uses and benefits of a cocrystal/co-crystal warrant discussion much more than a grammatical term, the definition however is important. Aakeroy et al[2] came up with the following, in which the industry seems settled; 'A cocrystal is a structurally homogeneous crystalline material that contains two or more neutral building blocks that are present in stoichiometric amounts'. This is now often extended to the definition that these building blocks are solid at room temperature.

Cocrystals have many uses, such as electronic and optical materials[3,4] and within the paint and agrochemical industry, although their main potential use and the primary focus of this project is their use as an alternative formulation of active pharmaceutical ingredients (APIs) within

the pharmaceutical industry[5]. The pharmaceutical industry has become increasingly interested in the use of cocrystals as API formulations because they have the ability to provide optimal physical properties whilst retaining the chemical properties of the individual cocrystal components[6,7]. Physicochemical properties such as melting point, stability and solubility of an API can be tuned through cocrystal formation[8] and a number of examples are given in section 1.7.

There are a number of synthetic methods for attempting cocrystallisation experiments, with solvent evaporation being the most common. For solution cocrystallisation to be successful, the solubilities of all starting materials need to be similar to avoid the recrystallisation of one cocrystal former before cocrystallisation has occurred[9]. The ternary phase diagram below (figure 1.1) shows the importance of the coformers having similar solubilities and clearly indicates that the area relating to cocrystal formation being thermodynamically favourable significantly reduces when the relative solubilities of the coformers have a larger difference.

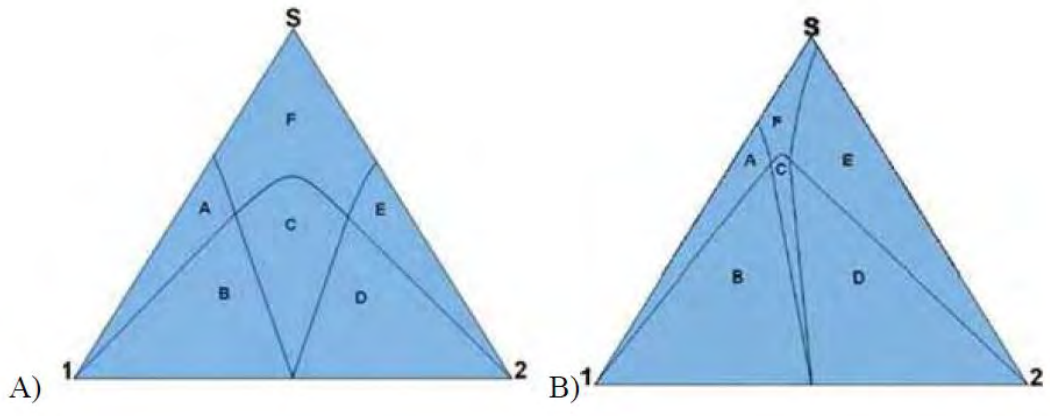

Figure 1.1: A ternary phase diagram for solvent mediated cocrystallisation. A) shows similar solubilities of the coformers whilst B) represents solubilities between the coformers with a greater difference. Region **A** represents coformer 1, region **B** represents coformer 1 and cocrystal, region **C** represents cocrystal, region **D** represents coformer 2 and cocrystal, region **E** represents coformer 2 and region **F** represents solution. Figure taken from reference 9

Other possible cocrystallisation methods are available such as liquid assisted grinding (LAG), dry grinding and sonic slurry, some of which can reduce the issue of non-comparable solubilities between the coformers.

Dry grinding and LAG is becoming increasingly popular. It is a 'greener' method as it uses only a few drops of solvent, but more importantly it can lead to formation of new polymorphic forms (section 1.3), alternative stoichiometries or a solvent free adduct[10,11]. The technique involves grinding stoichiometric amounts of the coformers by hand, using a pestle and mortar or using a ball mill. It has been found that the presence of a small amount of solvent (LAG) can increase the kinetics of the cocrystallisation and gives more polymorphic control[10,12]. The sonic slurry method also reduces the amount of solvent required for cocrystallisation and removes the problem of coformers having a large difference in solubilities. This method involves suspending the coformers in a small amount of solvent which undergoes intense bursts of heat and pressure. This allows the growth and collapse of 'bubbles' giving rise to a new cocrystalline phase[13]. The ability to form heteromeric synthons (synthetic building blocks) is the key to cocrystallisation as this has to be more energetically favourable than remaining as a mixture of coformers[2].

Whilst cocrystals are the desired result of a cocrystallisation experiment, there are other possible outcomes[14]. Not only could the materials recrystallise as a mixture of the coformers, salt formation or the production of hydrates and solvates are also possible. A salt results when a proton is transferred between the two coformers[15]. Hydrates and solvates form when either water or solvent molecules are present within the crystalline structure[12]. All of these different forms exhibit different physical properties to that of an anhydrous neutral cocrystal[12].

All of the above will be discussed and explored in much more detail further in the chapter.

1.3 Polymorphism

A crystalline polymorph is defined as a crystal with more than one crystalline arrangement of molecules or structure. In terms of a cocrystal, a polymorphic cocrystal has the same stoichiometry but a different structure[16]. Polymorphic cocrystals attracts extensive study due to its ability to change the physicochemical properties such as melting point, density and solubility the material[17,18]. Whilst at times the changes in these properties may be beneficial, it can also reduce desired properties such as good bioavailability, e.g. the antiretroviral drug ritonavir[19,20] there is also the possibility of it having a much more dangerous affect for example increasing the toxicity[18]. There are many examples of both single component systems and cocrystals forming polymorphs. Carbamazepine, for example, has multiple polymorphic forms as a single component[21] and also as a cocrystal with isonicotinamide, which forms the 1:1 cocrystal structure shown in figure 1.2 (a) and whilst the second 1:1 polymorphic form has yet to have its structure solved it is believed to be isostructural to that of carbamazepine : nicotinamide, figure 1.2 (b)[22].

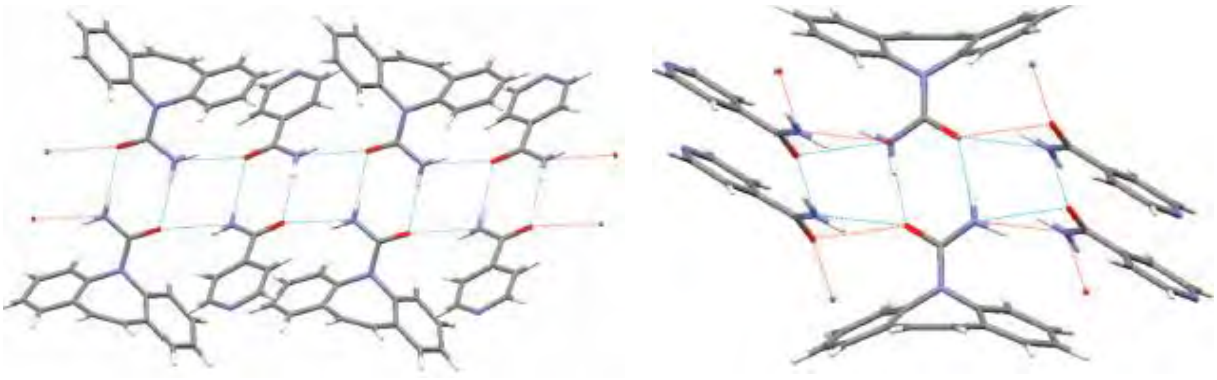

(a) (b)

Figure 1.2: The crystal structures of (a) 1:1 carbamazepine : isonicotinamide and (b) carbamazepine : nicotinamide believed to be isostructural to the second polymorphic form of carbamazepine : isonicotinamide. Figures taken from reference 22

An extensive CSD (Cambridge Structural Database) search carried out by Aitipamula *et al* in 2010 found that 1.2% of the 3624 cocrystals in the database are polymorphic[23]. As a consequence, pharmaceutical companies have required vigorous polymorph screening of single components to take place before they select an active pharmaceutical ingredient. This screening involves several stages including crystallisation using a wide variety of experimental techniques and reaction conditions, followed by subjecting the samples to a number of analytical techniques. Property comparisons are then made before the polymorph selection[24]. This is a process that will be used routinely in cocrystal screening as these materials become more widespread.

Solvent evaporation (the most common cocrystallisation technique) is a technique also used within polymorph screening, utilising various different solvents and solvent mixtures as this can affect nucleation and crystal growth. The resultant crystals are examined whilst they remain wet and in the solvent and once dried[24,25]. Different reaction vessels should be utilised within a vigorous polymorph screen, for example, capillary crystallisation provides a wide range of supersaturation levels, which in turn can affect the nucleation[24]. Along with the solvent evaporation technique, other experimental methods such as grinding, thermomicroscopy, compression, sublimation and vapour and heat stressing of crystalline forms should be employed[24]. Upon crystal formation, full characterization of the adduct is required often using multiple techniques such as powder X-ray diffraction and Raman spectroscopy, both being efficient as neither requires a large sample size[24,25].

1.4 Cocrystals and salts

Cocrystals and salts are both multi component crystalline materials, though a salt is formed if proton transfer occurs between the two components e.g. an acid and an amide (figure 1.3). Study of the pK_a difference between the coformers can often indicate whether proton transfer is likely, with a difference of greater than 2 - 3 often resulting in salt formation[15].

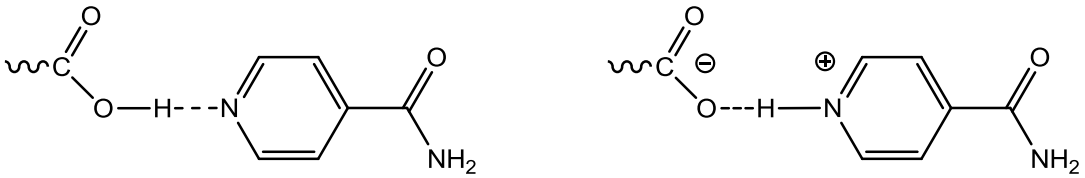

(a) (b)

Figure 1.3: An example of a cocrystal (a) and a salt (b) in which proton transfer has occurred

The question of whether the position of this hydrogen atom affects the physical properties and the reliability of the crystalline material has attracted much attention, with Aakeroy *et al* investigating the reliability and predictability of salts versus cocrystals[25]. This study involved the inspection of 85 crystalline structures of which 65 were cocrystals and the remaining 20 salts. Of this sample selection, 45% of the salts showed either an unexpected stoichiometry or lattice combination (including the presence of solvates) compared to 5% of the cocrystals. This trend was continued in the CSD searches that they carried out, demonstrating a significant advantage of cocrystals over salts in reliability and predictability of design within the pharmaceutical industry[25].

However, the location of the hydrogen atom is not always clear cut; a salt-cocrystal continuum exists in which the hydrogen could be disordered or partially occupy multiple sites[15]. Physical effects such as temperature, solvent choice and stoichiometric ratio of the

coformers are also known to have an effect on this salt-cocrystal continuum. In one case, a variable temperature neutron diffraction study of pentachlorophenol : 4-methylpyridine (ΔpK_a = 0.77) showed that as the temperature increases the adduct becomes more cocrystal 'like' with the shared hydrogen moving closer towards the pentachlorophenol oxygen (figure 1.4)[15,26].

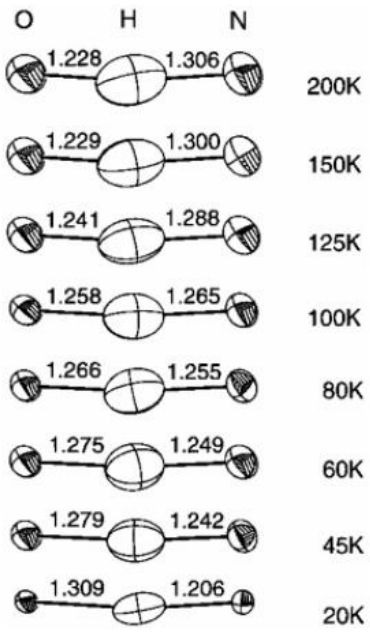

Figure 1.4: The location of the hydrogen atom at varying temperatures in the pentachlorophenol : 4-methylpyridine complex measured using neutron diffraction. Figure taken from reference 15

Proton migration to become more cocrystal like in character at elevated temperatures is a behaviour also seen in the 1:1 salt of urea : phosphoric acid in which the proton moved towards the phosphate oxygen to become more centered between the two components. The choice of solvent used in the cocrystallisation synthesis can also influence the extent of proton transfer, with the use of more polar solvents favouring proton transfer[27]. 2,3-lutidine : fumaric acid is an example of a crystalline system that can form both cocrystal and salt forms by

variation of the stoichiometric ratio of starting materials. A 1:2 salt is obtained from a 1:1 ratio of coformers, whereas a 2:1 cocrystal is formed from a 2:1 lutidine : fumaric acid starting material ratio (figure 1.5)[28].

(a) (b)

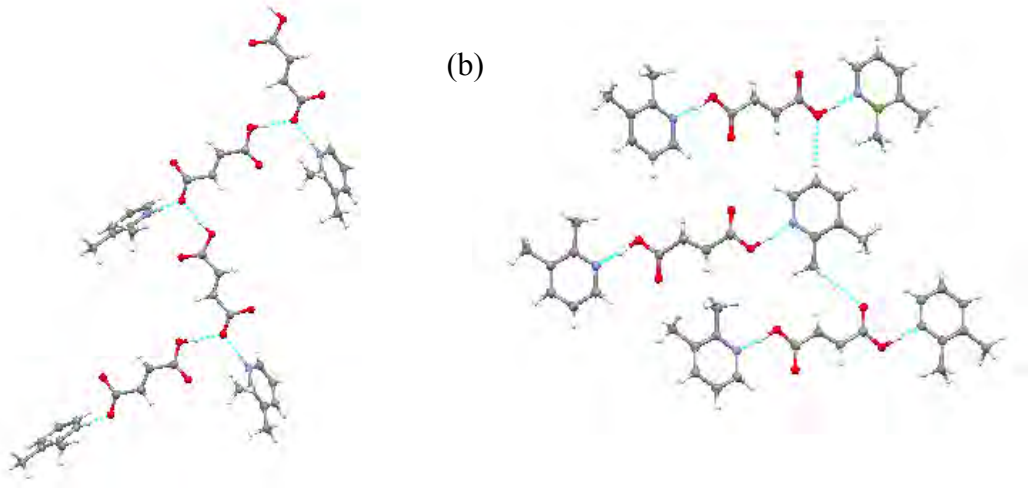

Figure 1.5: The crystal structure of (a) 2,3-lutidine : fumarate salt, 1:2 and (b) 2,3-lutidine : fumaric acid 2:1[28]

These examples clearly indicate the importance of being able to locate the acidic proton. Structure solution of the multi-component materials discussed in this thesis was carried out using both single crystal and powder X-ray diffraction analysis, although these techniques are not always sufficient to fully classify the new crystalline adducts as either cocrystals or salts. As a result, complementary techniques will be employed, such as inspection of certain bond lengths and angles of the atoms involved and comparison with other known structures. Infrared spectroscopy is also a technique that can aid classification of these materials based on the observation of O-H, N-H, C-O and C=O bands[29]. Neutron diffraction is suitable for the investigation of the position of light atoms such as hydrogen atoms, but the requirement of deuteration by recrystallisation limits the application of this technique when materials are available only from solvent free synthetic methods[30].

1.5 Hydrates and solvates

The stability and other physical properties of both hydrates and solvates differ from that of the unsolvated forms, and can be either detrimental or beneficial to a pharmaceutical product[12]. The majority of cocrystallisation experiments are from solution, so the presence of solvent within the crystal lattice is not surprising. Water molecules are small and can form multiple hydrogen bonds and hence inclusion as a hydrate within a crystal structure is frequently observed[31]. The CSD database search carried out by Aitipamula *et al* also investigated the number of cocrystal structures that exist as either solvates or hydrates[23]. The results of this search showed that ~12% of the 3624 entries were hydrates with a further ~11% being solvates (with methanol, ethanol and acetonitrile being the most common solvate to be incorporated into the structure)[23].

It has been reported that in certain systems where there is an imbalance of donor and acceptor molecules, that the presence of water can stabilize the structure[32.33]. Work carried out by Aakeroy *et al*[33] on the cocrystallisation of two hydrazones (which have limited hydrogen bond donor sites) with a range of carboxylic acids showed that all twelve of the adducts formed were hydrates indicating that the inclusion of water within the structure is driven by the desire to even out the donor/acceptor balance. The thermal stability of a range of hydrated cocrystals was investigated by Clarke *et al*[32] which observed that the more tightly bound the water molecules, the higher the temperature required before the water is lost. For example the samples in which the water was held in channels was lost at temperatures less than 100ºC, though temperatures greater than 120ºC were required before dehydration of the samples in which the water was tightly bound within the crystalline lattice[33].

1.6 Synthon formation and crystal engineering

Cocrystal formation relies on the formation of heteromeric synthons, with this supramolecular assembly being energetically more favourable than the existence of the pure coformers[2,7] Several homomeric and heteromeric synthons have been identified as 'strong', 'stable' and 'robust' and are frequently observed in many cocrystal structures. Examples of supramolecular synthons that are applicable to this thesis are acid-heterocyclic nitrogen, acid-amide, amide-amide and acid-acid and amide-heterocyclic nitrogen[7,34-37] (figure 1.6)

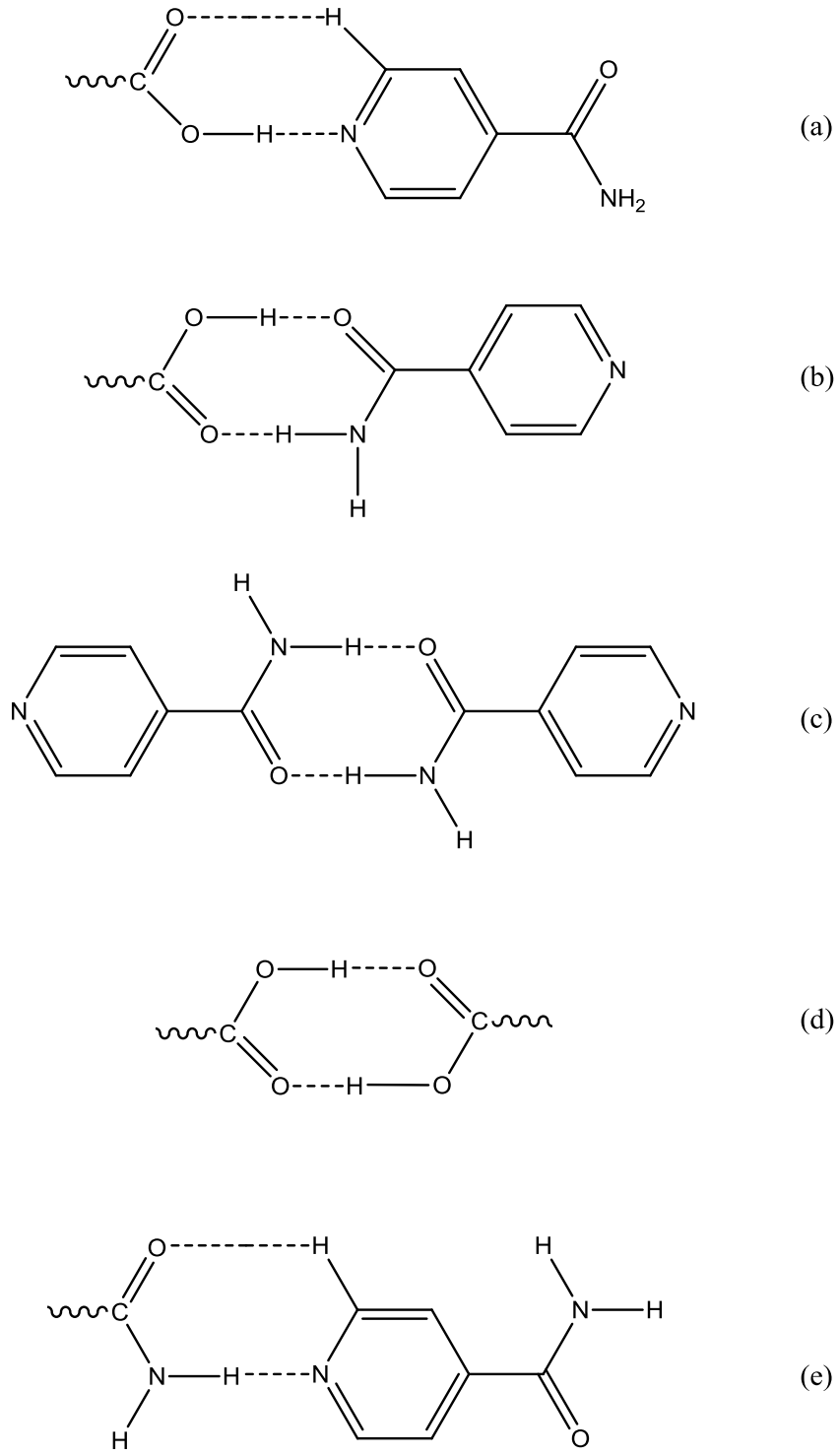

Figure 1.6: Five robust synthons formed between isonicotinamide and a carboxylic acid; (a) an acid-heterocyclic nitrogen synthon reinforced by a C-H...O=C to form a ring motif, (b) an acid-amide synthon, (c) an amide-amide synthon, (d) an acid-acid synthon and (e) an amide-pyridine synthon again reinforced by a soft C-H...O=C to form a ring motif

These robust synthons exist as they contain strong hydrogen bond donor and acceptor sites and they follow guidelines set out by Etter[38], suggesting a hierarchy of hydrogen bond formation (see list below):

1. All good proton donors and acceptors are used in hydrogen bonding
2. Six-membered ring intramolecular bonds form in preference to intermolecular hydrogen bonds
3. The best proton donors and acceptors remaining after intramolecular hydrogen bond formation form intermolecular hydrogen bonds to one another

Synthon energy studies were carried out by Vishweshwar *et al*[39] in which it was found that the heterosynthons (a, b and c in figure 1.6) are more likely to be formed before the homosynthons (d and e in figure 1.6).

Crystal engineering is the term used for 'crystal design' by studying such synthons and supramolecular interactions with the aim of being able to control the crystalline state along with its physical properties[7,34,35,40,41]. Potential hydrogen bond donor and acceptor sites and the possibility of robust synthon formation has been explored in detail for the coformers selected in this thesis, and their behaviour will be discussed further in the relevant chapters.

1.7 Properties of cocrystals

Both academic and industrial study and research into cocrystals has increased significantly in the last few years, owing mainly to the fact that cocrystals have the ability to change the physical properties of a material whilst a coformer retains its chemical properties, giving the potential to tune certain desirable bulk properties[6,8,42-44]. These potential uses and tunability of properties of cocrystals arise because crystalline materials obtain their physical properties from the molecular arrangement and the relative placement of the interactions between molecules[8]. There are a number of physical properties that are especially important when selecting an API, including melting point, solubility, dissolution, stability, bioavailability, compressability and wettability[8,43].

The melting point is important as it is directly related to the solubility with a higher melting point implying that the new material is thermodynamically stable[8]. There are several studies that have investigated the melting points of cocrystals and compared them to that of their coformers. Dicarboxylic acids, for example, display alternating melting point with increasing or decreasing chain length due to conformational packing differences between those with an even number of carbon atoms and those with an odd number, a trend which remains when these acids are cocrystallised with another material[29,41]. For example, melting point measurements on ten AMG cocrystals showed that the melting point of each cocrystal was related to the coformer[45], further indicating that if an API was required with a specific melting point, selection of a cocrystal former with a melting point in the desired range would be a solution. What is not clear however, is whether the melting point of the cocrystal can be predicted as above both coformers, below both coformers or between the two, with reports illustrating all of these possibilities[8,29,39,46].

Many APIs have poor solubility and one of the primary interests in cocrystal research is to investigate the potential of improving this situation. Solubility is a property with many considerations, including the hydrogen bonding strength and melting point of the cocrystal along with the temperature and polarity of the solvent[45]. Cocrystal studies that have involved the measurement of solubility have found that upon cocrystallisation of an API the solubility does in most cases increase[43,45].

The dissolution of an API is directly related to the solubility and when considering drugs for oral consumption, a good dissolution rate is key. A study by McNamare *et al*[47] investigated the cocrystallisation of glutaric acid with the poorly soluble 2-[4-(4-chloro-2-fluorophenoxy)phenyl]pyrimidine-4-carboxamide, which is a potential candidate for treating surgical, chronic and neuropathic pain. Upon cocrystallisation dissolution rate experiments were carried out in pure water, with the intrinsic dissolution rate of the cocrystal being about 18 times faster than the coformer[47].

Both chemical and physical stability is also an important factor when selecting APIs as it effects properties such as shelf life in which it is important that the API is in the most stable form (i.e. not undergoing polymorphism). Stability measurements can be carried out in stability chambers, for example, the AMG 517 (an antagonist of the protein TRPV1) cocrystals which showed no change after being subjected to the chamber for a month[45], along with looking at moisture sorption measurements[6, 45].

Bioavailability is the measure of both the rate and extent of the activity of the drug when reaching systematic circulation[8], another highly important factor to consider during API selection. The study by McNamara *et al* not only found better dissolution rates when the API

was cocrystallised with glutaric acid but also that the bioavailability increased when testing the drug in dogs[47].

These are just a few examples highlighting the significant advantages that cocrystals can provide to the pharmaceutical industry, specifically due to the ability to 'select' the optimum properties and obtain them via cocrystallisation.

1.8 Structure solution of cocrystals

Structure solution is an integral part of cocrystal research; it confirms (or not!) synthon design principles, it allows the determination of whether the adduct is a salt or cocrystal, it aids the discovery of solvent or water molecules that may be present within the crystal lattice and facilitates the determination of structure-property relationships. Single crystal X-ray diffraction is currently the most widely used technique for cocrystal structure solution, though NMR spectroscopy and solid state IR spectroscopy are all techniques used to complement this method. Powder X-ray diffraction and neutron diffraction are also used within this field. Powder X-ray diffraction is used more as a 'screening' technique for new materials although it does have the potential for full structure analysis.

1.9 Crystallography; the fundamentals

X-ray crystallography is a powerful technique with the ability to determine the crystal structure of both molecular and inorganic crystalline solids. It can provide details such as the contents of the sample, packing of the atoms or molecules and structural details such as bond lengths and angles. This technique involves placing the crystalline material in a beam of X-rays, which then diffracts in all directions (figure 1.7). The diffracted beams are collected by a detector generating a unique diffraction fingerprint (no two distinct crystalline solids will have the same diffraction pattern).

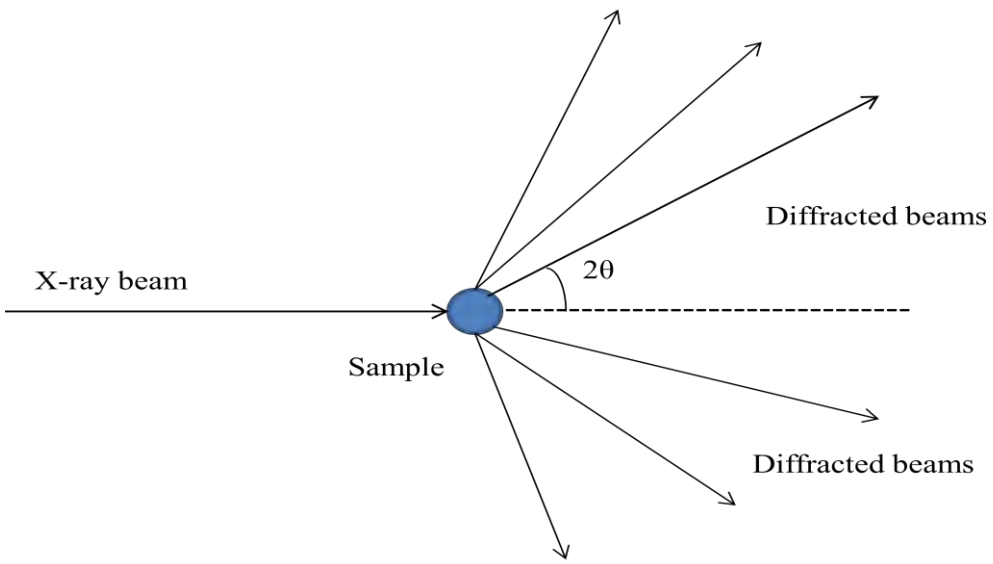

Figure 1.7: A schematic of the X-ray diffraction experiment

1.9.1 The crystalline material

In order for X-ray crystallography to be successful the sample must be crystalline; i.e. have periodic long range order. A crystal lattice is formed of unit cells; a unit cell contains the smallest repeating unit and is connected to other identical unit cells in three dimensions. It has parameters which define both the axes (*a, b* and *c*) and the angles (*α, β,* and *γ*). This labelling of parameters is the standardised scheme for a unit cell (figure 1.8).

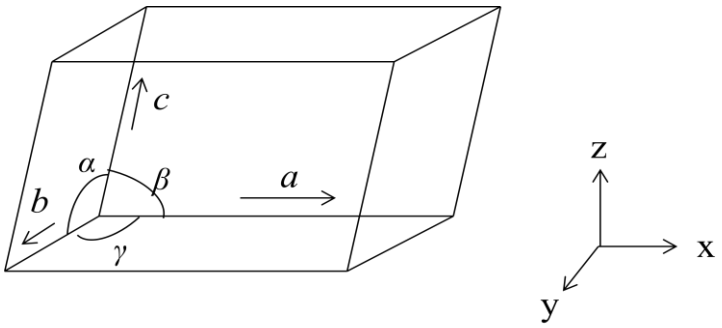

Figure 1.8: A unit cell

The contents of the unit cell can often be reduced to sub-units known as the asymmetric unit. Each asymmetric unit is related to others by symmetry elements (rotation, reflection, inversion etc) to form the complete crystal structure. Sets of imaginary planes can also be defined, running through the crystal lattice. The planes within a set are parallel and equidistant (interplanar distance known as *d*-spacing) and are labelled by Miller indices (*h,k,l*); integer values which are mathematically related to the unit cell parameters.

The combination of various different symmetries places restrictions on the unit cell parameters. There are seven different crystal systems (table 1.1) and in addition to this there

are four different lattice types; primitive (P), body-centred (I), face-centred (F) and base-centred (A,B or C) shown in figure 1.9.

Table 1.1: The seven crystal systems

Crystal system	**Restrictions on Unit Cell parameters**	**Possible Bravais lattice types**
Cubic	$a = b = c$ $\alpha = \beta = \gamma = 90^o$	P, I, F
Hexagonal	$a = b \neq c$ $\alpha = \beta = 90^o \ \ \gamma = 120^o$	P
Trigonal	$a = b = c$ $\alpha = \beta = \gamma \neq 90^o$	R
Tetragonal	$a = b \neq c$ $\alpha = \beta = \gamma = 90^o$	P, I
Orthorhombic	$a \neq b \neq c$ $\alpha = \beta = \gamma = 90^o$	P, I, F, A, B, C
Monoclinic	$a \neq b \neq c$ $\alpha = \gamma = 90^o \ \ \beta \neq 90^o$	P, C
Triclinic	$a \neq b \neq c$ $\alpha \neq \beta \neq \gamma \neq 90^o$	P

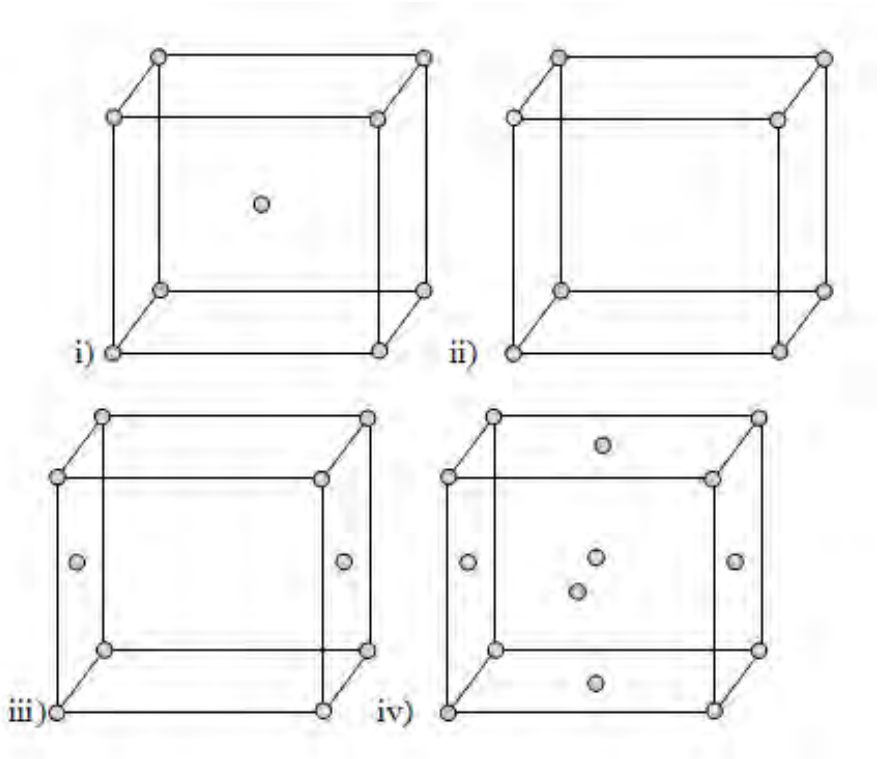

Figure 1.9: The four Bravais lattice types; (i) Body centered, (ii) primitive, (iii) A centered and (iv) face centered[48]

A crystal structure is assigned a space group which represents all of the symmetry elements within the system. The combination of possible symmetry elements, the seven crystal systems and fourteen Bravais lattices mean there are only 230 different space groups. The possible symmetry elements include inversion, rotation, reflection, screw axes and glide planes.

1.9.2 The diffraction experiment

Wilhelm Conrad Röntgen first discovered X-rays in 1895, receiving a Nobel prize for his work[49]. The X-ray crystallography experiment is possible because X-rays have wavelengths of the same order as intramolecular bond lengths.

During the X-ray experiment, the crystalline sample is irradiated with X-rays, which get diffracted in all directions. The diffracted beams are measured by a detector to give a diffraction pattern. In single crystal X-ray diffraction, the sample is one crystallite, with minimum dimension normally 0.01 mm.

Braggs law explains how diffraction patterns are produced (equation 1.1 and figure 1.10)

$$2d\sin\theta = n\lambda$$

Equation 1.1: Bragg's law

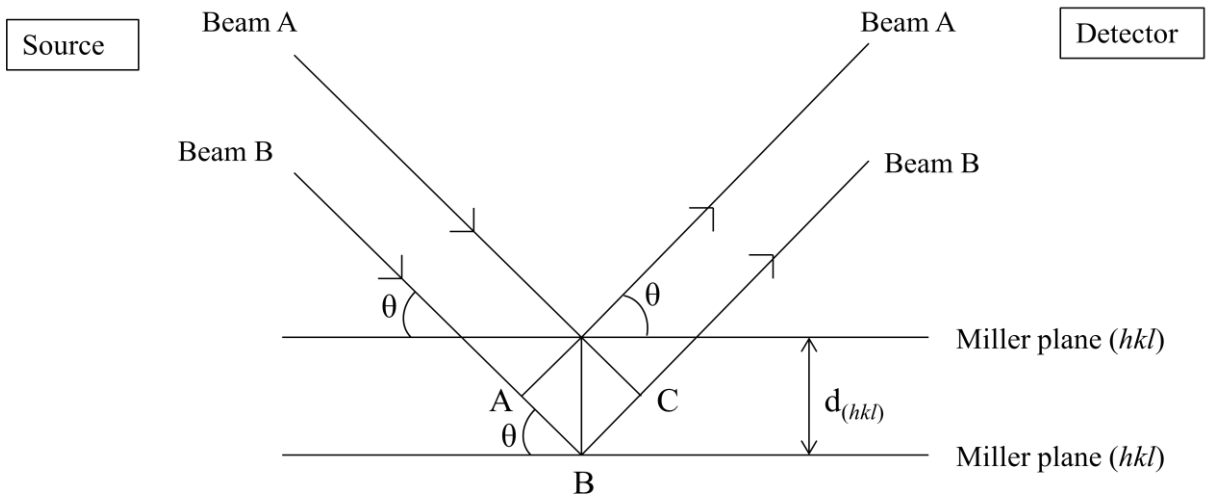

Figure 1.10: Bragg's law

The derivation of Bragg's law is a mathematical construct in which diffraction can be thought of in terms of reflection of the incident beam from the lattice planes. For constructive interference to occur, and thus intensity observed on the detector, beams A and B (figure 1.10) must be in phase when they reach the detector. The difference in path length from source to detector of beams A and B is equal to AB + BC (figure 1.10) and for the beams to be in phase this must be equal to $n\lambda$ (where n is an integer and λ is the X-ray wavelength). Using trigonometry, AB + BC is found to be equal to twice the d-spacing multiplied by $\sin\theta$ where θ is the angle of incidence, hence Bragg's law (equation 1.1). As the X-ray diffraction experiment can be easily understood in terms of reflection, it is common for diffraction peaks to be referred to as reflections.

X-rays are produced when an excited electron relaxes back to its ground state. In a standard X-ray crystallography experiment, X-rays are produced in a sealed tube in which an electron beam is generated by an electric current and accelerated towards a metal target (usually copper or molybdenum dependent on wavelength requirements). The X-ray beam is produced as a by-product of this collision. Three wavelengths of radiation are produced; $K\alpha_1$, $K\alpha_2$ and $K\beta$. A monochromator can be used to remove some of the unwanted $K\alpha_2$ and $K\beta$ radiation to produce a monochromatic beam.

A peak (reflection) occurs when a set of lattice planes (*hkl*) satisfies Bragg's law. Each set of planes gives rise to one diffraction peak. The relative intensities of the peaks and the peak positions (2θ values figure 1.7) give information on the contents of the unit cell, the cell parameters and crystal system. The first stage is indexing in which each measured peak is assigned (*hkl*) values. The *d*-spacing of the (*hkl*) reflection (calculated using Bragg's law) can be related to the unit cell parameters allowing them to be calculated. The Bravais lattice type

and space group are determined by investigation of absences within the diffraction pattern which occur because of symmetry related atoms. There are two types of absence, a general absence relating to Bravais lattice type and a systematic absence relating to translational space group symmetry. The different lattice types place different conditions of when there will be a general absence, for example, an absence will occur for a body centred lattice if $h + k + l$ is odd. Systematic absences only occur for translational space group symmetry and pose similar conditions. For example a 2_1 screw axis in the *a* direction will have a systematic absence at (*h*, 0, 0) where h is odd and absent. This information allows the symmetry to be determined and a space group to be assigned.

1.9.3 Structure solution and refinement

Each peak in the diffraction pattern has a structure factor, F_{hkl} which is related to the relative intensity (equation 1.2).

$$I_{hkl} \propto |Fhkl|^2$$

Equation 1.2: Relationship between structure factors and intensities

The structure factors are related to the electron density which is required for structure solution. The diffraction pattern is a Fourier transform of electron density, although before the electron density map can be obtained the phase problem has to be overcome. Electron density, *ρ(xyz)* is obtained by summing all of the structure factors and phase angles (equation 1.3).

$$\rho(xyz) = \frac{1}{V} \sum_{h,k,l} F(hkl) \times \exp[-2\pi i(hx + ky + lz)]$$

Equation 1.3: Reverse Fourier transform of the diffraction pattern

The phase problem exists because only the intensities can be recorded in the diffraction pattern and not the phases. The most traditional method of overcoming this is by using direct methods in which possible phase angles are estimated. This approach is used mainly for small molecules without heavy metals. Patterson methods are also available, these use trial structures; once a 'trial' structure is obtained it undergoes refinement to compare it with the experimental data, refining lattice parameters, atomic positions etc. Once an initial structure solution has been obtained the most common method of refinement is the least squares method which gives a numerical representation of the 'goodness' of fit between the experimental data and the structure.

1.10 Single crystal X-ray diffraction

Single crystal X-ray diffraction (SXRD) is the most commonly used technique to determine a crystal structure[50], however it does come with certain requirements. This method is reliant on the quality of crystal; small crystals are often poorly diffracting and data collections can be quite time consuming[30]. SXRD is routinely carried out at low temperatures as it can yield better quality data than at room temperature[50]; this approach is potentially vital for reliable location of hydrogen atoms in a crystal structure.

1.10.1 Potential problems in single crystal analysis

Disorder and twining both provide challenges and problems in the structure refinement stage. Disorder occurs when atoms are in different orientations or positions in neighbouring unit cells and hence a perfect translational repeat is not obeyed. The percentage occupancy of these different orientations can be variable, particularly with changes in temperature. The refined crystal structure will contain all orientations of the disordered groups and is derived from diffraction data from all the unit cells in the sample as this is the diffraction average. Twinning occurs when a single dataset includes more than one diffraction pattern superimposed on one another. There are two types; firstly merohedral twinning which occurs when the symmetry of a crystal lattice is such that unit cells can be orientated in two ways leading to datasets that overlap exactly. It normally arises from systems in which the unit cell parameters are very close to higher symmetry values (such as a monoclinic unit cell with β very close to 90°). Non-merohedral twinning occurs when two orientations of a crystal lattice are present in the same sample and give rise to superimposed diffraction patterns which do not overlap. Polymorphism (section 1.3) is another phenomenon that can cause crystallographers further challenges.

1.10.2 Structure validation

Once a crystal structure has been solved, there are several parameters and visual inspections that can be used to validate that the structure is chemically sensible and correct. The first values to consider are the R factors and the goodness-of-fit. The R factor is a measure of agreement between the diffraction pattern calculated from the model and experimental data and, ideally should be less than 5 % but is normally acceptable if less than 10 %. The weighted R factor (wR_2), which will have a higher value, though still be less than 25 %, takes

into account the precision of the measured quantities by weighting them accordingly. The goodness-of-fit is another weighted statistical measure of the agreement between the calculated and raw data. This value should be close to 1 with the range 0.8 - 2 being acceptable. The completeness of data (the percentage of the unique reflections that have been measured out to the maximum diffraction angle) is another value used to validate the crystal structure with > 97% being ideal. The final parameter to check is the remaining difference electron density, (electron density that has not been assigned in the model) with values below 0.6 $e^-/Å^3$ for organic structures indicating that all atoms have been assigned.

Visual checks of the bond lengths and angles should be made to ensure that they are all within sensible parameters for that bond type. The thermal parameters should also be visually checked as comparatively large or small ellipsoids will highlight any potential disorder or incorrect atom assignment.

All of these checks along with the use PLATON[51] will validate the structure and highlight any issues.

1.11 Powder diffraction

Powder X-ray diffraction data contains the same structural information as single crystal X-ray data, though whereas the latter is in three dimensions, powder data is compressed into one dimension[30]. In powder diffraction, many crystallites satisfy the Bragg criterion for diffraction from planes (*hkl*). Therefore cone-shaped Debye rings are formed (figure 1.11).

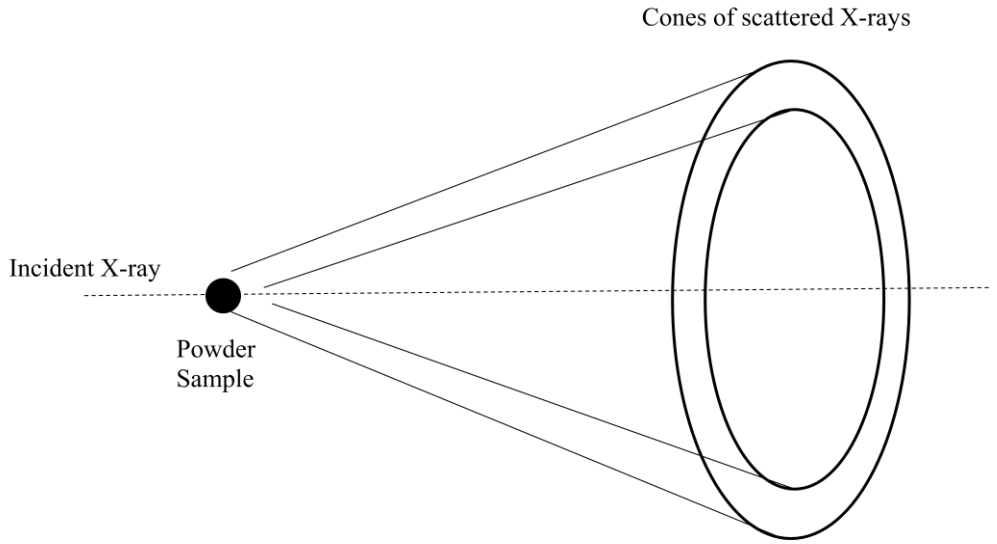

Figure 1.11: The diffraction cones formed from the scattered X-rays in powder X-ray diffraction

The diffraction data is collected by taking a slice through the Debye ring along 2θ and is then compressed into one dimension. This leads to both systematic and accidental peak overlap within a powder diffraction pattern and is particularly a problem when the structure has either a large unit cell or low symmetry as this gives rise to a higher density of peaks[52]. The ability to be able to solve structures from powder diffraction data is important when single crystals of suitable quality or size are difficult to obtain. As in single crystal X-ray diffraction challenges do arise, although for the powder method, preferred orientation is the most common sample preparation issue. Preferred orientation occurs when the crystallites favour certain orientations

as opposed to being randomly oriented. It can potentially be avoided or minimised if a capillary tube is used for sample mounting during data collection as opposed to a disc especially if the crystallites show a plate-like morphology.

To solve a crystal structure from powder diffraction data the following process is followed[30];

1. Indexing to obtain lattice parameters, crystal system and space group
2. Structure solution by producing an approximate model with atomic positions
3. Structure refinement

Unlike in single crystal structure determination, these steps are often complex due to the lack of data.

Crystal structure solution from powder diffraction data is limited. Synchrotron data can be used to give a better signal/noise ratio and with higher resolution can be used to resolve peak overlap to an extent[30]. Direct space methods are now the most common approach to the solution of molecular structures from PXRD. These differ significantly from traditional structure solution methods as they approach the problem by movement of a structural model around the unit cell, using some form of optimisation algorithm and identify the correct structure by agreement with the experimental data. These methods do not use integrated intensities directly and utilize information gained from knowledge of the chemical structure (more details in chapter 2)[53].

1.12 Neutron diffraction

Neutron diffraction data can also be used in the determination of crystal structures and can be advantageous when investigating the position of light atoms or distinguishing between isotopes. However the requirement of deuteration by recrystallisation can limit the application of this technique particularly when investigating cocrystal structures[30]. As discussed previously in this chapter, recrystallisation of crystals can lead to other polymorphic forms and the recrystallisation of cocrystals could lead to the formation of alternative stoichiometries, or potentially solvated forms of the adduct (particularly if the cocrystal was formed using a technique such as grinding where solvent was not required). Another problem with neutron diffraction is that it requires a much larger sample size.

1.13 Other complementary techniques

Solution state ^{1}H NMR spectroscopy is a useful technique in this area as it has the ability to indicate the cocrystal stoichiometry by looking at the relevant integration of the different hydrogen environments. The NMR spectra will also identify any solvent peaks. Whilst solvent could be present in a sample that is not properly dry, it could be that the solvent is located within the crystal lattice and forms part of the structure. Solid state NMR spectroscopy is a technique that can be used to aid location of hydrogen atoms and crystal symmetry, a technique used in many polymorphic studies[54].

Solid state infra-red spectroscopy is a technique that is regularly used to provide vital information on the salt vs cocrystal issue, based on the observation of O-H, N-H, C-O and C=O bands[29] with a direct comparison of the adduct and its coformers indicating whether proton transfer could have occurred.

1.14 Aims and materials used

The work reported in this thesis is based upon molecular crystallography and cocrystal design with several aims. The field of crystal engineering has expanded significantly within recent years and this project aims to provide more structures and results towards the prediction of hydrogen bond networks and the relation of properties between coformers and molecular adducts. The other primary aim was to develop the ability to solve the structures of multi-component molecular adducts by powder diffraction and other complementary techniques. This would be a significant advantage to the pharmaceutical industry, not only making the process quicker and cheaper but enabling the use of alternative methods of cocrystallisation such as grinding in which single crystal X-ray diffraction analysis is not always possible. The determination of accurate packing and even the determination of salt or cocrystal form from powder diffraction is the goal.

This research focuses on the potential crystalline adducts that can be formed using dicarboxylic acids ($HO_2C(CH2)_{n-2}CO_2H$) as a series of coformers (table 1.2). These dicarboxylic acids were chosen due to their potential to form strong hydrogen bonds at each end of the acid and their ability to form the strong synthons discussed in section 1.7. Isonicotinamide, nicotinamide and adenine (table 1.2) were selected as the other coformer for adduct formation. All three have pK_a values that will enhance the probability of obtaining a cocrystal rather than a salt with the majority of the acids. Nicotinamide and isonicotinamide contain a heterocyclic nitrogen and an amide group which will form strong hydrogen bonds and the adenine molecule provides three strong hydrogen bond acceptor and two strong hydrogen bond donor sites.

Table 1.2: A table of the coformers studied in this project with their relative pK_a values[55]. pK_a^1 refers to the first deprotonation and pK_a^2 the second deprotonation.

Coformer	Molecular structure	pK_a^1	pK_a^2
Oxalic acid n = 2	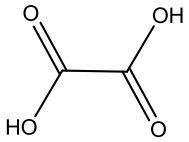	1.27	4.29
Malonic acid n = 3	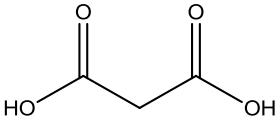	2.85	5.70
Succinic acid n = 4	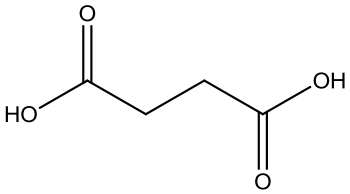	4.21	5.64
Fumaric acid n = 4	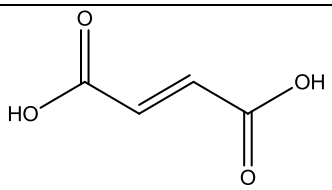	3.02	4.38
Maleic acid n = 4	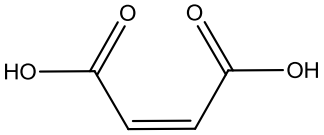	1.97	6.24
Glutaric acid n = 5	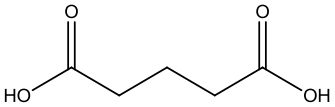	4.34	5.41
Adipic acid n = 6	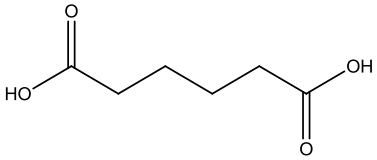	4.43	5.41
Pimelic acid n = 7	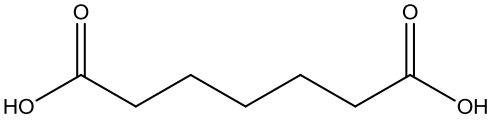	4.50	5.43

Suberic acid n = 8	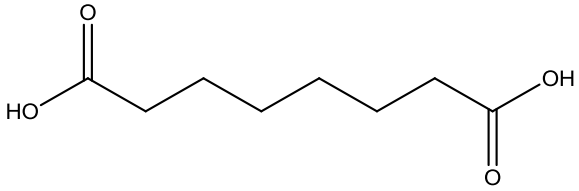	4.53 5.50
Azelaic acid n = 9	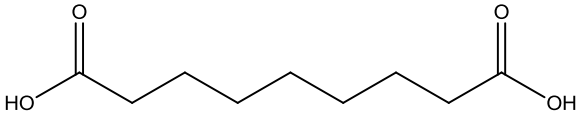	4.55 5.50
Sebacic acid n = 10	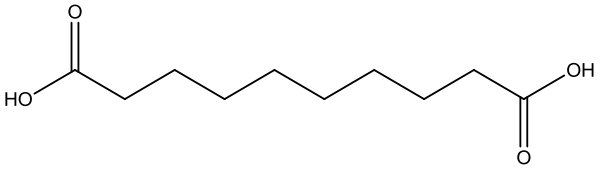	4.72 5.45
Undecanedioic acid n = 11	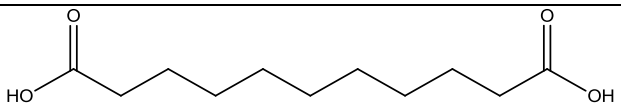	4.48
Isonicotinamide	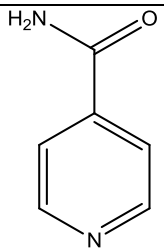	Heterocyclic N: 3.4 Amide: 13.7
Nicotinamide	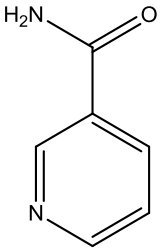	Heterocyclic N: 3.6 Amide: 13.3
Adenine	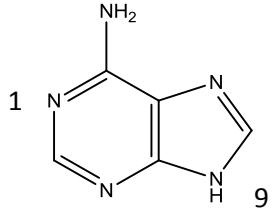	N1 - 4.1 N9 - 9.8

1.15 References

1. L. Ling Ooi, *Principles of X-ray Crystallography*, Oxford University Press, 2010

2. C. B. Aakeroy and D. J. Salmon, *CrystEngComm*, 2005, **7**, 439

3. A. N. Sokolov, T. Friscic and L. R. MacGillivray, *J. Am. Chem. Soc.*, 2006, **128**(9), 2806

4. G. S. Papaefstathiou, Z. M. Zhong, L. Geng and L. R. MacGillivray, *J. Am. Chem. Soc.*, 2004, **126**(30), 9158

5. D. R. Weyna, T. Shattock, P. Vishweshwar, M. J. Zaworotko, *Cryst. Growth. Des.*, 2009, **9**(2), 1106

6. S. F. Chow, M. Chen, L. M. Shi, A. H. L. Chow and C. C. Sun, *Pharm, Res.*, 2012**,** **29**(7), 1854

7. N. Blagden, M. De Matas, P. T. Gavan and P. York, *Adv. Drug. Del. Rev.*, 2007, **59**(7), 617

8. N. Blagden, D. J. Berry, A. Parkin, H. Javed, A. Ibrahim, P. T. Gavan, L. L. De Matos and C. C. Seaton, *New. J. Chem.*, 2008, **32**(10), 1659

9. N. Schultheiss and A. Newman, *Cryst. Growth .Des.*, 2009, **9**(6), 2950

10. A. V. Trask, N. Shan, W. D. S .Motherwell, W. Jones, S. H. Feng, R. B. H. Tan and K. J. Carpenter, *Chem.Commun.*, 2005, **7**, 880

11. A. V. Trask, W. D. S. Motherwell and W. Jones, *Chem.Commun.*, 2004**, 7,** 890

12. P. Vishweshwar, J. A. McMahon, J. A. Bis and M. J. Zaworotko, *J. Pharm. Sci.*, 2006, **95**(3), 499

13. D. K. Bucar and L. R. MacGillivray, *J. Am. Chem. Soc.*, 2007, **129**(1), 32

14. S. Aitipamula, R. Banerjee, A. K. Bansal, K. Biradha, M. L. Cheney, A. R. Choudhury, G. R. Desiraju, A. G. Dikundwar, R. Dubey, N. Duggirala, P. P. Ghogale, S. Ghosh, P. K. Goswani, N. R. Goud, R. Jeti, P. Karpinski, P. Kaushik, D. Kumar, V. Kumar, B. Moulton, A. Mukherjee, G. Mukherjee, A. S. Myerson, V. Puri, A. Ramanan, T. Rajamannar, C. M. Reddy, N. Rodriguez-Hornedo, R. D. Rogers, T. N. G. Row, P. Sanphui, N. Shan, G. Shete, A. Singh, C. Q. C. Sun, J. A. Swift, R. Thaimattam, T.S. Thakur, R. K. Thaper, S. P. Thomas, S. Tothadi, V. R. Vangala, N. Variankaval, P. Vishweshwar, D. R. Weyna and M. J. Zaworotko, *Cryst. Growth. Des.*, 2012, **12**(5), 2147

15. S. L. Childs, G. P. Stahly and A. Park, *Mol. Pharm.*, 2007, **4**(3), 323

16. J. H. terHorst and P. W. Cains, *Cryst. Growth. Des.*, 2008, **8**(7), 2537

17. N. Chieng, T. Rades and J. Aaltonen, *J. Pharmaceut. Biomed.*, 2011, **55**(4), 618

18. S. R. Chemburkar, J. Bauer, K. Deming, H. Spiwek, K. Patel, J. Morris, R. Henry, S. Spanton, W. Dziki, W. Porter, J. Quick, P. Bauer, J. Donaubauer, B. A. Narayanan, M. Soldani, D. Riley and K. McFarland, *Org. Process. Res. Dev.*, 2000, **4**(5), 413

19. J. Bauer, S. Spanton, R. Henry, J. Quick, W. Dziki, W. Porterand J. Morris, *Pharm. Res.*, 2001, **18**(6), 859

20. E. Gagniere, D. Mangin, F. Puel, A. Rivoire, O. Monnier, E. Garcia and J. R. Klein, *J. Cryst. Growth*, 2009, **311**(9), 2689

21. S. L. Childs, P. A. Wood, N. Rodriguez-Hornedo, S. Reddy and K. I. Hardcastle, *Cryst. Growth. Des.*, 2009, **9**(4), 1869

22. J. H. terHorst and P. W. Cains, *Cryst. Growth. Des.*, 2008, **8**(7), 2537

23. S. Aitipamula, P. S. Chow and R. B. H. Tan, *Cryst. Growth. Des.*, 2010, **10**(5), 2229

24. R. Hilfiker, J. Berghausen, F. Blatter, A. Burkhard, S. M. De Paul, B. Freiermuth, A. Geoffroy, U. Hofmeier, C. Marcolli, B. Siebenhaar, M. Szelagiewicz, A. Vit and M. Von Raumer, *J. Therm. Anal.Calorim.*, 2003, **73**(2), 429

25. C. B. Aakeroy, M. E. Fasulo and J. Desper, *Mol. Pharm.*, 2007**, 4**(3), 317

26. I. Majerz, Z. Malarski and L. Sobczyk, *Chem. Phys. Lett.*, 1997, **274**(4), 361

27. J. H. Clark and C. W. Jones, *ChemComm.*, 1990, **24**, 1786

28. D. A. Haynes, W. Jones and W. D. S. Motherwell, *CrystEngComm.*, 2006**, 8**(11), 830

29. C. B. Aakeroy, I. Hussain and J. Desper, *Cryst. Growth. Des.*, 2006, **6**(2), 474

30. K. D. M. Harris and M. Tremayne, *Chem. Mater.*, 1996**, 8**(11), 2554

31. S. Aitipamula, P. S. Chow and R. B. H. Tan, *CrystEngComm.*, 2012**, 14**(7), 2381

32. H. D. Clarke, K. K. Arora, H. Bass, P. Kavuru, T. T. Ong, T. Pujari, L. Wojitas and M. J. Zaworotko, *Cryst.Growth.Des.*, 2010, **10**(5), 2152

33. C. B. Aakeroy, S. Forbes and J. Desper, *CrystEngComm.*, 2012, **14**(7), 2435

34. A. M. Moragues-Bartolome, W.J ones and A. J. Cruz-Cabeza, *CrystEngComm.*, **2012, 14**(7), 2552

35. N. Shan and M. J. Zaworotko, *Drug Disc. Today*, 2008**, 13**(9-10), 440

36. D. R. Weyna, M. L. Cheney, N. Shan, M. Hanna, L. Wojtas and M. J. Zaworotko, *CrystEngComm.*, 2012, **14**(7), 2377

37. B. Das and, J. B. Baruah, *Cryst. Growth. Des.*, 2011, **11**(12), 5522

38. M. C. Etter, *Acc. Chem. Res.*, 1990, **23**(4), 120

39. P. Vishweshwar, A. Nangia and V. M. Lynch, *Cryst. Growth. Des.*, 2003, **3**(5), 783

40. D. Braga and F. Grepioni, *Chem.Commun.*, 2005, **29**, 3635

41. A. Nangia and G. R. Desiraju, *Acta. Crystallogr. Sect. A.*, 1998, **1**(54), 934

42. N. Issa, S. A. Barnett, S. Mohamed, D. E. Braun, R. C. B. Copley, D. A. Tocher and S. L. Price, *CrystEngComm.*, 2012, **14**(7), 2454

43. M. R. Caira, S. A. Bourne, H. Samsodien, E. Engel, W. Liebenberg, N. Stieger and M. Aucamp, *CrystEngComm.*, 2012, **14**(7), 2541

44. S. Ghosh and C. M. Reddy, *CrystEngComm.*, 2012, **14**(7), 2444

45. M. K. Stanton and A. Bak, *Cryst. Growth. Des.*, 2008**, 8**(10), 3856

46. L .S. Reddy, A. Nangia and V. M. Lynch, *Cryst. Growth. Des.*, 2004, **4**(1), 89

47. D. P. McNamara, S. L. Childs, J. Giordano, A. Iarriccio, J. Cassidy, M. S. Shet, R. Mannion, E. O'Donnell and A. Park, *Pharm. Res.*, 2006, **23**(8), 1888

48. A. Cowell, *An investigation into the synthesis, structural characterisation, thermal and polymorphic behaviour of organic crystalline materials*, PhD thesis, University of Birmingham, 2011

49. The Nobel Foundation, *Nobel Lectures, Physics 1901-1921*, Elsevier, Amsterdam, 1967

50. A. E. Goeta, J. A. K. Howard, *Chem. Soc. Rev.*, 2004, **33**(8), 490

51. A. L. Spek, *PLATON*, Bijvoet Centre for Biochemical Research, Vakgroep Kristal-en Structure-Chemie, University of Utrecht, Netherlands

52. M. I. McMahon, *J. Sync. Rad.*, 2005**, 12**, 549

53. M. Tremayne, J. J. Novoa, D. Braga, L. Addadi, *Engineering of Crystalline Materials Properties*, Springer, 2008

54. R. K. Harris, *Analyst*, 2006, **131**, 351

55. R. M. C. Dawson, D. C. Elliott, W. H. Elliott and K. M. Jones, *Data for biochemical research*, **2 ed**, Oxford Clarendon Press, 1969

2. Methodology

2.1 Single crystal structure solution and refinement

Structure solution and refinement, by a full-matrix least-squares procedure on F^2, were carried out using SHELXS97 and SHELXL97 respectively[1]. All non-hydrogen atoms were refined with anisotropic displacement parameters. Electron density maps were used to locate the positions of the carboxyl hydrogen atoms, confirming that the crystalline adduct is either in neutral cocrystal form or protonated salt form. H atoms were then added at calculated positions and refined by use of a riding model with isotropic displacement parameters based on the equivalent isotropic displacement parameter (U_{eq}) of the parent atom. The hydrogen atoms that are part of the water molecules in the hydrated structures were manually added and fixed as they could not be treated in the same way. WinGX[2] was used to prepare the material for discussion in the following results chapters for all structures except adenine : pimelic acid in which OLEX2[3] was used. Details of intermolecular interactions occurring in all structures were analysed with the aid of *PLATON*[4]. *DIAMOND*[5] and ORTEP3[6] were used to produce all of the figures displaying the crystal packing. Details of data collection are given in chapter 3.

2.2 Structure solution from powder diffraction data

2.2.1: Data handling

Powder X-ray diffraction data were collected as RAW files and converted to a UXD format using Diffract file exchange [XCH], with an in-house Perl-based converter used to create XY, GSA and XDD files required for other crystallographic software used later in the structure solution process.

Information about previously published crystal structures was downloaded from the Cambridge Structural Database (CSD) in crystallographic information file (CIF) format[7].

2.2.2: Unit cell and space group determination

The unit cell is determined from the X-ray powder diffraction pattern by means of indexing, which generates possible sets of lattice parameters from the selected peak positions with a figure of merit used to rank the results. The first 20 peaks in the diffraction pattern were selected using XFIT[8] and this information was used as an input in CRYSFIRE[9]. CRYSFIRE runs a series of indexing programs using the selected peak positions and collates a summary file detailing possible sets of lattice parameters including a figure of merit and unit cell volume. Chekcell[10] was then used to verify that the peak selection from XFIT and the results from CRYSFIRE matched. The space group was determined by examining the systematic absences in the diffraction pattern, using the international crystallographic tables and Chekcell[10].

2.2.3: Pattern decomposition

Pattern decomposition was carried out following identification of the unit cell and space group in both GSAS[11] via the EXPGUI[12] platform to create a Le Bail fit[13], and in Topas[14] to create a Pawley fit[14]. Pattern decomposition is a 'structureless' refinement, used in this work to achieve more accurate lattice parameters, zero-point and peak shape before structure solution is attempted. In this stage of the process, the peak intensities are treated as variables to be refined. An R factor (% R_{wp}) is produced and represents a target agreement that the structure solution and refinement steps later in the process aim to achieve.

2.2.4: Direct space methods

Traditional and direct space methods are two distinct approaches that can be used to solve a crystal structure once the lattice parameters and space group have been assigned. Traditional methods involve extracting individual intensities, I(*hkl*), from each individual reflection and whilst this approach has been successful in solving crystal structures from powder X-ray diffraction[15-17] the issue of peak overlap in powder X-ray diffraction (section 1.11) makes it more difficult to extract reliable intensities from the individual peaks.

Direct space methods, which have been utilised within this project (chapter 7), are techniques in which a 'trial' structure is produced. Trial structures are evaluated using the experimental diffraction pattern and assigned a figure of merit (% R_{wp}) or in some cases evaluated using chi-squared. The R-factor is a measure of similarity between the 'trial' structure and the experimental data, comparing the whole diffraction pattern point by point (equation 2.1).

$$\% R_{wp} = 100x \sqrt{\frac{\sum_i w_i (y_{iobs} - y_{icalc})^2}{\sum_i w_i (y_{iobs})^2}}$$

Equation 2.1: % R_{wp}, where y_{iobs} is the experimentally observed intensity at a value of 2θ and y_{icalc} is the calculated intensity at 2θ

A number of variables or structural parameters need to be considered when defining a problem using direct space methods. These are commonly categorized in three groups; the position of the molecule(s) or fragment(s) within the unit cell (*x,y,z*), the orientation of the molecule(s) or fragment(s) (θ,Φ,Ψ) and any freely rotating sections within the molecule(s) (τ_1-τ_n). The dimensionality of hypersurface of R_{wp} is then defined by these variables. Incorporation of prior crystallographic and chemical knowledge reduces the dimensionality and makes this process more efficient, e.g. prior chemical knowledge of benzene means only

6 parameters need to be considered as opposed to 18 if treated as six individual atoms. In this project, the molecular model was created in Chem 3D pro[18] and then converted and described by a list of elements. POSSUM[19] (a cross-platform suite program package) was used to input the different variables defining the structural model (such as the number of freely rotating bonds in the molecules), starting points for the calculation and other data before undergoing an optimisation.

A number of optimisation techniques are available for direct space methods including Monte Carlo[20,21], simulated annealing[22,23], genetic algorithms[24,25] and grid searches[26]. This study uses the differential evolution method, an evolutionary algorithm using a population based optimisation technique (described further in section 2.2.5).

2.2.5: Differential evolution

Differential evolution (DE) is a population based optimisation technique that maintains a number of trial structures which produce offspring through a combination of mutation and recombination (equation 2.2).

$$\text{Offspring} = \text{Parent} + K\,(\text{Random}_1 - \text{Parent}) + F\,(\text{Random}_2 - \text{Random}_3)$$

Equation 2.2: The creation of a trial structure from members of the previous population. K is the recombination factor and F the mutation factor

The calculation begins with trial structures spread across the hypersurface, each described by a set of elements with the structural parameters ($x,y,z,\theta,\Phi,\Psi,\tau_1$-$\tau_n$) chosen at random. Each member of the population is a trial structure whose fitness is measured by % R_{wp} (comparison of the trial structure to the experimental data). Each member then produces an offspring

structure using equation 2.2. If the offspring is fitter than its parent, i.e. has a lower R_{wp}, it replaces the parent structure which is then discarded; if not the parent remains in the population and the offspring is discarded. This process continues with the mean % R_{wp} of each generation and the best individual % R_{wp} been monitored. Convergence is achieved when these two values are equal. The process is fast and relatively efficient although local minima are sometimes located rather than the global minimum (figure 2.1)

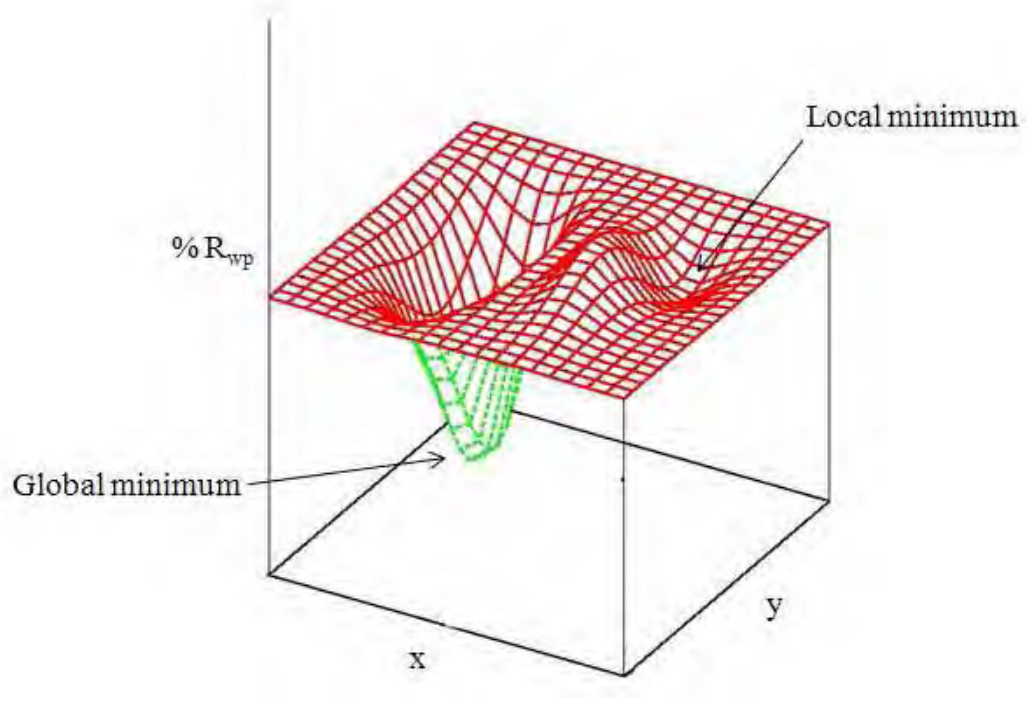

Figure 2.1: An example of local minimum and the global minimum on an energy hypersurface. Figure taken from reference 27

To try and avoid this problem, a diverse initial population is used. The initial recombination and mutation vectors between the population are likely to be large due to the random diverse distribution, and will consequently produce diverse offspring. Progression of the calculation will result in the population becoming less diverse, leading to a shortening of vectors, and eventually convergence of the calculation (figure 2.2).

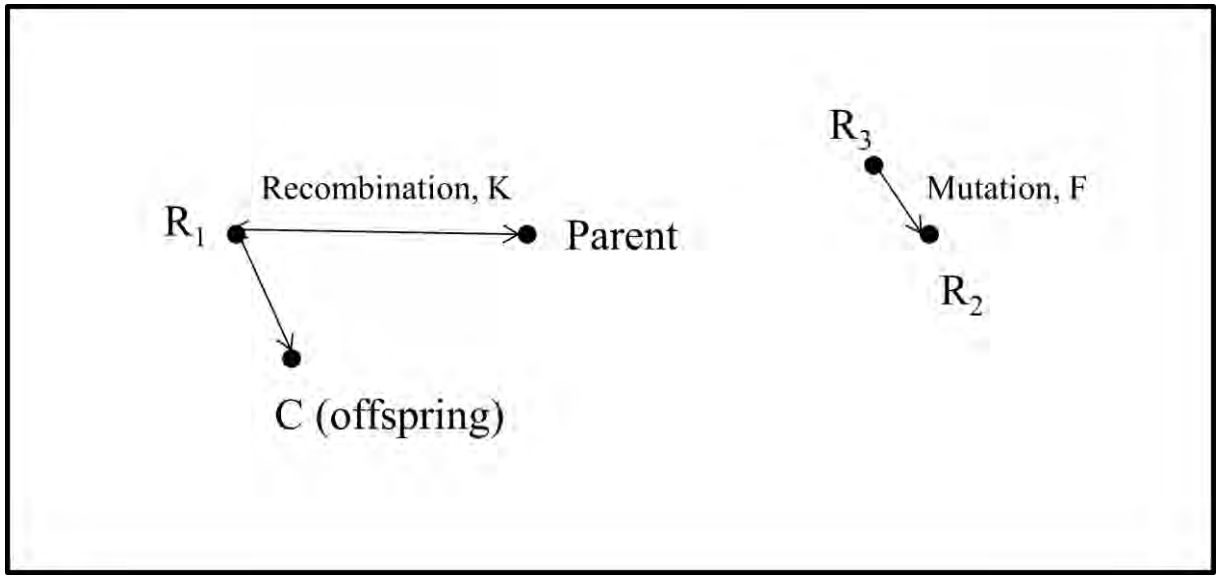

Figure 2.2: Production of an offspring trial structure using a combination of variables of the parent and randomly selected individuals (R_1, R_2 and R_3)

The recombination vector K, represents the difference between genetic material from the parent to one random member, R_1. The mutation vector F, represents the difference in parameters between two random members of the population, R_2 and R_3. The mutation component establishes significant differences between the child and its original parent to avoid premature convergence in local minima. The scaling of these vectors (values of K and F) can be defined in POSSUM[19] along with other data. A vector that is too large may miss narrow minima, whereas if it is too small, convergence may lead to a local minima. The DE calculation also uses boundary conditions to keep the search within a defined space, using prior crystallographic knowledge to direct the search. The DE process can be used to give a structure solution that is used as the starting point for Rietveld refinement[28] in which more flexible structural features are introduced.

2.2.6: Rietveld refinements

Rietveld refinement uses a least-squares approach to obtain an optimal fit between an observed experimental diffraction pattern and a calculated diffraction pattern simulated from the model structure such as that obtained from DE. The refinement considers every point in the powder diffraction pattern as an individual intensity and compares it to the simulated data, again using % R_{wp} as a figure of merit. Variables relating to both the crystal structure and instrumentation are adjusted to achieve the optimal fit[28]. To ensure refinements are chemically acceptable, geometric restraints can be applied to the bond lengths and angles based upon prior chemical knowledge and standard molecular geometries[29]. Rietveld refinement can be carried out using a number of different software packages. In this project GSAS[11] and Topas[14] were the programs of choice.

2.3 References

1. G. M. Sheldrick, *Acta. Crystallogr., Sect. A: Found. Crystallogr.*, 2008, **64**, 112
2. L. J. Farrugia, *J. Appl. Crystallogr.*, 1999, **32**, 837
3. O. V. Dolomanov, L. J. Bourhis, R. J. Gildea, J. A. K. Howard and H. Puschmann, *J. Appl. Cryst.*, 2009, **42**, 339
4. A. L. Spek, *PLATON*, Bijvoet Centre for Biochemical Research, Vakgroep Kristal-en Structure-Chemie, University of Utrecht, Netherlands
5. K. Brandenburg, *Diamond, Version 3.0*, Crystal Impact GbR, Bonn, Germany, 1997-2004
6. L. J. Farrugia, *J. Appl. Crystallogr.*, 1997, **30**, 565
7. S. R. Hall, F. H. Allen and I. D. Brown, *Acta Crystallogr. Sect. A*, 1991, **47**, 655
8. R. W. Cheary and A. A. Collis, Deposited in the CCP14 Powder Diffraction Laboratory, Engineering and Physical Science Research Council, Daresbury Laboratory, Warrington, England, 1996

9. R. A. Shirley, CRYSFIRE Powder Indexing System, University of Surrey, England, 2000,

10. J. Laugier and B. Bochu, Labatoire des Materiaux and Genie Physique Ecole Nationale Superieure de Physique de Grenoble (INPG). Domaine Universitaire BP 46, 38402, Saint Martin d'Heres, France

11. A. C. Larson and R. B. Von Dreele, *General Structure Analysis System (GSAS),* Los Alamos National Labouratory Report LAUR 86-748, Los Alamos. New Mexico, USA, 1994

12. B. H. Toby, *J. Appl. Crystallogr.*, 2001, **34**, 210

13. A. LeBail, H. Droy and J. L. Fourquet, *Mat. Res, Bull.*, 1988, **23**, 447

14. G. S. Pawley, *J. Appl. Crystallogr.*, 1981, **14**, 357

15. R. J. Cernik, A. K. Cheetham, C. K. Prout, D. J. Watkin, A. P. Wilkinson and B. T. M. Willis, *J. Appl. Crystallogr.*, 1991, **24**, 222

16. K. D. Knudsen, P. Pattison, A. N. Fitch and R. J. Cernik, *Angewandte Chemie-International Edition*, 1998, **37**(17), 2340

17. P. Lightfoot, M. Tremayne, K. D. M. Harris and P. G. Bruce, *J. Chem. Soc. Chem. Comm.*, 1992, **14**, 1012

18. *CS Chem 3D pro(tm) Molecular modelling and analysis*, Copyright 1986-1996

19. C. C. Seaton and M. Tremayne, *Possum Programs fro Direct-Space Structure Solution from Powder Diffraction Data*, 2002, School of Chemistry, University of Birmingham, UK

20. K. D. M. Harris, M. Tremayne, P. Lightfoot and P. G. Bruce, *J. Am. Chem. Soc.*, 1994, **116**(8), 3543

21. M. Tremayne, B. M. Kariuki and K. D. M. Harris, *J. Appl. Crystallogr.*, 1996, **29**, 211

22. M. Rajeswaran, T. N. Blanton, N. Zumbulyadis, D. J. Giesen, C. Conesa-Moratilla, S. T. Misture, P. W. Stephens and A. Huq, *J. Am. Chem. Soc.*, 2002, **124**(48), 14450

23. A. Huq and P. W. Stephens*, J. Pharm. Sci.*, 2003, **92**(2), 244

24. B. M. Kariuki, P. Calcagno, K. D. M. Harris, D. Philp and R. L. Johnston, *Angewandte Chemie-International Edition*, 1999, **38**(6), 831

25. B. M. Kariuki, G. L. Bauer, K. D. M. Harris and S. J. Teat, *Angewandte Chemie-International Edition*, 2000, **39**(24), 4485

26. S. Y. Ryabova, N. A. Rastorgueva, E. J. Sonneveld, R. Peschar, H. Schenk, V. A. Tafeenko L. A. Aslanov and V. V. Chernyshev, *Acta. Crystallogr. Sect. B*, 2005, **61**, 192

27. A. Cowell, *An investigation into the synthesis, structural characterisation, thermal and polymorphic behaviour of organic crystalline materials*, PhD thesis, University of Birmingham, 2011

28. H. M. Rietveld, *J. Appl. Crystallogr.*, 1969, **22**, 65

29. F. H. Allen, O. Kennard, D. G. Watson, L. Brammer, A. G. Orpen and R. Taylor, *J. Chem. Soc. Perk. T. 2*, 1987, S1

3. Experimental

3.1 Synthesis by solvent-mediated crystallisation

Stoichiometric amounts of the cocrystal components (approximately 0.1 g) were dissolved in a suitable solvent added dropwise (approximately 20 ml, though when dissolving adenine significantly more solvent was required, approximately 50 ml). The solutions were heated and stirred until all starting material had dissolved and the solutions were both filtered (through hot filtration) into the same conical flask. The solution was allowed to crystallise over time before being dried under suction for approximately one hour. All experiments were carried out at room temperature and pressure. The experiments were repeated using a different solvent. This experimental procedure was followed for all systems presented in this thesis using both methanol and ethanol as initial and repeat choice of solvent unless otherwise stated. The length of time for cocrystallisation varies from two days to two months with the longer chain acid cocrystals taking the longest.

3.2 Synthesis by solvent-mediated crystallisation using multi-reaction rack

Stoichiometric amounts (approximately 0.05 g) of the cocrystal components were added to a 20ml vial suitable for use in a multi-reaction rack. The Anachem Reactarray Microvate multi-reaction rack, model RAR-12 can hold 24 samples and allows accurate temperature control over each strip of four holders with a global stirring control. A suitable solvent (methanol) was added dropwise and the vial placed into the rack. The multi-reaction rack was programmed to heat from room temperature to 60 ºC at a ramp rate of 5 ºC per minute, to hold for 1 hour allowing the starting materials to dissolve and then to drop to 25 ºC at a ramp rate

of 5 ºC per minute, with stirring for the first 75 minutes. The resultant solution was left over time to crystallise and was then dried under suction for approximately one hour. All experiments were carried out at room temperature and pressure.

3.3 Powder X-ray diffraction

3.3.1 Laboratory diffraction data

Datasets were collected using a Bruker AXS D8 high resolution powder diffractometer in transmission mode. The sample was mounted on clear transparent tape and held in place on a PMMA transmission sample ring as a thin disc of approxiamately 8mm diameter. The wavelength used was λ = 1.5406 Å ($CuK\alpha_1$) generated by a sealed-tube X-ray source and selected using a germanium crystal monochromator. A 1mm exit slit and 1° mototrised divergence slit were used and the detector was a solid-state LynxEye position sensitive detector (PSD) covering 3º in 2θ. The data were collected over a 2θ range of 5º <2θ <70º and the step size was 0.0198º. The data were collected over 20 minutes.

3.3.2 High resolution diffraction data

The high resolution synchrotron X-ray powder diffraction data was obtained from beamline I11 at Diamond Light Source over a 2θ range of 0.955˚– 151.74˚ (λ = 1.035467 Å). Data were collected at room temperature at various positions of the sample to avoid beam damage (three positions at 4mm intervals if the amount of sample permitted) with the datasets combined. The data were collected for either 10 minutes or 15 minutes at each position.

3.4 Single crystal X-ray diffraction

Single crystal X-ray diffraction data collection has been carried out using five different diffractometers, including one at a synchrotron source. Details of the instruments used and a list of which diffractometer was used for each data collection are given overleaf (table 3.1).

3.4.1 Diffractometer 1; Bruker APEX II CCD

Data were collected from suitable crystals on a Bruker APEX II CCD diffractometer at the window of a Bruker FR591 rotating anode ($\lambda_{Mo\text{-}K\alpha}$ = 0.71073 Å) at 120 K by the UK National Crystallography Service[1]. The data collections were driven by *COLLECT*[2] and processed by *DENZO*[3]. Absorption corrections were applied using SADABS[4]. Structure solution and refinement details are given in chapter 2.

3.4.2 Diffractometer 2; Bruker CCD

Data were collected from suitable crystals on a Bruker CCD diffractometer at the window of a Bruker FR591 rotating anode ($\lambda_{Mo\text{-}K\alpha}$ = 0.71073 Å) at 120 K by the UK National Crystallography Service[1]. The data collections were driven by *COLLECT*[2] and processed by *DENZO*[3]. Absorption corrections were applied using SADABS[4]. Structure solution and refinement details are given in chapter 2.

3.4.3 Diffractometer 3; Bruker SMART 6000

Data were collected from suitable crystals on a Bruker SMART 6000 diffractometer ($\lambda_{Cu\text{-}K\alpha}$ = 1.54184 Å) at 120 K in the School of Chemistry at the University of Birmingham. The data collections were driven by SMART[5] and processed by SAINT[6]. Absorption corrections were applied using SADABS[4]. Structure solution and refinement details are given in chapter 2.

3.4.4 Diffractometer 4; Rigaku Kappa 3 circle

Data were collected from suitable crystals on a Kappa 3 circle diffractometer equipped with a Rigaku Saturn 724 CCD detector (λ = 0.71075 Å) at the UK National Crystallography Service[1]. The data were collected at 100 K, and the data collections were driven and processed by CrystalClear-SM Expert 2.0r7[7]. Absorption corrections were applied using CrystalClear-SM Expert 2.0r7[7]. Structure solution and refinement details are given in chapter 2.

3.4.5 Diffractometer 5; Synchrotron 4-circle

Data were collected from a suitable crystal on a Crystal Logic 4-circle kappa diffractometer equipped with a Rigaku Saturn 724 CCD detector using synchrotron radiation (λ = 0.68890 Å) at beamline I19 at Diamond Light Source by the UK National Crystallography Service[1]. The data were collected at 100 K, and the data collection was driven and processed by CrystalClear-SM Expert 2.0r5[8]. Structure solution and refinement details are given in chapter 2.

Table 3.1: Details of the single crystal diffractometers used for data collection of specific crystal structures

System	Chapter	Diffractometer
Adeninium : malonate	4	Diffractometer 3; Bruker SMART 6000
Adenine : succinic acid	4	Diffractometer 1; Bruker APEX II CCD
Adenine : fumarate	4	Diffractometer 1; Bruker APEX II CCD
Adeninium : hydrogen maleate	4	Diffractometer 5; Synchrotron 4-circle
Adeninium : hydrogen maleate methanolate	4	Diffractometer 3; Bruker SMART 6000
Adenine : pimelic acid	4	Diffractometer 4; Rigaku Kappa 3 circle
Adenine : suberic acid	4	Diffractometer 4; Rigaku Kappa 3 circle
Azelaic acid	4	Diffractometer 3; Bruker SMART 6000
Adenine : sebacic acid	4	Diffractometer 3; Bruker SMART 6000
Isonicotinamide : pimelic acid	5	Diffractometer 2; Bruker CCD
Isonicotinamide :suberic acid	5	Diffractometer 1; Bruker APEX II CCD
Isonicotinamide : azelaic acid	5	Diffractometer 1; Bruker APEX II CCD
Nicotinamide : succinic acid	6	Diffractometer 1; Bruker APEX II CCD
Nicotinamide : undecanedioic acid	6	Diffractometer 3; Bruker SMART 6000

3.5 Solution ^{1}H NMR Spectroscopy

The solution state ^{1}H NMR spectra were recorded on a Bruker AVIII300 spectrometer. The spectra were recorded at 300.18 MHz with a 5 mm quad probe using residual solvent as a reference. A small amount of each sample (approximately 5 – 25 mg) was used, dissolved in d^{6} DMSO.

3.6 Melting point measurements

Melting point measurements were made on a Stuart Scientific Melting Point SMP1 machine. The sample were placed into a 100 mm long capillary tube with inner dimension of 1.3 mm before being inserted into the melting point machine along with a standard thermometer that measures up to 360°. The melting point machine was turned on to heat gently and the melting point read. Each melting point was measured twice with an average taken.

3.7 References

1. S. J. Coles and P. A. Gale, *Chem. Sci.*, 2012, **3**(3), 683
2. R. W. W. Hooft, *COLLECT Data Collection Software*, Nonius B.V., Delft, 1998
3. Z. Otwinowski and W. Minor, in *Methods in Enzymology*, ed. C. W. Carter and R. M. Sweet, Academic Press, New York, 1997, vol. 276, Pt A, pp. 307-326
4. G. M. Sheldrick, *SADABS*, Bruker AXS Inc., Madison, Wisconsin, USA, 2007
5. Bruker, *SMART Version 5*, Bruker AXS, Inc.: Madison, WI, USA, 1997
6. Bruker, *SAINT Version 6*, Bruker AXS, Inc.: Madison, WI, USA, 1997
7. Rigaku, *CrystalClear Version 2*, Rigaku Corporation, Tokyo, Japan, 2011
8. Rigaku, *CrystalClear Version 2*, Rigaku Corporation, Tokyo, Japan, 2010

4. Adenine: tautomerism, cocrystallisation, salt formation and solvation

4.1 Introduction

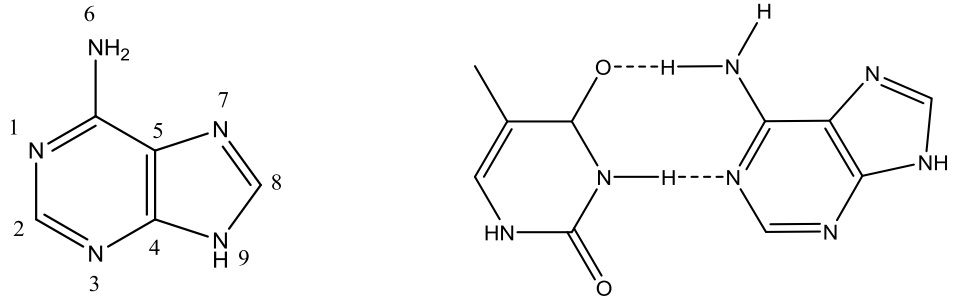

(a) (b)

Figure 4.1: (a) The most stable tautomer of adenine, showing the numbering scheme used when discussing tautomeric forms and (b) the adenine-thymine base pair

Adenine (figure 4.1 (a)), a nucleobase with several uses in biochemistry[1], is an integral part of both DNA and RNA. Adenine hydrogen bonds with thymine (figure 4.1 (b)) to form a base pair stabilising the DNA double helix (along with a guanine-cytosine base pair) and forms a base pair with uracil in RNA, aiding protein synthesis[2,3]. Not only does it play an important part within the structure of DNA, it has multiple hydrogen bond donor and acceptor sites, giving it the opportunity to form strong heteromeric synthons between itself and other molecules.

Adenine exists in fourteen different tautomeric forms which can be problematic, for example it can cause spontaneous mutations in DNA[4,5]. Investigation of twelve of these different tautomers, focussing on the relative stabilities and ionisation energies found that the natural form of adenine, tautomer 9*H* (figure 4.2), is the most stable, followed by tautomers 3*H* and 7*H* respectively[5].

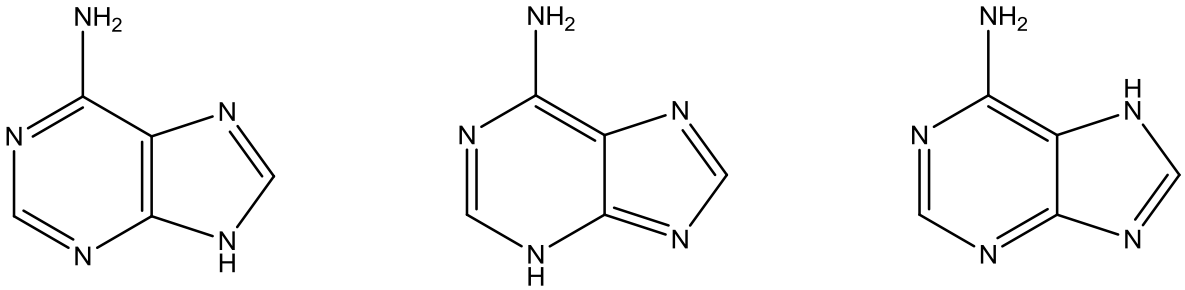

(a) (b) (c)

Figure 4.2: The three most stable tautomers of adenine; (a) 9*H*, (b) 3*H* and (c) 7*H*

Whilst there is limited previous research into adenine complexes, it has been identified as a good cocrystal former as it contains a number of strong hydrogen bond donor and acceptor sites and is known to form crystalline complexes, for example with metal ions[6] and hydrated crystalline complexes such as adenine : riboflavin[7]. Appendix 1.1 and 1.2 contain tables displaying the results of a CSD (Cambridge Structural Database) of all known adenine complexes to date (both neutral and protonated adeninium ion forms) and their relative tautomeric form. Previous publications have reported that adenine has formed crystalline complexes with three dicarboxylic acids; oxalic acid[8], maleic acid[1,9] and adipic acid[10] and these will be discussed in detail later in the chapter.

This chapter focuses on the synthesis and characterisation of a number of crystalline adducts formed by adenine and a range of dicarboxylic acids, $HO_2C(CH2)_{n-2}CO_2H$ with a carbon chain length (*n*) between two and ten. There are a few cocrystals and salts reported for adenine but relatively few of these contain dicarboxylic acids. As such, no trend in structure or properties has yet been established for adenine : dicarboxylic acid adducts, although a number of possible motifs between adenine and the dicarboxylic acid along with possible dimer formations of adenine have been identified for the most stable three tautomers of adenine as shown in table 4.1.

Table 4.1: Possible adenine - acid and adenine - adenine bonding motifs

9H tautomer	
Adenine - acid	
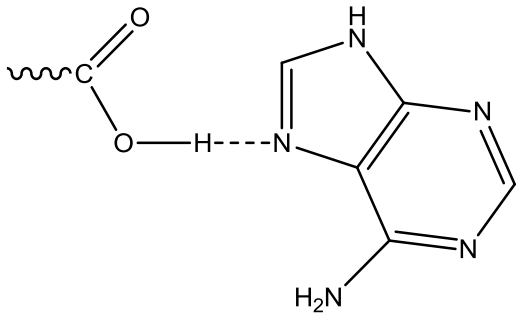 **9*H*-I**	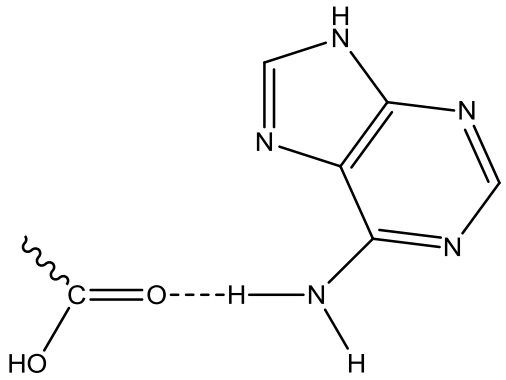 **9*H*-II**
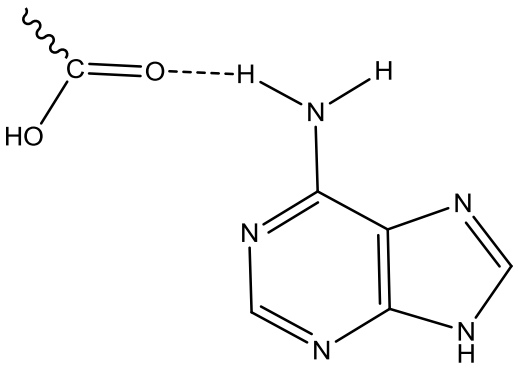 **9*H*-III**	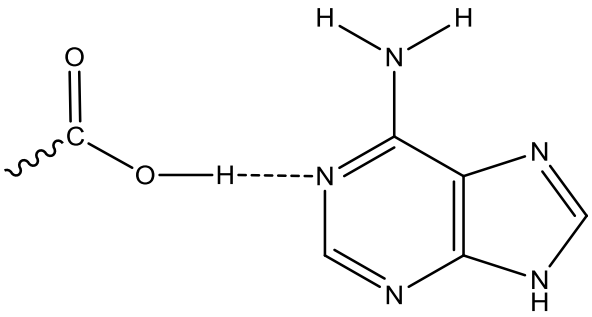 **9*H*-IV**
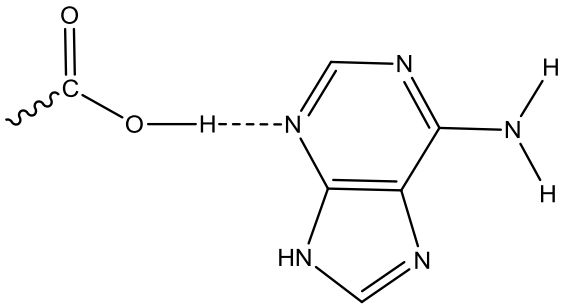 **9*H*-V**	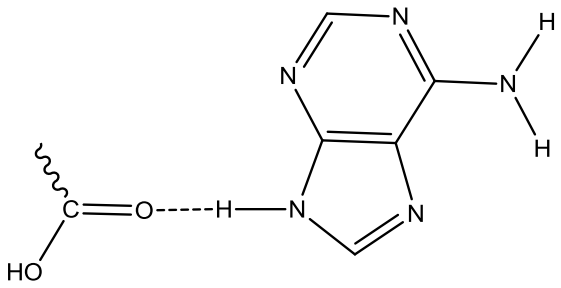 **9*H*-VI**

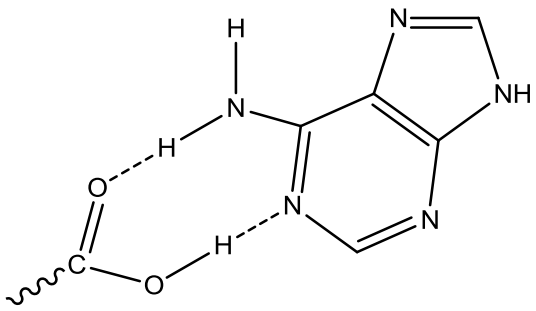

9*H*-VII

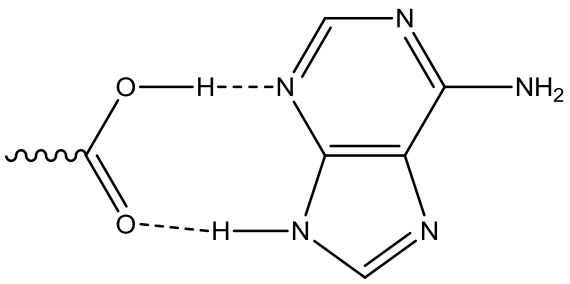

9*H*-VIII

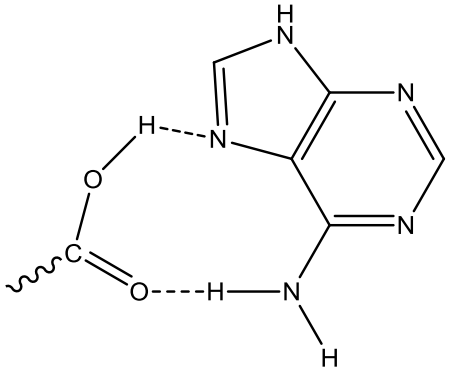

9*H*-IX

Adenine dimers

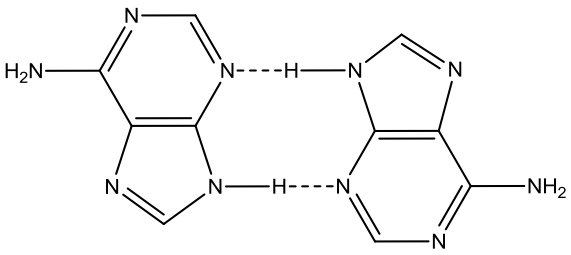

9*H*-X

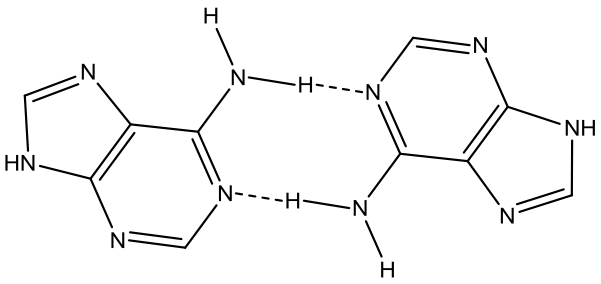

9*H*-XI

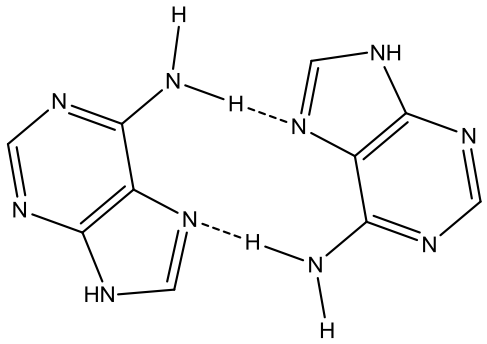

9*H*-XII

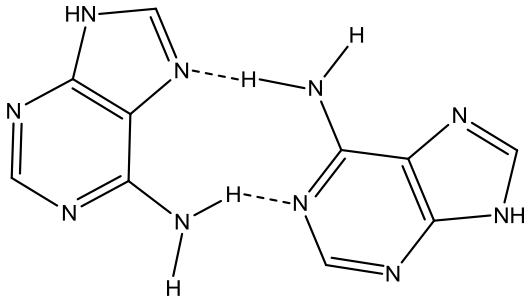

9*H*-XIII

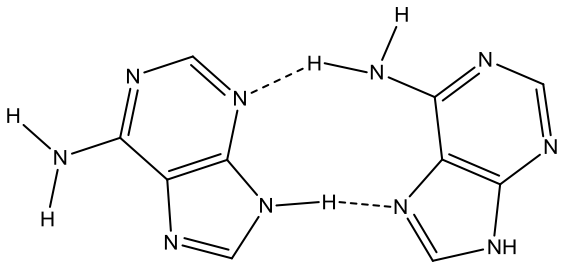 **9*H*-XV**	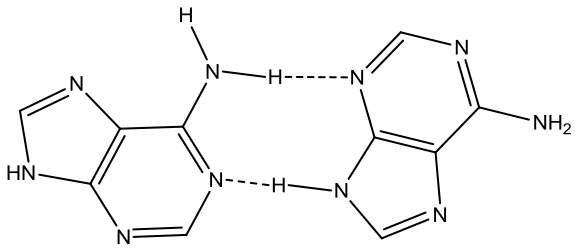 **9*H*-XVI**

3H tautomer	
Adenine - acid	
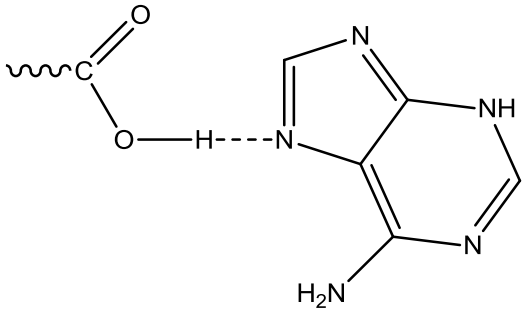 **3*H*-I**	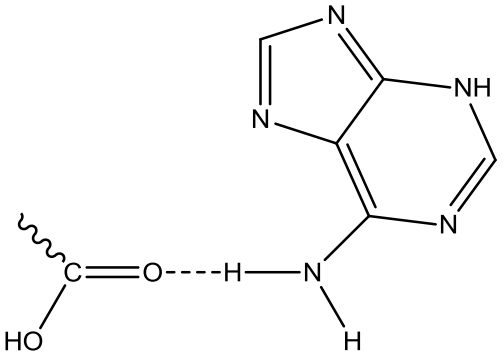 **3*H*-II**
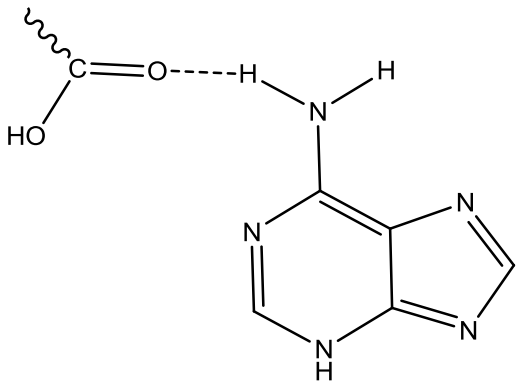 **3*H*-III**	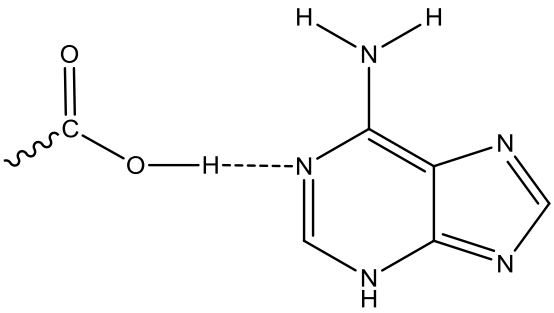 **3*H*-IV**

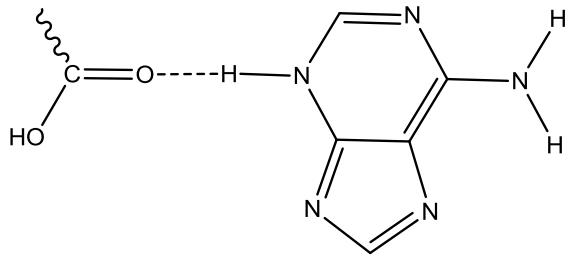

3*H*-V

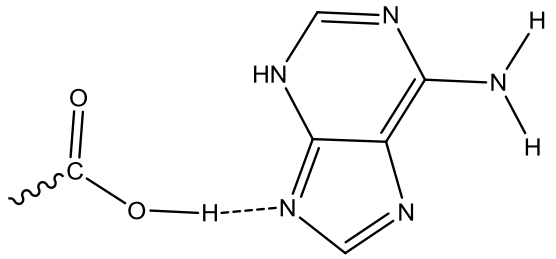

3*H*-VI

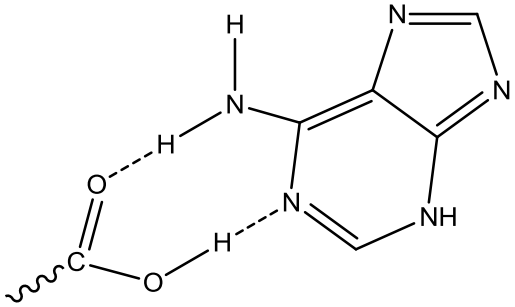

3*H*-VII

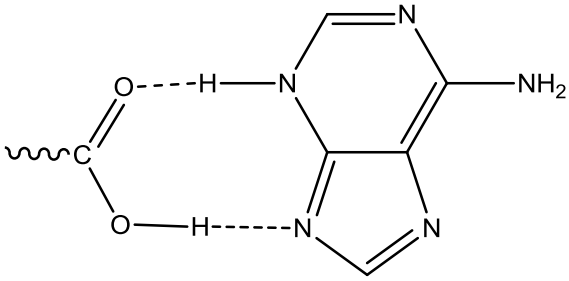

3*H*-VIII

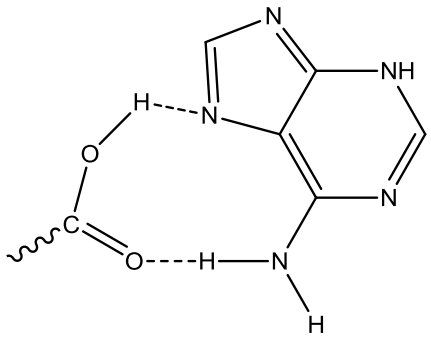

3*H*-IX

Adenine dimers

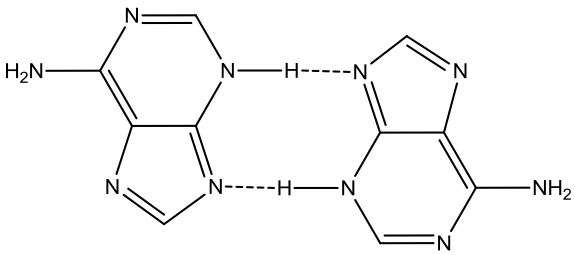

3*H*-X

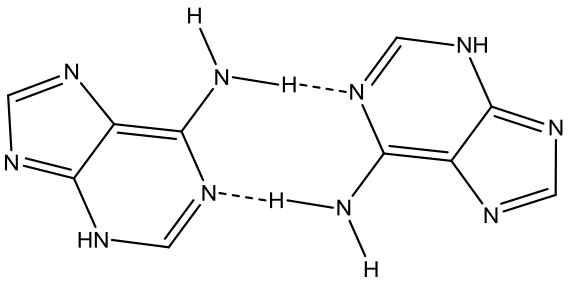

3*H*-XI

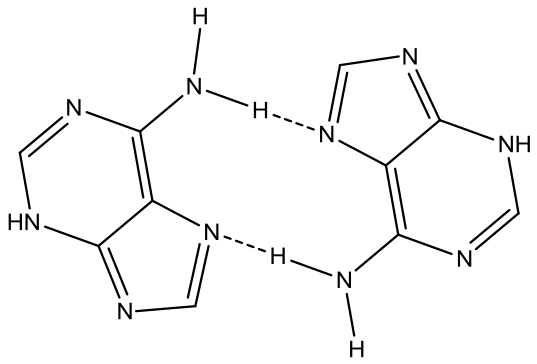

3*H*-XII

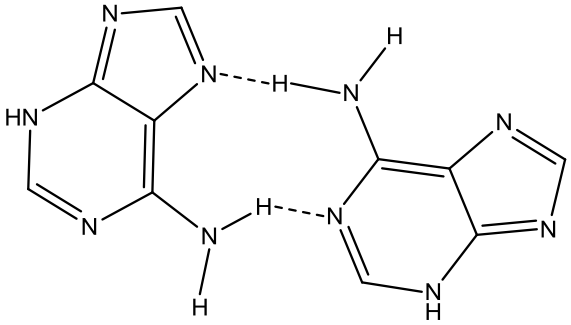

3*H*-XIII

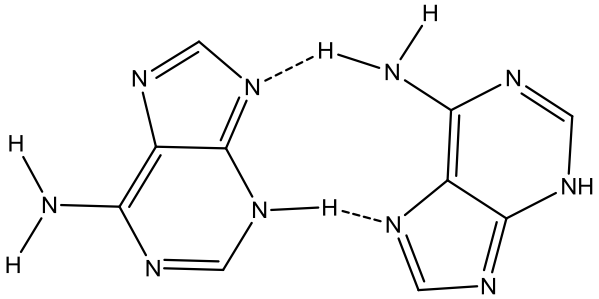

3*H*-XIV

7H tautomer	
Adenine - acid	
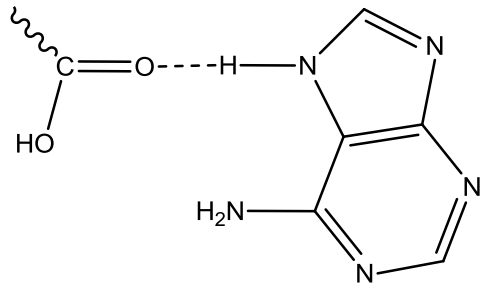	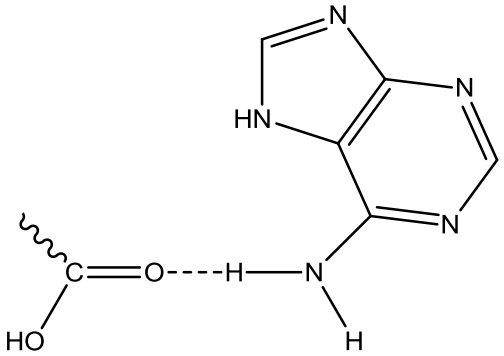
7*H*-I	**7*H*-II**
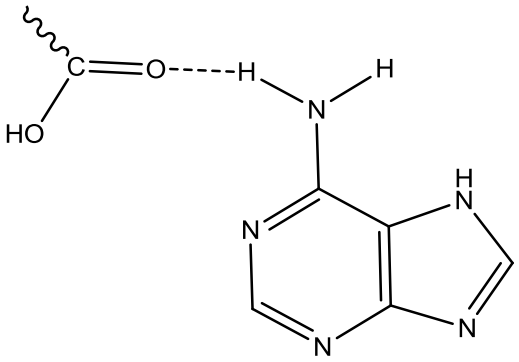	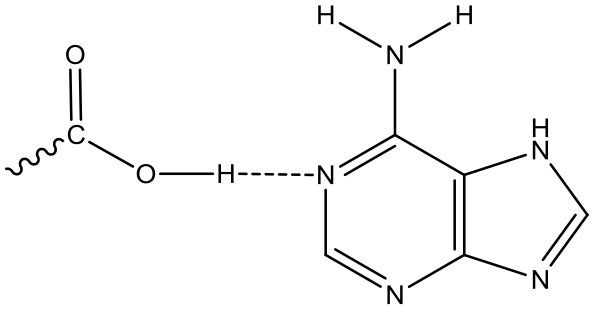
7*H*-III	**7*H*-IV**
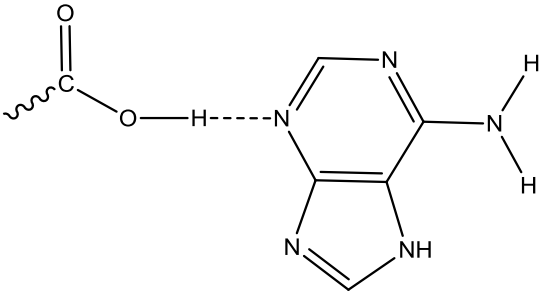	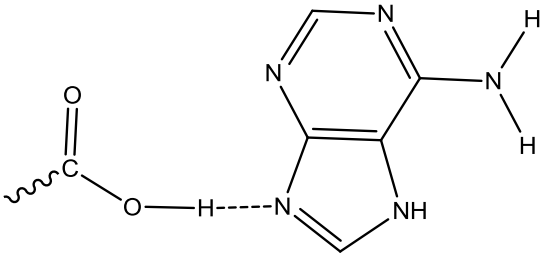
7*H*-V	**7*H*-VI**
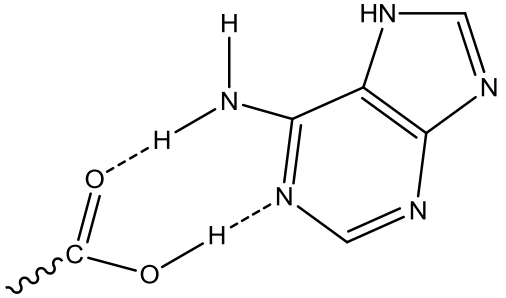	
7*H*-VII	

Adenine dimers	
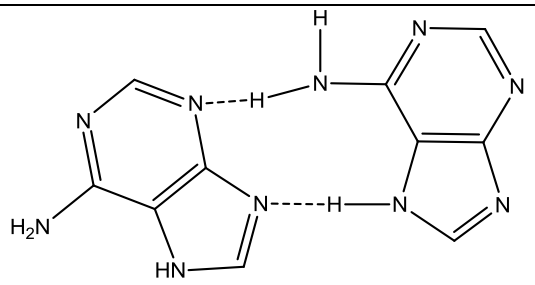 **7*H*-VIII**	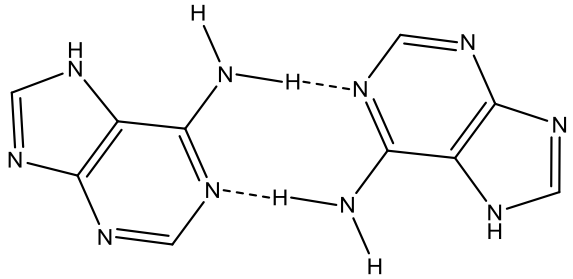 **7*H*-IX**
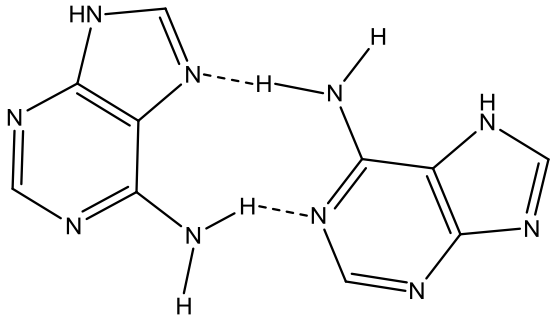 **7*H*-X**	

It is clear from this table that there are many possible motifs for the different tautomers, including a number of dimer options, with additional alternatives possible for the adeninium form. From the study of both previously reported adenine complexes and the structure of adenine itself it is found that an adenine dimer motif is very popular[1,2,6,7,9,10]. Structure descriptions of adenine complexes are often described using base pairs, Watson-Crick and Hoogsteen edges. Figure 4.3 shows an example of carboxylic acids bonding to an adenine molecule on the base (B), Watson-Crick edge (W-C) and the Hoogsteen edge (H).

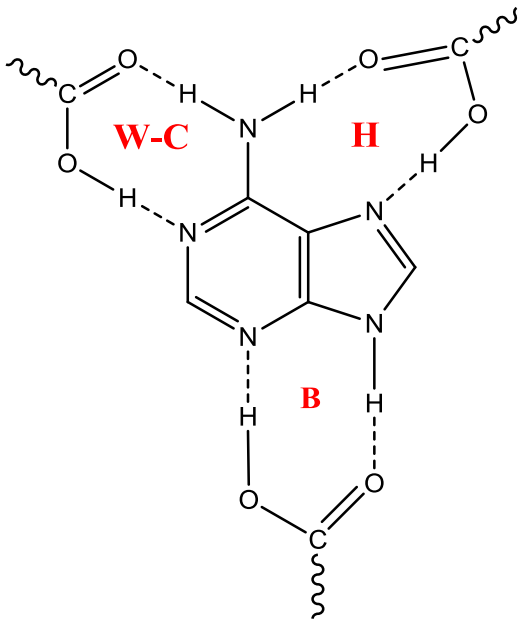

Figure 4.3: An example of adenine molecule as the 9*H* tautomer forming motifs with carboxylic acids on the base (b), Watson-Crick (WC) and Hoogsteen (H) edges

The consideration of possible hydrogen bonding motifs is not the only variable in prediction of the structure of a crystalline adduct; the pK_a difference of the coformers can also give insight into whether proton transfer is likely to occur, thus resulting in salt (in this case adeninium) rather than cocrystal formation. A pK_a difference greater than 2 - 3 is often used to indicate that salt formation will dominate[11], although there are anomalies to this 'rule'. The pK_a values of all of the coformers investigated in this chapter are given in table 4.2.

Table 4.2: A table of pK_a values for the coformers investigated[12]. pK_a^1 refers to the pK_a of the first acid deprotonation and pK_a^2 then refers to that of the second.

Coformer	Chemdraw	pK_a
Adenine	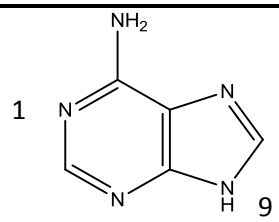	N1 - 4.1 N9 - 9.8
		pK_a^1 pK_a^2
Oxalic acid	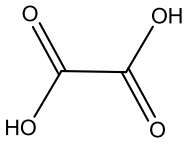	1.27 4.29
Malonic acid	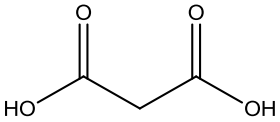	2.85 5.70
Succinic acid	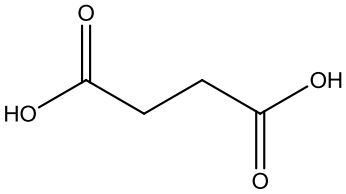	4.21 5.64
Fumaric acid	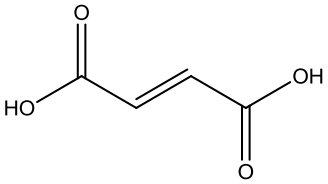	3.02 4.38
Maleic acid	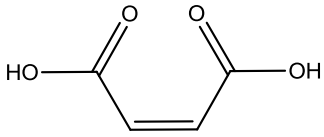	1.97 6.24
Glutaric acid	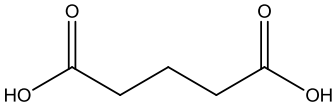	4.34 5.41
Adipic acid	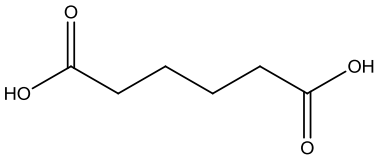	4.43 5.41

Pimelic acid	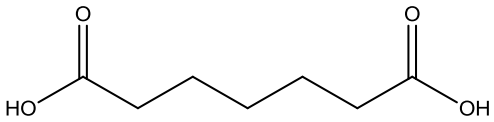	4.50	5.43
Suberic acid	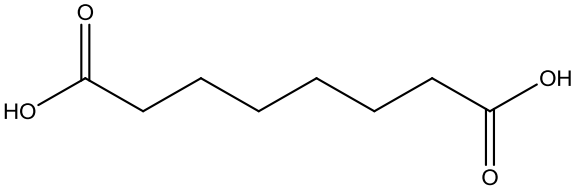	4.53	5.50
Azelaic acid	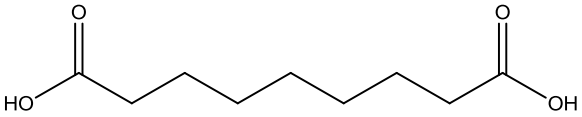	4.55	5.50
Sebacic acid	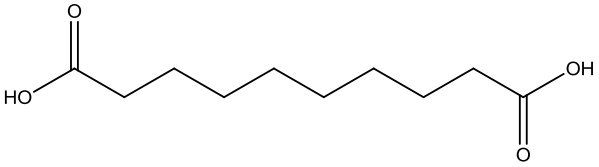	4.72	5.45
Undecanedioic acid	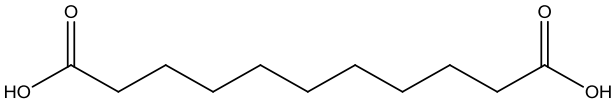	4.48	

These pK_a values suggest that cocrystal formation will predominate for adducts of adenine with carboxylic acids with n≥5, and that cocrystals will most likely be formed with malonic, succinic acid and fumaric acid, but that for oxalic and maleic acid, salt formation is the most likely outcome.

4.2 Previously known structures

There are five previously reported adenine adducts with dicarboxylic acids from the set of coformers considered here; two adeninium : oxalate (n = 2) salts, one of which is chlorinated and the other hydrated[8], an adeninium : adenine : maleate (n = 4) hydrated salt[1], a second adeninium : maleate hydrated salt (incorrectly reported in the literature as adeninium : succinate)[9] and an adenine : adipic acid (n = 6) 2:1 solvated cocrystal[10]. As comparison of the motifs and hydrogen bonded networks of both published and new structures is essential the crystal packing found within these published adducts along with the structure of pure adenine will be discussed in detail first.

4.2.1 – Adenine

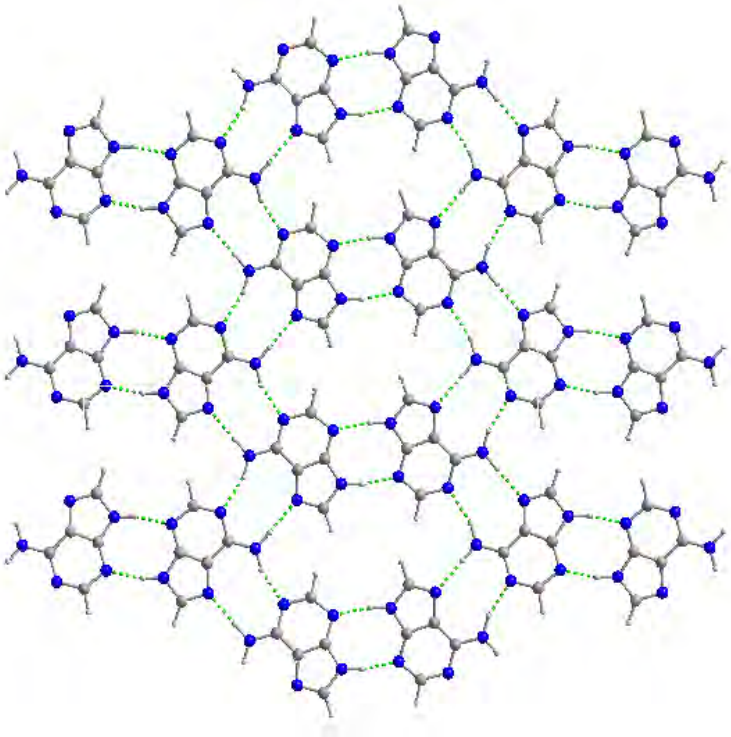

Figure 4.4: A view of the pure adenine structure, displaying the two adenine dimer motifs present which form infinite sheets. Hydrogen bonds are shown as dashed lines.

The structure of adenine has been published by Mahaptra *et al*[2], though it has since been found to be disordered by a Tremayne and co-workers who successfully solved the structure from powder X-ray diffraction[13] (figure 4.4). Infinite hydrogen bonded sheets are formed through two different adenine dimer motifs, which stack to form the adenine structure. The dimers present in this structure are based on the 9*H* tautomer motifs 9*H*-X and 9*H*-XIII, both of which are observed in the structures presented later in this chapter.

4.2.2 – Adeninium : oxalate : chlorine solvate 2:1:2

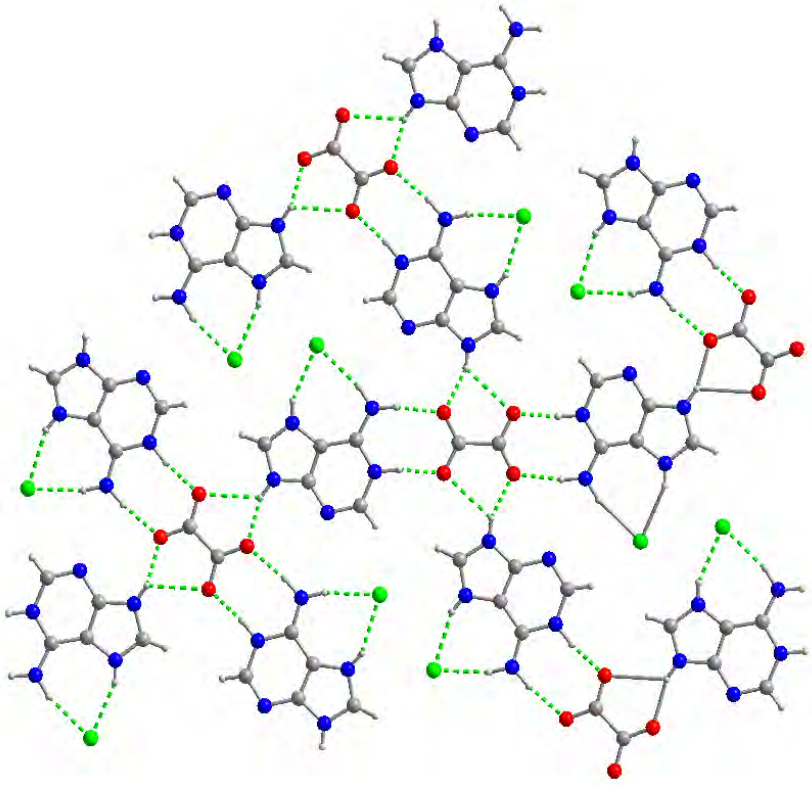

Figure 4.5: A view of the chlorinated adeninium : oxalate salt[8]. Hydrogen bonds are shown as dashed lines

The chlorinated adeninium : oxalate salt has a 2:1:2 adeninium : oxalate : chlorine stoichiometry in which the oxalic acid has been bideprotonated (figure 4.5). The pK_a difference between these two coformers is greater than two, therefore the formation of a salt as opposed to a cocrystal was to be expected, although surprisingly the structure does not contain adenine dimers as seen in many other adenine and adeninium structures. With both of the carboxyl groups on the oxalic acid deprotonated, the adeninium ions exist in the 1*H*,7*H*,9*H* tautomeric form. The adeninium and oxalate molecules link to form $R_2^2(8)$ ring motifs[14] based on motif 9*H*-VII but in an alternative tautomeric form. A secondary ring motif

is formed where N9 acts as a double donor, donating to two oxygen molecules to the oxalates. The chlorine molecules bond only to the adeninium molecules and not to the oxalates[8].

4.2.3 – Adeninium : hydrogen oxalate : oxalate : hydrate 2:2:1:2

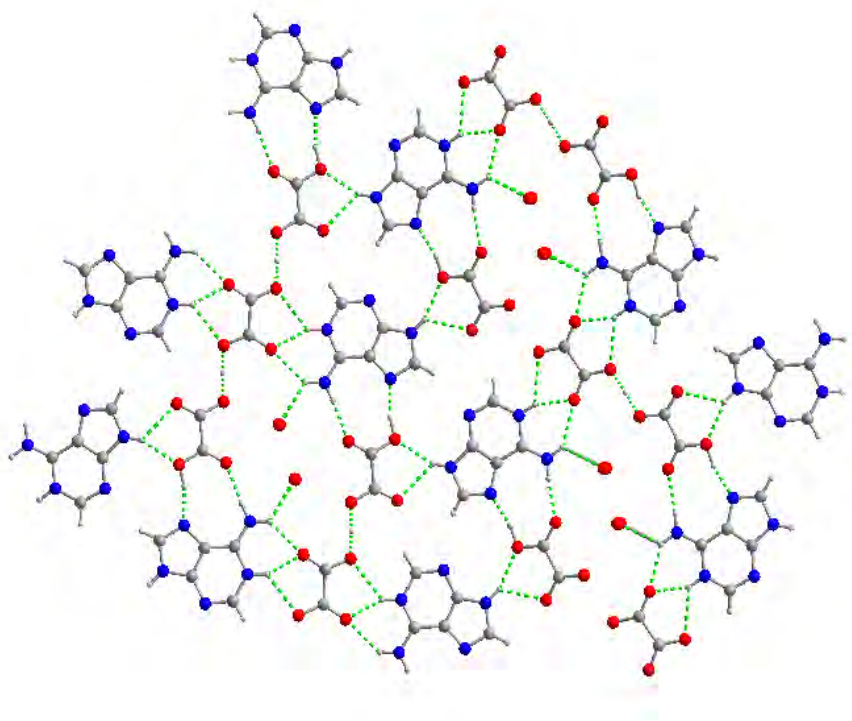

Figure 4.6: A view of the hydrated adeninium : oxalate salt structure[8]. Hydrogen bonds are shown as dashed lines

The hydrated adeninium : hydrogen oxalate salt structure is similar to the chlorinated structure in that no adenine dimer is present. The adeninium molecules exist in the 1*H*,9*H* tautomeric form with the asymmetric unit containing one adeninium cation, one hydrogen oxalate anion, half an oxalic acid and a disordered water molecule (figure 4.6). The structure consists of a $R_2^2(9)$ acid-Hoogsteen ring motif between the adeninium and the oxalate based on motif 9*H*-IX but with a protonated adeninium. A second ring motif is present similar to one seen in the

chlorinated structure in which N9 acts as a double donor. Like the chlorine molecules in the previous oxalate structure, the water molecules bond solely to the adeninium ions[8].

4.2.4 – Adeninium : adenine : hydrogen maleate : hydrate 2:2:1:2

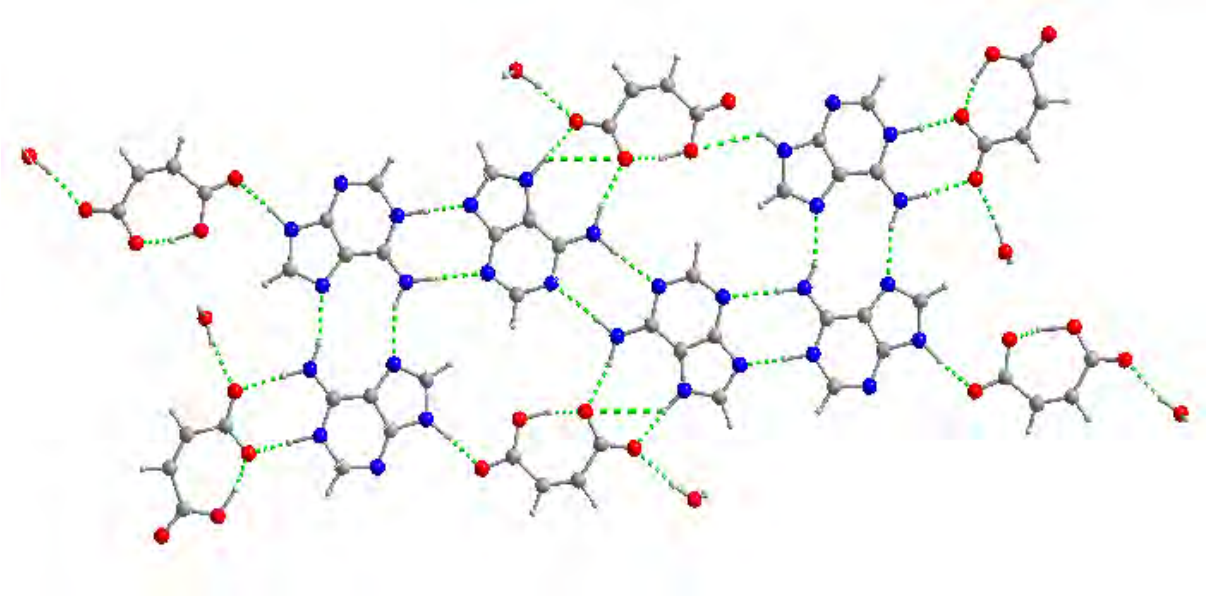

Figure 4.7: A view of the adeninium : hydrogen maleate hydrated structure[1] with a mixture of neutral and protonated adenine units, hydrogen bonding to the hydrogen maleate anions[1]. Hydrogen bonds are shown as dashed lines

The McHugh *et al* hydrated salt of adeninium : adenine : hydrogen maleate has an asymmetric unit containing two adeninium cations, two hydrogen maleate anions, one neutral adenine and two water molecules. The neutral adenine molecule exists in a less stable tautomeric form than the adenine starting material (not 9*H* but 7*H*) with the adeninium cations existing as the 1*H*,9*H* tautomer (figure 4.7). The structure is built up of trimer units of adenine and adeninium, based on a $R_2^2(10)$ ring motif between the two adeninium cations (motif 9*H*-XII) and a second $R_2^2(8)$ ring motif formed between the neutral 7*H* adenine molecule and a 1*H*,9*H* adeninium dimer using a protonated Watson-Crick to adenine base synthon. As this adenine-

adeninium dimer motif is formed between molecules of different tautomeric form, this motif is not displayed in table 4.1 with the other adenine dimer synthons. This trimer unit is linked to another trimer through the formation of an adenine – adenine $R_2^2(8)$ dimer, 7*H*-IX, and is surrounded by maleate ions bonded either via $R_2^2(9)$ or $R_2^2(8)$ ring motifs or as a chain. There is a water molecule interacting with each maleate ion but never to an adenine unit[1].

4.2.5 – Adeninium : hydrogen maleate : hydrate 1:1:1

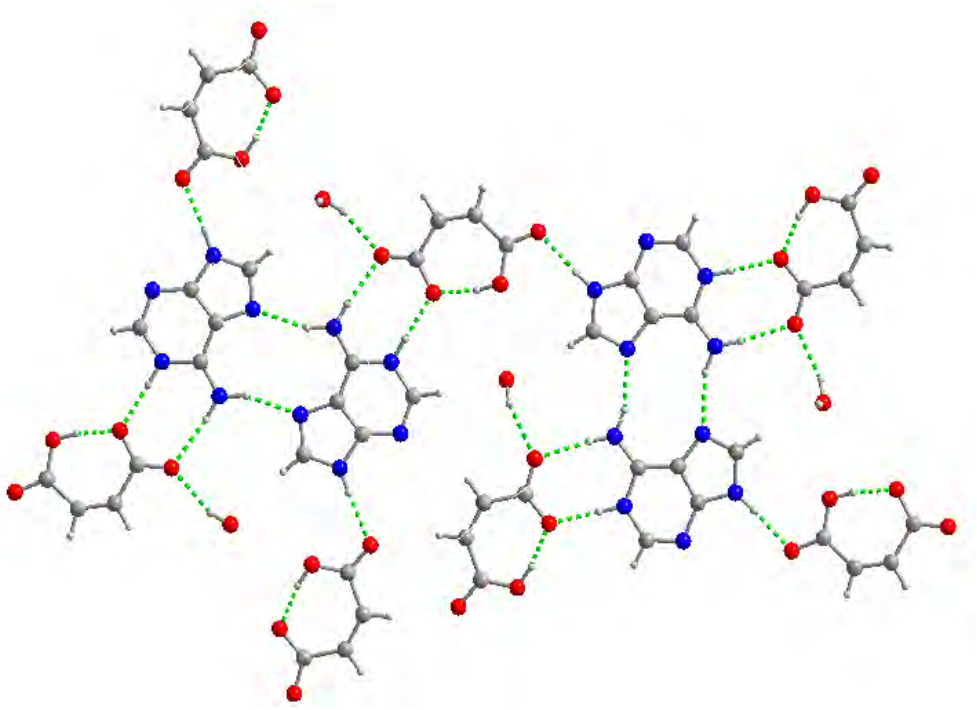

Figure 4.8: A view of the adeninium : maleate hydrated salt structure[8] with adeninium dimer units hydrogen bonding to hydrogen maleate anions. Hydrogen bonds are shown as dashed lines

The Sridhar *et al* hydrated adeninium : hydrogen maleate structure is a 1:1:1 salt with the adeninium in the most stable 1*H*,9*H* tautomeric form (figure 4.8). The structure contains an adeninium based $R_2^2(10)$ dimer, motif 9*H*-XII (table 4.1), with each adeninium ion interacting

with two hydrogen maleates. One linkage is an acid-amide $R_2^2(8)$ ring motif, motif 9*H*-VII, whereas the other is an acid-pyridine chain motif, motif 9*H*-VI. Again the water molecules are involved in hydrogen bonds only to the maleate ions[9].

4.2.6 – Adenine : adipic acid : methanolate 2:1:2

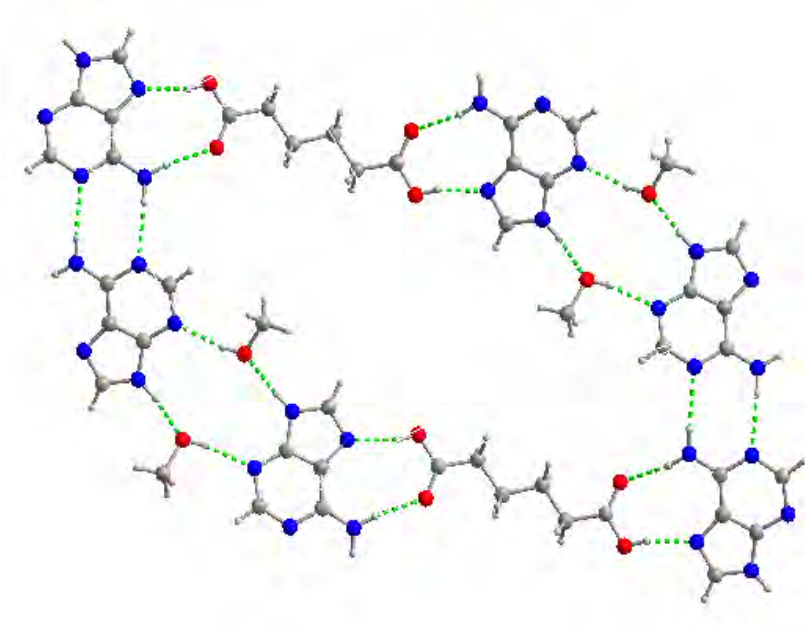

Figure 4.9: A view of the solvated adenine : adipic acid : methanolate cocrystal structure[10]. Hydrogen bonds are shown as dashed lines

The adenine : adipic acid : methanolate structure (2:1:2) contains adenine as the 9*H* tautomer. Two adenine molecules form an adenine $R_2^2(8)$ dimer, motif 9*H*-XI, with a third adenine molecule interacting with the dimer through two methanol molecules in a $R_4^4(12)$ ring (figure 4.9). The solvate molecules essentially disrupt the formation of a second adenine dimer (9*H*-X). These units are capped at each end by adipic acid molecules which form adenine-acid $R_2^2(9)$ ring motifs (motif 9*H*-IX). The overall structure forms a large $R_{10}^{10}(42)$ ring motif[10].

4.3 Adenine : oxalic acid

With both a hydrated and chlorinated adeninium : oxalate salt structure already known, the focus of this study was to synthesise an anhydrous, neutral cocrystal. The experimental procedure followed is described in chapter 3, using methanol, ethanol and ethyl acetate as solvents. Figure 4.10 shows the powder X-ray diffraction patterns for the products of crystallisation, compared with those of the starting materials and the published salt structures.

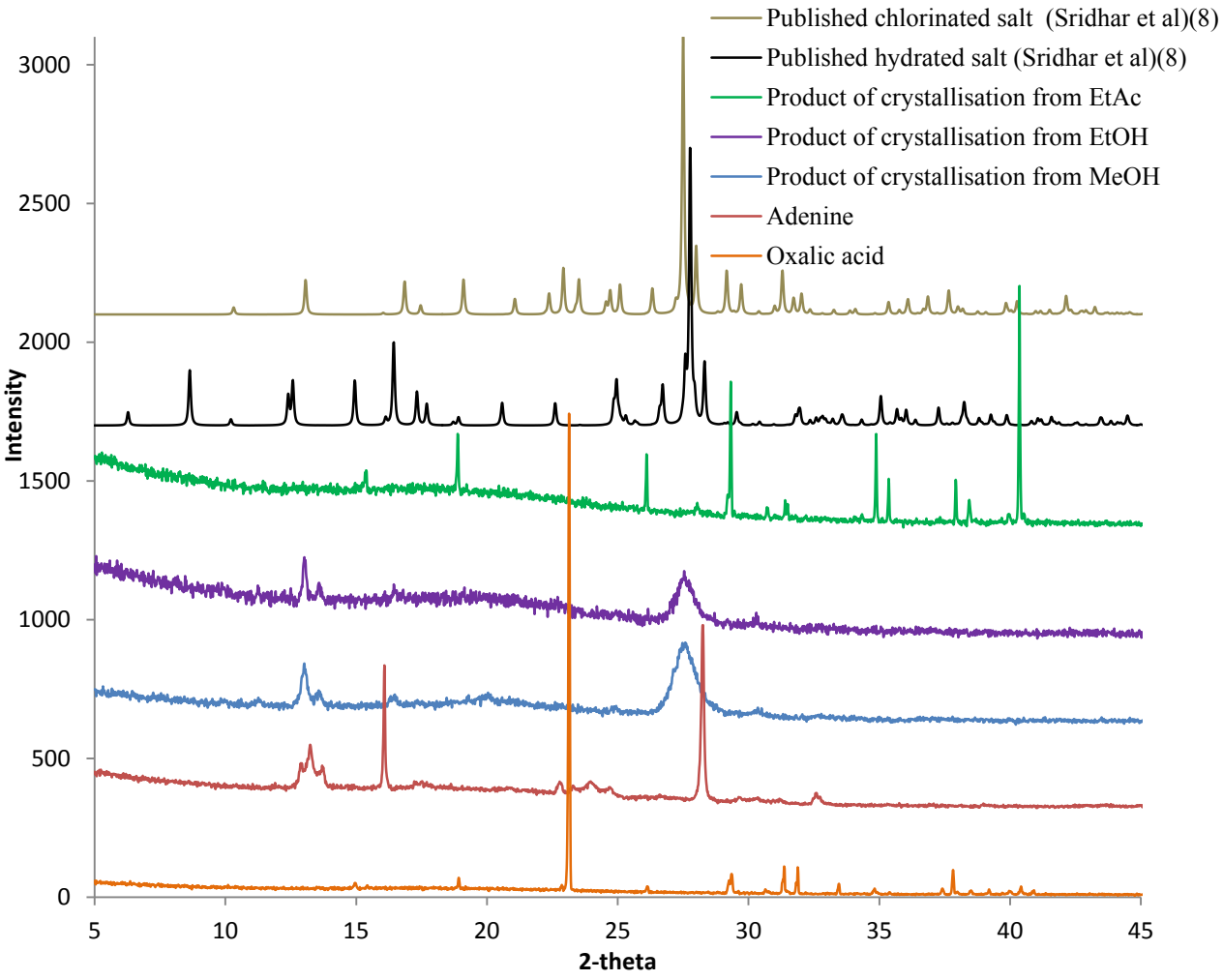

Figure 4.10: Powder diffraction patterns of the products of crystallisation compared to those of the starting materials and published salt structures

From this comparison it can be easily identified that none of the three adducts formed are the same as the published structures or the starting materials. Whilst the resultant adducts from methanol and ethanol are the same, that synthesised from ethyl acetate is different, suggesting the formation of two distinct materials, though those from methanol and ethanol may be a very poor quality adenine. Solution ^{1}H NMR analysis on the product of ethyl acetate crystallisation has not been possible to date, but is the next stage of structure solution on what may be another new and exciting system. The published materials were synthesised in a similar way, using hydrochloric acid as the solvent for the chloride structure and water as the solvent for the hydrated form[8].

4.4 Adeninium : hydrogen malonate

Adenine was crystallised with malonic acid following the synthetic procedure detailed in chapter 3 and produced a new material as confirmed by powder X-ray diffraction below (figure 4.11).

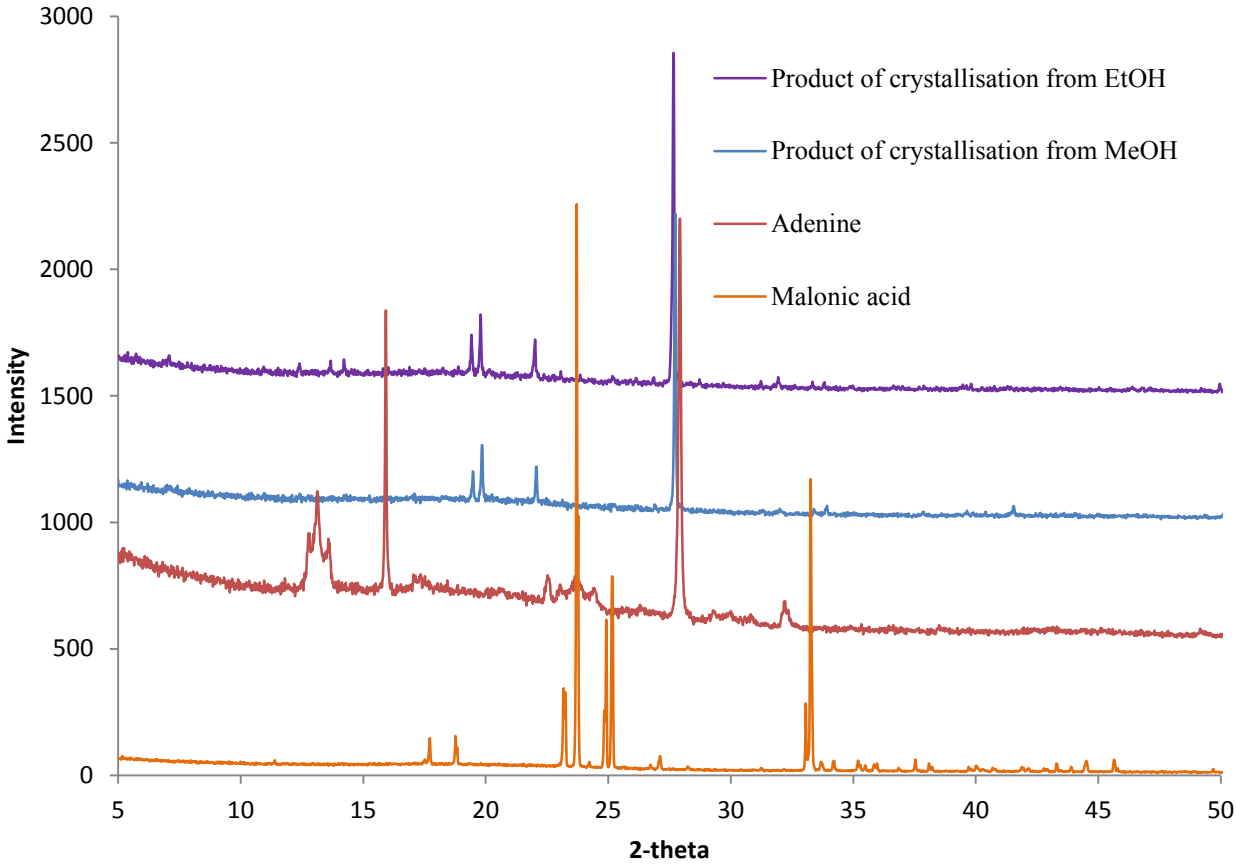

Figure 4.11: Powder X-ray diffraction data for the product of adenine and malonic acid cocrystallisation and the starting materials

The data shows that both products of crystallisation differ from the starting materials. The diffraction pattern of the product from ethanol displays small peaks at 10 - 15° in 2-theta that are not apparent in the pattern of the sample obtained from methanol. This could indicate that two new materials have formed or that one sample is a mixture. Solution ^{1}H NMR spectroscopy was carried out on both samples (appendix 2.1) and it was found that both consisted of both adenine and malonic acid, both with a 1:1 stoichiometry, though the ratios

obtained from the NMR signals for the sample crystallised in ethanol are not as exact as in the methanol sample, providing further indication of the ethanol sample being a mixture.

A crystal of suitable quality from the sample synthesised in ethanol was identified and selected for structure determination by single crystal diffraction. The structure solution established this adduct as an anhydrous 1:1 salt crystallising in a triclinic cell with space group P-1 (table 4.3). However, the quality of the dataset was poor and consequently the structure has a low completeness and a high excess of electron density, although it is good enough to enable study of the hydrogen bond motifs and the crystal packing.

Table 4.3: Cell parameters for adeninium : hydrogen malonate, 1:1

Compound	Adeninium :hydrogen malonate 1:1
a (Å)	4.8942(3)
b (Å)	8.1034(4)
c (Å)	12.5052(6)
α (°)	82.944(3)
β (°)	86.677(3)
γ (°)	79.855(4)
Volume ($Å^3$)	484.17(4)
Z	2
T (K)	120(2)
Reflections collected	4730
Independent reflections	1725
R(int)	0.0288
Goodness of fit	1.168
R_1 (observed)	0.0991
R_1 (all)	0.1097
wR_2 (observed)	0.12512
wR_2 (all)	0.2680

The position of the hydrogen atoms were determined by an electron density map confirming the structure to be a salt, since proton transfer occurred from the malonic acid to the adenine. The diffraction pattern simulated from the structure solved by single crystal methods is the same as that of the experimental laboratory powder X-ray diffraction pattern confirming that the crystal chosen is representative of the bulk material (appendix 2.2). Table 4.4 lists the nine intermolecular and intramolecular hydrogen bonds, whilst table 4.5 details selected bond lengths and angles (full crystallographic details and intramolecular bonds are given in appendix 2). Figure 4.12 shows the numbering scheme used.

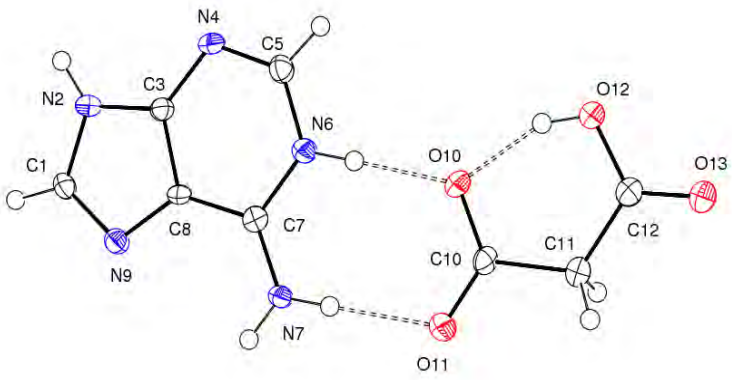

Figure 4.12: The independent molecules of adeninium : hydrogen malonate acid showing the atom-numbering scheme and the hard intermolecular hydrogen-bonds (shown as dashed lines). Displacement ellipsoids are drawn at 50% probability level

Table 4.4: Hydrogen bond table for adeninium : hydrogen malonate, 1:1

D-H...A	d(D-H)	d(H...A)	d(D...A)	<(DHA)
O12-H12...O10	0.84	1.68	2.461(3)	154.0
N2-H2...N4^{i}	0.88	2.10	2.926(4)	157.2
N2-H2...O13^{ii}	0.88	2.65	3.074(4)	110.6
N6-H6...O10	0.88	1.78	2.662(4)	176.6
N7-H7A...O11	0.88	1.93	2.807(4)	174.5
N7-H7B...N9^{iii}	0.88	2.01	2.872(4)	164.3
C1-H1...O13^{ii}	0.95	2.36	2.977(5)	121.8
C5-H5...O12^{ii}	0.95	2.37	3.297(5)	165.0
C5-H5...O13^{ii}	0.95	2.44	3.222(4)	139.8

Symmetry transformations used to generate equivalent atoms:

(i) –x-1, -y+1, -z+1 (ii) x-1, y, z-1 (iii) -x+1, -y, -z+1

Table 4.5: Selected intramolecular bond lengths (Å) and angles (°) for adeninium : hydrogen malonate, 1:1

Bond lengths (Å)		Bond angles (°)		Torsion angles (°)	
C10-O10	1.267(4)	O10-C10-O11	124.4(3)	O10-C10-C12-O12	-0.4(3)
C10-O11	1.248(4)	O12-C12-O13	120.7(3)	O11-C10-C13-O14	-1.6(9)
C12-O12	1.319(4)	C1-N9-C8	104.0(3)	H7B-N7-C7-N6	-180.0(3)
C12-O13	1.205(5)	C1-N2-C3	106.5(3)	H7B-N7-C7-C8	0.4(6)
		C3-N4-C5	112.2(3)	O10-C10-C12-O12	-0.4(3)
		C5-N6-C7	124.0(3)		
		C1-N9-C8	104.0(3)		
		C1-N2-C3	106.5(3)		

The asymmetric unit contains an adeninium cation along with a hydrogen malonate anion. The adeninium exists in its most stable 9*H* tautomeric form, with protonation on the 1*H* position; the 1*H*,9*H* tautomer is commonly seen in other molecular salts as can be seen from the table displayed in appendix 1.2. The coformers hydrogen bond to one another to form a

popular $R_2^2(8)$ ring motif (motif 9*H*-VII) on the Watson-Crick edge. The C10-O10 and C10-O11 bond lengths show no clear distinction, indicative of a deprotonated carboxyl, suggesting the deprotonation of the hydrogen to the adenine molecule, further confirmed by the larger endocyclic angle around the protonated site; C5-N6-C7 of 124.0(3)°, approximately 4° larger than in a neutral adenine structure.

The coformers are linked by the amide N7 donating H7A to O11 and the heterocyclic N6 donating H6 to O10. There is one further hydrogen bond within the asymmetric unit, an intermolecular interaction between the carboxyl groups on the hydrogen malonate, donated by O12 through H12 to O10 (figure 4.12). The adeninium forms a chain with neighbouring adeninium molecules, the first linkage formed through a complementary hydrogen bond donated by N7 to N9 via H7B, creating an $R_2^2(10)$ ring motif (motif 9*H*-XII) and the second, motif 9*H*-X, formed by a complementary bond being donated by N2 to N4 via H2, resulting in an $R_2^2(8)$ ring motif. This can be viewed as a unit of repeating adeninium dimers creating an infinite chain of adeninium cations which are linked to other adeninium chains through hydrogen malonate molecules to form a planar sheet. These linkages arise through the adeninium : malonate $R_2^2(8)$ ring motif within the asymmetric unit along with a further two hydrogen bond motifs. The first of these is an $R_2^1(5)$ ring formed by combination of a hard hydrogen bond donated by the heterocyclic N2 via H2 to O13 and a soft hydrogen bond, also accepted by O13, but formed by donation of H1 by heterocyclic C1. The second utilises the heterocyclic C5 as a double donor of H5 to both O12 and O13, forming an $R_1^2(5)$ ring motif (figure 4.13). All strong hydrogen bond donors and acceptors are used within this structure, with N2 and C5 being double donors and O13 an acceptor of three hydrogen bonds.

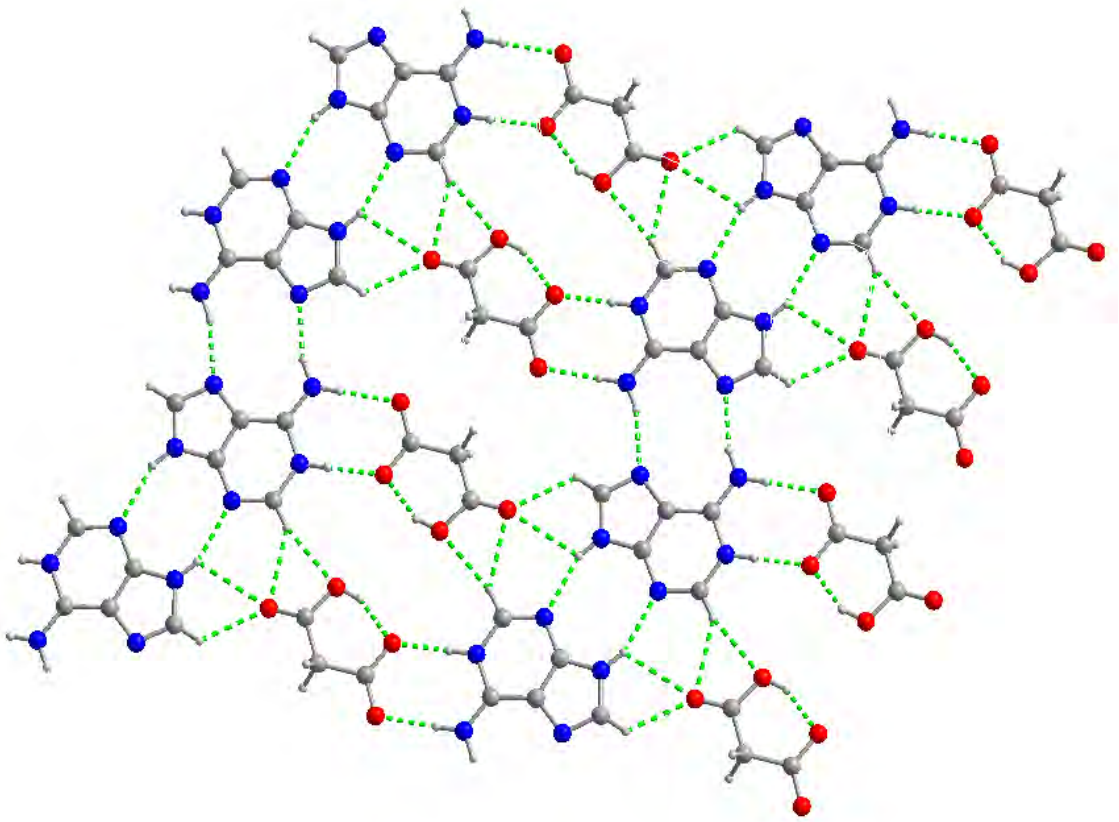

Figure 4.13: A view of adeninium : hydrogen malonate, 1:1. Hydrogen bonds are shown as dashed lines

4.5 Adenine : succinic acid

Adenine was cocrystallised with succinic acid following the experimental procedure outlined in chapter 3, to produce a new material as confirmed by powder X-ray diffraction below (figure 4.14).

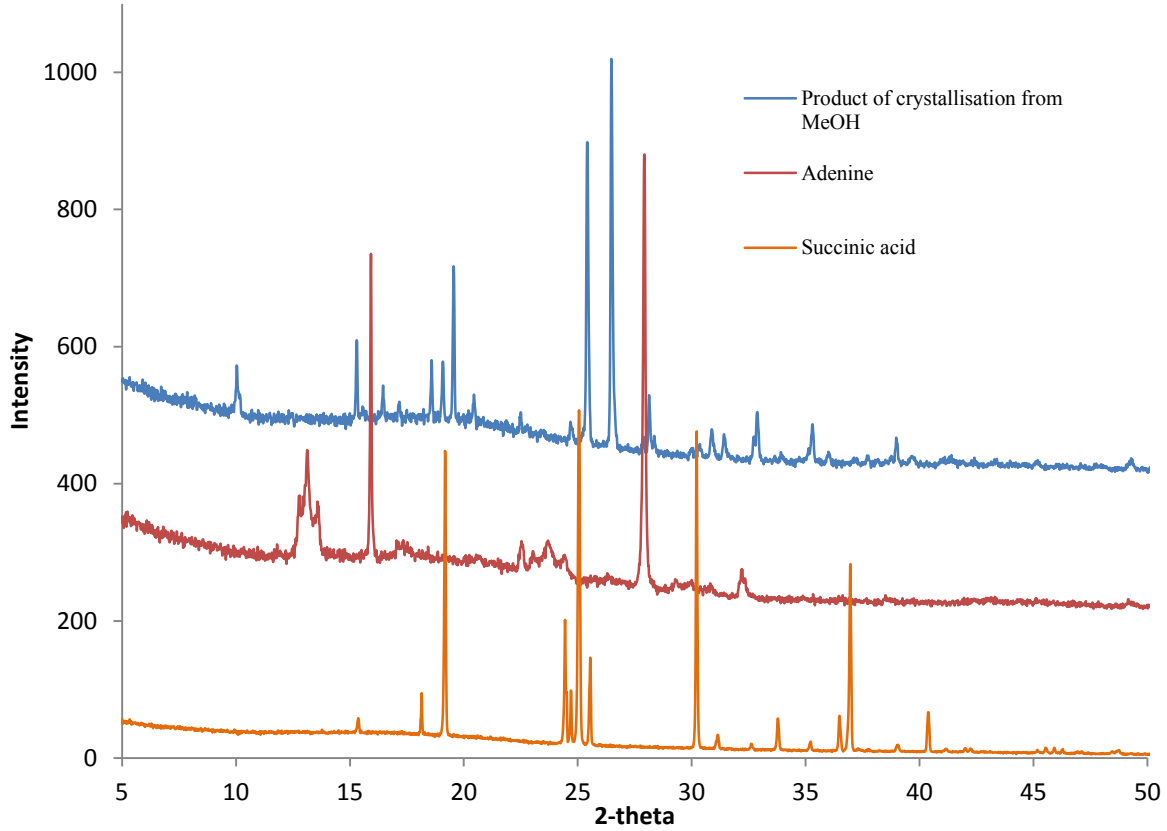

Figure 4.14: Powder X-ray diffraction data for the product of adenine and succinic acid cocrystallisation and the starting materials

It is clear from the above powder diffraction patterns that a new material has been formed, with a stoichiometry of 1:1 of both coformers determined by ^{1}H NMR spectroscopy (appendix 3.1).

Single crystal X-ray diffraction data were collected at the UK National Crystallography Service[15] and the adduct was found to crystallise in a monoclinic cell with a space group of $P2_1/n$ (table 4.6).

Table 4.6: Cell parameters for adenine : succinic acid, 1:1

Compound	Adenine : succinic acid 1:1
a (Å)	9.4902(4)
b (Å)	5.3041(3)
c (Å)	21.2846(8)
α (°)	90
β (°)	92.398(3)
γ (°)	90
Volume ($Å^3$)	1070.46(9)
T (K)	120(2)
Z	4
Reflections collected	8933
Independent reflections	2426
R(int)	0.0485
Goodness of fit	1.114
R_1 (observed)	0.0586
R_1 (all)	0.0817
wR_2 (observed)	0.1123
wR_2 (all)	0.1257

The position of the hydrogen atoms were determined by an electron density map confirming the structure to be a cocrystal, since no proton transfer occurred from the acid to the adenine. The powder diffraction pattern simulated from the structure solved from single crystal data is the same as that of the experimental laboratory powder X-ray diffraction pattern confirming that the crystal chosen is representative of the bulk material (appendix 3.2). Table 4.7 lists the seven intermolecular hydrogen bonds that make up the cocrystal structure; Table 4.8 details

selected bond lengths and angles and figure 4.15 shows the numbering scheme used. Full crystallographic details and intramolecular bonds and angles can be found in appendix 3.

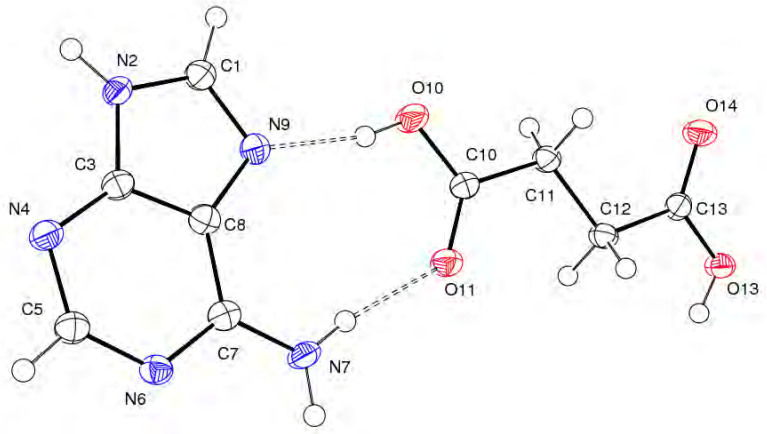

Figure 4.15: The independent molecules of adenine : succinic acid showing the atom-numbering scheme and the hard intermolecular hydrogen-bonds (shown as dashed lines). Displacement ellipsoids are drawn at 50% probability level

Table 4.7: Intermolecular hydrogen bonding (Å) for adenine : succinic acid, 1:1

D-H...A	d(D-H)	d(H...A)	d(D...A)	<(DHA)
N2-H2...N4^{i}	0.88	1.96	2.825(3)	166.4
N7-H7A...O11^{ii}	0.88	2.04	2.875(2)	157.3
N7-H7B...O11	0.88	2.05	2.924(3)	171.7
O10-H10...N9	0.84	1.80	2.630(3)	167.0
O13-H13...N6^{iii}	0.84	1.87	2.686(2)	162.9
C1-H1...O14^{iv}	0.95	2.38	3.077(3)	129.9
C5-H5...O14^{v}	0.95	2.43	3.213(2)	139.9

Symmetry transformations used to generate equivalent atoms:

(i) –x, -y+3, -z (ii) –x+0.5, y+0.5, -z+0.5 (iii) –x+0.5, y+1.5, -z+0.5

(iv) –x+1, -y+1, -z (v) x-1, y+2, z

Table 4.8: Selected bond lengths (Å) and angles (°) for adenine : succinic acid, 1:1

Bond lengths (Å)		Bond angles (°)		Torsion angles (°)	
C10-O10	1.304(3)	O10-C10-O11	122.8(2)	O10-C10-C13-O13	-176.4(2)
C10-O11	1.220(3)	O13-C13-O14	120.0(2)	O11-C10-C13-O14	-177.0(2)
C13-O13	1.330(3)	C1-N9-C8	103.6(2)	H7B-N7-C7-N6	-180.0(2)
C13-O14	1.206(3)	C1-N2-C3	106.7(2)	H7B-N7-C7-C8	-180.0(2)
		C3-N4-C5	111.1(2)	O10-C10-C13-O13	-176.4(2)
		C5-N6-C7	119.2(2)		
		O10-C10-O11	122.8(2)		
		O13-C13-O14	120.0(2)		

In the crystal structure of adenine : succinic acid, the asymmetric unit consists of one neutral adenine molecule in the most stable and expected 9*H* tautomeric form and one succinic acid (figure 4.15). There is clear discrimination between the length of the C-OH and C=O bonds in the succinic acid molecule (table 4.7) indicating that both carboxyl groups have retained their acidic protons, and the endocyclic C-N-C angles further confirm the presence of the 9*H* tautomer with C1-N2-C3 of 106.7(2)° approximately 3° larger than the unprotonated nitrogen site (C1-N9-C8 of 103.6(2)°) (table 4.8).

The two coformer molecules are hydrogen bonded through two hard hydrogen bonds; the first formed by the amide N7 acting as a donor via H7B to O11 and the second in which the heterocyclic nitrogen N9 acts as an acceptor of H10 donated by O10, together creating an $R_2^2(9)$ ring formed along the Hoogsteen edge of the adenine molecule (9H-IX). Each adenine forms a dimer through complementary hydrogen donation from N2 via H2 to N4 on the neighbouring adenine molecule, resulting in an $R_2^2(8)$ ring. This dimer motif (9*H*-X) is common to other crystalline adenine structures, and acts to form a small supramolecular building block of four molecules containing alternating ring motifs (figure 4.16).

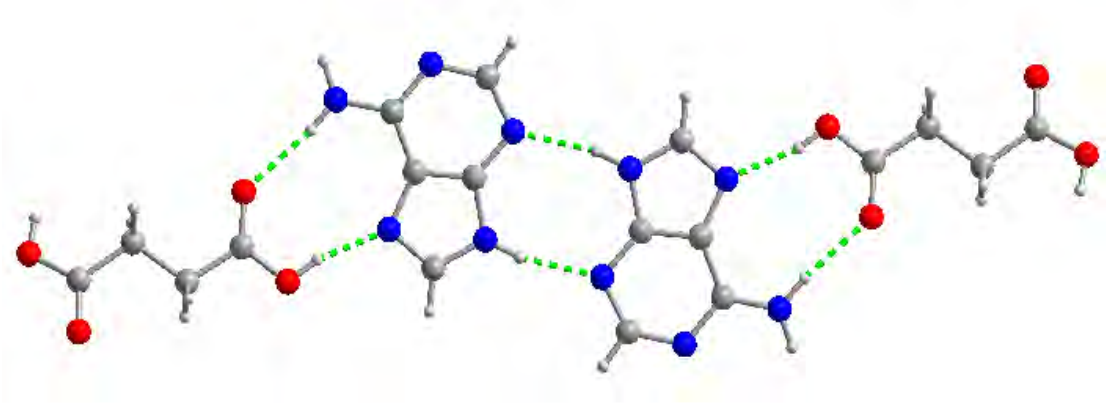

Figure 4.16: A view of the chain units formed by an adenine dimer capped at each end by a succinic acid molecule. Hydrogen bonds are shown as dashed lines

These units are linked to others through two soft hydrogen bonds in which O14 acts as a double acceptor (C1 on one adenine acts as a donor via H1 while C5 on the neighbouring adenine, within the dimer, acts as the second donor via H5) forming $R_3^2(8)$ rings above and below the adenine dimer (figure 4.17). The result is the formation of an infinite hydrogen-bonded ribbon running in the [-120] direction.

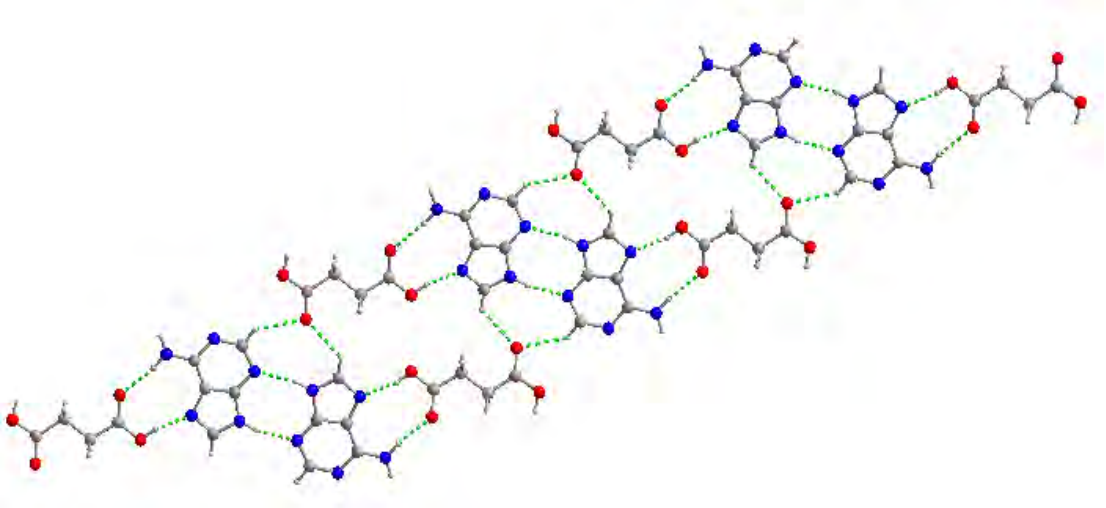

Figure 4.17: The infinite hydrogen-bonded ribbon of adenine dimers and alternating succinic acid molecules. Hydrogen bonds are shown as dashed lines

Each ribbon is then linked to two others running in the same direction through a 'layer' of other ribbons running in the [120] direction in a sandwich-type arrangement containing alternating layers of ribbons (figure 4.18).

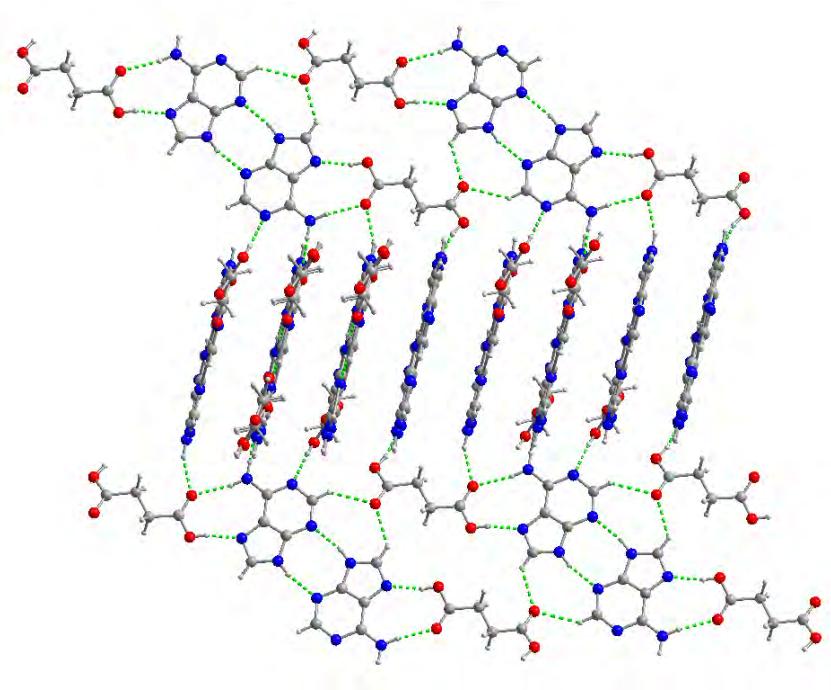

Figure 4.18: The extensive hydrogen bonded network of alternating perpendicular layers of infinite hydrogen-bonded ribbons of adenine and succinic acid molecules. Hydrogen bonds are shown as dashed lines

This architecture is formed by the two remaining hard hydrogen bonds; one formed by donation of H7A from N7 to O11 and the second from O13 via H13 to N6. In this extensive hydrogen bond network (table 4.7), each adenine molecule is involved in eight intermolecular interactions with five succinic acid and one adenine molecule, such that all hydrogen bond donors and acceptor sites on the adenine are used. Each succinic acid molecule is hydrogen bonded to five adenine molecules with both carboxylic OH groups acting as donors and both C=O groups as double acceptors. In this structure, parallel ribbons are stacked with an interplanar distance of 3.56 Å, with each ribbon also cross-linked by eight others (figure 4.19).

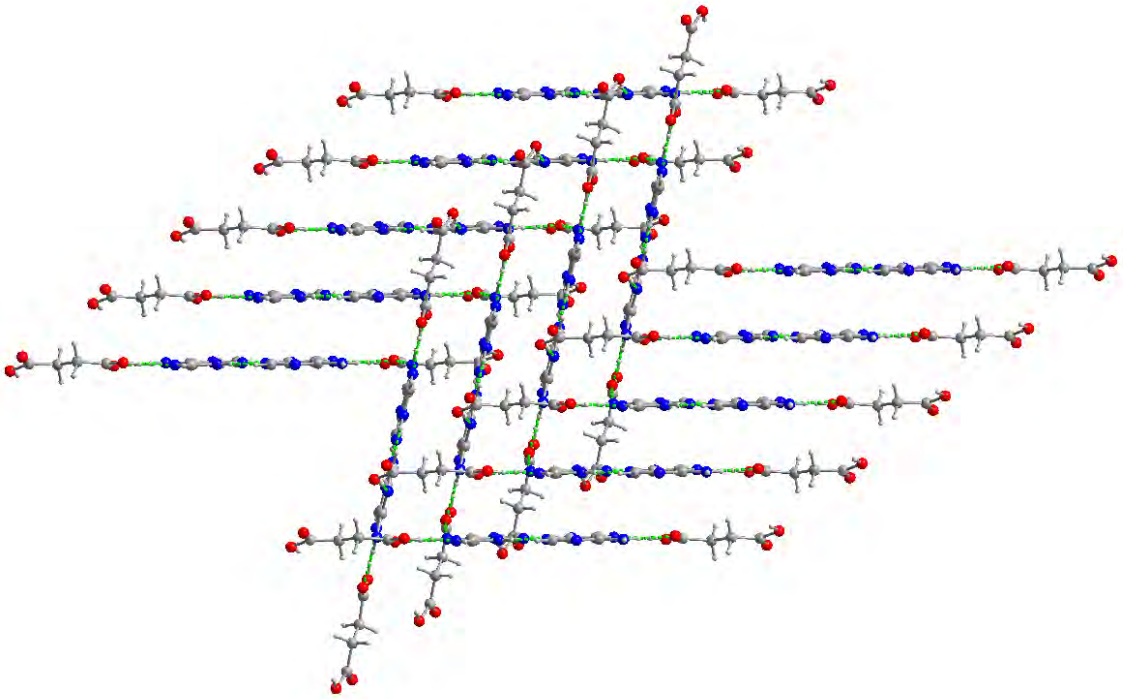

Figure 4.19: A view showing the stacking and cross-linking of ribbons in the crystal structure of adenine : succinic acid, 1:1

4.6 Adeninium : hydrogen fumarate

Adenine was cocrystallised with fumaric acid following the synthetic procedure described in chapter 3, to produce a new crystalline material as confirmed by powder X-ray diffraction below (figure 4.20).

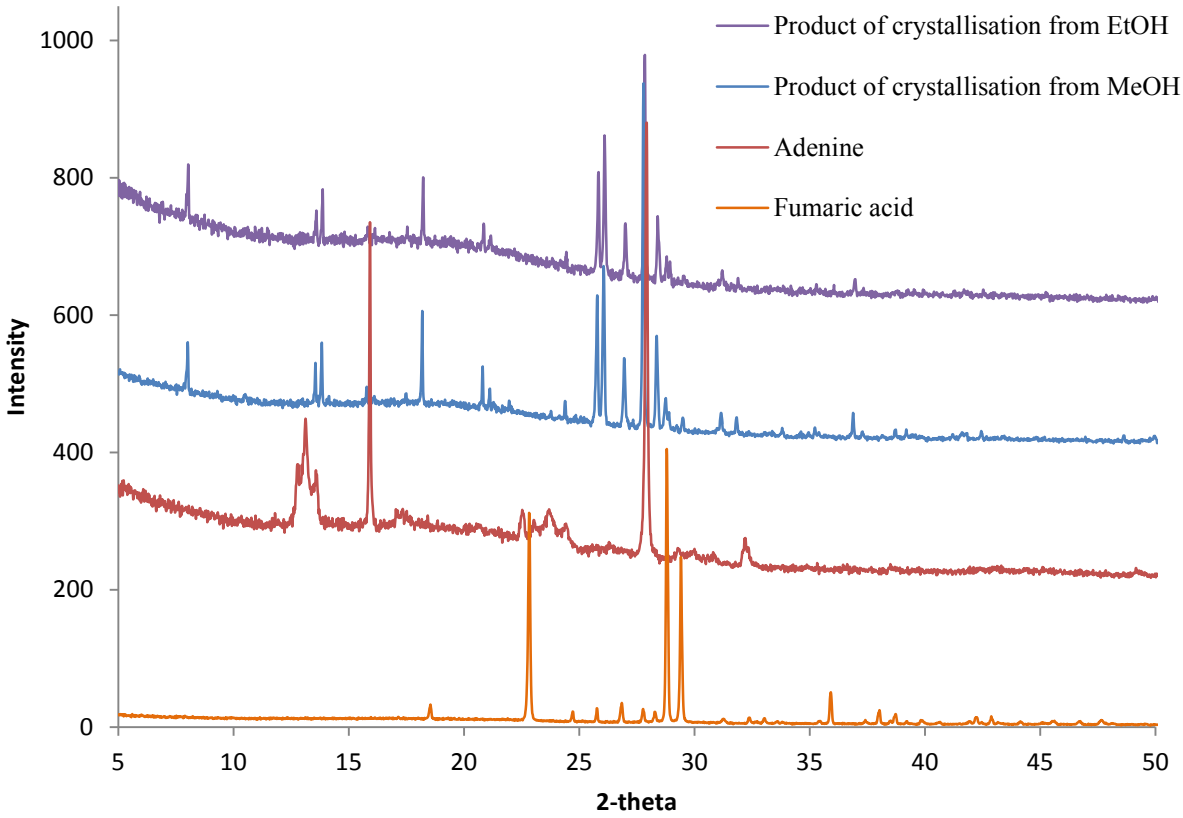

Figure 4.20: Powder X-ray diffraction data for the product of adenine and fumaric acid cocrystallisation and the starting materials

The diffraction patterns show that both products of crystallisation are the same and differ from the starting materials. Solution ^{1}H NMR spectroscopy was used to confirm both adenine and fumaric acid are present in the new material in a 1:1 stoichiometry (appendix 4.1).

A crystal of suitable quality for single crystal structural analysis was selected from the sample synthesised in methanol, with a dataset then being collected at the UK National Crystallography Service[15] (chapter 3). The dataset exhibited merohedral twinning;

consequently this structure was solved by Dr Louise Male. The structure of the new material is a 1:1 salt, crystallising in the monoclinic cell with space group, $P2_1/c$ (table 4.9).

Table 4.9: Cell parameters for adeninium : hydrogen fumarate, 1:1

Compound	Adeninium : hydrogen fumarate 1:1
a (Å)	3.61600(10)
b (Å)	13.0730(6)
c (Å)	22.0296(9)
α (°)	90
β (°)	94.633(3)
γ (°)	90
Volume ($Å^3$)	1037.98(7)
T (K)	120(2)
Z	4
Reflections collected	10663
Independent reflections	1872
R(int)	0.0778
Goodness of fit	1.114
R_1 (observed)	0.0574
R_1 (all)	0.0813
wR_2 (observed)	0.1071
wR_2 (all)	0.1206

The position of the hydrogen atoms was determined by an electron density map confirming the structure to be a salt, since proton transfer occurred from the fumaric acid to the adenine. The powder diffraction pattern simulated from the structure solved by single crystal analysis is the same as that of the experimental laboratory powder X-ray diffraction pattern confirming that the crystal chosen is representative of the bulk material (appendix 4.2). Table 4.10 lists

the seven intermolecular hydrogen bonds that make up the salt structure, with table 4.11 detailing selected intramolecular bond lengths and angles. Figure 4.21 shows the numbering scheme used. Appendix 4 contains a full table of intramolecular bond lengths and angles and crystallographic details.

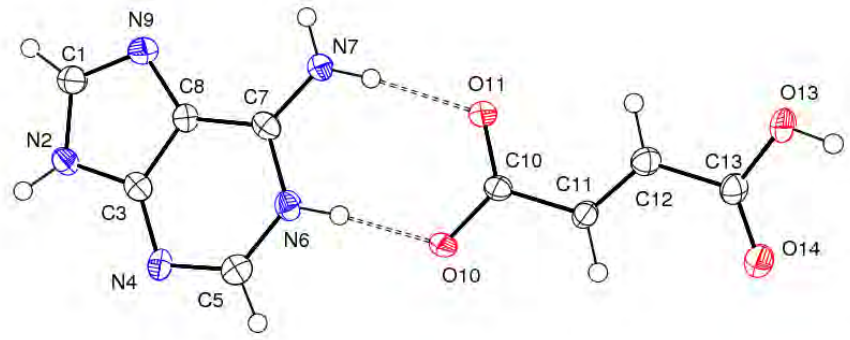

Figure 4.21: The independent molecules of adeninium : hydrogen fumarate showing the atom-numbering scheme and the hard intermolecular hydrogen-bonds (shown as dashed lines). Displacement ellipsoids are drawn at 50% probability level

Table 4.10: Intermolecular hydrogen bonding (Å) for adeninium : hydrogen fumarate, 1:1

D-H...A	d(D-H)	d(H...A)	d(D...A)	<(DHA)
N2-H2...N4^{i}	0.88	2.06	2.892(4)	158.5
N7-H7A...O11	0.88	1.92	2.795(4)	170.9
N7-H7B...O11^{ii}	0.88	2.07	2.809(4)	140.8
N6-H10...O10	0.88	1.77	2.604(3)	171.3
O13-H13...O10^{iii}	0.84	1.76	2.577(4)	172.0
C5-H5...O14^{iv}	0.95	2.52	3.175(5)	135.5
C5-H5...O14^{v}	0.95	2.55	3.244(5)	130.9

Symmetry transformations used to generate equivalent atoms:

(i) –x-1, -y+2, -z+1 (ii) –x+1, -y+1, -z+1 (iii) –x+1, y-0.5, -z+0.5

(iv) –x, y+0.5, -z+0.5 (v) –x+1, y+0.5, -z+0.5

Table 4.11: Selected bond lengths (Å) and angles (°) for adeninium : hydrogen fumarate, 1:1

Bond length (Å)		Bond angle (°)		Torsion angles (°)	
C10-O10	1.280(4)	O10-C10-O11	123.5(3)	O10-C10-C13-O13	-149.5(4)
C10-O11	1.246(4)	O13-C13-O14	123.8(3)	O11-C10-C13-O14	-161.3(3)
C13-O13	1.324(4)	O10-C10-O11	123.5(3)	H7B-N7-C7-N6	180.0(3)
C13-O14	1.215(4)	C1-N9-C8	103.3(3)	H7B-N7-C7-C8	180.0(3)
		C1-N2-C3	106.1(3)		
		C3-N4-C5	111.9(3)		
		C5-N6-C7	123.8(3)		

The asymmetric unit of the adeninium : hydrogen fumarate structure shows that in this case, proton transfer has taken place so that the crystal structure contains an adeninium ion in the 9*H* tautomeric form protonated at the 1*H* position, again forming the most common 1*H*,9*H* adeninium tautomer (appendix 1.2). The adeninium is hydrogen bonded to the hydrogen fumarate ion through the formation of a $R_2^2(8)$ ring on the Watson-Crick edge (9*H*-VII). The intramolecular geometry of the adeninium ion again confirms the presence of this tautomer with a larger endocyclic angle around the protonated nitrogen N2 site and the C5-N6-C7 angle of 123.8° approximately 4° larger than that in the unprotonated adenine : succinic acid cocrystal. There is clear discrimination again between the C-OH and C=O bond lengths at the protonated C13 end of the hydrogen fumarate ion, but much less so at the carboxylate end (table 4.11).

The coformers are linked by a hard hydrogen bond from the amide N7 acting as a donor via H7A to O11, with the ring motif completed by the formation of an acid-pyridine interaction from the protonated heterocyclic nitrogen N6 within the adeninium six-membered ring via H6 to the carboxylate O10 as shown in figure 4.21. The adeninium dimer $R_2^2(8)$ ring motif, 9*H*-X is also present in this structure, formed by complementary hydrogen bond donation from N2

to N4 via H2. This creates a small supramolecular building block of four molecules containing alternating acid-adeninium and adeninium-adeninium ring motifs (figure 4.22).

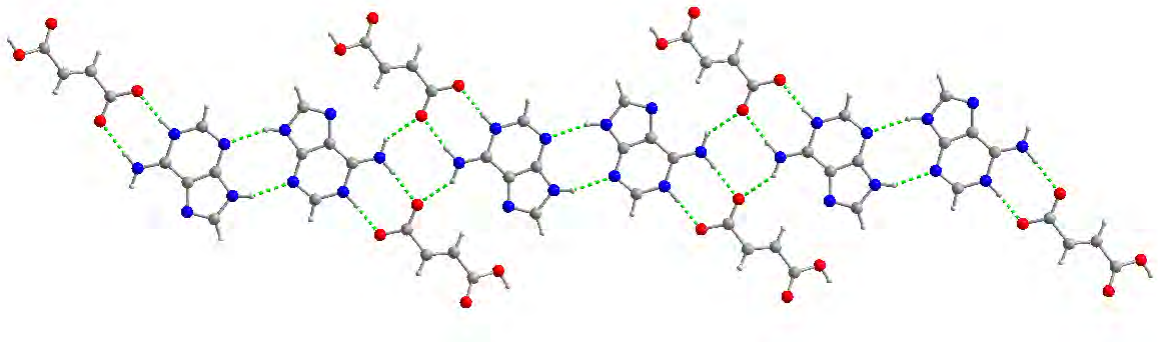

Figure 4.22: The infinite hydrogen-bonded chain of adeninium dimers and alternating hydrogen fumarate molecules in this cocrystal structure. Hydrogen bonds are shown as dashed lines

These supramolecular units are then linked together to form an infinite chain by a complementary hydrogen bond donated by N7 via H7B to O11 creating an additional $R_4^2(8)$ ring (figure 4.22). Unlike in the crystal structure of adenine : succinic acid, N9 and C1 in the adenine unit are not involved in any significant intermolecular interactions. The hydrogen fumarate ion that could be in a position to form these additional interactions is instead bent out of plane, such that half the fumarate is either above or below the plane of the chain shown in figure 4.22, with intramolecular carboxylate-to-carboxyl torsion angles O10-C10-C13-O13 and O11-C10-C13-O14 of -149.5° and -161.3° respectively (table 4.11). The result is an infinite hydrogen-bonded non-planar chain running in the [-210] direction. A reason for this marked geometric distortion of the hydrogen fumarate ion becomes clear after consideration of how these chains are then linked to others. Each fumarate ion links to three other chains running in the [210] direction (figure 4.23); in the first case, the fumarate acts as both a hydrogen bond donor from O13 via H13 to O10 and as an acceptor of a soft hydrogen bond

from C5 via H5 to O14 forming two interactions which in combination create a further $R_3^3(9)$ ring; O14 acts as a double acceptor as an interaction is also formed between a second adeninium dimer in a neighbouring chain, also denoted as C5-H5...O14 but with a slightly shorter H...A distance of 2.42 Å; finally, a complementary O13-H13...O10 hydrogen bond in which O10 of the fumarate ion under consideration acts as an acceptor forms the interaction with a third chain.

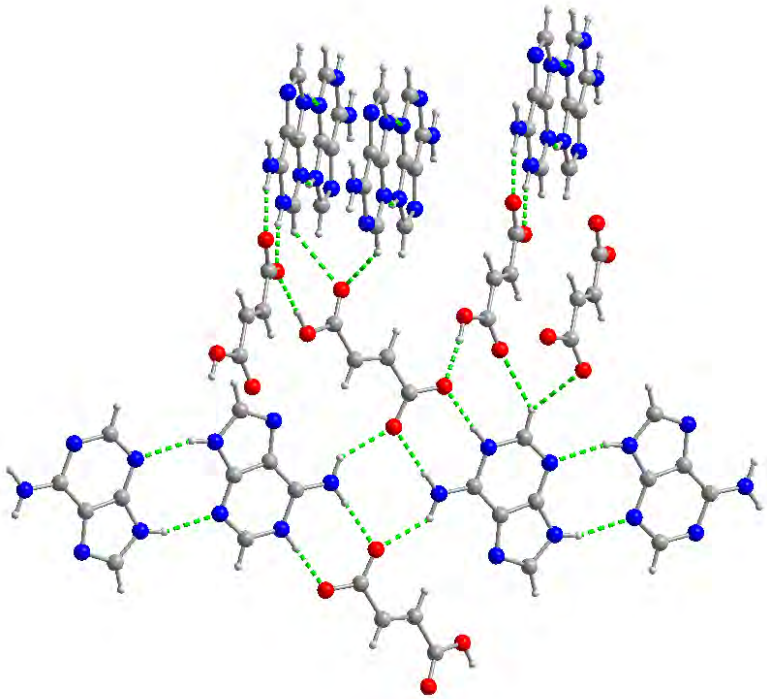

Figure 4.23: A view of part of the extensive hydrogen bond network formed by the adeninium dimers and hydrogen fumarate molecules showing a number of the criss-cross chains that form the alternating layer structure. Hydrogen bonds are shown as dashed lines

Each adeninium is involved in seven interactions including a bifurcated C-H donation, but both the strong acceptor N9 and the weak donor C1 are not used. Each hydrogen fumarate ion is also involved in seven interactions; all three unprotonated oxygens act as double acceptors with the carboxylic OH acting as a donor. In a similar way to adenine : succinic acid, these chains form a sandwich-type structure in which there are alternating 'layers' of

chains running in opposing directions, with each asymmetric unit pair of coformers within a chain, involved in interactions with four others. However, in this structure the ribbons themselves are bent above and below the plane (due to the fumarate conformation discussed earlier) and parallel ribbons are stacked with an interplanar distance of 3.62 Å (figure 4.24).

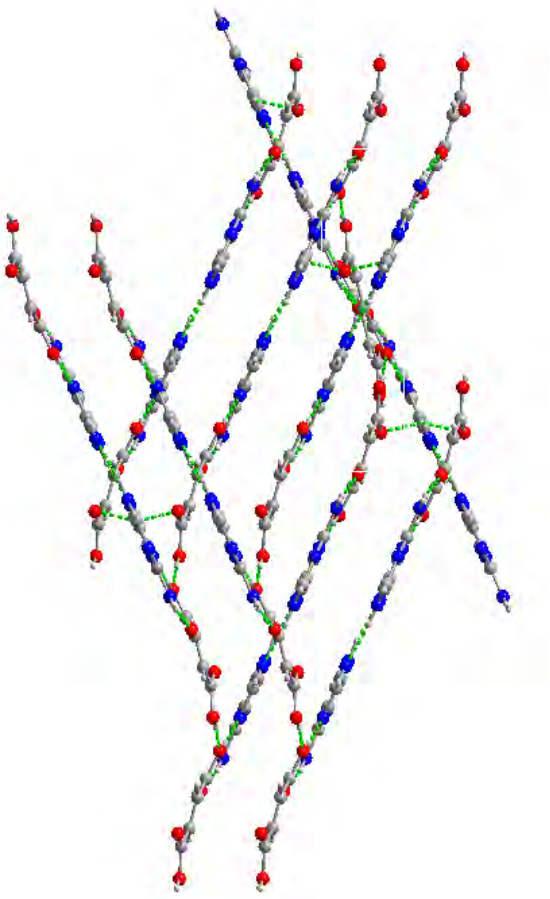

Figure 4.24: A view showing the stacking and cross-linking of ribbons in the crystal structure of the adeninium : hydrogen fumarate salt. Hydrogen bonds are shown as dashed lines

Whilst the structure of adeninium : hydrogen fumarate exhibits similarities to that of the adenine : succinic acid structure, the architecture of these two cocrystals is clearly distinct. They both contain neutral adenine molecules in its most stable tautomeric form and contain the common adenine dimer motif, motif 9*H*-X. Both structures consist of small four molecule

units that bond to form either infinite chains or ribbons, which in turn form a sandwich type layer structure, however the networks present in these structures are very different.

4.7 Adeninium : hydrogen maleate

Two adeninium : hydrogen maleate structures have previously been reported as hydrated salts, so adenine was cocrystallised with maleic acid following the experimental procedure outlined in chapter 3 to investigate the possibility of an anhydrous, neutral adenine : maleic acid adduct. Powder X-ray diffraction was used to confirm that a new material had been formed (figure 4.25).

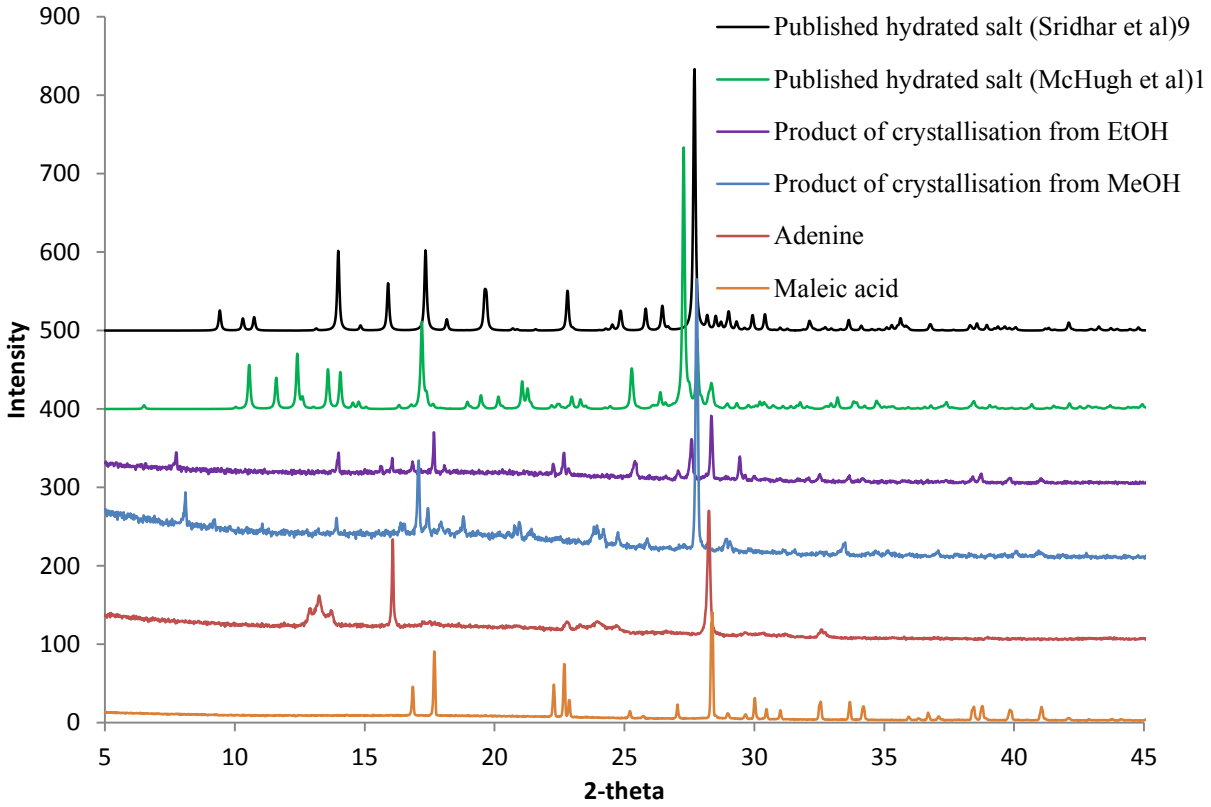

Figure 4.25: Powder X-ray diffraction data for the product of adenine and maleic acid cocrystallisation, the starting materials and the published materials

The powder diffraction patterns of the two products of crystallisation are not only different from the powder patterns of the published structures, but also differ from both the starting materials and each other, indicating the formation of a further two new crystalline materials.

The powder diffraction pattern of the product from ethanol shows the presence of some excess maleic acid. The reported hydrated salt published by Sridhar *et al*[9](9) was crystallised using water as the solvent, the other published maleate salt does not report the solvent used. ^{1}H NMR spectra of the product crystallised in methanol indicates a 1:1 stoichiometry of adenine and maleic acid, along with the presence of methanol. ^{1}H NMR spectra of the product crystallised from ethanol indicates a 1:3 adenine : maleic acid stoichiometry, but with maleic acid starting material present in the diffraction pattern, a reliable stoichiometry cannot be obtained in this way. The spectra also show impurity peaks at ~1.25ppm which are currently unidentified (appendix 5.1).

Single crystal X-ray diffraction data were collected on suitable crystals of both products, confirming that the product crystallised from ethanol (**1**) is an unsolvated salt which crystallises in a monoclinic cell with space group $P2_1/c$, and the product from methanol (**2**) is a solvated salt crystallising in the triclinic cell with space group P -1. Due to the small size of the crystals (0.09 x 0.01 x 0.01) of (**1**), the data were collected on beamline I19 at the Diamond Light Source[15] (chapter 3). Table 4.12 shows the cell parameters for both (**1**) and (**2**).

Table 4.12: Cell parameters for both adeninium : hydrogen maleate salts

Compound	Adeninium : hydrogen maleate (**1**)	Adeninium : hydrogen maleate methanolate (**2**)
a (Å)	3.610(3)	5.28150(10)
b (Å)	13.323(11)	10.0506(2)
c (Å)	22.187(19)	22.0125(4)
α (°)	90	78.1910(10)
β (°)	92.258(7)	85.1600(10)
γ (°)	90	80.0170(10)
Volume ($Å^3$)	1066.3(15)	1124.98(4)
T (K)	100(2)	120(2)
Z	4	4
Reflections collected	10172	7965
Independent reflections	2401	3745
R(int)	0.0556	0.0212
Goodness of fit	1.052	1.067
R_1 (observed)	0.0416	0.0345
R_1 (all)	0.0582	0.0404
wR_2 (observed)	0.1020	0.0900
wR_2 (all)	0.1108	0.0937

The position of the hydrogen atoms were determined by an electron density map confirming both structures to be salts, since proton transfer occurred from the maleic acid molecules to the adenine. The powder diffraction patterns simulated from the structures solved from the single crystal diffraction data is the same as that of the experimental laboratory powder X-ray diffraction pattern confirming that the crystals chosen are representative of the bulk material (appendix 5.2). Table 4.13 lists the intermolecular and intramolecular hydrogen bonds that make up the salt structures, whilst table 4.14 details selected bond lengths and angles. Figure

4.26 shows the numbering schemes used. Appendix 5 includes full crystallographic details and intramolecular bonds and angles for both (**1**) and (**2**).

(**1**)

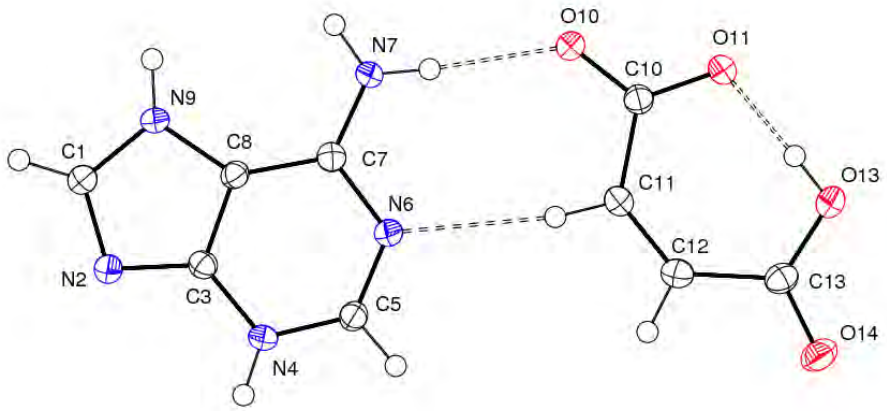

(**2**)

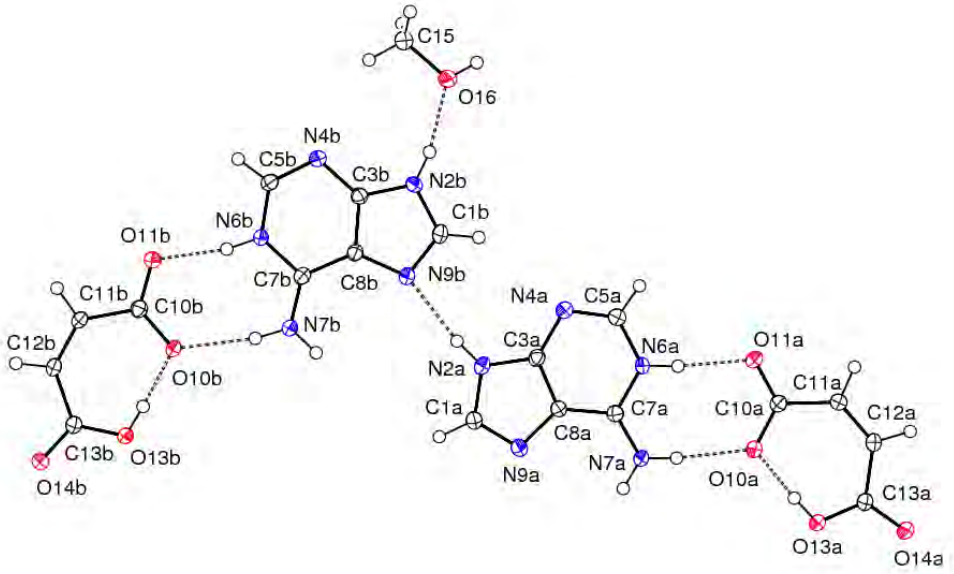

Figure 4.26: The independent molecules of anhydrous adeninium : maleate, 1:1 (**1**) and the independent molecules of adeninium : maleate : methanolate, 2:2:1 (**2**) showing the atom-numbering scheme and the hard intermolecular hydrogen-bonds (shown as dashed lines). Displacement ellipsoids are drawn at 50% probability level

Table 4.13: Intermolecular hydrogen bonding (Å) for both adeninium : maleate salts

D-H...A	d(D-H)	d(H...A)	d(D...A)	<(DHA)
		(**1**)		
O13-H13...O11	0.84	1.62	2.464(2)	177.4
N7-H7A...O10	0.88	2.07	2.946(3)	171.3
N7-H7B...O11^{i}	0.88	2.07	2.922(2)	163.2
N9-H9...O10^{i}	0.88	1.87	2.721(2)	161.6
N9-H9...O11^{i}	0.88	2.56	3.288(2)	140.1
N4-H4...N2^{ii}	0.88	1.95	2.808(2)	162.9
C11-H11...N6	0.9496(16)	2.4325(22)	3.374(3)	170.936(116)
C5-H5...O14^{iii}	0.9493(16)	2.7549(20)	3.054(3)	99.213(98)
C1-H1...O13	0.9505(16)	2.8564 (20)	3.417(3)	118.739(104)
		(**2**)		
N7A-H7AA...O10A	0.88	1.93	2.799(2)	169.3
N7A-H7AB...O14A^{iv}	0.88	2.01	2.865 (2)	163.8
N6A-H6A...O11A	0.88	1.90	2.772(2)	174.3
N2A-H2A...N9B	0.88	2.05	2.921(2)	171.5
O13A-H13A...O10A	0.84	1.59	2.430(1)	173.0
N7B-H7BA...O10	0.88	2.00	2.873(2)	170.1
N7B-H7BB...O14B^{v}	0.88	1.97	2.808(2)	158.1
N6B-H6B...O11B	0.88	1.82	2.687(2)	168.9
N2B-H2B...O16	0.88	1.83	2.696(2)	168.4
O13B-H13B...O10B	0.84	1.61	2.448(2)	174.6
O16-H16...O14A^{vi}	0.84	1.82	2.659(2)	173.4
C5A-H5A...O11A^{vi}	0.95	2.39	3.330(2)	172.4
C1A-H1A...O14B^{v}	0.95	2.33	3.130(2)	141.7
C5B-H5B...O11B^{vii}	0.95	2.35	3.293(2)	169.7

Symmetry transformations used to generate equivalent atoms:

(i) –x+5, -y+1, -z+1 (ii) x+2, y+1/2, -z+1/2 (iii) x+1, -y+1, -z

(iv) –x+1, -y, -z (v) -x, -y+2, -z (vi) –x+3, -y+2, -z+1

(vii) –x+2, -y+1, -z

Table 4.14: Selected bond lengths (Å) and bond angles (°) for both adeninium : maleate salts

	(**1**)	(**2**) molecules A	(**2**) molecules B
C10-O10	1.254(2)	1.275(2)	1.281(2)
C10-O11	1.280(2)	1.248(2)	1.249(2)
C13-O13	1.309(2)	1.288(2)	1.303(2)
C13-O14	1.226(2)	1.241(2)	1.230(2)
O10-C10-O11	122.4(2)	121.1(1)	121.3(1)
O13-C13-O14	121.2(1)	123.4(1)	123.05(1)
O10-C10-C13-O13	177.6(2)	1.0(1)	2.9(1)
O11-C10-C13-O14	2.4(3)	7.5(9)	7.4(8)
H7B-N7-C7-N6	180.0(2)	180.0(1)	180.0(1)
H7B-N7-C7-C8	180.0(2)	0.2(2)	-1.1(3)
C1-N9-C8	106.4(1)	103.2(1)	103.6(1)
C1-N2-C3	103.4(1)	106.4(1)	106.1(1)
C3-N4-C5	116.2(1)	111.9(1)	111.8(1)
C5-N6-C7	120.1(1)	123.6(1)	123.8(1)

4.7.1 Crystal structure of adeninium : hydrogen maleate, (1)

In this crystal structure, proton transfer has taken place, giving an asymmetric unit containing an adeninium cation and a hydrogen maleate anion. The hydrogen maleate anion displays the planar conformation commonly found in other hydrogen maleate structures[1,9] (1, 9) stabilised by formation of a short intramolecular hydrogen bond O13-H13...O11 involving the remaining carboxyl proton (figure 4.26 (**1**)). Comparison of the carboxylate C-O bond lengths again indicates the presence of the acidic proton (involved in the intramolecular hydrogen bond) on O13 and loss of a proton from the other carboxylate end of the hydrogen maleate. However, the adeninium ion in is in the less common 3*H*,7*H* tautomeric form, with the endocyclic angles C1-N9-C8 and C1-N2-C3 reversed so that the protonated N9 site is

approximately 3° larger than N2. Protonation of N4 also results in an endocyclic angle significantly larger than the other structures reported in this chapter (table 4.14).

The two components interact through a hard hydrogen bond formed by the amide N7 acting as a donor via H7A to O10 and a soft hydrogen bond formed by C11 via H11 in which the heterocyclic N6 acts as the acceptor (figure 4.26 (**1**)). The adeninium and hydrogen maleate ions combine to form a $R_2^2(8)$ ring on the Watson-Crick site, similar to that seen in the fumarate structure although the synthon itself is clearly formed by an alternative combination of interactions with a soft interaction forming part of the motif (based on motif 7*H*-VII). In this structure, the adeninium dimer $R_2^2(8)$ motif is formed through complementary donation from N4 via H4 to N2. Although the supramolecular effect of this adeninium synthon is similar to the succinic acid and fumarate structures, the nature of this dimer differs due to the alternative tautomeric form giving the motif 3*H*-X. Each adeninium is hydrogen bonded to a second hydrogen maleate through formation of an $R_2^2(9)$ ring motif on the Hoogsteen edge of the adeninium ion (this motif is similar to that of 9*H*-IX but with a different tautomeric form); hard hydrogen bonds are formed by N7 acting as a donor via H7B to O11 and N9 via H9 to O10, with a further reinforcing hydrogen bond between N9 and O11 also via H9 (but not shown on the crystal packing diagram) (figure 4.27). This results in the formation of chains of alternating adeninium and hydrogen maleate ions linked through alternating hydrogen bonded rings in the Watson-Crick and Hoogsteen modes, running parallel to the *b*-axis.

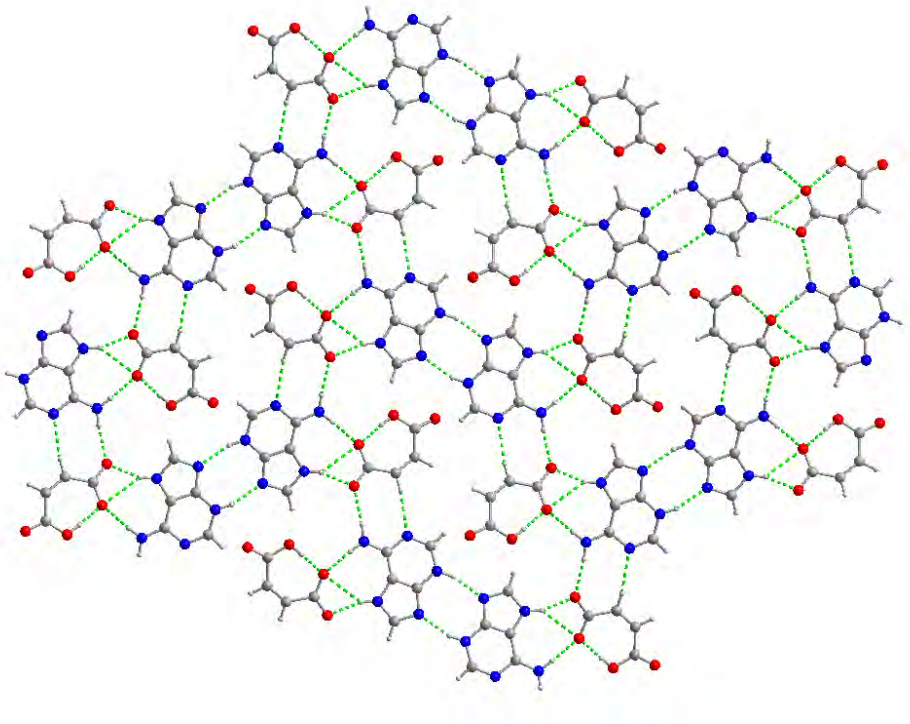

Figure 4.27: A view of the crystal structure showing the chains of alternating $R_2^2(8)$ and $R_2^2(9)$ rings linked together in an infinite sheet with an extensive hydrogen-bonded network. Hydrogen bonds are shown as dashed lines

These chains are linked together by the adeninium dimers to give an infinite hydrogen bonded sheet lying in the (211) plane (figure 4.27). While the carboxylate end of the hydrogen maleate is involved in the strong hydrogen bonds discussed above, the protonated end lies either above or below the plane and is involved in the formation of soft hydrogen bonds with adeninium dimers in neighbouring layers. The first of these is formed by C1 of one adeninium acting as a donor via H1 to O13 and the second by C5 on the other adeninium within the dimer, via H5 to O14 generating a puckered $R_3^3(10)$ ring (Figure 4.28).

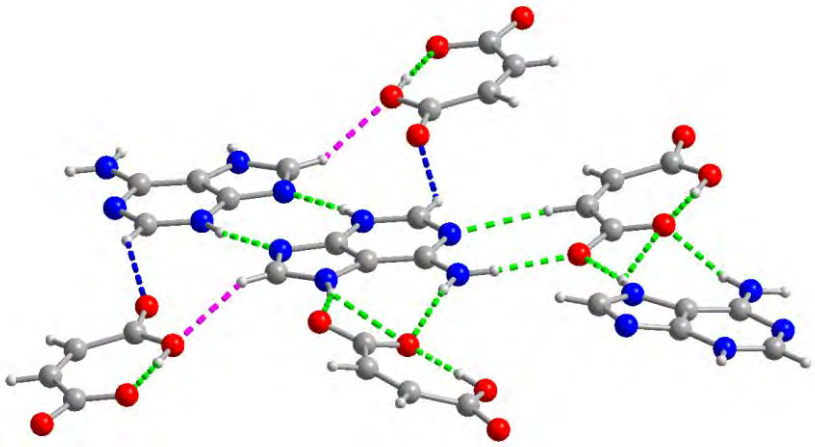

Figure 4.28: The intermolecular interactions surrounding each 3*H*7*H* adeninium molecule in (1). This view shows the adeninium dimer and chains of alternating $R_2^2(8)$ and $R_2^2(9)$ rings within a layer (green dashed lines) with soft hydrogen bonds between the dimer and hydrogen maleate anions above and below this plane shown as dashed pink and blue lines

All strong hydrogen bond donors and acceptors are used in this structure, with each adeninium ion involved in nine intermolecular interactions including N9 acting as a bifurcated donor and both weak C-H donors also used. Each hydrogen maleate ion interacts with four adeninium ions and is involved in eight hydrogen bonds such that O10 acts as a double acceptor, O11 as a triple acceptor (including the intramolecular interaction) and O13 as both a donor and acceptor.

4.7.2 Crystal structure of adeninium : hydrogen maleate : methanolate, (2)

The crystal structure shows that proton transfer has again taken place, but that in this case, the asymmetric unit contains two symmetrically independent adeninium cations, both in the more common 1*H*,9*H* tautomeric form, and two symmetrically independent hydrogen maleate anions, with one methanol molecule also present (figure 4.26 (**2**)). The intramolecular geometry of both adeninium ions (A and B with atom labels a and b respectively) is similar, with the endocyclic angles C1-N2-C3 again larger than the unprotonated N9 site, and the C5-N6-C7 angle significantly larger than in the unprotonated N6 structures (table 4.14). Both adeninium cations (A and B) are hydrogen bonded to the hydrogen maleate anions (A and B respectively) through the formation of $R_2^2(8)$ rings on each Watson-Crick site. The hydrogen maleate ions are again planar, stabilised by the short intramolecular hydrogen bonds formed by O13-H13…O10. The C-O bond lengths in maleate B again indicate the presence or not of the acidic proton (as in structure (1)), although this distinction is not clear in maleate A.

The distinctive $R_2^2(8)$ rings between the coformers in this structure are formed by a combination of the amide N7 acting as a donor via H7A to O10 and a second hard hydrogen bond in which the protonated heterocyclic nitrogen N6 acts as a donor of H6 to the carboxylate O11 in each pair. This motif (9H-VII) is similar to that seen in the adeninium hydrogen fumarate structure rather than the anhydrous maleate structure (**1**). The two adeninium ions are linked through the formation of a hard hydrogen bond donated by N2A on adeninium A via H2A to N9B on adeninium B (with a soft reinforcing interaction, not shown in figure 4.26, formed between C1B-H1B and N4A), and hence the typical dimer motif seen in many other adenine adduct structures is not formed here. The eighth hard hydrogen bond found within the asymmetric unit of this crystal structure is formed between adeninium B and

the methanol molecule, by donation of H2B from the remaining strong donor N2B to the methanol hydroxyl O16 acting as an acceptor.

The asymmetric unit is linked to others by a combination of hard and soft hydrogen bonds generating an infinite hydrogen bonded sheet lying in the (123) plane. This structure can be viewed as parallel ladders of $R_2^2(8)$ rings formed independently by the adeninium and hydrogen maleate A and B pairs (figure 4.29).

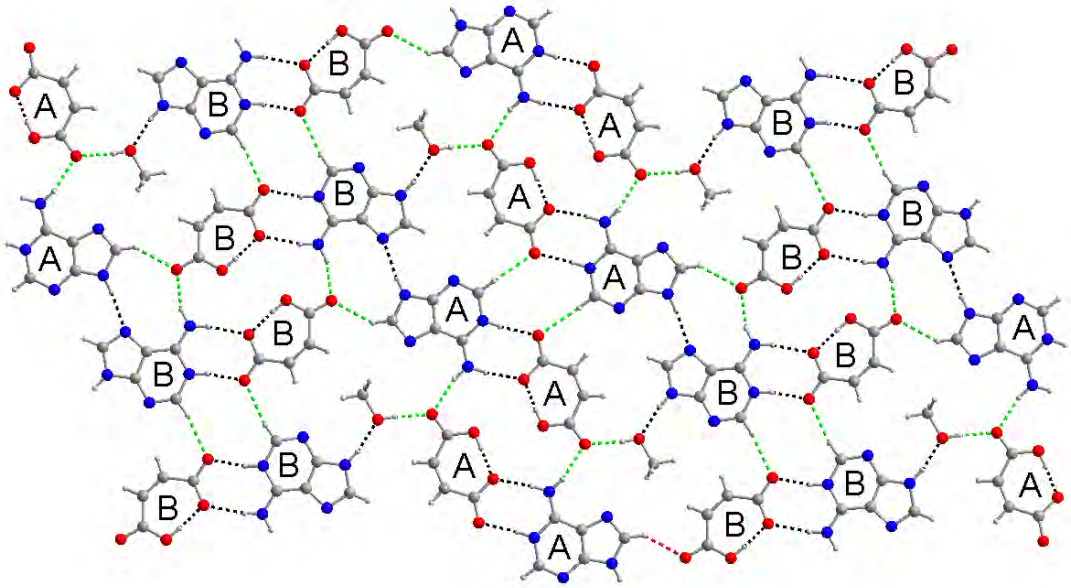

Figure 4.29: A view of the crystal structure showing the hydrogen-bonded sheet formed by the crystallographically independent adeninium (A and B) and the hydrogen maleate (A and B) ions with methanol. Intermolecular hydrogen bonds are shown as dashed lines

In the 'A' ladder, the amide N7 on adeninium A acts as a donor via H7B to form a hydrogen bond with the O14 acceptor on the hydrogen maleate A; generation of the complementary hydrogen bond around an inversion centre forms a $R_6^4(16)$ ring. The C5 on adeninium A acts as a donor of H5 forming a soft hydrogen bond with O11 which then acts as a double

acceptor; generation of the complementary hydrogen bond around an inversion centre forms a $R_4^2(10)$ ring. The overall effect is the formation of a ladder running in the [2-10] direction comprised of $R_2^2(8)$ rings interspersed by alternating $R_6^6(16)$ and $R_4^2(10)$ rings (figure 4.29). A similar architecture is generated by the adeninium and hydrogen maleate B ions in which complementary hydrogen bonds N7-H7...O14 and C5-H5...O11 form the 16-membered and 10-membered rings. There are two further interactions that link the 'A' and 'B' ladders to form an infinite sheet. The first of these is a soft hydrogen bond formed by C1 of adeninium A via H1 to O14 of the neighbouring hydrogen maleate B; the second is an O-H...O hydrogen bond formed by donation of H16 by O16 of the methanol to the hydrogen maleate A O14 making it a double acceptor (figure 4.29). As in previous structures, the adeninium and hydrogen maleate ions are involved in an extensive hydrogen bonding network. All the acceptors in both hydrogen maleate ions act as double acceptors with the carboxyl donor involved in a strong intramolecular interaction. Both adeninium ions are involved in six intermolecular interactions that are marked on the structure packing diagram, however, the remaining N acceptors and weak C-H donors are all in the correct geometry to be involved in weak C-H...N interactions with neighbouring maleates, adeniniums and the methanol hydrogens, although these are not discussed in any more detail.

4.8 Adenine : glutaric acid

Adenine and glutaric acid were cocrystallised following the experimental procedure outlined in chapter 3. Powder X-ray diffraction was used to confirm the formation of a new material below (figure 4.30).

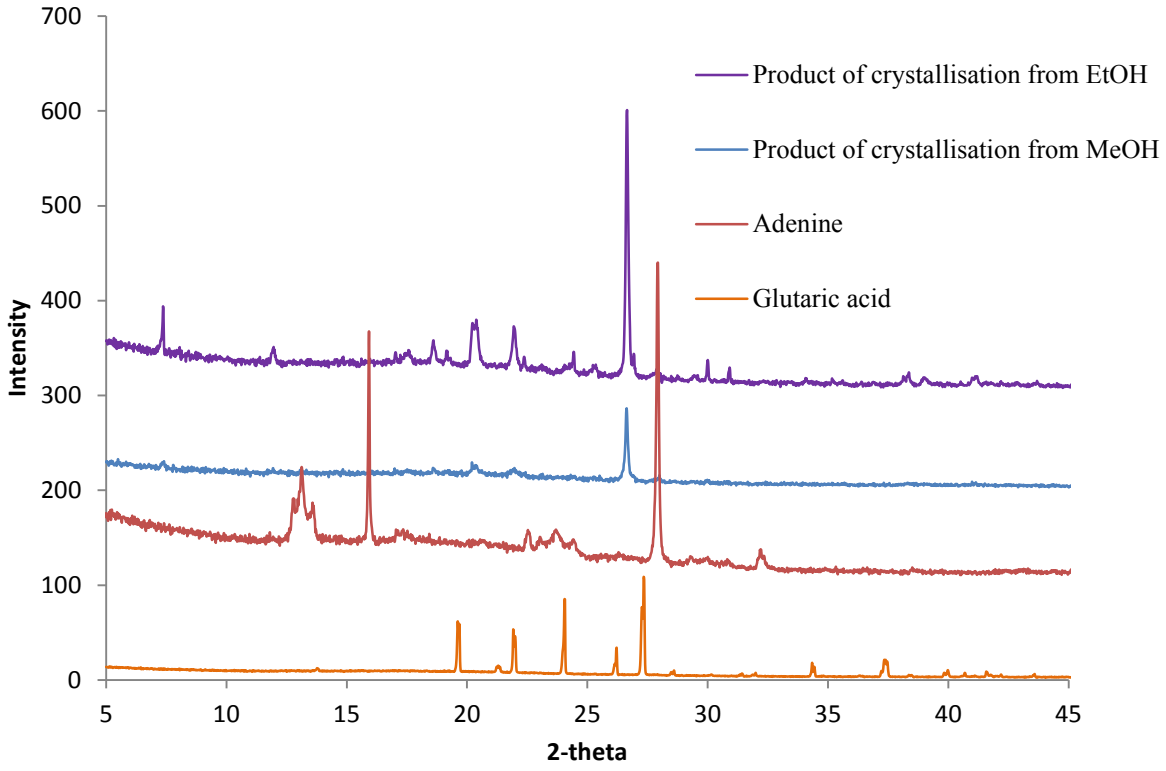

Figure 4.30: Powder X-ray diffraction data for the product of adenine and glutaric acid cocrystallisation and the starting materials

The two products of crystallisation from different solvents have identical patterns differing from those of the coformers indicating the formation of a new material. As the product obtained from methanol is much less crystalline, further study on this adduct was carried out on the sample formed from ethanol. Solution NMR spectroscopy was used to identify that both adenine and glutaric acid are present in a 1:1 stoichiometry (appendix 6.1).

The single crystals in this sample of the adenine : glutaric acid adduct are very small, so while a suitable crystal is not available for single crystal diffraction analysis, indexing was carried out using the powder X-ray diffraction data to identify the unit cell. Indexing provides a list of various possible unit cells for the crystalline material providing unit cell parameters, the volume of the cell and each option is given a figure of merit. The unit cell selected (table 4.15) was chosen because it has the correct volume for a 1:1 triclinic cell if it has space group P-1 and has sensible cell parameters. It also has the highest figure of merit of all of the results given (shown in appendix 6.2). Further work on this material includes attempting to solve the crystal structure from the powder X-ray diffraction data by firstly doing either a le bail or pawley fit (chapter 2)

Table 4.15: Cell parameters obtained for adenine : glutaric acid, 1:1

Parameter	Adenine : glutaric acid
a (Å)	5.2672
b (Å)	11.1084
c (Å)	18.1065
α (°)	137.836
β (°)	84.602
γ (°)	89.534
Volume ($Å^3$)	703.162

4.9 Adenine : adipic acid

A solvated adenine : adipic acid cocrystal has previously been reported[10], however unsolvated forms of cocrystals and salts are preferable when designing materials for the pharmaceutical industry, so following the experimental procedure outlined in chapter 3 the synthesis of an anhydrous adenine : adipic acid material was attempted. Powder X-ray diffraction of the resultant adducts was used to confirm that a new material has been formed (figure 4.31).

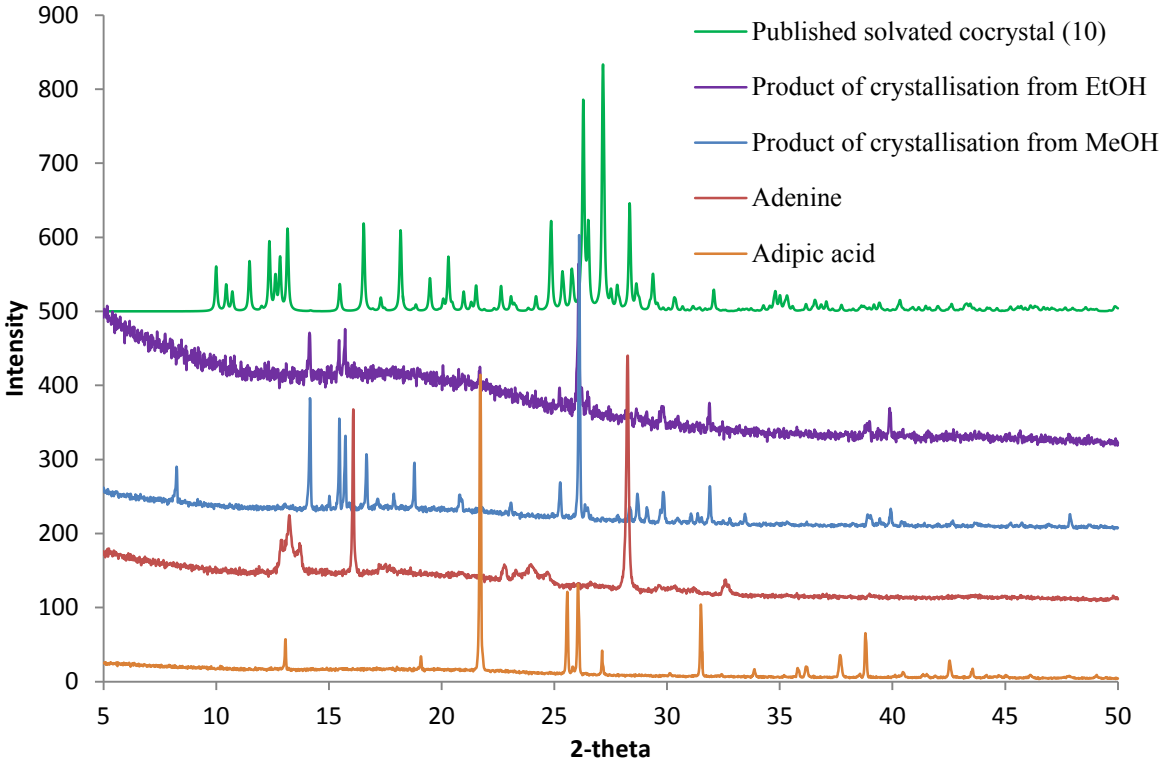

Figure 4.31: Powder X-ray diffraction data for the product of adenine and adipic acid cocrystallisation, the simulated powder pattern from the published solvated cocrystal structure[10] and the starting materials

The powder diffraction patterns show that the product from crystallisation from methanol is different to that of the published solvated cocrystal and the starting materials. The diffraction pattern of the product of crystallisation from ethanol is similar to that obtained from methanol but less crystalline. A 1:1 stoichiometry for this new material (synthesised in methanol) was

determined from ^{1}H NMR spectroscopy. The spectrum shows only peaks relating to the coformers and the DMSO (the solvent in which the NMR spectra were obtained from). The lack of a methanol solvent peak in the NMR spectrum suggests that the new material is anhydrous (appendix 7.1).

The crystal structure has yet to be solved, however indexing from the powder diffraction data has been carried out. The indexing results are given in appendix 7.2, though the unit cell selected is shown in table 4.16. This unit cell was chosen due to it having the correct volume for a 1:1 crystal structure of adenine : adipic acid if it has space group P-1. It also has sensible unit cell parameters and a relatively high figure of merit. Single crystals of adenine : adipic acid have since been grown and are awaiting single crystal X-ray diffraction analysis.

Table 4.16: Cell parameters obtained for adenine : adipic acid, 1:1

Parameter	Adenine : adipic acid
a (Å)	11.5146
b (Å)	11.8849
c (Å)	6.483
α (°)	100.388
β (°)	103.01
γ (°)	65.44
Volume (Å^3)	782.437

4.10 Adenine : pimelic acid

Adenine was cocrystallised with pimelic acid following the synthetic procedure described in chapter 3. Powder X-ray diffraction was used to identify whether the resultant product is a new material (figure 4.32).

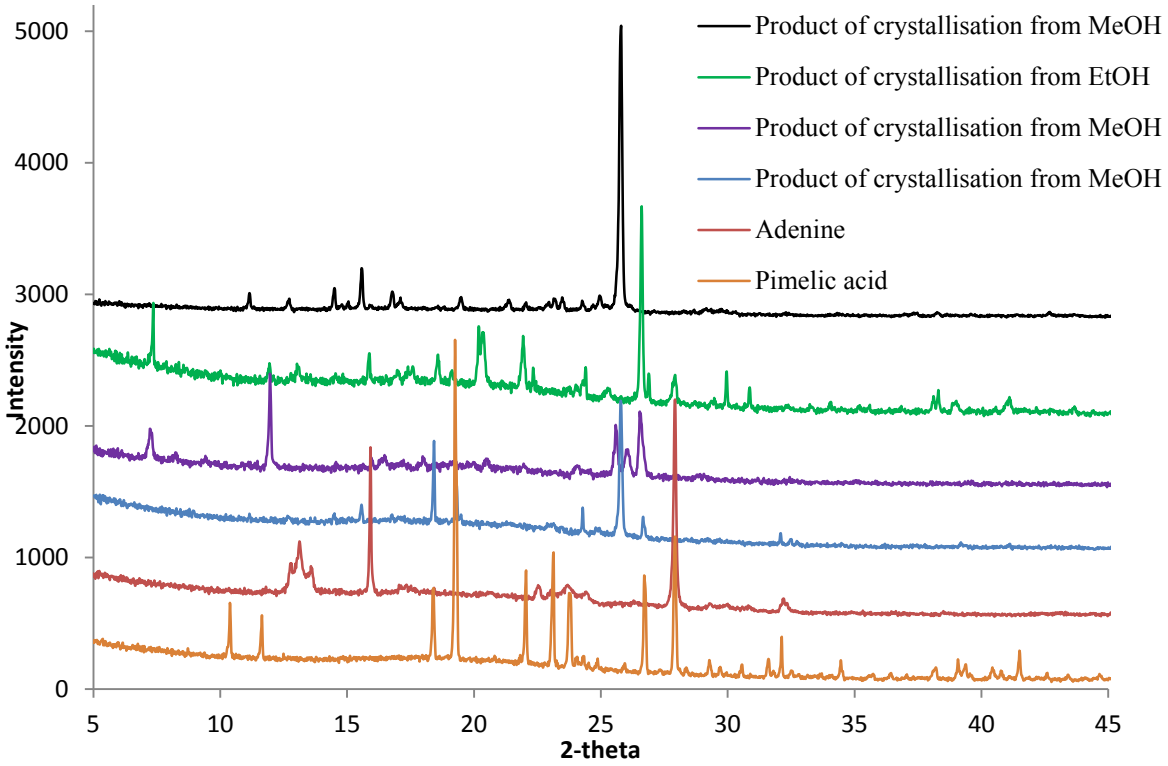

Figure 4.32: Powder X-ray diffraction data for the product of adenine and pimelic acid cocrystallisation and the starting materials

This synthesis was repeated a number of times and of the four adducts synthesised, two new materials have formed. The first of these is the final product of crystallisation from methanol (black line) in which the diffraction pattern shows the formation of a new material without any excess of starting material. The second new material formed is that of the product from ethanol (green line) although this sample does contain peaks indicating the presence of some starting material. The other two products formed from methanol show either a mixture of the

two new materials (purple line) or a mixture of the new product from methanol and pimelic acid (blue line) and in both cases show reduced crystallinity. Further work on the new product from ethanol has not yet been carried out, although ^{1}H NMR spectroscopy has been used to determine the stoichiometry of the new material from methanol. Whilst this NMR spectrum is not absolutely conclusive, it does suggest a 1:1 stoichiometry (appendix 8.1).

A suitable crystal was identified and selected from the sample synthesised in methanol (black line in figure 4.32) for analysis by single crystal X-ray diffraction, though due to the poor quality of these crystals and the difficulty of the sample, both the data collection and the structure solution were carried out by Dr Mateusz Pitaz at the UK National Crystallography Service[15]. The adenine : pimelic acid adduct was found to form a 1:1 cocrystal, crystallising in a monoclinic cell with space group $P2_1/c$. The cell parameters are given in table 4.17.

Table 4.17: Cell parameters for adenine : pimelic acid, 1:1

Compound	Adenine : pimelic acid 1:1
a (Å)	12.438(11)
b (Å)	31.49(3)
c (Å)	7.237(6)
α (°)	90
β (°)	102.635(13)
γ (°)	90
Volume ($Å^3$)	2766(4)
T (K)	100(2)
Z	8
Reflections collected	11224
Independent reflections	4802
R(int)	0.1653
Goodness of fit	0.832
R_1 (observed)	0.0757
R_1 (all)	0.2554
wR_2 (observed)	0.1443
wR_2 (all)	0.2055

The positions of the hydrogen atoms were determined by an electron density map confirming that the structure is a cocrystal, since no proton transfer occurred from the pimelic acid to the adenine. The powder diffraction pattern simulated from the structure solved by single crystal analysis is the same as that of the experimental laboratory powder X-ray diffraction pattern confirming that the crystal chosen is representative of the bulk material (appendix 8.2). Table 4.18 lists the 14 intermolecular hydrogen bonds that make up the cocrystal structure, whilst table 4.19 details selected bond lengths and angles. Figure 4.33 shows the numbering scheme used. Full crystallographic details and tables of all intramolecular bonds and angles are given in appendix 8.

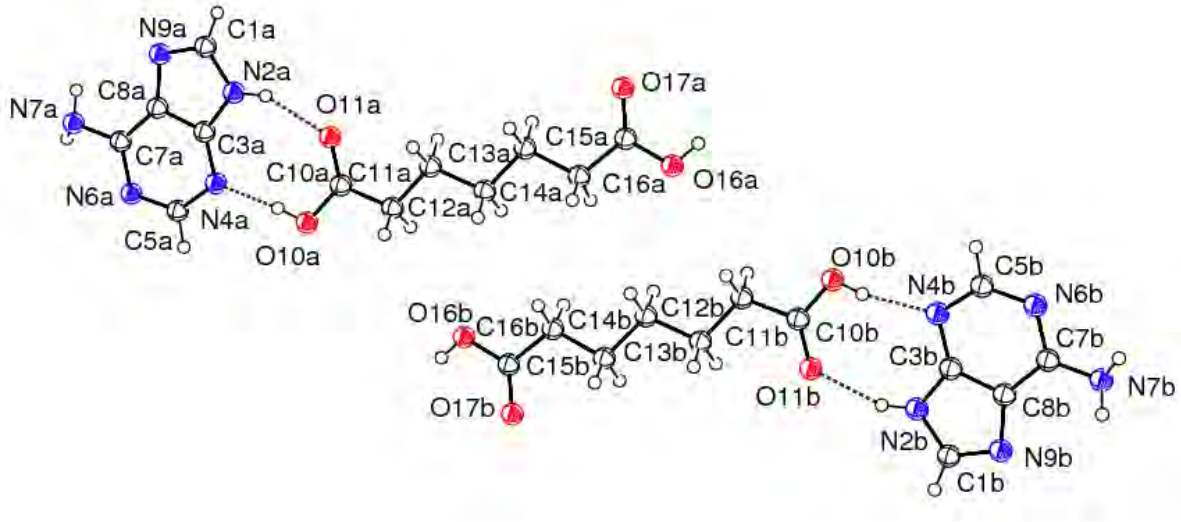

Figure 4.33: The independent molecules of adenine and pimelic acid showing the atom-numbering scheme. Displacement ellipsoids are drawn at 50% probability level

Table 4.18: Intermolecular hydrogen bonding (Å) for adenine : pimelic acid, 1:1

D-H...A	d(D-H)	d(H...A)	d(D...A)	<(DHA)
N2A-H2A...O11A	0.88	1.96	2.777(7)	152.9
N7A-H7AB...O17A^{iv}	0.86	2.26	3.048(7)	152.8
N7A-H7AA...O17B^{iii}	0.86	2.52	3.090(7)	124.6
O10A-H10A...N4A	0.84	1.87	2.693(7)	168.0
O16A-H16A...N9A^{ii}	0.84	1.87	2.696(6)	159.2
C1A-H1A...O10B^{iv}	0.95	2.41	3.265(8)	149.0
C5A-H5A...O11B^{iii}	0.95	2.81	3.765(9)	178.9
N2B-H2B...O11B	0.88	1.92	2.752(7)	156.7
N7B-H7BA...O17A^{ii}	0.86	2.57	3.145(7)	125.2
N7B-H7BB...O17B^{i}	0.86	2.35	3.047(7)	137.3
O10B-H10B...N4B	0.84	1.88	2.707(7)	166.1
O16B-H16B...N9B^{iii}	0.84	1.83	2.633(7)	160.1
C1B-H1B...O10A^{i}	0.95	2.46	3.339(8)	153.8
C5B-H5B...O11A^{ii}	0.95	2.81	3.720(8)	160.1

Symmetry transformations used to generate equivalent atoms:

(i) –x+2, y-0.5, -z+0.5 (ii)–x+1, y-0.5, -z-0.5 (iii) –x+2, y+0.5, -z+0.5

(iv) –x+1, y+0.5, -z-0.5

Table 4.19: Selected bond lengths (Å) and angles (°) for adenine : pimelic acid, 1:1

Bond lengths (Å)			Bond angles (°)		
	Molecules A	Molecules B		Molecules A	Molecules B
C10-O10	1.344(7)	1.319(7)	O10-C10-O11	122.3(6)	124.1(6)
C10-O11	1.237(7)	1.239(7)	O16-C16-O17	122.6(6)	122.9(6)
C16-O16	1.327(7)	1.333(7)	O10-C10-O11	122.3(6)	124.1(6)
C16-O17	1.236(7)	1.243(7)	O16-C16-O17	122.6(6)	122.9(6)
			C1-N9-C8	105.0(5)	104.8(6)
			C1-N2-C3	107.1(5)	106.9(6)
			C3-N4-C5	112.1(6)	110.6(6)
			C5-N6-C7	117.2(6)	119.7(6)
			O10-C10-C16-O16	9.1(9)	4.3(9)
			O11-C10-C16-O17	0.5(6)	-0.9(6)
			H7B-N7-C7-N6	-160.5(6)	-144.0(7)
			H7B-N7-C7-C8	22.5(9)	-40.2(9)

In the crystal structure of adenine : pimelic acid, the asymmetric unit contains two symmetrically independent neutral adenine molecules in the most stable 9*H* tautomeric form and two symmetrically independent pimelic acid molecules (figure 4.33). The intramolecular geometry of both adenine molecules (A and B with atom labels a and b respectively) is similar in terms of the endocyclic angles C1-N2-C3 are approximately 2° larger than the unprotonated N9 site and there is clear discrimination between the bond lengths of the C-OH and C=O bonds in both pimelic acid molecules indicating that all four carboxyl groups in the asymmetric unit have retained their acidic protons (table 4.19). In this structure there is a slight difference in the O10-O16 angles in the different pimelic acid molecules and a large difference in the adenine amide group to the adenine ring angle in the two independent

molecules with a difference of ~20º (torsion angles H7B-N7-C7-N6 and H7B-N7-C7-C8 in table 4.19).

Both adenine molecules A and B are hydrogen bonded to the pimelic acid molecules A and B respectively through two hard hydrogen bonds; the first formed by the heterocyclic N2 acting as a donor via H2 to O11 and the second in which O10 on the acid donates H10 to N4, creating a $R_2^2(8)$ ring based on motif 9*H*-VIII (figure 4.33).

A second ring motif is formed between the adenine and a second pimelic acid molecule via the donation of H7B from the amide N7 to O17 and the heterocyclic N9 acting as an acceptor of H16 from O16 forming a $R_2^2(9)$ ring, motif 9*H*-IX. The combination of these two rings form infinite zigzag chains of either entirely A or B adenine and pimelic acid molecules (figure 4.34).

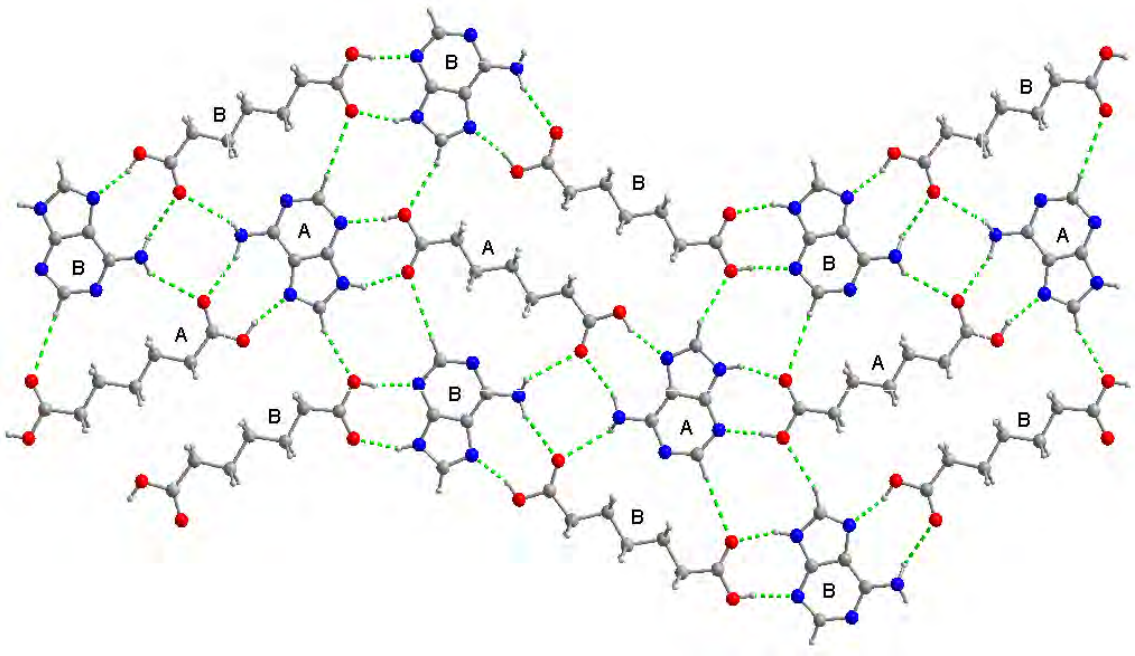

Figure 4.34: A view of the infinite sheet formed through the linking of the adenine : pimelic acid chains. Hydrogen bonds are shown as dashed lines

The chains are linked into an infinite sheet involving both hard and soft hydrogen bonds. An $R_4^2(8)$ ring motif is formed between the chains; two interactions as part of the A and B chains respectively and the two complementary hydrogen bonds formed by donation from heterocyclic N7A via H7AA to O17B and from N7B via H7BA to O17A. Formation of this sheet is reinforced by four soft hydrogen bonds; the first pair of interactions are formed between C1B and O10A via H1B and C5A and O11B via H5A, these create another ring motif, $R_4^2(10)$, when combined with hard interactions already discussed as part of the A and B chains. An equivalent ring is formed taking into account the other soft hydrogen bonds; C5B and O11A via H5B and C1A and O10B via H1A.

The NH_2 group in both the adenine molecules in this structure are out of the plane of the ring, in turn causing the sheets in this structure to deviate from planar. The full crystal structure of this adenine : pimelic acid cocrystal is generated by the stacking of these sheets, however no hard hydrogen bond interactions are formed between them, the only linkages are short contact bonds between the carbons in the pimelic acid chain and a short linkage between the bent NH_2 and the carbon chain in the acid. The majority of strong hydrogen bond donors and acceptors are used in this structure with the exception of one heterocyclic N acceptor N6 on both the A and B adenine molecules. Whilst this cocrystal structure exhibits favourable adenine : acid ring motifs, the lack of an adenine dimer is surprising. The majority of previously published crystalline adenine complexes, and those reported here, involve either the formation of an adenine dimer, or at least the formation of hydrogen bond interactions between adenine molecules. The lack of this supramolecular feature is especially surprising in a solvent free structure.

4.11 Adenine : suberic acid

Adenine and suberic acid were cocrystallised following the synthetic procedure detailed in chapter 3. Powder X-ray diffraction was used to identify that the resultant adducts are new materials (figure 4.35).

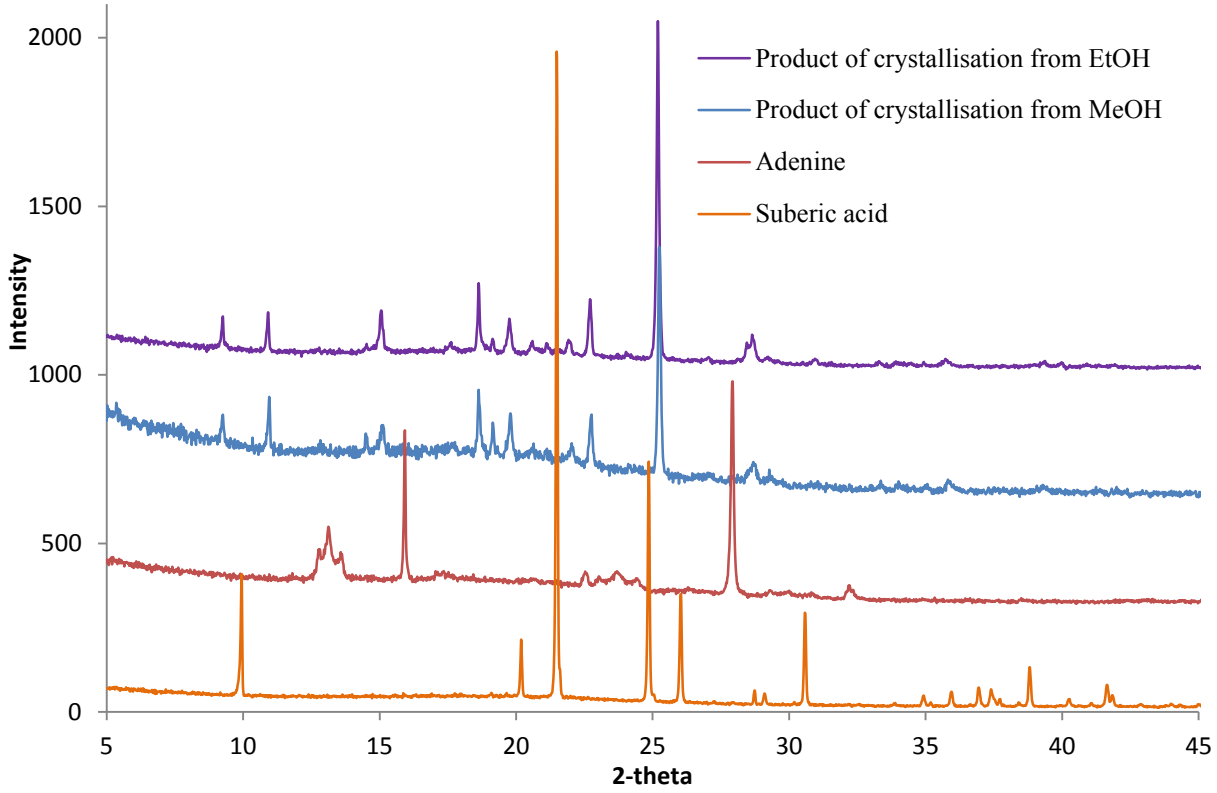

Figure 4.35: Powder X-ray diffraction data for the product of adenine and suberic acid cocrystallisation and the starting materials

The above powder diffraction patterns show that both adducts obtained from methanol and ethanol are the same and do not contain any starting materials. ^{1}H NMR spectroscopy was used to confirm the presence of both adenine and suberic acid in a 1:1.5 ratio (appendix 9.1). Attempts were made to index the powder diffraction pattern to obtain a possible unit cell for this adenine : suberic acid structure as the crystals obtained are of poor quality, making

structure determination from single crystal X-ray diffraction data difficult. Appendix 9.2 gives the results of this indexing although a reliable unit cell could not be identified.

A selection of crystals was sent to the UK National Crystallography Service[15] as it was hoped that the more powerful diffractometer would enable a single crystal dataset to be collected from the smaller crystals. It was reported that the sample was formed of a large crystal made up of a number of smaller ones intergrown together, with some microcrystalline crystals grown on the surface. Upon smashing this cluster, small fragments were identified, though they gave poor and smeared diffraction and not a single diffraction pattern (figure 4.36). The service did however manage to obtain a suitable single crystal from the sample synthesised in ethanol, allowing a dataset to be collected from which structure solution and refinement was possible, though with poor R factors. The structure was found to be a neutral 1:1:1 hydrated cocrystal, crystallising in a triclinic unit cell with space group P-1. Table 4.20 gives the cell parameters and refinement values for this cocrystal.

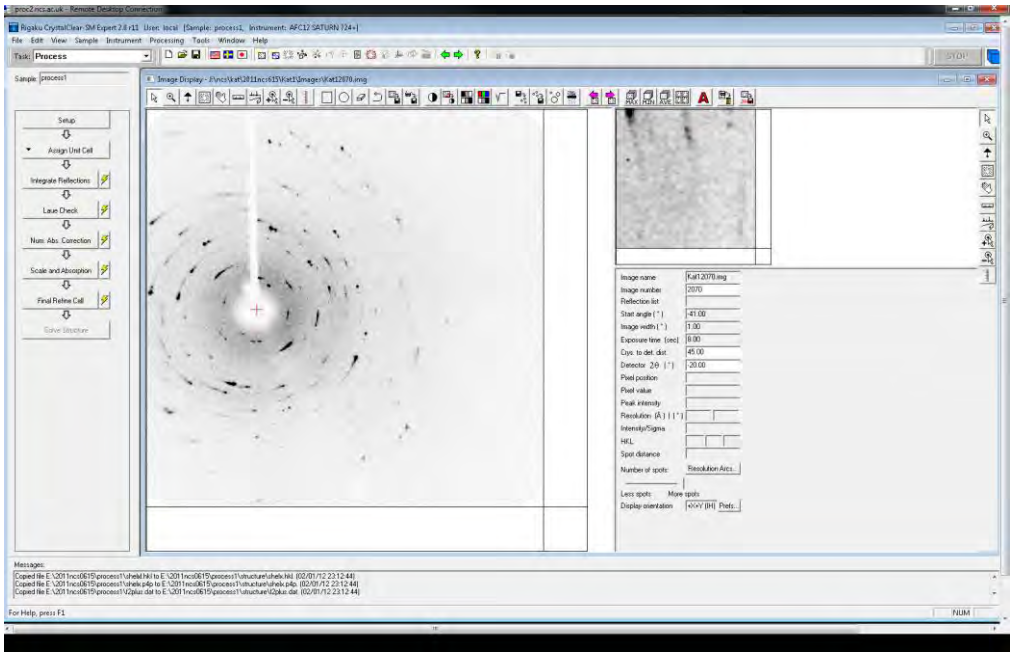

Figure 4.36: A screen shot showing the poor diffraction obtained from the small fragments of the large adenine : suberic acid cluster-like crystals

Table 4.20: Cell parameters and refinement values for adenine : suberic acid : hydrate, 1:1:1

Compound	Adenine : suberic acid : water 1:1:1
a (Å)	8.080(17)
b (Å)	9.76(2)
c (Å)	10.49(2)
α (°)	104.43(4)
β (°)	99.88(4)
γ (°)	92.014(19)
Volume ($Å^3$)	786(3)
T (K)	100
Z	2
Reflections collected	4634
Indepentdent reflections	2343
R(int)	0.2197
Goodness of fit	1.479
R_1 (observed)	0.1415
R_1 (all)	0.1600
wR_2 (observed)	0.3573
wR_2 (all)	0.3840

This cell was not identified from the powder diffraction data, although comparison of the simulated powder X-ray diffraction pattern from the single crystal data and the experimental laboratory powder data confirms that the single crystal chosen was representative of the bulk (appendix 9.3). The 1:1.5 stoichiometry assumed from the ^1H NMR spectrum is incorrect as the cocrystal has a 1:1:1 adenine : suberic acid : hydrate stoichiometry. This discrepancy could be caused by the hydration of the cocrystal. The position of the hydrogen atoms were determined by an electron density map confirming the structure to be a cocrystal, since no proton transfer occurred from the suberic acid to the adenine. Table 4.21 gives details on the

eight intermolecular bonds, with figure 4.37 showing the atom numbering scheme used. Appendix 9 contains a full list of intermolecular bond lengths and angles, though selected ones are given in table 4.22.

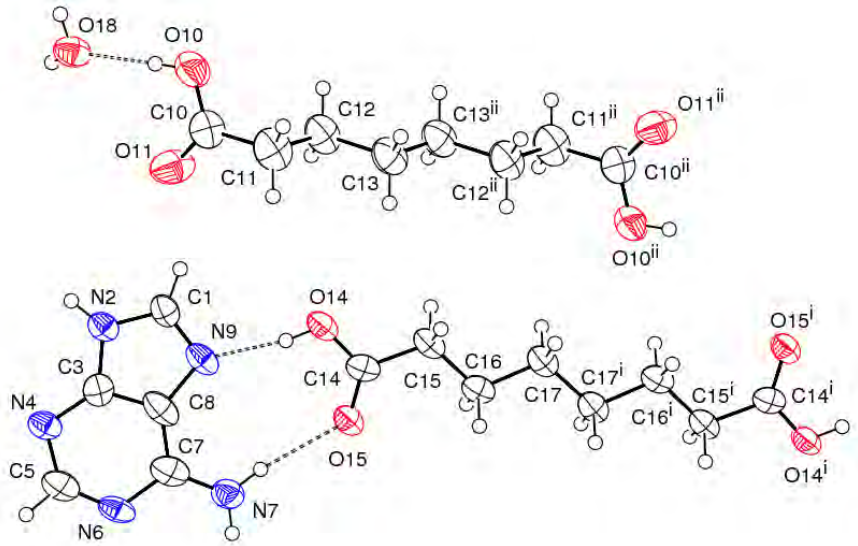

Figure 4.37: The independent molecules of adenine and suberic acid, showing the atom-numbering scheme. Displacement ellipsoids are drawn at 50% probability level

Table 4.21: Intermolecular hydrogen bonding (Å) for adenine : suberic acid : hydrate, 1:1:1

D-H...A	d(D-H)	d(H...A)	d(D...A)	<(DHA)
N2-H2...N4^{i}	0.88	2.03	2.909(8)	172.8
N7-H7A...O15	0.88	2.16	3.035(7)	172.1
N7-H7B...N6^{ii}	0.88	2.23	3.108(8)	173.2
O10-H10...O18	0.84	1.78	2.604(7)	168.2
O14-H14...N9	0.84	1.82	2.647(6)	138.3
O18-H18A...O11^{iii}	0.86(2)	1.97(2)	2.818(8)	170(6)
O18-H18B...O15^{iv}	0.86(2)	1.92(2)	2.768(7)	172(6)
C1-H1...O11^{iv}	0.95	2.16	3.045(9)	155

Symmetry transformations used to generate equivalent atoms:

(i) –x, -y+1, -z+1 (ii) –x, -y, -z (iii) –x, -y+2, -z+1

(iv) x, y+1, z+1

Table 4.22: Selected intermolecular bond lengths (Å) and angles (°) for adenine : suberic acid : hydrate, 1:1:1

Bond lengths (Å)		Bond lengths (°)		Torsion lengths (°)	
C10-O10	1.289(8)	O10-C10-O11	122.0(6)	O10-C10-C10^{i}-O10^{i}	-180.0(5)
C10-O11	1.202(7)	O14-C15-O15	123.3(5)	O11-C10-C10^{i}-O11^{i}	-180.0(6)
C14-O14	1.307(7)	C1-N9-C8	103.6(5)	O14-C14-C14^{i}-O14^{i}	180.0(6)
C14-O15	1.223(6)	C1-N2-C3	108.2(4)	O15-C14-C14^{i}-O15^{i}	180.0(4)
		C3-N4-C5	109.4(4)	H7A-N7-C7-N6	179.8(5)
		C5-N6-C7	119.3(5)	H7A-N7-C7-C8	0.01(9)
				O10-C10-C11-C12	-80.2(7)
				O11-C10-C11-C12	97.0_8)
				O14-C14-C15-C16	179.6(5)
				O15-C14-C15-C16	-0.6(8)

The size and shape of the ellipsoids (figure 4.37) are both large and elongated suggesting disorder within the structure. The ellipsoids in the adenine molecule and one of the acids are all elongated in the c direction and the other acid has very large ellipsoids for the carbon atoms. The asymmetric unit consists of one neutral adenine molecule, in the most stable 9*H* tautomeric form, two half symmetrically independent suberic acid molecules and a molecule of water. As can be seen from table 4.22 there is clear distinction between the C-OH and C=O bonds in the suberic acid molecules, indicating that both the carboxyl groups have retained their acidic protons, and the endocyclic adenine C-N-C angles further confirm the presence of the 9*H* tautomer with C1-N2-C3 having a bond angle significantly larger than that of the unprotonated N9 site. It is clear from table 4.22 that whilst one of the acid molecules is planar (O14-C14-C15-C16 and O15-C14-C15-C16) the other is twisted (O10-C10-C11-C12 and O11-C10-C11-C12). There are three hard hydrogen bonds within the asymmetric unit of this structure. The first is between the twisted suberic acid molecules and the water moleucule and

is formed by donation of H10 from O10 to O18. The other two hydrogen bonds form a linkage between the adenine and the second, more planar suberic acid molecule, forming the popular adenine : acid $R_2^2(9)$ ring motif, 9*H*-IX, on the Watson-Crick edge. This ring motif is formed by N7 acting as a donor of H7A to O15 and the heterocyclic N9 acting as an acceptor of H14 donated by O14.

The adenine molecule forms a dimer with a neighbouring adenine through a complementary hydrogen bond donated by N2 to N4 via H2 to form the 9*H*-X motif, common in other adenine crystalline structures. This interaction creates infinite chains of alternating adenine dimers and planar suberic acid molecules. These chains are linked together through the formation of a further adenine - adenine $R_2^2(8)$ ring, motif 9*H*-XI created by a further complementary hydrogen bond donated by N7 to N6 via N7B. This part of the structure combines to create an infinite hydrogen bonded sheet (figure 4.38) in which infinite chains of adenine molecules are a distinct supramolecular feature.

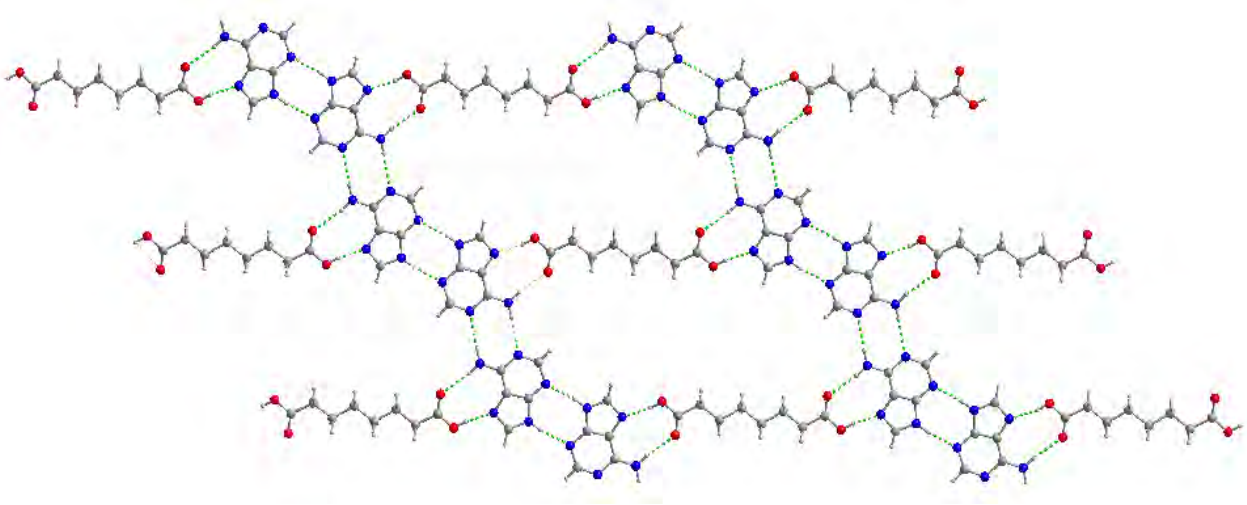

Figure 4.38: A view of part of the crystal structure of adenine : suberic acid showing the infinite chains that link to form sheets of adenine and planar suberic acid components. Hydrogen bonds are shown as dashed lines

The twisted suberic acid moiety that is linked to the water molecules also form hydrogen bond chains which cross and link to the adenine : suberic acid sheets. Each of these chains is formed by two of the twisted suberic acid molecules linked by two water molecules to create a large $R_4^4(12)$ ring motif. This motif is formed by a complementary hydrogen bond donated by O18 through H18A to O11 in combination with the O10-H10...O18 suberic acid : water hydrogen bond present in the asymmetric unit, hence the water acts as both a hydrogen bond donor and acceptor. These acid : water chains link to the adenine : acid chains through a further hard hydrogen bond donated by the water to the more suberic acid by O18 to O15 via H18B, and a soft hydrogen bond donated from the adenine C1 via H1 to O11 on the twisted suberic acid.

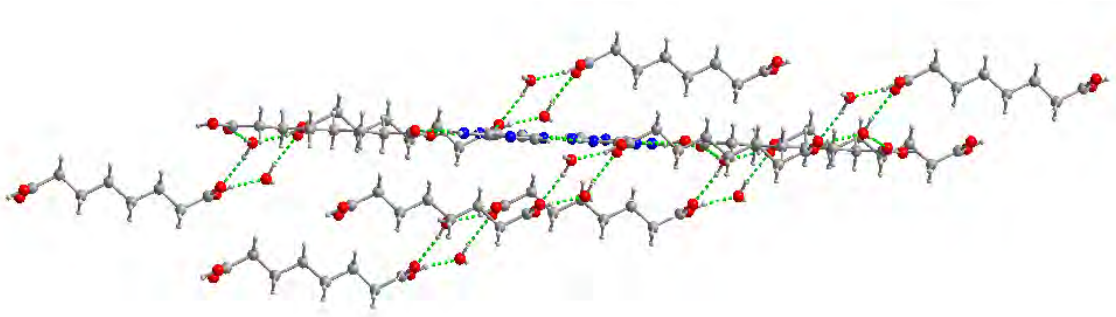

Figure 4.39: A view to show the crossing of the adenine : acid with the acid : water chains. Hydrogen bonds are shown as dashed lines

This structure utilises all strong hydrogen bond donor and acceptor sites and contains both common adenine dimers and a common adenine : acid ring motif.

4.12 Adenine : azelaic acid

The experimental procedure described in chapter 3 was followed as part of a BSc project in which the project student attempted to cocrystallise an adenine and azelaic acid crystalline adduct[16]. Powder X-ray diffraction was used to confirm the formation of an new material (figure 4.40)

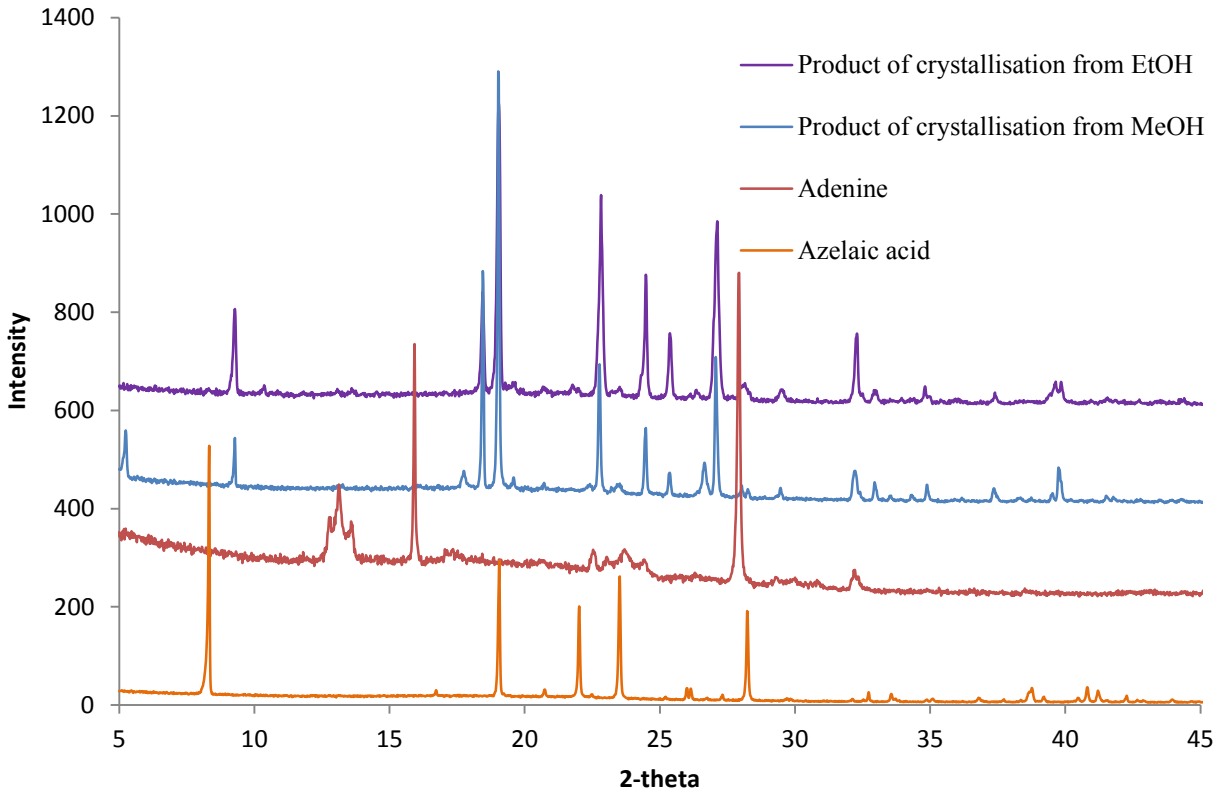

Figure 4.40: Powder X-ray diffraction data for the product of adenine and azelaic acid cocrystallisation and the starting materials

From the powder diffraction patterns above it can be determined that a new material has been formed. The two diffraction patterns are very similar, although there is an unidentified peak at ~5° in the pattern of the product synthesised in methanol[16]. ^{1}H NMR spectroscopy was used to identify what coformers are present and in what ratio they exist. In this case it is clear from the NMR data (appendix 10.1), that there is a minimal amount of adenine present and that

azelaic acid is the only coformer present in any meaningful amount. A suitable crystal was therefore selected for single crystal X-ray diffraction analysis from the sample synthesised in ethanol, and a dataset collected. It was found that the resultant adduct was in fact a different, previously unpublished azelaic acid polymorph, with no adenine present in the crystal structure. The structure crystallises in the monoclinic cell with space group $P2_1/c$. Table 4.23 gives the cell parameters for this azelaic acid polymorph.

Table 4.23: Cell parameters for azelaic acid polymorph

Compound	Azelaic acid
a (Å)	5.51140(10)
b (Å)	9.4563(2)
c (Å)	18.8814(4)
α (°)	90
β (°)	95.994(2)
γ (°)	90
Volume ($Å^3$)	978.67(3)
T(K)	120(2)
Z	4
Reflections collected	13150
Independent reflections	1697
R(int)	0.0358
Goodness of fit	1.069
R_1 (observed)	0.0472
R_1 (all)	0.0525
wR_2 (observed)	0.1217
wR_2 (all)	0.1288

The position of the hydrogen atoms was determined by an electron density map. The powder diffraction pattern simulated from the structure solved by single crystal analysis is essentially the same as that of the experimental laboratory powder X-ray diffraction pattern although there may be some impurity or preferred orientation. However, this does confirm that the crystal chosen is representative of the bulk material (appendix 10.2). Table 4.24 lists the three intermolecular hydrogen bonds that are formed in the crystal structure, table 4.25 list selected bond lengths and angles, whilst Figure 4.41 shows the numbering scheme used. Full bond lengths and angles are shown in appendix 10.

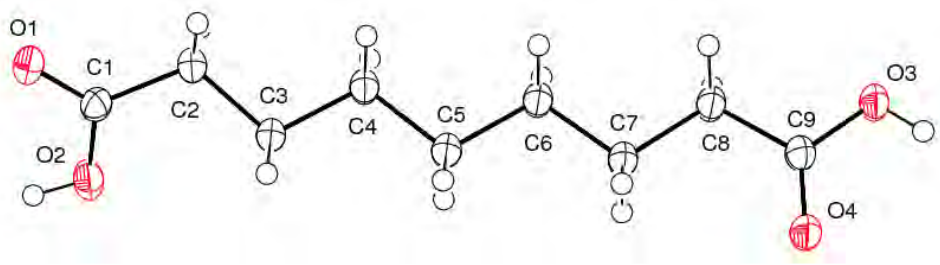

Figure 4.41: The asymmetric unit of the azelaic acid polymorph showing the atom-numbering scheme. Displacement ellipsoids are drawn at 50% probability level

Table 4.24: Intermolecular hydrogen bonding and weak interactions (Å) for the azelaic acid polymorph

D-H...A	d(D-H)	d(H...A)	d(D...A)	<(DHA)
O2-H2...O1^{i}	0.84	1.84	2.672(1)	169.2
O3-H3...O4^{ii}	0.84	1.82	2.659(1)	175.7
C2-H2B...O4^{iii}	0.99	2.68	3.343(2)	124.8
C8-H8A...O1^{iv}	0.99	2.42	3.388(2)	167

Symmetry transformations used to generate equivalent atoms:

(i) -x+4,-y+1,-z+1 (ii) -x,-y+1,-z (iii) –x+2, y-0.5, -z+0.5

(iv) x-1, -y+0.5, z-0.5

Table 4.25: Selected intramolecular bond lengths (Å) and angles (°) for the azleaic acid polymorph

Bond lengths (Å)		Bond lengths (°)		Torsion lengths (°)	
C1-O1	1.230(2)	O1-C1-O2	122.8(1)	O1-C1-C9-O4	104.1(2)
C1-O2	1.308(2)	O3-C9-O4	123.0(1)	O2-C1-C9-O3	132.5(2)
C9-O4	1.221 (2)			O1-C1-C2-C3	145.8(2)
C9-O3	1.321(2)			O2-C1-C2-C3	-36.5(2)
				O7-C8-C9-O4	-1.9(1)
				O7-C8-C9-O3	178.7(1)

There is a clear distinction between the C-OH and C=O bond lengths (table 4.25) further confirming the correct placing of the carboxyl hydrogen. The azelaic acid molecules in this structure are twisted (table 4.25), a feature common within the longer chain acids with an odd number of carbon atoms[17]. In previously published structures, this twisting is a consequence of the packing observed within the structures, which consist of chains involving carboxy dimers, which are in close proximity to the carboxy dimers in the chains either side of it. The twisting occurs to reduce repulsion between these dimers. This is a property also seen in azelaic acid cocrystals, for example isonicotinamide : azelaic acid[18].

The overall crystal structure is formed of infinite chains of azelaic acid molecules, hydrogen bonding together to form infinite sheets, with soft hydrogen bonds linking the sheets together. The azelaic acid chains are built up of $R_2^2(8)$ acid dimers formed at each end of the molecule. The first consists of a hydrogen bond donated by O2 via H2 to O1 with propagation around an inversion centre creating an $R_2^2(8)$ ring motif. The second is formed by donation of H3 from O3 to O4, again with propagation around an inversion centre forming an $R_2^2(8)$ ring motif.

These infinite chains are then linked together via a soft hydrogen bond donated by C2 to O4 through H2B (figure 4.42).

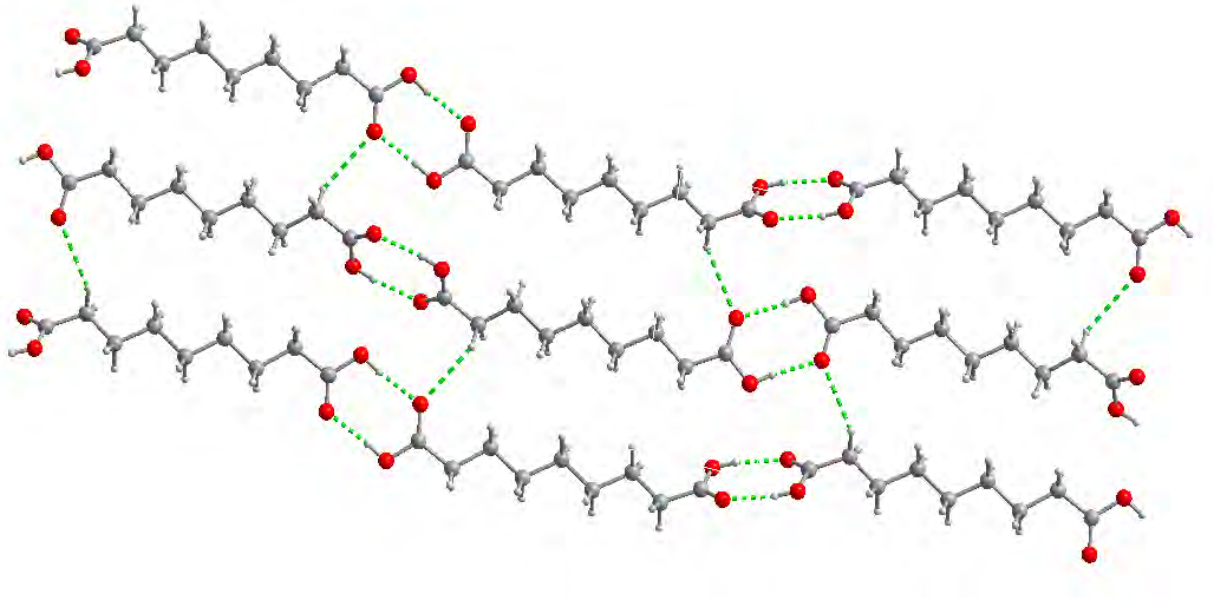

Figure 4.42: A view of the chain units bonding to form an infinite sheet. Hydrogen bonds are shown by dashed lines

A soft bond donated by C8 to O1 via H8A completes this structure to bond the infinite sheets as seen in figure 4.43.

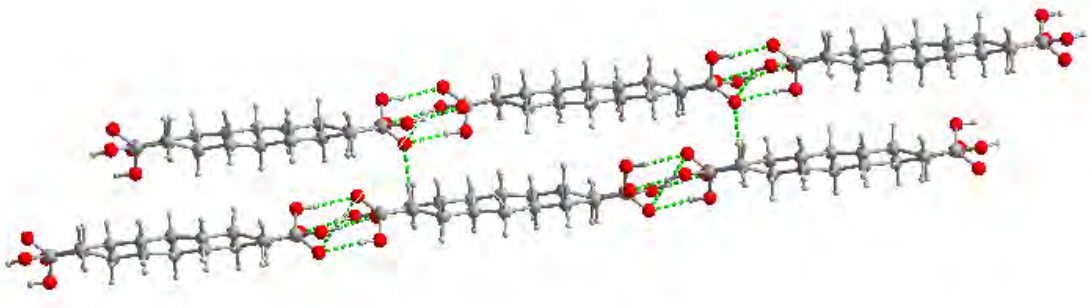

Figure 4.43: A view of the infinite sheets linking via a soft hydrogen bond. Hydrogen bonds are shown by dashed lines

There are five previously published azelaic acid polymorph structures[17,19,20], differing from the structure reported here in a number of ways. All are monoclinic, though four of the five have the space group C2/c, the fifth is in $P2_1/c$. The other polymorphs of azelaic acid also differ to this one as the two C-OH groups on the carboxyl are on the same side (figure 4.44) as compared to the structure reported here where they are on opposing sides (figure 4.41). Whilst there are differences between these polymorphic structures, there are some similarities, for example all of them form infinite chains, though they do not all contain strong hydrogen bonds linking these chains to form sheets. The twisting present in this polymorph is a feature seen in all of them.

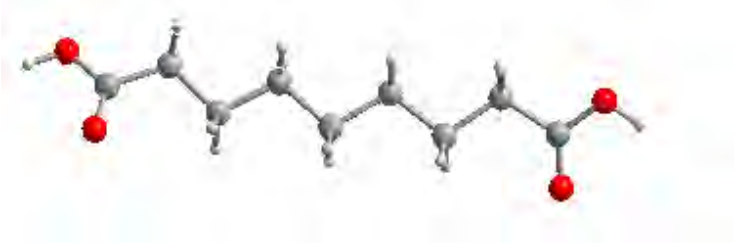

Figure 4.44: A view of a differing azelaic acid polymorph, showing the C-OH groups on the same side

Polymorph screening is very important within the pharmaceutical industry as different polymorphs exhibit different properties, with numerous examples of drugs having multiple forms and becoming problematic with potentially dangerous results[21]. The most common method of polymorph screening is simple recrystallisation of the single component from a wide range of different solvents or using differing experimental conditions[22]. To discover a different polymorph through an attempted cocrystallisation experiment is rare, but it opens up a whole new method of polymorph screening available to the pharmaceutical industry.

Since no adenine was present in the result of the initial cocrystallisation attempt, a repeat of the synthesis outlined in chapter 3 was carried out in the hope of forming an adenine : azelaic

acid crystalline adduct. Powder X-ray diffraction was used to determine whether a new adduct material had been formed (figure 4.45).

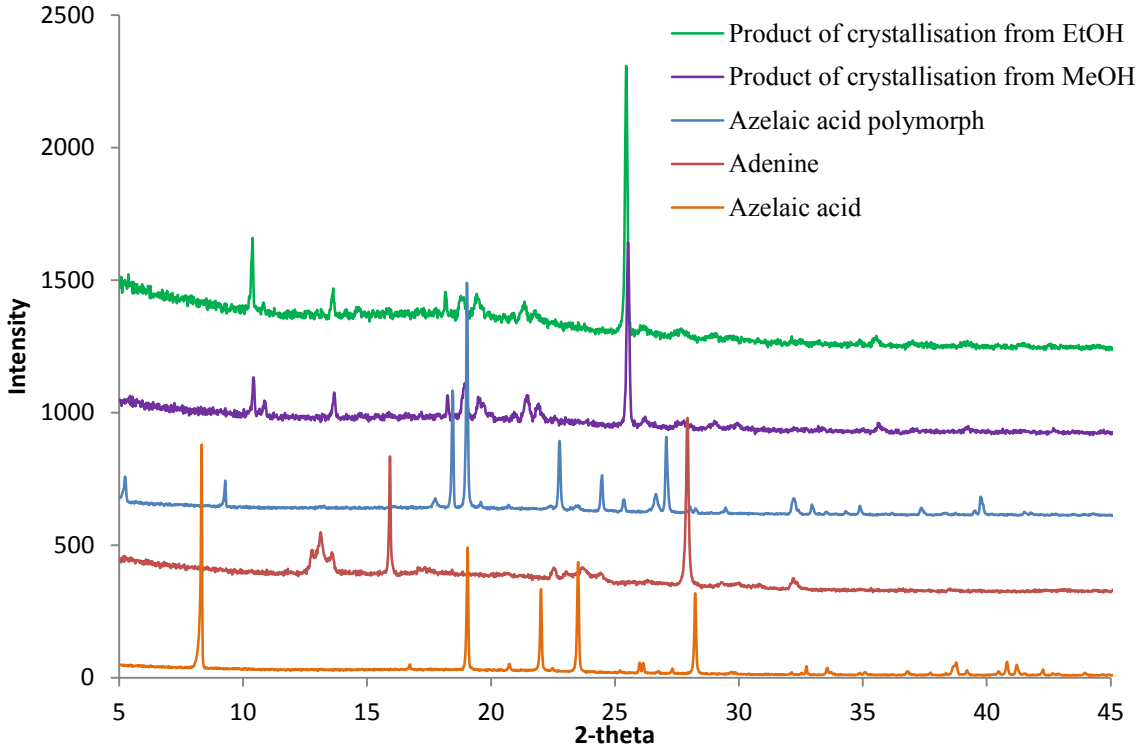

Figure 4.45: Powder X-ray diffraction data for the product of adenine and azelaic acid cocrystallisation compared with the powder pattern of the azelaic acid polymorph and the starting materials

The diffraction patterns above show that upon repeating the synthesis, a new material which is differs from both the azelaic acid polymorph and the starting materials has been formed. Solution ^{1}H NMR spectroscopy of these new materials confirm the presence of both adenine and azelaic acid and indicate a 1:1 adenine : azelaic acid stoichiometry. This suggests that an adenine : azelaic acid adduct has also been formed (appendix 10.6). Single crystal X-ray diffraction analysis has not yet been attempted, though indexing the powder X-ray diffraction pattern has been carried out. A table of results is shown in appendix 10.7, though the cell selected is given in table 4.26. This cell was selected because the volume is correct for a 1:1

adenine : azelaic acid adduct with monoclinic symmetry. Whilst the figure of merit for the chosen cell is low, cells with much higher figures of merit have volumes that would not be correct being either too low for a triclinic cell or having a volume representative of monoclinic but unit cell parameters representative of triclinic. The low figure of merit does suggest that this may not be correct but it is a good basis. Single crystals of this adduct have been obtained and are awaiting single crystal x-ray diffraction analysis.

Table 4.26: Cell parameters obtained from indexing of adenine : azelaic acid, 1:1

Parameter	Adenine : azelaic acid
a (Å)	18.2318
b (Å)	4.6715
c (Å)	16.3596
α (°)	90
β (°)	111.414
γ (°)	90
Volume ($Å^3$)	1297.161

4.13 Adenine : sebacic acid

Adenine was cocrystallised with sebacic acid following the experimental procedure described in chapter 3. Powder X-ray diffraction was used to confirm the formation of a new material. As can be seen from the diffraction patterns below in figure 4.46, the products of crystallisation are different from different solvents as well as from the coformers, suggesting that two new materials have been formed, although the product from ethanol looks like it may also contain some of the product obtained from methanol.

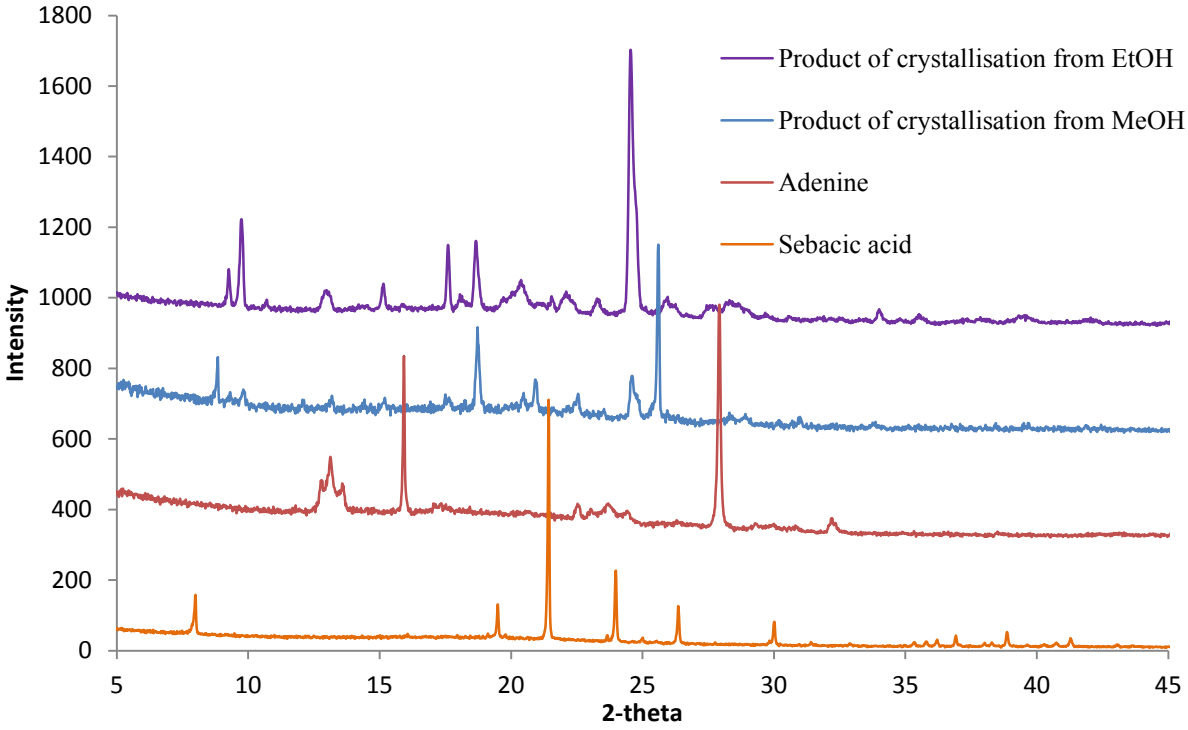

Figure 4.46: Powder X-ray diffraction data for the product of adenine and sebacic acid cocrystallisation and the starting materials

Solution ^{1}H NMR spectroscopy was carried out on both of these crystalline adducts (appendix 11.1), suggesting that adenine and sebacic acid are present in both of these new materials in a 1:1 ratio from ethanol but a 4:3 adenine : acid ratio from methanol.

Single crystal X-ray diffraction analysis has been used to solve the crystal structure of the new material from methanol, although a suitable crystal of the product from ethanol has not been obtained. The dataset collected for the product of crystallisation from methanol resulted in a hydrated cocrystal structure in a 4:3:4 adenine : sebacic acid : water stoichiometry. The structure crystallises in a triclinic cell with a space group of P -1. Table 4.27 gives the cell parameters for this hydrated structure.

Table 4.27: Cell parameters for adenine : sebacic acid : hydrate 4:3:4

Compound	Adenine : sebacic acid : hydrate 4:3:4
a (Å)	10.3417(2)
b (Å)	12.4896(3)
c (Å)	12.7894(3)
α (°)	101.134(2)
β (°)	107.272(2)
γ (°)	104.6200(10)
Volume ($Å^3$)	1460.72(6)
T (K)	120(2)
Z	2
Reflections collected	14245
Indepentdent reflections	5019
R(int)	0.0254
Goodness of fit	1.044
R_1 (observed)	0.0360
R_1 (all)	0.0429
wR_2 (observed)	0.0877
wR_2 (all)	0.0918

The position of the hydrogen atoms was determined by an electron density map confirming that the structure is a cocrystal, since no proton transfer has occurred from the sebacic acid to the adenine. The powder diffraction pattern simulated from the structure solved by single crystal analysis is similar to that of the experimental laboratory powder X-ray diffraction pattern although the peaks at 25 - 27° in 2-theta may suggest that there is some anisotropic thermal behaviour evident in this comparison. (appendix 11.2). The crystal is however assumed to be representative of the bulk material. Table 4.28 lists the 15 intermolecular interactions that are formed in this cocrystal structure, whilst figure 4.47 shows the numbering scheme used. A full table of intramolecular bonds and angles can also be found in appendix 11, with selected values given in table 4.29.

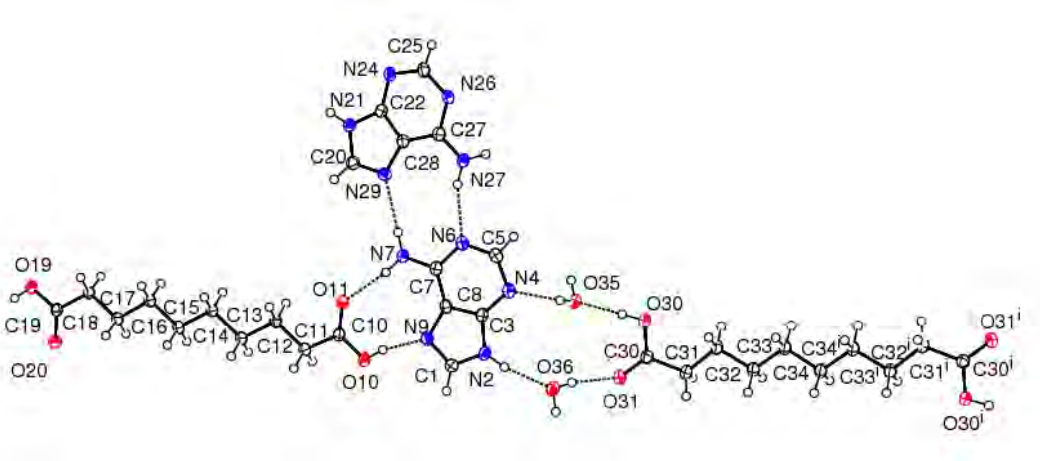

Figure 4.47: The independent molecules of adenine : sebacic acid : hydrate 4:3:4 synthesised from methanol showing the atom-numbering scheme and the hard intermolecular hydrogen-bonds (shown as dashed lines). Displacement ellipsoids are drawn at 50% probability level

Table 4.28: Intermolecular hydrogen bonding (Å) for adenine : sebacic acid : hydrate 4:3:4

D-H...A	d(D-H)	d(H...A)	d(D...A)	<(DHA)
N2-H2...O36	0.88	1.91	2.782(2)	168.6
N7-H7A...N29	0.88	2.14	3.018(2)	178.5
N7-H7B...O11	0.88	2.04	2.909(2)	171.5
O10-H10...N9	0.84	1.84	2.669(2)	167.8
O19-H19...N26^{ii}	0.84	1.76	2.589(2)	169.3
N21-H21...N24^{iii}	0.88	2.03	2.869(2)	160.3
N27-H27A...O20^{iv}	0.88	2.08	2.940(2)	164.3
N27-H27B...N6	0.88	2.11	2.958(2)	161.3
O30-H30...O35	0.84	1.76	2.601(1)	177.0
O35-H35A...O11^{v}	0.87 (2)	1.92 (2)	2.776(2)	165.3(19)
O35-H35B...N4	0.88 (2)	2.04(2)	2.852(2)	153.0(18)
O36-H36A...O31	0.85(2)	2.02(2)	2.851(2)	169.6(19)
O36-H36B...O20	0.86(2)	1.94(2)	2.772(2)	164(2)
C20-H20...O35	0.95	2.50	3.335(2)	146.0
C25-H25...O31	0.95	2.42	3.257(2)	146.0

Symmetry transformations used to generate equivalent atoms:

(i) -x, -y+2, -z+1 (ii) x+2, y, z+1 (iii) - x+2, -y, -z

(iv) x-2, y, z-1 (v) -x+2, -y+1, -z+1

Table 4.29: Selected intramolecular bond lengths (Å) and angles (°) for adenine : sebacic acid : hydrate, 4:3:4

Bond lengths (Å)		Bond lengths (°)		Torsion lengths (°)	
C10-O10	1.309(2)	O10-C10-O11	113.5(1)	O10-C10-C19-O19	179.4(2)
C10-O11	1.222(2)	O19-C20-O19	123.4(1)	O11-C10-C19-O20	-176.6(1)
C19-O19	1.302(2)	O30-C30-O31	123.0(1)	O30-C30-C30^{i}-O30^{i}	-180.0(1)
C19-O20	1.226(2)	C1-N9-C8	103.8(1)	O31-C31-C31^{i}-O31^{i}	180.0(2)
C30-O30	1.312(2)	C1-N2-C3	106.6(1)	H7B-N7-C7-N6	-180.0(1)
C30-O31	1.222(2)	C3-N4-C5	110.5(1)	H7B-N7-C7-C8	0.2(3)
		C5-N6-C7	118.8(1)	H27B-N27-C27-N6	180.0(1)
		C20-N29-C28	103.6(1)	H27B-N27-C27-C28	-0.3(3)
		C20-N21-C22	106.7(1)		
		C22-N24-C25	111.1(1)		
		C25-N26-C27	120.7(1)		

The asymmetric unit of the adenine : sebacic acid hydrated cocrystal, 4:3:4 contains two symmetrically independent adenine molecules, both in the most stable 9*H* tautomeric form, one complete and one half symmetrically independent sebacic acid molecule with two molecules of water (figure 4.47). There is clear discrimination between the length of the C-OH and C=O bonds in both the sebacic acid molecules (table 4.27) indicating that all carboxyl groups have retained their acidic protons, and the endocyclic C-N-C angles further confirming the presence of the 9*H* tautomer with C1-N2-C3 and C20-N21-C22 having angles approximately 3° larger than the unprotonated nitrogen sites (C1-N9-C8 and C20 N29 C28) (table 4.27). The intramolecular angles between the two independent molecules are similar, however it is believed that z' for this structure is two because it may be the only way to accomodate the water molecules.

The coformer molecules hydrogen bond to form an adenine dimer and two adenine : acid ring motifs within the asymmetric unit. One of which also integrates both water molecules (figure 4.48). One of the most common adenine dimers, 9*H*-XIII, is formed by the amide groups on the two adenine molecules N7 and N27 acting as hydrogen bond donors of H7A and H27B to N29 and N6 respectively to give an $R_2^2(9)$ ring. The first of the adenine : acid ring motifs is formed on the Hoogsteen edge of one adenine by the amide N7 donating its second hydrogen H7B, to O11, with the adenine heterocyclic N9 also accepting a hydrogen bond from O10 via H10 resulting in another $R_2^2(9)$ ring, (motif 9*H*-IX). The second adenine : acid ring motif (formed by the same adenine molecule) also encompasses the water molecules. This motif is formed by the heterocyclic N2 donating H2 to O36 on one water molecule, which in turn donates H36A to the sebacic acid acceptor O31. The adenine also accepts a hydrogen bond at N4 donated by O35 via H35B on the second water molecule, which in turn accepts H30 from O30 from the sebacic acid, altogether creating a large $R_4^4(12)$ ring motif, similar to motif 9*H*-VIII shown in table 4.1.

The adenine dimer unit is hydrogen bonded to three sebacic acid molecules; the two present in the asymmetric unit and a third $R_2^2(8)$ motif formed by the donation of H27A from amide N27 O20, with heterocyclic N26 acting as an acceptor for H19 donated from O19. This seven unit architecture (two adenine molecules, three sebacic acid molecules and two water molecules) links to a further unit through the formation of a second adenine dimer to create a small chain unit of four adenine molecules. This dimer is formed through a complementary hydrogen bond donated by N21 to N24 via H21, forming an $R_2^2(8)$ ring, motif 9*H*-X.

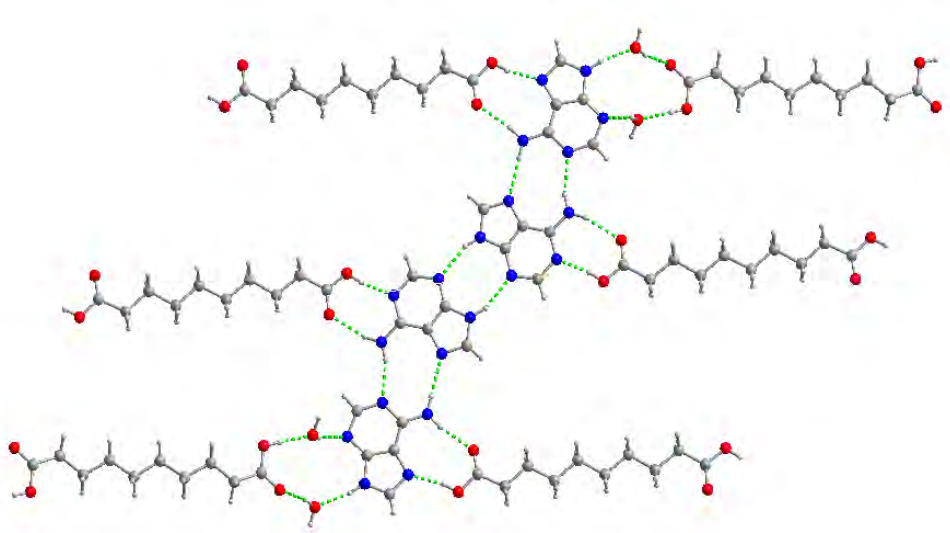

Figure 4.48: A view of the adenine : sebacic acid cocrystal structure showing the adenine dimer units as small four unit chains. Hydrogen bonds are shown as dashed lines

The adenine : sebacic acid structure consists of multiple layers with the water molecules acting as a step and linking these layers together (figure 4.49). The water molecules each hydrogen bond to further sebacic acid molecules; the first donated by O35 through H35A to O11 and the second formed by O36 donating a hydrogen bond via H36B to O20. The structure is completed by the presence of two soft hydrogen bonds, one of which donated by C20 to O35 via H20 and the second donated by C25 via H25 to O31.

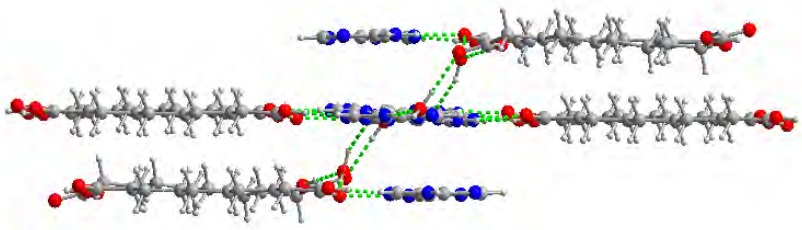

Figure 4.49: A view of the layered structure of adenine : sebacic acid. Hydrogen bonds are shown as dashed lines

This cocrystal structure utilises all strong hydrogen bond donor and acceptor sites, containing adenine dimer units commonly found in a number of adenine structures along with three different adenine : acid ring motifs.

4.14 Adenine : undecanedioic acid

Adenine was synthesised with undecanedioic acid following the experimental procedure outlined in chapter 3. Currently no crystals have formed in the solution; further work includes repeating this procedure using a range of different solvents along with investigating possible other methods of synthesis such as solvent drop grinding.

4.15 Discussion

In this chapter we have presented the structures of eight new adenine : dicarboxylic acid adducts in addition to a new polymorphic form of an acid and introduced the structures of five previously published adenine : dicarboxylic acid adducts. Of the new adenine adducts reported, four are cocrystals and four are salts. When predicting the possibility of proton transfer by investigation of their pK_a values, it was correctly predicted that malonic acid and maleic acid are more likely to form a salt as opposed to a cocrystal. However, the adeninium : hydrogen fumarate salt is an anomaly to the generic rule that a pK_a difference of less than 3 would suggest cocrystal formation (table 4.2). This shows that although the difference in pK_as may be an indicator of adduct form when values are at the extremes, a more robust solid-state parameterisation is required if this prediction of solid state form is to be more reliable.

In addition to the study of electron density maps for location of the proton in question, detailed investigation of the carboxyl bond lengths can be utilised to confirm whether these adducts are cocrystal or salt. From table 4.30 it can be seen that if the structure is a salt, only one of the C-OH carboxyl bond lengths is ~1.3 Å, the other is much shorter and more representative of a C=O bond, confirming the deprotonation.

Table 4.30: Carboxylic acid bond lengths in the adenine : dicarboxylic acid adducts. The highlighted cells show the much shorter C-OH bond lengths in the salt structures

	C=O	C-OH	C=O	C-OH
Adenine : hydrogen malonate	1.205(5)	1.319(4)	1.248(4)	1.267(4)
Adenine : succinic acid	1.220(3)	1.304(3)	1.206(3)	1.330(3)
Adenine : hydrogen fumarate	1.215(4)	1.324(4)	1.246(4)	1.280(4)
Adenine : hydrogen maleate	1.226(2)	1.309(2)	1.280(2)	1.254(2)
Adenine : hydrogen maleate : malonate Mol A	1.241(2)	1.288(2)	1.248(2)	1.275(2)
Mol B	1.230(2)	1.303(2)	1.249(2)	1.281(2)
Adenine : pimelic acid	1.236(7)	1.327(7)	1.237(7)	1.344(7)
Adenine : suberic acid	1.223(6)	1.307(7)	1.202(7)	1.289(8)
Adenine : sebacic acid	1.226(2)	1.302(2)	1.222(2)	1.309(2)

Investigation of the intramolecular geometry within the adenine molecule can also be used. Table 4.31 shows the bond angles within the adenine molecule. It can be seen that when a nitrogen atom in adenine is protonated, the angle becomes approximately 3° larger. This observation helps with both the confirmation of whether there has been proton transfer from the acid as well as confirming the existence of a specific tautomer.

The anhydrous adeninium : hydrogen maleate structure for example contains adeninium cations in the less stable 3*H*,7*H* tautomeric form, and the table clearly shows that for this structure the bond angles around N9 and N4 are greater than in the other structures based on the more stable 9*H* or 1*H*,9*H* tautomers.

Table 4.31: Selected intramolecular bond angles around the heterocyclic nitrogen of the adenine : dicarboxylic acid adducts. The protonated nitrogen positions are highlighted in orange

	C1-N9-C8	C1-N2-C3	C3-N4-C5	C5-N6-C7
Adenine : hydrogen malonate	104.0(3)	106.5(3)	112.2(3)	124.0(3)
Adenine : succinic acid	103.6(2)	106.7(2)	111.1(2)	119.2(2)
Adenine : hydrogen fumarate	103.3(3)	106.1(3)	111.9(3)	123.8(3)
Adenine : hydrogen maleate	106.4(1)	103.4(1)	116.2(1)	120.1(1)
Adenine : hydrogen maleate : malonate	103.2(1)	106.4(1)	119.1(1)	123.6(1)
Adenine : pimelic acid	105.0(5)	107.1(5)	112.1(6)	117.2(6)
Adenine : suberic acid	103.6(5)	108.2(4)	109.4(4)	119.3(5)
Adenine : sebacic acid	103.8(1)	106.6(1)	110.5(1)	118.8(1)

The study by Guerra *et al*[5] established that the three most stable tautomers of neutral adenine are 9*H* > 3*H* > 7*H*. All four structures in which there are neutral adenine molecules detailed in this chapter exist in its most stable 9*H* tautomeric form. As can be seen in appendix 1.1, in the previously reported adenine adducts in which the adenine molecule is neutral, all exist in the 9*H* form except for four in the 7*H* tautomeric form.

In the four salt structures formed, three contain adeninium cations in the most common 1*H*,9*H* tautomeric form (as shown in appendix 1.2). The anhydrous adeninium : hydrogen maleate structure however contains adeninium cations in the 3*H*,7*H* tautomeric form. There are only two adeninium complexes previously reported containing this tautomeric form[23], both containing metal ions. This adeninium : hydrogen maleate structure is the first purely organic adduct to contain 3*H*,7*H* adeninium cations. DFT (density functional theory) calculations have been reported on various adeninium tautomeric forms[24] and it was concluded that the 1*H*,9H form is the most stable followed by the 3*H*,7*H*. The remaining adeninium tautomer options have the following stabilities 3*H*,9*H* > 7*H*,9*H* > 1*H*,7*H* > 6*H*,9*H* > 6*H*,7*H*, though of the structures currently known, there are only examples of 1*H*,7*H* and 6*H*,9*H* (appendix 1.2). The hydrogen bonding network in adenine : hydrogen maleate results in a crystalline arrangement that stabilizes this uncommon tautomer. The lack of protonation at the N2 adeninium position enables the formation of a C-H...N interaction on the Watson-Crick site enabling the hydrogen maleate in this structure to form an additional intermolecular interaction. The presence of a hydrogen on N4 necessitates movement of the proton from N2 to N9 so the expected adeninium dimer (3*H*-X, figure 4.1) can from. The overall combination of these structural requirements results in the adoption and stabilization of the unusual 3*H*,7*H* tautomer.

The vast majority of adenine : dicarboxylic crystalline adducts reported contain the adenine dimer motif as shown in table 4.1. The exceptions are the previously published adeninium : oxalate structures, the adenine : pimelic acid cocrystal reported here and the solvated adeninium : hydrogen maleate salt (although this latter structure does contain strong hydrogen bonds between the adenine molecules). Two of the cocrystal structures discussed in this chapter (adenine : suberic acid and adenine : sebacic acid) contain ribbons of adenine molecules, a supramolecular feature formed by dimers linked together forming chains, similar to the structure of pure adenine. The adenine : acid ring motifs are also popular within this set of crystalline adducts with all of these structures involving at least one of these networks. Table 4.32 lists the different motifs present in both the previously known structures and those reported here.

Table 4.32: The motifs found in the adenine structures discussed

Structure	Tautomer	Adenine motifs		Adenine-acid motifs		Adenine-acid single bond
Adenine	9*H*	9*H*-X 9*H*-XIII	B-B H-WC			
Adeninium : oxalate : chlorine[8]	1*H*9*H*			9*H*-VII[a]	WC-acid	N9H-O=C $R_2^1(5)$
Adeninium : hydrogen oxalate : oxalate : hydrate[8]	1*H*9*H*			9*H*-IX	H-acid	N9H-O=C $R_2^1(5)$
Adeninium : adenine : hydrogen maleate : hydrate[1]	7*H* 1*H*9*H*	9*H*-XII 7*H*-IX 9*H*-XVI[a]	H-H WC-WC B-WC	9*H*-IX 9*H*-VII[a]	H-acid WC-acid	9*H*-VI N9H-O-C
Adeninium : hydrogen maleate : hydrate[9]	1*H*9*H*	9*H*-XII	H-H	9*H*-VII[a]	WC-acid	9*H*-VI N9H-O=C
Adenine : adipic acid : methanolate[10]	9*H*	9*H*-XI	WC-WC	9*H*-IX	H-acid	
Adenine : hydrogen malonate	1*H*9*H*	9*H*-XII 9*H*-X	H-H B-B	9*H*-VII[a]	WC-acid	9*H*-VI N9H-O=C
Adenine : succinic acid	9*H*	9*H*-X	B-B	9*H*-IX	H-acid	9*H*-IV 9*H*-III N1-CO_2H NH-C=O
Adenine : hydrogen fumarate	1*H*9*H*	9*H*-X	B-B	9*H*-VII[a]	WC-acid	9*H*-III NH-C=O
Adenine : hydrogen maleate (**1**)	3*H*7*H*	3*H*-X	B-B	9*H*-IX[a] 7*H*-VII	H-acid WC-acid	
Adenine : hydrogen maleate : methanolate (**2**)	1*H*9*H*			9*H*-VII[a]	WC-acid	
Adenine : pimelic acid	9*H*			9*H*-VIII 9*H*-IX	B-acid H-acid	9*H*-II 9*H*-III NH-C=O NH-C=O
Adenine : suberic acid	9*H*	9*H*-X 9*H*-XI	B-B WC-WC	9*H*-IX	H-acid	
Adenine : sebacic acid	9*H*	9*H*-XIII 9*H*-X	H-WC B-B	9*H*-VIII 9*H*-IX	B-acid H-acid	

B – base of adenine or adeninium, WC – Watson-Crick edge, H – Hoogsteen edge

a – based on this motif, though with either different tautomeric forms or adeninium cations as opposed to neutral adenine molecules

Whilst there are some similarities between the structures presented in this chapter (for example the existence of an adenine-acid ring motif), it is clear from the above table that many of the hydrogen bonding networks are distinct. There are six possible adenine dimer motifs (B-B, H-H, WC-WC, B-H, B-WC, H-WC) and whilst the base-Hoogsteen dimer does not occur in these structures, the remaining options are similarly represented, with a slight emphasis on a base-base pair arising from adenine : acid linkages on the Watson-Crick and Hoogsteen sites. An adenine-acid ring motif is present in all structures discussed here, with all three options (B-acid, H-acid and WC-acid) represented. These adenine structures all exhibit extensive hydrogen bonded networks that do not show an obvious trend, however some common features have emerged. All anhydrous adducts have a B-B adenine dimer and a H-acid linkage whilst all hydrated forms contain a H-H adenine dimer. When studying the cocrystal motifs as a comparison to the salt structures, it was noted that the H-acid linkage is present in all cocrystals whereas the salt structures contain the WC-acid motif, with the B-acid linkage not occurring. Further structures within this series would be required to determine whether these patterns would continue to allow prediction of the packing and hydrogen bonding networks of future adenine structures.

The synthesis of new materials and a preference for the neutral anhydrous forms of these adducts is for their potential use within the pharmaceutical industry. Adenine is a nucleobase, but as reported in both previous work and the work reported here, its ability to tautomerise can be problematic. In addition to its very high melting point and poor solubility adenine is not an ideal solid state material for pharmaceutical application. Cocrystal formation provides a potential route for tuning certain physicochemical properties such as melting point, solubility and stability of an active pharmaceutical ingredient, whilst retaining the chemical properties of the cocrystal formers. Melting point studies of these materials has been started,

although further work is needed for completion of this, and investigation into relative solubilities is also needed. As can be seen from Table 4.33, the melting points of the crystalline adducts are significantly lower than that of adenine and in some cases lower than its pure acid as well, an advantage when considering adenine for pharmaceutical application. The melting points of the other adenine adducts not included in this table was attempted, however at 360ºC the samples had not melted implying that these samples may have degraded and not be fully representative. This analysis was attempted significantly later than the preparation of the sample, in some cases, more than a year.

Table 4.33: The melting points of a selection of adenine : dicarboxylic acids and their coformer materials

Material	**Melting point (˚C)**
Adenine	> 360
Maleic acid	141-143
Succinic acid	179-181
Fumaric acid	286 – 288
Adenine : succinic acid	241 – 244
Adeninium : fumarate	242 – 244
Adeninium : maleate	132 – 136
Adeninium : maleate: methanolate	192 - 195

Further work into this series of cocrystals will involve attempts to synthesise neutral, anhydrous cocrystal forms of adenine with all of the materials in this set including investigating different methods of synthesis and alternative stoichiometries. Solvent drop grinding is another possible experimental method and should be utilised as it creates the possibility for solvent free forms to be obtained. It could also yield adenine adducts of differing stoichiometries to those discussed and it would be interesting to determine whether tautomerisation occurs using this technique as opposed to from solution. Study into the properties of these new materials also requires further work; solubility and reliable melting

point measurements for the whole set of materials are to be taken. There are also a number of materials that were not fully characterised so structure solution from powder diffraction data would prove beneficial where the quality of these crystals for single crystal X-ray diffraction is poor.

4.16 Footnote

1. Since submission of this thesis, two further adenine adduct structures have been solved; an adenine : adipic acid cocrystal (that differs from the published solvated structure[10]) and an adenine : azelaic acid cocrystal structures. Both of these structures follow the patterns highlighted in the above discussion (appendix12).

2. The adenine : succinic acid, adenine : hydrogen fumarate, adenine : hydrogen maleate and adenine : hydrogen maleate : malonate structures discussed within this chapter have been drafted into a paper for publication to be entitled 'The supramolecular behaviour of adenine with succinic, fumaric and maleic acids; tautomerisation, cocrystallisation, salt formation and solvation' (appendix 13)

4.17 References

1. C. McHugh and A. Erxleben. *Cryst. Growth. Des.*, 2011, **11**(11), 5096
2. S. Mahapatra, S. K. Nayak, S. J. Prathapa and T. N. G. Row, *Cryst. Growth. Des.*, 2008, **8**(4), 1223
3. P. Yakovchuk, E. Protozanova and M. D. Frank-Kamenetskii, *Nucleic Acids Res.*, 2006, **34**(2), 564
4. M. Hanus, M. Kabelac, J. Rejnek, F. Ryjacek and P. Hobza, *J. Phys. Chem. B.*, 2004, **108**(6), 2087
5. C. Fonseca Guerra, F. M. Bickelhaupt, S. Saha and F. Wang, *J. Phys. Chem. A.*, 2006, **110**(11), 4012

6. J. P. Garcia-Teran, O. Castillo, A. Luque, U. Garcia-Couceiro, P. Roman and F. Lloret, *Inorg. Chem.*, 2004, **43**(18), 5761

7. S. Fujii, K. Kawasaki, A. Sato, T. Fujiwara and K. L. Tomita, *Arch. Biochem. Biophys.*, 1977, **181**(2), 363

8. B. Sridhar, K. Ravikumar and B. Varghese, *Acta Crystallogr. Sect. C*, 2009, **65**, O202

9. B. Sridhar and K. Ravikumar, *Acta Crystallogr. Sect. C*, 2007, **63**, O415

10. M. Byres, P. J. Cox, G. Kay and E. Nixon, *CrystEngComm.*, 2009, **11**(1), 135

11. S. L. Childs, G. P. Stahly and A. Park, *Mol. Pharmaceut.*, 2007, **4**(3), 323

12. R. M. C.Dawson, D. C.Elliott, W. H. Elliott and K. M. Jones, *Data for biochemical research*, **2 ed**, Oxford Clarendon Press, 1969

13. M. Tremayne, L. V. Vella-Zarb, A. Bond and S. L. Price, *Personnal Communication*

14. J. Bernstein, R. E. Davis, L. Shimoni and N. L. Chang, *Angew. Chem. Int.*, 1995, **34**(15), 1555

15. S. J. Coles and P. A. Gale, *Chem. Sci.*, 2012, **3**(3), 683

16. D. Narsi, *The synthesis and structural characterisation of organic co-crystals and salts*, BSc project, University of Birmingham, 2011

17. V. R. Thalladi, M. Nusse and R. Boese, *J. Am. Chem. Soc.*, 2000, **122**(38), 9227

18. L. J. Thompson, R. S. Voguri, L. Male and M. Tremayne, *CrystEngComm.*, 2011, **13**(12),. 4188

19. J. Housty and M. Hospital, *Acta Crystallogr.*, 1967, **22**, 288

20. A. D. Bond, M. R. Edwards and W. Jones, *Acta Crystallogr. Sect. E*, 2001, **57**, o143

21. N. Chieng, T.Rades, J.Aaltonen, *J.Pharm.Biomed.Anal.*, 2011, *55*(4), 618

22. J. M. Miller, B. M. Collman, L. R. Greene, D. J. W. Grant and A. C. Blackburn, *Pharm. Dev. Technol.*, 2005, **10**(2), 291

23. J. P. Garcia-Teran, O. Castillo, A. Luque, U. Garcia-Couceiro, G. Beobide and P. Roman, *Inorg. Chem.*, 2007, **46**(9), 3593

24. C. Marian, D. Nolting and R. Weinkauf, *Phys. Chem. Chem. Phys.*, 2005, **7**(18), 3306

5. The Crystal Structures and Melting Point Properties of Isonicotinamide Cocrystals with Alkanediacids

5.1 Introduction

Isonicotinamide (pyridine-4-carboxamide, figure 5.1) has also been identified as a good candidate for cocrystallisation with the alkanediacids used in chapter 4 for the adenine complexes. This molecule also has a number of strong hydrogen bond donor and acceptor sites present and demonstrates a propensity to form crystalline adducts with other materials. The strong hydrogen bond donor and acceptor sites present in this structure make it ideal for forming the robust acid-pyridine heteromeric synthon seen in many of the amide-acid cocrystal combinations discussed later in this chapter.

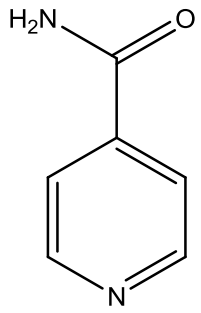

Figure 5.1: Isonicotinamide

Previously published isonicotinamide : dicarboxylic acids adduct structures include 2:1 cocrystals of isonicotinamide : oxalic acid[1], isonicotinamide : malonic acid (cocrystal and salt mix)[1], isonicotinamide : succinic acid[1], isonicotinamide : fumaric acid[2], isonicotinamide : glutaric acid[1] and isonicotinamide : adipic acid[1]. Isonicotinamide : glutaric acid and

isonicotinamide : adipic acid also exist in a 1:1 stoichiometry. All of these published structures contain a dicarboxylic acid $HO_2C(CH2)_{n-2}CO_2H$ with a carbon chain length (*n*) of between two and six carbon atoms.

This chapter focuses on the cocrystallisation of six new potential isonicotinamide : dicarboxylic acid adducts; isonicotinamide with maleic acid, pimelic acid, suberic acid, azelaic acid, sebacic acid and undecanedioic acid. Maleic acid, like succinic acid and fumaric acid, has a carbon chain length of four carbon atoms, whilst the remaining acids have much longer chain lengths with *n* being between seven and eleven respectively (table 5.1). The hydrogen bonding patterns of these potential complexes were predicted by studying the possible hydrogen bonding motifs and networks that these structures could form along with an understanding of the packing of similar isonicotinamide : diacid complexes. The pK_a values of these coformers were also examined to monitor the possibility of the formation of salts rather than cocrystals (see section 1.4).

Three possible hydrogen bonding motifs were identified for these materials, including an isonicotinamide dimer, and two heteromeric motifs, one of which contains the very strong acid-pyridine synthon, (figure 5.2).

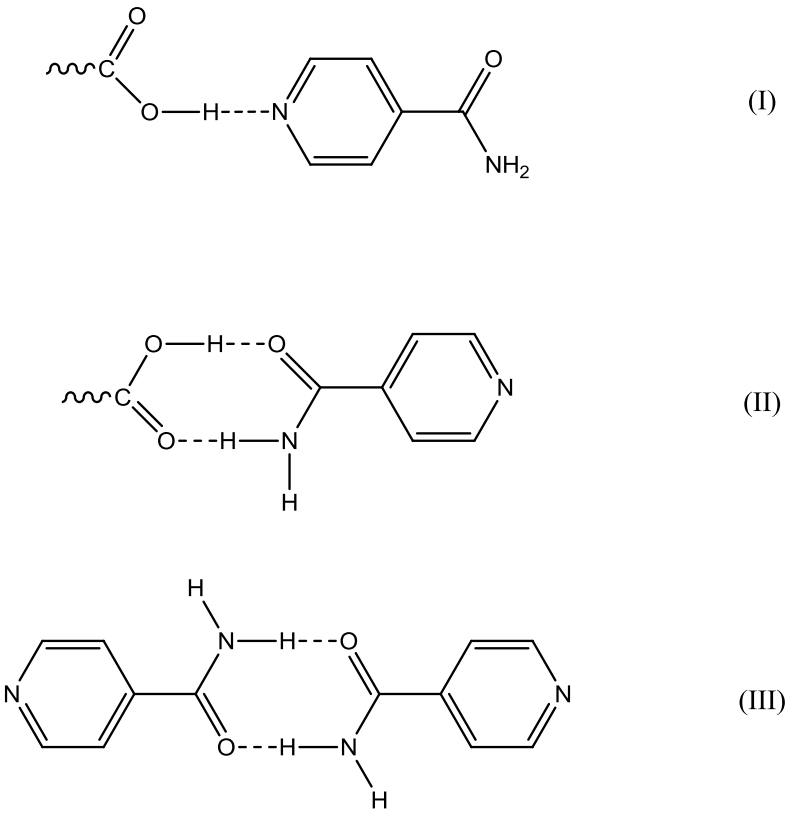

Figure 5.2: Possible hydrogen bonding motifs for isonicotinamide : dicarboxylic acids; (I) acid-pyridine, (II) acid-amide and (III) amide-amide.

In appendix 14, the hydrogen bond motifs and packing diagrams for all of the previously reported isonicotinamide : dicarboxylic acid cocrystals are shown. As can be seen from these figures, a clear trend exists. All these structures contain the acid-pyridine hydrogen bonding motif I (shown in figure 5.2) with the 1:1 complexes exhibiting the acid : amide motif II and the 2:1 complexes containing the amide dimer synthon III.

The relative pK_a values of all these materials are given in table 5.1Table 5.1: . From this data we can predict that the new materials formed and presented in this chapter will be in cocrystal form as the pK_a difference is less than 2 - 3 (perhaps with the exemption of maleic acid as this pK_a difference is close to the borderline). Using our knowledge of motifs we would predict that all will contain motif I and either II or III dependent on the stoichiometry.

Table 5.1: A table of pK_a values for the coformers investigated[3]. pK_a^1 refers to the first deprotonation and pK_a^2 the second deprotonation.

Coformer	Chemdraw	pK_a^1	pK_a^2	Cocrystal (C) or salt (S)	Previously reported?
Isonicotinamide	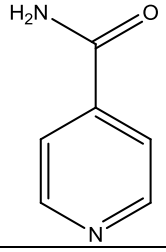	Heterocyclic N: 3.4 Amide: 13.7			
Oxalic acid	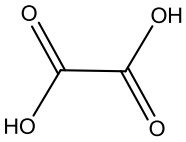	1.27	4.29	2:1 C	Y
Malonic acid	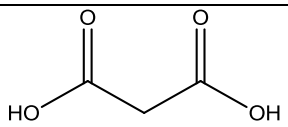	2.85	5.70	2:1 C and S mixed	Y
Succinic acid	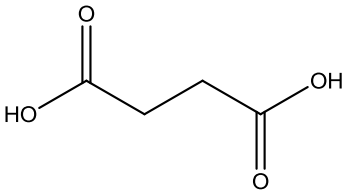	4.21	5.64	2:1 C	Y
Fumaric acid	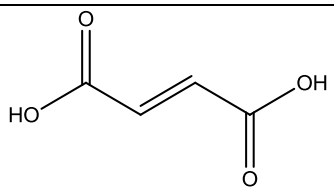	3.02	4.38	2:1 C	Y
Maleic acid	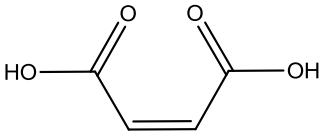	1.97	6.24	1:1 S	N
Glutaric acid	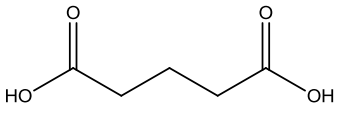	4.34	5.41	2:1 and 1:1 C	Y

Adipic acid	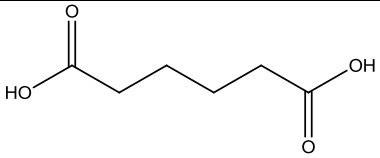	4.43	5.41	2:1 and 1:1 C	Y
Pimelic acid	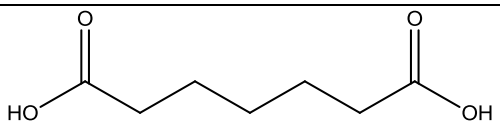	4.50	5.43	1:1 C	N
Suberic acid	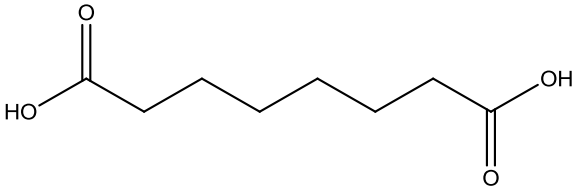	4.53	5.50	1:1 C	N
Azelaic acid	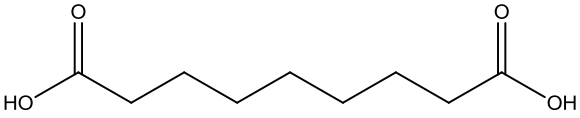	4.55	5.50	1:1 C	N
Sebacic acid	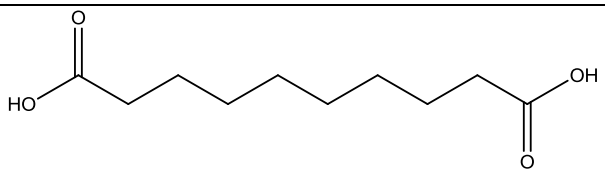	4.72	5.45	2:1	N
Undecanedioic acid	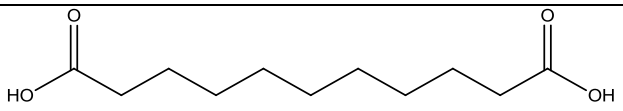	4.48		1:1	N

In addition to the synthesis and crystal structure determination of these materials, a melting point study of all the isonicotinamide : dicarboxylic acid adducts and their respective coformers was undertaken with the aim of enhancing the understanding of how the physical properties of a cocrystal relate to the two different coformers, and consequently aide the tuning of physical properties of materials by cocrystallisation. The melting point of the pure acids shows an alternating pattern with the acids containing an odd number of carbon atoms in the chain length having a lower melting point (figure 5.3). This alternation is well documented[4] and is discussed in detail later in this chapter. The melting point study here will

address whether the cocrystals have the same alternating pattern and the relative placing of these melting points with respect to their coformers.

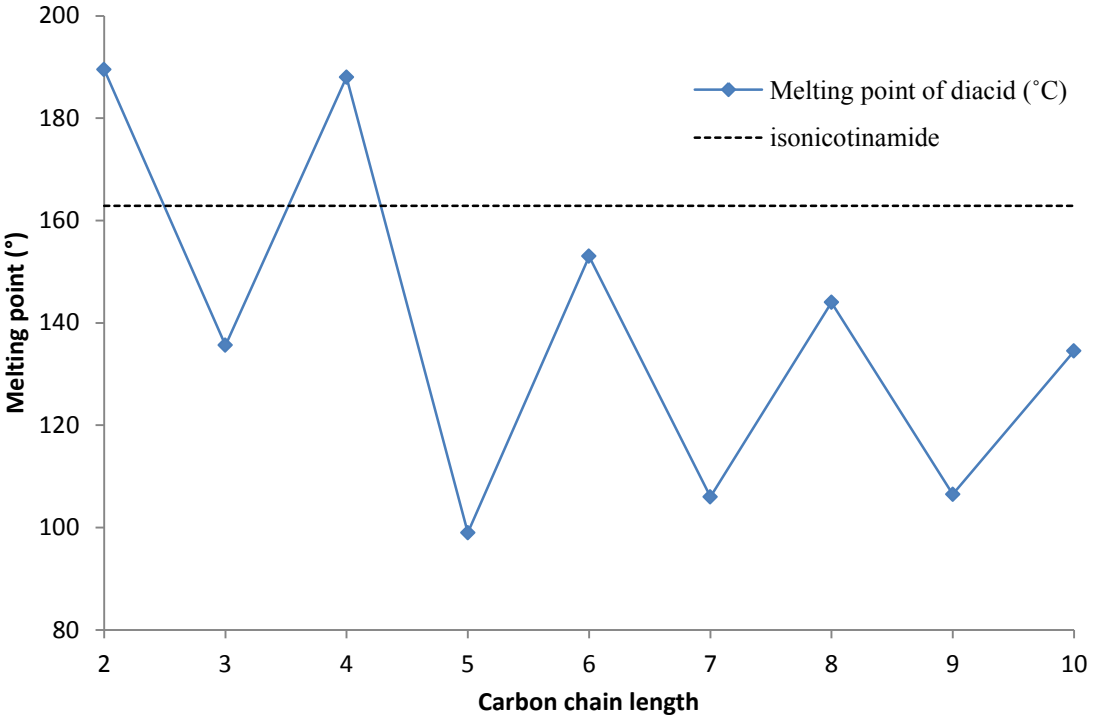

Figure 5.3: Melting point of the coformers used in this study

5.2 Isonicotinamide : hydrogen maleate

An isonicotinamide : hydrogen maleate salt structure has been previously identified by a member of our research group[5] (see appendix 14.5). However, maleic acid has been reported to isomerise to fumaric acid[6] during cocrystal formation, for example in the cocrystallisation of nicotinamide and maleic acid as discussed in chapter 6.

With this in mind, a range of experimental techniques were employed by myself and an undergraduate project student to investigate the possibility of maleic acid isomerising to give an isonicotinamide : fumaric acid cocrystal structure. Isonicotinamide was cocrystallised with maleic acid following the procedure outlined in section 3.2 (multi-reaction rack) and powder X-ray diffraction was used to identify whether new the adduct formed was isonicotinamide : maleic acid, isonicotinamide : fumaric acid or an alternative material (figure 5.4).

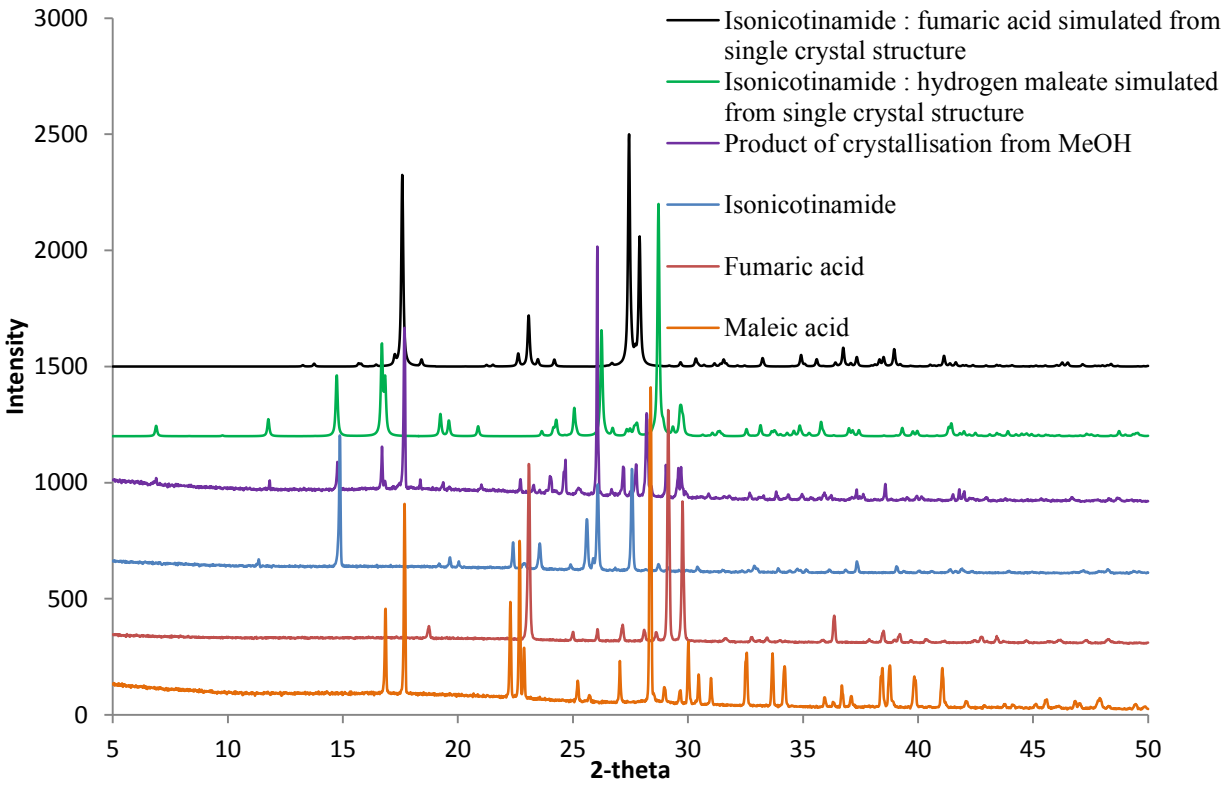

Figure 5.4: Powder X-ray diffraction patterns of the isonicotinamide : hydrogen maleate, isonicotinamide : fumaric acid, the new adduct formed and the corresponding coformers.

The powder diffraction patterns above show that the product of crystallisation is a mixture of both isonicotinamide : hydrogen maleate and isonicotinamide : fumaric acid with a possibility of a small amount of starting material also present. This indicates that some of the maleic acid did indeed isomerise to fumaric acid in the cocrystal process. This research was then taken further by the project student who investigated the outcome of standard cocrystallisation using a wide range of solvents. His research employed eight different solvents and yielded some very interesting results (table 5.2) in which a study of the crystallisation process (how long before crystals formed etc) allowed prediction of the resulting material (maleate or fumaric acid adduct)[7].

Table 5.2: Resultant adducts from the isonicotinamide : maleic acid cocrystallisation experiments with a variation of solvents[7]

Solvent	Resultant material
Methanol	Isonicotinamide : fumaric acid
Ethanol	Mixture of isonicotinamide : hydrogen maleate and isonicotinamide : fumaric acid
Propan-1-ol	Isonicotinamide : hydrogen maleate
Ethyl acetate	Isonicotinamide : hydrogen maleate
Butan-1-ol	Isonicotinamide : hydrogen maleate
Methyl acetate	Isonicotinamide : hydrogen maleate
Acetonitrile	Isonicotinamide : hydrogen maleate
Dimethylsulfoxide	No product reported

5.3 Isonicotinamide : pimelic acid

Isonicotinamide was cocrystallised with pimelic acid following the experimental procedure outlined in chapter 3.1. Powder X-ray diffraction was used to confirm that a new material had been formed (figure 5.5).

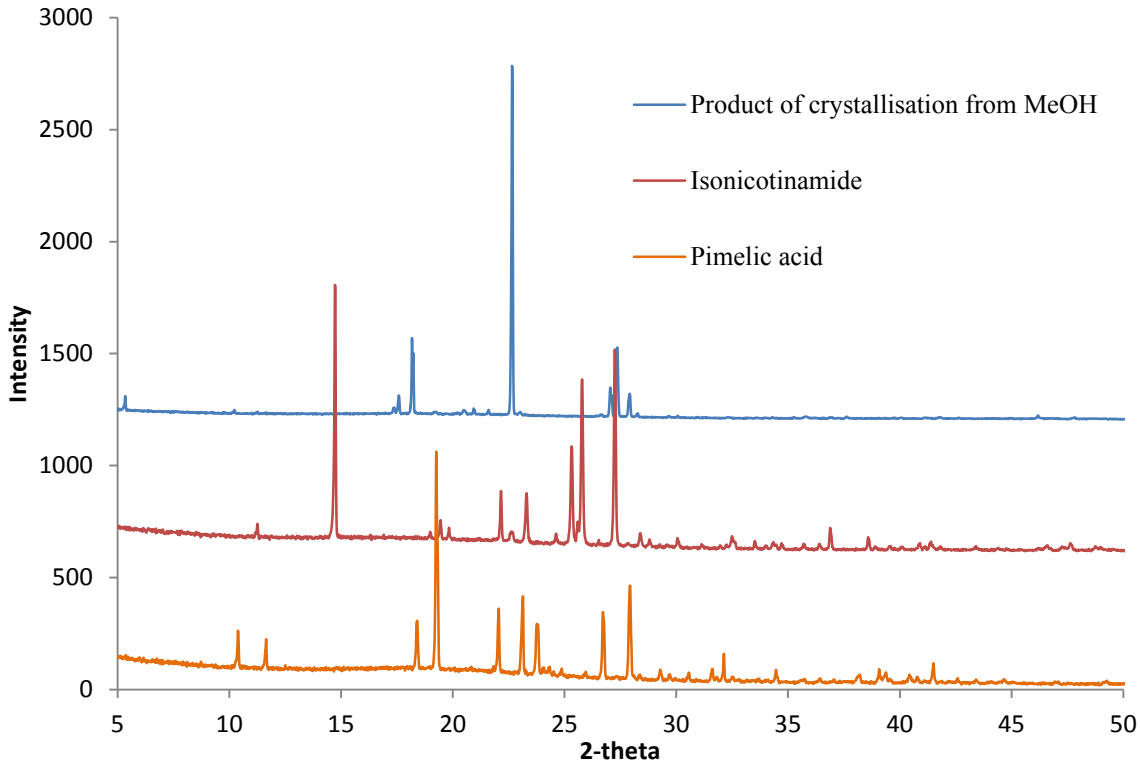

Figure 5.5: Powder X-ray diffraction data for the product of isonicotinamide and pimelic acid cocrystallisation and the starting materials

The diffraction patterns above show that the product of crystallisation is a new material though there may be a small amount of excess pimelic acid starting material also present, indicated by the presence of a peak at ~19°. ^{1}H NMR spectroscopy was used to confirm the presence of both isonicotinamide and pimelic acid in this material and to identify a 1:1 stoichiometry (with a small amount of excess pimelic acid present), appendix 15.1.

Single crystal X-ray diffraction analysis was carried out on a crystal of suitable quality. The data collection was carried out at the UK National Crystallography Service[8], with structure solution completed by myself. The structure solution of this anhydrous, neutral 1:1 cocrystal shows crystallisation in a monoclinic cell with space group P2/*c*. Table 5.3 Table 5.3gives the cell parameters for this structure.

Table 5.3: Cell parameters for isonicotinamide : pimelic acid, 1:1

Compound	Isonicotinamide : pimelic acid 1:1
a (Å)	8.2223(5)
b (Å)	5.1437(3)
c (Å)	33.38946(2)
α (°)	90
β (°)	93.873(3)
γ (°)	90
Volume ($Å^3$)	1408.9(2)
T (K)	120(2)
Z	4
Reflections collected	13904
Independent reflections	2480
R(int)	0.0742
Goodness of fit	1.077
R_1 (observed)	0.0557
R_1 (all)	0.0901
wR_2 (observed)	0.1184
wR_2 (all)	0.1337

The positions of the hydrogen atoms were determined by an electron density map confirming the structure to be a cocrystal, as no proton transfer occurred from the acid to the

isonicotinamide. The diffraction pattern simulated from the single crystal structure is the same as the laboratory experimental powder diffraction pattern confirming that the crystal selected was representative of the bulk material (appendix 15.2). Table 5.4 gives details of the six intermolecular hydrogen bonds that are formed in this structure whilst table 5.5 lists selected intramolecular bonds and angles in the structure. The numbering scheme used for the structure description is shown in figure 5.6. For full crystallographic details and intramolecular bonds and angles see appendix 15.

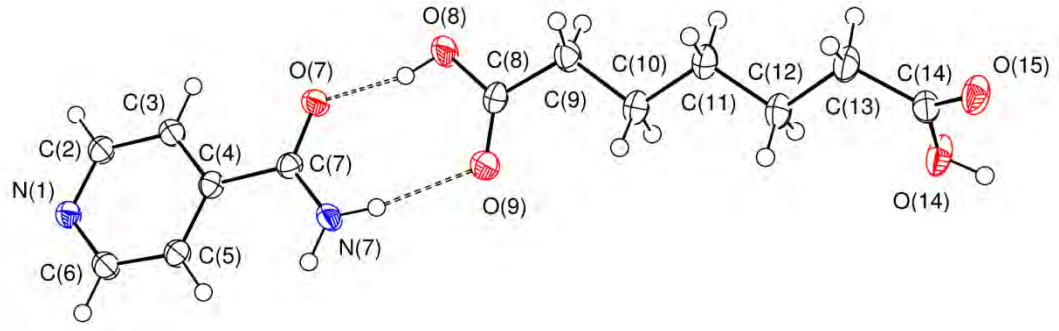

Figure 5.6: The independent molecules in the asymmetric unit isonicotinamide : pimelic acid showing the atom-numbering scheme and the hard intermolecular hydrogen-bonds (showed as dashed lines)

Table 5.4: Hydrogen bonding (Å) for isonicotinamide : pimelic acid, 1:1

D-H...A	d(D-H)	d(H...A)	d(D...A)	<(DHA)
N7-H7A...O9	0.88	2.05	2.917(2)	168
N7-H7B...O15^{i}	0.88	2.08	2.927(3)	162
O8-H8...O7	0.84	1.77	2.586(2)	165
O14-H14...N1^{ii}	0.84	1.80	2.634(2)	174
C5-H5...O15^{i}	0.95	2.38	3.310(3)	166
C6-H6...O15^{iii}	0.95	2.56	3.221(3)	127

Symmetry transformations used to generate equivalent atoms:

(i) –x+1, y-1, z-0.5 (ii) x-1, -y, -z-0.5 (iii) x+1, -y, z+0.5

Table 5.5: Selected bond lengths (Å) and angles (°) for isonicotinamide : pimelic acid, 1:1

Bond length	Bond length (Å)	Torsion angle	Torsion angle (°)
C7-O7	1.246(3)	C3-C4-C7-N7	-179.0(2)
C7-N7	1.322(3)	O8-C8-C9-C10	-169.6(2)
C8-O8	1.322(3)	C12-C13-C14-O14	35.4(3)
C8-O9	1.209(3)	O8-C8-C14-O14	-116.6(3)

The crystal structure of isonicotinamide : pimelic acid, 1:1 consists of infinite chains of alternating isonicotinamide and acid molecules linked together by the acid-pyridine and acid-amide synthons (I and II respectively) expected for a 1:1 cocrystal structure of this type with these coformers.

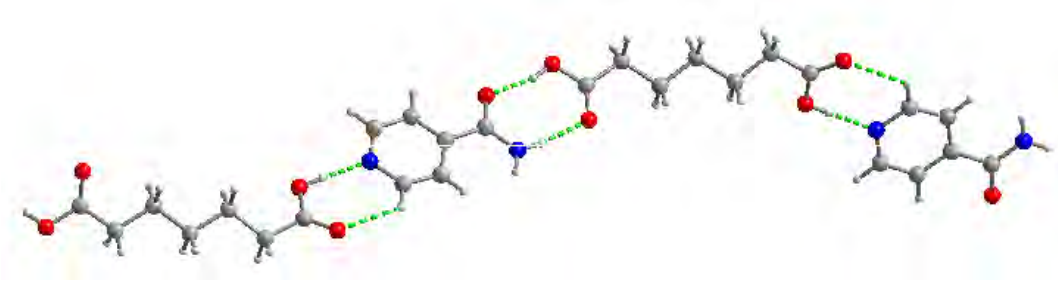

Figure 5.7: A view of the chain formed by alternating isonicotinamide and pimelic acid molecules. Hydrogen bonds are shown as dashed lines

The distinctive supramolecular chain motif (figure 5.7) is formed by alternating isonicotinamide and pimelic acid molecules involved in four intermolecular interactions; two hard hydrogen bonds N-H...C=O and O-H...C=O, one hard O-H...N(heterocyclic) interaction and one soft C-H...O=C interaction. The heterocyclic nitrogen N1 acts as a hydrogen bond

acceptor of H14 donated by O14 from the pimelic acid and is reinforced by a soft hydrogen bond from C6 via H6 to the other carboxyl oxygen O15 creating an $R_2^2(7)$ ring. Each isonicotinamide molecule interacts with a second pimelic acid molecule to form an $R_2^2(8)$ acid-amide synthon in which the amide nitrogen N7 acts as a donor via H7A to the carboxyl oxygen O9, while the amide oxygen O7 accepts a second hydrogen bond from the other carboxyl oxygen O8 via H8. All the isonicotinamide molecules within a chain face in the same direction along the *c*-axis but the orientation of the amide group alternates up and down along the chain. Although the isonicotinamide molecules themselves are planar, the chain motif is crinkled due to the twisted conformation of the pimelic acid molecules (Table 5.5:). The interplanar angles between the alkyl chain and the acid groups at both ends O8-C8-C9-C10 and C12-C13-C14-O14 are -162.6(2)° and 35.4(3)° respectively, with the full extent of the twisting illustrated by an interplanar angle between the two acid groups O8-C8-C14-O14 of -116.6(3)°.

The hydrogen bonded chains are cross-linked via a further N-H...O=C hydrogen bond donated by N7 through H7B to O15 of a pimelic acid in the chain above, and reinforced by another soft hydrogen bond from C5 via H5 to O15 (figure 5.8).

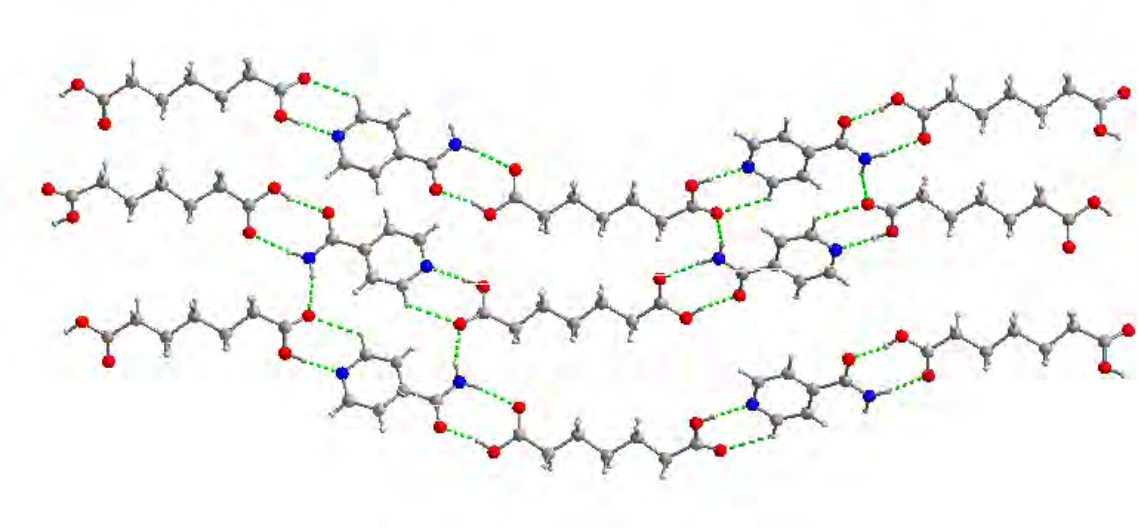

Figure 5.8: A view of the chains cross-linked by N-H...O hydrogen bonds. Hydrogen bonds are shown as dashed lines. The weak C5-H5...O15 hydrogen bond has been omitted from this figure

The chains are aligned in alternate directions such that the isonicotinamide molecules in each chain are stacked above and below each other, and with the twisted conformation of the acid in the chain, this cross-linking results in the formation of a 'step-like' sheet in which complementary pairs of isonicotinamide and pimelic acid molecules form $R_4^2(16)$ rings in alternating orientations. All strong hydrogen bonding donor and acceptor sites are involved in the hydrogen bonding network in this structure.

5.4 Isonicotinamide : suberic acid

Isonicotinamide was cocrystallised with suberic acid following the experimental procedure outlined in chapter 3.1. Powder X-ray diffraction was used to confirm the production of a new material (figure 5.9).

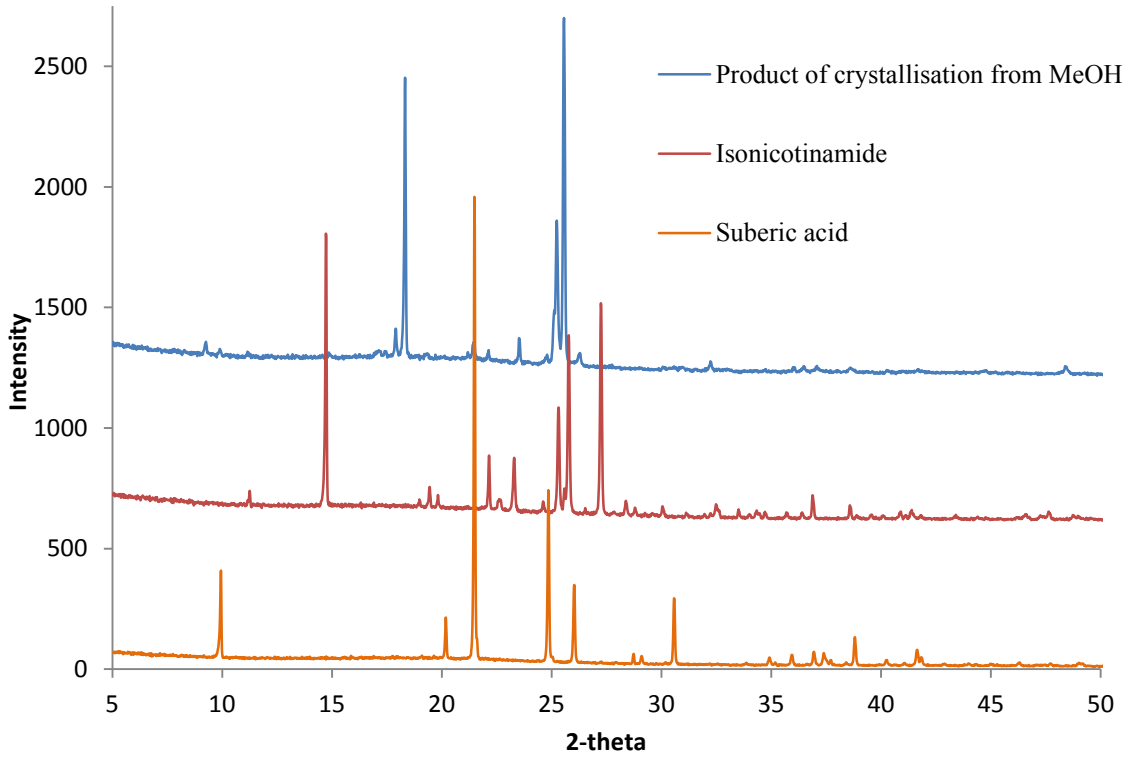

Figure 5.9: Powder X-ray diffraction data for the product of isonicotinamide and suberic acid cocrystallisation and the starting materials

The above diffraction patterns show that a new material has been formed although there is indication that it also contains a small amount of isonicotinamide and suberic acid starting material. ^{1}H NMR spectroscopy was used to obtain the stoichiometry of the new material formed; it shows that both isonicotinamide and suberic acid are present in a 1:1 stoichiometry (with a small amount of excess suberic acid present), appendix 16.1.

A crystal of suitable quality was isolated for single crystal analysis and a dataset collected at the UK National Crystallography Service[8]. Structure determination was carried out and it was found to be an anhydrous neutral cocrystal with a 1:1 stoichiometry, however, unlike isonicotinamide : pimelic acid, this structure has triclinic symmetry with space group P-1. Crystallographic details are given in table 5.6.

Table 5.6: Cell parameters for isonicotinamide : suberic acid , 1:1

Compound	Isonicotinamide : suberic acid 1:1
a (Å)	8.943(2)
b (Å)	9.537(1)
c (Å)	10.135(2)
α (°)	86.653(1)
β (°)	66.031(7)
γ (°)	66.571(1)
Volume ($Å^3$)	719.1(2)
T (K)	120(2)
Z	2
Reflections collected	9503
Independent reflections	2516
R(int)	0.0719
Goodness of fit	1.105
R_1 (observed)	0.0724
R_1 (all)	0.1055
wR_2 (observed)	0.1604
wR_2 (all)	0.1837

The positions of the hydrogen atoms were determined by an electron density map confirming this structure to be a cocrystal, as no proton transfer occurred from the acid to the

isonicotinamide. The diffraction pattern simulated from the single crystal structure is the same as that of the laboratory experimental powder diffraction pattern confirming that the crystal selected was representative of the bulk material (although there are clearly starting materials also present), appendix 16.2. Table 5.7 gives details of the six intermolecular hydrogen bonds that are formed in this structure whilst table 5.8 details selected intramolecular bonds and angles in the structure. The numbering scheme used for the structure description is shown in figure 5.10 Figure 5.10: with full crystallographic details given in appendix 16.

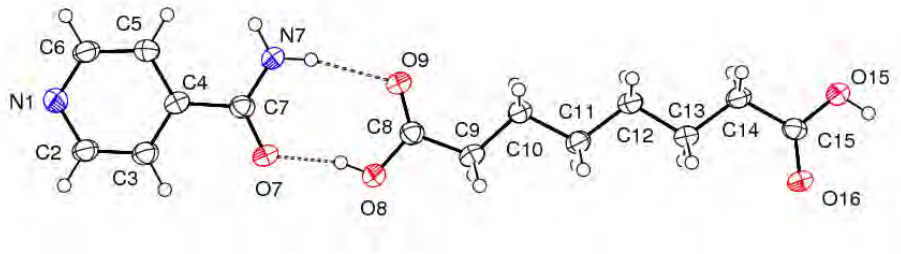

Figure 5.10: The independent molecules in the asymmetric unit of isonicotinamide : suberic acid showing the atom-numbering scheme and the hard intermolecular hydrogen-bonds (showed as dashed lines)

Table 5.7: Hydrogen bonding (Å) for isonicotinamide : suberic acid, 1:1

D-H...A	d(D-H)	d(H...A)	d(D...A)	<(DHA)
N7-H7A...O9	0.88	2.10	2.963(4)	167
N7-H7B...O16^{i}	0.88	2.08	2.939(4)	165
O8-H8...O7	0.84	1.76	2.583(3)	164
O15-H15...N1^{ii}	0.84	1.84	2.648(4)	162
C2-H2...O9^{iii}	0.95	2.60	3.379(3)	140
C5-H5...O16^{ii}	0.95	2.40	3.304(5)	160

Symmetry transformations used to generate equivalent atoms:

(i) x, y+1, z+1 (ii) x-1, y-1, z-1 (iii) x+1, y, z

Table 5.8: Selected bond lengths (Å) and angles (°) for isonicotinamide : suberic acid, 1:1

Bond length	Bond length (Å)	Torsion angle	Torsion angle (°)
C7-O7	1.241(4)	C3-C4-C7-N7	172.2(3)
C7-N7	1.325(5)	O8-C8-C9-C10	179.2(3)
C8-O8	1.321(5)	C13-C14-C15-O15	176.8(3)
C8-O9	1.213(4)	O8-C8-C15-O15	168.8 (4)

The crystal structure of isonicotinamide : suberic acid, 1:1 is also formed of chains that consist of alternating isonicotinamide and acid molecules. The structure has a 1:1 stoichiometry, and as expected the molecules are linked by acid-amide and acid-pyridine interactions (I and II), but the more planar conformation of the suberic acid molecules (table 5.8) means that the chain itself differs to that of the isonicotinamide : pimelic acid chain structure (figure 5.11).

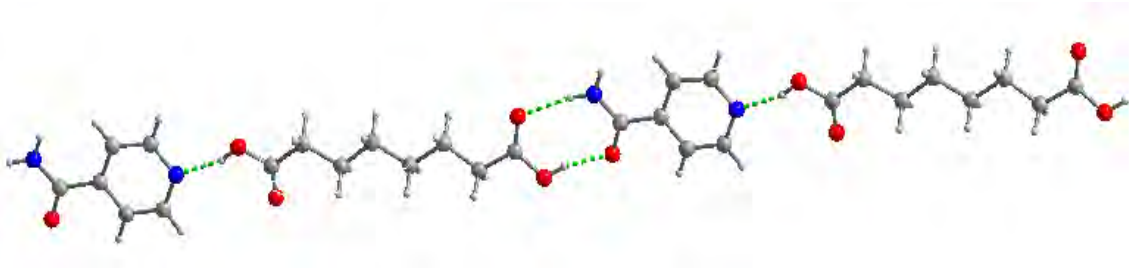

Figure 5.11: A view of the chain formed of alternating isonicotinamide and suberic acid molecules. Hydrogen bonds are shown as dashed lines

Within each chain, each isonicotinamide molecule faces in the same direction with the amide group in the same orientation, and is involved in the formation of three hard hydrogen bonds. Two of these, N-H...O=C and O-H...O=C form the same acid-amide $R_2^2(8)$ motif seen in the isonicotinamide : pimelic acid structure, with the third a hard O-H...N(heterocyclic) interaction in which N1 acts as a hydrogen bond acceptor of H15 donated by O15 from the other suberic acid molecule. However, the planar conformation of the suberic acid molecule and the relative orientation of the acid and amide within the chains in this structure are not conducive to the formation of the $R_2^2(7)$ ring motif seen in the isonicotinamide : pimelic acid structure. The way in which these chains pack is also distinct from the other structure, as in this case the adjacent chains are aligned in the same direction and staggered. An N-H...O=C bond is formed between adjacent chains from N7 through H7B to O16 of a suberic acid molecule in the chain above and reinforced by two soft hydrogen bonds, one from C5 via H5 also to O16 in the chain above and the other from C2 via H2 to O9 of a suberic acid molecule in the chain below. The overall result is a planar hydrogen bonded sheet in the (011) plane (figure 5.12). All strong hydrogen bond donors and acceptors are involved in the intermolecular network displayed in this structure.

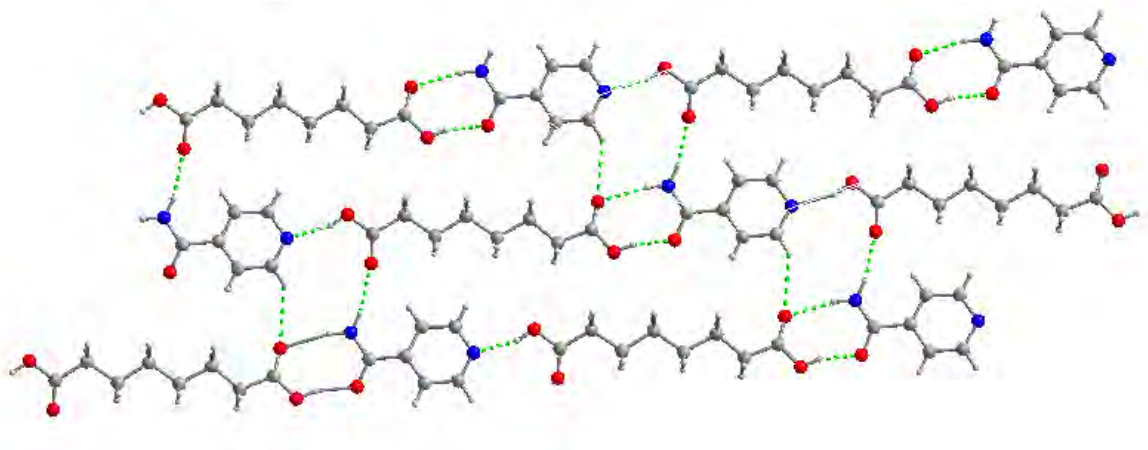

Figure 5.12: A view of the planar hydrogen bonded sheet. Hydrogen bonds are shown as dashed lines. The weak C5-H5...O16 hydrogen bond has been omitted from this figure

5.5 Isonicotinamide : azelaic acid

Isonicotinamide was cocrystallised with azelaic acid following the experimental procedure detailed in chapter 3.1. Powder X-ray diffraction was used to confirm the formation of a new material (figure 5.13).

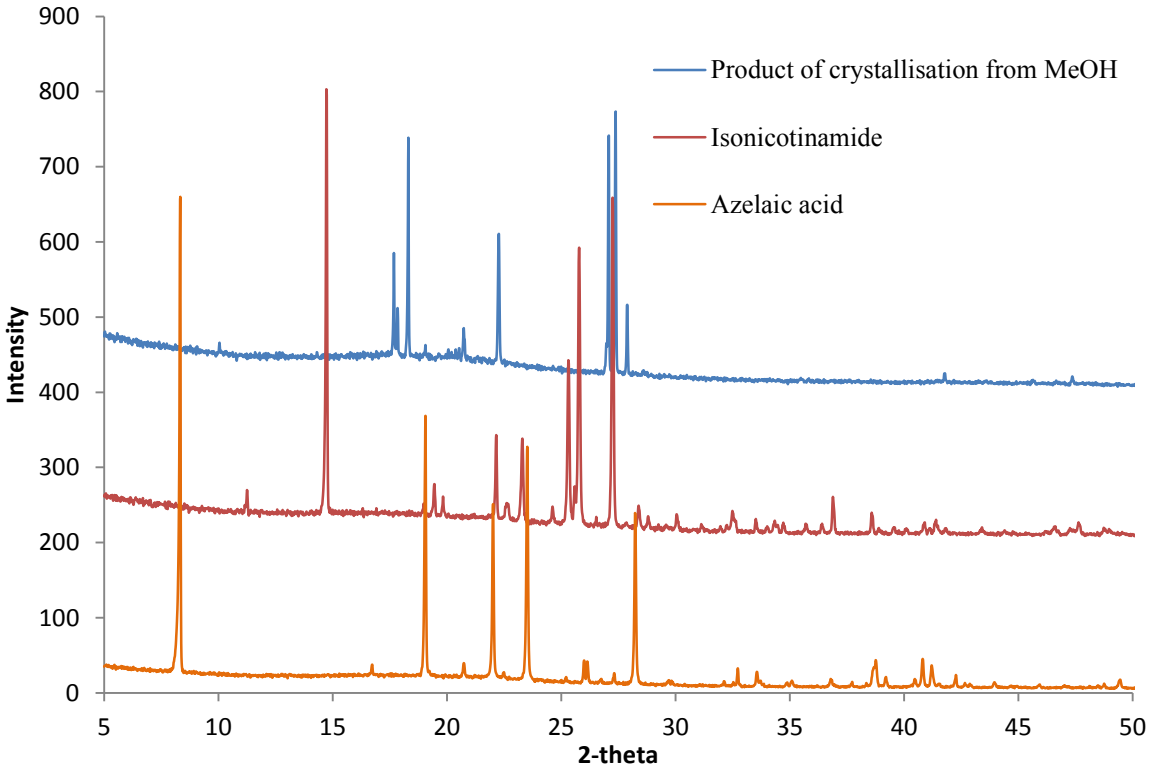

Figure 5.13: Powder X-ray diffraction data for the product of isonicotinamide and azelaic acid cocrystallisation and the starting materials

The X-ray powder diffraction patterns shown above prove that a new material has formed without any excess starting material. Solution ^{1}H NMR spectroscopy was used to identify the 1:1 stoichiometry of this new isonicotinamide : azelaic acid material (appendix 17.1).

A crystal of suitable quality was identified and a single crystal dataset collected on this sample at the UK National Crystallography Service[8]. The crystal structure determination

(completed by myself) identified that the material is a 1:1 cocrystal in a monoclinic cell with space group P2/*c*. Table 5.9 shows the cell parameters and certain crystallographic details.

Table 5.9: Cell parameters for isonicotinamide : azelaic acid, 1:1

Compound	Isonicotinamide : azelaic acid 1:1
a (Å)	8.2118(1)
b (Å)	5.0680(7)
c (Å)	38.683(5)
α (°)	90
β (°)	93.264(6)
γ (°)	90
Volume ($Å^3$)	1607.3(4)
T (K)	120(2)
Z	4
Reflections collected	11278
Independent reflections	2761
R(int)	0.0748
Goodness of fit	1.283
R_1 (observed)	0.0872
R_1 (all)	0.1217
wR_2 (observed)	0.1966
wR_2 (all)	0.2217

The positions of the hydrogen atoms were determined by an electron density map confirming that this structure was also a cocrystal, as no proton transfer occurred from the acid to the isonicotinamide. The diffraction pattern simulated from the single crystal structurea is the same as that of the laboratory experimental powder diffraction pattern confirming that the crystal selected was representative of the bulk material, al there is clearly a shift in peak positions arising from the different temperatures at which the data is 'collected' (appendix

17.2). Table 5.10 gives details of the six intermolecular hydrogen bonds that form this structure whilst table 5.11 lists selected intramolecular bonds and angles in this structure. The numbering scheme used for structure description is shown in figure 5.14 and full crystallographic details are given in appendix 17.

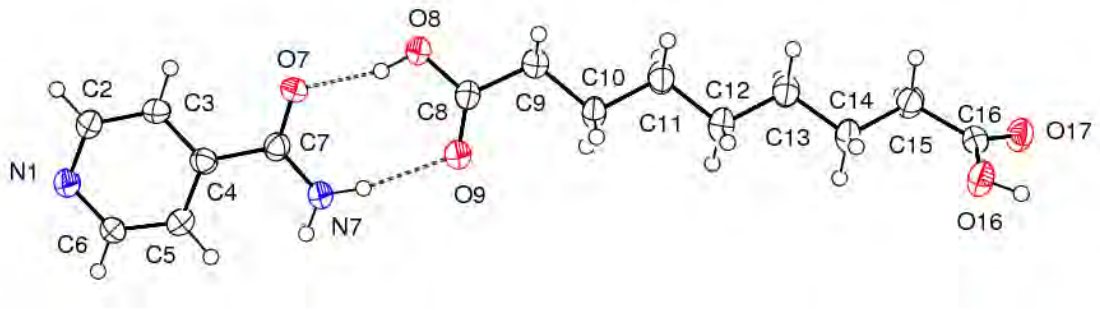

Figure 5.14: The independent molecules in the asymmetric unit of isonicotinamide : azelaic acid showing the atom-numbering scheme and the hard intermolecular hydrogen-bonds (showed as dashed lines)

Table 5.10: Hydrogen bonding (Å) for isonicotinamide : azelaic acid, 1:1

D-H...A	d(D-H)	d(H...A)	d(D...A)	<(DHA)
N7-H7A...O9	0.88	2.03	2.899(5)	169
N7-H7B...O17^{i}	0.88	2.06	2.905(5)	162
O8-H8...O7	0.84	1.77	2.586(4)	164
O16-H16...N1^{ii}	0.84	1.79	2.626(4)	175
C5-H5...O17^{ii}	0.95	2.37	3.296(5)	166
C6-H6...O17^{iii}	0.95	2.53	3.192(5)	127

Symmetry transformations used to generate equivalent atoms:

(i) –x+1, y+1, -z+0.5 (ii) x-1, -y+2, z-0.5 (iii) x+1, -y+2, z+0.5

Table 5.11: Selected bond lengths (Å) and angles (°) for isonicotinamide : azelaic acid, 1:1

Bond length	Bond length (Å)	Torsion angle	Torsion angle (°)
C7-O7	1.248(5)	C3-C4-C7-N7	178.4(4)
C7-N7	1.322(5)	O8-C8-C9-C10	-171.5(4)
C8-O8	1.318(5)	C14-C15-C16-O16	30.6(6)
C8-O9	1.216(6)	O8-C8-C16-O16	-115.0 (5)

Isonicotinamide : azelaic acid, 1:1 is essentially isostructural to isonicotinamide : pimelic acid, 1:1. It is formed of infinite chains of alternating isonicotinamide and acid molecules (figure 5.15) and includes the predicted acid-pyridine and acid-amide motifs (I and II) forming both the $R_2^2(8)$ and $R_2^2(7)$ ring motifs expected in a 1:1 stoichiometry.

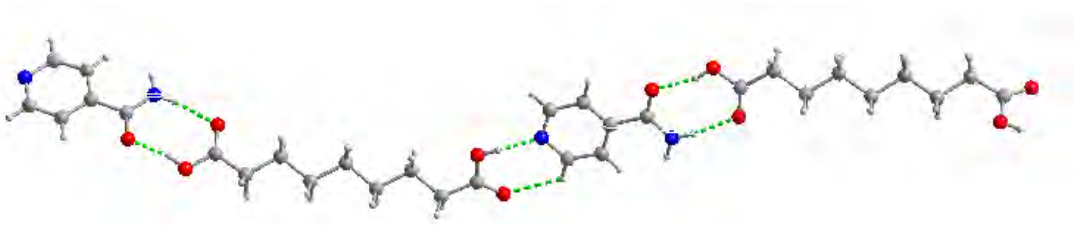

Figure 5.15: A view of the alternating isonicotinamide and azelaic acid molecules to form the infinite chain. Hydrogen bonds are shown as dashed lines

The azelaic acid molecules in this structure (figure 5.16) also exhibit the twisting seen in the pimelic acid cocrystal (table 5.11) giving rise to crinkled chains, that form the same cross-linked hydrogen bonded network seen in the isonicotinamide : pimelic acid structure. All strong hydrogen bond donors and acceptors are used in this structure.

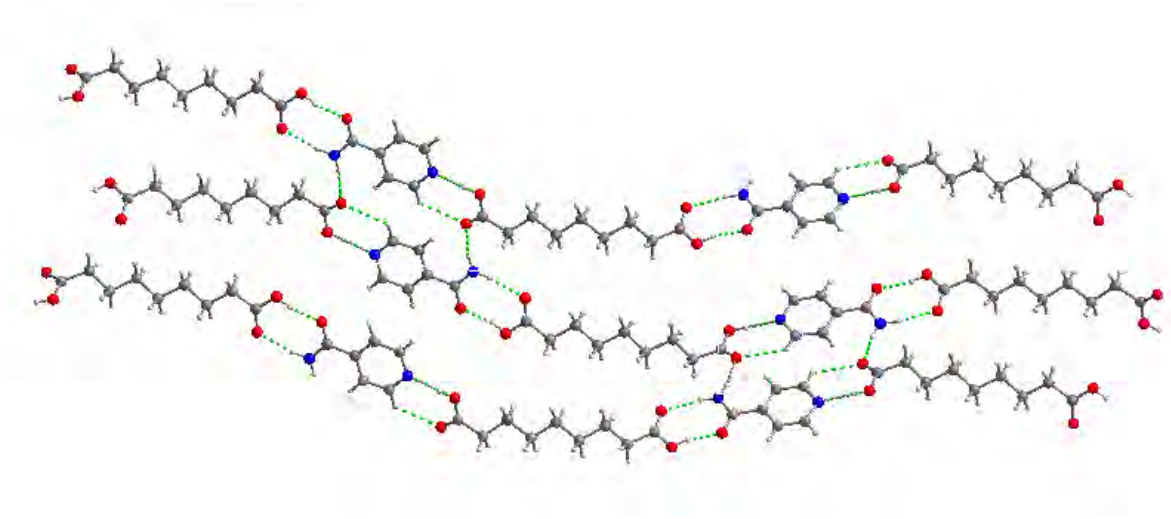

Figure 5.16: A view of the cross-linked isonicotinamide : azelaic acid sheet. Hydrogen bonds are shown as dashed lines. The weak C5-H5...O17 hydrogen bond has been omitted from this figure

5.6 Isonicotinamide : sebacic acid

Isonicotinamide was cocrystallised with sebacic acid following the experimental procedure described in chapter 3. Powder X-ray diffraction was used to identify whether a new material had been formed (figure 5.17).

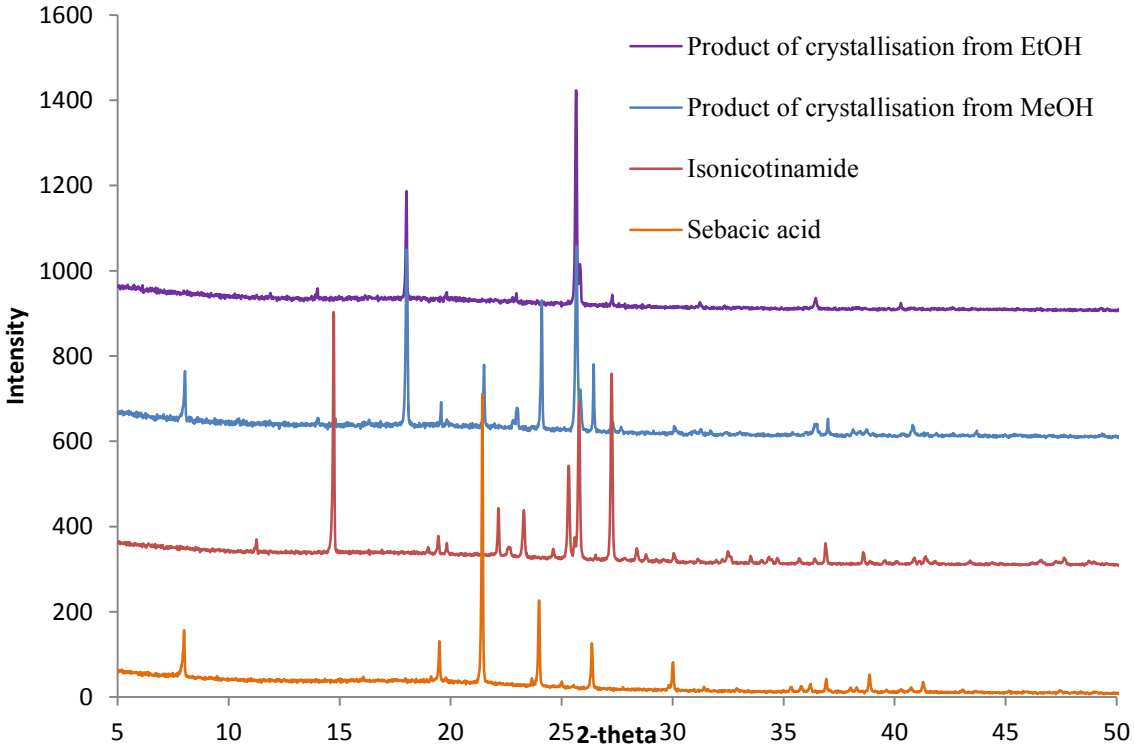

Figure 5.17: Powder X-ray diffraction data for the product of isonicotinamide and sebacic acid cocrystallisation and the starting materials

It can be seen from the diffraction patterns above that a new material has been formed from both methanol and ethanol. The product from methanol also contains a significant amount of starting material (sebacic acid) whereas that from ethanol seems a higher purity material. ^{1}H NMR spectroscopy confirmed the presence of both isonicotinamide and sebacic acid in this material and determined the stoichiometry as 2:1 isonicotinamide : sebacic acid (appendix 18.1). Several crystals were selected for single crystal X-ray diffraction analysis, however, the

crystals were so small and weakly diffracting that it was not possible even to obtain a unit cell. Further work on this material would include further attempt at the synthesis of a crystal of suitable quality for single crystal X-ray diffraction by growth in an incubator with controlled conditionss during the solvent evaporation step of the experimental procedure. Structure solution from powder diffraction data is unlikely to be successful in this case as there is little diffraction data available for a relatively complex structure.

5.7 Isonicotinamide : undecanedioic acid

Isonicotinamide was cocrystallised with undecanedioic acid following the experimental procedure detailed in chapter 3. Powder X-ray diffraction was used to identify whether a new material had been formed (figure 5.18).

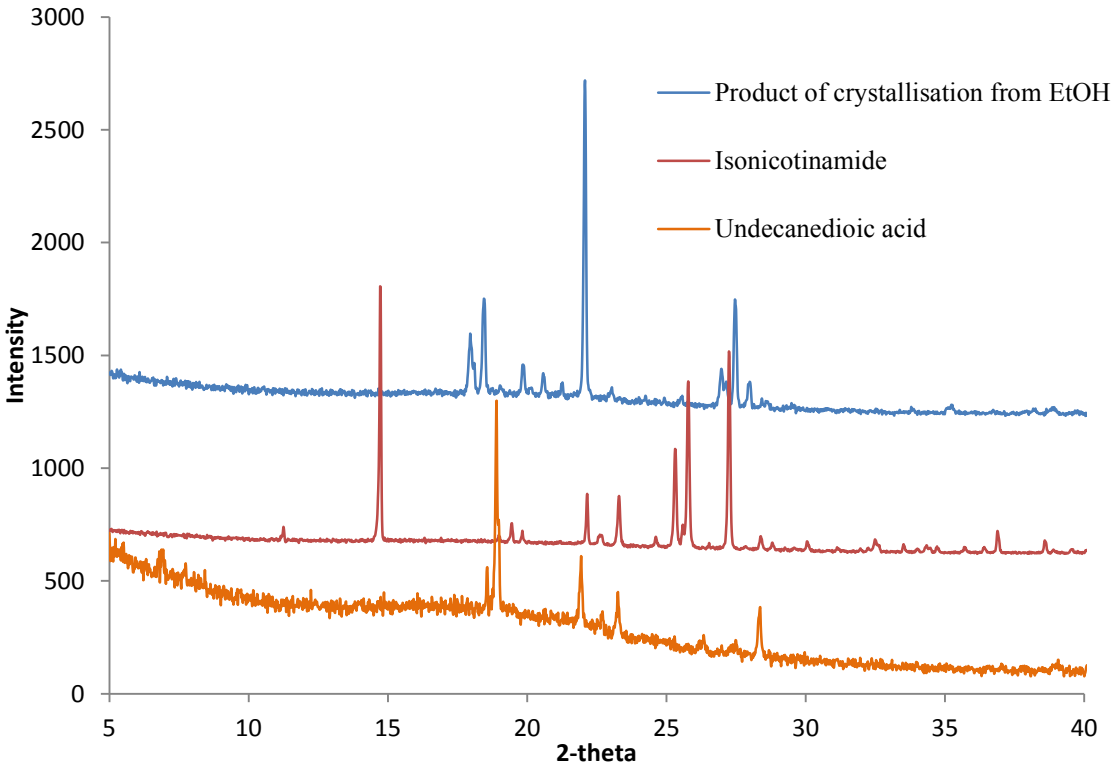

Figure 5.18: Powder X-ray diffraction data for the product of isonicotinamide and undecanedioic acid cocrystallisation and the starting materials

The diffraction patterns in figure 5.18 confirm that a new material has been formed ant that no starting materials are present. ^{1}H NMR spectroscopy was used to confirm the presence of isonicotinamide and undecanedioic acid in this material in a 1:1 stoichiometry (appendix19.1). However, in a similar way to isonicotinamide : sebacic acid, 2:1, crystals of this adduct have been placed on the single crystal X-ray diffractometer but they were not of

suitable quality to enable data collection. Attempts have not been made to solve the structure of this material from powder diffraction data.

5.8 Discussion

The published isonicotinamide : alkanediacid adducts were reported as cocrystals as opposed to salts. A further three cocrystal structures and a salt structure have been discussed in this chapter; correctly predicted earlier in the chapter when studying the relative pK_a values displayed in table 5.1.

The hydrogen bonding networks in crystalline structures in this series of cocrystal materials are similar. As previously discussed, all the previously known structures contain the acid-pyridine synthon I, with synthon II present in 1:1 structures and synthon III present in the 2:1 structures (figure 5.2); a trend that is continued in the isonicotinamide: diacid crystalline structures presented here. The structures all contain infinite hydrogen bonded chains consisting of alternating isonicotinamide and dicarboxylic acid molecules in the 1:1 structures and alternating isonicotinamide dimers and dicarboxylic acid molecules in the 2:1 structures. These infinite chains then link via further hydrogen bonds to create an infinite sheet.

The three new cocrystal structures with the longer chain acids (isonicotinamide : pimelic acid, isonicotinamide : suberic acid and isonicotinamide : azelaic acid) all have a 1:1 stoichiometry. Before the structure solution was undertaken, the hydrogen bond network was correctly predicted involving both the acid-pyridine and acid-amide heteromeric synthons. Although the predicted heteromeric synthons are present in all three of these structures, the chain motifs and resultant crystal packing in both the pimelic acid and azelaic acid cocrystal structures differ significantly from other published isonicotinamide : alkanediacid cocrystals. The twisted conformation of the acid molecules in the pimelic and azelaic acid structures is a feature not observed in other isonicotinamide : alkanediacid materials in which a geometry more like that found in the isonicotinamide : suberic acid structure is adopted, regardless of whether the acid has an odd or even chain length. Twisting of the alkyl chain is a feature that

has been reported in the pure α,ω-alkanedicarboxylic acids[4] in which it was related to the melting point behaviour of these materials. Although lower chain length diacids display significant polymorphic behaviour, it was found that those with a chain length greater than five displayed packing regularities. The longer chain acids with an even number of carbon atoms adopt a fully extended all-*trans* planar conformation, whereas the odd acids display twisted conformations (table 5.12).

Table 5.12: Selected torsion angles (°) of the pimelic, suberic and azelaic acid cocrystals with isonicotinamide and the related angles in the pure acid structures

			Pure acid[a]
Isonicotinamide : pimelic acid	O8-C8-C9-C10	-169.6(2)	-163.14(8)
	C12-C13-C14-O14	35.4(3)	-163.14(8)
	O8-C8-C14-O14	-116.6(3)	70.2(1)
Isonicotinamide : suberic acid	O8-C8-C9-C10	179.2(3)	178.33(8)
	C13-C14-C15-O15	176.8(3)	178.33(8)
	O8-C8-C15-O15	168.8(4)	180
Isonicotinamide : azelaic acid	O8-C8-C9-C10	-171.5(4)	-163.33(6)
	C14-C15-C16-O16	30.6(6)	-163.33(6)
	O8-C8-C16-O16	-115.0(5)	68.08(9)

a Data taken from[4]

In all cases, the pure diacid molecules are linked together through dimers to form an infinite hydrogen bonded chain, but it is the different backbone conformation and different packing of these chains between odd and even acids that has been related to the melting point properties. In the even members of the series, adjacent chains are shifted, resulting in an offset so that the carboxy dimers are not in repulsive proximity. This shift is not adopted by the odd numbered acids[4] and so the alkyl chain twists to accommodate the alternate orientations of the carboxy groups. This results in the formation of the energetically unfavourable conformations and hence the odd acids display lower melting points than the even members seen in figure 5.3[4].

The melting points of the isonicotinamide cocrystals (both these previously published and those synthesised in this project) were recorded and compared against their starting materials (figure 5.19).

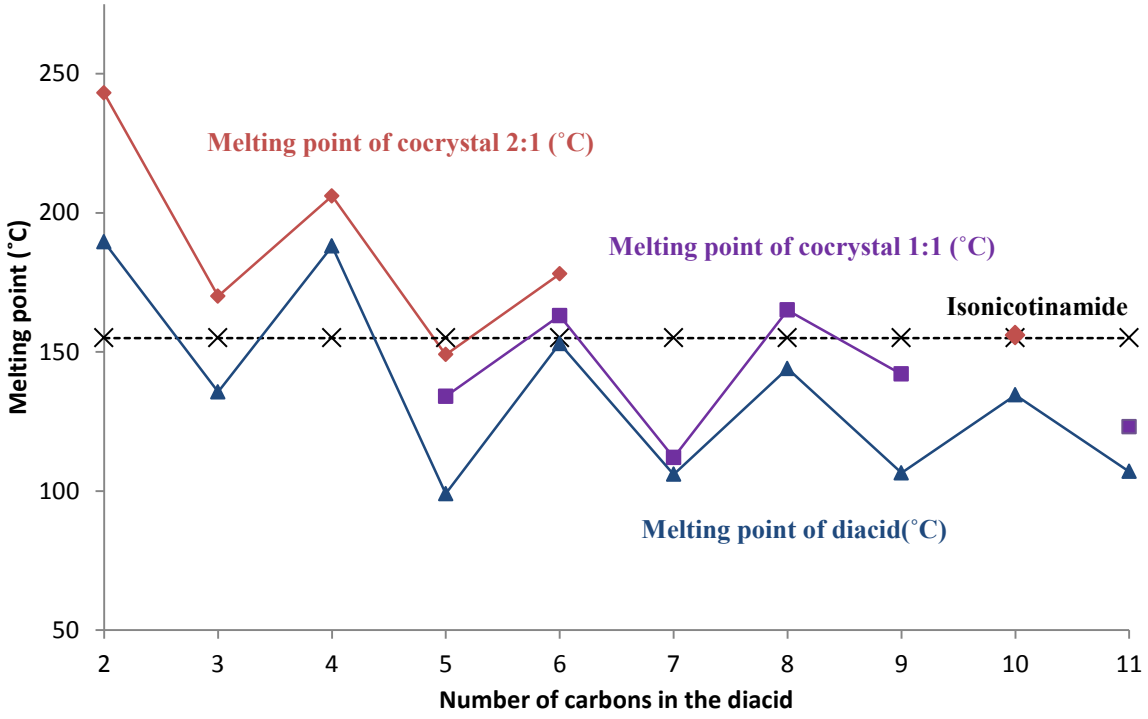

Figure 5.19: Melting point (°C) of the isonicotinamide : diacid cocrystals and their respective coformers

It can be seen from figure 5.20 that the melting points of the cocrystals mimic the alternation behaviour of the pure acids. The melting points of the 1:1 cocrystals are higher than the pure acids but lower than the 2:1 cocrystals. Both this study and others[1,9,10] demonstrate that the melting point alternation behaviour of pure α,ω-alkanedicarboxylic acids is a reliable property that is retained within each homologous series after cocrystallisation. However, the relative placement of each melting point series i.e. pure acid vs 1:1 cocrystal vs 2:1 cocrystal is not easy to rationalise. It could be expected that both the 1:1 and 2:1 cocrystal series have higher melting points than both the pure components as the strong intermolecular interactions that are formed in preference to those between molecules of individual components stabilise the cocrystal structure and raise the melting point. Whilst this behaviour is observed in some cases[1,11], including most of the 2:1 and the odd 1:1 cocrystal adducts discussed here, there are many other examples of cocrystals with melting points between those of the pure components[12] and others in which the melting point is significantly lower than both[9,11]. Melting point behaviour of cocrystals containing one of these dicarboxylic acids in which the alternating trend is reversed has also been reported[13]. This case involves cocrystallisation with 1,2-bis(4-pyridyl)propane and reports that cocrystals with dicarboxylic acids with an odd number of carbons have higher melting points than those with an even carbon chain length[13]. Melting point is clearly linked to crystal packing, intermolecular forces and molecular conformation (as demonstrated by pure odd diacids[4], the isonicotinamide : pimelic acid and isonicotinamide : azelaic acid adducts discussed here), but other factors such as entropy considerations make any correlation complicated; even more so when considering the relative melting points of cocrystal systems with differing stoichiometries, in which there seems to be no correlation between the strength of hydrogen bonds and which cocrystal stoichiometry is formed. When studying the crystal density and packing fraction (calculated using platon[13]) of

the isonicotinamide cocrystals with pimelic, suberic and azelaic acids we found no direct relationship between these properties and the relative placement of the melting point series (figure 5.20). For a table of these values see appendix 20.

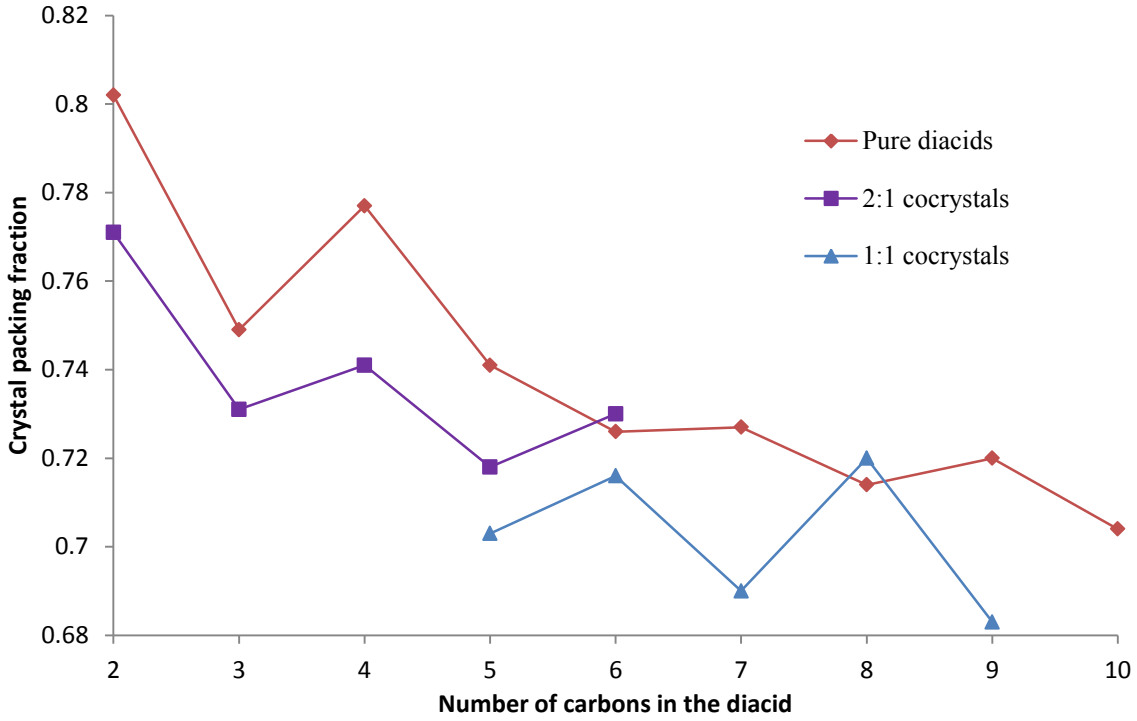

Figure 5.20: Packing fraction of the isonicotinamide cocrystals and their respective coformers

Although the 2:1 isonicotinamide : diacid cocrystals show a good correlation between these parameters within a series in respect of the packing fraction, both the pure acids and our 1:1 cocrystal results show that this is not always the case i.e. the increase in melting point between isonicotinamide : pimelic acid to isonicotinamide : azelaic acid is matched by a relative decrease rather than an increase in packing fraction (figure 5.20). Consideration of the relative strength of intermolecular hydrogen-bond interactions within the supramolecular unit of isostructural systems within a series also gives disparate results. The 2:1 cocrystals containing even diacids show a decrease in melting point with an increasing number of carbon atoms that correlates with a decrease in intermolecular hydrogen-bond strength quantified by

an increase in total H...A distance within the supramolecular building block defining the cocrystal unit (appendix 20). In the case of isonicotinamide : pimelic acid and isonicotinamide : azelaic acid, in which there was no correlation with packing fraction, the increase in melting point is mirrored by an increase in relative hydrogen-bond strength. Unfortunately, similar analysis of pure diacid components, whether within the odd or even series, shows a contradictory almost systematic increase of hydrogen-bond strength with decrease in melting point. Hence, whilst it has not been possible to rationalise the relative placements of the melting points, it has been found that the reliable melting point alternation of the pure alkanediacids can be used as a potential tool in the tunability of the properties of new crystalline materials through cocrystal formation within a homologous series and that in the structures reported here at least, the key structural feature displayed by the twisting of odd acids is retained in the isonicotinamide cocrystal with longer chain acids.

5.9 Footnote

The results presented in this chapter (structures and properties of isonicotinamide : pimelic acid, isonicotinamide : suberic acid and isonicotinamide : azelaic acid) have been published in L.J.Thompson, R.S.Voguri, L.Male, M.Tremayne, *CrystEngComm.*, 2011, **13**(12), 4188 (appendix 20)

5.10 References

1. P. Vishweshwar, A. Nangia and V. M. Lynch, *Cryst. Growth. Des.*, 2003, **3**, 783

2. C. B. Aakeroy, A. M. Beatty and B. A. Helfrich, *J. Am. Chem. Soc.*, 2002, **124**, 14425

3. R. M. C. Dawson, D. C. Elliott, W. H. Elliott and K. M. Jones, *Data for biochemical research*, **2 ed**, Oxford Clarendon Press, 1969

4. V. R. Thalladi, M. Nusse and R.Boese, *J. Am. Chem. Soc.*, 2000, **122**, 9227

5. A. Cowell, *An investigation into the synthesis, structural characterisation, thermal and polymorphic behaviour of organic crystalline materials*, PhD thesis, University of Birmingham, 2011

6. S. Chatterjee, V. R. Pedireddi and C. N. R. Rao, *Tetrahedron Lett.*, 1998, **39**, 2843

7. G. Cutts, *Synthesis and structure determination of molecular cocrystals*, M.Sci project report, University of Birmingham, 2011

8. S. J. Coles and P. A. Gale, *Chem. Sci.*, 2012, **3**(3), 683

9. D. Braga, L. Maini, G. de Sanctis, K. Rubini, F. Grepioni, M.R. Chierotti and R. Gobetto, *Chem.-Eur. J.*, 2003, **9**, 5538

10. C. B. Aakeroy, I. Hussain and J. Desper, *Cryst. Growth. Des.*, 2006, **6**, 474

11. L. S. Reddy, A. Nangia and V. M. Lynch, *Cryst. Growth. Des.*, 2004, **4**, 89

12. N. Schultheiss and A. Newman, *Cryst. Growth. Des.*, 2009, **9**, 2950

13. D. Braga, E. Dichiarante, G. Palladino, F. Grepioni, M. R. Chierotti, R. Gobetto and L. Pellegrino, *CrystEngComm*, 2010, **12**, 3534

14. A. L. Spek, *PLATON*, Bijvoet Centre for Biochemical Research, Vakgroep Kristal-en Structure-Chemie, University of Utrecht, Netherlands

6. The Crystal Structures of Nicotinamide Cocrystals with Alkanediacids

6.1 Introduction

Nicotinamide (3-pyridinecarboxamide, vitamin B3) is "generally recognized as safe" (GRAS), a term used and requires for materials used within both food and pharmaceutical products. It has a molecular structure similar to that of isonicotinamide, with the amide on the 3-position as opposed to the 4-position, and is also a good candidate for cocrystallisation with the alkanediacids used in chapters 4 and 5 for the adenine and isonicotinamide adducts (figure 6.1).

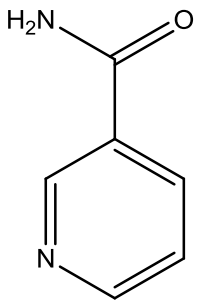

Figure 6.1: Nicotinamide

In a similar way to isonicotinamide, nicotinamide contains both strong hydrogen bond donors and acceptors and has shown a propensity to form crystalline complexes with a number of materials including the dicarboxylic acids studied in this project. Previously published nicotinamide : dicarboxylic acids include 1:1 and 2:1 cocrystal stoichiometries for nicotinamide : fumaric acid[1], nicotinamide : adipic acid[2] and nicotinamide : suberic acid[2]. 2:1 cocrystal structures have been reported for nicotinamide : malonic acid[2] and nicotinamide : sebacic acid[2] with 1:1 cocrystal structures known for nicotinamide : glutaric acid[2],

nicotinamide : pimelic acid[2] and nicotinamide : azelaic acid[2]. A 1:1 nicotinamide : oxalic acid salt has also been reported[3] along with a 2:1 nicotinamide : oxalic adduct, in which the structure was unable to be solved[2]. All these published structures contain a dicarboxylic acid with a carbon chain length, *n* ($HO_2C(CH2)_{n-2}CO_2H$) of between two and ten carbon atoms.

This chapter focuses on the cocrystallisation of three new potential nicotinamide : dicarboxylic acid adducts; nicotinamide with succinic acid, maleic acid and undecanedioic acid. The structure of these potential complexes can again possibly be predicted by studying the possible hydrogen bonding motifs and networks that these structures could form based on an understanding of similar nicotinamide : diacid complexes. The pK_a values of these coformers can also be examined to identify the possibility of the formation of a salt or a cocrystal (section 1.4).

Three possible hydrogen bonding motifs were identified for these adduct materials, including a nicotinamide dimer and two acid : amide motifs, including the very strong acid pyridine motif (figure 6.2). These are similar to those formed by isonicotinamide, although there is now a possibility of alternate packing arrangements of nicotinamide adopting either the *anti* or *syn*, amide-pyridine N conformation.

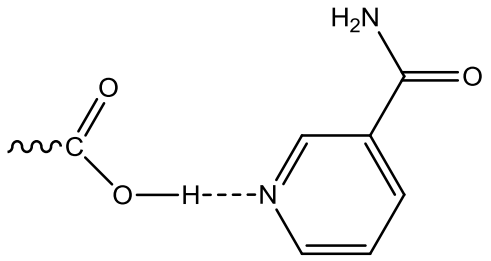

(I)

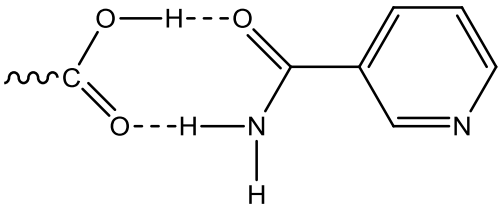

(II)

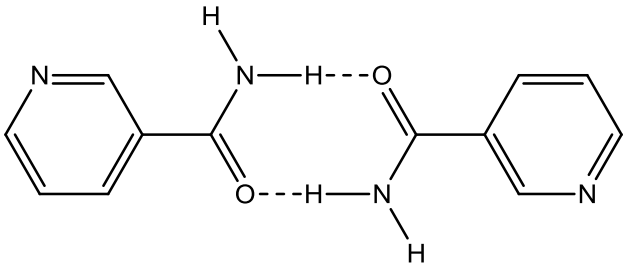

(III)

Figure 6.2: Possible hydrogen bonding motifs for nicotinamide : dicarboxylic acids; (I) acid-pyridine, (II) acid-amide and (III) amide-amide

Appendix 22 contains crystal packing diagrams and synthon figures for all the previously reported nicotinamide : dicarboxylic acid cocrystal structures. These figures show a clear trend; all structures contain the strong acid-pyridine hydrogen bonding motif shown in figure 6.2 (I), however, the 1:1 complexes exhibit the acid : amide motif (II), whilst the amide dimer (III) can be seen in all 2:1 complexes. The exception to this are the salt structures (nicotinamide : hydrogen oxalate and nicotinamide : hydrogen maleate) in which the nicotinamide dimer is present despite its 1:1 stoichiometry. With this knowledge, we can predict that all three adducts studied in this chapter will contain the strong acid-pyridine

synthon (I) along with one of the other motifs dependent upon the stoichiometry. The published nicotinamide : azelaic acid (n = 9) structure displays twisting of the acid conformation. This compares favourably with the conclusion from the isonicotinamide series, and would be expected as it has an odd chain length, however, the nicotinamide : pimelic acid structure does not exhibit the same twisting. There are no melting point values reported for these nicotinamide cocrystal structures, so no further structure-property relationships can be discussed.

The relative pK_a values of all these materials are given in table 6.1. From these values we can predict that cocrystals are likely to predominate for the nicotinamide : acid adducts in this series although the ΔpK_a for nicotinamide with maleic acid and oxalic acid is in the less predictable region.

Table 6.1: A table of pK_a values for the coformers investigated[4]. pK_a^1 refers to the first deprotonation and pK_a^2 the second deprotonation.

Coformer	Chemdraw	pK_a^1	pK_a^2	Cocrystal (C) or salt (S)	Previously reported?
Nicotinamide	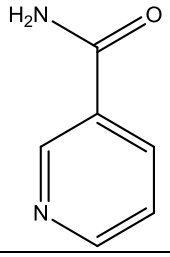	Heterocyclic N: 3.6 Amide: 13.3			
Oxalic acid	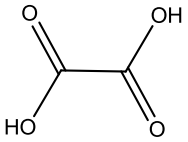	1.27	4.29	2:1 adduct and 1:1 S	Y
Malonic acid	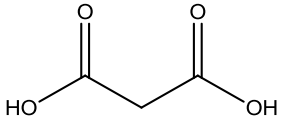	2.85	5.70	2:1 C	Y
Succinic acid	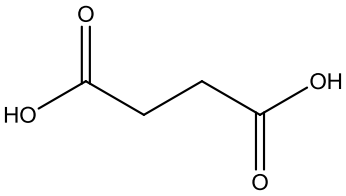	4.21	5.64	2:1 and 1:1 C	N
Fumaric acid	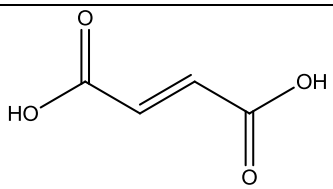	3.02	4.38	2:1 and 1:1 C	Y
Maleic acid	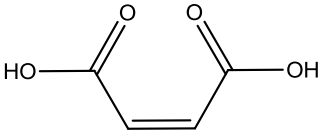	1.97	6.24	1:1 S	N
Glutaric acid	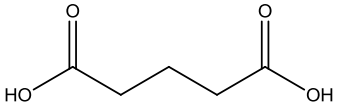	4.34	5.41	1:1 C	Y

Adipic acid	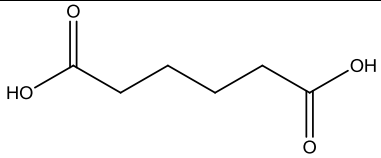	4.43	5.41	2:1 and 1:1 C	Y
Pimelic acid	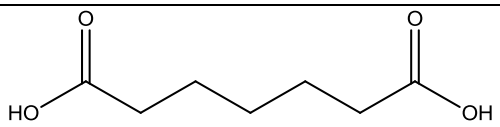	4.50	5.43	1:1 C	Y
Suberic acid	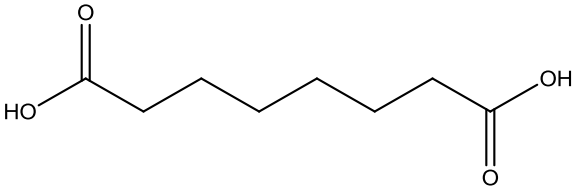	4.53	5.50	2:1 and 1:1 C	Y
Azelaic acid	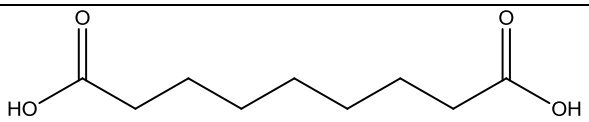	4.55	5.50	1:1 C	Y
Sebacic acid	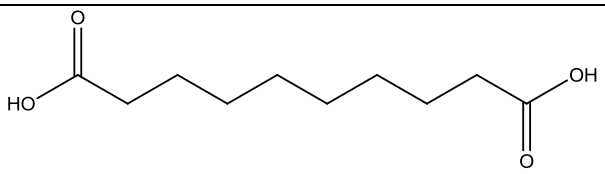	4.72	5.45	2:1	Y
Undecanedioic acid	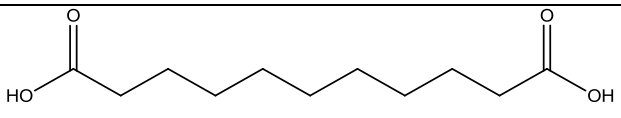	4.48		1:1	N

6.2 Nicotinamide : succinic acid

Nicotinamide was cocrystallised with succinic acid following the experimental procedure outlined in chapter 3.1. Powder X-ray diffraction was used to identify whether the resulting material was distinct from the starting components (figure 6.3).

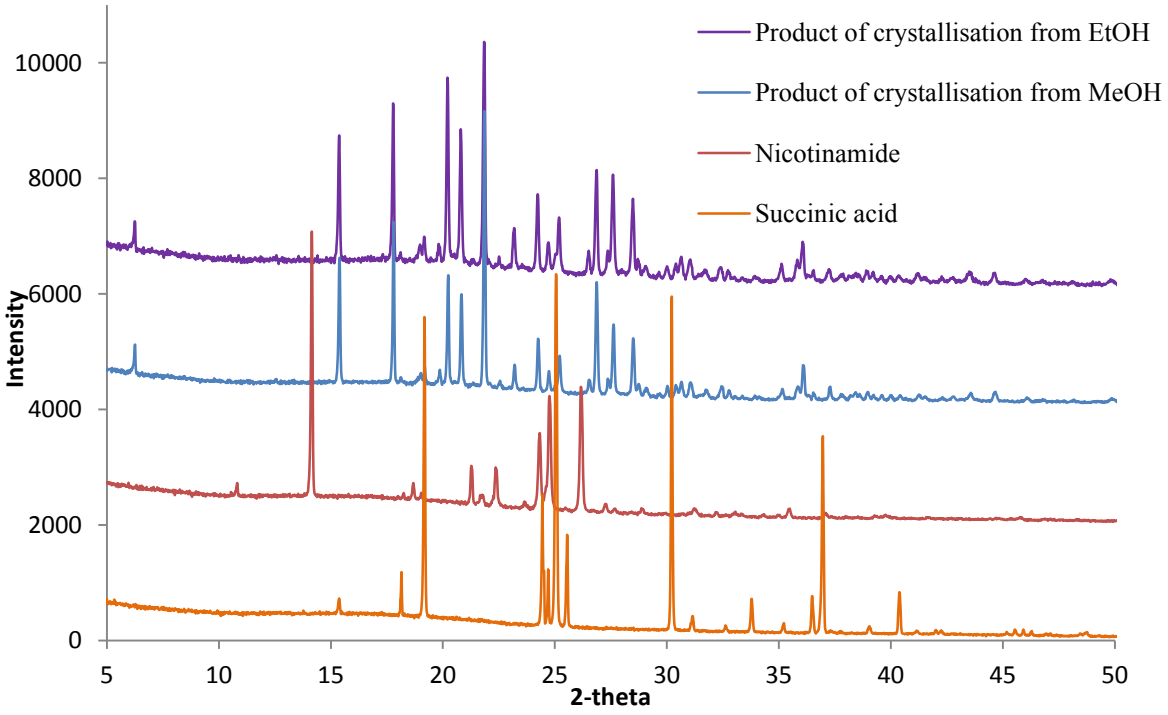

Figure 6.3: Powder X-ray diffraction data for the product of nicotinamide and succinic acid cocrystallisation and the starting materials

The diffraction patterns above show that both products of crystallisation are the same new material with no starting material present. ^{1}H NMR spectroscopy was carried out to determine the stoichiometry of the new nicotinamide : succinic acid adduct and to confirm the presence of both coformers in the material. The resultant spectrum shown in appendix 23.1 suggests a 2:1 nicotinamide : succinic acid stoichiometry.

Single crystal X-ray diffraction analysis was attempted several times on crystals selected from these samples, however the crystals were not of suitable quality to obtain a unit cell and allow

data collection. This was a problem reported by other researchers who also attempted the structure solution of this 2:1 nicotinamide : succinic acid adduct[2]. Consequently cocrystallisation was repeated using a more controlled experimental procedure as detailed in chapter 3.2, with the aim of producing better quality crystals. Powder X- ray diffraction was again used to determine the outcome of this new experimental method, figure 6.4.

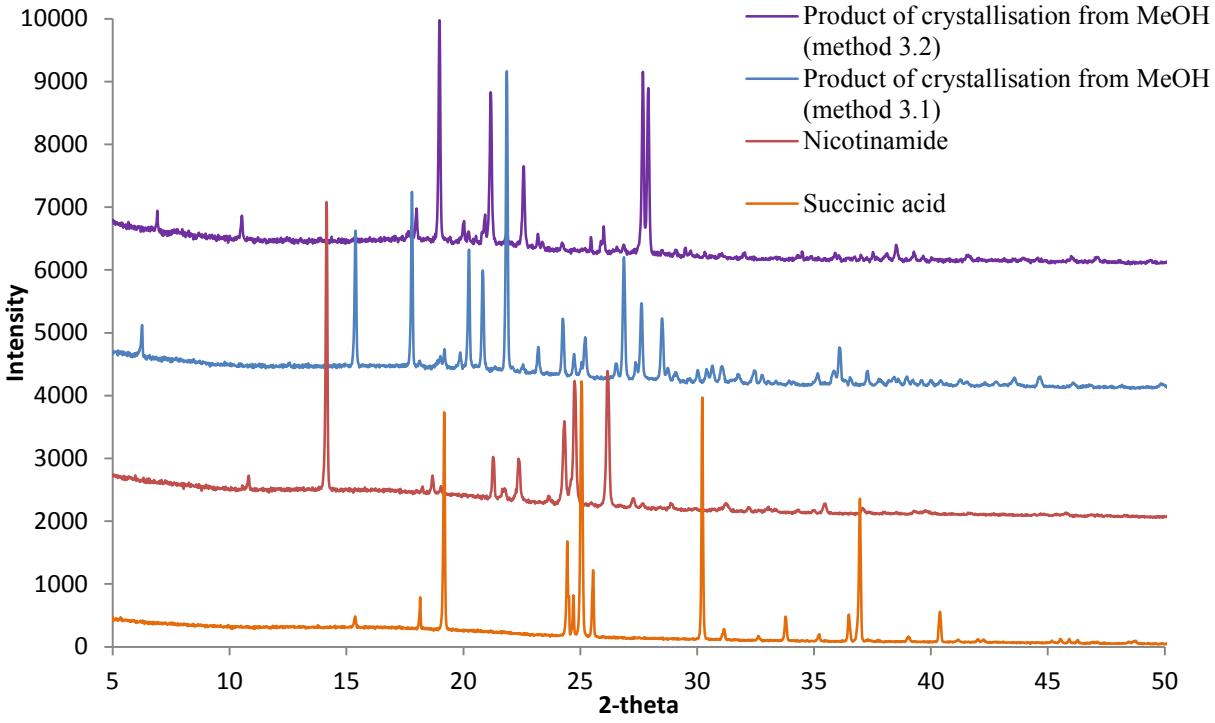

Figure 6.4: Powder X-ray diffraction data for the product of nicotinamide and succinic acid cocrystallisation using the two different cocrystallisation methods and their respective starting materials

It can be seen from this figure that the crystalline adduct formed when using the different experimental method 3.2, that a second new material has been formed, again with no traces of the 2:1 adduct or the starting materials present. The ^{1}H NMR spectra of this second adduct suggests a 1:1 stoichiometry (appendix 23.2). Crystals of suitable quality were selected for single crystal X-ray diffraction, a dataset was collected at the UK National Crystallography Service[5] and the structure solution undertaken. However, this resulted in the structure a 2:1

cocrystal even though the ^{1}H NMR spectra of this sample had implied a 1:1 stoichiometry. A powder diffraction pattern was simulated from this structure and compared to the laboratory powder diffraction pattern, (figure 6.5). It can be seen the crystal chosen for single crystal analysis was not representative of the bulk material obtained from the experimental procedure 3.2, but does match the bulk pattern obtained from experiment 3.1 from which no crystals could be obtained.

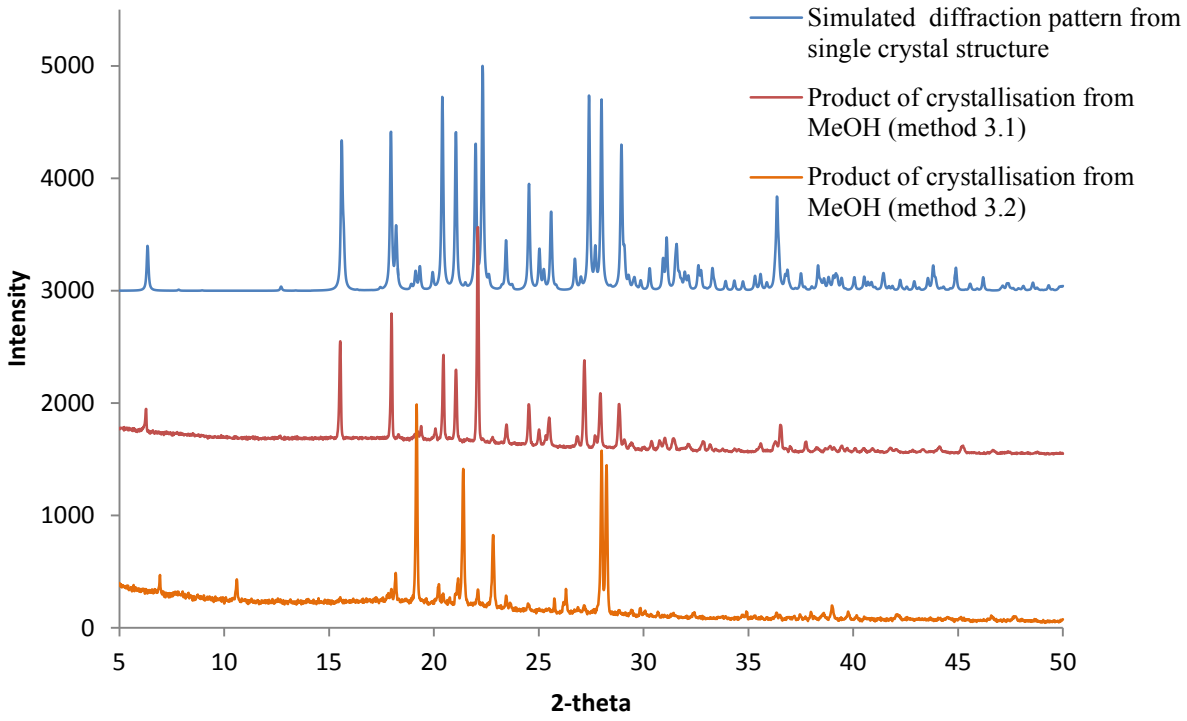

Figure 6.5: The diffraction pattern simulated from the single crystal structure compared to that of the laboratory experimental powder diffraction patterns of the products of crystallisation using experimental methods 3.1 and 3.2

It was not possible to obtain a crystal structure for the 1:1 nicotinamide : succinic adduct by single crystal X-ray diffraction, so it was solved from high quality powder diffraction data collected at a synchrotron source. Full details of this procedure and the structure description are discussed in chapter 7.

6.2.1 Nicotinamide : succinic acid, 2:1 structure description

The single crystal dataset for the 2:1 crystal was collected at the national crystallography service (chapter 3). Structure solution confirmed the adduct to be a cocrystal, crystallising in a triclinic cell with space group P-1. Table 6.2 gives the cell parameters for the 2:1 nicotinamide : succinic acid structure.

Table 6.2: Cell parameters for nicotinamide : succinic acid, 2:1

Compound	Nicotinamide : succinic acid 2:1
a (Å)	5.0872(2)
b (Å)	11.5569(5)
c (Å)	14.2784(5)
α (°)	77.433(2)
β (°)	86.726(2)
γ (°)	89.418(2)
Volume ($Å^3$)	818.01(6)
T (K)	120(2)
Z	2
Reflections collected	12664
Independent reflections	3205
R(int)	0.0610
Goodness of fit	1.106
R_1 (observed)	0.0555
R_1 (all)	0.0803
wR_2 (observed)	0.1162
wR_2 (all)	0.1320

The positions of the hydrogen atoms were determined by an electron density map, confirming the structure to be a cocrystal with no proton transfer from the succinic acid to the nicotinamide. Table 6.3 lists the eight intermolecular hydrogen bond interactions that are formed in this cocrystal structure, whilst table 6.4 gives selected intramolecular bond lengths and angles. Figure 6.6 shows the numbering scheme used in the discussion. Full crystallographic details are given in appendix 23.

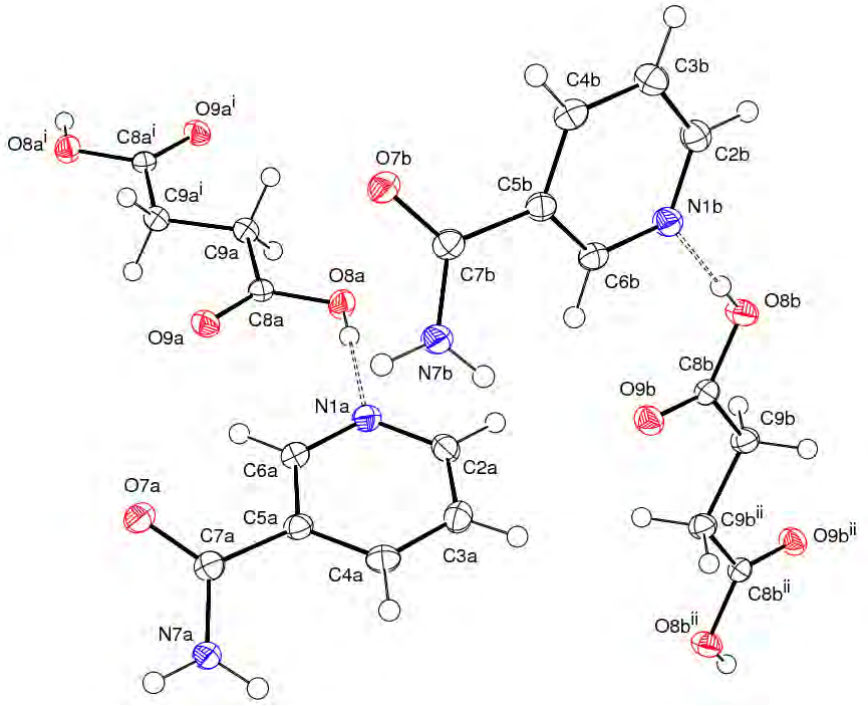

Figure 6.6: The independent molecules of nicotinamide : succinic acid, 2:1 showing the atom-numbering scheme and the hard intermolecular hydrogen-bonds (shown as dashed lines). Displacement ellipsoids are drawn at 50% probability level

Table 6.3: Intermolecular hydrogen bonding (Å) for nicotinamide : succinic acid, 2:1

D-H...A	d(D-H)	d(H...A)	d(D...A)	<(DHA)
O8A-H8A...N1A	0.84	1.85	2.691(3)	174.1
C6A-H6A...O9A	0.95	2.52	3.206(3)	129.5
N7A-H7AA...O7A^{i}	0.88	2.10	2.953(2)	164.1
N7A-H7AB...O7A^{ii}	0.88	2.15	2.899(3)	142.2
O8B-H8B...N1B	0.84	1.84	2.682(3)	176.0
C6B-H6B...O9B	0.95	2.61	3.268(3)	126.9
N7B-H7BA...O7B^{iii}	0.88	2.06	2.941(3))	173.6
N7B-H7BB...O7B^{ii}	0.88	2.22	2.947(3)	139.1

Symmetry transformations used to generate equivalent atoms:

(i) –x+1, -y+2, -z+2 (ii) x-1, y, z (iii) –x+2, -y+1, -z+2

Table 6.4: Selected bond lengths (Å) and angles (°) for nicotinamide : succinic acid, 2:1

Bond lengths (Å)				Bond angles (º)	
	Molecules A	Molecules B		Molecules A	Molecules B
C7-O7	1.241(3)	1.242(3)	O7-C7-N7	121.8(2)	122.2(2)
C7-N7	1.332(3)	1.331(3)	O9-C8-O8	123.6(2)	123.3(2)
C8-O9	1.213(3)	1.212(3)	C6-C5-C7-N7	151.9(2)	26.5(3)
C8-O8	1.328(3)	1.334(3)	O8-C8-C9-C10	174.6(2)^{i}	-176.6(2)^{ii}

Symmetry transformations used to generate equivalent atoms:

(i) –x+3, -y+2, -z+1 (ii) -x, -y+1,-z+1

The crystal structure of 2:1 nicotinamide : succinic acid displays an extended hydrogen bond network generated by the acid-pyridine and amide-amide synthons (I and III) expected in a cocrystal of this composition in a 2:1 stoichiometry, but unlike other nicotinamide : acid cocrystals, this one contains two crystallographically different nicotinamide molecules with different conformations. Nicotinamide molecule A (donated by 'a' in figure 6.6) adopts an

anti conformation with the heterocyclic N and the amide N on opposite sides of the molecule whereas nicotinamide molecule B (denoted by 'b' in figure 6.6) adopts a *syn* conformation.

Each nicotinamide molecule (A and B) is involved in four intermolecular hydrogen bonds with A and B molecules respectively; one hard O-H...N(heterocyclic) interaction and one soft C-H...O=C hydrogen bond to a succinic acid molecule, and two hard N-H...O=C hydrogen bonds to other nicotinamide molecules of the same conformation. More specifically, the carboxyl O8A acts as a hydrogen-bond donor via H8A to heterocyclic N1A of nicotinamide molecule A at (x, y, z) with the acid-pyridine packing motif (figure 6.2 (I)) reinforced by a C6A in the nicotinamide acting as a soft hydrogen-bond donor through H6A to the other carboxyl oxygen O9A at (x, y, z). Propagation of this motif through inversion within the succinic acid molecule generates the 2:1 nicotinamide : succinic acid unit in which the succinic acid A is capped at both ends by molecules of nicotinamide A. These units are then linked together through the complementary amide dimer $R_2^2(8)$ motif, figure 6.2 (III) formed by N7A via H7AA to O7A at (1-x, 2-y, 2-z) to generate a chain running in the $[20\bar{1}]$ direction. The chains are linked through a second complementary N-H...O interaction formed by N7A through H7AB to O7A resulting in the formation of ladders of alternating $R_4^2(8)$ and $R_2^2(8)$ rings and the generation of an extended corrugated hydrogen-bonded sheet in the *ac* plane, figure 6.7.

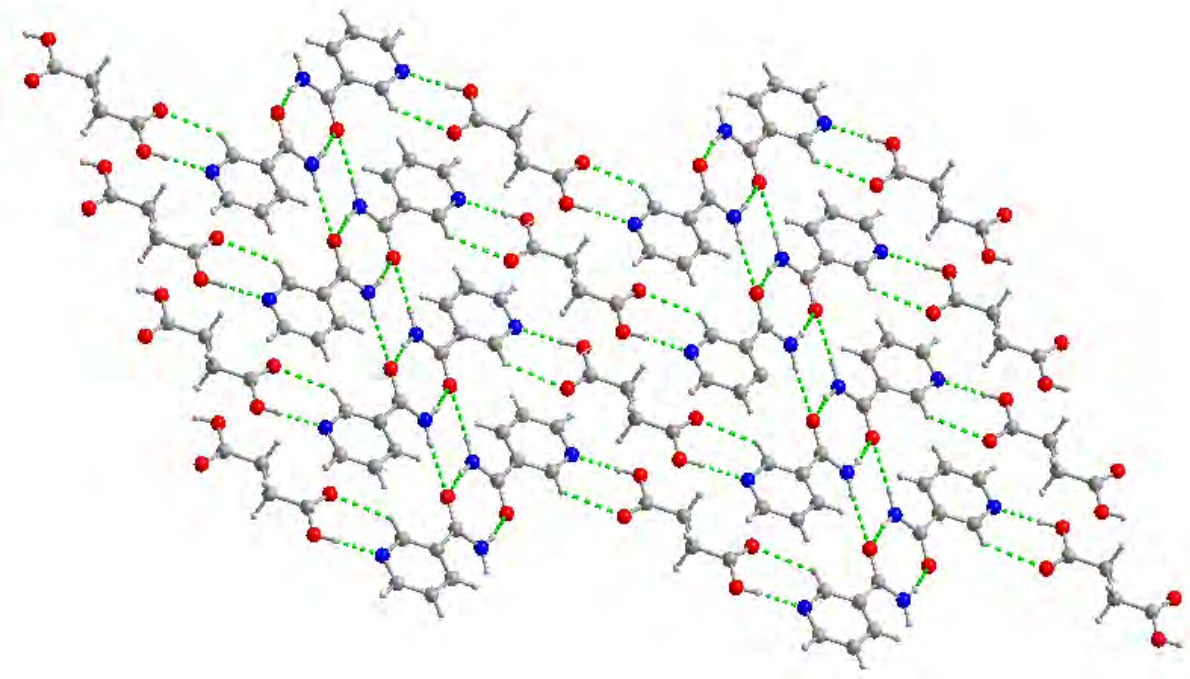

Figure 6.7: A view of the corrugated hydrogen-bonded sheet in the *ac* plane formed by nicotinamide A and succinic acid A molecules. Hydrogen bonds are shown as dashed lines

Nicotinamide B is involved in a similar set of intermolecular interactions with succinic acid B and other nicotinamide B molecule, generating the same synthons and motifs as nicotinamide A. The formation of a dimer with nicotinamide B at (2-x, 1-y, -z) generates a chain linking the nicotinamide B succinic acid B units, which in this case runs in the [201] direction. These chains are linked to others to give a second corrugated hydrogen-bonded sheet also in the *ac* plane. Hence, the structure contains alternating sheets comprised purely of A molecules and then purely of B molecules in which the chains run in opposing directions. There are no strong interactions between alternating sheets and all strong hydrogen-bond donors and acceptors are used in the hydrogen-bond network. Figure 6.8 shows a stereoview of this crystal structure showing the chains formed by nicotinamide A and succinic acid A running along [20-1] and nicotinamide B and succinic acid B running along [201].

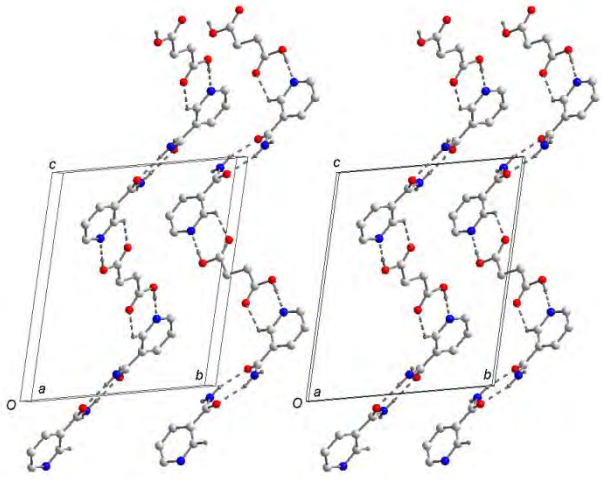

Figure 6.8: A stereoview of part of the crystal structure of nicotinamide : succinic acid 2:1 showing the chains formed by nicotinamide A and succinic acid A running along [20-1] (right) and nicotinamide B and succinic acid B running along [201] (left). Hydrogen bonds are shown as dashed lines

6.3 Nicotinamide : maleic acid

Cocrystallisation of nicotinamide and maleic acid has yielded some more interesting findings, resulting in extensive further work carried out by myself, a previous group member and an undergraduate project student. Nicotinamide was cocrystallised with maleic acid using the solvent evaporation experimental method (chapter 3) from both methanol and ethanol but resulting in different crystalline materials. From methanol, a nicotinamide : hydrogen maleate salt was formed, with the maleate undergoing isomerisation to form a 1:1 nicotinamide : fumaric acid cocrystal if the initial crystals were left to redissolve in the solvent. The crystals of the maleate salt were white and able to be isolated for single crystal X-ray diffraction analysis[6] whereas the fumaric cocrystal crystals were yellow. From ethanol, the yellow nicotinamide : fumaric acid cocrystal formed without appearance of the maleate crystals first. Isomerisation of maleic acid to fumaric acid in cocrystallisation has previously been reported[7], in which it was suggested that the use of a highly polar solvent was the cause of this isomerisation. Consequently, investigation of solvent effect was undertaken, initially using dichloromethane and acetone to identify whether the isomerisation occurs using aprotic solvents. Powder X-ray diffraction was used to compare and identify the adducts formed from these solvents (figure 6.9). Appendix 22.3 shows the crystal structure and packing motif for the hydrogen maleate salt structure[6] and the fumaric acid cocrystal structures[1].

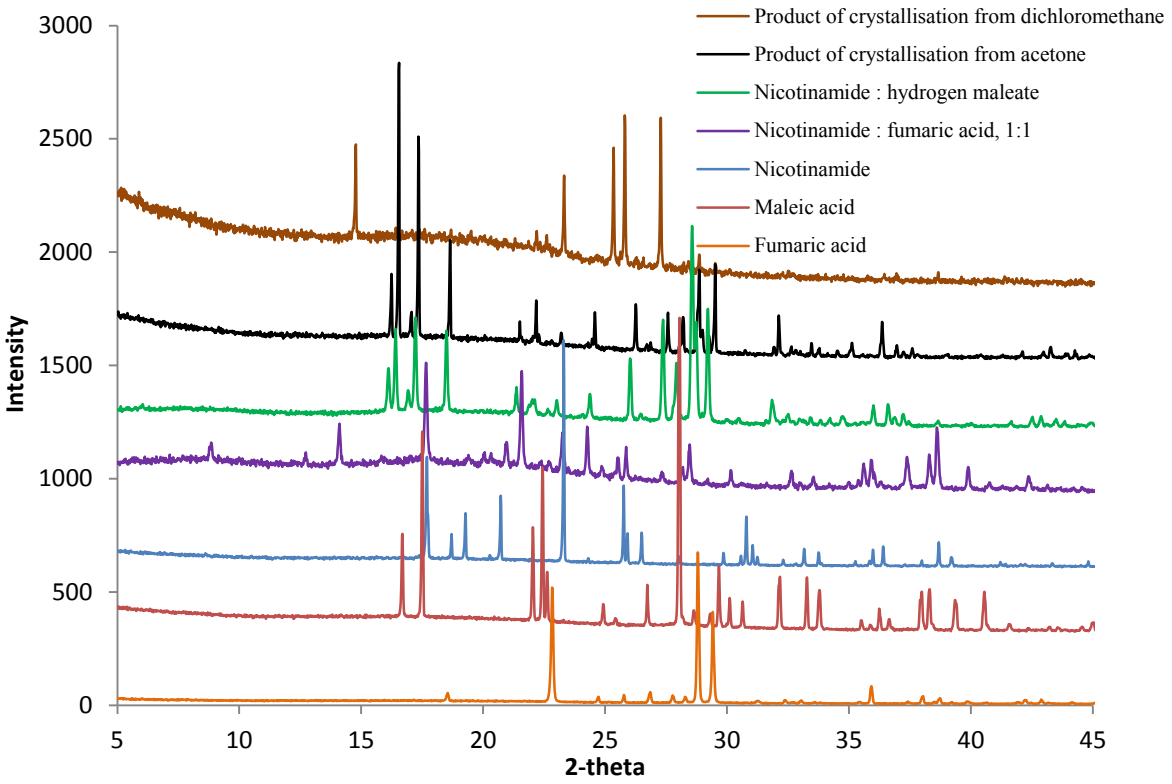

Figure 6.9: Powder X-ray diffraction pattern of the products of crystallisation from the aprotic solvents compared to those of the starting materials, the nicotinamide : hydrogen maleate 1:1 salt and nicotinamide : fumaric acid 1:1 cocrystal

The powder diffraction patterns above clearly show that the product of crystallisation from acetone is the nicotinamide : hydrogen maleate salt. The diffraction pattern of the product of crystallisation from dichloromethane indicates the formation of a further new material with the pattern consisting of peaks which clearly differ to those of the adduct structures and starting materials.

A undergraduate student took this project further and investigated a range of other solvents including propan-1-ol, ethyl acetate, butan-1-ol, methyl acetate, acetonitrile and dimethylsulfoxide[8]. The nicotinamide : hydrogen maleate salt formed in all of these solvents, except for dimethylsulfoxide, which produced no crystalline material. The product of crystallisation from propan-1-ol also contained the nicotinamide : fumaric acid cocrystal. The

project concluded that the length of time taken for the crystals to form allowed some prediction of the resultant product. It was found that the white nicotinamide hydrogen maleate crystals form quickly (less than 1 day) as opposed to the yellow nicotinamide : fumaric acid crystals which took up to a month to form[8]. Both the cocrystal and the salt adducts formed in these polar protic and polar aprotic solvents, and hence further work will include the use of non polar solvents to investigate the effect on this isomerisation.

6.4 Nicotinamide : undecanedioic acid

Nicotinamide was cocrystallised with undecanedioic acid following the experimental procedure discussed in chapter 3.1. Powder X-ray diffraction was used to determine whether the resultant adduct was a new material, figure 6.10.

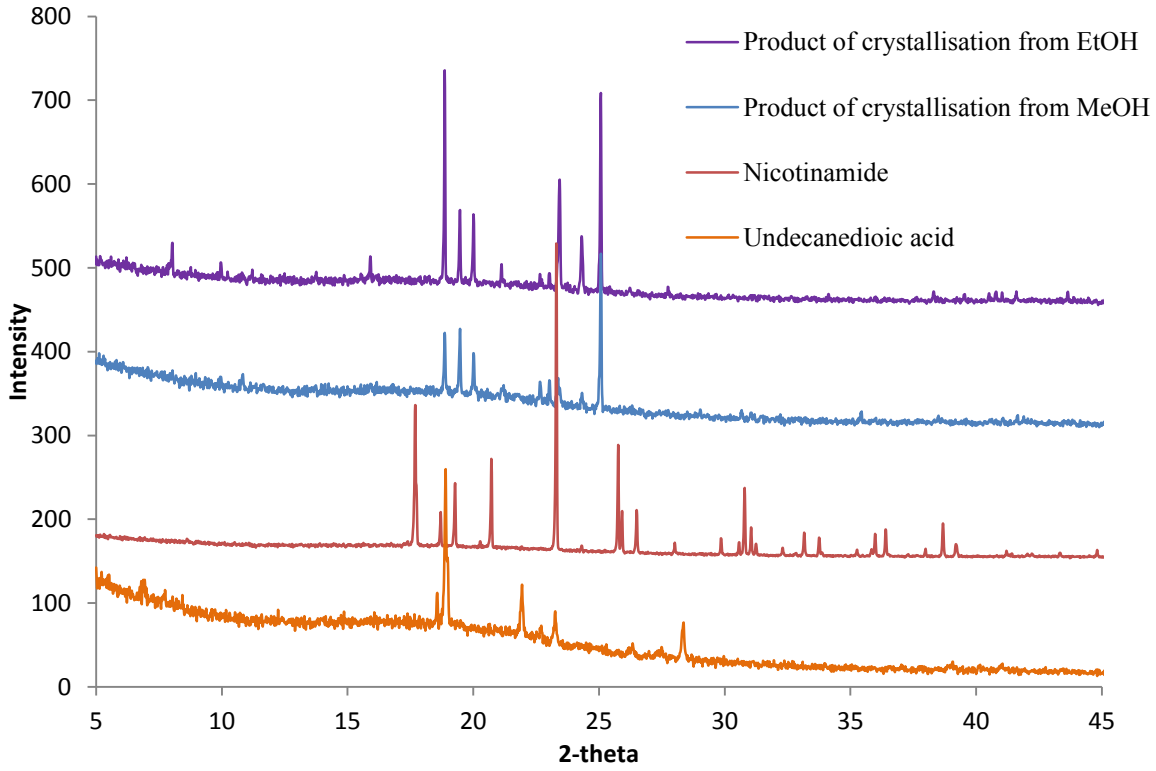

Figure 6.10: Powder X-ray diffraction data for the product of nicotinamide and undecanedioic acid cocrystallisation and the respective starting materials

The diffraction patterns above show that a new material has been formed. The adducts from methanol and ethanol are the same, although there may be some differences due to prefererred orientation or some impurity in the sample from ethanol. ^{1}H NMR spectroscopy was used to confirm the presence of both nicotinamide and undecanedioic acid in this new material in a 1:1 stoichiometry (appendix 24.1).

A suitable crystal was selected for single crystal X-ray diffraction analysis, a unit cell was determined and a dataset collected. The structure crystallises in a triclinic with space group P-1, table 6.5 gives the cell parameters for the nicotinamide : undecanedioic acid 1:1 structure.

Table 6.5: Cell parameters for nicotinamide : undecanedioic acid, 1:1

Compound	Nicotinamide : undecanedioic acid 1:1
a (Å)	9.1939(1)
b (Å)	11.6336(2)
c (Å)	17.6109(3)
α (°)	106.738(1)
β (°)	90.588(1)
γ (°)	105.479(1)
Volume ($Å^3$)	1730.63(5)
T (K)	120(2)
Z	4
Reflections collected	15786
Independent reflections	5925
R(int)	0.0288
R_1 (observed)	0.0442
R_1 (all)	0.0373
wR_2 (observed)	0.0985
wR_2 (all)	0.1047

The position of the hydrogen atoms were determined by an electron density map confirming the structure as a cocrystal, since no proton transfer occurred from the acid to the nicotinamide. The diffraction pattern simulated from the single crystal structure matches the experimental powder X-ray diffraction pattern confirming that the crystal chosen is representative of the bulk material (appendix 24.2). Table 6.6 lists the eight intermolecular

hydrogen bonds in this structure, whilst table 6.7 lists selected bond lengths and angles (full crystallographic details are given in appendix 24. Figure 6.11 shows the numbering scheme used in this discussion.

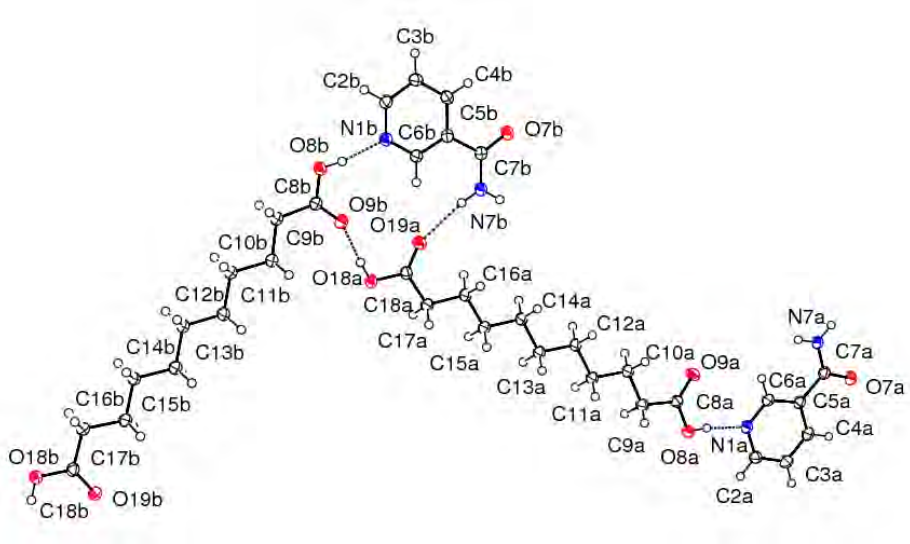

Figure 6.11: The independent molecules of nicotinamide and undecanedioic acid showing the atom-numbering scheme and the hard intermolecular hydrogen-bonds (shown as dashed lines). Displacement ellipsoids are drawn at 50% probability level

Table 6.6: Hydrogen bond table for nicotinamide : undecanedioic acid, 1:1

D-H...A	d(D-H)	d(H...A)	d(D...A)	<(DHA)
N7A-H7AA...O7A[i]	0.88	2.08	2.952(2)	173
N7A-H7AB...O19B[ii]	0.88	2.09	2.954(2)	168
O8A-H8A...N1A	0.84	1.78	2.613(1)	173
O18A-H18A...O9B	0.84	1.83	2.662(4)	174
C6A-H6A...O19B[iii]	0.95	2.34	3.277(2)	170
N7B-H7BA...O7B[iv]	0.88	2.10	2.975(2)	170
N7B-H7BB...O19A	0.88	2.10	2.963(2)	165
O8B-H8B...N1B	0.84	1.79	2.622(1)	171
O18B-H18B...O9A[v]	0.84	1.84	2.673(1)	175
C6B-H6B...O19A[vi]	0.95	2.37	3.292(2)	164

Symmetry transformations used to generate equivalent atoms:

(i) -x+3, -y+1, -z+1 (ii) x+1, y-1, z+1 (iii) x+1, y, z

(iv) –x, -y+1, -z+1 (v) x-1, y+1, z-1 (vi) –x+2, -y+1, -z+1

Table 6.7: Selected intramolecular bond lengths (Å) and angles (°) for nicotinamide : undecanedioic acid, 1:1

	Bond lengths (Å)			Bond angles (°)	
	Molecules A	Molecules B		Molecules A	Molecules B
C7-O7	1.238(2)	1.237(2)	O7-C7-N7	122.8(1)	122.5(1)
C7-N7	1.329(2)	1.329 (2)	O9-C8-O8	122.2(1)	122.4(1)
C8-O9	1.214(2)	1.220(2)	O19-C18-O18	122.6(1)	122.6(1)
C8-O8	1.316(2)	1.309(2)	C6-C5-C7-N7	-177.0(1)	-177.7(1)
C18-O18	1.335(2)	1.334(2)	O8-C8-C9-C10	178.7(1)	-170.4(1)
C18-O19	1.207(2)	1.209(2)	O18-C18-C19-C20	174.1(1)	175.6(1)
			O8-C8-C18-O18	-15.7(2)	10.7(2)

The asymmetric unit of nicotinamide : undecanedioic acid, 1:1 contains two symmetrically independent undecanedioic acid molecules (A and B) and two symmetrically independent nicotinamide molecules (A and B), though unlike the nicotinamide : succinic acid 2:1 structure, both nicotinamide molecules adopt the *syn* conformation, figure 6.11. It is clear from the bond lengths and angles listed in table 6.7 that nicotinamide molecules A and B have the same conformation with the bond lengths and angles similar. The same cannot be said for the acid molecules in which the torsion angles O8-C8-C9-C10, O18-C18-C19-C20 and O8-C8-C18-O18 are very different in molecule B compared to molecule A. From the C-OH and C=O bond angles given in table 6.7, it can be seen that there is a clear distinction between them, confirming again that this is a cocrystal as all carboxyl groups have retained their acidic protons.

Each nicotinamide molecule (A and B) is involved in two intermolecular hydrogen bonds to molecules of the same type; one hard O-H...N(heterocyclic) interaction and a self complementary N-H...O=C hydrogen bond. More specifically the heterocyclic N1 acts as a hydrogen bond acceptor of H8 donated by the carboxyl O8 to form the acid-pyridine motif I, as expected in a cocrystal structure composed of these coformers. Propagation of this motif through the nicotinamide dimer (packing motif III) formed by a complementary bond donated by the amide N7 through H7A to O7, creates the four unit chains that can be viewed as the basic building block of this crystalline structure. Figure 6.12 shows an example of this supramolecular unit formed from molecules B; molecules A form a similar unit with the same bonding and motifs.

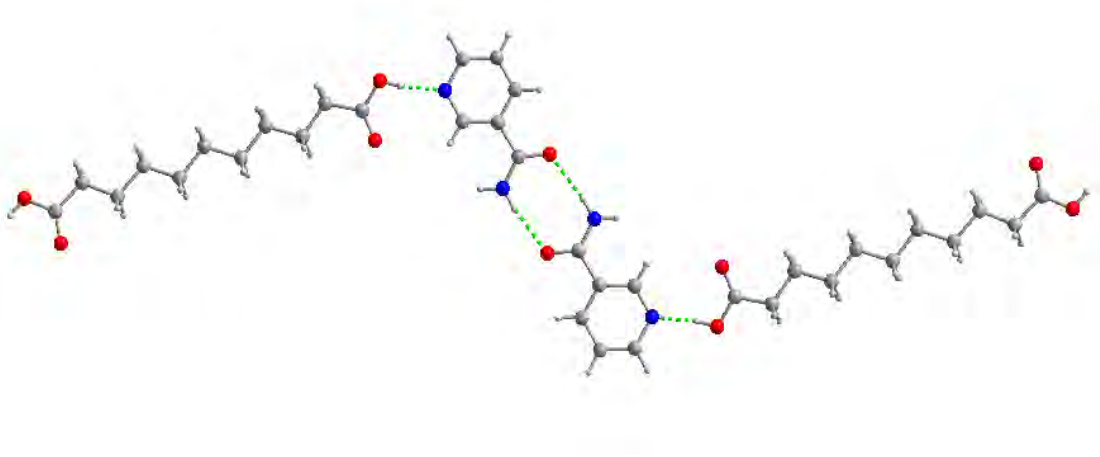

Figure 6.12: A view of the small four unit chains formed by the acid-pyridine and amide-amide packing motifs I and III

Each nicotinamide molecule (A and B) is involved in three hard intermolecular hydrogen bonds and one reinforcing weak hydrogen bond; one hard O-H...N(heterocyclic) interaction between respective molecules and a hard self complementary N-H...O=C hydrogen bond are present. The final two hydrogen bonds are a hard N-H...O interaction and a soft reinforcing C-H...O linkage formed between an acid and an amide of differeing types. More specifically the heterocyclic N1 acts as a hydrogen bond acceptor of H8 donated by the carboxyl O8 to form the acid-pyridine motif I, as expected in a cocrystal structure composed of these coformers. Propagation of this motif through the nicotinamide dimer (packing motif III) formed by a complementary bond donated by the amide N7 through H7A to O7, creates the four unit chains that can be viewed as the basic building block of this crystalline structure. Figure 6.12 shows an example of this supramolecular unit formed from molecules B; molecules A form a similar unit with the same bonding and motifs.

These units form hydrogen bonds to other units of the opposite type (A or B) via two strong hydrogen bonds and a reinforcing soft bond, including the nicotinamide using amide N7 as a donor to the carboxyl O9 as an acceptor with the undecanedioic molecules on the second

chain. Specifically N7 will donate H7B to O19 on the opposite type chain, with the acids from different chains also interacting through the donation of H18 from O18 to the acceptor O9 ion the neighbouring chain unit. The amide-acid linkage is reinforced by the soft hydrogen bond donated by C6 via H6 to O19 creating a $R_2^1(7)$ ring motif, though the two hard interactions in combination with the acid-pyridine linkage form a much larger $R_3^3(14)$ ring motif (figure 6.13). Each supramolecular chain unit of molecules A forms hydrogen bond interactions to four chains of molecules B, which in turn are linked to four units of molecule A etc to form the overall crystal structure shown in figure 6.13.

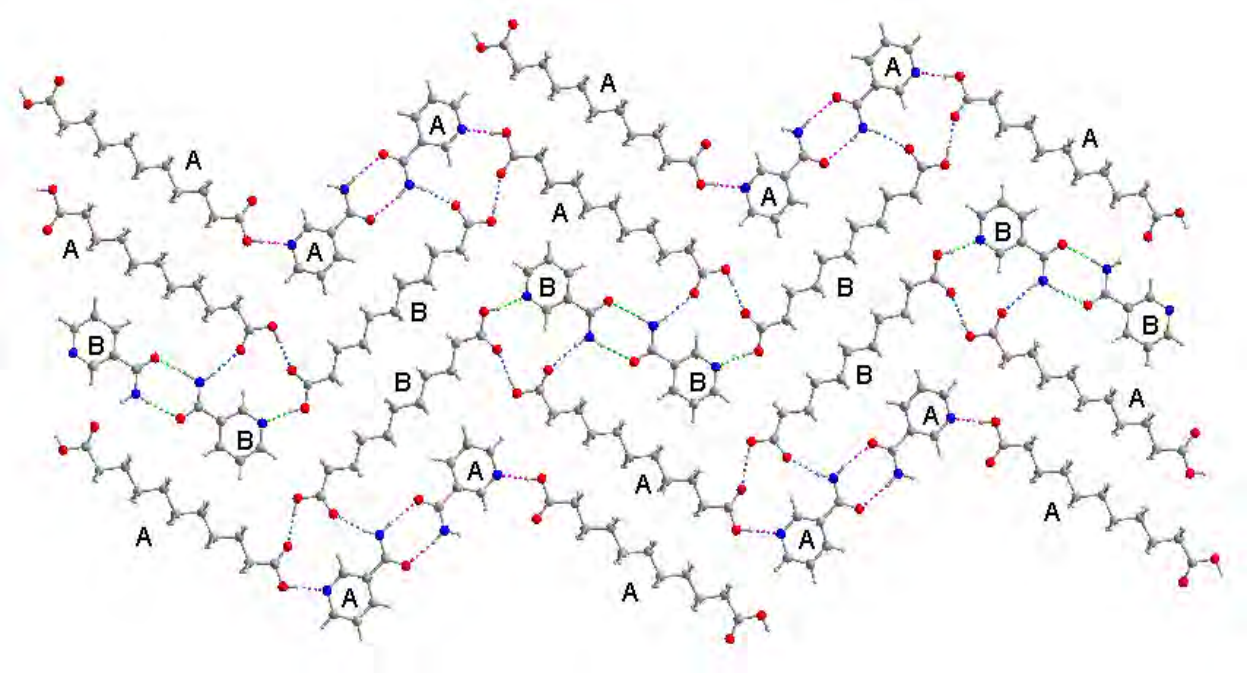

Figure 6.13: A view of the hydrogen bonding network of the nicotinamide : undecanedioic acid cocrystal. Hydrogen bonds are shown as dashed lines with the pink lines referring to bonding between the A molecules, green lines between the B molecules and the blue lines represent the hydrogen bonds that link these chains together.

All strong hydrogen bond donors and acceptors are utilised within this cocrystal structure forming an extensive hydrogen bonded network that differs significantly from other nicotinamide and isonicotinamide cocrystals with dicarboxylic acids. The first major difference is that whilst this has a 1:1 stoichiometry, the amide-amide synthon (III) is present whereas the amide-acid synthon (II) is not. In other cases the dimer is only formed in the 2:1 cocrystal structures. The other packing feature that is different in this structure is that it consists of small four-unit chains rather than the infinite chains formed in other cocrystals of this series.

6.5 Discussion

The published nicotinamide : dicarboxylic acid cocrystals follow the same trend in packing motifs as the isonicotinamide : dicarboxylic acid cocrystals; all contain the strong acid-pyridine synthon and then either an acid-amide motif for 1:1 adducts or the amide-amide linkage in the 2:1 adducts. This trend is followed by the nicotinamide : succinic acid 2:1 cocrystal, however the two nicotinamide molecules within this structure exist in two different conformations. A study of the Cambridge Structural Database[9] revealed that not only is this a feature unobserved in other cocrystals within this series, but it has not been previously reported in other nicotinamide adducts which display only one conformation. Results from the database highlighted that there are more examples of structures adopting the *anti* rather than the *syn* conformation, as indicated by the structures discussed in this chapter, with the hydrogen-bonded sheet formed by nicotinamide A in the *anti* conformation being the common supramolecular unit found in other 2:1 nicotinamide dicarboxylic acid cocrystals such as nicotinamide : adipic acid, nicotinamide : suberic acid and nicotinamide : sebacic acid[2]. There are no other reports of the *syn* conformation in this series of cocrystals, although it is found in the 1:1 structures within this series; nicotinamide : glutaric acid and nicotinamide : pimelic acid[2].

The nicotinamide : undecanedioic acid cocrystal structure presented in this chapter goes against all of the trends previously discussed. The structure does contain the acid-pyridine packing motif, however, the acid-amide synthon that is expected in the 1:1 cocrystals is not present; instead the amide-amide packing motif, usually seen in the 2:1 cocrystal structures is formed. The short four-unit supramolecular chains are another feature not observed in the other structures within this series, all of which contain infinite chains that link to form infinite sheets.

In the isonicotinamide chapter, twisting of the acid conformations is seen within the longer chain dicarboxylic acids containing an odd number of carbon atoms. The isonicotinamide : pimelic and isonicotinamide : azelaic acid 1:1 (n = 7 and 9 respectively) structures contained similar twisting to that seen in the pure acids; however only the published nicotinamide : azelaic acid cocrystal exhibits this twisting and not the pimelic acid adduct[2]. Undecanedioic acid contains eleven carbon atoms on its backbone and hence it would be predicted that twisting would be present. The O8-C8-O18-C18 torsion angles shown in table 6.7 show that twisting is present in this structure, though not to the same extent as the pure acids or the isonicotinamide : pimelic and isonicotinamide : azelaic acid 1:1 structures. The reason for this can be rationalised by study of the structure. The twisting is present in the pure acids to avoid repulsion between the carboxy dimers[10] and is present in the cocrystal structures to avoid repulsion between the acid-amide ring motifs[11]. The twisting is energetically unfavourable and with this structure not following the packing trends; the motifs are not within a close enough range for repulsion so the acid molecules do not need to twist.

A melting point of 106-108 ºC has been obtained for nicotinamide : undecanedioic, this is in the same range as the acid which was recorded to melt at 107ºC. Unfortunately the published nicotinamide : dicarboxylic acids did not report the melting points so it has not been possible to determine whether the alternating trend displayed by the pure acids and isonicotinamide cocrystals is followed in this series of cocrystals.

Further work would include further attempts at obtaining a structure for isonicotinamide : undecanedioic acid to see whether the structure would be similar to the nicotinamide : undecanedioic acid structure or whether it follows the initial trend set out by all other crystalline adducts within the series of materials studied within this project.

Study into the formation of hydrogen maleate salt structures from cocrystallisation experiments with both nicotinamide and isonicotinamide also yielded some exciting results. It was found that within both systems, the maleic acid would isomerise to fumaric acid within the crystal structure when using certain solvents. Table 6.8 lists the different solvents used and the resultant material formed when both isonicotinamide and nicotinamide are cocrystallised with maleic acid. It is clear from this table that the hydrogen maleate structure is more common.

Table 6.8: A table listing the resultant crystalline adducts when maleic acid is cocrystallised with isonicotinamide and nicotinamide[8]

Solvent	Resultant material with isonicotinamide	Resultant material with nicotinamide
Methanol	Isonicotinamide : fumaric acid	Nicotinamide : hydrogen maleate that recrystallises to nicotinamide : fumaric acid
Ethanol	Mixture of isonicotinamide : hydrogen maleate and isonicotinamide : fumaric acid	Nicotinamide : fumaric acid
Propan-1-ol	Isonicotinamide : hydrogen maleate	Mixture of nicotinamide : hydrogen maleate and nicotinamide : fumaric acid
Butan-1-ol	Isonicotinamide : hydrogen maleate	Nicotinamide : hydrogen maleate
Acetonitrile	Isonicotinamide : hydrogen maleate	Nicotinamide : hydrogen maleate
Methylacetate	Isonicotinamide : hydrogen maleate	Nicotinamide : hydrogen maleate
Ethyl acetate	Isonicotinamide : hydrogen maleate	Nicotinamide : hydrogen maleate
Dimethylsulfoxide	No product reported	No product reported

6.6 Footnote

The results presented in this chapter (structure of nicotinamide : succinic acid 2:1) have been published in L.J.Thompson, R.S.Voguri, A. Cowell, L.Male, M.Tremayne, *Acta Crystallogr. C*, 2010, **C66**, 0421 (appendix 25)

6.7 References

1. L. Orola and M. V. Veidis, *CrystEngComm.*, 2009, **11**(3), 415
2. S. Karki, T. Friscic and W.Jones, *CrystEngComm.*, 2009, **11**(3), 470
3. S. Athimoolam and S. Natarajan, *Acta Crystallogr. Sect. C*, 2007, **63**, o263
4. R. M. C. Dawson, D. C. Elliott, W. H. Elliott and K. M. Jones, *Data for biochemical research*, **2 ed**, Oxford Clarendon Press, 1969
5. S. J. Coles and P. A. Gale, *Chem. Sci.*, 2012, **3**(3), 683
6. A. Cowell, *An investigation into the synthesis, structural characterisation, thermal and polymorphic behaviour of organic crystalline materials*, PhD thesis, University of Birmingham, 2011
7. S.Chatterjee, V.R.Pedireddi, C.N.R.Rao, *Tetrahedron Lett.*, 1998, **39**(18), 2843
8. G. Cutts, *Synthesis and structure determination of molecular cocrystals*, M.Sci project report, University of Birmingham, 2011
9. F.H.Allen, *Acta Crystallogr. Sect. B*, 2002, **58**, 380
10. V.R.Thalladi, M.Nusse, R.Boese, *J. Am. Chem. Soc.*, 2000, **122**(38), 9227
11. L.J. Thompson, R.S. Voguri, L. Male and M. Tremayne, *CrystEngComm.*, 2011, **13**(12), 4188

7. Structure solution from X-ray powder diffraction

7.1 Introduction

This chapter focuses on the structure solution of crystalline adducts from powder diffraction using high resolution X-ray diffraction data collected on beamline I11 at Diamond Light Source (section 3.3.2). The unknown nicotinamide : succinic acid 1:1 structure (as discussed in chapter 6) has successfully been solved using this data and a variation of methods has been used on both a room temperature and low temperature dataset of the known nicotinamide : fumaric acid structure[1].

7.2 Nicotinamide : succinic acid

It was found in chapter 6 that different experimental cocrystallisation methods (section 3.1 and 3.2) form nicotinamide : succinic acid crystalline adducts of different stoichiometry; 2:1 and 1:1 respectively, though single crystals could only be formed for the 2:1 adduct. Therefore high quality powder diffraction data was collected on these crystals with the primary aim to solve the structure without needing good quality single crystals.

7.2.1 Unit cell and space group determination

The laboratory X-ray diffraction pattern of the 1:1 nicotinamide : succinic acid adduct (figure 7.1) shows that the crystalline sample contains no starting material with solution ^{1}H NMR spectroscopy confirming the presence of both nicotinamide and succinic acid in a 1:1 stoichiometry (appendix 23.2).

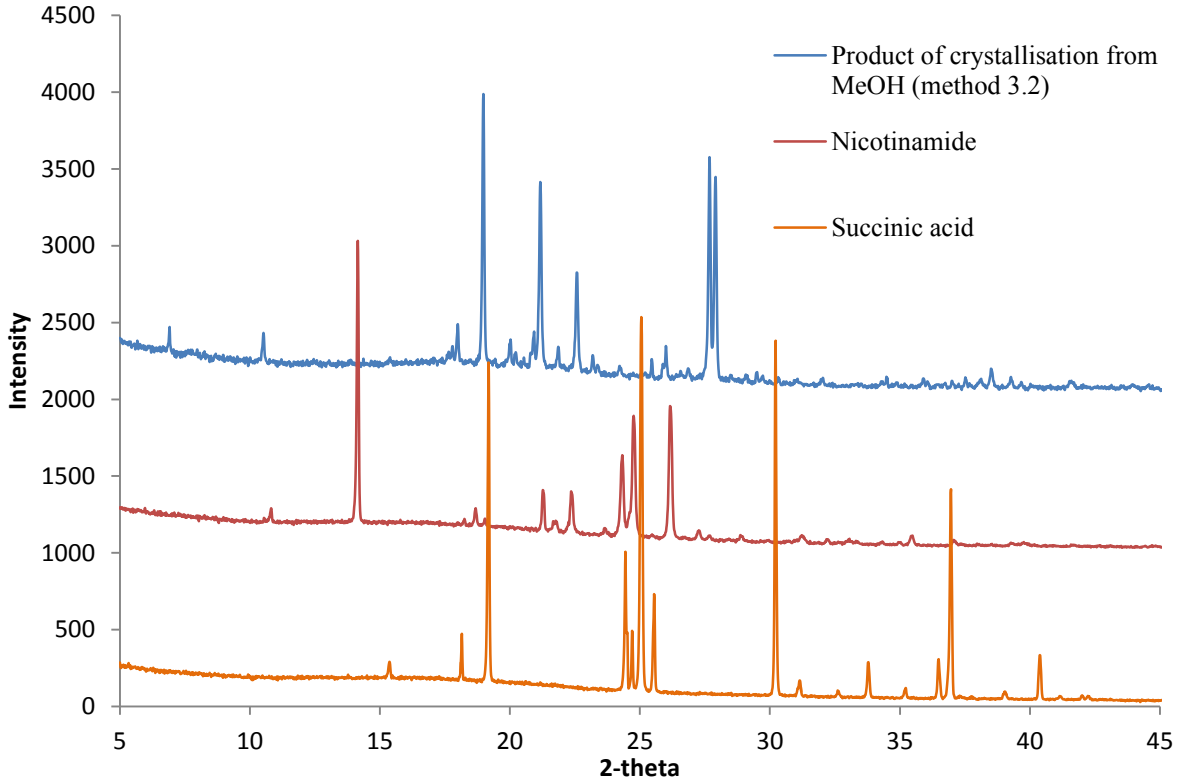

Figure 7.1: Powder X-ray diffraction data for the product of nicotinamide and succinic acid cocrystallisation using the cocrystallisation experimental method 3.2 and the respective starting materials

As discussed in section 1.11, high resolution X-ray diffraction data collected from a synchrotron source can be used to give better signal/noise ratio and can resolve peak overlap to an extent[2]. Diffraction data were collected on beamline I11 at Diamond Light Source at room temperature (section 3.3.2) and indexed (section 2.2.2) allowing a unit cell to be determined (table 7.1).

Table 7.1: The selected unit cell for nicotinamide : succinic acid, 1:1 from the initial indexing results

Parameter	Nicotinamide : succinic acid, 1:1
a (Å)	8.8832
b (Å)	25.4316
c (Å)	5.0191
α (º)	90
β (º)	93.761
γ (º)	90
V	1131.44

7.2.2 Pattern decomposition

A le bail fit on the high resolution diffraction data was formed in GSAS[3] (section 2.2.3). As can be seen from the screenshot below (figure 7.2), the le bail fit is very poor with both peak height and peak width fitting badly. The poor fit is believed to be caused by anisoptropic peak broadening, a feature often found to be present in X-ray powder diffraction data sets collected from synchrotron light sources[4].

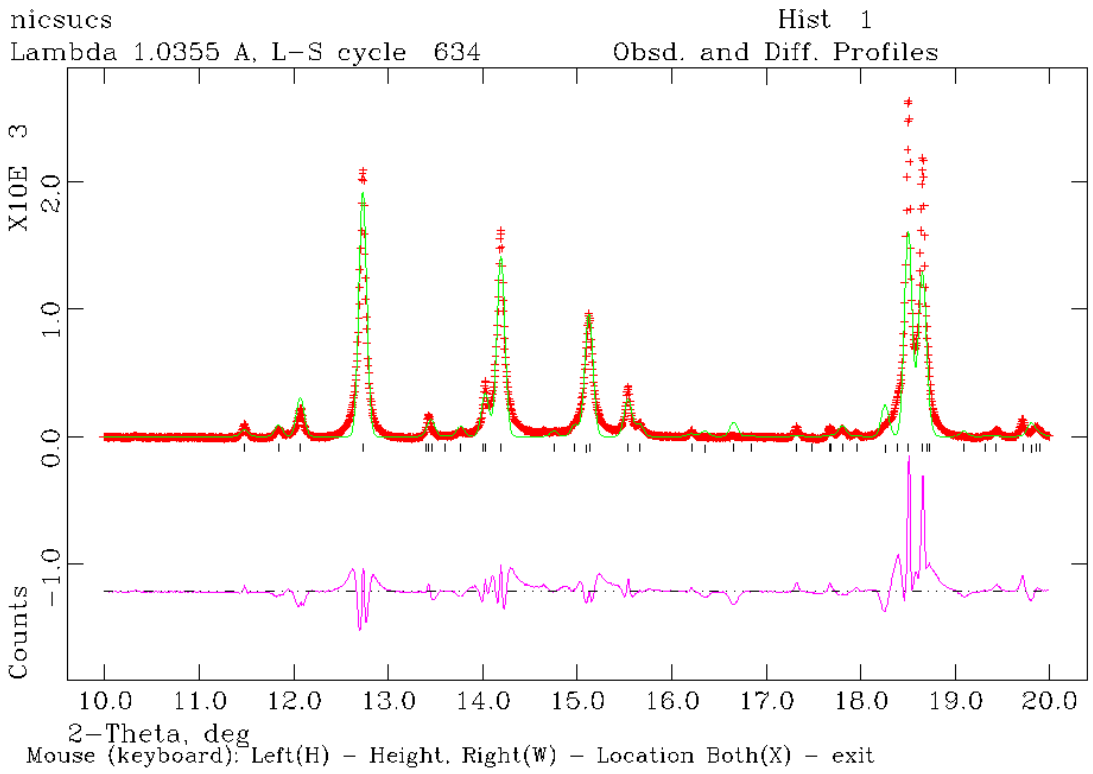

Figure 7.2: A screenshot of the le bail fit of nicotinamide : succinic acid 1:1. The experimental pattern is represented by the red crosses, the calculated pattern by the green line and the pink line represents the difference of the two

Since anisotropic peak broadening could not be overcome in GSAS, a le bail fit was carried out on the laboratory X-ray diffraction pattern using the unit cell obtained from indexing the high resolution data. This yielded a slightly better fit (figure 7.3) and did allow for a basic structure solution, though not good enough for publication. However, structure solution with both reliable and publishable results has been obtained by using Topas[5] in which a good quality pawley fit was achieved (figure 7.4).

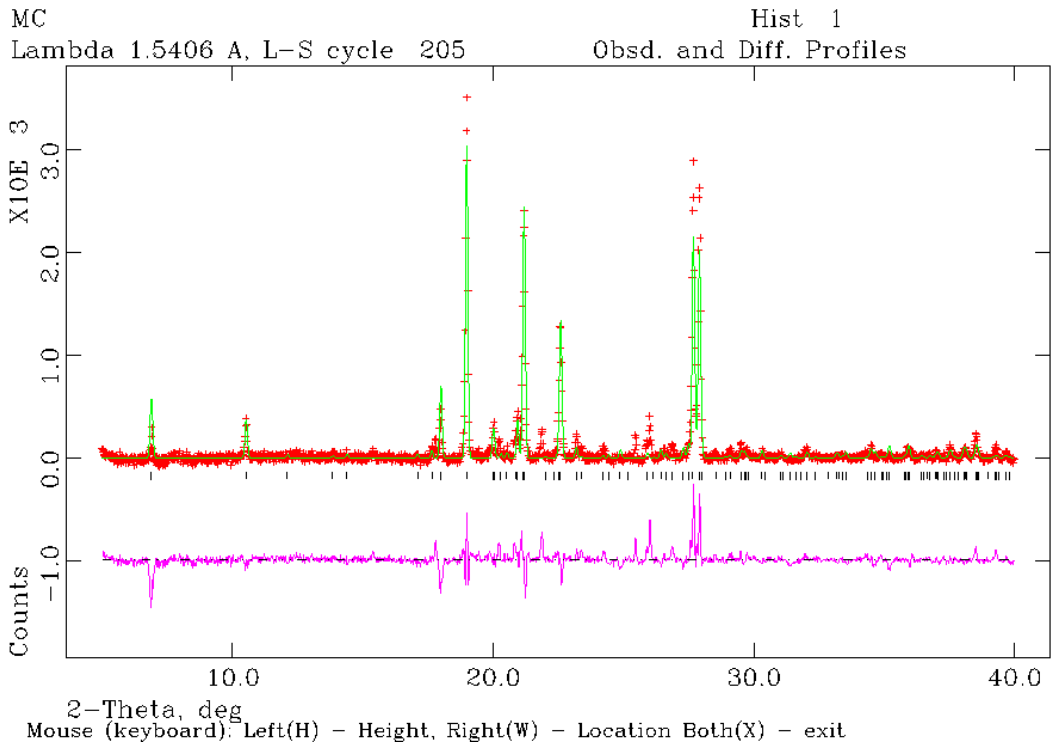

Figure 7.3: Le bail fit of the nicotinamide : succinic acid laboratory X-ray diffraction data. The experimental pattern is represented by the red crosses, the calculated pattern by the green line and the pink line represents the difference of the two

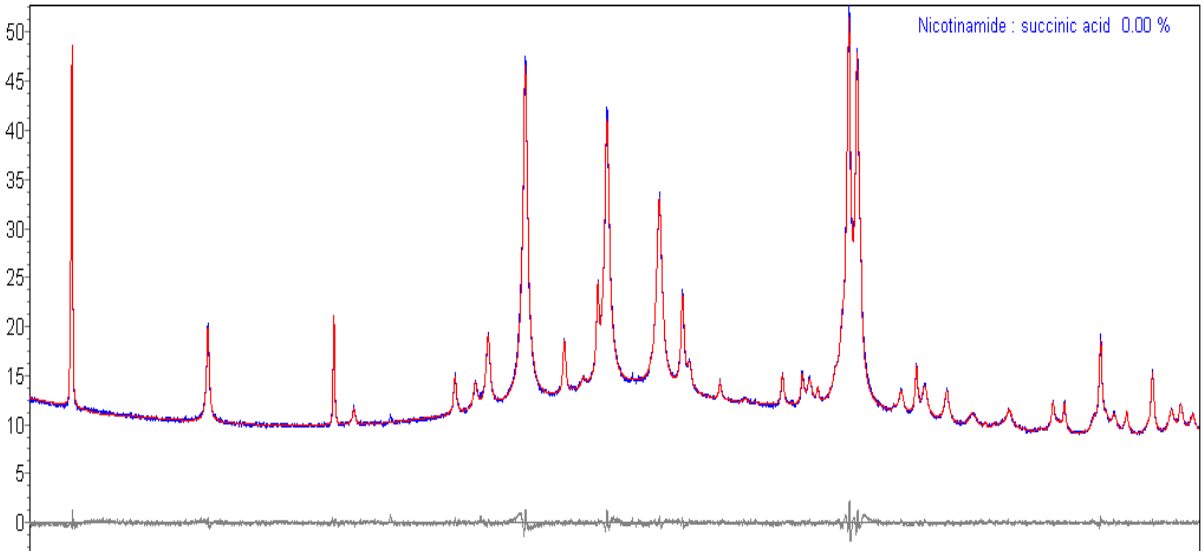

Figure 7.4: Pawley fit of nicotinamide : succinic acid on the high resolution synchrotron data. The experimental pattern is represented by the blue line, the calculated pattern by the redline and the grey line represents the difference of the two

7.2.3 Structure solution

A basic structure solution was obtained from the le bail fit of the laboratory X-ray diffraction pattern. Whilst it did not yield results good enough for publication, it did provide a good understanding of the crystal packing and molecular arrangement within the structure. The structure solution which yielded reliable results was solved from the pawley fit of the high resolution synchrotron data by inputting all of the different possible conformations for the nicotinamide : succinic acid 1:1 adduct as Z matrices. These models were refined to obtain an R-factor (measure of agreement between the model and the experimental data). Sixteen different possible conformations were identified; eight cocrystals and eight salts with the amide group and the heterocyclic nitrogen on the nicotinamide and carboxylic acid groups on the acid being altered (figure 7.5).

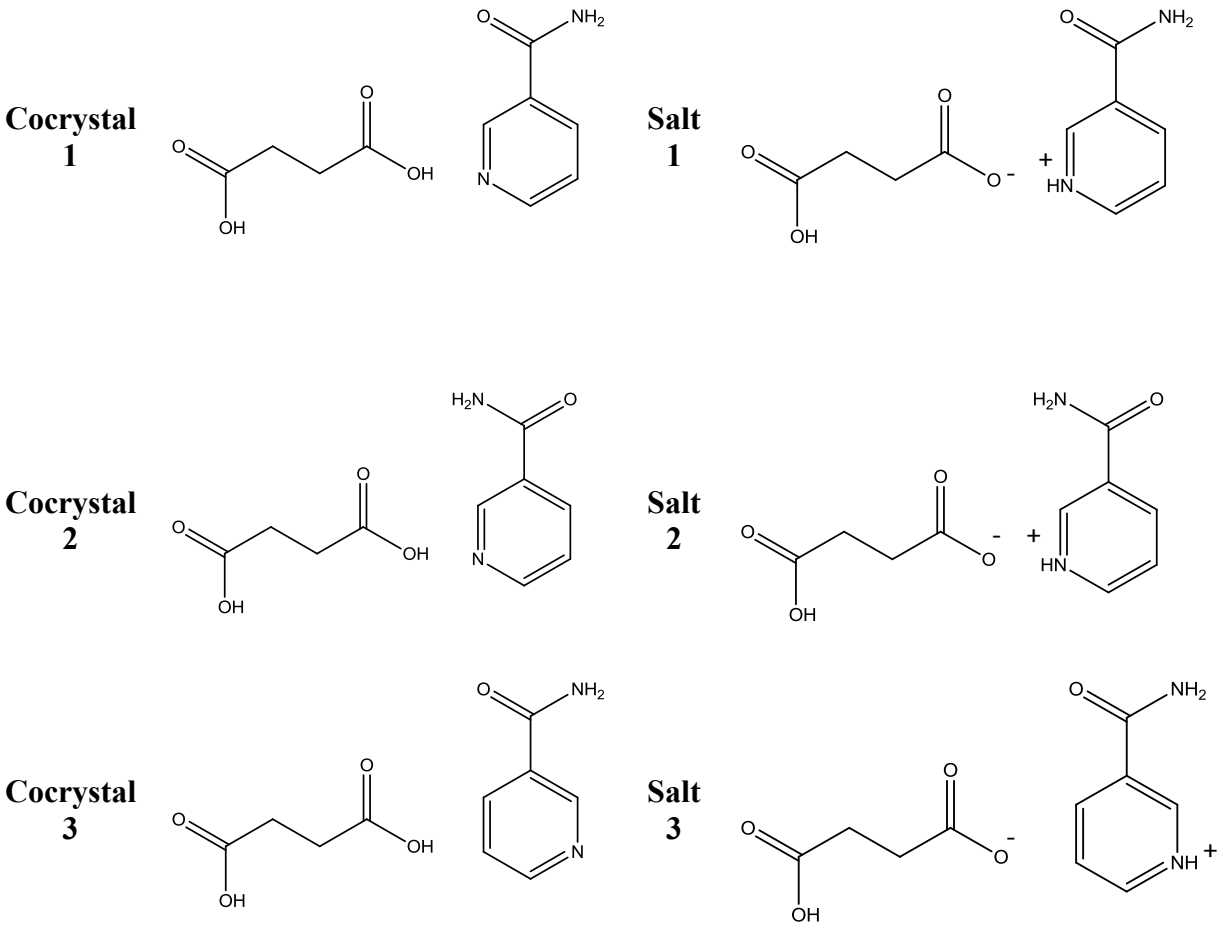

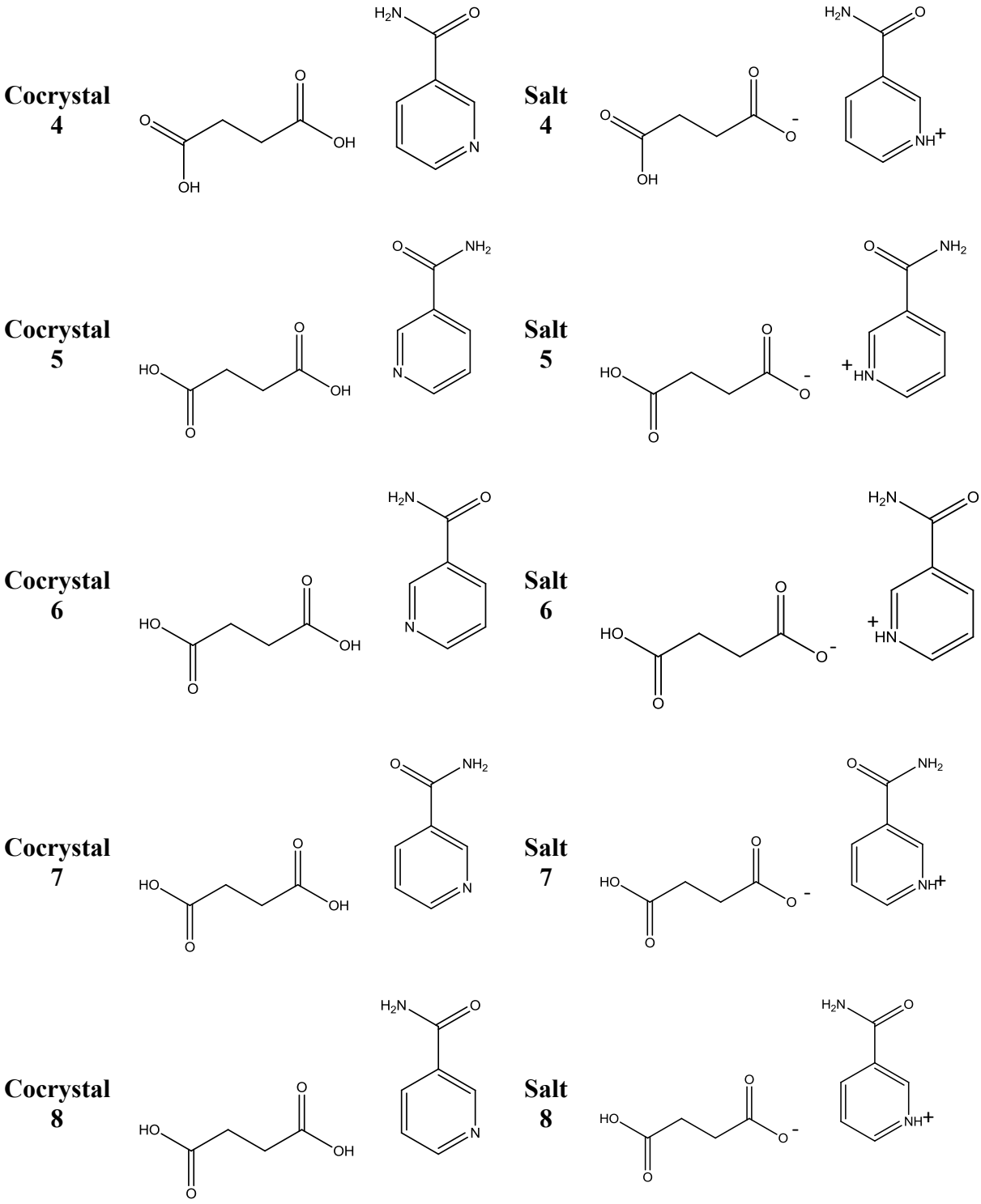

Figure 7.5: The sixteen possible cocrystal and salt conformations for nicotinamide : succinic acid 1:1

Restraints were applied to all bond lengths and angles to ensure the results were chemically sensible. Table 7.2 shows the resultant R factors for all sixteen conformational models.

Table 7.2: A table of R factors for all sixteen nicotinamide : succinic acid 1:1 conformations

Model	R_{wp}	Model	R_{wp}
Cocrystal 1	3.96	Salt 1	4.04
Cocrystal 2	4.77	Salt 2	4.95
Cocrystal 3	5.02	Salt 3	4.81
Cocrystal 4	5.63	Salt 4	5.46
Cocrystal 5	3.99	Salt 5	4.13
Cocrystal 6	4.64	Salt 6	4.81
Cocrystal 7	4.91	Salt 7	4.76
Cocrystal 8	5.37	Salt 8	5.46

Inspection of these results was initially done in groups of four (conformations 1-4 and 5-8) to enable the conformation of the nicotinamide molecule to be confirmed, in which the amide group and the position of the heterocyclic nitrogen was different (nicotinamide conformation the same for 1 and 5, 2 and 6, 3 and 7 and 4 and 8). The R factors for models 1 and 5 are the lowest in all four cases. Further confirmation of this being the correct nicotinamide model was obtained from removing the bond length restraints on the amide and pyridine ring with the results displayed in table 7.3.

Table 7.3: The amide and pyridine bond lengths for the different conformations of the nicotinamide molecule once the restraints on bond lengths were removed

Model	Amide bond length (Å)	Pyridine bond length (Å)	Conformation
Cocrystal 1	C=O 1.250 C-N 1.396	C-C 1.481 C-N 1.300 C-C 1.390 C-N 1.341 C-C 1.365	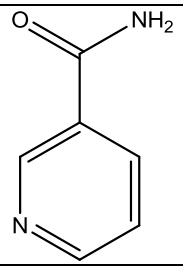
Cocrystal 2	C=O 1.422 C-N 1.162		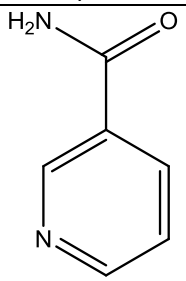
Cocrystal 3		C-C 1.275 C-N 1.435 C-C 1.299 C-N 1.411 C-C 1.380	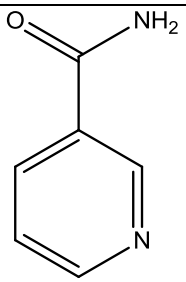

It was found that removing the bond length restraints for the amide group for model 2 that the C=O bond length elongated to a length more representative of a C-N and the opposite happens to the C-N, which contracts to a length more representative of a C=O. A similar elongation and contraction occurs to the C-N and C-C bond lengths around the pyridine ring in cocrystal 3 upon removal of the restraints in which the C-N bond lengths elongate to be more representative of C-C and the relevant two C-C bonds contract to be more representative of C-N.

The conformation of the succinic acid molecule was then able to be confirmed in a similar manner. From inspection of the R factors, cocrystal and salt 1 have lower values than the

respective cocrystal and salt 5 models. Removal of the bond length restraints found a contraction of C-OH and an elongation of C=O, table 7.4.

Table 7.4: The carboxylic acid bond lengths for the different conformations of the succinic acid molecule once the restraints on bond lengths were removed

Model	Carboxylic acid bond length (Å)		Conformation
Cocrystal 1	C=O C-OH	1.200 1.270	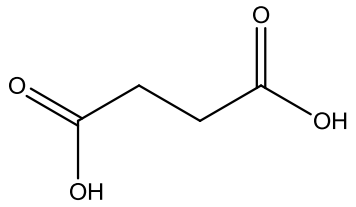
Cocrystal 5	C=O C-OH	1.302 1.161	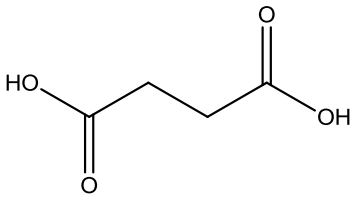

The remaining unknown with this structure is whether it is a cocrystal or salt? Inspection of the R factors indicate that it is a cocrystal, however when removing the restraints on this hydrogen atom, it sits equidistant to both the nicotinamide and succinic acid molecules. Solid state infrared spectroscopy data were collected although it was inconclusive. When considering all factors including the trend in all other nicotinamide : dicarboxylic acid adducts and the pK_a difference between the coformers (chapter 6, table 6.1) it has been deduced that the correct structure is that of model cocrystal 1.

7.2.4 Rietveld refinement

Rietveld refinement (section 2.2.6) was carried out after the structure solution, obtaining fully refined cell parameters, thermal parameters and bond lengths and angles (section 7.2.5).

Rietveld refinement was also carried out on the basic structure solution obtained from the le bail fit. The models were then manually changed so to 'test' the possible different conformations and obtain an R factors (table 7.5). The R factors for these results are all very close, and the lowest of indicates cocrystal 2 to be the correct model.

Table 7.5: Comparison of the R factors relating to each possible conformational model collected from the lab data

Model	R_{wp}
Cocrystal 1	0.1132
Cocrystal 2	0.1114
Cocrystal 3	0.1135
Cocrystal 4	0.1116

7.2.5 Structure description

An example of the numbering system used in this description can be seen in figure 7.6 with the crystallographic details, hydrogen bonding and selected bond lengths and angles given in tables 7.6, 7.7 and 7.8 respectively.

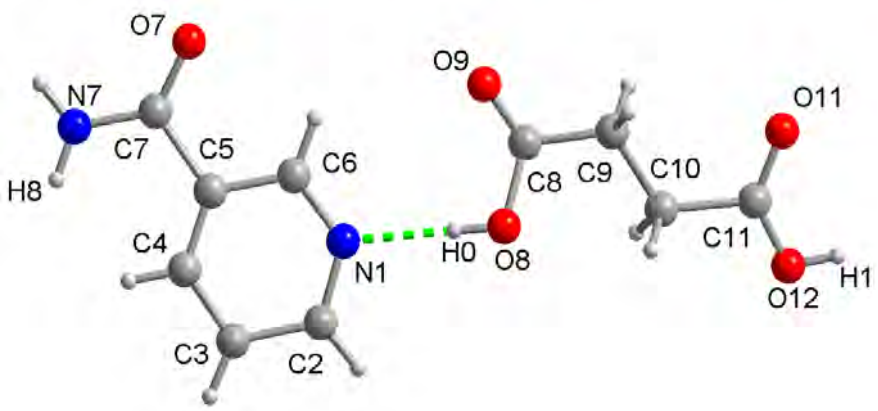

Figure 7.6: The numbering scheme used for the nicotinamide : succinic acid 1:1 structure description

Table 7.6: Refined cell parameters for nicotinamide : succinic acid, 1:1

Cocrystal	Nicotinamide : succinic acid
Formula	$(C_6H_6N_2O)(C_4H_6O_4)$
M_r	240.21
T (K)	298
Crystal system	Monoclinic
Space group	$P2_1/n$
a (Å)	10.49 (0.00014)
b (Å)	25.44 (0.00032)
c (Å)	5.02 (0.00006)
α (˚)	90
β (˚)	122.31 (0.00066)
γ (˚)	90
Z	2
2θ (˚)	3.37 - 25.02
Goodness of fit	1.077
Final R_1 and wR_2	0.0557, 0.1184
R_1 (all data)	0.0901

Table 7.7: Intermolecular hydrogen bonding (Å and °) in nicotinamide : succinic acid, 1:1

D-H...A	D(D-H)	D(H...A)	D(D...A)	<(DHA)
O8-H0...N1	0.84	1.86	2.70	177
N7-H7...O11^{i}	0.88	2.11	2.94	159
O12-H11...O7^{i}	0.84	1.78	2.7	167
N7-H8...O9^{ii}	0.88	2.14	2.99	165

Table 7.8: Selected intramolecular bond lengths and angles in nicotinamide : succinic acid, 1:1

Bond length	Bond length (Å)	Angle	Angle (°)
C7-O7	1.250	O7-C7-N7	126.82
C7-N7	1.371	O9-C8-O8	125.00
C8-O8	1.377	O11-C11-O12	125.95
C8-O9	1.150	C4-C5-C7-O7	170.01
C11-O11	1.200	O9-C8-C9-C10	170.00
C11-O12	1.207	O12-C11-C10-C9	170.69

The distinctive supramolecular chain motif is formed by alternating nicotinamide and succinic acid molecules involved in three intermolecular interactions; one of which is a hard hydrogen bond between the heterocyclic nitrogen and the acid, more specifically O8 acts as a hydrogen bond donor via H0 to N1. Each nicotinamide molecule interacts with a second succinic acid molecule to form a $R_2^2(8)$ acid-amide synthon in which the amide nitrogen N7 acts as a donor via H7 to the carboxyl oxygen O11, whilst the amide oxygen O7 accepts a second hydrogen bond from the other carboxyl oxygen O12 via H11 (figure 7.7). The nicotinamide molecules within the chain all face the same direction with the amide groups alternating between pointing up and down.

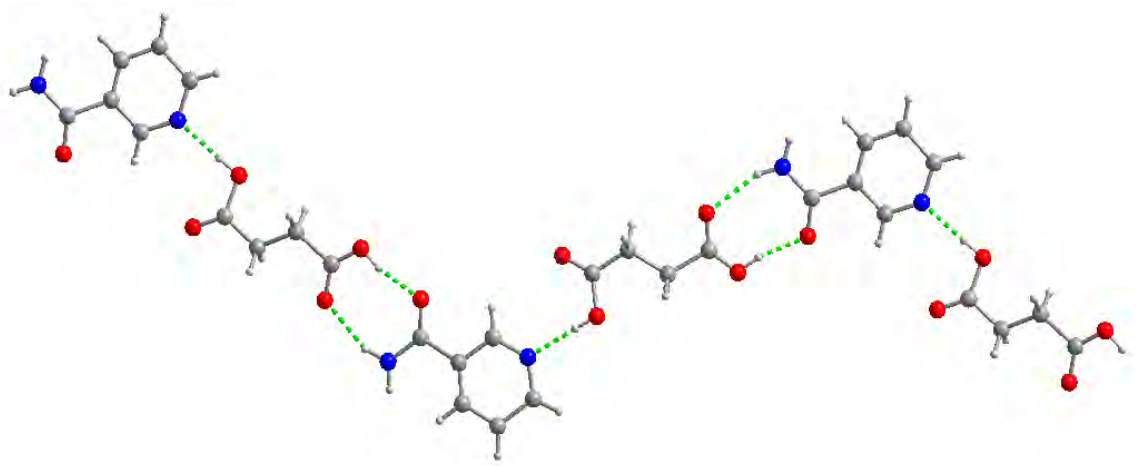

Figure 7.7: A view of the chain formed by alternating nicotinamide and succinic acid molecules. Hydrogen bonds are shown as dashed lines

These infinite chains are linked through a second complementary N-H…O interaction formed by N7 through H8 to O9 resulting in the formation of a corrugated hydrogen bonded sheet (figure 7.8). In the different chains of this corrugated sheet the nicotinamide molecules face the opposite way from one another.

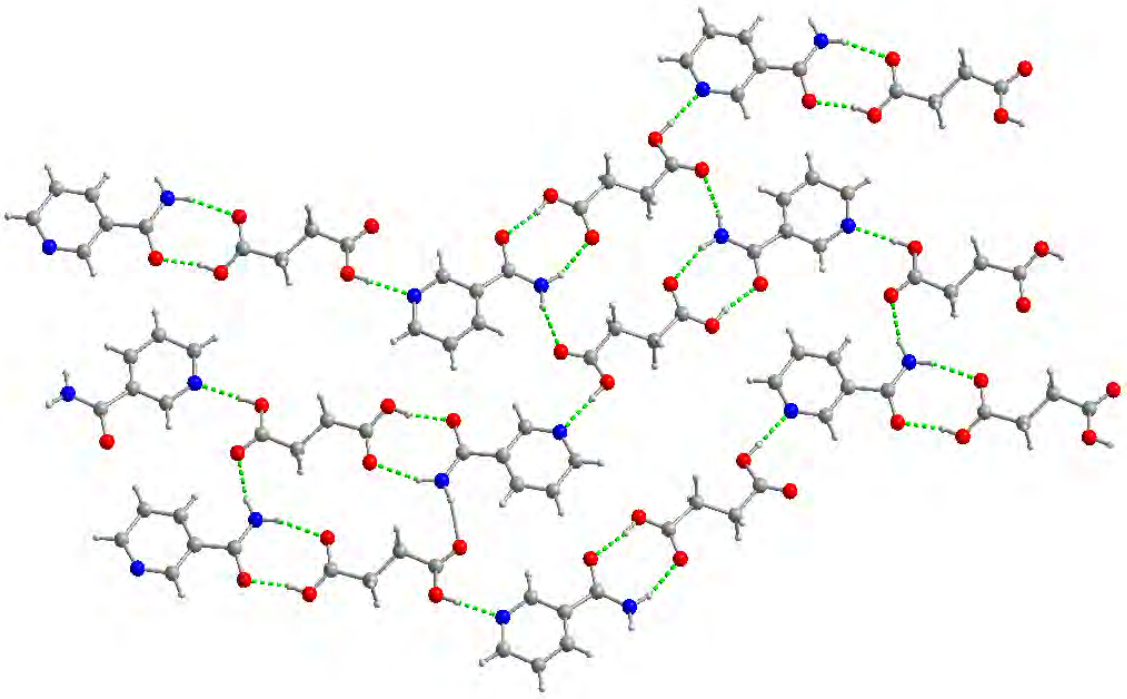

Figure 7.8: A view of the hydrogen bonded sheet formed by the chains linking via hard hydrogen bonds. Hydrogen bonds are represented by dashed lines

All hydrogen bond donors and acceptors are utilised within this structure, which contains the acid-pyridine and acid-amide synthons expected for a 1:1 nicotinamide : dicarboxylic acid cocrystal (chapter 6).

7.3 Nicotinamide : fumaric acid

Upon the success of the structure solution of the unknown nicotinamide : succinic acid 1:1 cocrystal, structure solution of the known nicotinamide : fumaric acid structure was attempted.

7.3.1 Pattern decomposition

A good quality pawley fit was obtained from room temperature data of nicotinamide : fumaric acid. The specific sample used was one that was synthesised with maleic acid, undergoing isomerisation in the cocrystallisation process (section 6.3). The cell parameters after the pawley fit refinements are shown in table 7.9.

Table 7.9: The refined pawley fit unit cell for nicotinamide : fumaric acid, 1:1

Parameter	Nicotinamide : fumaric acid
a (Å)	5.5629
b (Å)	13.8113
c (Å)	14.3808
α (º)	90
β (º)	93.5493
γ (º)	90
Space group	P21/*c*

7.3.2 Structure solution

The structure of nicotinamide : fumaric acid 1:1 has previously been reported[1] and is known to form infinite chains of alternating nicotinamide and acid molecules that link to form hydrogen bonded sheets (appendix 22.4).

Sixteen different conformational models were identified for nicotinamide : fumaric acid 1:1 (figure 7.9), though it is known from the previously reported single crystal structure that it is a cocrystal with the conformation of the nicotinamide and fumaric acid being that of model 1[1].

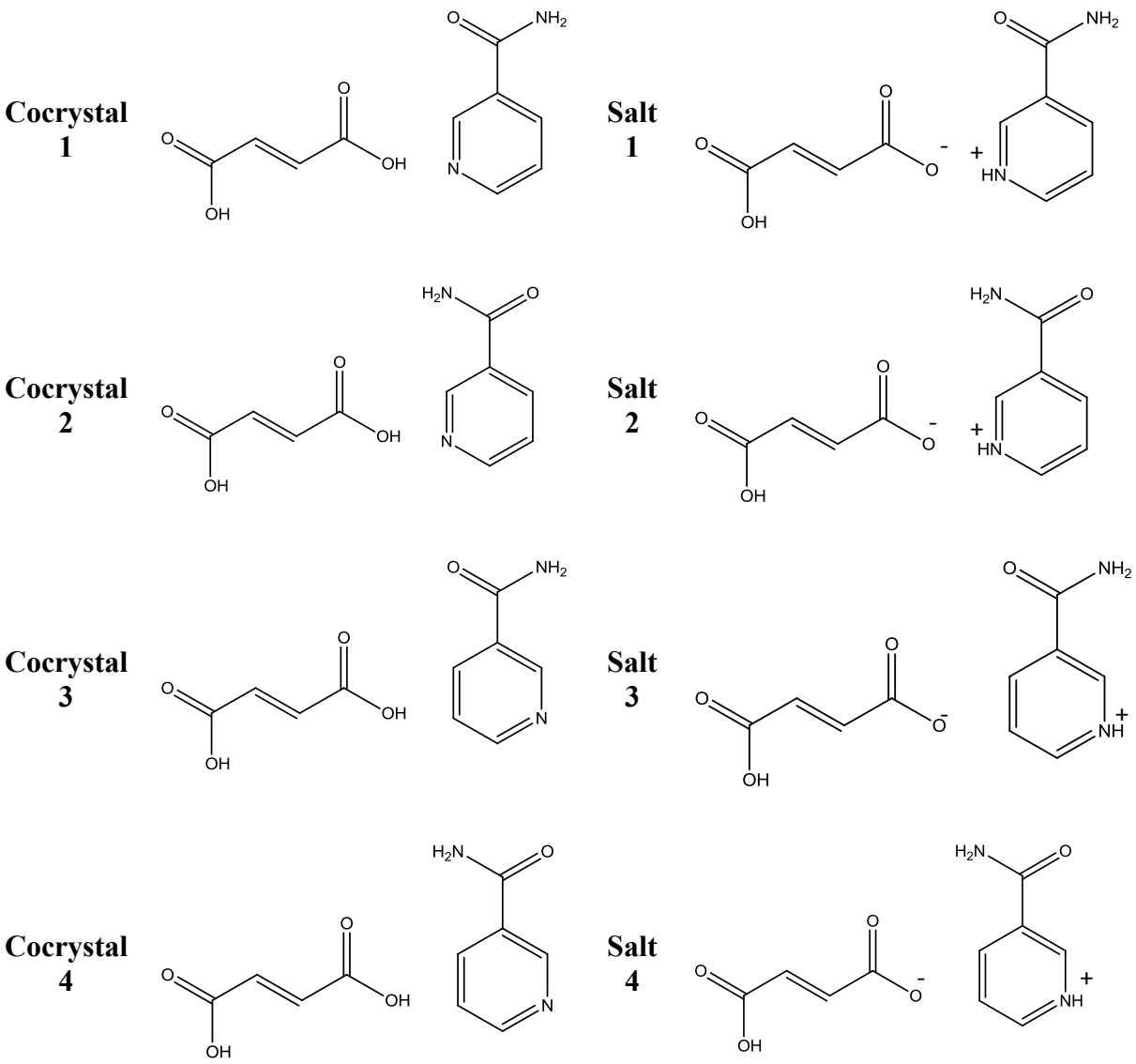

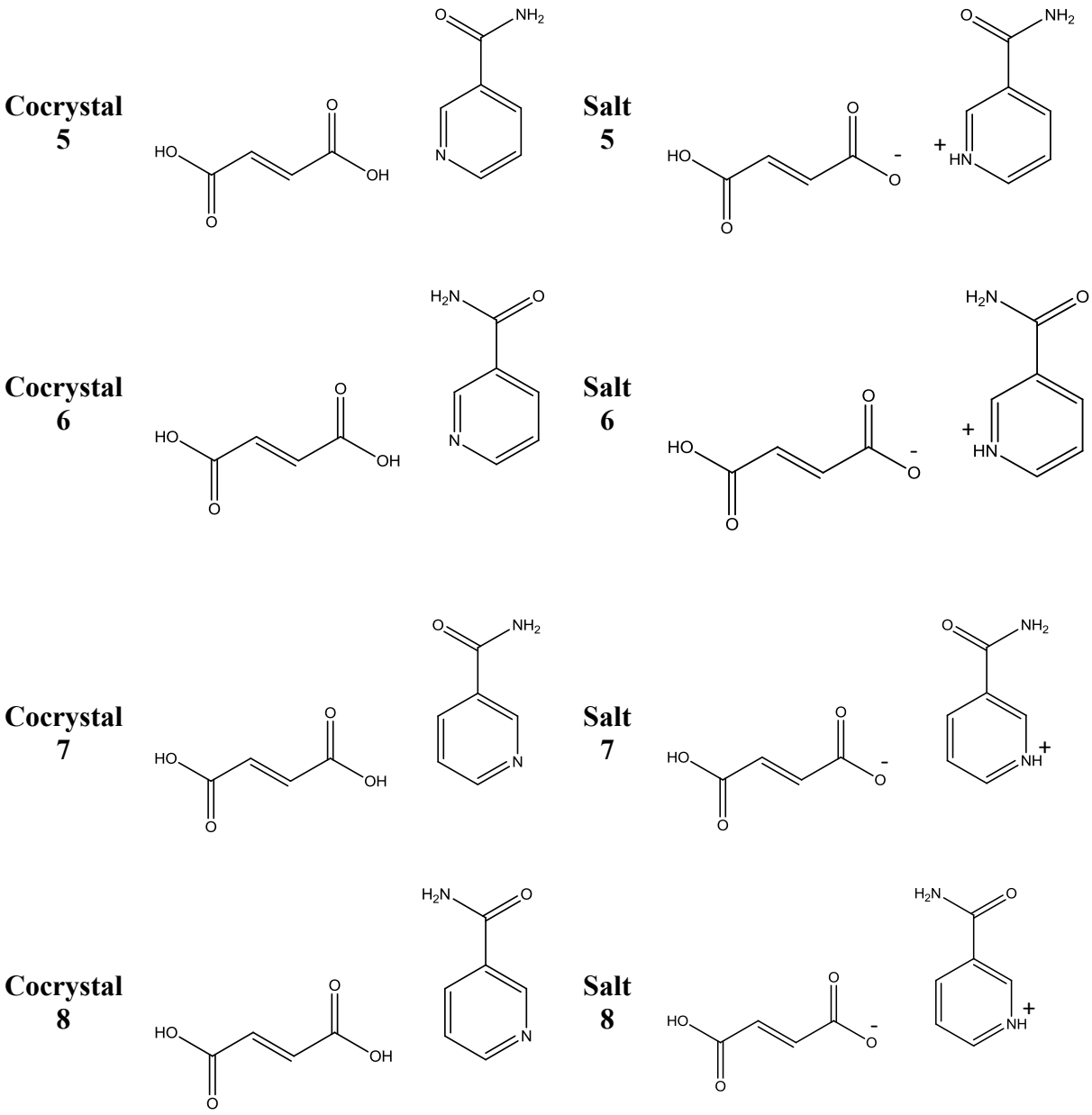

Figure 7.9: The sixteen possible cocrystal and salt conformations for nicotinamide : fumaric acid 1:1

All of the conformational models above were used as Z-matrices in sixteen different structure solutions with R factors collected (table 7.10). Like with nicotinamide : succinic acid, restraints were placed on all of the bond lengths and angles.

Table 7.10: A table of R factors for all sixteen nicotinamide : fumaric acid 1:1 conformations

Model	R_{wp}	Model	R_{wp}
Cocrystal 1	9.89	Salt 1	9.76
Cocrystal 2	10.50	Salt 2	10.31
Cocrystal 3	10.41	Salt 3	10.55
Cocrystal 4	11.22	Salt 4	11.42
Cocrystal 5	9.63	Salt 5	9.57
Cocrystal 6	10.14	Salt 6	10.08
Cocrystal 7	10.43	Salt 7	10.52
Cocrystal 8	11.13	Salt 8	11.36

As previously mentioned, it is known from the single crystal structure that nicotinamide : fumaric acid is a cocrystal and has the conformation seen in model 1. The resultant R factors do not fully represent this, with cocrystal and salt 5 having lower values than model 1 and that of the salt being slightly lower, although the R factors of these four models (cocrystals 1 and 5 and salts 1 and 5) are all very close. Once again the bond lengths were studied and bond length restraints removed to further confirm the conformation of nicotinamide and to obtain a clearer idea about the fumaric acid molecule (tables 7.11 and 7.12 respectively).

Table 7.11: The amide and pyridine bond lengths for the different conformations of the nicotinamide molecule once the restraints on bond lengths were removed

Model	Amide bond length (Å)	Pyridine bond length (Å)	Conformation
Cocrystal 1	C=O 1.220 C-N 1.330	C-C 1.399 C-N 1.310 C-C 1.360 C-N 1.350 C-C 1.360	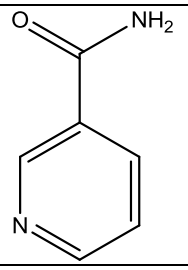
Cocrystal 2	C=O 1.160 C-N 1.133		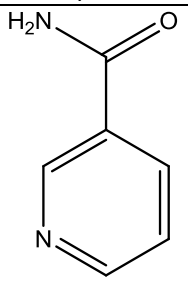
Cocrystal 3		C-C 1.195 C-N 1.448 C-C 1.307 C-N 1.354 C-C 1.329	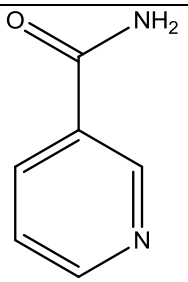

Table 7.12: The carboxylic acid bond lengths for the different conformations of the fumaric acid molecule once the restraints on bond lengths were removed

Model	Carboxylic acid bond length (Å)	Conformation
Cocrystal 1	C=O 1.215 C-OH 1.290	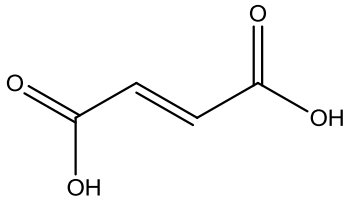
Cocrystal 5	C=O 1.199 C-OH 1.290	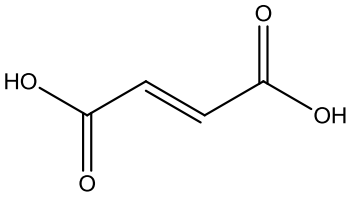

The bond lengths for the nicotinamide molecule have shown the same elongation and contraction that was found in the nicotinamide : succinic acid structure solution in which the bond length becomes more representative of its opposite. When inspecting the bond lengths of the fumaric acid molecule, we do not see this, concluding that with this dataset the method has not been as conclusive on the conformation of the acid molecule or the placement of the acidic proton.

7.3.3 Rietveld refinement

The final call parameters for nicotinamide : fumaric acid 1:1 after rietveld refinement are given in table 7.13 along with a comparison of the cell parameters obtained from single crystal analysis.

Table 7.13: The refined unit cell parameters for nicotinamide : fumaric acid, 1:1 compared to those obtained from single crystal analysis of the cocrystal 1 model

Parameter	Nicotinamide : fumaric acid from powder diffraction analysis	Nicotinamide : fumaric acid from single crystal analysis[3]
a (Å)	5.5627	5.550(1)
b (Å)	13.8108	13.792(1)
c (Å)	14.3811	14.360(2)
α (º)	90	90
β (º)	93.5549	93.41(1)
γ (º)	90	90
Space group	$P2_1/c$	$P2_1/c$

As the structure solution resulted in an incorrect model being the preferred one, R factors were obtained for all of the different conformational possibilities of nicotinamide : fumaric acid by entering the known atomic coordinates from the single crystal structure[1] and allowing them to refine within tight restraints. New atomic coordinates for the atoms that will be in different positions were calculated so that all sixteen models could be used. The results of this are given in table 7.14

Table 7.14: A table of R factors for all sixteen nicotinamide : fumaric acid 1:1 conformations using atomic coordinates

Model	**R_{wp}**	**Conformation**	**R_{wp}**
Cocrystal 1	9.32	Salt 1	9.27
Cocrystal 2	9.74	Salt 2	9.73
Cocrystal 3	9.77	Salt 3	9.67
Cocrystal 4	10.51	Salt 4	10.41
Cocrystal 5	9.79	Salt 5	9.75
Cocrystal 6	9.82	Salt 6	9.80
Cocrystal 7	10.36	Salt 7	10.10
Cocrystal 8	10.63	Salt 8	10.52

This has resulted in the correct conformational model of both the nicotinamide and fumaric acid molecules having the lowest R factors, though the salt versus cocrystal result is still questionable.

7.3.4 Low temperature data

The room temperature data resulted in the best R factor for a model with the correct conformation of nicotinamide molecule but incorrect fumaric acid conformation therefore both of the above methods (z matrix of all conformations as method 1 and refinement of atomic positions from single crystal structure being method 2) were applied to the low temperature high resolution data. The resulting R factors for both methods are given in table 7.15.

Table 7.15: A table of R factors for all sixteen nicotinamide : fumaric acid 1:1 conformations using method 1 (z matrices of all conformational models) and method 2 (atomic positions from the single crystal structure)

Model	R_{wp} method 1	R_{wp} method 2	Model	R_{wp} method 1	R_{wp} method 2
Cocrystal 1	8.34	9.54	Salt 1	8.33	9.53
Cocrystal 2	9.17	10.49	Salt 2	9.08	10.39
Cocrystal 3	8.83	10.10	Salt 3	8.99	10.29
Cocrystal 4	9.87	11.30	Salt 4	10.04	11.49
Cocrystal 5	8.35	9.55	Salt 5	8.37	9.58
Cocrystal 6	9.03	10.34	Salt 6	9.04	10.34
Cocrystal 7	9.04	10.35	Salt 7	9.16	10.49
Cocrystal 8	9.92	11.35	Salt 8	9.96	11.40

As can be seen from these results the R factors for models 1 and 5 are again very close, though this data has a better R factor for model 1 compared to 5 in both structure solution methods. Both the nicotinamide and fumaric acid conformations are correct though the position of the acidic proton is unconfirmed as the structure is known to be a cocrystal and these results indicate a salt. The refined unit cell parameters for the low temperature data are shown in table 7.16 along with those obtained from the room temperature data and single crystal structure.

Table 7.16: The refined unit cell parameters for nicotinamide : fumaric acid, 1:1 compared to those obtained from single crystal analysis

Parameter	Nicotinamide : fumaric acid low temperature	Nicotinamide : fumaric acid room temperature	Nicotinamide : fumaric acid from single crystal analysis[1]
a (Å)	5.5221	5.5627	5.550(1)
b (Å)	13.7652	13.8108	13.792(1)
c (Å)	14.1250	14.3811	14.360(2)
α (º)	90	90	90
β (º)	92.2912	93.5549	93.41(1)
γ (º)	90	90	90
Space group	$P2_1/c$	$P2_1/c$	$P2_1/c$

7.4 Discussion

Several conclusions can be drawn from this initial work in solving crystalline adducts from powder diffraction. The nicotinamide : succinic acid structure solution has shown the importance of collecting powder X-ray diffraction data from a synchrotron source and how much extra detail can be obtained from it particularly when comparing the results of this to the results obtained from the laboratory X-ray diffraction data.

It is clear from both systems studied that the location of the acidic proton is not able to be reliably confirmed from this method alone, it will require further analysis by either solid state infrared spectroscopy, studying the COOH and NH bands or NMR spectroscopy.

The nicotinamide : fumaric acid system shows the differences between low temperature and room temperature, in this case with the low temperature data being more reliable.

7.5 Footnote

The nicotinamide : succinic acid, 1:1 structure will be drafted into a communication paper for publication.

7.6 References

1. L. Orola and M. V. Veidis, *CrystEngComm.*, 2009, 11(3), 415

2. K. D. M. Harris and M. Tremayne, *Chem.Mater.*, 1996**, 8**(11), 2554

3. A. C. Larson and R. B. Von Dreele, *General Structure Analysis System (GSAS),* Los Alamos National Labouratory Report LAUR 86-748, Los Alamos. New Mexico, USA, 1994

4. A. LeBail and A. Jouanneaux, *J. Appl. Crystallogr.*, 1997, **30**, 265

5. G. S. Pawley, *J. Appl. Cryst.*, 1981, **14**, 357

8. Conclusions and further work

The work presented and discussed in this thesis has covered a variety of areas within crystallography, more specifically, molecular crystallography. A number of results have been generated that have enabled better understanding and provided advances in certain subject areas.

It has been shown that in certain structures studied within this project that it is possible to link the properties of the crystalline adduct with their relative coformers, a significant advantage for the pharmaceutical industry in which the requirement of optimal physical properties is vital. The continuation of this section of the project will include obtaining measurements for other physical properties (e.g. solubility) and comparing the results to that of their relative coformers, providing further evidence that the properties of a cocrystal can be tuned from those of the coformers.

Chapter four presented the structures of several new adenine cocrystals and salts to add to the relatively short list of previously reported adenine adducts. It yielded some very interesting results with the adenine undergoing tautomerisation in some structures and the existence of a vast number of hydrogen bonding motifs. This area of research has room for further developments. Single crystals were not obtained for all adducts, therefore there are still structures yet to be solved. It would also be interesting to try multiple different cocrystallisation methods to investigate whether it is possible to obtain anhydrous forms of all of the structures and to determine whether tautomerisation would occur in different conditions.

It has been shown from the initial work completed in this project that it is possible to solve a cocrystal structure from powder diffraction data, though it did have some problems. In both

the nicotinamide : succinic acid and nicotinamide : fumaric acid structure the relative placing of the acidic proton was not easily obtained. The nicotinamide : fumaric acid dataset had further problems with the wrong model being obtained in the initial stages. This work needs to be continued with significantly more datasets to ensure that this method is reliable and other complementary techniques need to be utilised to aide the salt or cocrystal problem.

In conclusion this project has been successful in making advances and further confirming certain hypotheses that have been previously reported along with initiating exciting areas of research within small molecule crystallography.

9. Appendices

Appendix 1:

1.1: Table of adenine complexes known to date and their relative tautomeric forms

9*H*

CSD code	Chemical	Tautomers	References
ADRBFT10	Adenine-riboflavin trihydrate	9H	1
BETNOD	tris(Adenine) phthalic acid hexahydrate	9H 1H9H	2
BIGHIJ	Diaqua-bis(quinoline-2-carboxylato)-manganese bis(adenine)	9H	3
CODYOJ	Adenine hydrochloride hemihydrate	9H	4
COFBUU	Adenine bis(N-methyl-2-pyrrolidone)	9H	5
COFBUU10	Adenine bis(N-methyl-2-pyrrolidone)	9H	6
DXCADM10	Deoxycorticosterone-adenine monohydrate	9H	7
EVIFIY	Adeninium adenine perchlorate dihydrate	9H 1H9H	8
FUSVAQ	Adenine trihydrate	9H	9
FUSVAQ01	Adenine trihydrate	9H	9
GUNQUB	bis(Adenine) hexahydroxytellurium tetrahydrate	9H	10
JOZZED	Adenine hydrogen peroxide	9H	11
LAFSUH	catena-(bis((m2-Oxalato)-aqua-adenine-cobalt(ii)) adenine solvate dihydrate)	9H	12
LAFTAO	catena-(bis((m2-Oxalato)-aqua-adenine-zinc(ii)) adenine solvate dihydrate)	9H	12
LOLCUL	bis(9H-Purin-6-amine) adipic acid methanol solvate	9H	13
MUBRAD	tris(2-Hydroxybenzoic acid) 9H-purin-6-amine	9H	14
NILNUS	(Adenin-7-yl)-(tris(2-aminoethyl)amino)-(perchlorato-O)-nickel adenine solvate	9H	15
TAZWOH	9H-purin-6-amine benzoic acid	9H	16
TAZWOH01	9H-Purin-6-amine bis(benzoic acid)	9H	13
VIGVEM	Adenine-adeninium tetrafluoroborate dihydrate	9H 1H9H	17
VILLIM	Hexa-aqua-magnesium(ii) diperchlorate bis(adenine)	9H	18
WUPGOE	5-Methylpyrimidine-2,4(1H,3H)-dione 9H-purin-6-amine dihydrate	9H	19
WUPGUK	5-Methylpyrimidine-2,4(1H,3H)-dione 9H-purin-6-amine tetrahydrate	9H	19
YUWMUY	Adenine 7-oxide monohydrate	9H	20
ZZZEGG	Adenine 1-N-oxide	9H	21
OYEFUU	Adeninium 2,6-dihydroxybenzoate monohydrate	9H	22

7H

CSD code	Chemical	Tautomers	References
SEGCOX	catena-(bis(m2-oxalato)-tetraaqua-di-manganese(ii) bis(adenine) dihydrate)Trichloroguaninium zinc	7H	23
VILLAE	Hexa-aqua-magnesium(ii) dichloride bis(adenine)	7H	18
VILLEI	Hexa-aqua-magnesium(ii) dibromide bis(adenine)	7H	18
PANSAA	6-Amino-9H-purin-1-ium hydrogen maleate hemikis(9H-purin-6-amine) monohydrate	7H 1H9H	24
ADAQCU	Diaqua-tetrakis(m2-adenine-N,N')-di-copper(ii) tetraperchlorate dihydrate	7H	25
PEKPEA	3-Adenyl-tris((2-aminoethyl)amine)-chloro-nickel(ii) chloride	7H	26
VILLOS	Tetra-aqua-bis(adenine)-manganese(ii) diperchlorate	7H	18
VILLUY	bis((m2-Aqua)-(m2-adenine-N,N'))-tetra-aqua-di-manganese(ii) tetranitrate dihydrate	7H	18

References

1. S. Fujii, K. Kawasaki, A. Sato, T. Fujiwara and K. I. Tomita, *Arch .Biochem. Biophys.*, 1977, **181**(2), 363
2. A. Takenaka and Y. Sasada, *Bull. Chem. Soc. Japan*, 1982, **55**(3), 680
3. D. Dobrzynska and L. B. Jerzykiewicz, *J. Am. Chem. Soc.*, 2004, **126**(36), 11118
4. M. D. Poojary and H. Manohar, *Acta Crystallogr. Sect. A*, 1984, **40**, C87
5. V. Langer and K. Huml, *Acta Crystallogr. Sect. A*, 1984, **40**, C86
6. V. Langer, K. Huml and J. Zachova, *Acta Crystallogr. Sect. C*, 1984, **40**, 2080
7. C. M. Weeks, D. C. Rohrer and W. L. Duax, *Science*, 1975, **190**(4219), 1096
8. V. Zelenak, Z. Vargova and I. Cisarova, *Acta Crystallogr. Sect. E*, 2004, **60**, O742
9. S. M. Tretjak, V. V. Mitkevich and L. F.Sukhodub, *Kristallografiya*, 1987, **32**(5), 1268
10. M. Driess, K. Merz and R. B. Rowlings, *Z. Anorg. Allg. Chem.*, 2001, **627**(2), 213-7.
11. M. A. Serra, B. K. Dorner and M. E. Silver, *Acta Crystallogr. Sect. C*, 1992, **48**, 1957
12. J. P. Garcia-Teran, O. Castillo, A. Luque, U. Garcia-Couceiro, P. Roman and F. Lloret, *Inorg. Chem.*, 2004, **43**(18), 5761
13. M. Byres, P. J. Cox, G. Kay and E. Nixon, *CrystEngComm.*, 2009, **11**(1), 135
14. L. C. Du, W. L .Zeng, X. Y. Liu and F. F. Jian, *Acta Crystallogr. Sect. E*,, 2009, **65**, O1791
15. K. Aoki, M. A. Salam, C. Munakata and I. Fujisawa, *Inorg. Chim. Acta.*, 2007, **360**(12), 3658
16. S. R. Perumalla, E. Suresh and V. R. Pedireddi, *Angew. Chem. Int. Ed.*, 2005, **44**(47), 7752
17. A. C. M. Young, J. C. Dewan and A. J. Edwards, *Acta Crystallogr. Sect. C*, 1991, **47**, 580
18. T. F. Mastropietro, D. Armentano, N. Marino and G. De Munno, *Polyhedron*, 2007, **26**(17), 4945
19. S. Chandrasekhar, T. R. R. Naik, S. K. Nayak and T. N. G.Row, *Bioorg. Med. Chem. Lett.*, 2010, **20**(12), 3530

20. T. Fujii, K. Ogawa, T. Saito, K. Kobayashi, T. Itaya and T. Date and K. Okamura *Chem. Pharm. Bull.*, 1995, **43**(1), 53
21. M. A. Stevens and G. B. Brown, *J. Am. Chem. Soc.*, 1958, **80**(11), 2759
22. J. C. Garcia-Ramos, A. Tovar-Tovar, J. Hernandez-Lima, F. Cortes-Guzman, R. Moreno-Esparza and L. Ruiz-Azuara, *Polyhedron*, 2011, **30**(16), 2697
23. J. P. Garcia-Teran, O. Castillo, A. Luque, U. Garcia-Couceiro, G. Beobide and P. Roman, *Dalton Trans.*, 2006, **7**, 902
24. C. McHugh and A. Erxleben. *Cryst.Grow.Des.*, 2011, **11**(11), 5096
25. A. Terzis, A. L. Beaucham and R. Rivest, *Inorg. Chem.*, 1973, **12**(5), 1166
26. A. Marzotto, D. A. Clemente, A. Ciccarese and G. Valle, *J. Cryst .Specrosc.*, 1993. **23**(2), 119

1.2: Table of adeninium complexes known to date and their relative tautomeric forms 1*H*,9*H*

CSD code	Chemical	Tautomers	References
ADALEW	Adenine (46,63-di-t-butyl-44,65-dimethyl-4,6(1,2)-dibenzena-1,3,2-dioxaphosphacyclohexaphane 2,2-dioxide) methanol solvate	1H9H	1
ADENBH	Adeninium hydrobromide hemihydrate	1H9H	2
ADENCH	Adenine hydrochloride hemihydrate	1H9H	3
ADENCH01	Adenine hydrochloride hemihydrate	1H9H	4
ADENCH02	Adenine hydrochloride monohydrate	1H9H	5
ADENCH03	Adenine hydrochloride hemihydrate	1H9H	6
ADENOH	bis(Adeninium nitrate) monohydrate	1H9H	7
ADENOH10	bis(Adeninium) dinitrate monohydrate	1H9H	7
ADENPH	Adeninium phosphate	1H9H	8
ADESUL	Adeninium hemisulfate monohydrate	1H9H	9
ADNCHG10	Adeninium catena(trichloro-mercury(ii)) sesquihydrate	1H9H	10
BOTSIN	9H-Adenin-1-ium oxalate hemikis(oxalic acid) monohydrate	1H9H	11
BUDJAM	Adeninium 3-carboxyanilinium diperchlorate trihydrate	1H9H	12
BUDVUR	Adenine 1-(2-carboxyethyl)-uracil	1H9H	13
BUDVUR10	Adenine 1-(2-carboxyethyl)-uracil	1H9H	14
CADENZO2	Trichloro-adeninium-zinc(ii)	1H9H	15
CADENZ10	Trichloro-adeninium-zinc	1H9H	16
CADENZ20	(Adeninium-N)-trichloro-zinc(ii)	1H9H	17
COFBUU10	Adeninium chloroacetate chloroacetic acid solvate	1H9H	18
EGOWIG	Adeninium aqua-(ethylenediamine-N,N,N'-triacetato-N'-acetic acid)-copper(ii) dihydrate	1H9H	19
GADPOS	catena-(bis(6-amino-9H-purine-1,7-diium) bis(m2-pyridine-2,3-dicarboxylato)-manganese(ii) tetrahydrate)	1H9H	20
IKAFOQ	6-amino-9H-purin-1-ium perchlorate	1H9H	21
LEZHIH	bis(Adenine) 7-hydroxy-8-(phenylazo)-1,3-naphthalene-disulfonate pentahydrate	1H9H	22
LICGIO	bis(adeninium) phthalate phthalic acid hydrate	1H9H	23
LOLDAS	Adeninium 2,6-dihydroxybenzoate	1H9H	24
LOLDEW	Adeninium 2,6-dihydroxybenzoate monohydrate	1H9H	24
LOLDIA	Adeninium 2-hydroxybenzoate methanol solvate	1 H9H	24
LOLDOG	Adeninium hydroxonium 3,5-dihydroxybenzoate hydroxide	1H9H	24
MUCCOD	Adeninium cytosinium sulphate	1H9H	25
RIGMEA	Adeninium phenylacetate phenylacetic acid monohydrate	1H9H	26
RIGMIE	Adeninium 3-carboxypropionate monohydrate	1H9H	26
SOLCOM	bis(Adeninium) aqua-bis(2-methylmalonato)-copper	1H9H	27
SOLCOM01	bis(adeninium) aqua-bis(methylmalonato)-copper(ii)	1H9H	28
SOLDAZ	catena-(bis(Adeninium) bis(m2-malonato)-copper dihydrate)	1H9H	27
SOLDAZ01	catena-[bis(Adeninium) bis(m2-malonato)-copper(ii)	1H9H	28

	dihydrate]		
TINYIZ	Bis(adeninium) chloranilate dihydrate	1H9H	29
TUDLOT	2-Aminopurinium 2-fluorobenzoate monohydrate	1H9H	30
UDIJEX	bis(1H,9H-Adeninium) aqua-bis(oxalato)-copper(ii)	1H9H	31
ZETGOU	bis(1H-Adeninium) pentachloroantimonate monohydrate	1H9H	32
ZETGUA	1H-Adeninium (propylen-1,2-diaminetetra-acetato)-antimony dihydrate	1H9H	32

3*H*,7*H*

CSD code	Chemical	Tautomers	References
UDIJIB	Bis(3H,7H-adeninium) diaqua-bis(oxalate)-cobalt (ii) dehydrate	3H7H	33
UDIJOH	Bis(3H,7H-adeninium) diaqua-bis(oxalate)-zinc (ii) dehydrate	3H7H	33

1*H*,7*H*

CSD code	Chemical	Tautomers	References
CUZGOT	6-Amino-8-mercaptopurinium chloride	1H7H	34
CUZGUZ	bis(6-Amino-8-mercaptopurinium) (6-amino-8-mercaptopurinium-S)-pentachloro-bismuth chloride pentahydrate	1H7H	34
CUZHAG	(6-Amino-8-mercaptopurinium) (6-amino-8-mercaptopurinium-S)-pentachloro-bismuth dihydrate	1H7H	34
OCIQUM	Adeninium tri-iodide di-iodine monohydrate	1H7H	35
PIDQIC	tetrakis(Adeninium) p-sulfonatocalix(4)arene tetradecahydrate clathrate	1H7H	36
BRADCU	Dibromo-di(adeninium) copper(ii) dibromide	1H7H	37

6*H*,9*H*

CSD code	Chemical	Tautomers	References
BEZSII	bis(Adeninium) hydrogen phosphate dihydrate	NH_3 9H	38
FESWUW	bis(Adeninium) (m2-hydrogen phosphato)-tetracosakis(m2-oxo)-dodecaoxo-dodeca-tungsten dimethylformamide solvate dihydrate	NH_3 9H	39

Mixture of tautomers

CSD code	Chemical	Tautomers	References
ADHCOS10	bis(Adeninium) trans-tetra-aqua-bis(adenine-N9)-cobalt(ii) sulfate hexahydrate	1H9H 7H	40
PANSAA	6-Amino-9H-purin-1-ium hydrogen maleate hemikis(9H-purin-6-amine) monohydrate	1H9H 7H	41
BETNOD	tris(Adenine) phthalic acid hexahydrate	1H9H 9H	42
EVIFIY	Adeninium adenine perchlorate dihydrate	1H9H 9H	43
VIGVEM	Adenine-adeninium tetrafluoroborate dihydrate	1H9H 9H	44
ADENZN	Trichloro-adeninium-zinc(ii) N7-H-adeninium chloride monohydrate	1H9H 1H7H	45
QUTJAR	(1H,9H)-Adeninium (3H,7H)-adeninium bis(pyridine-2,6-dicarboxylato)-copper(ii) trihydrate	1H9H 3H7H	46
QUTJEV	(1H,9H)-Adeninium (3H,7H)-adeninium bis(pyridine-2,6-dicarboxylato)-manganese(ii) trihydrate	1H9H 3H7H	46
QUTKEW	(1H,9H)-Adeninium (3H,7H)-adeninium tris(pyridine-2,6-dicarboxylato)-cerium tetrahydrate	1H9H 3H7H	46
APUHEZ	tris(adeninium) hexafluoro-aluminium hydrate	1H9H 3H7H	47

References

1. K. C. K. Swamy, S. Kumaraswamy and P. Kommana, *J. Am. Chem. Soc.*, 2001, **123**(50), 12642
2. V. Langer and K. Huml, *Acta Crystallogr. Sect. B*, 1978, **34**, 1881
3. J. M. Broomhead, *Acta Crystallogr.*, 1948, **1**(1-6), 324
4. W. Cochran *Acta Crystallogr.*, 1951, **4**(2), 81
5. T. J. Kistenma and T. Shigemat, *Acta Crystallogr. Sect. B*, 1974, **30**, 166
6. L. M. Cunane and M. R. Taylor, *Acta Crystallogr. Sect. B*, 1993, **49**, 524
7. B. E. Hingerty, J. R. Einstein and C. H. Wei, *Acta Crystallogr. Sect. B*, 1981, **37**, 140
8. V. Langer, K. Huml and J. Zachova, *Acta Crystallogr. Sect. B*, 1979, **35**, 1148
9. V. Langer, K. Huml and L. Lessinger, *Acta Crystallogr. Sect. B*, 1978, **34**, 2229
10. M. Authiermartin and A. L. Beauchamp, *Can. J. Chem*, 1975, **53**(15), 2345
11. B. Sridhar, K. Ravikumar and B. Varghese, *Acta Crystallogr. Sect. C*, 2009, **65**, O202
12. L. Bendjeddou, A. Cherouana, N. Hadjadj, S. Dahaoui and C. Lecomte, *Acta Crystallogr. Sect. E*, 2009, **65**, O2303
13. A. Takenaka, S. Fujita and Y. Sasada, *Nucl. Acid. S.*, 1982, **11**, 281
14. S. Fujita, A. Takenaka and Y. Sasada, *Bull. Chem. Soc. Japan*, 1983, **56**(8), 2234

15. P. T. Muthiah, S. K. Mazumdar and S. Chaudhuri, *J. Inorg. Bio.*, 1983, **19**(3), 237
16. M. R. Taylor, *Acta.Cryst.B*, 197, **29**, 884
17. M. R. Taylor, L. M.Vilkins and M. J. McCall, *Acta Crystallogr. Sect. C*, 1989, **45**, 1625
18. J. Maixner, J. Zachova and K. Huml, *Collect. Czech. Chem. Comm.*, 1993, **58**(4), 861
19. E. Serrano-Padial, D. Choquesillo-Lazarte, E. Bugella-Altamirano, A. Castineiras, R. Carballo and J. Niclos-Gutierrez, *Polyhedron*, 2002, **21**(14-15), 1451
20. B. Das, A. K. Boudalis and J. B. Baruah, *Inorg. Chem. Comm.*, 2010, **13**(11), 1244
21. H. K. Fun, J. H. Goh, A. C. Maity and S. Goswami, *Acta Crystallogr. Sect. E*, 2011, **67**, O427
22. W. H. Ojala, W. B. Gleason, T. I. Richardson and R. E. Lovrien, *Acta Crystallogr. Sect. C*, 1994, **50**, 1615
23. B. Sridhar and K. Ravikumar, *Acta Crystallogr. Sect. C*, 2007, **63**, O212
24. M. Byres, P. J. Cox, G. Kay and E. Nixon, *CrystEngComm.*, 2009, **11**(1), 135
25. A. Cherouana, R. Bousboua, L. Bendjeddou, S. Dahaoui and C. Lecomte, *Acta Crystallogr. Sect. E*, 2009, **65**, O2285
26. B. Sridhar and K. Ravikumar, *Acta Crystallogr. Sect. C*, 2007, **63**, O415
27. A. Castineiras, I. Garcia-Santos, J. M. Gonzalez-Perez and J. Niclos-Gutierrez, *Private Communication*, 2008
28. S. Perez-Yanez, O. Castillo, J. Cepeda, J. P. Garcia-Teran, A. Luque and P. Roman, *Eur. J. Inorg. Chem.*, 2009, **26**, 3889
29. K. Gotoh, R. Ishikawa and H. Ishida, *Acta Crystallogr. Sect. E*, 2007, **63**, O4433
30. J. JaiNhuknan, A. G. Karipides and J. S. Cantrell, *Acta Crystallogr. Sect. C*, 1997, **53**, 454
31. J. P. Garcia-Teran, O. Castillo, A. Luque, U. Garcia-Couceiro, G. Beobide and P. Roman, *Inorg. Chem.*, 2007, **46**(9), 3593
32. L. Zhi-Xian, T. Lian-Dong, H. Sheng-Zhi, J. Huaxue, *Chin. J. Struct. Chem*., 1995, **14**, 423, 1995
33. J. P. Garcia-Teran, O. Castillo, A. Luque, U. Garcia-Couceiro, G. Beobide and P. Roman, *Inorg. Chem.*, 2007, **46**(9), 3593
34. L. P. Battaglia and A. B. Corradi, *Dalton. Trans.*, 1984, **11**, 2401
35. Z. M. Wang, Y. J. Cheng, C. S. Liao and C. H. Yan, *CrystEngComm.*, 2001, **50**
36. J. L. Atwood, L. J. Barbour, E. S. Dawson, P. C. Junk and J. Kienzle, *Supramol. Chem.*, 1996, **7**(4), 271
37. P. D. Meester and A. C. Skapski, *Dalton. Trans*, 1973, 1596
38. R. J. Walker, P. Tollin and J. N. Low, *Cryst. Struct. Comm.*, 1982, **11**(2) 579
39. J. Li, Y. Fei Qi, Z. Han, E. Wang, J. Li, X. Wu, H. Wang, *Chem. Res. Chin. Univ.*, 2004, **20**,258
40. P. D. Meester and A. C. Skapski, *Dalton. Trans.*, 1973, **15**, 1596
41. C. McHugh and A. Erxleben. *Cryst. Growth .Des.*, 2011, **11**(11), 5096
42. A. Takenaka and Y. Sasada, *Bull. Chem. Soc. Japan*, 1982, **55**(3), 680
43. V. Zelenak, Z. Vargova and I. Cisarova, *Acta Crystallogr. Sect. E*, 2004, **60**, O742
44. A. C. M.Young, J. C. Dewan and A. J. Edwards, *Acta Crystallogr. Sect. C*, 1991, **47**, 580
45. M. R. Taylor and J. A. Westphalen, *Acta Crystallogr. Sect. A*, 1981, **37**, C63
46. B. Das and J. B. Baruah, *Cryst. Growth. Des.*, 2010, **10**(7), 3242
47. A. Cadiau, K. Adil, A. Hemon-Ribaud, M. Leblanc, A. Jouanneaux, A. M. Z.Slawin, P. Lightfoot and V. Maisonneuve, *Solid State Sciences*, 2011, **13**(1), 151

Appendix 2:

2.1.1: ^{1}H NMR spectra of adenine : malonic acid adduct synthesised from methanol (solvent – DMSO)

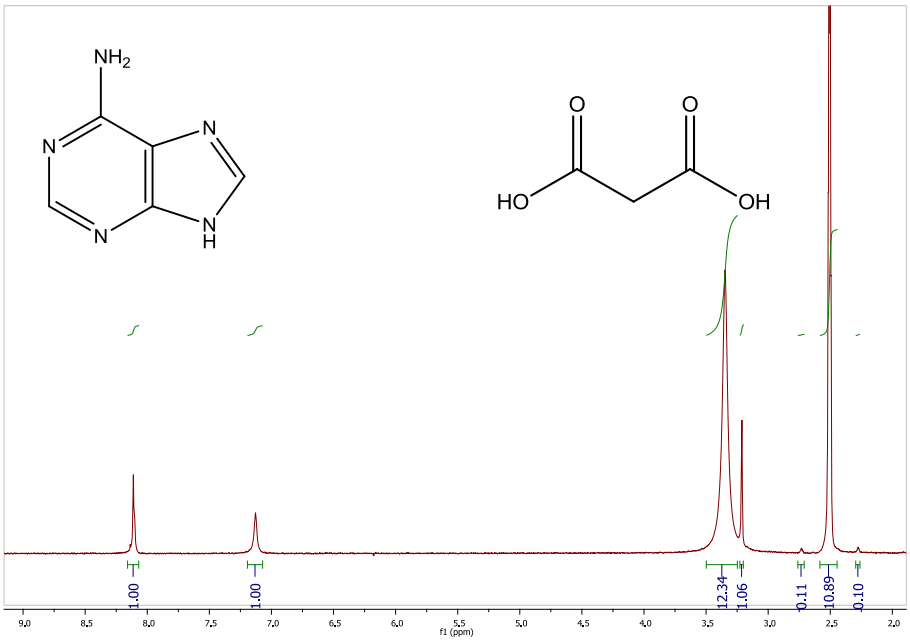

Adenine: 7.10 (2H,s), 8.10 (2H,d), 12.80 (1H,s),
Malonic acid: 3.2 (2H, s)

2.1.2: ^{1}H NMR spectra of adenine : malonic acid adduct synthesised from ethanol (solvent – DMSO)

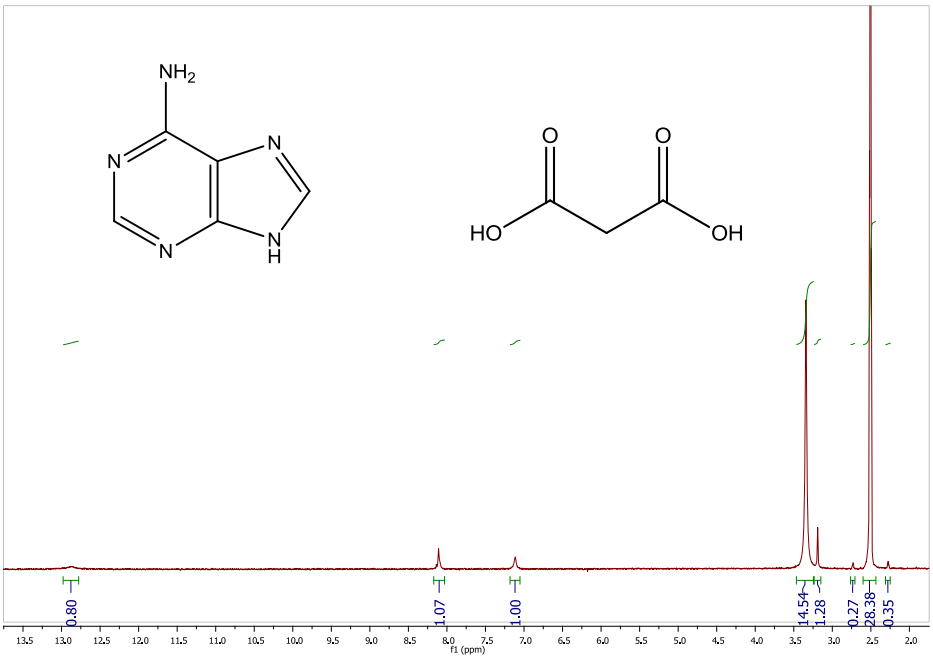

Adenine:	7.25 (2H,s),	8.20 (2H,d),	12.80 (1H,s)
Malonic acid:	3.25 (2H, s)		

2.2: The diffraction pattern simulated from the single crystal structure compared to that of the laboratory experimental powder diffraction pattern of adeninium : hydrogen malonate

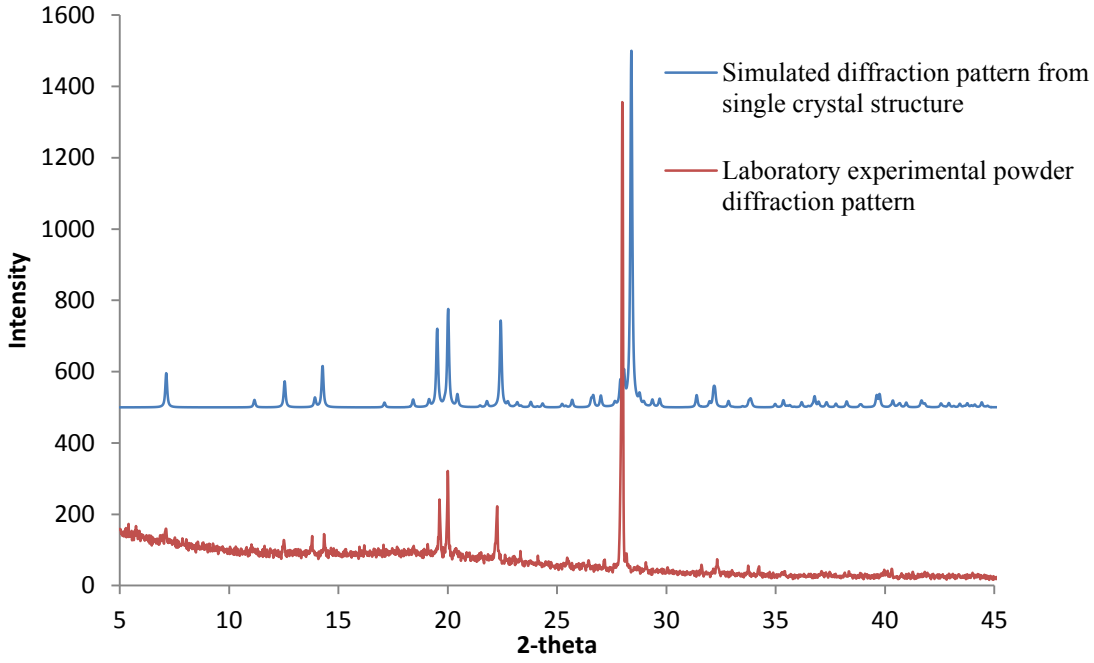

2.3: Ortep of adeninium : hydrogen malonate, 1:1

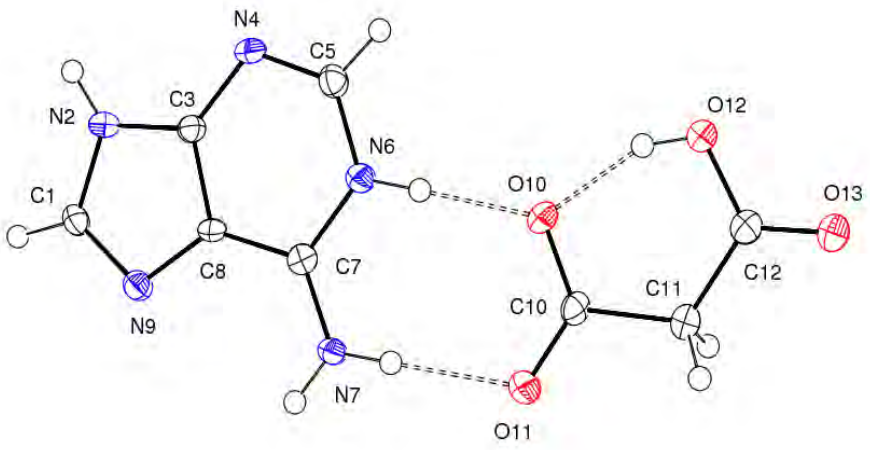

2.4: Crystallographic details of adeninium : hydrogen malonate, 1:1

Empirical formula	$C_8 H_9 N_5 O_4$	
Formula weight	239.20	
Temperature	120(2) K	
Wavelength	1.54184 Å	
Crystal system	Triclinic	
Space group	P -1	
Unit cell dimensions	a = 4.8942(3) Å b = 8.1034(4) Å c = 12.5052(6) Å	α = 82.944(3)° β = 86.677(3) ° γ = 79.855(4)°
Volume	484.17(4) $Å^3$	
Z	2	
Density (calculated)	1.641 Mg/m^3	
Absorption coefficient	1.159 mm^{-1}	
F(000)	248	
Crystal size	0.15 x 0.08 x 0.04 mm^3	
Theta range for data collection	6.97 to 70.03°.	
Index ranges	-5<=h<=5, -9<=k<=9, -14<=l<=14	
Reflections collected	4730	
Independent reflections	1725 [R(int) = 0.0288]	
Completeness to theta = 70.03°	94.6 %	
Absorption correction	Semi-empirical from equivalents	
Max. and min. transmission	0.9551 and 0.8453	
Refinement method	Full-matrix least-squares on F^2	
Data / restraints / parameters	1725 / 0 / 155	
Goodness-of-fit on F^2	1.168	
Final R indices [I>2sigma(I)]	R_1 = 0.0991, wR_2 = 0.2512	
R indices (all data)	R_1 = 0.1097, wR_2 = 0.2680	
Largest diff. peak and hole	2.005 and -0.567 $e.Å^{-3}$	

2.5: Intramolecular bond lengths (Å) and angles (°) in adeninium : hydrogen malonate, 1:1

Bond length (Å)		Bond length (Å)		Bond length (Å)	
C10-O11	1.248(4)	C1-N9	1.302(4)	C7-N7	1.302(4)
C10-O10	1.267(4)	C1-N2	1.370(4)	C7-N6	1.379(4)
C10-C11	1.525(4)	C1-H1	0.950	C7-C8	1.426(5)
C11-C12	1.518(5)	C3-N2	1.349(5)	C8-N9	1.375(4)
C11-H11A	0.990	C3-N4	1.368(4)	N2-H2	0.880
C11-H11B	0.990	C3-C8	1.394(5)	N6-H6	0.880
C12-O13	1.205(5)	C5-N4	1.310(4)	N7-H7A	0.880
C12-O12	1.319(4)	C5-N6	1.346(4)	N7-H7B	0.880
O12-H12	0.840	C5-H5	0.950		

Bond angle (°)		Bond angle (°)		Bond angle (°)	
O11-C10-O10	124.4(3)	N9-C1-N2	113.5(3)	N9-C8-C7	131.2(3)
O11-C10-C11	118.0(3)	N9-C1-H1	123.3	C3-C8-C7	118.2(3)
O10-C10-C11	117.6(3)	N2-C1-H1	123.3	C3-N2-C1	106.6(3)
C12-C11-C10	117.5(3)	N2-C3-N4	128.0(3)	C3-N2-H2	126.7
C12-C11-H11A	107.9	N2-C3-C8	105.4(3)	C1-N2-H2	126.7
C10-C11-H11A	107.9	N4-C3-C8	126.5(3)	C5-N4-C3	112.2(3)
C12-C11-H11B	107.9	N4-C5-N6	126.1(3)	C5-N6-C7	123.9(3)
C10-C11-H11B	107.9	N4-C5-H5	117.0	C5-N6-H6	118.0
H11A-C11-H11B	107.2	N6-C5-H5	117.0	C7-N6-H6	118.0
O13-C12-O12	120.7(3)	N7-C7-N6	120.5(3)	C7-N7-H7A	120.0
O13-C12-C11	122.4(3)	N7-C7-C8	126.6(3)	C7-N7-H7B	120.0
O12-C12-C11	116.9(3)	N6-C7-C8	113.0(3)	H7A-N7-H7B	120.0
C12-O12-H12	109.5	N9-C8-C3	110.5(3)	C1-N9-C8	104.0(3)

Torsion angle (°)		Torsion angle (°)	
O11-C10-C11-C12	-166.6(3)	N4-C3-N2-C1	178.8(3)
O10-C10-C11-C12	14.8(5)	C8-C3-N2-C1	-0.5(4)
C10-C11-C12-O13	166.9(3)	N9-C1-N2-C3	0.1(4)
C10-C11-C12-O12	-15.1(5)	N6-C5-N4-C3	-0.7(5)
N2-C3-C8-N9	0.6(4)	N2-C3-N4-C5	-179.6(3)
N4-C3-C8-N9	-178.6(3)	C8-C3-N4-C5	-0.5(5)
N2-C3-C8-C7	-178.2(3)	N4-C5-N6-C7	-0.2(5)
N4-C3-C8-C7	2.6(5)	N7-C7-N6-C5	-177.4(3)
N7-C7-C8-N9	-2.0(6)	C8-C7-N6-C5	2.2(5)
N6-C7-C8-N9	178.3(3)	N2-C1-N9-C8	0.2(4)
N7-C7-C8-C3	176.5(3)	C3-C8-N9-C1	-0.6(4)
N6-C7-C8-C3	-3.2(4)	C7-C8-N9-C1	178.0(3)

Appendix 3:

3.1: ^{1}H NMR spectra of adenine : succinic acid adduct (solvent – DMSO)

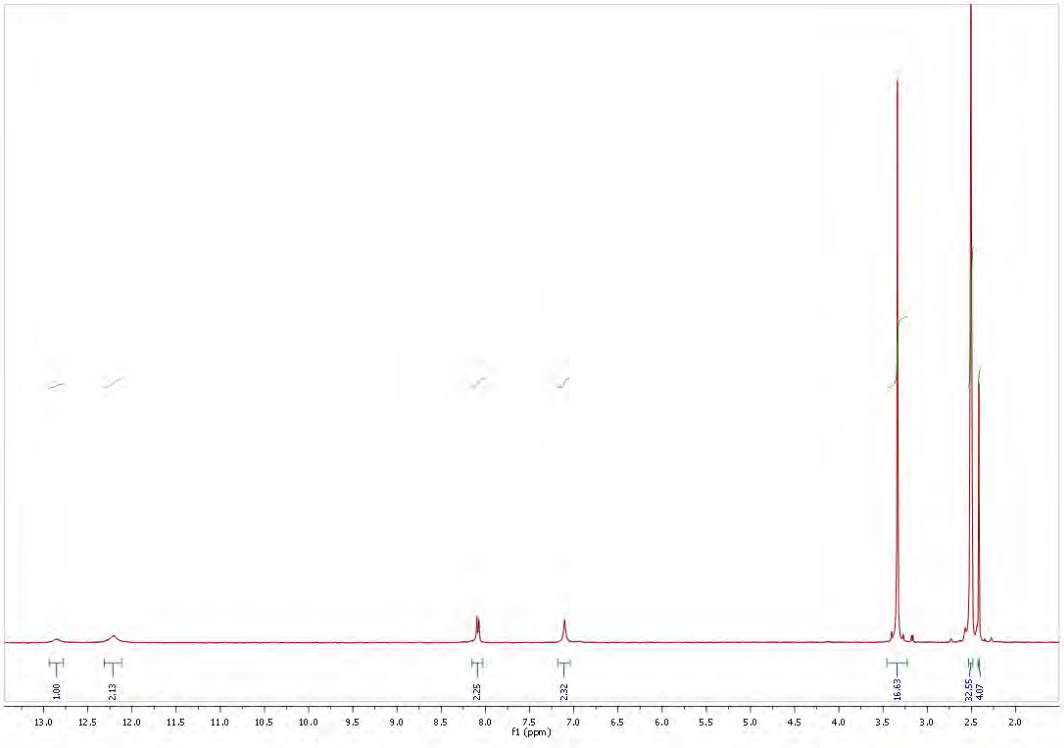

Adenine:	7.10 (2H,s),	8.10 (2H,d),	12.80 (1H,s)
Succinic acid:	2.42 (4H, s),	12.20 (2H, s)	

3.2: The diffraction pattern simulated from the single crystal structure compared to that of the laboratory experimental powder diffraction pattern of adenine : succinic acid

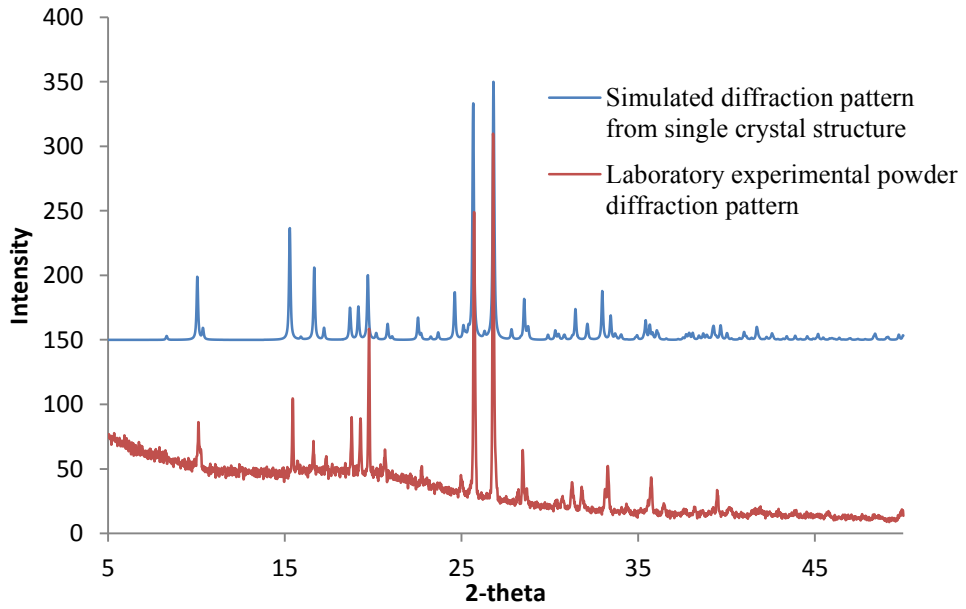

3.3: Ortep of adenine : succinic acid, 1:1

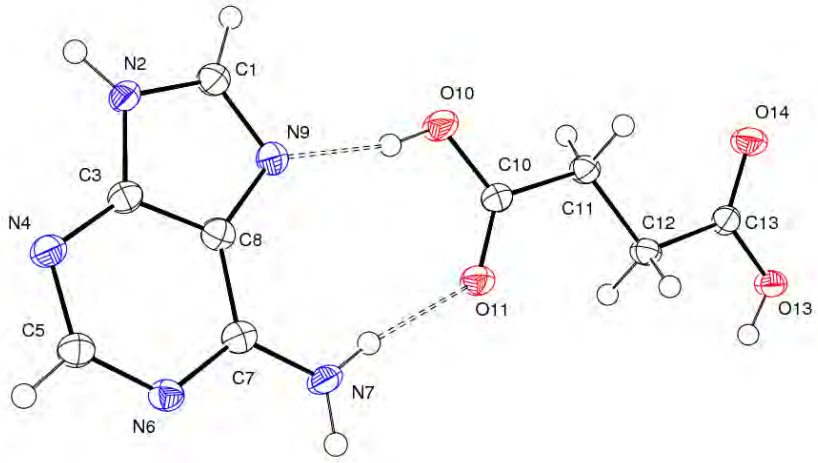

3.4: Crystallographic details of adenine : succinic acid, 1:1

Empirical formula	$C_9 H_{11} N_5 O_4$
Formula weight	253.23
Temperature	120(2) K
Wavelength	0.71073 Å
Crystal system	Monoclinic
Space group	$P2_1/n$
Unit cell dimensions	a = 9.4902(4) Å b = 5.3041(3) Å c = 21.2846(8) Å β = 92.398(3) °
Volume	1070.46(9) $Å^3$
Z	4
Density (calculated)	1.471 Mg/m^3
Absorption coefficient	0.126 mm^{-1}
F(000)	528
Crystal size	0.10 x 0.08 x 0.06 mm^3
Theta range for data collection	3.52 to 27.48°.
Index ranges	-12<=h<=12, -6<=k<=6, -27<=l<=27
Reflections collected	8933
Independent reflections	2426 [R(int) = 0.0485]
Completeness to theta = 27.48°	99.1 %
Absorption correction	Semi-empirical from equivalents
Max. and min. transmission	0.9925 and 0.9875
Refinement method	Full-matrix least-squares on F^2
Data / restraints / parameters	2426 / 0 / 165
Goodness-of-fit on F^2	1.114
Final R indices [I>2sigma(I)]	R_1 = 0.0586, wR_2 = 0.1123
R indices (all data)	R_1 = 0.0817, wR_2 = 0.1257
Largest diff. peak and hole	0.278 and -0.276 $e.Å^{-3}$

3.5: Intramolecular bond lengths (Å) and angles (°) in adenine : succinic acid, 1:1

Bond length (Å)		Bond length (Å)		Bond length (Å)	
C1-N9	1.324(3)	C7-N6	1.362(3)	C11-H11A	0.9900
C1-N2	1.351(3)	C7-C8	1.407(3)	C11-H11B	0.9900
C1-H1	0.9500	C8-N9	1.390(3)	C12-C13	1.509(3)
C3-N4	1.352(3)	N2-H2	0.8800	C12-H12A	0.9900
C3-N2	1.370(3)	N7-H7A	0.8800	C12-H12B	0.9900
C3-C8	1.382(3)	N7-H7B	0.8800	C13-O14	1.206(3)
C5-N4	1.325(3)	C10-O11	1.220(3)	C13-O13	1.330(3)
C5-N6	1.340(3)	C10-O10	1.304(3)	O10-H10	0.8400
C5-H5	0.9500	C10-C11	1.498(3)	O13-H13	0.8400
C7-N7	1.333(3)	C11-C12	1.526(3)		

Bond angle (°)		Bond angle (°)		Bond angle (°)	
N9-C1-N2	13.5(2)	C1-N2-C3	106.7(2)	C10-C11-H11B	108.9
N9-C1-H1	123.2	C1-N2-H2	126.7	C12-C11-H11B	108.9
N2-C1-H1	123.2	C3-N2-H2	126.7	H11A-C11-H11B	107.7
N4-C3-N2	27.4(2)	C5-N4-C3	111.1(2)	C13-C12-C11	111.7(2)
N4-C3-C8	126.8(2)	C5-N6-C7	119.2(2)	C13-C12-H12A	109.3
N2-C3-C8	105.8(2)	C7-N7-H7A	120.0	C11-C12-H12A	109.3
N4-C5-N6	28.6(2)	C7-N7-H7B	120.0	C13-C12-H12B	109.3
N4-C5-H5	115.7	H7A-N7-H7B	120.0	C11-C12-H12B	109.3
N6-C5-H5	115.7	C1-N9-C8	103.7(2)	H12A-C12-H12B	107.9
N7-C7-N6	119.9(2)	O11-C10-O10	122.8(2)	O14-C13-O13	119.8(2)
N7-C7-C8	122.8(2)	O11-C10-C11	124.0(2)	O14-C13-C12	123.2(2)
N6-C7-C8	117.2(2)	O10-C10-C11	113.1(2)	O13-C13-C12	117.0(2)
C3-C8-N9	110.3(2)	C10-C11-C12	113.5(2)	C10-O10-H10	109.5
C3-C8-C7	116.9(2)	C10-C11-H11A	108.9	C13-O13-H13	109.5
N9-C8-C7	132.7(2)	C12-C11-H11A	108.9		

Torsion angle (°)		Torsion angle (°)	
N4-C3-C8-N9	-179.3(2)	C8-C3-N4-C5	0.6(3)
N2-C3-C8-N9	0.0(3)	N4-C5-N6-C7	-0.9(4)
N4-C3-C8-C7	-1.1(4)	N7-C7-N6-C5	179.7(2)
N2-C3-C8-C7	178.2(2)	C8-C7-N6-C5	0.2(3)
N7-C7-C8-C3	-178.8(2)	N2-C1-N9-C8	0.6(3)
N6-C7-C8-C3	0.7(3)	C3-C8-N9-C1	-0.4(3)
N7-C7-C8-N9	-1.2(4)	C7-C8-N9-C1	-178.1(3)
N6-C7-C8-N9	178.3(2)	O11-C10-C11-C12	3.7(3)
N9-C1-N2-C3	-0.6(3)	O10-C10-C11-C12	-176.4(2)
N4-C3-N2-C1	179.6(2)	C10-C11-C12-C13	177.0 (2)
C8-C3-N2-C1	0.3(3)	C11-C12-C13-O14	12.6(3)
N6-C5-N4-C3	0.5(4)	C11-C12-C13-O13	-168.0(2)
N2-C3-N4-C5	-178.6(2)		

Appendix 4:

4.1: ^{1}H NMR spectra of adenine : fumaric acid adduct (solvent – DMSO)

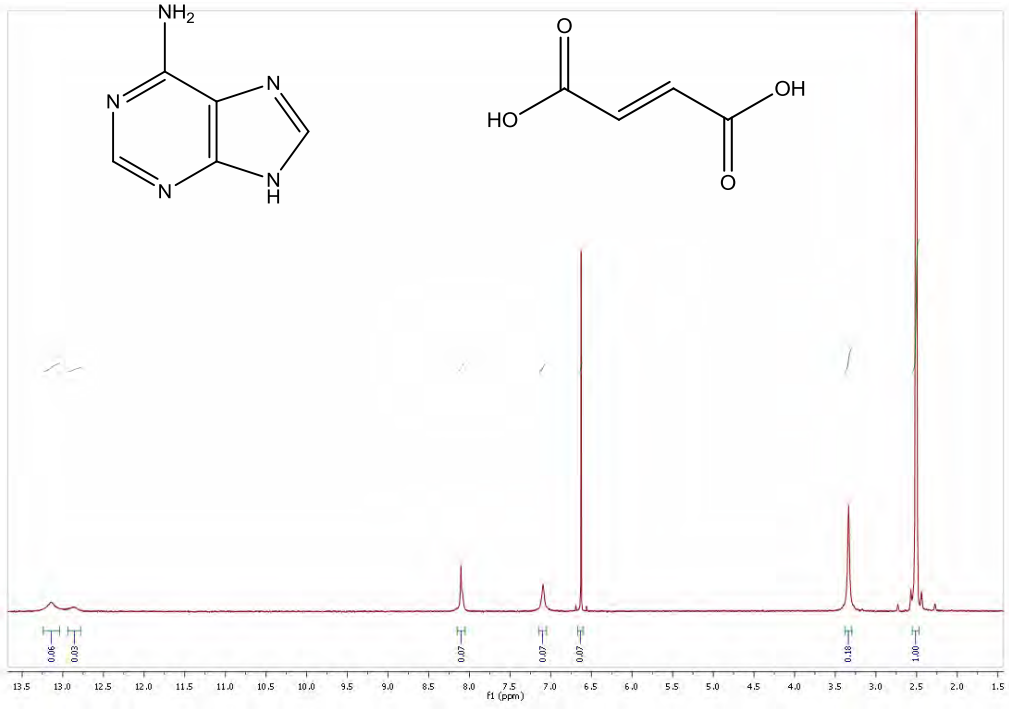

Adenine: 7.10 (2H,s), 8.10 (2H,d), 12.80 (1H,s)

Fumaric acid: 6.62 (2H, s), 13.20 (2H, s)

4.2: The diffraction pattern simulated from the single crystal structure compared to that of the laboratory experimental powder diffraction pattern of adeninium : hydrogen fumarate

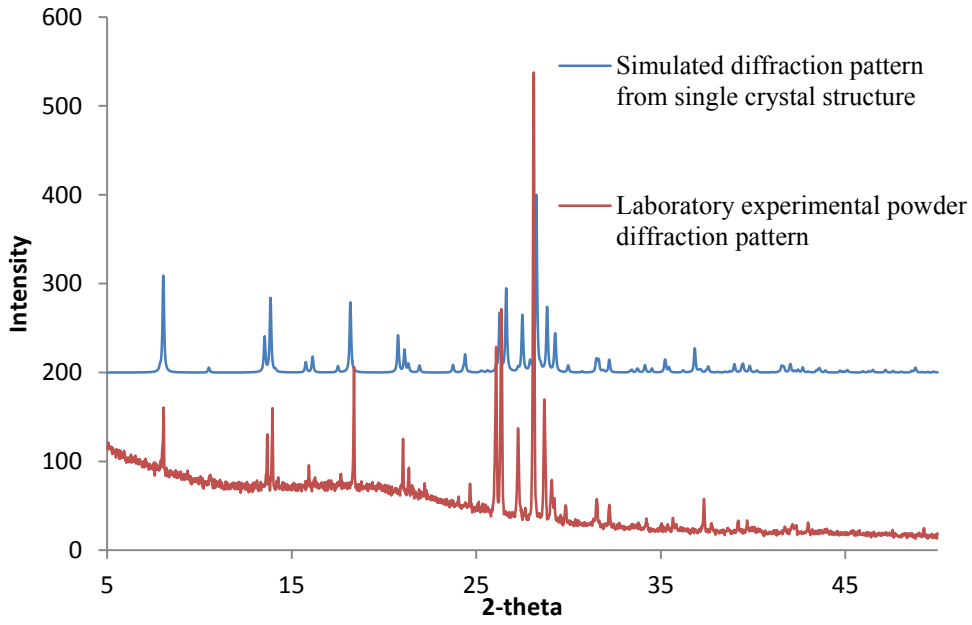

4.3: Ortep of adeninium : hydrogen fumarate, 1:1

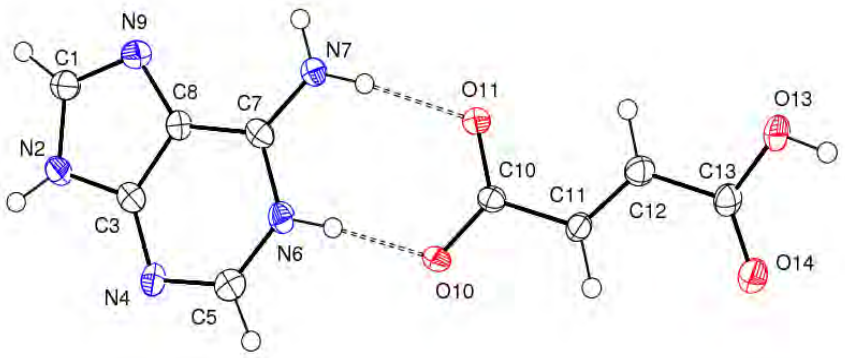

4.4: Crystallographic details of adeninium : hydrogen fumarate, 1:1

Empirical formula	$C_9 H_9 N_5 O_4$
Formula weight	251.21
Temperature	120(2) K
Wavelength	0.71073 Å
Crystal system	Monoclinic
Space group	$P2_1/c$
Unit cell dimensions	a = 3.6160(1) Å b = 13.0730(6) Å c = 22.0296(9) Å β = 94.633(3) °
Volume	1037.98(7) $Å^3$
Z	4
Density (calculated)	1.608 Mg/m^3
Absorption coefficient	0.130 mm^{-1}
F(000)	520
Crystal size	0.16 x 0.02 x 0.01 mm^3
Theta range for data collection	3.25 to 25.02°.
Index ranges	-4<=h<=4, -15<=k<=15, -26<=l<=26
Reflections collected	10663
Independent reflections	1872 [R(int) = 0.0778]
Completeness to theta = 25.02°	99.6 %
Absorption correction	Semi-empirical from equivalents
Max. and min. transmission	0.9987 and 0.9795
Refinement method	Full-matrix least-squares on F^2
Data / restraints / parameters	1872 / 0 / 166
Goodness-of-fit on F^2	1.114
Final R indices [I>2sigma(I)]	R_1 = 0.0574, wR_2 = 0.1071
R indices (all data)	R_1 = 0.0813, wR_2 = 0.1206
Largest diff. peak and hole	0.303 and -0.360 $e.Å^{-3}$

4.5: Intramolecular bond lengths (Å) and angles (°) in adeninium : hydrogen fumarate, 1:1

Bond length (Å)		Bond length (Å)		Bond length (Å)	
C1-N9	1.324(3)	C7-N6	1.362(3)	C11-H11A	0.9900
C1-N2	1.351(3)	C7-C8	1.407(3)	C11-H11B	0.9900
C1-H1	0.9500	C8-N9	1.390(3)	C12-C13	1.509(3)
C3-N4	1.352(3)	N2-H2	0.8800	C12-H12A	0.9900
C3-N2	1.370(3)	N7-H7A	0.8800	C12-H12B	0.9900
C3-C8	1.382(3)	N7-H7B	0.8800	C13-O14	1.206(3)
C5-N4	1.325(3)	C10-O11	1.220(3)	C13-O13	1.330(3)
C5-N6	1.340(3)	C10-O10	1.304(3)	O10-H10	0.8400
C5-H5	0.9500	C10-C11	1.498(3)	O13-H13	0.8400
C7-N7	1.333(3)	C11-C12	1.526(3)		

Bond angle (°)		Bond angle (°)		Bond angle (°)	
C1-N9	1.311(5)	C7-N7	1.309(5)	C10-O10	1.280(4)
C1-N2	1.370(5)	C7-N6	1.386(5)	C10-C11	1.489(5)
C1-H1	0.950	C7-C8	1.395(5)	C11-C12	1.316(5)
C3-N2	1.356(5)	C8-N9	1.380(4)	C11-H11	0.950
C3-N4	1.366(5)	N2-H2	0.880	C12-C13	1.481(5)
C3-C8	1.381(5)	N7-H7A	0.880	C12-H12	0.950
C5-N4	1.315(5)	N6-H6	0.880	C13-O14	1.215(5)
C5-N6	1.348(5)	N7-H7B	0.880	C13-O13	1.324(5)
C5-H5	0.950	C10-O11	1.246(4)	O13-H13	0.840

Torsion angle (°)		Torsion angle (°)	
N2-C3-C8-N9	0.3(4)	C8-C3-N4-C5	-0.1(6)
N4-C3-C8-N9	179.8(4)	N4-C5-N6-C7	-0.6(6)
N2-C3-C8-C7	-179.4(3)	N7-C7-N6-C5	-179.4(4)
N4-C3-C8-C7	0.1(6)	C8-C7-N6-C5	0.6(5)
N7-C7-C8-N9	0.1(7)	N2-C1-N9-C8	0.4(5)
N6-C7-C8-N9	-180.0(4)	C3-C8-N9-C1	-0.4(4)
N7-C7-C8-C3	179.7(4)	C7-C8-N9-C1	179.2(4)
N6-C7-C8-C3	-0.4(5)	O11-C10-C11-C12	13.6(6)
N4-C3-N2-C1	-179.6(4)	O10-C10-C11-C12	-165.6(4)
C8-C3-N2-C1	0.0(4)	C10-C11-C12-C13	177.5(4)
N9-C1-N2-C3	-0.3(5)	C11-C12-C13-O14	10.3(6)
N6-C5-N4-C3	0.3(5)	C11-C12-C13-O13	-168.7(4)
N2-C3-N4-C5	179.4(4)		

Appendix 5:

5.1.1: ^{1}H NMR spectra of adenine : maleic acid adduct (synthesised in EtOH) (**1**) (solvent – DMSO)

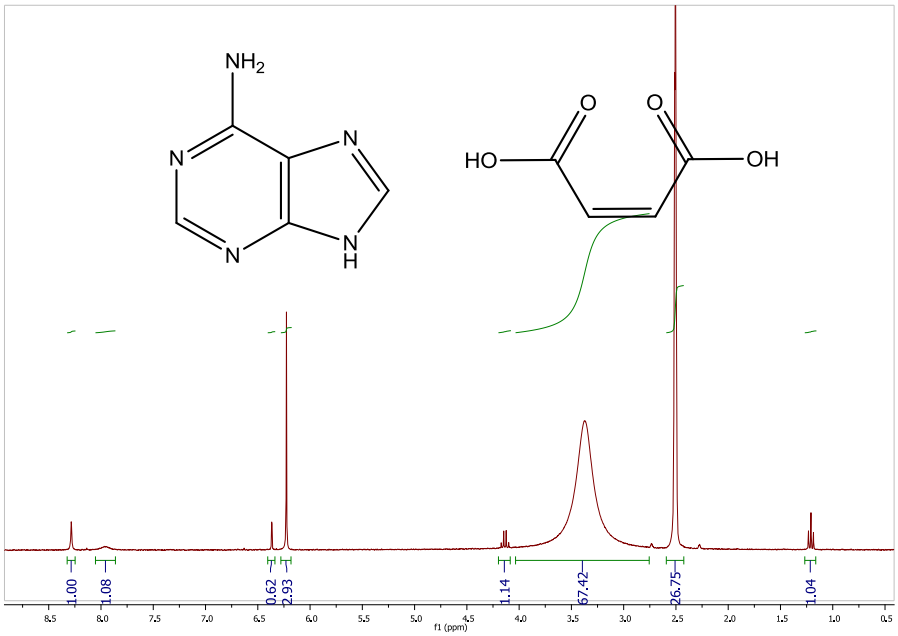

Adenine: 7.95 (2H,s), 8.25 (2H,s)
Maleic acid: 6.2 (2H, s),
Impurity: 1.25 (t)

5.1.2: ^{1}H NMR spectra of adenine : maleic acid adduct (synthesised in MeOH) (**2**) (solvent – DMSO)

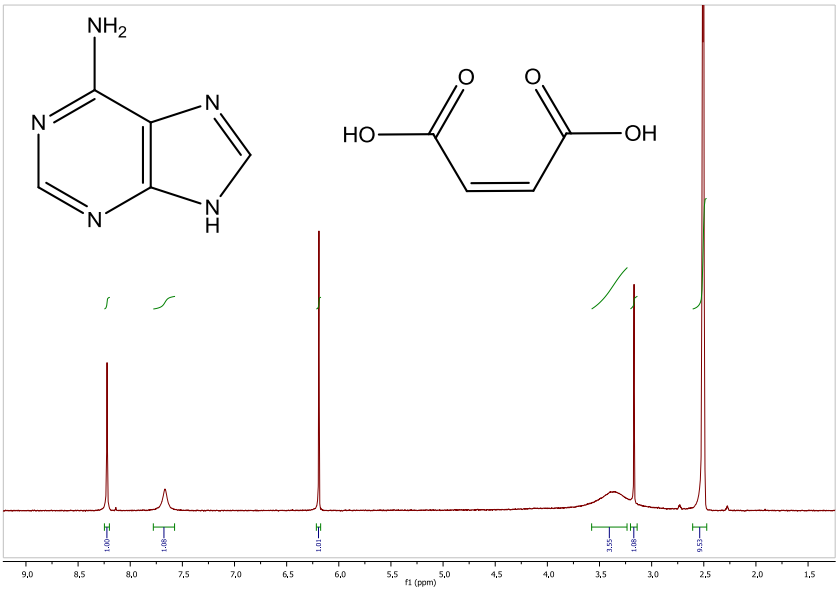

Adenine: 7.60 (2H,s), 8.20 (2H,d)
Maleic acid: 6.2 (2H, s)

5.2.1: The diffraction pattern simulated from the single crystal structure compared to that of the laboratory experimental powder diffraction pattern of anhydrous adeninium : hydrogen maleate (**1**)

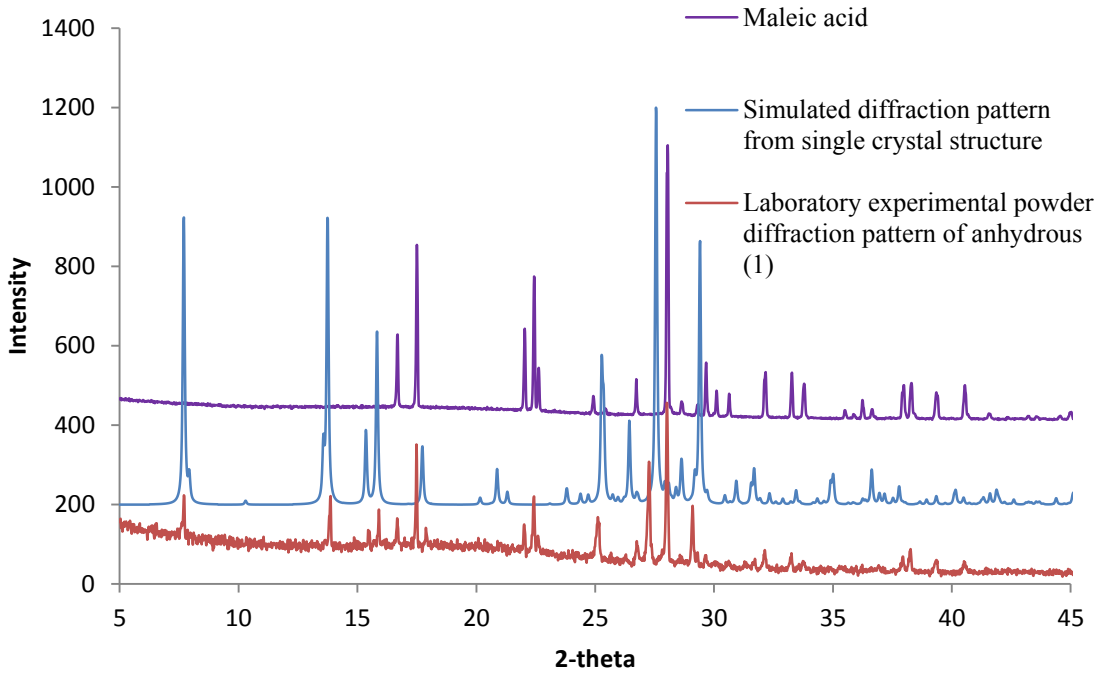

5.2.2: The diffraction pattern simulated from the single crystal structure compared to that of the laboratory experimental powder diffraction pattern of adeninium : hydrogen maleate methanolate (**2**)

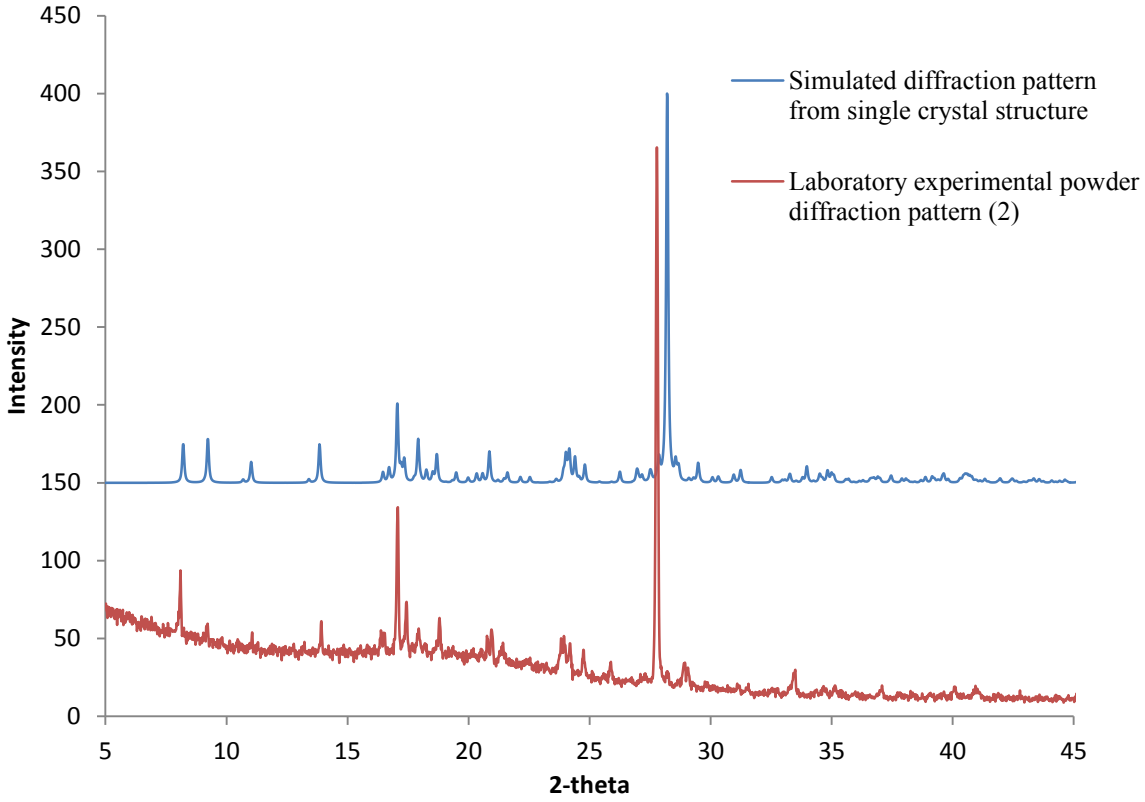

5.3: Ortep of anhydrous adeninium : hydrogen maleate (**1**), 1:1

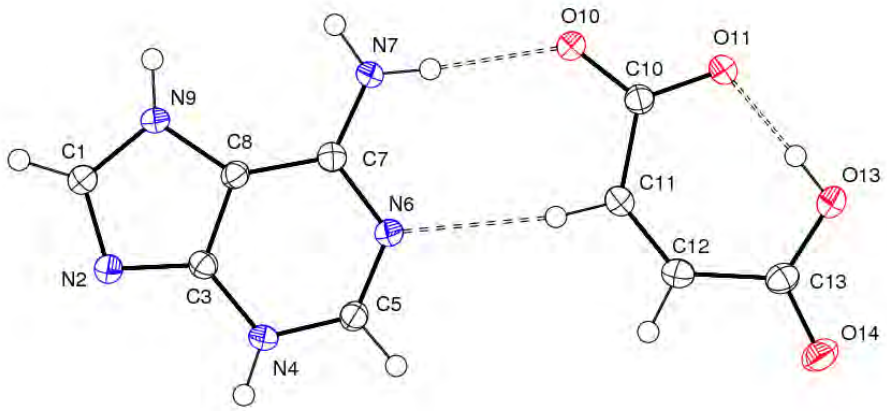

5.4: Crystallographic details of anhydrous adeninium : hydrogen maleate (**1**), 1:1

Empirical formula	$C_9 H_9 N_5 O_4$
Formula weight	251.21
Temperature	100(2) K
Wavelength	0.68890 Å
Crystal system	Monoclinic
Space group	$P2_1/c$
Unit cell dimensions	a = 3.610(3) Å b = 13.323(11) Å c = 22.187(19) Å β = 92.258(7) °
Volume	1066.3(15) $Å^3$
Z	4
Density (calculated)	1.565 Mg/m^3
Absorption coefficient	0.126 mm^{-1}
F(000)	520
Crystal size	0.09 x 0.01 x 0.01 mm^3
Theta range for data collection	2.96 to 26.56°.
Index ranges	-4<=h<=4, -17<=k<=17, -28<=l<=28
Reflections collected	10172
Independent reflections	2401 [R(int) = 0.0556]
Completeness to theta = 26.56°	98.1 %
Max. and min. transmission	0.9987 and 0.9887
Refinement method	Full-matrix least-squares on F^2
Data / restraints / parameters	2401 / 0 / 164
Goodness-of-fit on F^2	1.052
Final R indices [I>2sigma(I)]	R_1 = 0.0416, wR_2 = 0.1020
R indices (all data)	R_1 = 0.0582, wR_2 = 0.1108
Largest diff. peak and hole	0.234 and -0.255 e.$Å^{-3}$

5.5: Intramolecular bond lengths (Å) and angles (°) in anhydrous adeninium : hydrogen maleate (**1**), 1:1

Bond length (Å)		Bond length (Å)		Bond length (Å)	
O13-C13	1.309(2)	C12-H12	0.9500	N4-C5	1.348(2)
O13-H13	0.8400	N6-C5	1.311(2)	N4-C3	1.369(2)
O14-C13	1.226(2)	N6-C7	1.375(2)	N4-H4	0.8800
O11-C10	1.280(2)	N7-C7	1.316(2)	C8-C3	1.379(2)
O10-C10	1.254(2)	N7-H7A	0.8800	C8-C7	1.419(2)
C10-C11	1.496(2)	N7-H7B	0.8800	N2-C1	1.340(2)
C11-C12	1.342(2)	N9-C1	1.345(2)	N2-C3	1.363(2)
C11-H11	0.9500	N9-C8	1.392(2)	C1-H1	0.9500
C12-C13	1.501(2)	N9-H9	0.8800	C5-H5	0.9500

Bond angle (°)		Bond angle (°)		Bond angle (°)	
C13-O13-H13	109.5	C1-N9-C8	106.4(1)	N2-C3-C8	112.1(1)
O10-C10-O11	122.4(1)	C1-N9-H9	126.8	N4-C3-C8	121.0(1)
O10-C10-C11	117.2(1)	C8-N9-H9	126.8	N6-C5-N4	126.0(1)
O11-C10-C11	120.4(1)	C5-N4-C3	116.2(1)	N6-C5-H5	117.0
C12-C11-C10	130.0(2)	C5-N4-H4	121.9	N4C5-H5	117.0
C12-C11-H11	115.0	C3-N4-H4	121.9	C13B-C12B-H12B	114.2
C10-C11-H11	115.0	C3-C8-N9	104.6(1)	O14B-C13B-O13B	121.1(3)
C11-C12-C13	131.8(2)	C3-C8-C7	120.0(1)	O14B-C13B-C12B	118.1(1)
C11-C12-H12	114.1	N9-C8-C7	135.4(1)	O13B-C13B-C12B	20.6(1)
C13-C12-H12	114.1	C1-N2-C3	103.4(1)	C13B-O13B-H13B	109.5
O14-C13-O13	121.2(2)	N7-C7-N6	118.2(1)	O16-C15-H15A	109.5
O14-C13-C12	118.9(1)	N7-C7-C8	125.1(1)	O16-C15-H15B	109.5
O13-C13-C12	120.0(1)	N6-C7-C8	116.7(1)	H15A-C15-H15B	109.5
C5-N6-C7	120.1(1)	N2-C1-N9	113.4(1)	O16-C15-H15C	109.5
C7-N7-H7A	120.0	N2-C1-H1	123.3	H15A-C15-H15C	109.5
C7-N7-H7B	120.0	N9-C1-H1	123.3	H15B-C15-H15C	109.5
H7A-N7-H7B	120.0	N2-C3-N4	126.9(1)	C15-O16-H16	109.5

Torsion angle (°)		Torsion angle (°)	
O10-C10-C11-C12	177.6(2)	C3-N2-C1-N9	0.4(2)
O11-C10-C11-C12	-1.2(2)	C8-N9-C1-N2	-0.2(2)
C10-C11-C12-C13	2.4(3)	C1-N2-C3-N4	179.0(1)
C11-C12-C13-O14	177.2(2)	C1-N2-C3-C8	-0.5(2)
C11-C12-C13-O13	-2.1(3)	C5-N4-C3-N2	-179.2(1)
C1-N9-C8-C3	-0.1(2)	C5-N4-C3-C8	0.3(2)
C1-N9-C8-C7	179.1(2)	N9-C8-C3-N2	0.4(2)
C5-N6-C7-N7	-178.7(1)	C7-C8-C3-N2	-179.0(1)
C5-N6-C7-C8)	1.6(2)	N9-C8-C3-N4	-179.1(1)
C3-C8-C7-N7	177.9(1)	C7-C8-C3-N4	1.5(2)
N9-C8-C7-N7	-1.2(3)	C7-N6-C5-N4	0.2(2)
C3-C8-C7-N6	-2.4(2)	C3-N4-C5-N6	-1.2(2)
N9-C8-C7-N6	178.5(2)		

5.6: Ortep of adeninium : hydrogen maleate methanolate (**2**), 1:1:0.5

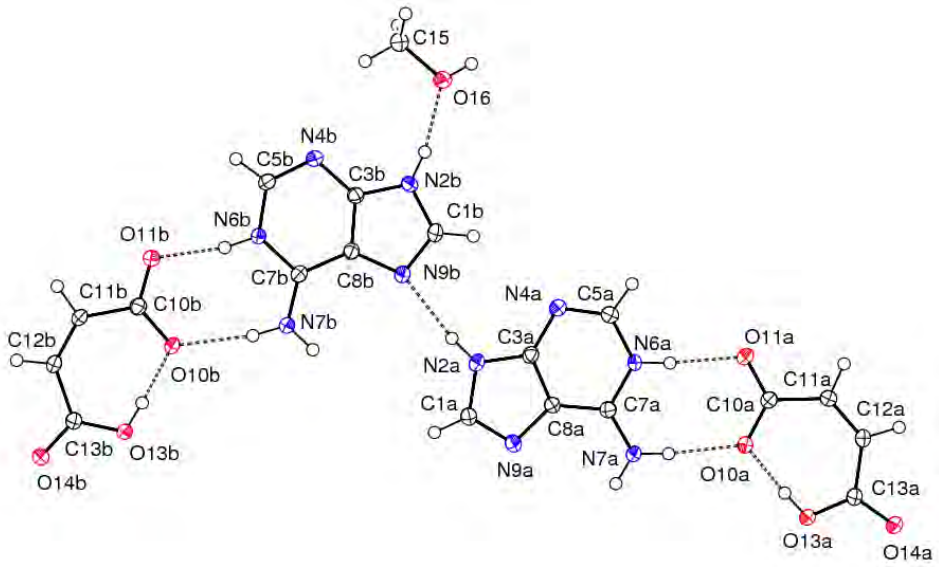

5.7: Crystallographic details of adeninium : hydrogen maleate methanolate (**2**), 1:1:0.5

Empirical formula	$C_{9.5}\ H_{11}\ N_5\ O_{4.5}$	
Formula weight	267.23	
Temperature	120(2) K	
Wavelength	1.54184 Å	
Crystal system	Triclinic	
Space group	P -1	
Unit cell dimensions	a = 5.2815(1) Å b = 10.0506(2) Å c = 22.0125(4) Å	α = 78.1910(1) ° β = 85.1600 (1) ° γ = 80.0170(1)°
Volume	1124.98(4) $Å^3$	
Z	4	
Density (calculated)	1.578 Mg/m^3	
Absorption coefficient	1.100 mm^{-1}	
F(000)	556	
Crystal size	0.15 x 0.05 x 0.05 mm^3	
Theta range for data collection	6.71 to 66.59°.	
Index ranges	-6<=h<=6, -11<=k<=11, -25<=l<=24	
Reflections collected	7965	
Independent reflections	3745 [R(int) = 0.0212]	
Completeness to theta = 66.59°	94.0 %	
Max. and min. transmission	0.9470 and 0.8524	
Refinement method	Full-matrix least-squares on F^2	
Data / restraints / parameters	3745 / 0 / 347	
Goodness-of-fit on F^2	1.064	
Final R indices [I>2sigma(I)]	R_1 = 0.0345, wR_2 = 0.0901	
R indices (all data)	R_1 = 0.0404, wR_2 = 0.0938	
Largest diff. peak and hole	0.256 and -0.346 e.$Å^{-3}$	

5.8: Intramolecular bond lengths (Å) and angles (°) in adeninium : hydrogen maleate methanolate (**2**), 1:1:0.5

Bond length (Å)		Bond length (Å)		Bond length (Å)	
C7A-N7A	1.312(2)	C12A-C11A	1.336(2)	N7B-H7BA	0.8800
C7A-N6A	1.367(2)	C12A-H12A	0.9500	N7B-H7BB	0.8800
C7A-C8A	1.407(2)	C11A-C10A	1.497(2)	N6B-H6B	0.8800
C5A-N4A	1.309(2)	C11A-H11A	0.9500	N2B-H2B	0.8800
C5A-N6A	1.363(2)	C10A-O11A	1.248(2)	C10B-O11B	1.249(2)
C5A-H5A	0.9500	C10A-O10A	1.276(2)	C10B-O10B	1.281(2)
C3A-N2A	1.358(2)	O13A-H13A	0.8400	C10B-C11B	1.492(2)
C3A-N4A	1.364(2)	C7B-N7B	1.308(2)	C11B-C12B	1.332(2)
C3A-C8A	1.389(2)	C7B-N6B	1.372(2)	C11B-H11B	0.9500
C1A-N9A	1.315(2)	C7B-C8B	1.408(2)	C12B-C13B	1.492(2)
C1A-N2A	1.374(2)	C5B-N4B	1.301(2)	C12B-H12B	0.9500
C1A-H1A	0.9500	C5B-N6B	1.358(2)	C13B-O14B	1.230(2)
C8A-N9A	1.375(2)	C5B-H5B	0.9500	C13B-O13B	1.303(2)
N7A-H7AA	0.8800	C3B-N4B	1.360(2)	O13B-H13B	0.8400
N7A-H7AB)	0.8800	C3B-N2B	1.362(2)	C15-O16	1.406(2)
N6A-H6A	0.8800	C3B-C8B	1.387(2)	C15-H15A	0.9800
N2A-H2A	0.8800	C1B-N9B	1.313(2)	C15-H15B	0.9800
C13A-O14A	1.241(2)	C1B-N2B	1.365(2)	C15-H15C	0.9800
C13A-O13A	1.288(2)	C1B-H1B	0.9500	O16-H16	0.8400
C13A-C12A	1.494(2)	C8B-N9B	1.390(2)		

Bond angle (°)		Bond angle (°)		Bond angle (°)	
N7A-C7A-N6A	121.1(1)	O14A-C13A-O13A	21.1(1)	C7B-N7B-H7BB	120.0
N7A-C7A-C8A	125.3(2)	O14A-C13A-C12A	117.7(1)	H7BA-N7B-H7BB	120.0
N6A-C7A-C8A	113.5(1)	O13A-C13A-C12A	121.3(1)	C5B-N6B-C7B	123.8(1)
N4A-C5A-N6A	125.6(2)	C11A-C12A-C13A	131.3(2)	C5B-N6B-H6B	118.1
N4A-C5A-H5A	117.2	C11A-C12A-H12A	114.4	C7B-N6B-H6B	118.1
N6A-C5A-H5A	117.2	C13A-C12A-H12A	114.4	C1B-N2B-H2B	126.9
N2A-C3A-N4A	128.0(1)	C12A-C11A-C10A	129.8(2)	C1B-N9B-C8B	103.7(1)
N2A-C3A-C8A	105.1(1)	C12A-C11A-H11A	115.1	O11B-C10B-O10B	123.1(1)
N4A-C3A-C8A	126.9(1)	C10A-C11A-H11A	115.1	O11B-C10B-C11B	116.9(1)
N9A-C1A-N2A	113.7(1)	O11A-C10A-O10A	123.4(1)	O10B-C10B-C11B	120.0(1)
N9A-C1A-H1A	123.2	O11A-C10A-C11A	117.7(1)	C12B-C11B-C10B	130.0(1)
N2A-C1A-H1A	123.2	O10A-C10A-C11A	118.9(1)	C12B-C11B-H11B	115.0
N9A-C8A-C3A	111.6(1)	C13A-O13A-H13A	109.5	C10B-C11B-H11B	115.0
N9A-C8A-C7A	129.9(1)	N7B-C7B-N6B	119.6(1)	C11B-C12B-C13B	131.6(2)
C3A-C8A-C7A	118.5(1)	N7B-C7B-C8B	127.0(1)	C11B-C12B-H12B	114.2
C7A-N7A-H7AA	120.0	N6B-C7B-C8B	113.4(1)	C13B-C12B-H12B	114.2
C7A-N7A-H7AB	120.0	N4B-C5B-N6B	125.5(1)	O14B-C13B-O13B	121.3(1)
H7AA-N7A-H7AB	120.0	N4B-C5B-H5B	117.2	O14B-C13B-C12B	118.1(1)
C5B-N4B-C3B	111.8(1)	N6B-C5B-H5B	117.2	O13B-C13B-C12B	120.6(1)
C3B-N2B-C1B	106.1(1)	N4B-C3B-N2B	126.3(1)	C13B-O13B-H13B	109.5

C3B-N2B-H2B	126.9	N4B-C3B-C8B	127.6(1)	O16-C15-H15A	109.5
C5A-N6A-C7A	123.6(1)	N2B-C3B-C8B	106.1(1)	O16-C15-H15B	109.5
C5A-N6A-H6A	118.2	N9B-C1B-N2B	113.9(1)	H15A-C15-H15B	109.5
C7A-N6A-H6A	118.2	N9B-C1B-H1B	123.0	O16-C15-H15C	109.5
C5A-N4A-C3A	111.9(1)	N2B-C1B-H1B	123.0	H15A-C15-H15C	109.5
C3A-N2A-C1A	106.4(1)	C3B-C8B-N9B	110.2(1)	H15B-C15-H15C	109.5
C3A-N2A-H2A	126.8	C3B-C8B-C7B	117.8(1)	C15-O16-H16	109.5
C1A-N2A-H2A	126.8	N9B-C8B-C7B	132.0(1)		
C1A-N9A-C8A	103.2(1)	C7B-N7B-H7BA	120.0		

Torsion angle (°)		Torsion angle (°)	
N2A-C3A-C8A-N9A	- 0.08(17)	N4B-C3B-C8B-N9B	179.6(1)
N4A-C3A-C8A-N9A	180.0(1)	N2B-C3B-C8B-N9B	-0.7(2)
N2A-C3A-C8A-C7A	-179.7(1)	N4B-C3B-C8B-C7B	-0.9(2)
N4A-C3A-C8A-C7A	0.4(2)	N2B-C3B-C8B-C7B	178.6(1)
N7A-C7A-C8A-N9A	1.6(3)	N7B-C7B-C8B-C3B	-176.4(2)
N6A-C7A-C8A-N9A	-178.2(2)	N6B-C7B-C8B-C3B	2.6(2)
N7A-C7A-C8A-C3A	-178.9(2)	N7B-C7B-C8B-N9B	2.9(3)
N6A-C7A-C8A-C3A	1.3(2)	N6B-C7B-C8B-N9B	-178.0(2)
N4A-C5A-N6A-C7A	2.0(2)	N4B-C5B-N6B-C7B	0.9(2)
N7A-C7A-N6A-C5A	177.8(1)	N7B-C7B-N6B-C5B	176.4(1)
C8A-C7A-N6A-C5A	-2.5(2)	C8B-C7B-N6B-C5B	-2.7(2)
N6A-C5A-N4A-C3A	-0.1(2)	N6B-C5B-N4B-C3B	1.0(2)
N2A-C3A-N4A-C5A	179.0(2)	N2B-C3B-N4B-C5B	179.4(2)
C8A-C3A-N4A-C5A	-1.1(2)	C8B-C3B-N4B-C5B	-1.0(2)
N4A-C3A-N2A-C1A	-179.9(2)	N4B-C3B-N2B-C1B	-179.7(2)
C8A-C3A-N2A-C1A	0.2(2)	C8B-C3B-N2B-C1B	0.6(2)
N9A-C1A-N2A-C3A	-0.2(2)	N9B-C1B-N2B-C3B	-0.3(2)
N2A-C1A-N9A-C8A	0.2(2)	N2B-C1B-N9B-C8B	-0.2(2)
C3A-C8A-N9A-C1A	-0.04(2)	C3B-C8B-N9B-C1B	0.5(2)
C7A-C8A-N9A-C1A	179.5(2)	C7B-C8B-N9B-C1B	-178.8(2)
O14A-C13A-C12A-C11A	-178.5(2)	O11B-C10B-C11B-C12B	-178.0(2)
O13A-C13A-C12A-C11A	0.9(3)	O10B-C10B-C11B-C12B	2.3(3)
C13A-C12A-C11A-C10A	-0.6(3)	C10B-C11B-C12B-C13B	1.5(3)
C12A-C11A-C10A-O11A	-179.0(2)	C11B-C12B-C13B-O14B	178.5(2)
C12A-C11A-C10A-O10A	1.1(3)	C11B-C12B-C13B-O13B	-1.1(3)

Appendix 6:

6.1: ^{1}H NMR spectra of adenine : glutaric acid adduct (solvent – DMSO)

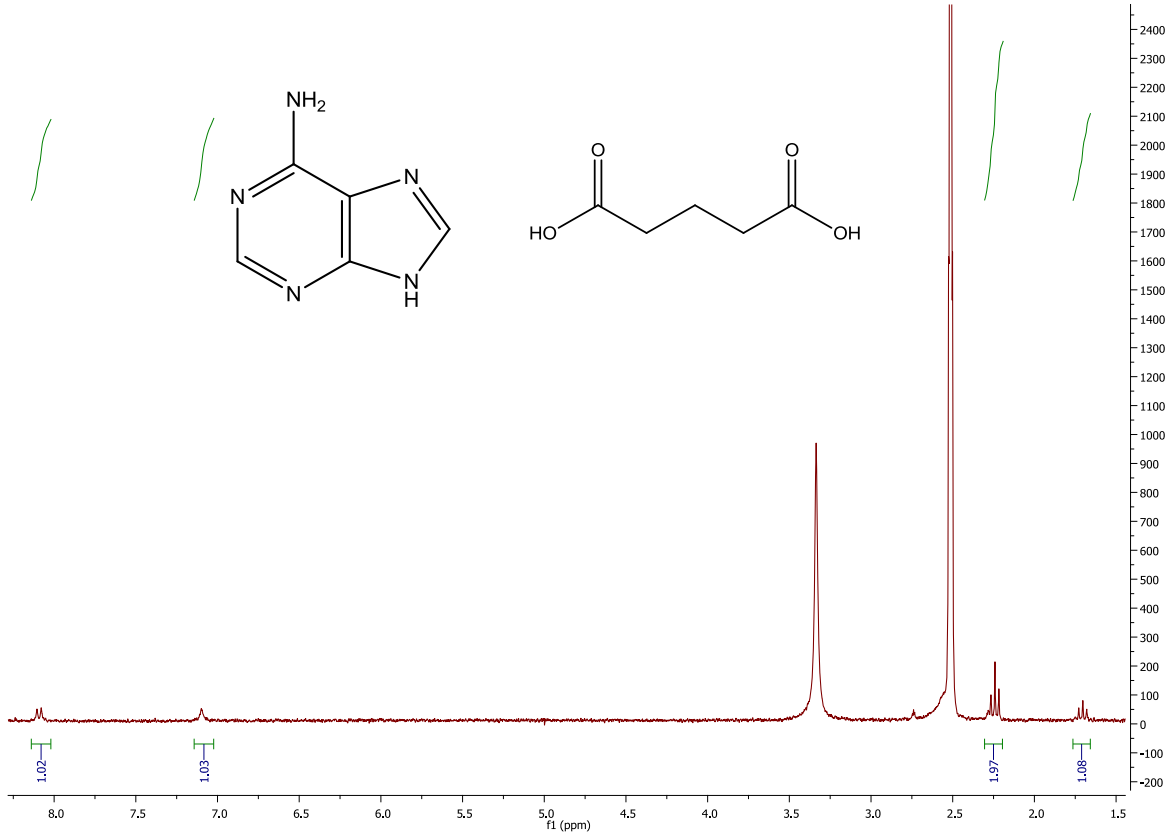

Adenine:	7.15 (2H,s),	8.10 (2H,d)
Glutaric acid:	1.7 (2H, t),	2.25 (4H, q)

6.2: Indexing results for adenine : glutaric acid 1:1, with the preferred unit cell highlighted in orange

I20	Merit	Volume	V/V1	a	b	c	alpha	beta	gamma
20	6.8	2037.407	1	20.615	5.7732	17.4311	90	100.859	90
20	6.8	2037.407	1	20.615	5.7732	17.4311	90	100.859	90
20	6	2038.286	1	24.3661	5.7742	17.4288	90	123.775	90
20	6	2038.286	1	24.3661	5.7742	17.4288	90	123.775	90
20	5.2	2348.391	1.15	24.0992	5.4323	17.9441	90	91.442	90
20	5.2	2348.391	1.15	24.0992	5.4323	17.9441	90	91.442	90
20	5	5889.011	2.89	51.8098	24.0917	4.7181	90	90	90
20	5	5889.011	2.89	51.8098	24.0917	4.7181	90	90	90
19	7	597.735	0.29	5.6897	8.7289	14.2471	57.883	89.827	93.411
19	6	644.747	0.32	5.7013	9.4646	15.2963	128.062	92.411	83.171
19	6	644.747	0.32	5.7013	9.4646	16.5475	127.652	112.547	83.171
19	6	597.233	0.29	5.6882	8.727	12.1144	84.653	87.379	86.64
19	5.1	1609.59	0.79	10.7059	15.5258	10.1946	102.638	90.999	102.64
19	4.7	1582.66	0.78	10.5341	15.1722	10.2637	102.276	97.606	93.258
18	10	703.162	0.35	5.2672	11.1084	18.1065	137.836	84.602	89.534
18	9	699.146	0.34	5.2658	11.0702	12.3288	100.439	81.853	89.323
18	8	1256.415	0.62	11.1715	12.0195	10.0587	90	111.528	90
18	7	1853.641	0.91	17.6333	16.282	6.4563	90	90	90
18	7	1853.641	0.91	17.6333	16.282	6.4563	90	90	90
18	7	1256.964	0.62	11.9828	12.0191	10.0671	90	119.895	90
18	7	701.865	0.34	5.2661	11.0977	12.3582	100.676	81.729	89.463
18	6	1468.344	0.72	17.4553	17.8027	5.0683	90	111.205	90
18	6	1468.343	0.72	16.321	17.8027	5.0683	90	94.376	90
18	6	1468.343	0.72	16.7164	17.8027	5.0683	90	103.22	90
18	6	948.076	0.47	9.0767	9.9572	19.4002	131.803	133.416	60.879
17	7	1703.444	0.84	17.8042	16.2749	5.8788	90	90	90
17	7	1336.301	0.66	24.5266	10.3271	5.3716	90	100.833	90
17	7	1336.301	0.66	24.1015	10.3271	5.3716	90	91.811	90
17	7	1085.32	0.53	12.1834	9.3567	9.5256	90	91.825	90
17	6.9	1039.31	0.51	10.8244	11.1459	9.6294	106.623	110.972	83.207
17	6	1263.348	0.62	11.1957	12.0044	9.5773	90	101.04	90
17	6	931.51	0.46	15.0059	6.299	10.1561	90	103.989	90
17	5.6	1390.75	0.68	10.8718	12.7984	10.5764	106.483	93.794	80.312
16	9.7	730.047	0.36	8.1431	12.4884	7.846	101.315	108.37	76.604

Appendix 7:

7.1: ^{1}H NMR spectra of adenine : adipic acid adduct (solvent – DMSO)

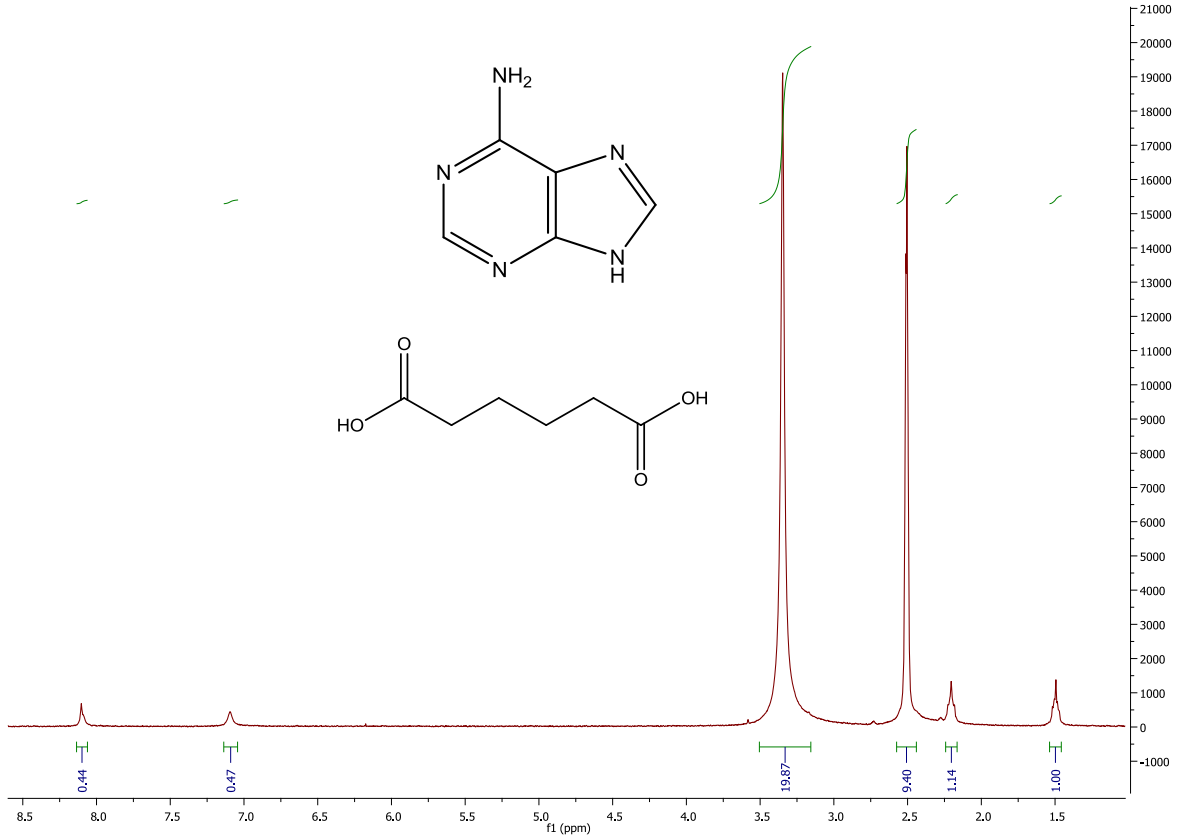

Adenine:	7.15 (2H,s),	8.15 (2H,d)
Adipic acid:	1.5 (4H, q),	2.2 (4H, t)

7.2: Indexing results for adenine : adipic acid 1:1, with the preferred unit cell highlighted in orange

I20	Merit	Volume	V/V1	a	b	c	alpha	beta	gamma
20	12.34	782.437	1	11.5146	11.8849	6.483	100.388	103.01	65.44
20	9.63	2082.011	2.66	11.8124	21.9384	8.2288	94.862	95.989	99.249
20	9.16	1542.753	1.97	12.6436	19.4839	6.3074	95.88	93.055	91.371
20	6.9	2462.008	3.15	17.6189	13.0139	12.962	90	124.067	90
20	6.9	2462.008	3.15	17.6189	13.0139	12.962	90	124.067	90
20	6.8	2462.43	3.15	14.9199	13.0154	12.9618	90	101.956	90
20	6.8	2462.43	3.15	14.9199	13.0154	12.9618	90	101.956	90
20	5.4	1495.23	1.91	11.8334	20.3964	6.4982	100.085	100.642	78.587
20	5.3	2553.391	3.26	26.4084	9.2588	12.805	90	125.36	90
20	5.3	2553.391	3.26	26.4084	9.2588	12.805	90	125.36	90
20	5.2	2553.396	3.26	23.8849	9.2588	12.805	90	115.618	90
20	5.2	2553.396	3.26	23.8849	9.2588	12.805	90	115.618	90
20	5.2	2553.384	3.26	21.6789	9.2588	12.805	90	96.563	90
20	5.2	2553.384	3.26	21.6789	9.2588	12.805	90	96.563	90
19	10	901.713	1.15	12.2863	12.8879	13.1215	63.899	62.886	29.336
19	9.94	908.44	1.16	7.0909	21.532	6.6711	92.471	116.774	89.521
19	9.45	1417.206	1.81	12.6297	19.4109	5.7931	93.045	91.227	88.192
19	8.3	1301.26	1.66	11.3726	19.169	6.4402	101.717	98.743	71.978
19	7.26	1759.631	2.25	12.7391	21.7388	6.4706	96.273	98.041	92.951
19	7.2	1315.52	1.68	11.401	19.0565	6.4328	96.108	99.036	105.255
19	7	1729.1	2.21	12.7725	14.1837	10.2489	91.188	101.265	107.626
19	7	2721.417	3.48	17.8809	13.4445	11.3204	90	90	90
19	7	2721.417	3.48	17.8809	13.4445	11.3204	90	90	90
19	6	2410.917	3.08	15.7927	11.8849	12.9707	90	97.986	90
19	6	2335.181	2.98	19.1791	11.3373	11.6722	90	113.062	90
19	6	1170.261	1.5	16.0937	10.7503	7.0159	90	105.398	90
19	6	1170.261	1.5	15.7565	10.7503	7.0159	90	100.024	90
19	6	1170.261	1.5	16.0937	10.7503	7.0159	90	105.398	90
19	5.9	1894.29	2.42	14.3358	21.3241	6.3669	97.612	90.63	100.715
19	5.5	1629.44	2.08	11.8715	21.8213	6.4968	97.589	101.006	82.984
18	14.19	1427.077	1.82	12.7432	19.3788	5.8439	93.395	97.673	91.247
18	13	1257.157	1.61	22.0742	9.3018	6.2978	90	103.543	90
18	13	1257.157	1.61	21.4901	9.3018	6.2978	90	93.011	90
18	11.07	848.203	1.08	6.623	21.5226	6.2313	91.169	107.209	90.452
18	10	1438.091	1.84	15.18	7.1497	13.3867	90	98.183	90
18	9.96	1214.944	1.55	8.8066	22.0775	6.5877	99.078	103.458	79.238
18	9.88	1049.069	1.34	7.5883	22.1721	6.8902	100.557	111.33	78.065
18	9.76	1439.609	1.84	15.1821	7.1496	13.4015	90	98.257	90
18	9.6	946.235	1.21	7.2245	21.672	6.8571	89.094	117.458	96.272
18	9.33	940.744	1.2	6.9939	21.7081	6.8218	88.54	113.804	96.761
18	9.16	1455.473	1.86	12.7676	19.4263	5.961	95.399	98.405	90.889

18	8	1438.09	1.84	18.7561	7.1497	13.3867	90	126.765	90
18	7	1542.944	1.97	23.791	6.1889	11.574	90	115.124	90
18	7	1542.944	1.97	23.791	6.1889	11.574	90	115.124	90
18	7	1542.944	1.97	23.791	6.1889	11.574	90	115.124	90
18	6.2	2493.95	3.19	33.4401	11.3355	6.5946	90	93.904	90
18	6.2	2493.95	3.19	33.4401	11.3355	6.5946	90	93.904	90
18	6	1158.208	1.48	15.5267	5.6828	13.2442	90	97.651	90
17	11	896.72	1.15	13.2285	13.7278	13.0783	57.353	55.516	27.402
17	10.15	1082.077	1.38	7.9621	21.5885	6.7362	89.63	110.535	93.557
17	10	996.052	1.27	11.9824	14.6456	6.3157	90	116.014	90
17	9	1238.211	1.58	10.7046	18.3838	6.3179	90	95.194	90
17	9	1221.964	1.56	12.7548	13.4399	8.0152	90	117.208	90
17	9	996.052	1.27	10.8205	14.6456	6.3157	90	95.624	90
17	8.77	1723.761	2.2	12.7017	21.543	6.3541	91.187	97.38	89.079
17	7.72	1765.895	2.26	12.799	21.9844	6.4401	97.527	95.952	80.562
17	6	2592.608	3.31	21.2757	11.3475	10.7387	90	90	90
17	6	1205.455	1.54	15.7991	10.7142	7.1895	90	97.9	90
17	6	1205.454	1.54	16.434	10.7142	7.1895	90	107.779	90
16	15.08	896.718	1.15	6.8719	21.6855	6.5011	92.488	111.149	95.242
16	14.67	918.717	1.17	11.4928	13.5113	6.4316	99.849	98.785	69.799
16	10.89	1475.89	1.89	12.8568	19.4541	6.0306	94.706	100.825	87.465
16	10.65	945.038	1.21	7.1807	21.5679	6.941	92.603	118.339	89.599
16	10.44	1922.006	2.46	14.139	21.829	6.382	89.493	98.597	99.261
16	10.22	1476.208	1.89	10.8609	21.7034	6.3407	91.616	96.027	83.37
16	8.47	1523.372	1.95	11.2084	22.1539	6.3392	92.233	95.741	76.606

Appendix 8:

8.1: ^{1}H NMR spectra of adenine : pimelic acid adduct (solvent – DMSO)

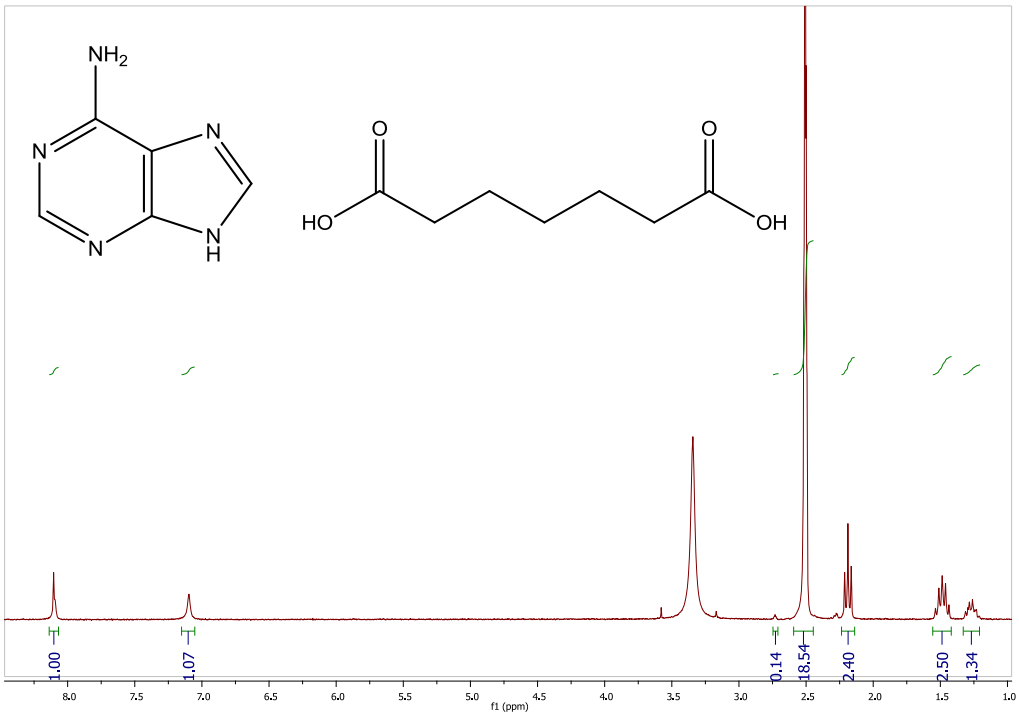

Adenine:	7.15 (2H,s),	8.15 (2H,d)	
Pimelic acid:	1.25 (2H, q),	1.5 (4H, q),	2.2 (4H, t)

8.2: The diffraction pattern simulated from the single crystal structure compared to that of the laboratory experimental powder diffraction pattern of adenine : pimelic acid, 1:1

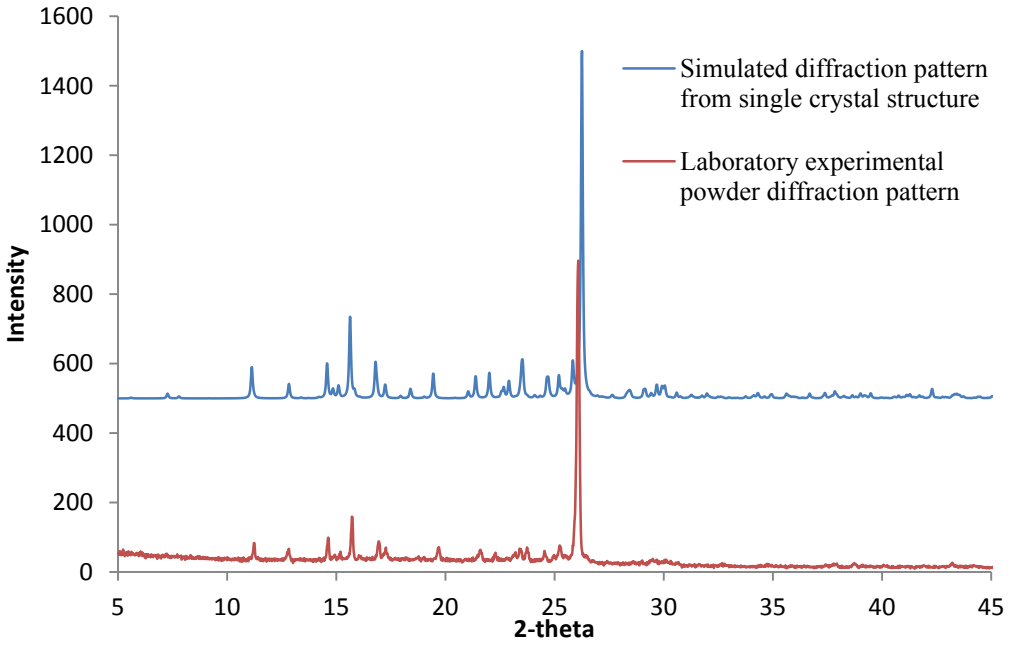

8.3: Ortep of adenine : pimelic acid, 1:1

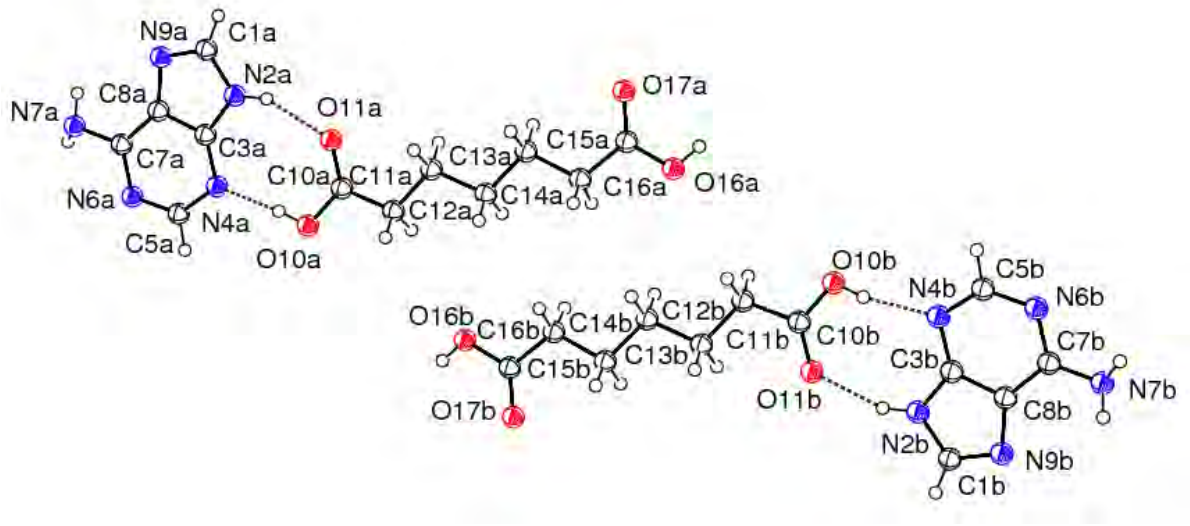

8.4: Crystallographic details for adenine : pimelic acid, 1:1

Empirical formula	$C_{12}\ H_{17}\ N_5\ O_4$
Formula weight	295.31
Temperature	100(2) K
Wavelength	0.71075 Å
Crystal system	Monoclinic
Space group	$P2_1/c$
Unit cell dimensions	a = 12.44 (1) Å b = 31.49(3) Å c = 7.237(6) Å β = 102.64(1) °
Volume	2766(4) $Å^3$
Z	8
Density (calculated)	1.419 Mg/m^3
Absorption coefficient	0.109 mm^{-1}
F(000)	1248
Crystal size	0.05 x 0.01 x 0.01 mm^3
Theta range for data collection	3.07 to 24.95°.
Index ranges	-11<=h<=14, -37<=k<=37, -8<=l<=7
Reflections collected	11224
Independent reflections	4802 [R(int) = 0.1653]
Completeness to theta = 24.95°	98.9 %
Absorption correction	Semi-empirical from equivalents
Max. and min. transmission	0.9989 and 0.9946
Refinement method	Full-matrix least-squares on F^2
Data / restraints / parameters	4802 / 0 / 385
Goodness-of-fit on F^2	0.832
Final R indices [I>2sigma(I)]	R_1 = 0.0757, wR_2 = 0.1443
R indices (all data)	R_1 = 0.2554, wR_2 = 0.2055
Largest diff. peak and hole	0.422 and -0.330 $e.Å^{-3}$

8.5: Intramolecular bond lengths (Å) and angles (°) for adenine : pimelic acid, 1:1

Bond length (Å)		Bond length (Å)		Bond length (Å)	
N6B–C5B	1.348(8)	O16B–H16B	0.8400	C11B–H11BA	0.9900
N6B–C7B	1.350(8)	O11B–C10B	1.239(7)	C5B–H5B	0.9500
N4B–C5B	1.323(8)	O10B–C10B	1.319(7)	C3B–C8B	1.426(9)
N4B–C3B	1.367(8)	O10B–H10B	0.8400	C1B–H1B	0.9500
N2B–C3B	1.357(8)	O11A–C10A	1.237(7)	C8B–C7B	1.402(9)
N2B–C1B	1.363(8)	O10A–C10A	1.344(7)	C10A–C11A	1.500(8)
N2B–H2B	0.8800	O10A–H10A	0.8400	C11A–C12A	1.499(8)
N9B–C1B	1.307(8)	O17A–C16A	1.236(7)	C11A–H11AA	0.9900
N9B–C8B	1.398(8)	O16A–C16A	1.327(7)	C11A–H11AB	0.9900
N7B–C7B	1.342(8)	O16A–H16A	0.8400	C12A–C13A	1.549(8)
N7B–H7BB	0.8647	C16B–C15B	1.486(8)	C12A–H12AA	0.9900
N7B–H7BA	0.8641	C15B–C14B	1.543(8)	C12A–H12AB	0.9900
N6A–C5A	1.349(8)	C15B–H15BA	0.9900	C13A–C14A	1.525(8)
N6A–C7A	1.369(7)	C15B–H15BB	0.9900	C13A–H13AA	0.9900
N4A–C5A	1.328(8)	C14B–C13B	1.525(8)	C13A–H13AB	0.9900
N4A–C3A	1.347(7)	C14–H14BA	0.9900	C14A–C15A	1.544(8)
N2A–C3A	1.347(7)	C14–H14BB	0.9900	C14A–H14AA	0.9900
N2A–C1A	1.369(8)	C13B–C12B	1.535(8)	C14A–H14AB	0.9900
N2A–H2A	0.8800	C13B–H13BA	0.9900	C15A–C16S	1.493(8)
N9A–C1A	1.322(7)	C13B–H13BB	0.9900	C15A–H15AA	0.9900
N9A–C6A	1.383(7)	C12B–C11B	1.513(8)	C15A–H15AB	0.9900
N7A–C7A	1.363(8)	C12B–H12BA	0.9900	C5A–H5A	0.9500
N7A–H7AA	0.8621	C12B–H12BB	0.9900	C3A–C8A	1.411(8)
N7A–H7AB	0.8623	C11B–C10B	1.509(8)	C1A–H1A	0.9500
O17B–C16B	1.243(7)	C11B–H11BB	0.9900	C6A–C7A	1.403(8)
O16B–C16B	1.333(7)				

Bond angle (°)		Bond angle (°)		Bond angle (°)	
C5B–N6B–C7B	119.7(6)	H13BA–C13B–H13BB	107.7	C11A–C12A–H12AA	109.0
C5B–N4B–C3B	110.6(6)	C11B–C12B–C13B	111.7(5)	C13A–C12A–H12AA	109.0
C3B–N2B–C1B	106.9(6)	C11B–C12B–H12BA	109.3	C11A–C12A–H12AB	109.0
C3B–N2B–H2B	126.5	C13B–C12B–H12BA	109.3	C13A–C12A–H12AB	109.0
C1B–N2B–H2B	126.5	C11B–C12B–H12BB	109.3	H12AB–C12A–H12AB	107.8
C1B–N9B–C8B	104.8(6)	C13B–C12B–H12BB	109.3	C14A–C13A–C12A	13.3(5)
C7B–N7B–H7BB	111.6	H12BA–C12B–H12BB	107.9	C14A–C13A–H13AA	108.9
C7B-N7B–H7BA	107.2	C10B–C11B–C12B	115.7(5)	C12A–C13A–H13AA	108.9
H7BB–N7B–H7BA	108.3	C10B–C11B–H11BA	108.4	C14A–C13A–H13AB	108.9
C5A–N6A–C7A	117.2(6)	C12B–C11B–H11BA	108.4	C12A–C13A–H13AB	108.9
C5A–N4A–C3A	112.1(6)	C10B–C11B–H11BB	108.4	H13AA–C13A–H13AB	107.7
C3A–N2A–C1A	107.1(5)	C12B–C11B–H11BB	108.4	C13A–C14A–C15A	109.9(5)
C3A–N2A–H2A	126.5	H11BA–C6–H11BB	107.4	C13A–C14A–H14AA	109.7
C1A–N2A–H2A	126.5	O11B–C10B–O10B	124.1(6)	C15A–C14A–H14AA	109.7
C1A–N9A–C8A	105.0(5)	O11B–C10B–C11B	121.9(5)	C13A–C14A–H14AB	109.7
C7A–N7A–H7AA	108.6	O10B–C10B–C11B	113.9(5)	C15A–C14A–H14AB	109.7
C7A–N7A–H7AB	108.8	N4B–C5B–N6B	129.2(6)	H14AA–C14A–H14AB	108.2
H7AA–N7A–H7AB	109.3	N4B–C5B–H5B	115.4	C16A–C15A–C14A	115.9(5)
C16B–O16B–H16B	109.5	N6B–C5B–H5B	115.4	C16A–C15A–H15AA	108.3
C10B–O10B–H10B	109.5	N2B–C3B–N4B	127.9(6)	C14A–C15A–H15AA	108.3
C10A–O10A–H10A	109.5	N2B–C3B–C8B	105.8(6)	C16A–C15A–H15AB	108.3
C16A–O16A–H16A	109.5	N4B–C3B–C8B	126.3(7)	C16A–C15A–H15AB	108.3
O17B–C16B–O16B	122.9(6)	N9B–C1B–N2B	114.0(6)	H15AA–C15A–H15AB	107.4
O17B–C16B–C15B	124.9(6)	N9B–C1B–H1B	123.0	O17A–C16A–O16A	122.6(6)
O16B–C16B–C15B	112.2(6)	N2B–C1B–H1B	123.0	O17A–C16A–C15A	125.5(6)
C16B–C15B–C14B	116.0(5)	N9B–C8B–C7B	135.4(7)	O16A–C16A–C15A	111.9(6)
C16B–C15B–H15BA	108.3	N9B–C8B–C3B	108.5(6)	N4A–C5A–N6A	129.4(6)
C14B–C15B–H15BA	108.3	C7B–C8B–C3B	116.1(7)	N4A–C5A–H5A	115.3
C16B–C15B–H15BB	108.3	N7B–C7B–N6B	120.9(6)	N6A–C5A–H5A	115.3
C14B–C15B–H15BB	108.3	N7B–C7B–C8B	120.9(7)	N2A–C3A–N4A	127.9(6)
H15BA–C15B–H15BB	107.4	N6B–C7B–C8B	118.1(6)	N2A–C3A–C8A	106.4(5)
C13B–C14B–C15B	109.5(5)	O11A–C10A–O10A	122.3(6)	N4A–C3A–C28A	125.7(6)
C13B–C14B–H14BA	109.8	O11A–C10A–C11A	124.3(6)	N9A–C1A–N2A	112.6(6)
C15B– C14B–H14BA	109.8	O10A–C10A–C11A	113.4(5)	N9A–C1A–H1A	123.7
C13B–C14B–H14BB	109.8	C12A–C111A–C10A	113.9(5)	N2A–C1A–H1A	123.7
C15B– C14B–H14BB	109.8	C12A–C11A–H11AA	108.8	N9A–C8A–C7A	134.8(6)
H14BA–C14B–H15BB	108.2	C10A–C11A–H11AA	108.8	N9A–C8A–C3A	108.9(5)
C14B–C13B–C12B	113.3(5)	C12A–C11A–H11AB	108.8	C7A–C8A–C3A	116.3(6)
C14B–C13B–H13BA	108.9	C10A–C11A–H11AB	108.8	N7A–C7A–N6A	119.2(6)
C12B–C13B–H13BA	108.9	H11AA–C11A–H11AB	107.7	N7A–C7A–C8A	121.5(6)
C14B–C13B–H13BB	108.9	C11A–C12A–C13A	112.7(5)	N6A–C7A–C8A	119.3(6)
C12B–C13B–H13BB	108.9				

Torsion angle (°)		Torsion angle (°)	
O17B–C16B–C15B–C14B	8.5(12)	O11A–C10A–C11A–C12A	3.3(10)
O16B– C16B–C15B–C14B	–170.9(6)	O10A– C10A–C11A–C12A	–177.3(6)
C16B–C15B–C14B–C13B	179.6(7)	C10A– C11A–C12A –C13A	–178.4(6)
C15B–C14B–C13B –C12B	178.0(6)	C11A–C12A –C13A –C14A	178.5(6)
C14B–C13B –C12B–C11B	–179.8(6)	C12A –C13A –C14A –C15A	–179.5(6)
C13B –C12B–C11B –C10B	179.1(7)	C13A –C14A –C15A–C16A	172.6(7)
C12B–C11B –C10 B–O11B	–6.6(10)	C14A –C15A–C16A –O17A	4.4(12)
C12B–C11B –C10 B–O10B	175.8(7)	C14A –C15A–C16A –O16A	–173.4(6)
C3B–N4B–C5B–N6B	0.3(12)	C3A–N4A–C5A–N6A	0.8(11)
C7B–N6B–C5B–N4B	–0.7(13)	C7A–N6A–C5A–N4A	–0.9(12)
C1B–N2B–C3B–N4B	178.8(8)	C1A–N2A –C3 A–N4A	–178.7(8)
C1B–N2B–C3B–C8B	–0.8(9)	C1A –N2A –C3A–C8A	–0.3(8)
C5B–N4B–C3B–N2B	–179.7(7)	C5A –N4A–C3A–N2A	178.1(7)
C5B–N4B–C3B–C8B	–0.2(11)	C5A –N4A–C3A–C8A	0.0(11)
C8B–N9B–C1B–N2B	–0.1(10)	C8A –N9A–C1A–N2A	2.7(8)
C3B–N2B–C1B–N9B	0.6(10)	C3A–N2A–C1A–N9A	–1.6(9)
C1B–N9B–C8B–C7B	–179.4(9)	C1A–N9A–C8A–C7A	178.4(8)
C1B–N9B–C8B–C3B	–0.4(9)	C1A–N9A–C8A–C3A	–2.8(8)
N2B–C3B–C8B–N9B	0.8(9)	N2A–C3A–C8A–N9A	1.9(9)
N4B–C3B–C8B–N9B	–178.9(7)	N4A–C3A–C8A–N9A	–179.6(7)
N2B–C3B–C8B–C7B	180.0(7)	N2A–C3A–C8A–C7A	–179.0(6)
N4B–C3B–C8B–C7B	0.3(12)	N4A–C3A–C8A–C7A	–0.5(12)
C5B–N6B–C7B–N7B	176.8(7)	C5A–N6A–C7A–N7A	–176.8(6)
C5B–N6B–C7B–C8B	0.8(11)	C5A–N6A–C7A–C8A	0.2(10)
N9B–C8B–C7B–N7B	2.3(15)	N9A–C8A–C7A–N7A	–3.9(13)
C3B–C8B–C7B–N7B	–176.6(7)	C3A–C8A–C7A–N7A	177.4(7)
N9B–C8B–C7B–N6B	178.3(8)	N9A–C8A–C7A–N6A	179.1(8)
C3B–C8B–C7B–N6B	–0.7(11)	C3A–C8A–C7A–N6A	0.4(10)

Appendix 9:

9.1: ^{1}H NMR spectra of adenine : suberic acid adduct (solvent – DMSO)

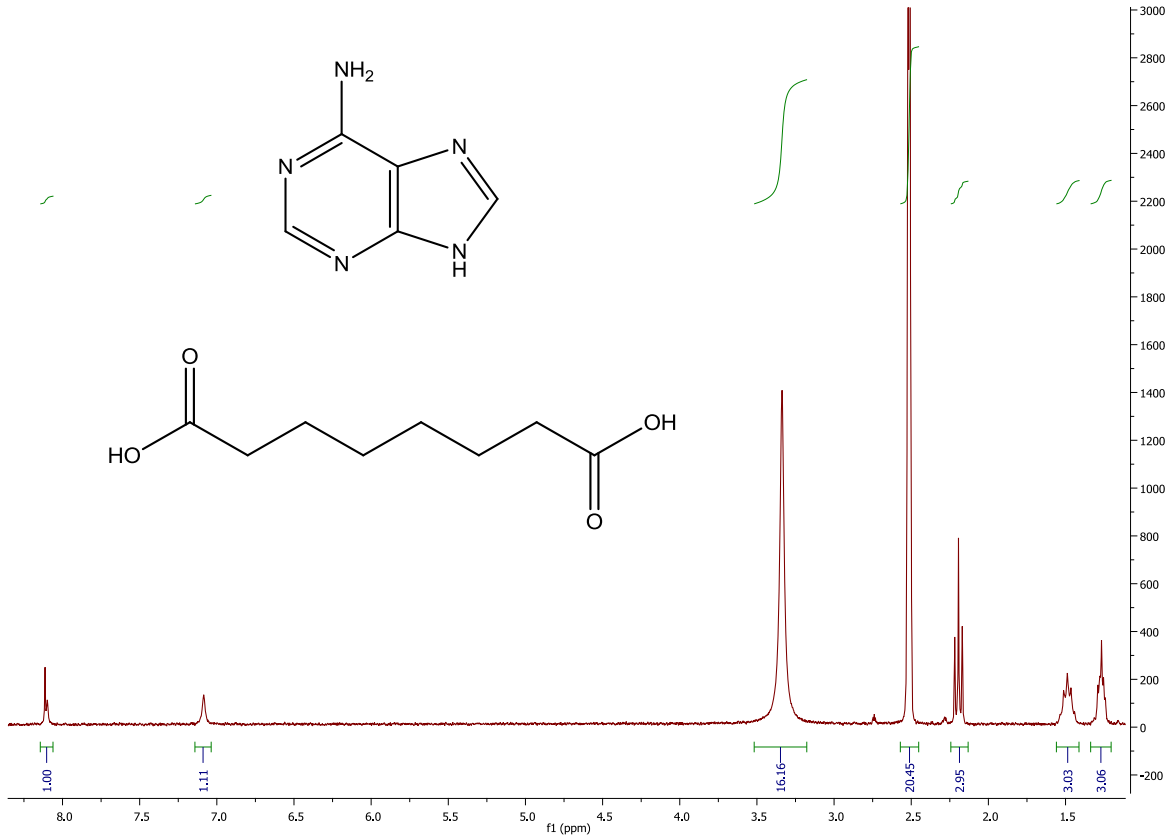

Adenine:	7.15 (2H,s),	8.10 (2H,d)	
Suberic acid:	1.25 (4H, q),	1.5 (4H, q),	2.2 (4H,t)

9.2: Indexing results for adenine : suberic acid, 1:1.5

I20	Merit	Volume	V/V1	a	b	c	alpha	beta	gamma
20	6.1	3562.37	1	46.2512	24.3184	3.1672	90	90	90
20	6.1	3562.37	1	46.2512	24.3184	3.1672	90	90	90
20	5.6	2801.482	0.79	20.1099	8.9383	19.2881	90	126.095	90
20	5.6	2801.482	0.79	20.1099	8.9383	19.2881	90	126.095	90
20	5.6	2801.478	0.79	20.1099	8.9383	17.8721	90	119.301	90
20	5.6	2801.478	0.79	20.1099	8.9383	17.8721	90	119.301	90
20	5.1	2801.211	0.79	19.2862	8.9394	17.874	90	114.631	90
20	5.1	2801.211	0.79	19.2862	8.9394	17.874	90	114.631	90
20	5	1972.54	0.55	10.042	16.2016	13.0826	92.802	111.899	88.955
20	5	1972.54	0.55	10.042	16.2016	13.0826	92.802	111.899	88.955
20	4.7	2019.73	0.57	13.0173	16.2223	10.2657	91.209	111.105	92.063
20	4.7	2019.73	0.57	13.0173	16.2223	10.2657	91.209	111.105	92.063
20	4.2	1953.39	0.55	13.1227	15.8363	10.1163	91.761	111.608	88.47
19	10.27	2325.452	0.65	13.6309	17.2214	11.2827	102.138	110.702	70.722
19	8	484.123	0.14	6.2146	8.2752	11.6128	88.845	56.026	79.319
19	8	484.122	0.14	6.2146	8.2752	9.6343	95.467	91.635	100.681
19	5.2	1974.48	0.55	10.0599	16.1452	13.102	92.662	111.744	89.014
18	11	657.985	0.18	6.6449	10.4081	12.2347	57.011	88.452	107.391
18	11	657.985	0.18	6.6449	10.5423	14.0795	50.2	60.302	70.414
18	11	657.985	0.18	6.6449	10.5423	12.2347	56.319	88.452	70.414
18	9.46	1792.196	0.5	11.2963	16.8112	10.4859	104.203	110.964	79.324
18	9	483.235	0.14	6.1995	9.3875	9.6291	95.921	91.787	60.131
18	9	483.235	0.14	6.1995	9.3875	9.6291	95.921	88.213	119.868
18	9	483.235	0.14	6.1995	9.3875	9.6291	84.079	88.213	60.131
18	9	483.234	0.14	6.1995	8.2821	9.6291	95.37	91.787	100.607
18	7	1333.113	0.37	24.3792	6.0865	9.5791	90	110.299	90
18	7	657.619	0.18	6.6393	10.3907	13.7724	51.135	62.749	72.733
18	6	1996.473	0.56	12.6243	16.6678	10.2381	90	112.067	90
18	6	1996.473	0.56	12.6243	16.6678	10.2381	90	112.067	90
18	6	1449.478	0.41	11.1944	13.1206	16.0972	58.005	122.444	130.811
18	6	1449.478	0.41	11.1944	13.1206	16.0972	58.005	57.556	49.189
18	6	1449.478	0.41	11.1944	13.1206	16.0972	121.995	57.556	130.811
18	6	1449.478	0.41	11.1944	13.1206	16.0972	121.995	122.444	49.189
18	5.2	3175.88	0.89	24.6237	6.4796	20.2522	90	100.625	90
18	4.8	2729.74	0.77	15.0354	14.3653	13.5375	90	111	90
17	13.82	482.507	0.14	8.2732	9.6267	6.1942	91.729	100.47	95.272
17	11	579.495	0.16	8.8575	7.454	14.5763	65.207	42.022	66.82
17	10.37	979.181	0.27	10.7641	13.0041	7.4825	96.646	89.715	109.641
17	10.28	1761.357	0.49	10.5402	16.7024	10.3136	102.543	89.494	96.317
17	10	1510.255	0.42	12.208	15.2745	10.367	90	128.626	90
17	10	1510.254	0.42	12.208	15.2745	9.9249	90	125.31	90
17	10	1240.418	0.35	9.0695	18.9898	21.5724	26.34	51.481	49.214

17	10	786.801	0.22	9.427	8.7709	11.2454	99.991	59.448	91.796
17	10	558.047	0.16	6.6806	8.9471	10.9188	66.537	79.756	102.623
17	9	1511.281	0.42	12.213	15.2742	10.3629	90	128.576	90
17	9	1211.491	0.34	9.5941	15.2786	8.3325	90	97.308	90
17	9	915.185	0.26	8.1615	10.7663	11.786	117.123	93.387	93.724
17	9	915.183	0.26	8.1615	10.7662	11.786	62.877	86.613	93.724
17	9	915.183	0.26	8.1615	10.7662	11.786	62.877	93.387	86.276
17	9	568.956	0.16	6.3367	9.4518	11.272	119.137	79.547	85.541
17	9	484.523	0.14	8.2777	6.2182	13.2785	84.54	46.24	79.3
17	8	1742.187	0.49	15.7719	11.9729	9.2329	90	92.227	90
17	8	580.464	0.16	7.4734	8.8657	9.9461	101.31	74.752	113.378
17	7	1472.132	0.41	12.0314	16.3612	13.6045	125.27	69.978	137.116
17	7	1390.382	0.39	18.575	8.9739	9.5738	90	119.396	90
17	6	1970.237	0.55	19.2272	15.2711	6.7555	90	96.646	90
17	6	1970.237	0.55	21.1043	15.2711	6.7555	90	115.185	90
17	6	1807.811	0.51	16.0464	9.5073	12.3299	90	106.038	90
17	6	1769.916	0.5	18.1976	11.7877	9.5788	90	120.527	90
17	6	1512.516	0.42	10.3773	15.2867	9.9175	90	105.974	90
17	6	1509.421	0.42	10.4036	15.2721	9.897	90	106.282	90
17	6	1390.383	0.39	16.1898	8.9739	9.5738	90	91.615	90
16	10.56	711.434	0.2	8.3711	11.9336	7.3615	89.799	98.96	101.543
16	10.17	1985.639	0.56	11.6058	16.3478	10.8745	97.032	103.682	84.858
16	10.14	727.459	0.2	9.737	10.3394	7.4967	102.804	97.209	83.651
16	9.32	3662.345	1.03	16.4389	13.7614	16.4114	90	99.44	90
16	7.82	1830.393	0.51	10.7227	16.4244	10.7047	97.084	100.188	82.63
16	7.03	1882.295	0.53	11.0614	16.3281	11.0123	94.236	107.388	94.495

9.3: The diffraction pattern simulated from the single crystal structure compared to that of the laboratory experimental powder diffraction pattern of adenine : suberic acid : hydrate, 2:2:1

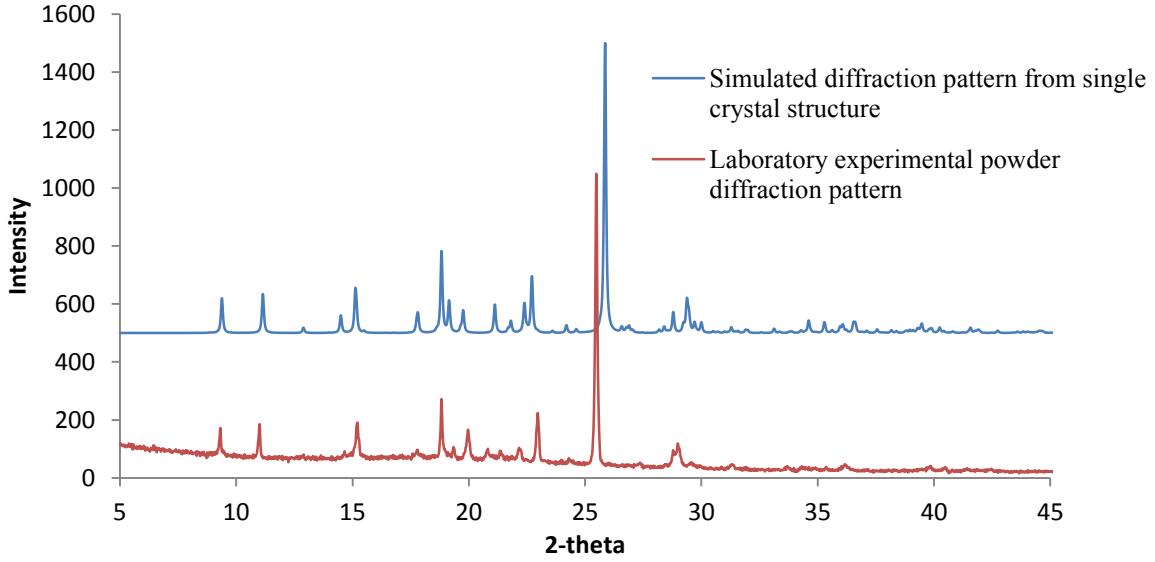

9.3: Ortep for adenine : suberic acid : hydrate, 2:2:1

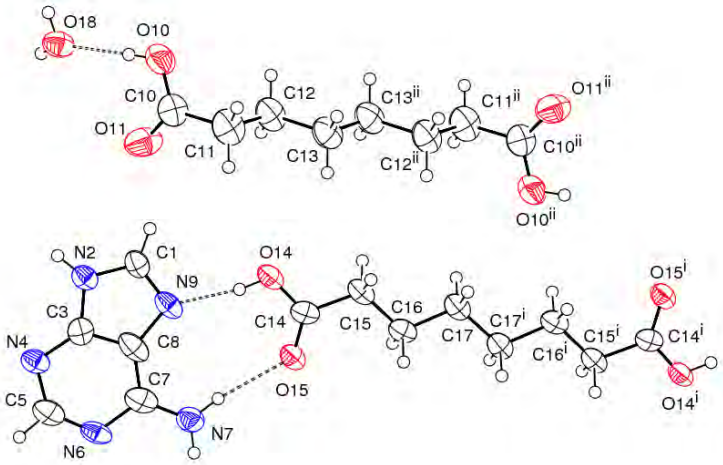

9.4: Crystallographic details for adenine : suberic acid : water, 2:2:1

Empirical formula	$C_{13}\ H_{21}\ N_5\ O_5$	
Formula weight	327.35	
Temperature	100 K	
Wavelength	0.71075 Å	
Crystal system	Triclinic	
Space group	P -1	
Unit cell dimensions	a = 8.08(2) Å b = 9.76(2) Å c = 10.49(2) Å	α = 104.43(4)° β = 99.88(4) ° γ = 92.01(2)°
Volume	786(3) $Å^3$	
Z	2	
Density (calculated)	1.383 Mg/m^3	
Absorption coefficient	0.108 mm^{-1}	
F(000)	348	
Crystal size	0.15 x 0.15 x 0.12 mm^3	
Theta range for data collection	3.22 to 23.81°.	
Index ranges	-9<=h<=9, -11<=k<=11, -11<=l<=11	
Reflections collected	4634	
Independent reflections	2343 [R(int) = 0.2197]	
Completeness to theta = 23.81°	97.4 %	
Absorption correction	Semi-empirical from equivalents	
Max. and min. transmission	1.000 and 0.667	
Refinement method	Full-matrix least-squares on F^2	
Data / restraints / parameters	2343 / 3 / 216	
Goodness-of-fit on F^2	1.479	
Final R indices [I>2sigma(I)]	R_1 = 0.0415, wR_2 = 0.3573	
R indices (all data)	R_1 = 0.1600, wR_2 = 0.38408	
Largest diff. peak and hole	0.656 and -0.484 $e.Å^{-3}$	

9.5: Intermolecular bond lengths (Å) and angles(°) for adenine : suberic acid : hydrate 2:2:1

Bond length (Å)		Bond length (Å)		Bond length (Å)	
C1-N9	1.320(7)	N7-H7B	0.8800	C14-O14	1.307(7)
C1-N2	1.341(6)	C10-O11	1.202(7)	C14-C15	1.510(7)
C1-H1	0.9500	C10-O10	1.289(8)	C15-C16	1.516(8)
C3-N4	1.357(6)	C10-C11	1.514(9)	C15-H15A	0.9900
C3-N2	1.368(7)	C11-C12	1.493(9)	C15-H15B	0.9900
C3-C8	1.389(9)	C11-H11A	0.9900	C16-C17	1.520(7)
C5-N6	1.317(8)	C11-H11B	0.9900	C16-H16A	0.9900
C5-N4	1.353(8)	C12-C13	1.547(9)	C16-H16B	0.9900
C5-H5	0.9500	C12-H12A	0.9900	C17-C17^{ii}	1.540(1)
C7-N7	1.359(8)	C12-H12B	0.9900	C17-H17A	0.9900
C7-C8	1.384(9)	C13-C13^{i}	1.501(1)	C17-H17B	0.9900
C7-N6	1.396(7)	C13-H13A	0.9900	O14-H14	0.8400
C8-N9	1.381(6)	C13-H13B	0.9900	O18-H18A	0.86(2)
N2-H2	0.8800	O10-H10	0.8400	O18-H18B	0.85(2)
N7-H7A	0.8800	C14-O15	1.223(6)		

Bond angle (°)		Bond angle (°)		Bond angle (°)	
N9-C1-N2	113.0(5)	C1-N2-H2	125.9	C13^{I}-C13-C12	113.4(6)
N9-C1-H1	123.5	C3-N2-H2	125.9	O15-C14-C15	124.1(5)
N2-C1-H1	123.5	C3-N4-C5	109.4(5)	O14-C14-C15	112.7(4)
N4-C3-N2	127.5(5)	C5-N6-C7	119.3(5)	C14-C15-C16	115.6(4)
N4-C3-C8	128.6(5)	C7-N7-H7A	120.0	C14-C15-H15A	108.4
N2-C3-C8	103.9(4)	C7-N7-H7B	120.0	C16-C15-H15A	108.4
N6-C5-N4	128.9(5)	H7A-N7-H7B	120.0	C14-C15-H15B	108.4
N6-C5-H5	115.6	C1-N9-C8	103.6(5)	C16-C15-H15B	108.4
N4-C5-H5	115.5	O11-C10-O10	122.0(6)	H15A-C15-H15B	107.4
N7-C7-C8	121.7(5)	O11-C10-C11	121.1(6)	C15-C16-C17	113.0(4)
N7-C7-N6	120.9(5)	O10-C10-C11	116.8(5)	C15-C16-H16A	109.0
C8-C7-N6	117.4(6)	C12-C11-C10	111.0(5)	C17-C16-H16A	109.0
N9-C8-C7	132.3(6)	C12-C11-H11A	109.4	C15-C16-H16B	109.0
N9-C8-C3	111.3(5)	C10-C11-H11A	109.4	C17-C16-H16B	109.0
C7-C8-C3	116.4(5)	C12-C11-H11B	109.4	H16A-C16-H16B	107.8
C1-N2-C3	108.2(5)	C10-C11-H11B	109.5	C16-C17-C17^{i}	114.3(5)
C13^{i}-C13-H13A	108.9	H11A-C11-H11B	108.0	C16-C17-H17A	108.7
C12-C13-H13A	108.9	C11-C12-C13	111.6(5)	C17^{ii}-C17-H17A	108.7
C13^{i}-C13-H13B	108.9	C11-C12-H12A	109.3	C16-C17-H17B	108.7
C12-C13-H13B	108.9	C13-C12-H12A	109.3	C17^{ii}-C17-H17B	108.7
H13A-C13-H13B	107.7	C11-C12-H12B	109.3	H17A-C17-H17B	107.6
C10-O10-H10	109.5	C13-C12-H12B	109.3	C14-O14-H14	109.5
O15-C14-O14	123.3(5)	H12A-C12-H12B	108.0	H18A-O18-H18B	110(4)

Torsion angle (°)		Torsion angle (°)	
N7-C7-C8-N9	-2.1(8)	N4-C5-N6-C7	1.8(7)
N6-C7-C8-N9	178.2(4)	N7-C7-N6-C5	180.0(4)
N7-C7-C8-C3	179.2(4)	C8-C7-N6-C5	-0.3(7)
N6-C7-C8-C3	-0.5(7)	N2-C1-N9-C8	1.0(5)
N4-C3-C8-N9	-178.9(4)	C7-C8-N9-C1	-179.8(5)
N2-C3-C8-N9	0.8(5)	C3-C8-N9-C1	-1.1(5)
N4-C3-C8-C7	0.1(7)	O11-C10-C11-C12	97.0(7)
N2-C3-C8-C7	179.8(4)	O10-C10-C11-C12	-80.2(7)
N9-C1-N2-C3	-0.5(5)	C10-C11-C12-C13	-178.3(5)
N4-C3-N2-C1	179.5(4)	C11-C12-C13-C13^{i}	-176.7(6)
C8-C3-N2-C1	-0.2(5)	O15-C14-C15-C16	-0.6(6)
N2-C3-N4-C5	-178.5(4)	O14-C14-C15-C16	179.5(4)
C8-C3-N4-C5	1.1(6)	C14-C15-C16-C17	177.4(3)
N6-C5-N4-C3	-2.1(6)	C15-C16-C17-C17^{ii}	177.0(4)

Appendix 10:

10.1: ^{1}H NMR spectra of adenine : azelaic acid adduct (solvent – DMSO)

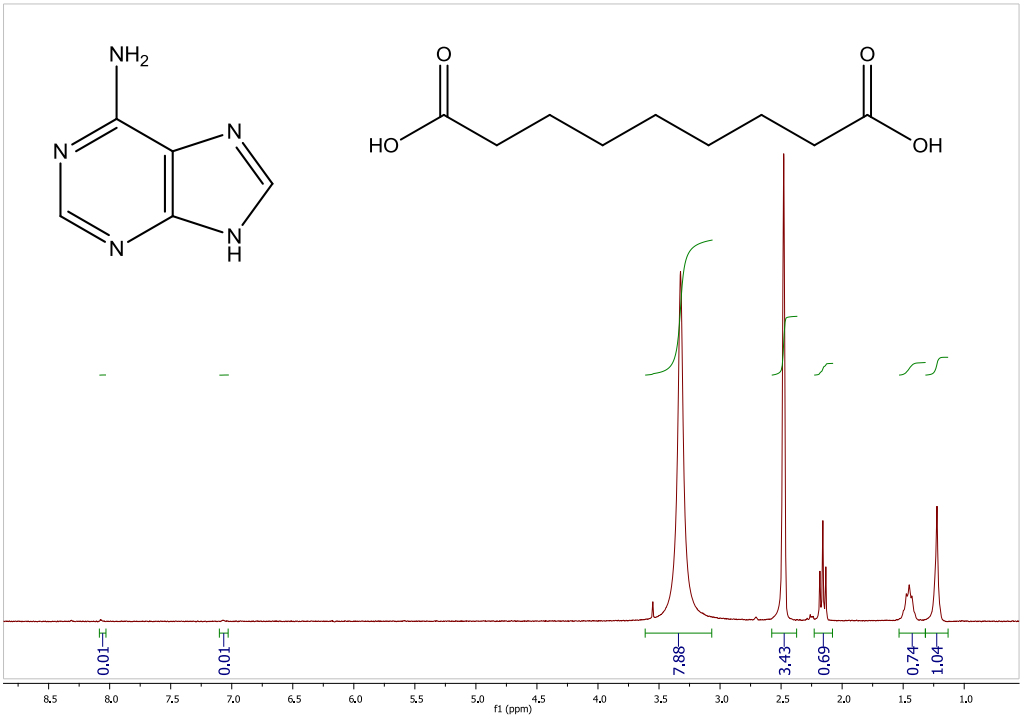

Adenine:	Not present		
Azelaic acid:	1.2 (6H,s),	1.4 (4H,t),	2.2 (4H,t)

10.2: The diffraction pattern simulated from the single crystal structure compared to that of the laboratory experimental powder diffraction pattern of the azelaic acid polymorph

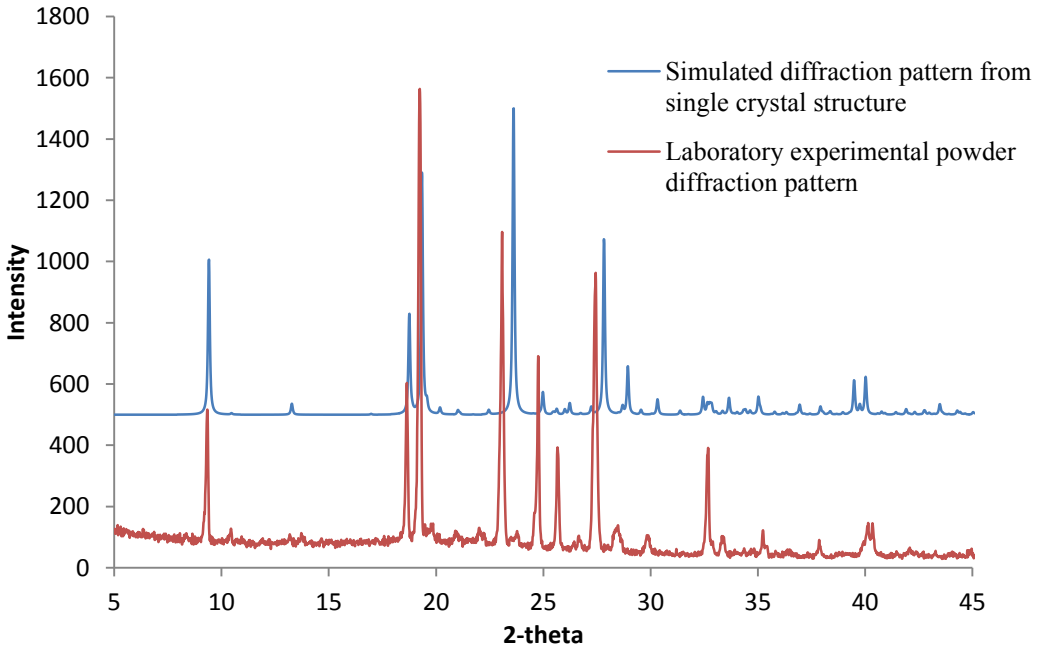

10.3: Ortep of the azelaic acid polymorph

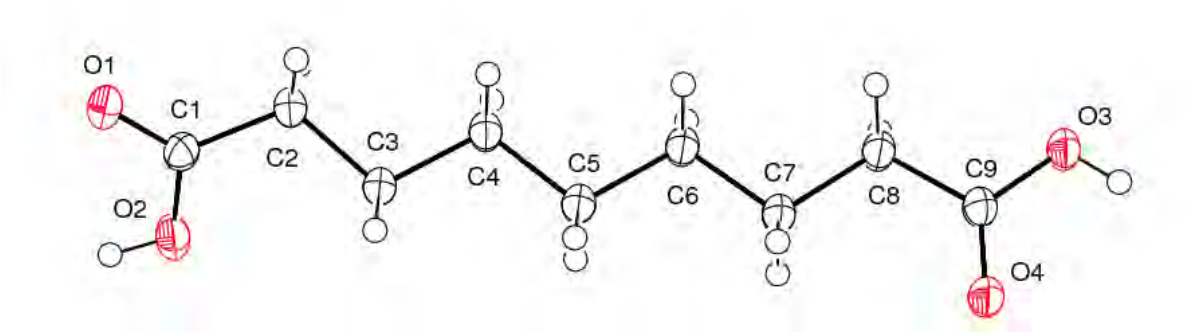

10.4: Crystallographic details for the azelaic acid polymorph

Empirical formula	$C_9 H_{16} O_4$
Formula weight	188.22
Temperature	120(2) K
Wavelength	1.54184 Å
Crystal system	Monoclinic
Space group	$P2_1/c$
Unit cell dimensions	a = 5.5114(1) Å b = 9.4563(2) Å c = 18.8814(4) Å β = 95.994(2) °
Volume	978.67(3) $Å^3$
Z	4
Density (calculated)	1.277 Mg/m^3
Absorption coefficient	0.832 mm^{-1}
F(000)	408
Crystal size	0.23 x 0.18 x 0.08 mm^3
Theta range for data collection	6.64 to 66.59°.
Index ranges	-6<=h<=6, -11<=k<=11, -22<=l<=22
Reflections collected	13150
Independent reflections	1697 [R(int) = 0.0358]
Completeness to theta = 66.59°	98.0 %
Absorption correction	Semi-empirical from equivalents
Max. and min. transmission	0.9364 and 0.8317
Refinement method	Full-matrix least-squares on F^2
Data / restraints / parameters	1697 / 0 / 122
Goodness-of-fit on F^2	1.069
Final R indices [I>2sigma(I)]	R_1 = 0.0472, wR_2 = 0.1217
R indices (all data)	R_1 = 0.0525, wR_2 = 0.1288
Largest diff. peak and hole	0.304 and -0.203 $e.Å^{-3}$

10.5: Intramolecular bond lengths (Å) and angles (°) for the azelaic acid polymorph

Bond length (Å)		Bond length (Å)		Bond length (Å)	
O3-C9	1.322(2)	C5-C4	1.525(2)	C9-C8	1.498(2)
O3-H3	0.8400	C5-H5A	0.9900	C4-H4A	0.9900
O2-C1	1.308(2)	C5-H5B	0.9900	C4-H4B	0.9900
O2-H2	0.8400	C3-C2	1.525(2)	C8-H8A	0.9900
O4-C9	1.221(2)	C3-C4	1.530(2)	C8-H8B	0.9900
C7-C6	1.525(2)	C3-H3A	0.9900	C1-C2	1.499(2)
C7-C8	1.525(2)	C3-H3B	0.9900	C2-H2A	0.9900
C7-H7A	0.9900	C6-H6A	0.9900	C2-H2B	0.9900
C7-H7B	0.9900	C6-H6B	0.9900		
C5-C6	1.524(2)	O1-C1	1.230(2)		

Bond angle (°)		Bond angle (°)		Bond angle (°)	
C9-O3-H3	109.5	C2-C3-H3B	109.4	H4A-C4-H4B	107.6
C1-O2-H2	109.5	C4-C3-H3B	109.4	C9-C8-C7	115.3(1)
C6-C7-C8	111.0(1)	H3A-C3-H3B	108.0	C9-C8-H8A	108.5
C6-C7-H7A	109.4	C5-C6-C7	114.1(1)	C7-C8-H8A	108.5
C8-C7-H7A	109.4	C5-C6-H6A	108.7	C9-C8-H8B	108.5
C6-C7-H7B	109.4	C7-C6-H6A	108.7	C7-C8-H8B	108.5
C8-C7-H7B	109.4	C5-C6-H6B	108.7	H8A-C8-H8B	107.5
H7A-C7-H7B	108.0	C7-C6-H6B	108.7	O1-C1-O2	122.8(1)
C6-C5-C4	112.5(1)	H6A-C6-H6B	107.6	O1-C1-C2	122.1(1)
C6-C5-H5A	109.1	O4-C9-O3	123.0(1)	O2-C1-C2	115.1(1)
C4-C5-H5A	109.1	O4-C9-C8	124.4(1)	C1-C2-C3	116.3(1)
C6-C5-H5B	109.1	O3-C9-C8	112.(1)	C1-C2-H2A	108.2
C4-C5-H5B	109.1	C5-C4-C3	114.0(1)	C3-C2-H2A	108.2
H5A-C5-H5B	107.8	C5-C4-H4A	108.8	C1-C2-H2B	108.2
C2-C3-C4	111.1(1)	C3-C4-H4A	108.8	C3-C2-H2B	108.2
C2-C3-H3A	109.4	C5-C4-H4B	108.8	H2A-C2-H2B	107.4
C4-C3-H3A	109.4	C3-C4-H4B	108.8		

Torsion angle (°)		Torsion angle (°)	
C4-C5-C6-C7	174.4(1)	O3-C9-C8-C7	178.7(1)
C8-C7-C6-C5	179.7(1)	C6-C7-C8-C9	174.0(1)
C6-C5-C4-C3	179.6(1)	O1-C1-C2-C3	145.8(2)
C2-C3-C4-C5	170.3(1)	O2-C1-C2-C3	-36.5(2)
O4-C9-C8-C7	-2.0(2)	C4-C3-C2-C1	177.9(1)

10.6.1: ^{1}H NMR spectra of adenine : azelaic acid adduct (product of crystallisation from methanol) repeat (solvent – DMSO)

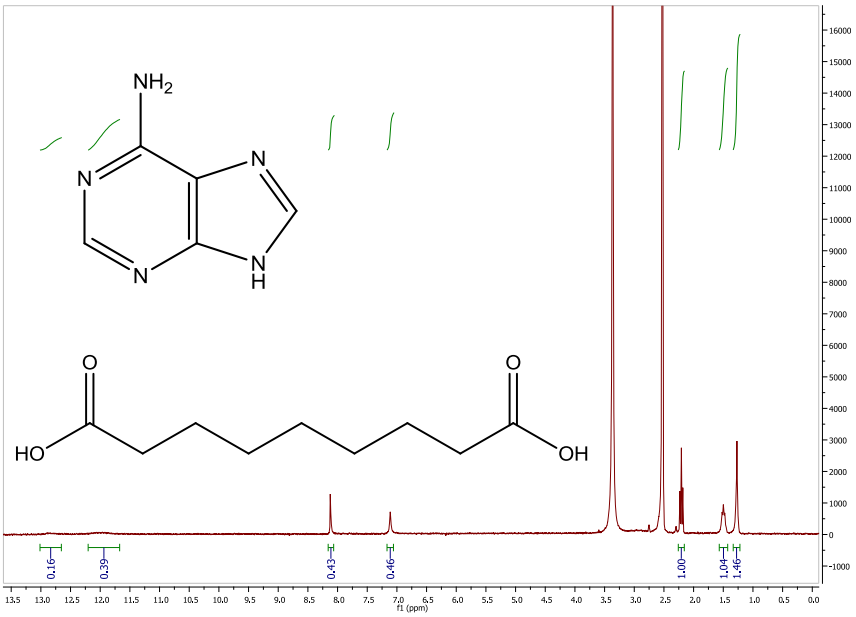

Adenine: 7.15 (2H,s), 8.15 (2H,d)
Azelaic acid: 1.25 (6H,s), 1.5 (4H,t), 2.25 (4H,t)

10.6.2: ^{1}H NMR spectra of adenine : azelaic acid adduct (product of crystallisation from ethanol) repeat (solvent – DMSO)

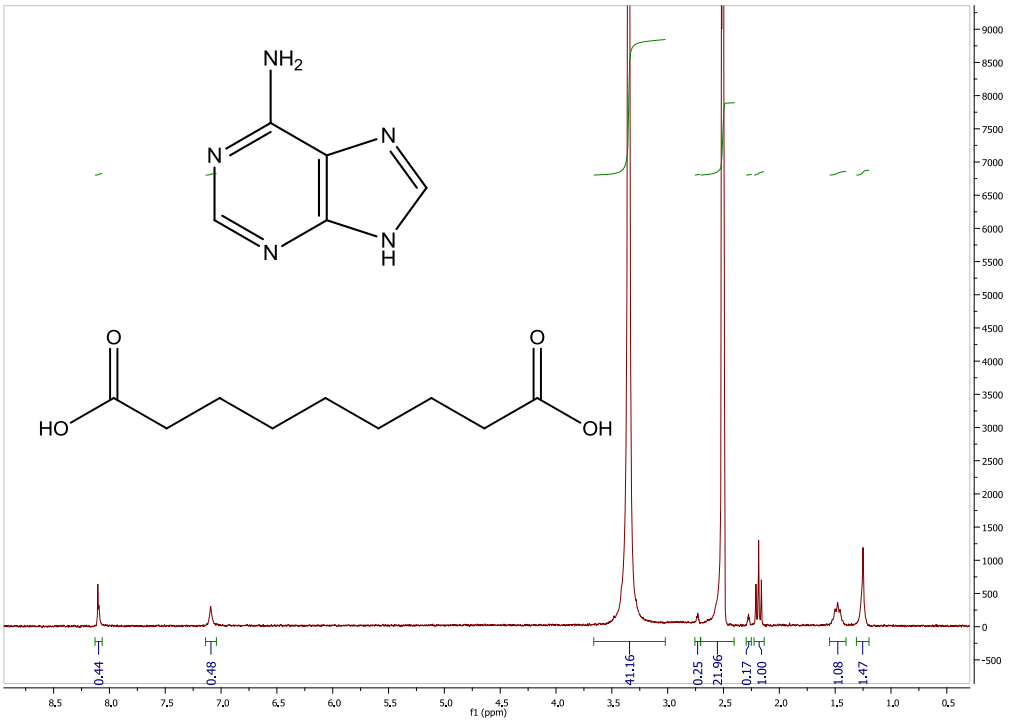

Adenine: 7.15 (2H,s), 8.15 (2H,d),
Azelaic acid: 1.25 (6H,s), 1.45 (4H,t), 2.20 (4H,t)

10.7: Indexing results for adenine : azelaic acid adduct, with the unit cell highlighted in orange

I20	Merit	Volume	V/V1	a	b	c	alpha	beta	gamma
17	7.1	1789.405	1	21.914	5.0149	20.9548	90	129.01	90
17	7.1	1789.405	1	21.914	5.0149	20.9548	90	129.01	90
17	7	1269.422	0.71	9.8836	10.8608	18.0716	95.918	60.624	58.814
17	6.3	4394.352	2.46	34.0165	28.0501	4.6054	90	90	90
17	6.3	4394.352	2.46	34.0165	28.0501	4.6054	90	90	90
17	6	1451.132	0.81	20.9083	9.3719	9.1299	90	125.792	90
17	6	1451.132	0.81	20.9083	9.3719	9.1299	90	125.792	90
17	5.4	4392.873	2.45	56.0465	17.0131	4.607	90	90	90
17	5.4	4392.873	2.45	56.0465	17.0131	4.607	90	90	90
17	4.31	2855.517	1.6	6.7166	8.5774	49.5658	90	90	90
16	12	547.189	0.31	7.1659	9.8778	9.8163	60.293	84.204	66.06
16	6	1297.161	0.72	18.2318	4.6715	16.3596	90	111.414	90
16	6	1297.161	0.72	18.2318	4.6715	16.3596	90	111.414	90
16	6	1297.161	0.72	18.2318	4.6715	16.3596	90	111.414	90
15	14	937.496	0.52	9.2242	10.8125	13.4039	91.446	63.374	57.137
15	14	530.951	0.3	6.837	9.3069	9.7017	114.5	79.493	80.16
15	14	530.95	0.3	6.837	9.3069	10.8016	118.727	62.019	99.84
15	12	1267.571	0.71	15.7558	10.8657	18.0229	95.93	146.835	63.687
15	12	1267.566	0.71	15.7557	14.8981	18.0228	60.956	33.165	38.816
15	12	945.183	0.53	12.5235	13.4668	10.8483	91.981	63.997	138.586
15	11	933.852	0.52	9.6918	10.8227	13.3423	91.762	117.3	53.108
15	9	1420.623	0.79	12.9814	11.2215	9.7834	90	94.574	90
15	9	1381.674	0.77	12.5685	12.9505	10.9615	90	129.249	90
15	9	932.169	0.52	13.3212	12.3582	12.346	52.089	44.16	41.951
15	9	932.167	0.52	13.3212	12.3582	9.6906	103.86	117.431	41.951
15	7	1657.955	0.93	11.1208	11.1513	23.6491	103.52	50.655	69.662
15	7	1314.606	0.73	17.6969	4.6902	16.544	90	106.795	90
15	7	1241.622	0.69	17.0757	14.0443	5.2171	90	97.076	90
15	7	1241.621	0.69	17.2294	14.0443	5.2171	90	100.412	90
15	7	932.166	0.52	9.2363	9.6906	13.3212	117.431	116.562	69.885
15	6	1310.357	0.73	16.9677	14.0157	5.5135	90	92.027	90
15	6	1275.021	0.71	14.3799	10.476	9.4307	90	116.172	90
14	22	531.392	0.3	6.9563	12.6683	10.4781	54.226	69.104	45.429
14	18	530.72	0.3	6.955	9.2161	14.4922	60.961	42.489	77.963
14	12	526.485	0.29	6.8975	9.1966	10.4215	58.123	110.275	101.476
14	11	1038.697	0.58	15.0559	8.1405	9.4591	90	116.37	90
14	9	1153.632	0.64	18.8301	5.2088	13.0157	90	115.357	90
14	8	1221.631	0.68	13.6737	10.4689	9.0015	90	108.547	90
14	8	1221.63	0.68	13.7731	10.4689	9.0015	90	109.741	90
14	7	2587.561	1.45	20.2569	13.6947	9.3275	90	90	90
14	7	1038.376	0.58	10.5462	16.2351	6.4298	90	109.404	90

14	6	1363.161	0.76	18.184	4.9204	16.3474	90	111.255	90
14	6	1350.881	0.75	18.2618	4.5408	17.537	90	111.732	90
14	6	1199.534	0.67	19.2476	7.5494	9.3638	90	118.164	90

Appendix 11:

11.1.1: ^{1}H NMR spectra of adenine : sebacic acid adduct (product of crystallisation from MeOH) (solvent – DMSO)

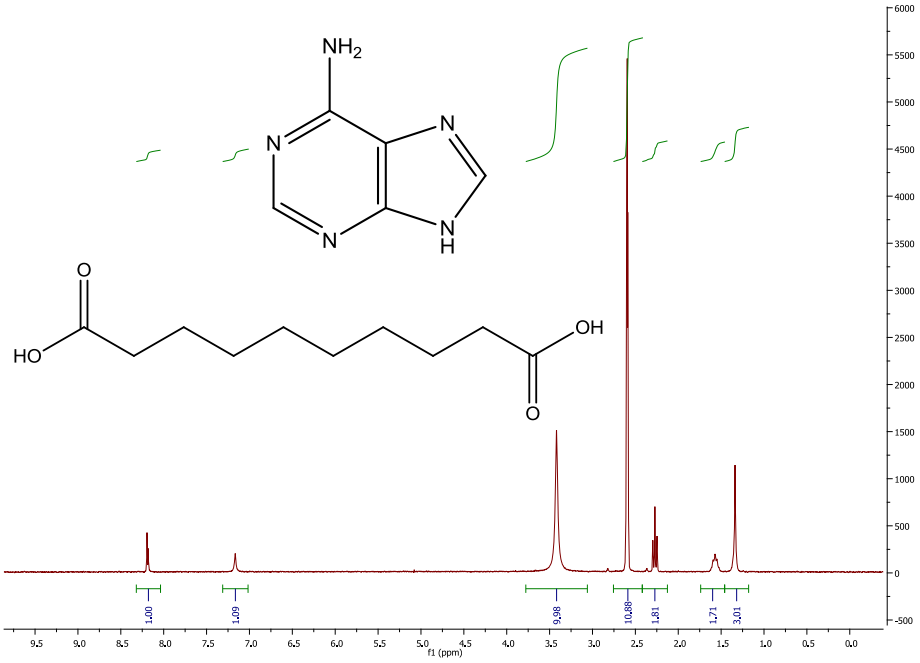

Adenine: 7.1 (2H,s), 8.10 (2H,d), Sebacic acid: 1.3 (8H, s), 1.55 (4H, q), 2.25 (4H,t)

11.1.2: ^{1}H NMR spectra of adenine : sebacic acid adduct (product of crystallisation from EtOH) (solvent – DMSO)

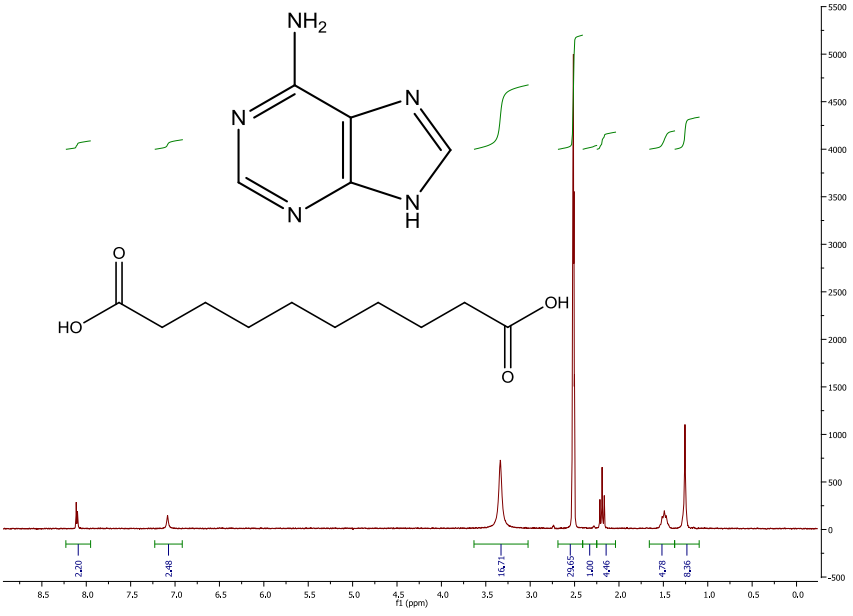

Adenine: 7.1 (2H,s), 8.10 (2H,d), Sebacic acid: 1.25 (8H, s), 1.5 (4H, q), 2.2 (4H,t)

11.2: The diffraction pattern simulated from the single crystal structure compared to that of the laboratory experimental powder diffraction pattern of adenine : sebacic acid : hydrate, 4:3:4

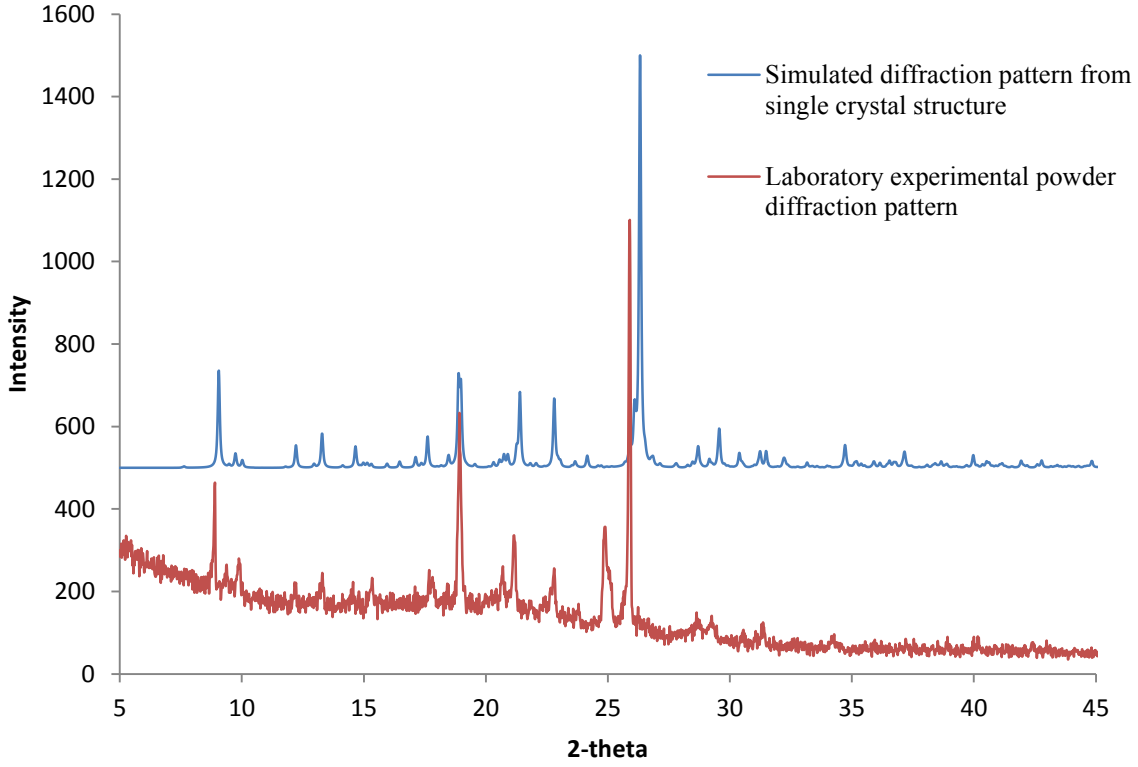

11.4: Ortep of adenine and sebacic acid hydrated cocrystal

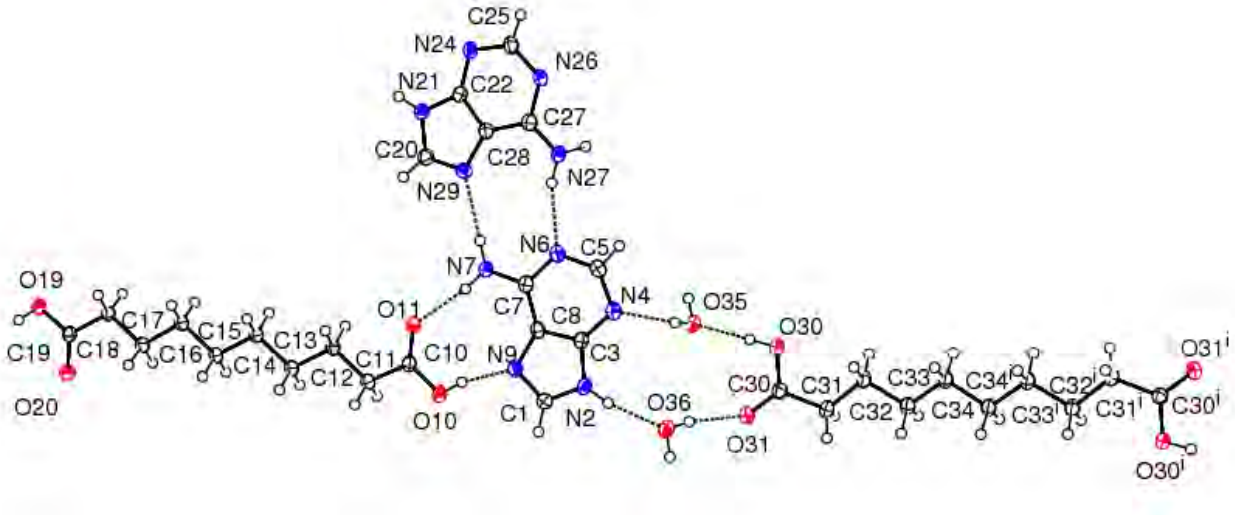

11.5: Crystallographic details for the adenine : sebacic acid : hydrate, 4:3:4

Empirical formula	$C_{25}\ H_{41}\ N_{10}\ O_8$	
Formula weight	609.68	
Temperature	120(2) K	
Wavelength	1.54184 Å	
Crystal system	Trioclinic	
Space group	P -1	
Unit cell dimensions	a = 10.3417(2) Å b = 12.4896(3) Å c = 12.7894(3) Å	α = 101.134(2) ° β = 95.994(2) ° γ = 104.620(1) °
Volume	1460.92(6) $Å^3$	
Z	2	
Density (calculated)	1.386 Mg/m^3	
Absorption coefficient	0.881mm^{-1}	
F(000)	650	
Crystal size	0.19 x 0.12 x 0.10 mm^3	
Theta range for data collection	6.49 to 66.60°.	
Index ranges	-12<=h<=12, -14<=k<=14, -15<=l<=15	
Reflections collected	14245	
Independent reflections	5019 [R(int) = 0.0254]	
Completeness to theta = 66.60°	97.2 %	
Absorption correction	Semi-empirical from equivalents	
Max. and min. transmission	0.9170 and 0.8504	
Refinement method	Full-matrix least-squares on F^2	
Data / restraints / parameters	5019 / 6 / 403	
Goodness-of-fit on F^2	1.044	
Final R indices [I>2sigma(I)]	R1 = 0.0360, wR2 = 0.0877	
R indices (all data)	R1 = 0.0429, wR2 = 0.0918	
Largest diff. peak and hole	0.286 and -0.214 e.$Å^{-3}$	

11.6: Intramolecular bond lengths (Å) and angles (°) for the adenine : sebacic acid : hydrate, 4:3:4

Bond length (Å)		Bond length (Å)		Bond length (Å)	
N2-C1	1.353(2)	C16-H16A	0.990	N27-H27A	0.880
N2-C3	1.369(2)	C16-H16B	0.990	N27-H27B	0.880
N2-H2	0.880	O20-C19	1.226(2)	C20-N21	1.364(2)
N7-C7	1.330(2)	O19-C19	1.302(2)	C20-H20	0.950
N7-H7A	0.880	O19-H19	0.840	N21-H21	0.880
N7-H7B	0.880	C14-C13	1.525(2)	C25-H25	0.950
C1-N9	1.320(2)	C14-H14A	0.990	C27-C28	1.411(2)
C1-H1	0.950	C14-H14B	0.990	O30-C30	1.312(2)
N4-C5	1.333(2)	C12-C13	1.522(2)	O30-H30	0.840
N4-C3	1.345(2)	C12-H12A	0.990	O31-C30	1.222(2)
C5-N6	1.334(2)	C12-H12B	0.990	C32-C33	1.522(2)
C5-H5	0.950	C19-C18	1.505(2)	C32-C31	1.523(2)
C3-C8	1.387(2)	C18-C17	1.518(2)	C32-H32A	0.990
C7-N6	1.358(2)	C18-H18A	0.990	C32-H32B	0.990
C7-C8	1.409(2)	C18-H18B	0.990	C31-C30	1.502(2)
N9-C8	1.387(2)	C17-H17A	0.990	C31-H31A	0.990
O10-C10	1.309(2)	C17-H17B	0.990	C31-H31B	0.990
O10-H10	0.840	C13-H13A	0.990	C34-C34^{i}	1.520(3)
O11-C10	1.222(2)	C13-H13B	0.990	C34-C33	1.521(2)
C11-C10	1.503(2)	N26-C25	1.340(2)	C34-H34A	0.990
C11-C12	1.518(2)	N26-C27	1.368(2)	C34-H34B	0.990
C11-H11A	0.990	C22-N24	1.355(2)	C33-H33A	0.990
C11-H11B	0.990	C22-N21	1.363(2)	C33-H33B	0.990
C15-C16	1.518(2)	C22-C28	1.386(2)	O35-H35A	0.873(2)
C15-C14	1.526(2)	N24-C25	1.326(2)	O35-H35B	0.881(2)
C15-H15A	0.990	N29-C20	1.314(2)	O36-H36A	0.845(2)
C15-H15B	0.990	N29-C28	1.380(2)	O36-H36B	0.860(2)
C16-C17	1.526(2)	N27-C27	1.324(2)		

Bond angle (°)		Bond angle (°)		Bond angle (°)	
C1-N2-C3	106.6(1)	C13-C14-H14A	109.0	N29-C20-H20	123.3
C1-N2-H2	126.7	C15-C14-H14A	109.0	N21-C20-H20	123.3
C3-N2-H2	126.7	C13-C14-H14B	109.0	C22-N21-C20	106.7(1)
C7-N7-H7A	120.0	C15-C14-H14B	109.0	C22-N21-H21	126.6
C7-N7-H7B	120.0	H14A-C14-H14B	107.8	C20-N21-H21	126.6
H7A-N7-H7B	120.0	C11-C12-C13	112.1(1)	N24-C25-N26	127.8(1)
N9-C1-N2	113.7(1)	C11-C12-H12A	109.2	N24-C25-H25	116.1
N9-C1-H1	123.2	C13-C12-H12A	109.2	N26-C25-H25	116.1
N2-C1-H1	123.2	C11-C12-H12B	109.2	N27-C27-N26	119.8(1)
C5-N4-C3	110.5(1)	C13-C12-H12B	109.2	N27-C27-C28	124.1(1)
N4-C5-N6	129.4(1)	H12A-C12-H12B	107.9	N26-C27-C28	116.2(1)
N4-C5-H5	115.3	O20-C19-O19	123.4(1)	N29-C28-C22	111.1(1)
N6-C5-H5	115.3	O20-C19-C18	123.0(1)	N29-C28-C27	132.0(1)
N4-C3-N2	127.4(1)	O19-C19-C18	113.6(1)	C22-C28-C27	116.9(1)
N4-C3-C8	126.9(1)	C19-C18-C17	114.4(1)	C30-O30-H30	109.5
N2-C3-C8	105.7(1)	C19-C18-H18A	108.7	C33-C32-C31	111.3(1)
N7-C7-N6	119.2(1)	C17-C18-H18A	108.7	C33-C32-H32A	109.4
N7-C7-C8	123.4(1)	C19-C18-H18B	108.7	C31-C32-H32A	109.4
N6-C7-C8	117.3(1)	C17-C18-H18B	108.7	C33-C32-H32B	109.4
C5-N6-C7	118.8(1)	H18A-C18-H18B	107.6	C31-C32-H32B	109.4
C1-N9-C8	103.8(1)	C18-C17-C16	112.8(1)	H32A-C32-H32B	108.0
C3-C8-N9	110.2(1)	C18-C17-H17A	109.0	C30-C31-C32	117.1(1)
C3-C8-C7	117.0(1)	C16-C17-H17A	109.0	C30-C31-H31A	108.0
N9-C8-C7	132.8(1)	C18-C17-H17B	109.0	C32-C31-H31A	108.0
C10-O10-H10	109.5	C16-C17-H17B	109.0	C30-C31-H31B	108.0
C10-C11-C12	115.0(1)	H17A-C17-H17B	107.8	C32-C31-H31B	108.0
C10-C11-H11A	108.5	C12-C13-C14	112.9(1)	H31A-C31-H31B	107.3
C12-C11-H11A	108.5	C12-C13-H13A	109.0	$C34^{i}$-C34-C33	113.5(2)
C10-C11-H11B	108.5	C14-C13-H13A	109.0	$C34^{i}$-C34-H34A	108.9
C12-C11-H11B	108.5	C12-C13-H13B	109.0	C33-C34-H34A	108.9
H11A-C11-H11B	107.5	C14-C13-H13B	109.0	$C34^{i}$-C34-H34B	108.9
C16-C15-C14	114.3(1)	H13A-C13-H13B	107.8	C33-C34-H34B	108.9
C16-C15-H15A	108.7	O11-C10-O10	123.0(1)	H34A-C34-H34B	107.7
C14-C15-H15A	108.7	O11-C10-C11	123.5(1)	C34-C33-C32	114.3(1)
C16-C15-H15B	108.7	O10-C10-C11	113.5(1)	C34-C33-H33A	108.7
C14-C15-H15B	108.7	C25-N26-C27	120.7(1)	C32-C33-H33A	108.7
H15A-C15-H15B	107.6	N24-C22-N21	127.5(1)	C34-C33-H33B	108.7
C15-C16-C17	112.0(1)	N24-C22-C28	127.4(1)	C32-C33-H33B	108.7
C15-C16-H16A	109.2	N21-C22-C28	105.2(1)	H33A-C33-H33B	107.6
C17-C16-H16A	109.2	C25-N24-C22	111.1(1)	O31-C30-O30	123.0(1)
C15-C16-H16B	109.2	C20-N29-C28	103.6(1)	O31-C30-C31	122.1(1)
C17-C16-H16B	109.2	C27-N27-H27A	120.0	O30-C30-C31	114.9(1)
H16A-C16-H16B	107.9	C27-N27-H27B	120.0	H35A-O35-H35	104.3(2)
C19-O19-H19	109.5	H27A-N27-H27B	120.0	H36A-O36-H36B	108.6(2)
C13-C14-C15	112.9(1)	N29-C20-N21	113.4(1)		

Torsion angle (°)		Torsion angle (°)	
C3-N2-C1-N9	-0.9(2)	C15-C14-C13-C12	177.8(1)
C3-N4-C5-N6	0.0(2)	C12-C11-C10-O11	4.1(2)
C5-N4-C3-N2	179.3(1)	C12-C11-C10-O10	-177.1(1)
C5-N4-C3-C8	1.2(2)	N21-C22-N24-C25	179.7(1)
C1-N2-C3-N4	-177.5(1)	C28-C22-N24-C25	1.1(2)
C1-N2-C3-C8	1.0(2)	C28-N29-C20-N21	-0.2(2)
N4-C5-N6-C7	-1.3(2)	N24-C22-N21-C20	-178.3(1)
N7-C7-N6-C5	-178.5(1)	C28-C22-N21-C20	0.5(2)
C8-C7-N6-C5	1.3(2)	N29-C20-N21-C22	-0.2(2)
N2-C1-N9-C8	0.4 (2)	C22-N24-C25-N26	1.0(2)
N4-C3-C8-N9	177.7(1)	C27-N26-C25-N24	-1.8(2)
N2-C3-C8-N9	-0.8(2)	C25-N26-C27-N27	-179.8(1)
N4-C3-C8-C7	-1.1(2)	C25-N26-C27-C28	0.5(2)
N2-C3-C8-C7	-179.5(1)	C20-N29-C28-C22	0.5 (2)
C1-N9-C8-C3	0.3(2)	C20-N29-C28-C27	-179.0(2)
C1-N9-C8-C7	178.8(2)	N24-C22-C28-N29	178.2(1)
N7-C7-C8-C3	179.6(1)	N21-C22-C28-N29	-0.6(2)
N6-C7-C8-C3	-0.3(2)	N24-C22-C28-C27	-2.2(2)
N7-C7-C8-N9	1.1(2)	N21-C22-C28-C27	178.9(1)
N6-C7-C8-N9	-178.7(1)	N27-C27-C28-N29	1.0(3)
C14-C15-C16-C17	-179.0(1)	N26-C27-C28-N29	-179.2(1)
C16-C15-C14-C13	-177.4(1)	N27-C27-C28-C22	-178.5(1)
C10-C11-C12-C13	-175.2(1)	N26-C27-C28-C22	1.3(2)
O20-C19-C18-C17	-8.2(2)	C33-C32-C31-C30	167.2(1)
O19-C19-C18-C17	172.6(1)	$C34^{i}$-C34-C33-C32	176.2 (2)
C19-C18-C17-C16	-179.7(1)	C31-C32-C33-C34	-174.6(1)
C15-C16-C17-C18	-178.1(1)	C32-C31-C30-O31	-157.9(2)
C11-C12-C13-C14	180.0(1)	C32-C31-C30-O30	23.0(2)

Appendix 12:

12.1: Crystalline structure of adenine : adipic acid 2:1

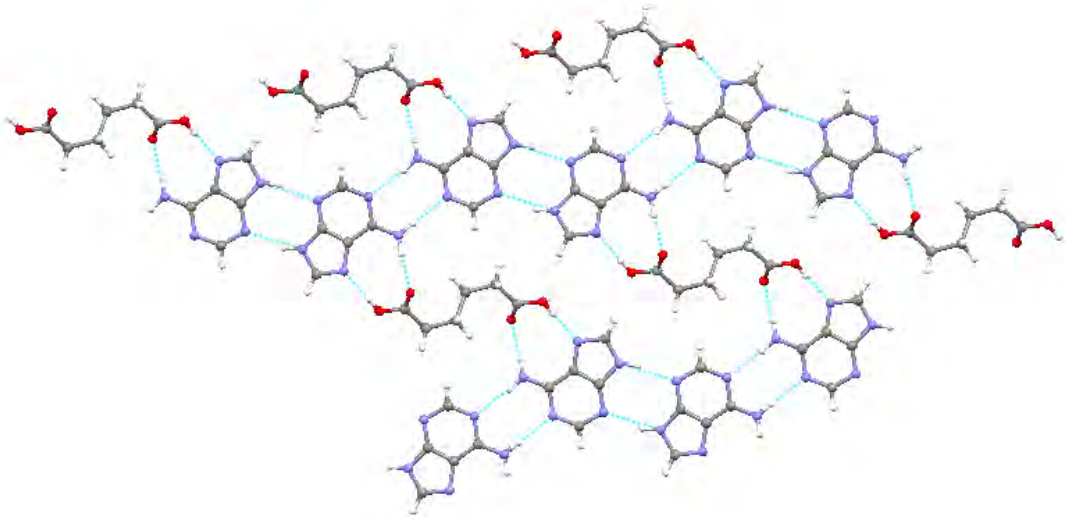

12.2: Crystalline structure of adenine : azelaic acid 1:1

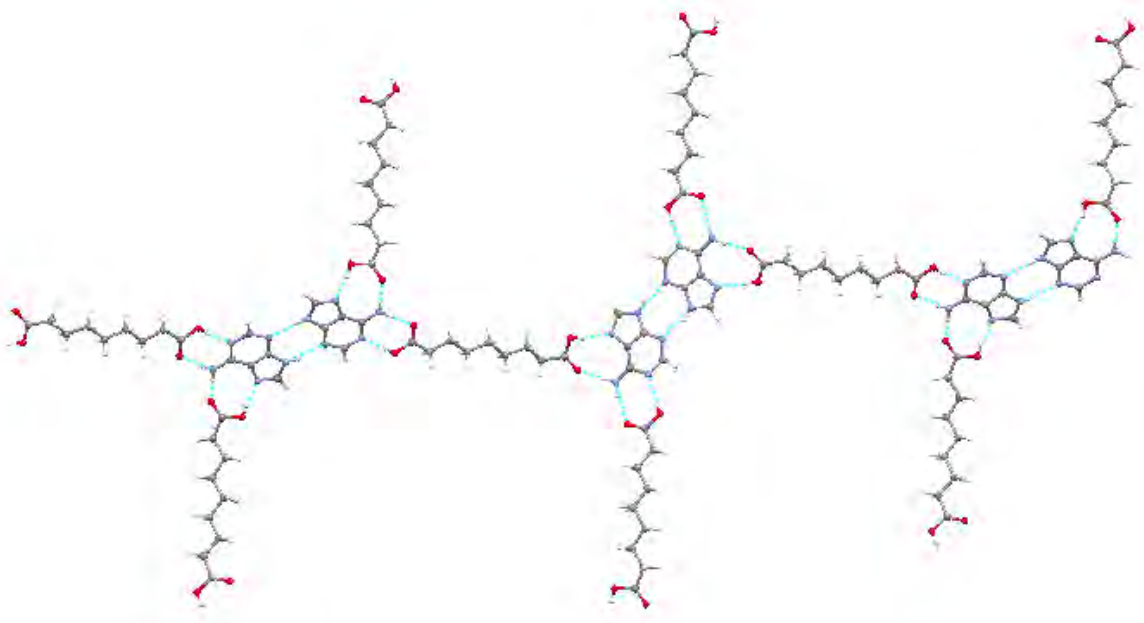

Appendix 13:

The supramolecular behaviour of adenine with succinic, fumaric and maleic acids; tautomerism, cocrystallisation, salt formation and solvation

*Laura J. Thompson, Norhanida Elias, Louise Male & Maryjane Tremayne**

School of Chemistry, University of Birmingham, Edgbaston, Birmingham, B15 2TT, UK

Email: m.tremayne@bham.ac.uk

ABSTRACT

The powerful hydrogen bonding capability of adenine makes it a key component of the DNA double helix, while as a crystalline molecular material, these hydrogen bond donors and acceptors make it a good potential cocrystal component possessing distinct physical properties. Here we report the preparation and structure determination of four adenine-based multicomponent adducts formed with a number of dicarboxylic acids; an anhydrous cocrystal with succinic acid (**1**), anhydrous salts with fumaric acid (**2**) and maleic acid (**3**), and a methanolated salt with maleic acid (**4**). The supramolecular behavior of adenine in these materials is discussed in terms of strong hydrogen bonded bidentate motifs formed between the adenine and acid components and the homomeric adenine synthons retained in these structures. The additional formation of an CH…N interaction on the Watson-Crick site in (**3**) enables the stabilization of the unusual *3H,7H* adeninium tautomer within a purely molecular material.

INTRODUCTION

Adenine (6-aminopurine) is a principal component of DNA and an important constituent of adenosine triphosphate (ATP), making it essential for the release of energy to be used by cells in living organisms. The structural aspects and supramolecular behaviour of adenine are diverse and intriguing. The multiple strong hydrogen bond donor and acceptor sites in the neutral adenine molecule make it a good potential cocrystal component able to form robust heteromeric synthons with other molecules. It forms a number of crystalline complexes, some with metals present [1-5] and other molecular cocrystal materials [6,7] including methanolated adenine : adipic acid [8] and anhydrous forms of adenine : benzoic acid [8,9] and adenine : 2-hydroxybenzoic acid [10]. In all these structures, adenine is present in its most stable and natural tautomeric 9*H* form (Scheme 1), although other less common adenine tautomers have been stabilised in structures in which metal ions are bound to the adenine [5,11,12] and the 7*H* tautomer found within the hydrogen bonding network of a molecular adduct [13]. The existence of multiple tautomeric forms of a nucleobase such as adenine can be problematic in spontaneous mutations in DNA [14], but may also be crucial, along with protonated adenine forms, in terms of high photostability and protection of DNA from UV damage [15].

Adenine also forms crystalline salts in which the adeninium cation itself can adopt a variety of tautomeric forms. A combined theoretical and experimental study placed the relative stability of the adeninium tautomers in their ground state as 1*H*,9*H* > 3*H*,7*H* > 3*H*,9*H* >> 7*H*,9*H* > 1*H*,7*H* [16,17] (Scheme 1) and hence it is unsurprising that the majority of crystalline adeninium salts contain the 1*H*,9*H* tautomer. It is this tautomer that is present in all the molecular adeninium : carboxylate salts reported to date, including oxalate [18], maleate [19] and hydroxybenzoate salts [8], and in combination with the non-canonical neutral 7*H* tautomer in a second hydrated maleate form [13]. Occurrence of the less stable 3*H*,7*H* adeninium tautomer in

the solid state is much less common. There are a few examples in which this tautomer exists in combination with the 1*H*,9*H* form in metal salts [20,21], but only in cobalt and zinc-oxalato frameworks [22] has the 3*H*,7*H* tautomer been reported as the only adeninium component present within the crystal structure. As far as we are aware, the anhydrous hydrogen maleate structure reported in this paper (**3**) is the first example in which the 3*H*,7*H* tautomer is stabilised within the hydrogen-bonding network of a purely molecular salt.

Scheme 1. Tautomers of adenine (top row) and the adeninium ion (bottom row) reported in the crystalline state and discussed in this work.

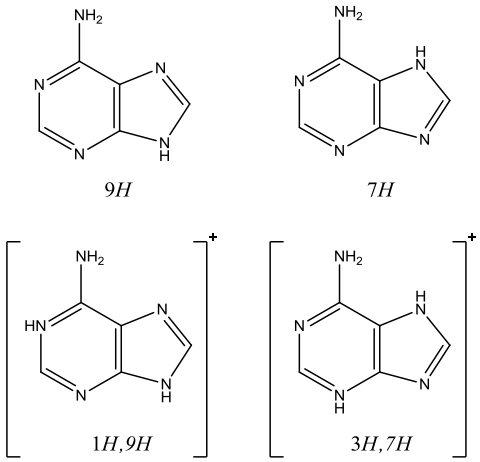

Combination of molecular components in the form of cocrystals or salts provides us with an alternative source of solid crystalline materials with the potential to provide optimal physical properties whilst retaining the chemical properties of the cocrystal components [23-26]. Physical properties can be changed dramatically by formulation in one of these alternative solid forms [27] and it has been shown that properties such as the transfer of melting point behaviour of pure aliphatic dicarboxylic acids can be tuned within a homologous series of cocrystals [28-31]. Although these effects are not always predictable [27,32], the ability to address poor hydration stability [33] and undesirable low or high solubility [28,34,35] by formulation in

cocrystal or salt form, makes these materials an essential tool in pharmaceutical material design and formulation.

Predictable synthesis of a cocrystal or a salt relies on the preferential formation of heteromeric synthons rather than the formation of strong intermolecular interactions between molecules within the individual components. Adenine contains several strong hydrogen bond donor and acceptor sites which are potentially available for interaction with suitable coformers containing complementary hydrogen bonding functionalities such as carboxylic acids. In this paper we report the synthesis and crystal structures of four new crystalline adducts formed by adenine and three dicarboxylic acids; adenine : succinic acid 1:1 (**1**), adeninium : hydrogen fumarate 1:1 (**2**), adeninium : hydrogen maleate 1:1 (**3**), and adeninium : hydrogen maleate : methanolate 2:2:1 (**4**). The supramolecular behaviour of adenine within these materials will be discussed in detail including the adoption of tautomeric form, formation of predicted hydrogen bond motifs, identification of any packing trends across the series and preference for cocrystal or salt formation.

Possible hydrogen bonding motifs in these adducts mimic the hydrogen bonding network in adenine itself [36] based primarily on the formation of strong bidentate synthons. In the pure *9H* form, adenine forms two motifs through complementary N-H...N interactions along the base of two molecules giving an $R_2^2(8)$ ring [37] (motif **I**) and between the Watson-Crick and Hoogsteen edges of neighbouring adenine molecules giving an $R_2^2(9)$ ring (motif **II**) (Scheme 2). Other adenine-adenine motifs include a Hoogsteen pairing generating an $R_2^2(10)$ ring (motif **III**), a Watson-Crick pairing generating an $R_2^2(8)$ ring (motif **IV**) and interaction of the Watson-Crick edge with the base of a neighbouring adenine forming another $R_2^2(8)$ ring (motif **V**). Adenine-acid motifs formed by N-H...O=C and O-H...N interactions include an $R_2^2(8)$ ring on the Watson-Crick edge (motif **VI**) and an $R_2^2(9)$ ring on the Hoogsteen edge

(motif **VII**). Maleic acid provides a possible alternative adenine-acid motif in which an $R_2^2(8)$ ring on the Watson-Crick site is formed by N-H...O(H) and C-H...N interactions rather than through the carboxylic group (motif **VIII**). In order to simplify the discussion and to aid identification of supramolecular trends within this series of structures, alternative motifs arising from tautomeric variation or proton transfer will be given a notation based on the *9H* form (as described above) but with an extension describing the hydrogen position within the motif. E.g: In scheme 2, the *3H,7H* adeninium tautomer is shown forming the motif **I(*3H*)** which denotes the $R_2^2(8)$ ring motif **I** with the hydrogen donated from the base of the adenine molecule on the *3H* position rather than *9H*; **VII(*7H*$^+$)** denotes an additional proton on *7H* of the adeninium ion in the $R_2^2(9)$ ring motif **VII**.

Five adenine : dicarboxylic acid salts or cocrystals have been reported; chlorinated and hydrated adeninium : oxalate structures [18], an adenine : adipic acid methanolate cocrystal [8], and two hydrated adeninium : maleate structures, including a mixed adenine-adeninium system [13] and a second hydrated maleate salt (which was incorrectly reported as adenine : succinate) [19]. All these structures contain one or more of the above motifs, but the hydrogen bonding network is disrupted by the presence of water, solvent or an additional ionic component resulting in the

Scheme 2. Bidentate hydrogen bond motifs found in adenine or adenine:carboxylic acid adducts. Motifs **I**, **II**, **III**, **IV** and **V** formed between adenine units, **VI** and **VII** formed by adenine with acids and **VIII** formed by adenine-maleic acid. Motifs **I(*3H*)** and **VII(*7H*$^+$)** denote alternative tautomer and adeninium motifs respectively.

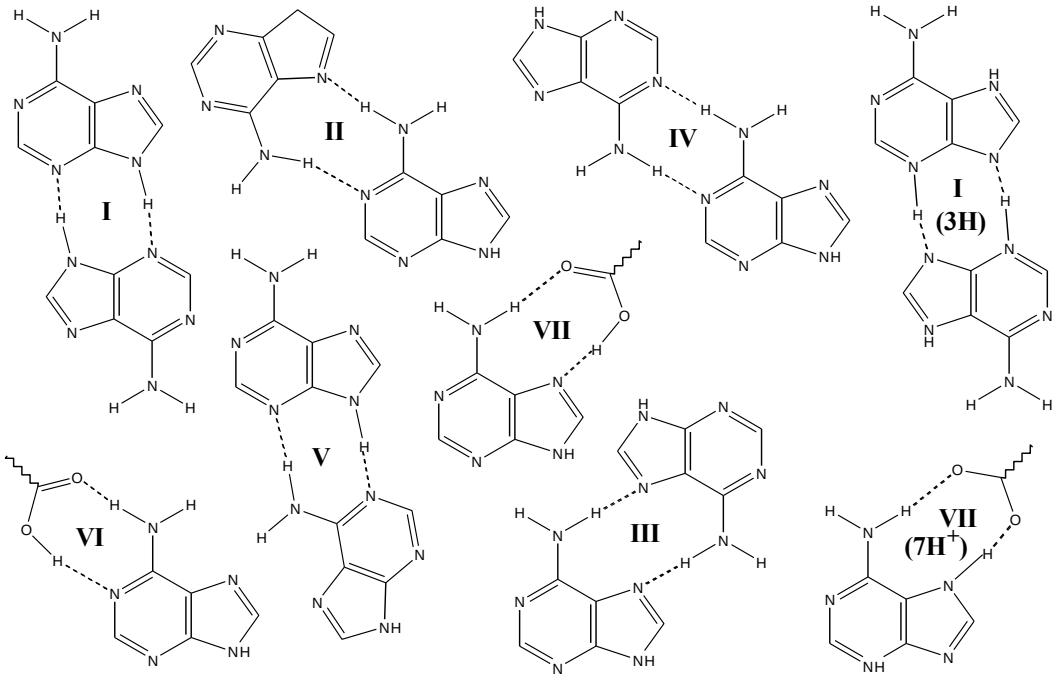

formation of single adenine-acid carboxylic O-H...N(hetero) (or C=O...H-N(adeninium) in salt form) and solvent-centred intermolecular interactions in addition to the bidentate motifs described above. As anhydrous adducts, structures (**1**), (**2**) and (**3**) reported in this paper, may display the formation of more predictable bidentate hydrogen bond motifs, whereas structure (**4**) is another new maleate adduct in which the solvent is retained. The hydrogen bonding network adopted by all these new materials will be analysed and the structural behaviour of all four maleate adducts discussed.

EXPERIMENTAL

*Preparation of compounds (**1**) to (**4**)*

All starting materials were purchased from Sigma Aldrich and used without purification. Equi-millimolar amounts of the two starting materials (approximately 0.6mmol), adenine and the respective dicarboxylic acid, were dissolved in warm solvent (10ml). The filtered solutions were mixed and allowed to cool to room temperature. On slow evaporation of the solvent, crystals were formed and obtained by filtration. For (**1**), (**2**) and (**4**), the crystals were obtained from methanol whereas (**3**) was obtained from an ethanolic solution.

Single crystal structure determination and refinement

Single crystal X-ray diffraction data were collected from suitable crystals of all four adducts. Data from crystals (**1**) and (**2**) were collected on a Bruker APEX II CCD diffractometer at the window of a Bruker FR591 rotating anode ($\lambda_{Mo\text{-}K\alpha}$=0.71073 Å) at 120K by the UK National Crystallography Service[38]. The data collections were driven by *COLLECT*[39] and processed by *DENZO*[40]. Absorption corrections were applied using SADABS[41]. Data for adduct (**3**) were collected on a Crystal Logic 4-circle kappa diffractometer equipped with a Rigaku Saturn 724 CCD detector using synchrotron radiation (λ = 0.68890 Å) at beamline I19 at the Diamond Light Source, UK. The data were collected at 100K and the data collection was driven and processed (including absorption correction) by CrystalClear-SM Expert 2.0 r5[42]. Data for (**4**) were collected on a Bruker SMART 6000 diffractometer (λ CuKα = 1.54184 Å) at 120K in the School of Chemistry at the University of Birmingham. The data collection was driven by SMART[43] and processed by SAINT[44]. An absorption correction was applied using SADABS[41].

All four structures were solved by direct methods and refined on F^2 by full-matrix least-squares refinement using *SHELXS97* and *SHELXL97*[45] respectively. All non hydrogen atoms were refined with anisotropic displacement parameters. Electron density maps were used to locate the positions of the hydrogen atoms thus confirming tautomeric form and whether or not proton transfer had taken place between the molecular components. All H atoms were then added at calculated positions and refined by use of a riding model with isotropic displacement parameters based on the equivalent isotropic displacement parameter (U_{eq}) of the parent atom. *WinGX*[46] was used to prepare the material for publication. The graphics were produced using *DIAMOND*[47] and *ORTEP3*[48] with details of intermolecular interactions analysed with the aid of *PLATON*[49] and geometrical analysis carried out in *MERCURY*[50]. The data from (**2**) are subject to merohedral twinning by 180° about the [100] direct lattice direction with the refined ratio of fractional contributions of the two components being 0.54:0.46. Crystallographic data for all four structures are given in Table 1.

RESULTS

The crystal structures of all four materials (**1**)-(**4**) contain extensive hydrogen bond networks in which the adenine and acid components form a range of possible synthons shown in Scheme 2. In these structures, adenine is present in both neutral form ((**1**)) and protonated forms ((**2**), (**3**) and (**4**)) in which two distinct tautomers are displayed. X-ray powder diffraction patterns were simulated from each single crystal structure and comparison with the experimental diffraction data showed a clear match between the crystals chosen for structural analysis and the bulk sample, although in (**3**) there is evidence of some excess maleic acid present (see Supplementary Information). Details of selected intramolecular bond lengths and angles for (**1**)-(**4**) confirming tautomeric form and acid conformation are given as Supplementary Information.

*Crystal structure of adenine:succinic acid 1:1 (**1**)*

In the crystal structure of (**1**), the neutral adenine molecule is in the most stable and expected *9H* tautomeric form confirmed by the endocyclic C4-N9-C8 angle being approximately 3° larger than the unprotonated nitrogen site C5-N7-C8 (Supplementary Information). There is also clear discrimination between the C-OH and C=O bonds in the succinic acid molecule indicating that both carboxyl groups have retained their acidic protons (Figure 1).

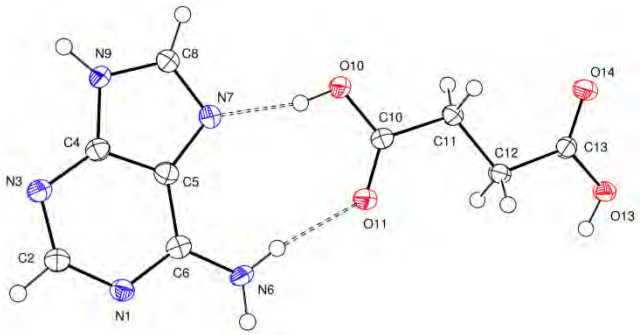

Figure 1. The asymmetric unit of adenine:succinic acid (**1**) showing the atom-numbering scheme and intermolecular hydrogen bonds (shown as dashed lines). Displacement ellipsoids are drawn at the 50% probability level.

The two coformer molecules are connected through two hydrogen bonds; N6-H6B…O11 and O10-H10…N7, together creating an $R_2^2(9)$ ring formed along the adenine Hoogsteen edge (Scheme 2, motif **VII**). Each adenine forms a dimer through complementary hydrogen donation from N9 via H9 to N3 resulting in an $R_2^2(8)$ ring. This dimer motif (motif **I**) is common to other

Table 1. Crystallographic data for adducts (**1**) to (**4**).

Cocrystal	(**1**)	(**2**)	(**3**)	(**4**)
Formula	$C_9H_{11}N_5O_4$	$C_9H_9N_5O_4$	$C_9H_9N_5O_4$	$C_{9.5}H_{11}N_5O_{4.5}$
M_r	253.23	251.21	251.21	267.23
T (K)	120	120	100	120
Crystal system	Monoclinic	Monoclinic	Monoclinic	Triclinic
Space group	$P2_1/n$	$P2_1/c$	$P2_1/c$	P -1
a (Å)	9.4902(4)	3.6160(1)	3.610(3)	5.2815(1)
b (Å)	5.3041(3)	13.0730(6)	13.323(11)	10.0506(2)
c (Å)	21.2846(8)	22.0296(9)	22.187(19)	22.0125(4)
α (˚)	90	90	90	78.191(1)
β (˚)	92.398(3)	94.633(3)	92.258(7)	85.160(1)
γ (˚)	90	90	90	80.017(1)
Volume (Å^3)	1070.46(9)	1037.98(7)	1066.3(15)	1124.98(4)
Z	4	4	4	4
D_{calc} (Mg/m^3)	1.571	1.608	1.565	1.578
μ (mm^{-1})	0.126	0.130	0.126	1.100
Crystal Shape	Fragment	Needle	Needle	Rod
Colour	Colourless	Colourless	Colourless	Colourless
Melting Pt (°C)	241-242	242-244	133-135	193-194
θ (˚)	3.52 – 27.48	3.25 – 25.02	2.96 – 26.56	6.71 – 66.59
Range of h	-12 – 12	-4 – 4	-4 – 4	-6 – 6
Range of k	-6 – 6	-15 – 15	-17 – 17	-11 – 11
Range of l	-27 – 27	-26 – 26	-28 – 28	-25 – 24
Reflections collected	8933	10663	10172	7965
Independent reflections	2426	1872	2401	3745
Goodness of fit	1.114	1.093	1.052	1.064
Final R_1 and wR_2 (I>2σ(I))	0.0586, 0.1123	0.0552, 0.1045	0.0416, 0.1020	0.0345, 0.0901
Final R_1 (all data)	0.0817	0.0792	0.0582	0.0404

crystalline adenine structures, and acts to form a small supramolecular building block containing alternating ring motifs (Figure 2a). These units are linked through two C-H…O interactions in which O14 acts as a double acceptor forming $R_3^2(8)$ rings above and below the adenine dimer (Figure 2a). The result is a hydrogen-bonded ribbon running in the [-120] direction, linked to two others running

in the same direction through a 'layer' of other ribbons running in the [120] direction in a sandwich-type arrangement (Figure 2b). This architecture is formed by the two remaining hydrogen bonds; N6-H6A…O11 and O13-H13…N1. In this extensive hydrogen bond network, each adenine molecule is involved in eight intermolecular interactions such that all hydrogen bond donors and acceptor sites are used, while in each succinic acid molecule, both carboxylic OH groups act as donors and both C=O groups as double acceptors (Table 2).

Table 2. Intermolecular hydrogen bonding and weak interactions (Å and ˚) in (**1**).

D-H…A	d(D-H)	d(H…A)	d(D…A)	<(DHA)
N6-H6A…O11[i]	0.88	2.04	2.875(2)	157.3
N6-H6B…O11	0.88	2.05	2.924(3)	171.7
N9-H9…N3[ii]	0.88	1.96	2.825(3)	166.4
O10-H10…N7	0.84	1.80	2.630(3)	167.0
O13-H13…N1[iii]	0.84	1.87	2.686(2)	162.9
C2-H2…O14[iv]	0.95	2.43	3.213(3)	140.0
C8-H8…O14[v]	0.95	2.38	3.077(3)	129.9

Symmetry transformations used to generate equivalent atoms:

(i) –x+0.5, y+0.5, -z+0.5 (ii) –x, -y+3, -z (iii) –x+0.5, y-1.5, -z+0.5

(iv) x-1, y+2, z (v) –x+1, -y+1, -z

(a)

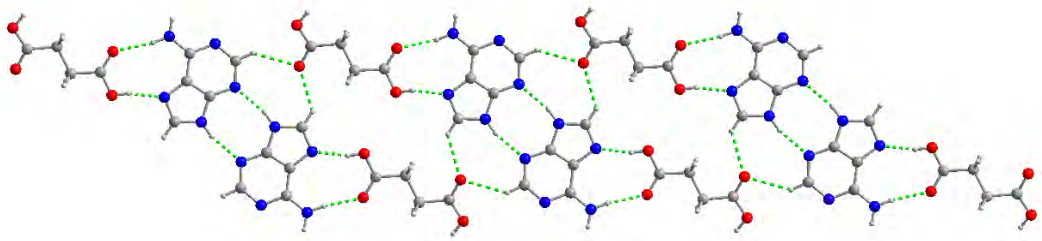

(b)

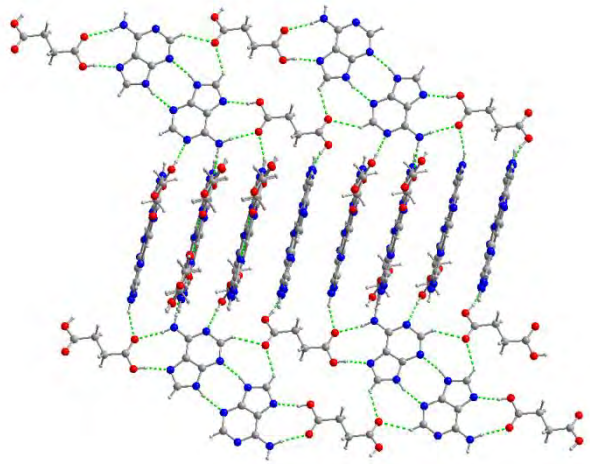

Figure 2. The hydrogen bond network of adenine and succinic acid molecules in (**1**) showing (a) the infinite ribbon of adenine dimers and succinic acid molecules, and (b) alternating perpendicular layers of these infinite hydrogen-bonded ribbons. Intermolecular hydrogen bonds are shown as dashed lines.

*Crystal structure of adeninium : hydrogen fumarate 1:1 (**2**)*

The asymmetric unit of (**2**) shows that in this case proton transfer has taken place and the adeninium ion is in the common *1H,9H* tautomeric salt form, confirmed by the larger endocyclic angle around the protonated nitrogen sites. There is clear discrimination again between the C-OH and C=O bond lengths at the protonated C13 end of the hydrogen fumarate ion, but not at the carboxylate C10 end (Figure 3).

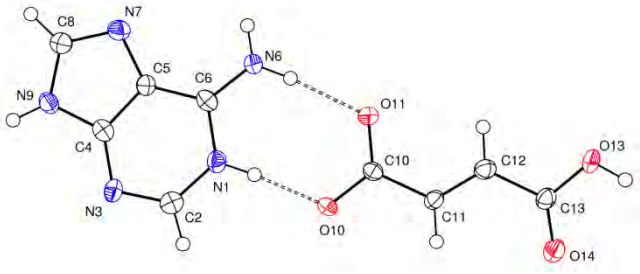

Figure 3. The asymmetric unit of adeninium : hydrogen fumarate (**2**) showing the atom-numbering scheme and intermolecular hydrogen bonds (shown as dashed lines). Displacement ellipsoids are drawn at the 50% probability level.

The coformers are linked by the hydrogen bonds N6-H6A…O11 and N1-H1…O10 forming an $R_2^2(8)$ ring on the Watson-Crick edge giving motif **VI(*1H*$^+$)** (Figure 3). The adeninium dimer $R_2^2(8)$ ring motif (motif **I**) is also formed in this structure, via complementary N9-H9…N3 interactions. This creates a supramolecular building block of alternating acid-adeninium and adeninium-adeninium ring motifs, distinct from that seen in (**1**), linked to form an infinite chain by complementary N6-H6B…O11 hydrogen bonds creating an additional $R_4^2(8)$ ring (Figure 4a). Unlike in the crystal structure of (**1**), this chain is not planar, with the hydrogen fumarate ion bent out of plane with intramolecular carboxylate-to-carboxyl torsion angles of -149.5° and
-161.3° (Supplementary Information). This marked geometric distortion of the hydrogen fumarate ion means that rather than the formation of strong interactions with the N7 or C8 in the adeninium units within the chain, each fumarate links to three neighbouring perpendicular chains (Figure 4b); the first through hydrogen bonds O13-H13…O10 and C2-H2…O14 which create a further $R_3^3(9)$ ring; the second also via a C2-H2…O14 interaction with an adeninium dimer but with a shorter H...A distance; finally, interaction with a third chain through a complementary O13-H13...O10 hydrogen bond (Table 3). In a similar way to (**1**), these chains form a sandwich-type structure with alternating ‘layers’ of chains running in

opposing directions. While there are the same total number of intermolecular interactions in structures (**1**) and (**2**), the coformer molecules play a different role in the network. In (**2**), each adeninium is involved in seven interactions including a bifurcated C-H donation, but with N7 and C8 not used. Each hydrogen fumarate ion is also involved in seven interactions with all three unprotonated oxygens acting as double acceptors and the carboxylic OH acting as a donor (Table 3).

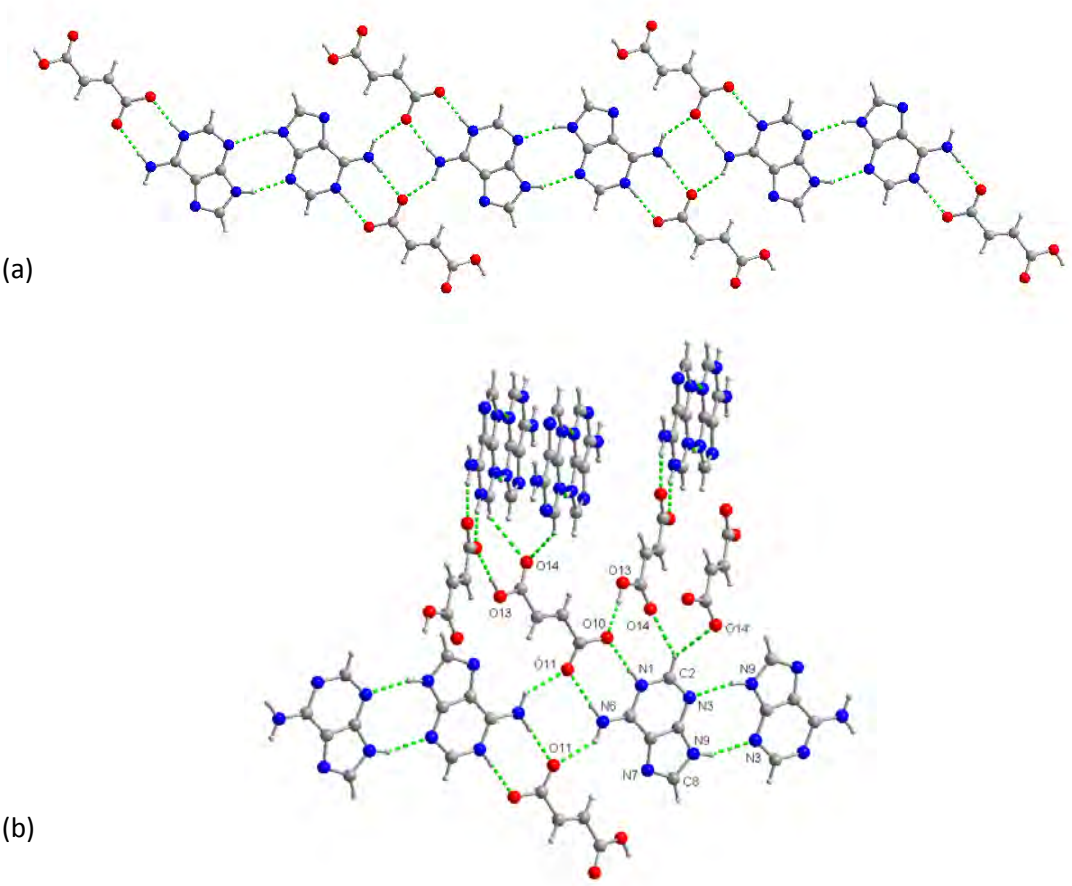

Figure 4. The hydrogen bond network of adeninium dimers and hydrogen fumarate ions in (**2**) showing (a) the infinite hydrogen-bonded chain of dimers and alternating ions, and (b) the criss-cross chains that form the alternating layer structure. Intermolecular hydrogen bonds are shown as dashed lines and selected atom labels are included in (b) to aid discussion.

Table 3. Intermolecular hydrogen bonding and weak interactions (Å and °) in (**2**).

D-H…A	d(D-H)	d(H…A)	d(D…A)	<(DHA)
N1-H1…O10	0.88	1.77	2.639(4)	171.3
N6-H6A…O11	0.88	1.92	2.795(4)	170.9
N6-H6B…O11^{i}	0.88	2.07	2.810(4)	140.8
N9-H9…N3^{ii}	0.88	2.06	2.892(4)	158.5
O13-H13…O10^{iii}	0.84	1.77	2.604(3)	172.0
C2-H2...O14^{iv}	0.95	2.42	3.172(5)	135.5
C2-H2...O14^{v}	0.95	2.54	3.238(5)	130.9

Symmetry transformations used to generate equivalent atoms:

(i) –x+1, -y+1, -z+1 (ii) –x-1, -y+2, -z+1 (iii) –x+1, y-0.5, -z+0.5

(iv) –x, y+0.5, –z+0.5 (v) –x+1, y+0.5, -z+0.5

*Crystal structure of adeninium : hydrogen maleate 1:1 (**3**)*

The crystal structure of (**3**) has an asymmetric unit containing an adeninium cation and a hydrogen maleate anion, the latter displaying the planar acid conformation stabilised by the short intramolecular hydrogen bond O13-H13...O11 commonly found in other hydrogen maleate structures [13,19] (Figure 5). However, the adeninium ion in (**3**) is in the unusual *3H,7H* tautomeric form with the endocyclic angles around N3 and N7 larger than the unprotonated N sites (Supplementary Information). The two components form an $R_2^2(8)$ ring on the adenine Watson-Crick edge which is similar to that seen in the fumarate structure (**2**) although the synthon itself is formed by an alternative combination of interactions N6-H6A…O10 and C11-H11…N1(Scheme 2, motif **VIII**) (Figure 5).

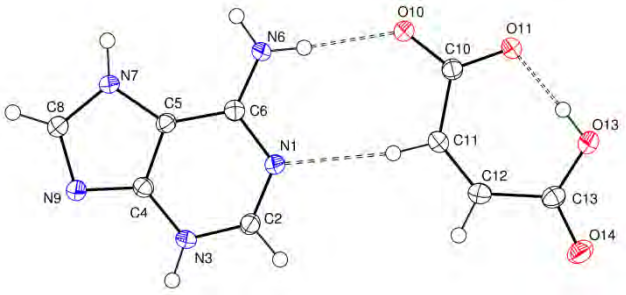

Figure 5. The asymmetric unit of adeninium : hydrogen maleate (**3**) showing the atom-numbering scheme and hydrogen bonds (shown as dashed lines). Displacement ellipsoids are drawn at the 50% probability level.

The adeninium dimer $R_2^2(8)$ motif is formed through complementary N3-H3…N9 interactions and differs in nature from the synthon in (**1**) and (**2**) due to the alternative tautomeric form giving the motif **I(*3H*)**. Each adeninium ion is hydrogen bonded to a second hydrogen maleate through N6-H6B…O11 and N7-H7…O10 interactions forming an $R_2^2(9)$ ring motif on the Hoogsteen edge (motif **VII(*7H*$^+$)**) (Figure 6a). The result is the formation of chains of alternating adeninium and hydrogen maleate ions linked through alternating hydrogen bonded rings in the Watson-Crick and Hoogsteen modes, running parallel to the *b*-axis. These chains are linked by the adeninium dimers to give an infinite hydrogen bonded sheet (Figure 6a). The protonated end of the hydrogen maleate lies either above or below the sheet and is involved in interactions with adeninium dimers in neighbouring sheets; a combination of C8-H8…O13 and C2-H2…O14 generating a puckered $R_3^3(10)$ ring (Figure 6b). All strong hydrogen bond donors and acceptors are used in this structure (Table 4), with each adeninium ion involved in nine intermolecular interactions (including N7 acting as a bifurcated donor) and each hydrogen maleate ion forming eight hydrogen bonds with O10 as a double acceptor, O11 as a triple acceptor and O13 as both a donor and acceptor.

(a)

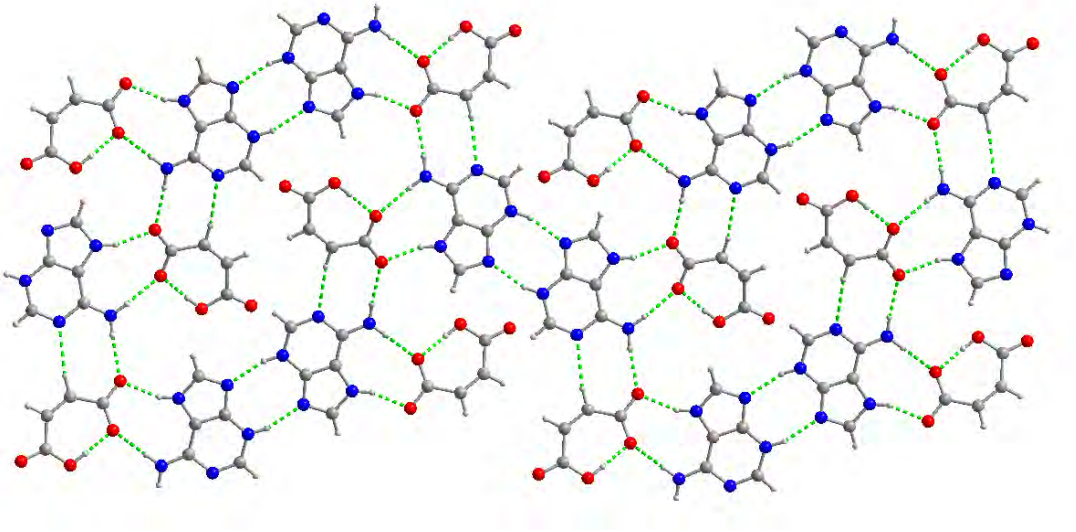

(b)

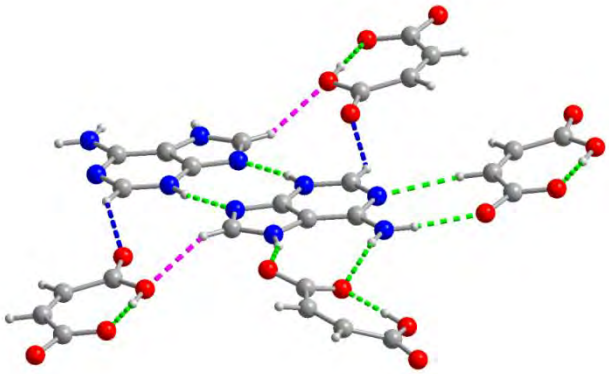

Figure 6. A view of the crystal structure of (**3**) showing (a) the chains of alternating $R_2^2(8)$ and $R_2^2(9)$ rings linked together in an infinite hydrogen-bonded sheet. Hydrogen bonds are shown as dashed lines and **(**b) interactions between the adeninium dimer and maleate anions above and below the plane shown as dashed pink and blue lines (hydrogen bonds within the layer are shown as green dashed lines).

Table 4. Intermolecular hydrogen bonding and weak interactions (Å and °) in (**3**).

D-H…A	d(D-H)	d(H…A)	d(D…A)	<(DHA)
N3-H3...N9[i]	0.88	1.95	2.808(2)	162.9
N6-H6A...O10	0.88	2.07	2.946(3)	171.3
N6-H6B...O11[ii]	0.88	2.07	2.922(2)	163.2
N7-H7...O10[ii]	0.88	1.87	2.721(2)	161.6
N7-H7...O11[ii]	0.88	2.56	3.288(2)	140.1
O13-H13...O11	0.84	1.62	2.464(2)	177.4
C2-H2...O14[iii]	0.95	2.39	3.154(3)	137.8
C8-H8...O13[iv]	0.95	2.35	3.231(3)	153.9
C11-H11...N1	0.95	2.43	3.374(3)	170.9

Symmetry transformations used to generate equivalent atoms:

(i) -x+1, -y+3, -z (ii) -x+2, y+1/2, -z+1/2 (iii) -x, -y, -z (iv) x+1, y+1, z

*Crystal structure of adeninium : hydrogen maleate : methanolate 2:2:1 (**4**)*

In the crystal structure of (**4**) the asymmetric unit contains two independent adeninium cations, two independent hydrogen maleate anions and one methanol molecule (Figure 7). Both adeninium ions (A and B with atom labels a and b respectively) are in the more common *1H,9H* tautomeric form and both hydrogen maleate ions are stabilised by intramolecular O13-H13…O10 hydrogen bonds. Both adeninium cations (A and B) are hydrogen bonded to the hydrogen maleate anions (A and B respectively) through the formation of $R_2^2(8)$ rings on each Watson-Crick site but via N1-H1…O11 and N6-H6A…O10 interactions within each pair (Figure 7 and Table 5) forming the **VI(*1H*$^+$)** motif, similar to that in the adeninium hydrogen fumarate structure (**2**) rather than the anhydrous maleate (**3**).

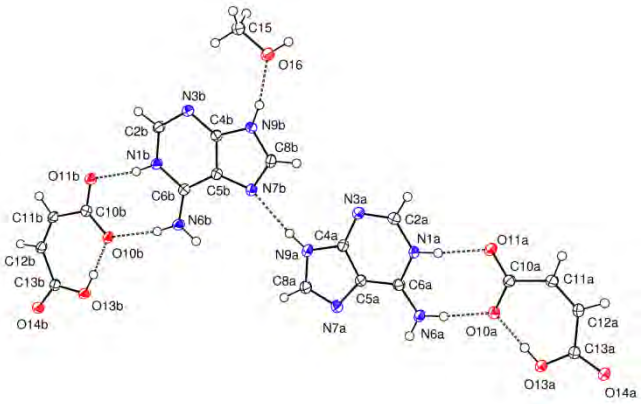

Figure 7. The asymmetric unit of adeninium : hydrogen maleate : methanolate (**4**) showing the atom-numbering scheme and hydrogen bonds (shown as dashed lines). Displacement ellipsoids are drawn at the 50% probability level.

The two adeninium ions are linked through N9A-H9A…N7B (reinforced by C8B-H8B…N3A, not shown in Figure 7), and hence the typical base edge dimer motif (**I**) is not formed here. The methanol is linked to adeninium B by N9B-N9B…O16.

The asymmetric unit is linked to others generating an infinite hydrogen bonded sheet that can be viewed as parallel ladders of $R_2^2(8)$ rings running in the [2-10] direction, formed independently by the adeninium and hydrogen maleate A and B pairs (Figure 8). These ladders contain alternating $R_6^4(16)$ and $R_4^2(10)$ rings formed by complementary N6-H6…O14 and C2-H2…O11 hydrogen bonds respectively. Two further interactions, C8A-H8A…O14B and O16-H16…O14 (the latter linking the methanol to hydrogen maleate A) bring together the 'A' and 'B' ladders to form an infinite sheet (Figure 8). In both hydrogen maleate ions all strong hydrogen bond donors and acceptors are used with the C-O groups acting as double acceptors. Both adeninium ions are involved in the six intermolecular interactions marked in Figure 8, whereas the heterocyclic N and C-H groups that are not marked as involved in intermolecular interactions are in positions conducive to the formation of weak interactions with neighbouring maleate or adeninium ions or methanol hydrogens.

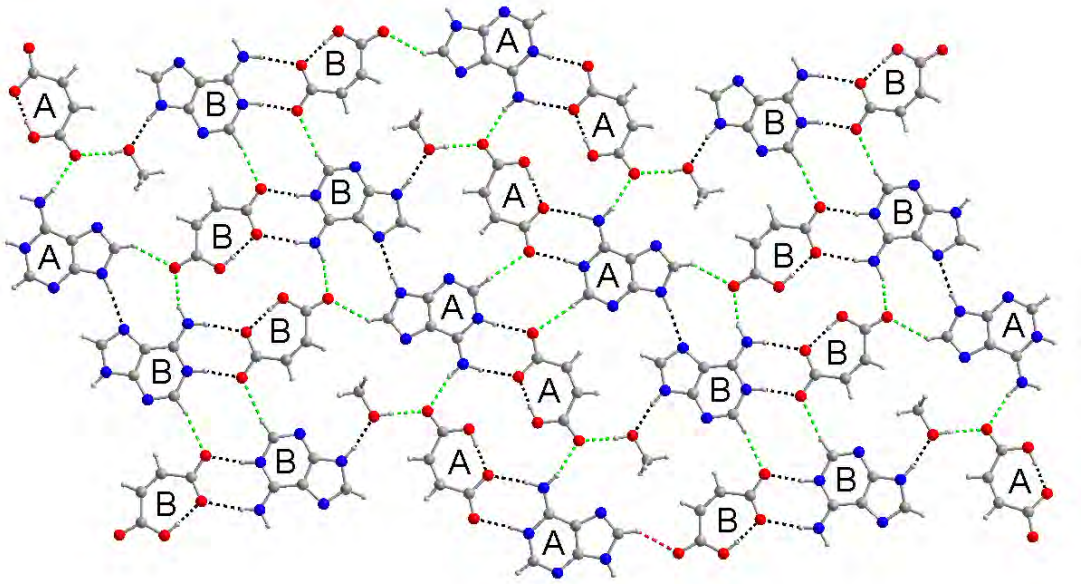

Figure 8. A view of the crystal structure of (**4**) showing the hydrogen-bonded sheet formed by the crystallographically independent adeninium (A and B) and the hydrogen maleate (A and B) ions with methanol. Hydrogen bonds are shown as dashed lines (black lines denote interactions within the asymmetric unit, green lines those between asymmetric units).

DISCUSSION

The structures presented in this paper illustrate the role that small dicarboxylic acids can play in disruption of the strong hydrogen bonding network in adenine in the crystalline solid state, resulting in the preferential formation of cocrystals or salts. There is general acceptance that if the pK_a difference ($\Delta pK_a = pK_a(base) - pK_a(acid)$) is greater than 2-3 then the salt will form, whereas if $\Delta pK_a < 0$ then the cocrystal product should predominate[51]. With aqueous pK_a

Table 5. Intermolecular hydrogen bonding and weak interactions (Å and °) in (**4**).

D-H…A	d(D-H)	d(H…A)	d(D…A)	<(DHA)
N1A-H1A...O11A	0.88	1.90	2.772(2)	174.3
N6A-H6AA...O10A	0.88	1.93	2.801(2)	169.3
N6A-H6AB...O14A^{i}	0.88	2.01	2.865(2)	163.7
N9A-H9A...N7B	0.88	2.05	2.921(2)	171.5
O13A-H13A...O10A	0.84	1.59	2.430(2)	173.1
C2A-H2A…O11A^{iii}	0.95	2.39	3.329(2)	172.4
C8A-H8A...O14B^{ii}	0.95	2.33	3.130(2)	141.7
N1B-H1B...O11B	0.88	1.82	2.688(2)	168.9
N6B-H6BA...O10B	0.88	2.00	2.875(2)	170.2
N6B-H6BB...O14B^{ii}	0.88	1.97	2.808(2)	158.1
N9B-H9B...O16	0.88	1.83	2.697(2)	168.4
O13B-H13B...O10B	0.84	1.61	2.448(2)	176.5
O16-H16...O14A^{iii}	0.84	1.82	2.658(2)	173.6
C2B-H2B…O11B^{iv}	0.95	2.35	3.292(2)	169.7
C8B-H8B…N3A	0.95	2.79	3.608(2)	144.9

Symmetry transformations used to generate equivalent atoms:

(i) -x, -y+2, -z (ii) –x+3, -y+2, -z+1 (iii) –x+2, -y+1, -z

(iv) –x+5, -y+1, -z+1

differences of -0.06, 1.13 and 2.23 between adenine and succinic, fumaric and maleic acids respectively[52], cocrystal formation is indeed expected in the case of adenine : succinic acid (**1**), and the maleic acid adducts (**3**) and (**4**) are most likely to be predicted as salts. However, with a ΔpK_a value within the range 0 to 3, the formation of an adenine fumarate salt (**2**) could not be predicted using this parameter. Although the difference in aqueous pK_as is a useful indicator of adduct form when values are at the extremes, an alternative indicator based on

features in the solid form or even consideration of pK_a behavior in the solvent of cocrystallization may prove to be more reliable in this narrow unpredictable region.

In (**2**) and (**4**), a single proton transfer from the acid takes place at the N6 position giving rise to the most common *1H,9H* adeninium tautomer. However, in the anhydrous hydrogen maleate structure (**3**), protonation of the natural *9H* adenine form is not observed, and generation of the less stable *3H,7H* adeninium tautomer is preferred. As far as we are aware, this is the first example in which the *3H,7H* tautomer is stabilized within the crystalline structure of a purely molecular material. The hydrogen-bonding network in (**3**) arises from a combination of intermolecular interactions that differs from the other reported structures and results in a crystalline arrangement that stabilizes this energetically unfavourable tautomer. The lack of protonation at the N1 position enables the formation of an additional C-H…N intermolecular interaction within motif **VIII** on the Watson-Crick site. The presence of a hydrogen on N3 necessitates movement of the proton from N9 to N7 so that the expected complementary adeninium dimer (motif **I(*3H*)**) can form. The overall combination of these structural requirements results in the adoption and stabilization of the unusual *3H,7H* tautomer. This tautomeric variation further illustrates the potential structural diversity displayed by adenine-based molecular adducts. This is evident even within the four hydrogen maleate structures that have now been reported; our work has produced the anhydrous hydrogen maleate (**3**) containing the *3H,7H* tautomer from ethanolic solution and the methanolate (**4**), based on the *1H,9H* tautomer from methanol. This *1H,9H* tautomer is also present in the hydrated form[19] from aqueous solution, whereas a second hydrate[13] from methanol in an open beaker has both *1H,9H* adeninium and neutral *7H* adenine forms present.

The supramolecular behaviour of (**1**)-(**4**) is dominated by strong bidentate motifs, similar to other adenine:carboxylic acid adducts (Table 6). All these structures contain either the $R_2^2(8)$ heterosynthon (motif **VI**) formed by NH…O=C and OH…N(hetero) interactions on

the Watson-Crick site, or the $R_2^2(9)$ heterosynthon (motif **VII**) on the Hoogsteen edge. Although adenine adducts containing monocarboxylic acids form both motifs[8], Table 6 highlights a preference for formation of the Hoogsteen-acid motif **VII** by cocrystals and the Watson Crick-acid motif **VI(*1H*$^+$)** by salts. This trend is also observed in the hydrated maleate structure[13] with the **VII(*7H*$^+$)** motif formed by the adenine *7H* tautomer and the **VI(*1H*$^+$)** motif generated by the adeninium ion. The only exception is structure (**3**), where the unusual *3H,7H* tautomer forms alternative interactions at the Watson-Crick site and protonation of the *7H* position gives the **VII(*7H*$^+$)** motif. Distinct adenine or adeninium dimer supramolecular units are also found in structures [(**1**)-(**4**)], mostly as the common $R_2^2(8)$ homosynthon (motif **I**). Formation of motif **I** is disrupted when the structure is solvated or hydrated, when alternative interactions are formed by the base edge of the adenine unit, e.g: in the solvated hydrogen maleate (**4**), in which a single NH…N(hetero) hydrogen bond is formed from the base of the adeninium to the Hoogsteen edge and reinforced by a CH…N(hetero) hydrogen bond to give an $R_2^2(7)$ ring. Hence, although the supramolecular behavior of these materials is not yet predictable, there are common features that emerge from the structures studied to date. All the dicarboxylic acid adduct structures in Table 6 contain at least two of the bidentate synthons discussed (although there may be some disruption to this network by solvation etc.), with the motif formed dependent on cocrystal, salt or tautomeric form. Consideration of the anhydrous adducts shows that only structure (**3**) utilizes a combination of three bidentate motifs, while the Watson-Crick edge in (**1**) is involved in alternative interactions to neighbouring supramolecular chains and the Hoogsteen site in (**2**) is blocked by twisting of the hydrogen fumarate ion.

Table 6. Intermolecular hydrogen bond motifs found in adenine: carboxylic acid adducts.

Material	Ad/Ad$^+$ motif		Bidentate Ad/Ad$^+$: acid motif		Single Ad/Ad$^+$: acid interaction	Reference
Adenine	**I**	**II**				35
Ad:benzoic acid	**I**		**VI**	**VII**		8
Ad:hydroxy benzoic acid			**VI**	**VII**	OH…N(3) N(9)H…O	8
Ad:succinic acid	**I**			**VII**	OH…N(1) N(6)H…O C(2)H…O C(8)H…O	this work (**1**)
Ad:adipic acid methanolate		**IV**		**VII**		8
Ad$^+$:hydrogen fumarate	**I**		**VI(*1H*$^+$)**		N(6)H…O C(2)H…O C(2)H…O	this work (**2**)
Ad$^+$:hydrogen maleate	**I(*3H*)**		**VIII**	**VII(*7H*$^+$)**	C(2)H…O C(8)H…O	this work (**3**)
Ad$^+$:hydrogen maleate methanolate	N(9)H…N(7) C(8)H…N(3)		**VI(*1H*$^+$)**		N(6)H…O C(2)H…O C(8)H…O	this work (**4**)
Ad$^+$:hydrogen maleate hydrate	**III**		**VI(*1H*$^+$)**		N(9)H…O	18
Ad$^+$:Ad:hydrogen maleate hydrate	**III**	**IV** **V(*1H*)**	**VI(*1H*$^+$)**	**VII(*7H*$^+$)**	N(9)H…O	13

Ad denotes neutral adenine and Ad+ denotes protonated adeninium species.

Finally, it is worth a comment on the effect of cocrystallisation and salt formation on physical properties as the primary concern of pharmaceutical formulation is often to tailor the solubility or transfer other desirable physical properties to a multi-component material. Adenine is poorly soluble in water and has a melting point > 360°C at which point it

decomposes, whereas succinic, fumaric and maleic acids have significantly lower melting points (184, 287 and 135°C respectively) and higher solubilities. The adenine : succinic acid cocrystal (**1**) has a melting point between the two individual components (~242°C) behaving in a similar way to the majority of pharmaceutical cocrystals[27]. The two anhydrous salts (**2**) and (**3**) display melting points lower than both the individual starting components, whereas the methanolated maleate salt (**4**) has a melting point between adenine and maleic acid (Table 1). Although the exact effect of cocrystallisation or salt formation on the physical properties of adenine is clearly unpredictable, this approach does provide a pathway to lowering the melting point and/or improving its poor solubility.

CONCLUSION

Adenine forms a variety of cocrystals and salts with small dicarboxylic acids. Those reported here include an anhydrous cocrystal with succinic acid, an anhydrous fumarate salt, an anhydrous maleate salt in which the adeninium adopts the unusual *3H,7H* tautomer and a methanolated maleate salt. The supramolecular behavior of adenine across this range of adducts can be rationalized through the formation of strong bidentate hydrogen bond synthons based around a number of predicted motifs, which adapt to accommodate salt formation or stabilization of uncommon tautomeric form.

ASSOCIATED CONTENT

Supporting Information. Full crystallographic data in CIF format and X-ray powder diffraction data for (**1**)-(**4**). This material is available free of charge via the Internet at http://pubs.acs.org.

AUTHOR INFORMATION

Corresponding Author

* Email: m.tremayne@bham.ac.uk. Phone: +44 121 414 3201.

Author Contributions

The manuscript was written through contributions of all authors. All authors have given approval to the final version of the manuscript.

ACKNOWLEDGMENT

We would like to thank the University of Birmingham and the EPSRC for the support for LJT and NE. The UK National Crystallography Service is thanked for collection of the single-crystal X-ray diffraction data. The powder diffraction facilities used in this research were obtained through the Science City Advanced Materials project with support from Advantage West Midlands (AWM) and part funded by the European Regional Development Fund (ERDF).

REFERENCES

1. Garcia-Teran, J. P.; Castillo, O.; Luque, A.; Garcia-Couceiro, U.; Roman, P.; Lloret, F.; *Inorg. Chem.*, **2004**, *43*, 5761-5770

2. Dobrzynska, D.; Jerzykiewicz, L. B.; *J. Am. Chem. Soc.*, **2004**, *126*, 11118-11119

3. Driess, M.; Merz, K.; Rowlings, R. B.; *Z. Anorg. Allg. Chem.*, **2001**, *627*, 213-217

4. Aoki, K.; Salam, M. A.; Munakata, C.; Fujisawa, I.; *Inorg. Chim. Acta*, **2007**, *360*, 3658-3670

5. Mastropietro, T. F.; Armentano, D.; Marino, N.; De Munno, G.; *Polyhedron*, **2007**, *26*, 4945-4954

6. Fujii, S.; Kawasaki, K.; Sato, A.; Fujiwara, T.; Tomita, K. I.; *Archives of Biochemistry and Biophysics*, **1977**, *181*, 363-370

7. Weeks, C. M.; Rohrer, D. C.; Duax, W. L.; *Science*, **1975**, *190*, 1096-1097

8. Byres, M.; Cox, P. J.; Kay, G.; Nixon, E.; *Crystengcomm*, **2009**, *11*, 135-142

9. Perumalla, S. R.; Suresh, E.; Pedireddi, V. R.; *Angew. Chem. Int. Ed. Engl.*, **2005**, *44*, 7752-7757

10. Du, L. C.; Zeng, W. L.; Liu, X. Y.; Jian, F. F.; *Acta Cryst. E*, **2009**, *65*, o1791

11. Fonseca Guerra, C.; Bickelhaupt, F. M.; Saha, S.; Wang, F.; *J. Phys. Chem. A*, **2006**, *110*, 4012 - 4020

12. Garcia-Teran, J. P.; Castillo, O.; Luque, A.; Garcia-Couceiro, U.; Beobide, G.; Roman, P.; *Dalton Trans.*, **2006**, *7*, 902-911

13. McHugh, C.; Erxleben, A.; *Cryst. Growth. Des.*, **2011**, *11*, 5096 – 5104

14. Hanus, M.; Kabeláč, M.; Rejnek, J.; Ryjáček, F.; Hobza, P; *J. Phys. Chem. B*, **2004**, *108*, 2087-2097

15. Crespo-Hernandez, C. E.; Cohen, B.; Hare, P. M.; Kohler, B; *Chem. Rev.*, **2004**, *104*, 1977-2019

16. Marian, C; Nolting, D.; Weinkauf, R.; *Phys. Chem. Chem. Phys*, **2005**, *7*, 3306-3316

17. Relative energies from density functional theory calculations (taken from ref 16): (a) neutral adenine tautomers; 9*H* (0 kcalmol^{-1}), 7*H* (7.675 kcalmol^{-1}), (b) protonated adeninium tautomers; 1*H*,9*H* (0 kcalmol^{-1}), 3*H*,7*H* (0.460 kcalmol^{-1}), 3*H*,9*H* (1.971 kcalmol^{-1}), 7*H*,9*H* (8.443 kcalmol^{-1}), 1*H*,7*H* (10.896 kcalmol^{-1}).

18. Sridhar, B.; Ravikumar, K; Varghese, B; *Acta. Cryst C*, **2009**, *C65*, o202-o206

19. Sridhar, B.; Ravikumar, K; *Acta. Cryst C*, **2007**, *C63*, o415-o418

20. Das, B.; Baruah, J. B.; *Cryst. Growth. Des.*, **2010**, *10*, 3242-3249

21. Cadiau, A.; Adil, K.; Hemon-Ribaud, A.; Leblanc, M.; Jouanneaux, A.; Slawin, A. M. Z.; Lightfoot, P.; Maisonneuve, V.; *Solid State Sci.*, **2011**, *13*, 151-157

22. Garcia-Teran, J. P.; Castillo, O.; Luque, A.; Garcia-Couceiro, U.; Beobide, G.; Roman, P.; *Inorg. Chem.*, **2007**, *46*, 3593-3602

23. Almarsson, O.; Zaworotko, M. J.; *Chem. Comm.*, **2004**, 1889-1896

24. Vishweshwar P.; McMahon, J. A.; Bis, J. A.; Zaworotko, M. J.; *J. Pharm. Sci.*, **2006**, *95*, 499-516.

25. Blagden, N.; Berry, D. J.; Parkin, A.; Javed, H.; Ibrahim, A.; Gavan, P.T.; De Matos, L. L.; Seaton, C. C.; *New J. Chem.*, **2008**, *32*, 1659-1672

26. Delori, A.; Friscic, T.; Jones, W.; *CrystEngComm.*, **2012**, *7*, 2350-2362

27. Schultheiss, N.; Newman, A.; *Cryst. Growth Des.*, **2009**, *9*, 2950-2967

28. Aakeroy, C. B.; Forbes, J.; Desper, J.; *J. Am. Chem. Soc.*, **2009**, *131*, 17048-17049

29. Vishweshwar, P.; Nangia, A.; Lynch, V. M.; *Cryst. Growth Des.*, **2003**, *3*, 783-790

30. Braga, D.; Maini, L.; de Sanctis, G.; Rubini, K.; Grepioni, F.; Chierotti, M. R.; Gobetto, R.; *Chem. Eur. J.*, **2003**, *9*, 5538-5548

31. Thompson, L. J.; Voguri, R. S.; Male, L.; Tremayne, M.; *CrystEngComm.*, **2011**, *13*, 4188-4195

32. Braga, D.; D'Agostino, S.; Dichiarante, E.; Maini, L.; Grepioni, F.; *Chem. Asian J.*, **2011**, *6*, 2214-2223

33. Trask, A. V.; Motherwell, W. D. S.; Jones, W.; *Int. J. Pharm.*, **2006**, *320*, 114-123

34. Bhatt, P. M.; Ravindra, N. V.; Banerjee, R.; Desiraju, G. R.; *Chem.Comm.*, **2005**, 1073-1075.

35. Cheney, M. L.; Shan, N.; Healey, E. R.; Hanna, M.; Wojtas, L.; Zaworotko, M. J.; Sava, V.; Song, S.; Sanchez-Ramos, J. R.; *Cryst. Growth Des.*, **2010**, *10*, 394-405

36. Mahapatra, S.; Nayak, S. K.; Prathapa, S. J.; Row, T. N. G.; *Cryst. Growth. Des.*, **2008**, *8*, 1223-1225

37. Bernstein, J.; Davis, R.E.; Shimoni, L.; Chang, N.L.; *Angew. Chem. Int. Ed.*, **1995**, *34*, 1555-1573

38. Coles, S.J.; Gale, P.A.; Chem. Sci., **2012**, *3*, 683-689

39. Hooft, R.W.W. *COLLECT.* Nonius BV, Delft, Holland, 1998

40. Otwinowski, Z.; Minor, W. *Methods in Enzymology, Vol. 276, Macromolecular Crystallography, Part A*, ed. C. W. Carter Jr and R. M. Sweet, Academic Press, New York, 1997, pp307-326

41. Sheldrick, G.M. *SADABS Version 2*. Bruker AXS Inc., Madison, Wisconsin, USA, 2007

42. Rigaku, *CrystalClear Version 2*, Rigaku Corporation, Tokyo, Japan, 2010

43. Bruker, *SMART Version 5*, Bruker AXS, Inc.: Madison, WI, USA, 1997

44. Bruker, *SAINT Version 6*, Bruker AXS, Inc.: Madison, WI, USA, 1997

45. Sheldrick, G.M. *Acta Crystallogr. A*, **2008**, *64*, 112-122

46. Farrugia, L.J. *J. Appl. Crystallogr*. **1999**, *32*, 837-838

47. Brandenburg, K. *Diamond Version 3.0*. Crystal Impact GbR, Bonn, Germany, 1997

48. Farrugia, L.J. *J. Appl. Crystallogr.* **1997**, *30*, 565

49. Spek, A.L. *PLATON, Bijvoet Centre for Biochemical Research, Vakgroep Kristal-en Structure-Chemie*, University of Utrecht, Netherlands, 2010

50. Macrae, C. F.; Edgington, P. R.: McCabe, P; Pidcock, E.; Shields, G. P.; Taylor, R.; Towler M.; van de Streek, J.; *J. Appl. Cryst.*, **2006**, *39*, 453-457

51. Childs, S. L.; Stahly, G. P.; Park, A.; *Mol. Pharm.*, **2007**, *4*, 323-338

52. Albert, A.; Serjeant, E. P.; *The Determination of Ionization constants*, Chapman and Hall: London, UK, 1971

FOR Table of Contents Use Only

SYNOPSIS (Word Style "SN_Synopsis_TOC"). If you are submitting your paper to a journal that requires a synopsis, see the journal's Instructions for Authors for details.

Appendix 14:

14.1: Crystalline structure of isonicotinamide : oxalic acid 2:1

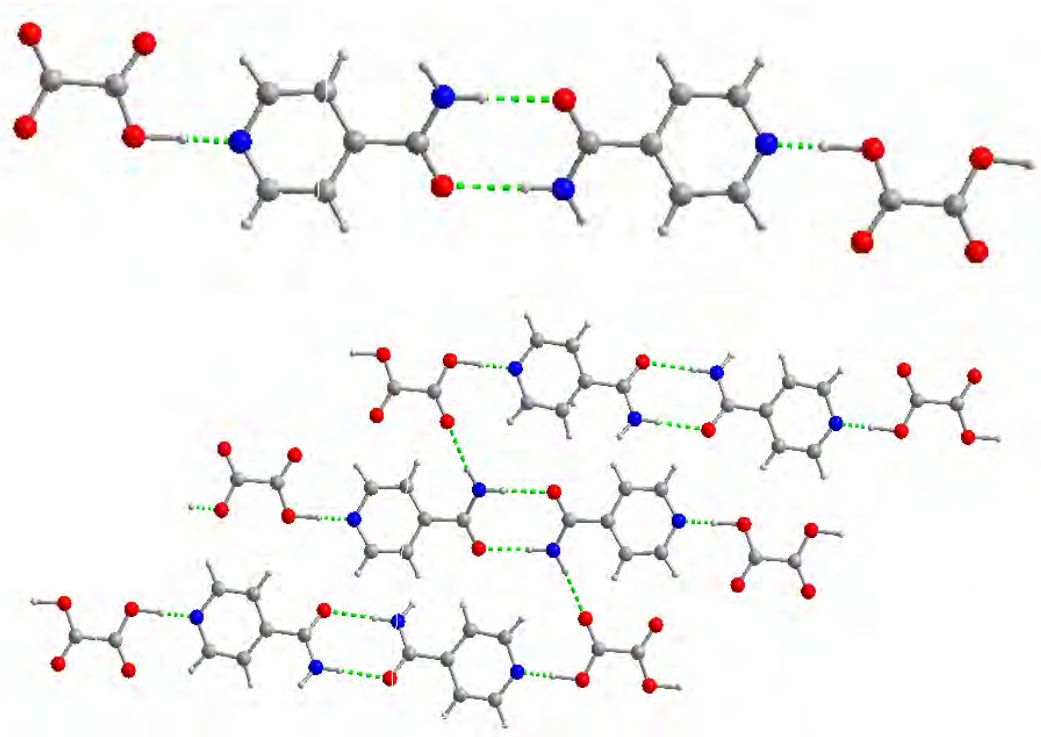

14.2: Crystalline structure of isonicotinamide : malonic acid 2:1

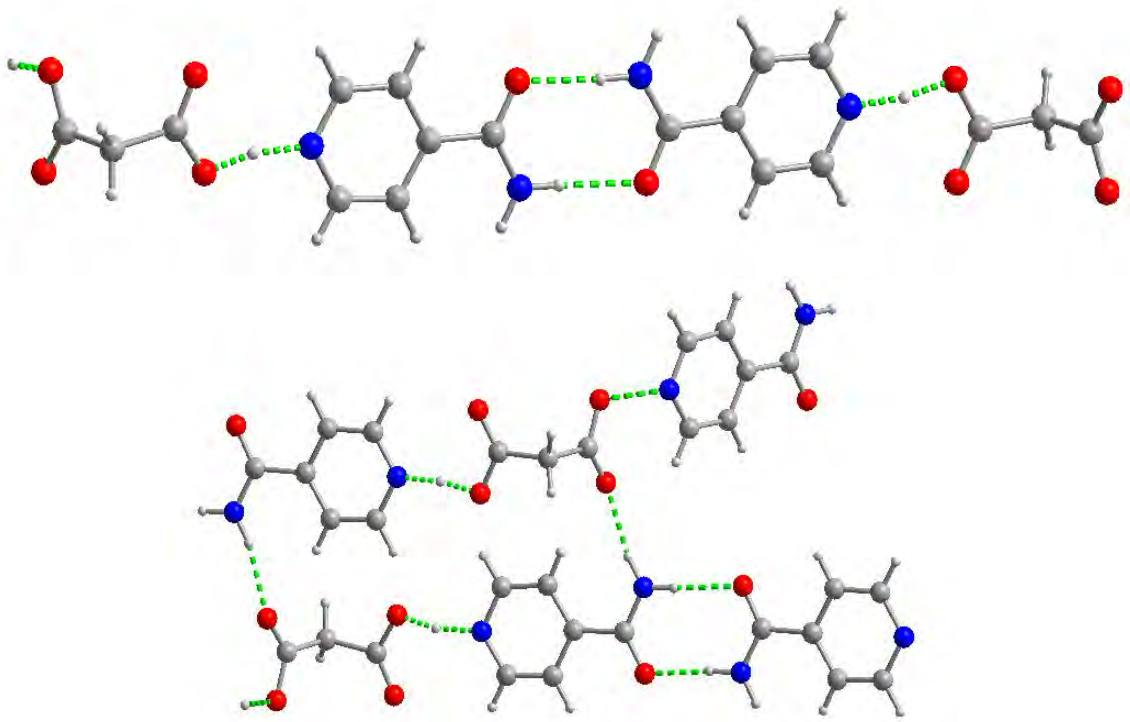

14.3: Crystalline structure of isonicotinamide : succinic acid 2:1

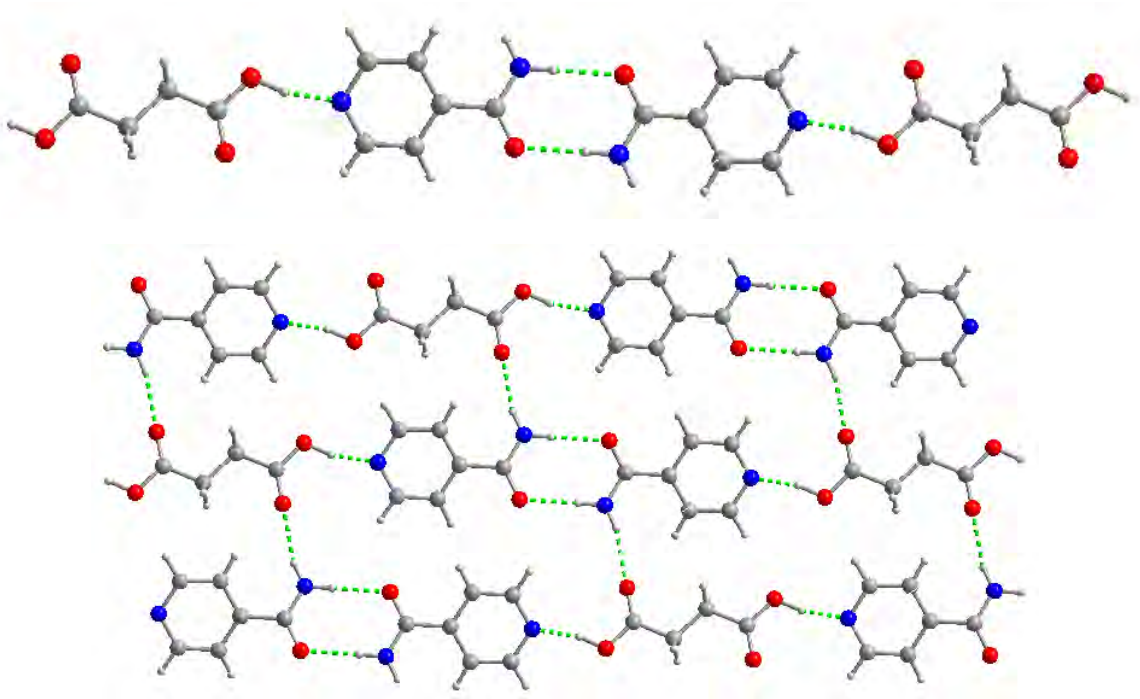

14.4: Crystalline structure of isonicotinamide : fumaric acid 2:1

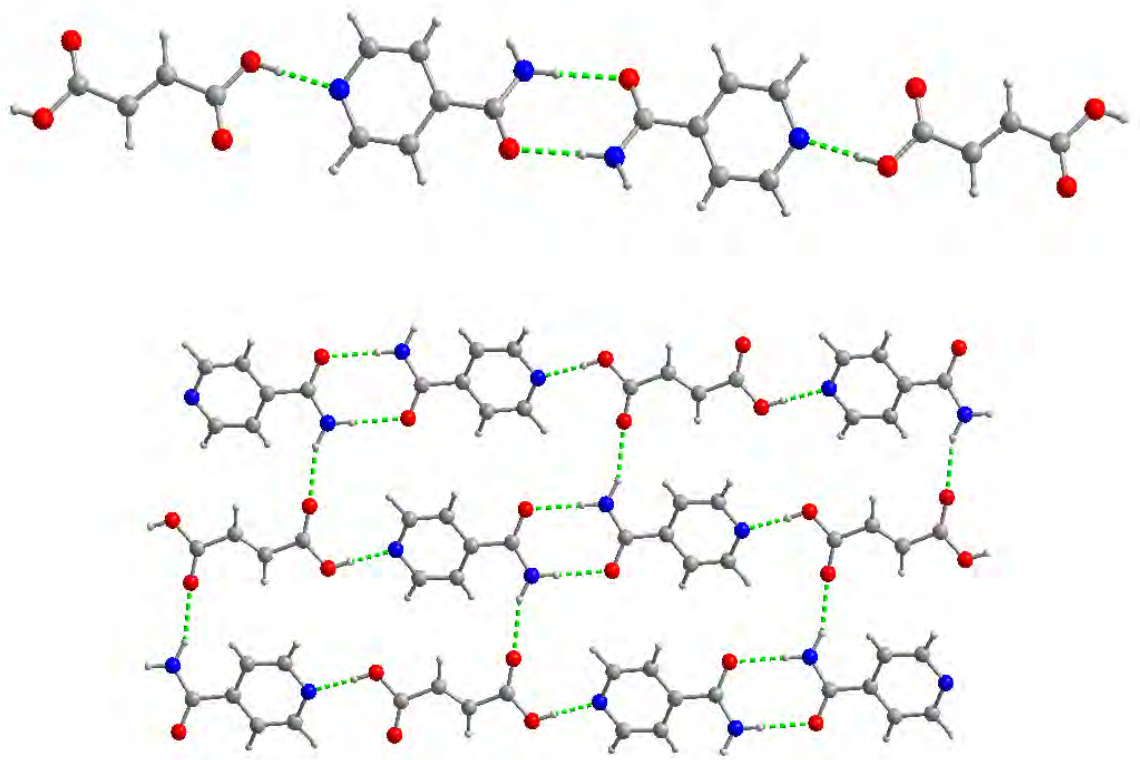

14.5: Crystalline structure of isonicotinamide : hydrogen maleate 1:1

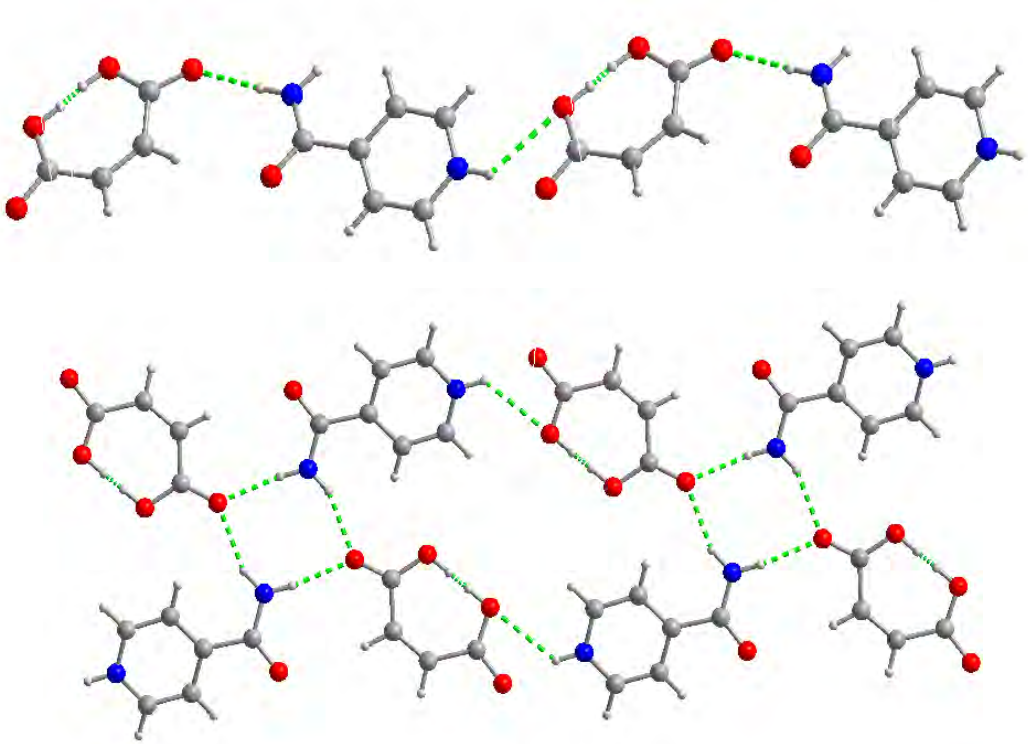

14.6: Crystalline structure of isonicotinamide : glutaric acid 2:1

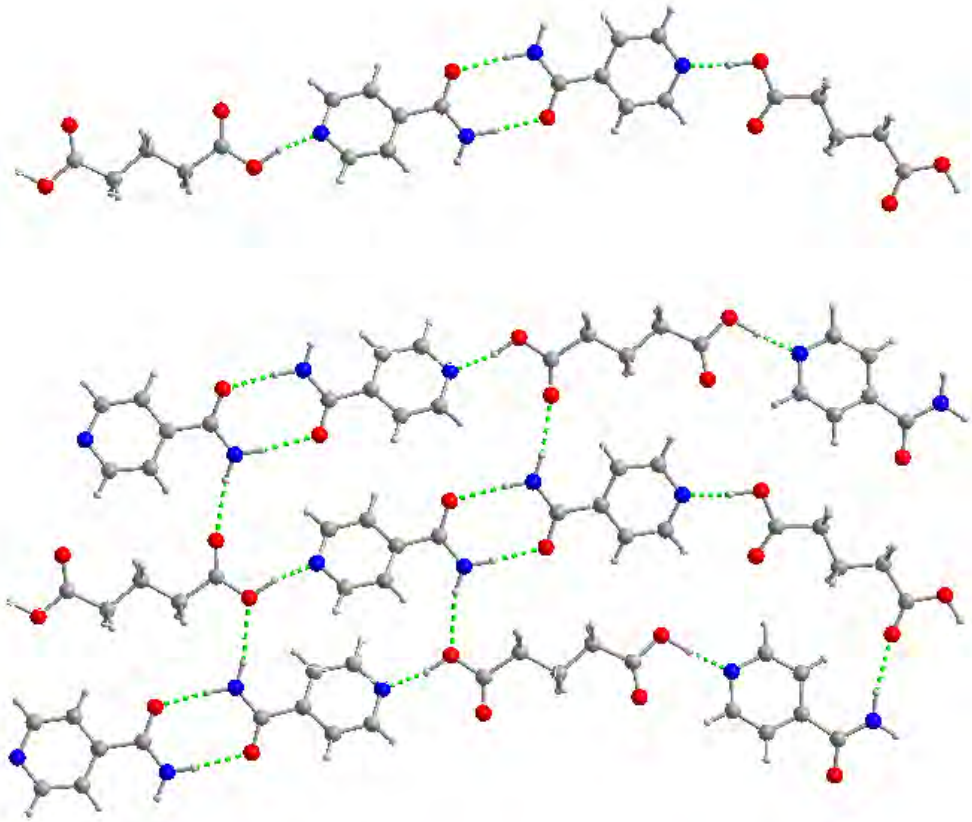

14.7: Crystalline structure of isonicotinamide : adipic acid 2:1

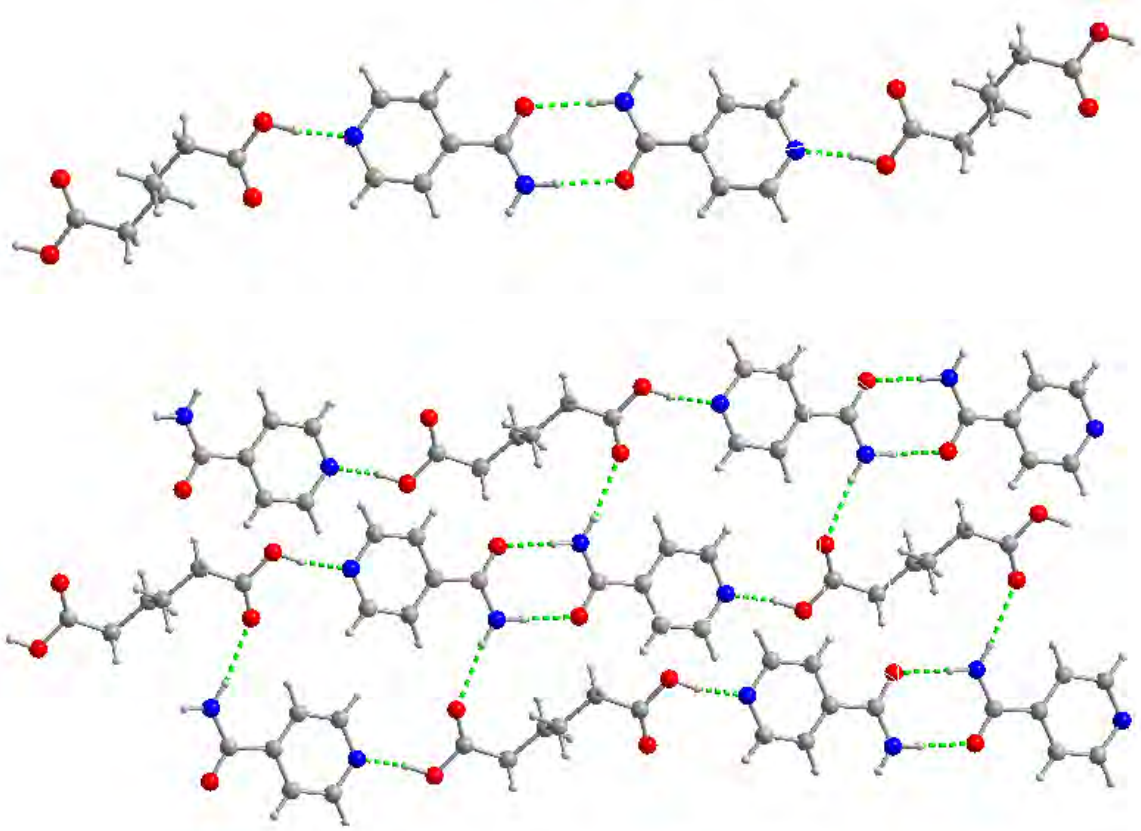

14.8: Crystalline structure of isonicotinamide : glutaric acid 1:1

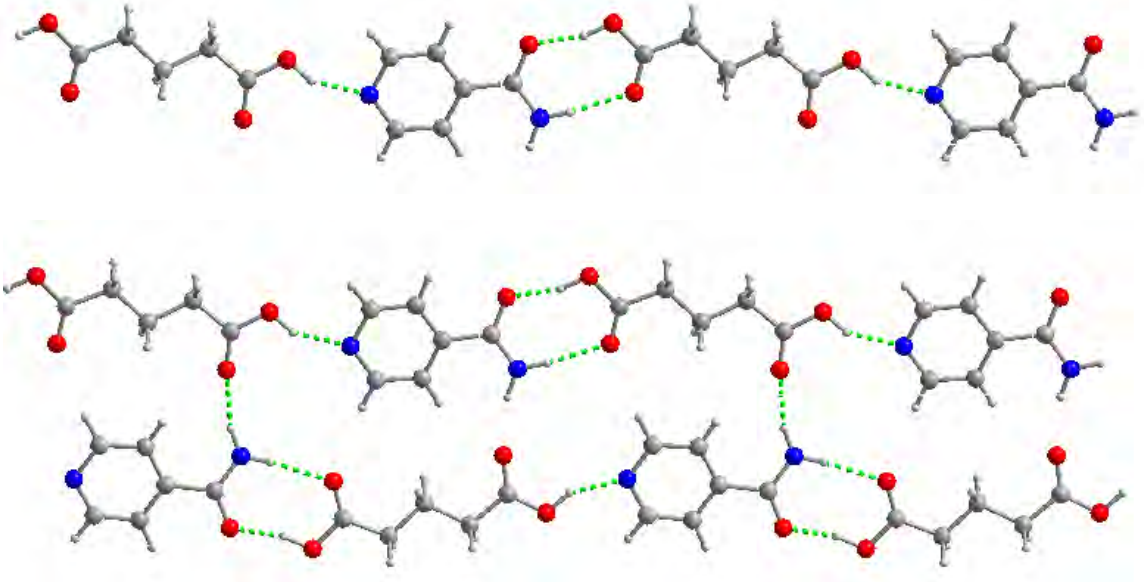

14.9: Crystalline structure of isonicotinamide : adipic acid 1:1

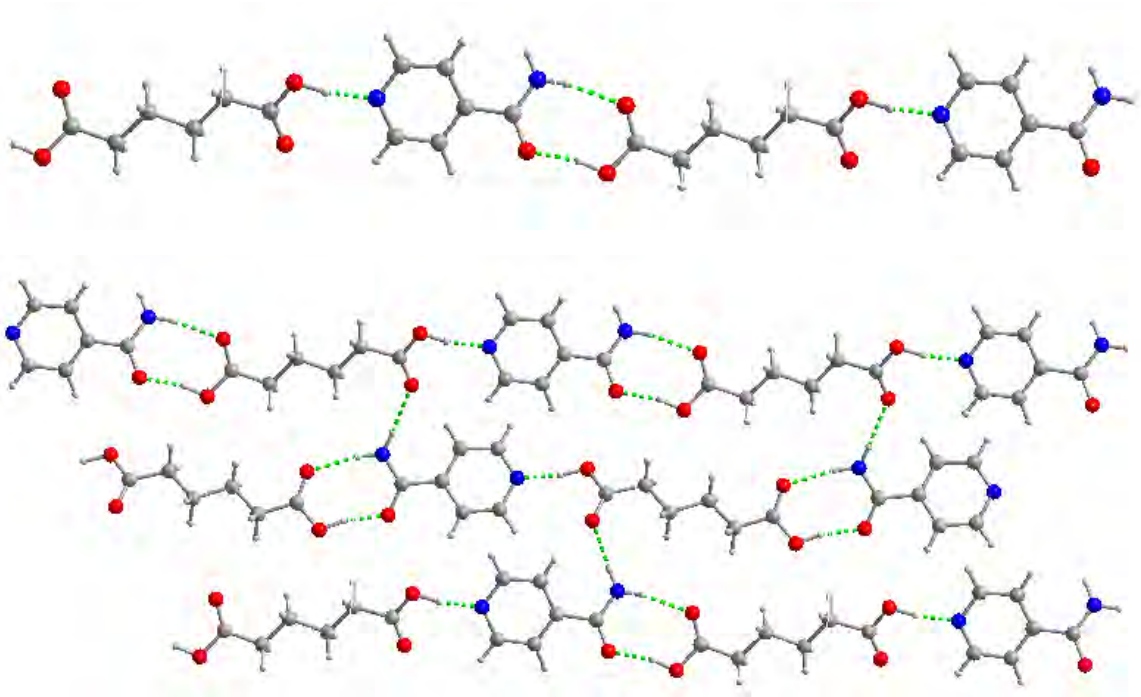

Appendix 15:

15.1: ^{1}H NMR spectra of isonicotinamide : pimelic acid (solvent – DMSO)

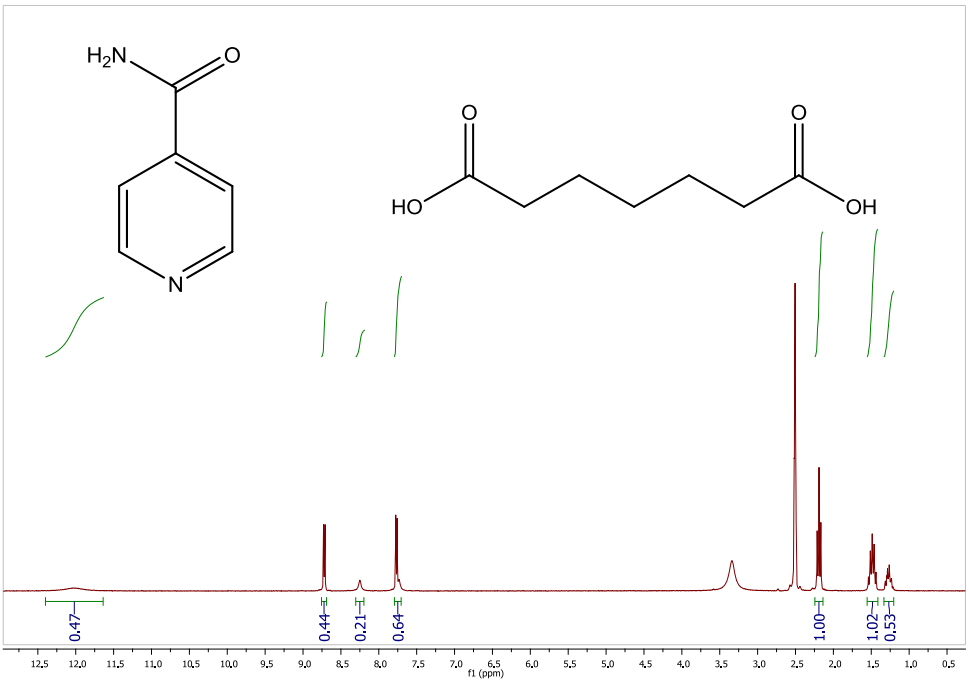

Isonicotinamide:	7.75 (3H,dd and s),	8.25 (1H,s),	8.72 (2H,dd)
Pimelic acid:	1.25 (2H, q),	1.5 (4H, q),	2.2 (4H,t)

15.2: The diffraction pattern simulated from the single crystal structure compared to that of the laboratory experimental powder diffraction pattern of isonicotinamide : pimelic acid, 1:1

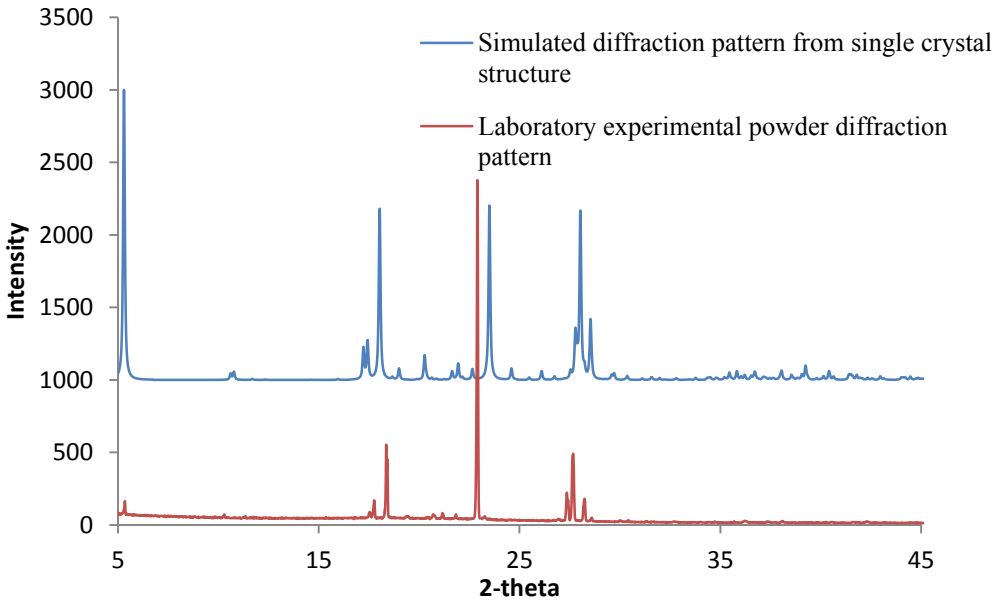

15.3: Ortep of isonicotinamide : pimelic acid, 1:1

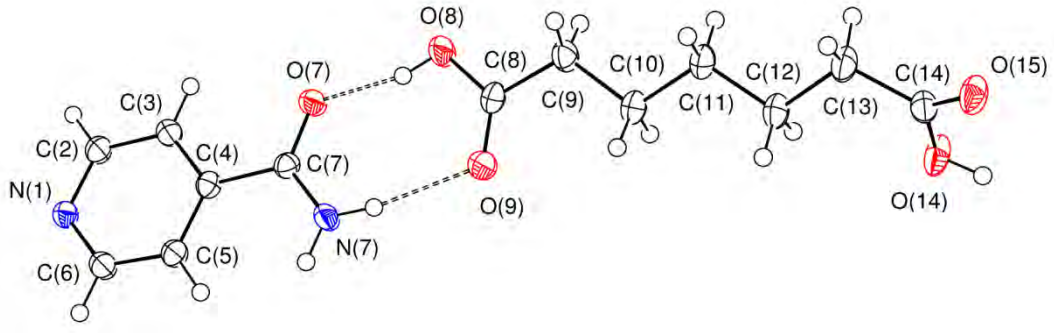

15.4: Crystallographic details for isonicotinamide : pimelic acid, 1:1

Empirical formula	$C_{13}\ H_{18}\ N_2\ O_5$
Formula weight	282.29
Temperature	120(2) K
Wavelength	0.71073Å
Crystal system	Monoclinic
Space group	P2/*c*
Unit cell dimensions	a = 8.2223(5) Å b = 5.1437(3) Å c = 33.389(2) Å α = 90° β = 93.873(3) ° γ = 90°
Volume	1408.9(2) $Å^3$
Z	4
Density (calculated)	1.331 Mg/m^3
Absorption coefficient	0.103 mm^{-1}
F(000)	600
Crystal size	0.10 x 0.08 x 0.05mm^3
Theta range for data collection	3.37 to 25.02°.
Index ranges	-9<=h<=9, -6<=k<=6, -39<=l<=39
Reflections collected	13904
Independent reflections	2480 [R(int) = 0.0742]
Completeness to theta = 25.02°	99.6%
Absorption correction	Semi-empirical from equivalents
Max. and min. transmission	0.9949 and 0.9898
Refinement method	Full-matrix least-squares on F^2
Data / restraints / parameters	2480 / 0 / 180
Goodness-of-fit on F^2	1.077
Final R indices [I>2sigma(I)]	R_1 = 0.0557, wR_2 = 0.1184
R indices (all data)	R_1 = 0.0901, wR_2 = 0.1337
Largest diff. peak and hole	0.311 and -0.305 e.$Å^{-3}$

15.5: Intramolecular bond lengths (Å) and angles (°) for isonicotinamide : pimelic acid, 1:1

Bond length (Å)		Bond length (Å)		Bond length (Å)	
C2-N1	1.333(3)	N7-H7A	0.8800	C12-C13	1.522(3)
C2-C3	1.390(3)	N7-H7B	0.8800	C12-H12A	0.9900
C2-H2	0.9500	C8-O9	1.209(3)	C12-H12B	0.9900
C3-C4	1.383(3)	C8-O8	1.322(3)	C13-C14	1.508(3)
C3-H3	0.9500	C8-C9	1.500(3)	C13-H13A	0.9900
C4-C5	1.385(3)	C9-C10	1.518(3)	C13-H13B	0.9900
C4-C7	1.504(3)	C9-H9A	0.9900	C14-O15	1.216(3)
C5-C6	1.380(3)	C9-H9B	0.9900	C14-O14	1.316(3)
C5-H5	0.9500	C10-C11	1.520(3)	O8-H8	0.8400
C6-N1	1.338(3)	C10-H10A	0.9900	O14-H14	0.8400
C6-H6	0.9500	C10-H10B	0.9900		
C7-O7	1.246(3)	C11-C12	1.522(3)		
C7-N7	1.322(3)				

Bond angle (°)		Bond angle (°)		Bond angle (°)	
N1-C2-C3	122.9(2)	C7-N7-H7B	120.0	C10-C11-H11B	108.8
N1-C2-H2	118.6	H7A-N7-H7B	120.0	C12-C11-H11B	108.8
C3-C2-H2	118.6	O9-C8-O8.	123.8(2)	H11A-C11-H11B	107.7
C4-C3-C2	119.3(2)	O9-C8-C9	124.5(2)	C13-C12-C11	112.1(2)
C4-C3-H3	120.4	O8-C8-C9	111.6(2)	C13-C12-H12A	109.2
C2-C3-H3	120.4	C8-C9-C10	114.9(2)	C11-C12-H12A	109.2
C3-C4-C5	117.9(2)	C8-C9-H9A	108.5	C13-C12-H12B	109.2
C3-C4-C7	118.9(2)	C10-C9-H9A	108.5	C11-C12-H12B	109.2
C5-C4-C7	123.2(2)	C8-C9-H9B	108.5	H12A-C12-H12B	107.9
C6-C5-C4	119.3(2)	C10-C9-H9B	108.5	C14-C13-C12	116.4(2)
C6-C5-H5	120.4	H9A-C9-H9B	107.5	C14-C13-H13A	108.2
C4-C5-H5	120.4	C9-C10-C11	112.2(2)	C12-C13-H13A	108.2
N1-C6-C5	123.2(2)	C9-C10-H10A	109.2	C14-C13-H13B	108.2
N1-C6-H6	118.4	C11-C10-H10A	109.2	C12-C13-H13B	108.2
C5-C6-H6	118.4	C9-C10-H10B	109.2	H13A-C13-H13B	107.3
O7-C7-N7	122.7(2)	C11-C10-H10B	109.2	O15-C14-O14	122.7(2)
O7-C7-C4	118.8(2)	H10A-C10-H10B	107.9	O15-C14-C13	123.2(2)
N7-C7-C4	118.5(2)	C10-C11-C12	113.9(2)	O14-C14-C13	114.1(2)
C2-N1-C6	117.5(2)	C10-C11-H11A	108.8	C8-O8-H8	109.5
C7-N7-H7A	120.0	C12-C11-H11A	108.8	C14-O14-H14	109.5

Torsion angle (°)		Torsion angle (°)	
N1-C2-C3-C4	0.0(4)	C3-C2-N1-C6	-0.3(4)
C2-C3-C4-C5	0.6(3)	C5-C6-N1-C2	0.0(4)
C2-C3-C4-C7	179.9(2)	O9-C8-C9-C10	12.4(4)
C3-C4-C5-C6	-0.9(3)	O8-C8-C9-C10	-169.6(2)
C7-C4-C5-C6	179.8(2)	C8-C9-C10-C11	-169.9(2)
C4-C5-C6-N1	0.7(4)	C9-C10-C11-C12	-176.0(2)
C3-C4-C7-O7	0.2(3)	C10-C11-C12-C13	-174.9(2)
C5-C4-C7-O7	179.5(2)	C11-C12-C13-C14	-175.6(2)
C3-C4-C7-N7	-178.9(2)	C12-C13-C14-O15	-146.7(2)
C5-C4-C7-N7	0.3(3)	C12-C13-C14-O14	35.4(3)

Appendix 16:

16.1: ^{1}H NMR spectra of isonicotinamide : suberic acid (solvent – DMSO)

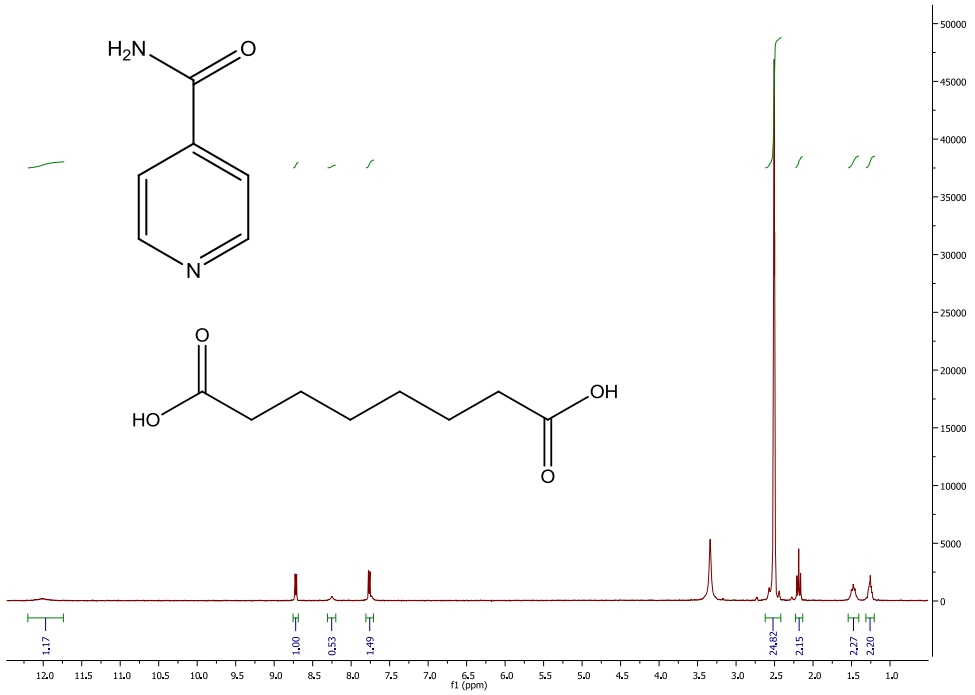

Isonicotinamide:	7.75 (3H,dd and s),	8.25 (1H,s),	8.70 (2H,dd)
Suberic acid:	1.25 (4H, q),	1.5 (4H, q),	2.2 (4H,t)

16.2: The diffraction pattern simulated from the single crystal structure compared to that of the laboratory experimental powder diffraction pattern of isonicotinamide : suberic acid, 1:1

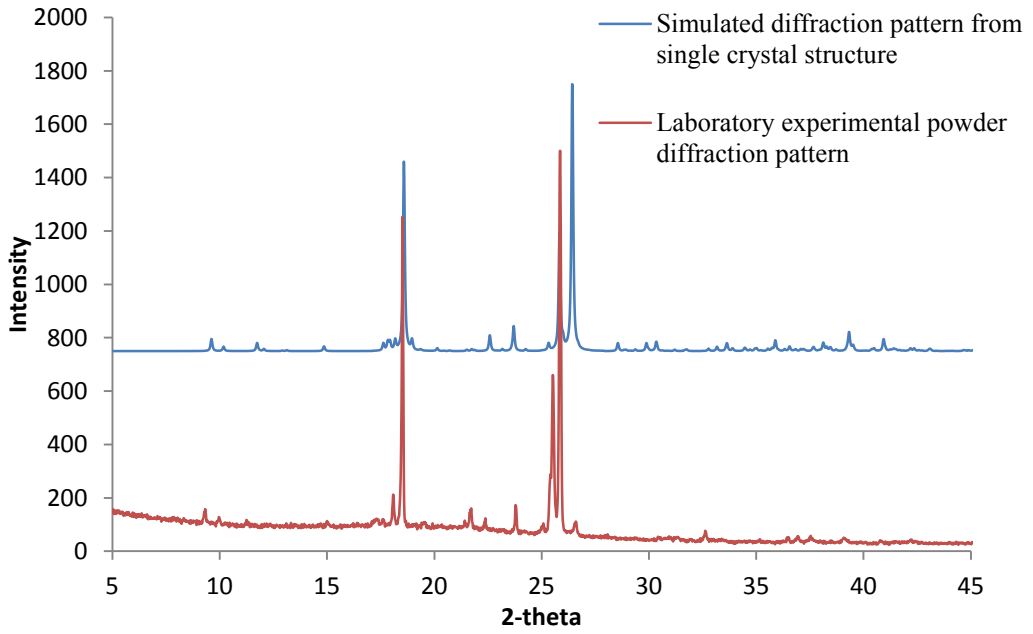

16.3: Ortep of isonicotinamide : suberic acid, 1:1

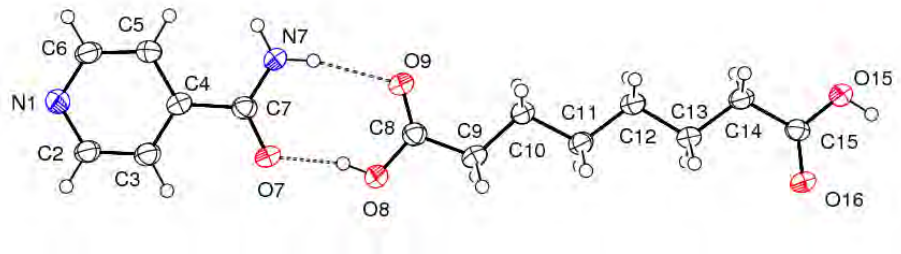

16.4: Crystallographic details for isonicotinamide : suberic acid, 1:1

Empirical formula	$C_{14}\ H_{20}\ N_2\ O_5$
Formula weight	296.32
Temperature	120(2) K
Wavelength	0.71073Å
Crystal system	Triclinic
Space group	P -1
Unit cell dimensions	a = 8.941 (2) Å b = 9.537(1) Å c = 10.135(2) Å α = 86.65(1)° β = 66.031(7) ° γ = 66.57(1)°
Volume	719.1(2) $Å^3$
Z	2
Density (calculated)	1.369 Mg/m^3
Absorption coefficient	0.104 mm^{-1}
F(000)	316
Crystal size	0.20 x 0.10 x 0.03mm^3
Theta range for data collection	2.97 to 25.02°.
Index ranges	-10<=h<=10, -11<=k<=11, -12<=l<=12
Reflections collected	9503
Independent reflections	2516 [R(int) = 0.0719]
Completeness to theta = 25.02°	99.0%
Absorption correction	Semi-empirical from equivalents
Max. and min. transmission	0.9969 and 0.9794
Refinement method	Full-matrix least-squares on F^2
Data / restraints / parameters	2516 / 0 / 192
Goodness-of-fit on F^2	1.105
Final R indices [I>2sigma(I)]	R_1 = 0.0724, wR_2 = 0.1604
R indices (all data)	R_1 = 0.1055, wR_2 = 0.1837
Largest diff. peak and hole	0.281 and -0.306 e.$Å^{-3}$

16.5: Intramolecular bond lengths (Å) and angles (°) for isonicotinamide : suberic acid, 1:1

Bond length (Å)		Bond length (Å)		Bond length (Å)	
C2-N1	1.332(4)	N7-H7B	0.8800	C12-H12A	0.9900
C2-C3	1.381(5)	C8-O9	1.214(4)	C12-H12B	0.9900
C2-H2	0.9500	C8-O8	1.321(4)	C13-C14	1.516(5)
C3-C4	1.385(5)	C8-C9	1.497(5)	C13-H13A	0.9900
C3-H3	0.9500	C9-C10	1.506(5)	C13-H13B	0.9900
C4-C5	1.381(5)	C9-H9A	0.9900	C14-C15	1.500(5)
C4-C7	1.500(5)	C9-H9B	0.9900	C14-H14A	0.9900
C5-C6	1.377(5)	C10-C11	1.528(4)	C14-H14B	0.9900
C5-H5	0.9500	C10-H10A	0.9900	C15-O16	1.215(4)
C6-N1	1.339(4)	C10-H10B	0.9900	C15-O15	1.309(4)
C6-H6	0.9500	C11-C12	1.517(5)	O8-H8	0.8400
C7-O7	1.241(4)	C11-H11A	0.9900	O15-H15	0.8400
C7-N7	1.326(4)	C11-H11B	0.9900		
N7-H7A	0.8800	C12-C13	1.520(4)		

Bond angle (°)		Bond angle (°)		Bond angle (°)	
N1-C2-C3	123.6(3)	O9-C8-O8	123.4(3)	C11-C12-H12A	109.2
N1-C2-H2	118.2	O9-C8-C9	125.8(3)	C13-C12-H12A	109.2
C3-C2-H2	118.2	O8-C8-C9	110.8(3)	C11-C12-H12B	109.2
C2-C3-C4	118.4(3)	C8-C9-C10	116.7(3)	C13-C12-H12B	109.2
C2-C3-H3	120.8	C8-C9-H9A	108.1	H12A-C12-H12B	107.9
C4-C3-H3	120.8	C10-C9-H9A	108.1	C14-C13-C12	112.8(3)
C5-C4-C3	118.5(3)	C8-C9-H9B	108.1	C14-C13-H13A	109.0
C5-C4-C7	118.3(3)	C10-C9-H9B	108.1	C12-C13-H13A	109.0
C3-C4-C7	123.2(3)	H9A-C9-H9B	107.3	C14-C13-H13B	109.0
C6-C5-C4	119.2(3)	C9-C10-C11	110.2(3)	C12-C13-H13B	109.0
C6-C5-H5	120.4	C9-C10-H10A	109.6	H13A-C13-H13B	107.8
C4-C5-H5	120.4	C11-C10-H10A	109.6	C15-C14-C13	114.5(3)
N1-C6-C5	122.9(3)	C9-C10-H10B	109.6	C15-C14-H14A	108.6
N1-C6-H6	118.6	C11-C10-H10B	109.6	C13-C14-H14A	108.6
C5-C6-H6	118.6	H10A-C10-H10B	108.1	C13-C14-H14B	108.6
O7-C7-N7	122.0(3)	C12-C11-C10	115.5(3)	H14A-C14-H14B	107.6
O7-C7-C4	119.2(3)	C12-C11-H11A	108.4	O16-C15-O15	122.8(3)
N7-C7-C4	118.7(3)	C10-C11-H11A	108.4	O16-C15-C14	124.8(3)
C2-N1-C6	117.4(3)	C12-C11-H11B	108.4	O15-C15-C14	112.4(3)
C7-N7-H7A	120.0	C10-C11-H11B	108.4	C8-O8-H8	109.5
C7-N7-H7B	120.0	H11A-C11-H11B	107.5	C15-O15-H15	109.5
H7A-N7-H7B	120.0	C11-C12-C13	112.0(3)		

Torsion angle (°)		Torsion angle (°)	
N1-C2-C3-C4	-1.5(5)	C5-C6-N1-C2	-0.2(5)
C2-C3-C4-C5	0.4(5)	O9-C8-C9-C10	-2.0(5)
C2-C3-C4-C7	179.8(3)	O8-C8-C9-C10	179.2(3)
C3-C4-C5-C6	0.6(5)	C8-C9-C10-C11	175.7(3)
C7-C4-C5-C6	-178.7(3)	C9-C10-C11-C12	178.0(3)
C4-C5-C6-N1	-0.8(5)	C10-C11-C12-C13	178.7(3)
C5-C4-C7-O7	-6.5(5)	C11-C12-C13-C14	178.6(3)
C3-C4-C7-O7	174.1(3)	C12-C13-C14-C15	179.6(3)
C5-C4-C7-N7	172.2(3)	C13-C14-C15-O16	-3.4(5)
C3-C4-C7-N7	-7.1(5)	C13-C14-C15-O15	176.8(3)
C3-C2-N1-C6	1.4(5)		

Appendix 17

17.1: ^{1}H NMR spectra of isonicotinamide : azelaic acid (solvent – DMSO)

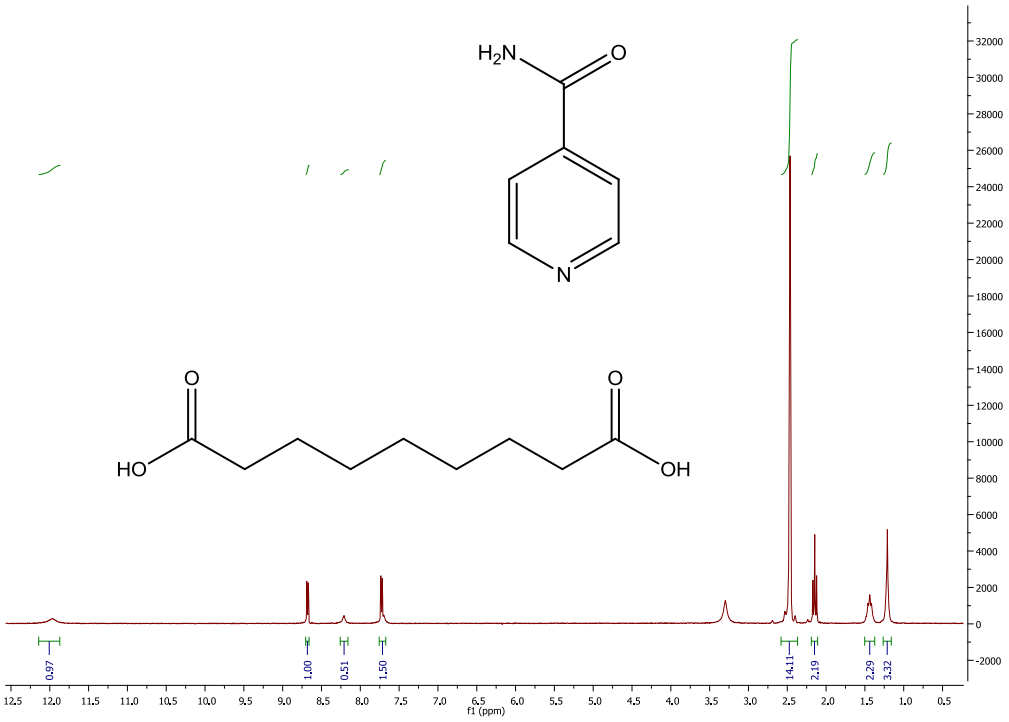

Isonicotinamide:	7.71 (3H,dd and s),	8.21 (1H,s),	8.68 (2H,dd)
Azelaic acid:	1.2 (6H, s),	1.42 (4H, q),	2.15 (4H,t)

17.2: The diffraction pattern simulated from the single crystal structure compared to that of the laboratory experimental powder diffraction pattern of isonicotinamide : azelaic acid, 1:1

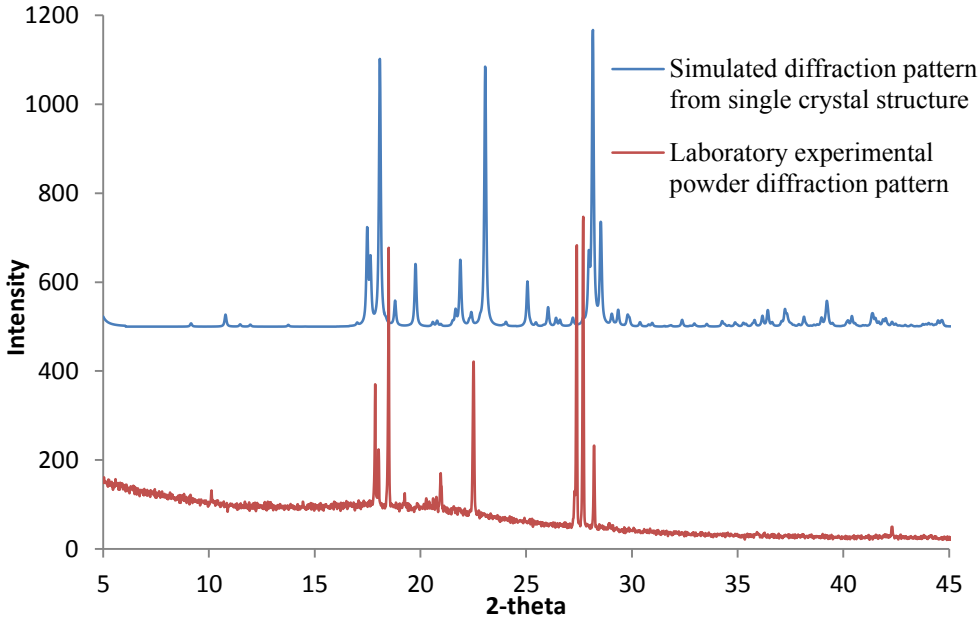

17.3: Ortep of isonicotinamide : azelaic acid, 1:1

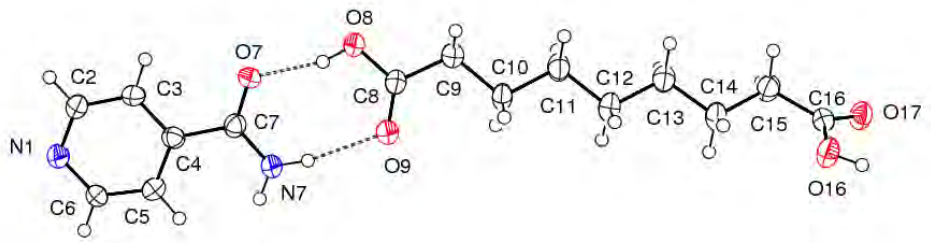

17.4: Crystallographic details for isonicotinamide : azelaic acid, 1:1

Empirical formula	$C_{15}\ H_{22}\ N_2\ O_5$
Formula weight	310.35
Temperature	120(2) K
Wavelength	0.71073Å
Crystal system	Monoclinic
Space group	P2/*c*
Unit cell dimensions	a = 8.212 (1) Å b = 5.068(7) Å c = 38.683(5) Å α = 90° β = 93.264(6) ° γ = 90°
Volume	1604.3(4) $Å^3$
Z	4
Density (calculated)	1.283 Mg/m^3
Absorption coefficient	0.097 mm^{-1}
F(000)	664
Crystal size	0.13 x 0.07 x 0.04mm^3
Theta range for data collection	3.16 to 25.03°.
Index ranges	-9<=h<=9, -6<=k<=6, -46<=l<=45
Reflections collected	11278
Independent reflections	2761 [R(int) = 0.0748]
Completeness to theta = 25.03°	97.3%
Absorption correction	Semi-empirical from equivalents
Max. and min. transmission	0.9961 and 0.9876
Refinement method	Full-matrix least-squares on F^2
Data / restraints / parameters	2761/ 0 / 201
Goodness-of-fit on F^2	1.186
Final R indices [I>2sigma(I)]	R_1 = 0.0879, wR_2 = 0.1966
R indices (all data)	R_1 = 0.1217, wR_2 = 0.2217
Largest diff. peak and hole	0.391 and -0.289 e.$Å^{-3}$

17.5: Intramolecular bond lengths (Å) and angles (°) for isonicotinamide : azelaic acid, 1:1

Bond length (Å)		Bond length (Å)		Bond length (Å)	
C6-N1	1.339(5)	C8-O9	1.216(5)	C13-C14	1.520(6)
C6-C5	1.379(6)	C8-O8	1.318(5)	C13-H13A	0.9900
C6-H6	0.9500	C8-C9	1.481(6)	C13-H13B	0.9900
C5-C4	1.393(6)	C9-C10	1.521(6)	C14-C15	1.521(6)
C5-H5	0.9500	C9-H9A	0.9900	C14-H14A	0.9900
C4-C3	1.394(6)	C9-H9B	0.9900	C14-H14B	0.9900
C4-C7	1.501(6)	C10-C11	1.523(6)	C15-C16	1.506(6)
C3-C2	1.381(6)	C10-H10A	0.9900	C15-H15A	0.9900
C3-H3	0.9500	C10-H10B	0.9900	C15-H15B	0.9900
C2-N1	1.336(6)	C11-C12	1.526(6)	C16-O17	1.222(5)
C2-H2	0.9500	C11-H11A	0.9900	C16-O16	1.313(5)
C7-O7	1.248(5)	C11-H11B	0.9900	O8-H8	0.8400
C7-N7	1.322(5)	C12-C13	1.523(6)	O16-H16	0.8400
N7-H7A	0.8800	C12-H12A	0.9900		
N7-H7B	0.8800	C12-H12B	0.9900		

Bond angle (°)		Bond angle (°)		Bond angle (°)	
N1-C6-C5	123.5(4)	O8-C8-C9	112.7(4)	H12A-C12-H12B	107.8
N1-C6-H6	118.3	C8-C9-C10	115.3(4)	C14-C13-C12	113.3(4)
C5-C6-H6	118.3	C8-C9-H9A	108.4	C14-C13-H13A	108.9
C6-C5-C4	118.8(4)	C10-C9-H9A	108.4	C12-C13-H13A	108.9
C6-C5-H5	120.6	C8-C9-H9B	108.4	C14-C13-H13B	108.9
C4-C5-H5	120.6	C10-C9-H9B	108.4	C12-C13-H13B	108.9
C5-C4-C3	118.0(4)	H9A-C9-H9B	107.5	H13A-C13-H13B	107.7
C5-C4-C7	123.0(4)	C9-C10-C11	112.5(4)	C13-C14-C15	112.3(4)
C3-C4-C7	119.0(4)	C9-C10-H10A	109.1	C13-C14-H14A	109.1
C2-C3-C4	118.9(4)	C11-C10-H10A	109.1	C15-C14-H14A	109.1
C2-C3-H3	120.6	C9-C10-H10B	109.1	C13-C14-H14B	109.1
C4-C3-H3	120.6	C11-C10-H10B	109.1	C15-C14-H14B	109.1
N1-C2-C3	123.4(4)	H10A-C10-H10B	107.8	H14A-C14-H14B	107.9
N1-C2-H2	118.3	C10-C11-C12	113.3(4)	C16-C15-C14	116.4(4)
C3-C2-H2	118.3	C10-C11-H11A	108.9	C16-C15-H15A	108.2
O7-C7-N7	122.8(4)	C12-C11-H11A	108.9	C14-C15-H15A	108.2
O7-C7-C4	118.9(4)	C10-C11-H11B	108.9	C16-C15-H15B	108.2
N7-C7-C4	118.3(4)	C12-C11-H11B	108.9	C14-C15-H15B	108.2
C2-N1-C6	117.4(4)	H11A-C11-H11B	107.7	H15A-C15-H15B	107.3
C7-N7-H7A	120.0	C13-C12-C11	112.8(4)	O17-C16-O16	122.8(4)
C7-N7-H7B	120.0	C13-C12-H12A	109.0	O17-C16-C15	122.7(4)
H7A-N7-H7B	120.0	C11-C12-H12A	109.0	O16-C16-C15	114.5(4)
O9-C8-O8	123.1(4)	C13-C12-H12B	109.0	C8-O8-H8	109.5
O9-C8-C9	124.2(4)	C11-C12-H12B	109.0	C16-O16-H16	109.5

Torsion angle (°)		Torsion angle (°)	
N1-C6-C5-C4	-0.4(7)	C5-C6-N1-C2	0.3(7)
C6-C5-C4-C3	0.4(6)	O9-C8-C9-C10	-9.6(7)
C6-C5-C4-C7	-179.5(4)	O8-C8-C9-C10	171.5(4)
C5-C4-C3-C2	-0.4(6)	C8-C9-C10-C11	169.3(4)
C7-C4-C3-C2	179.6(4)	C9-C10-C11-C12	175.7(4)
C4-C3-C2-N1	0.3(7)	C10-C11-C12-C13	173.6(4)
C5-C4-C7-O7	179.9(4)	C11-C12-C13-C14	174.2(4)
C3-C4-C7-O7	-0.1(6)	C12-C13-C14-C15	176.7(4)
C5-C4-C7-N7	-1.7(6)	C13-C14-C15-C16	175.8(4)
C3-C4-C7-N7	178.4(4)	C14-C15-C16-O17	150.4(4)
C3-C2-N1-C6	-0.3(7)	C14-C15-C16-O16	-30.6(6)

Appendix 18:

18.1: ^{1}H NMR spectra of the isonicotinamide : sebacic acid adduct (cocrystallised from ethanol) (solvent – DMSO)

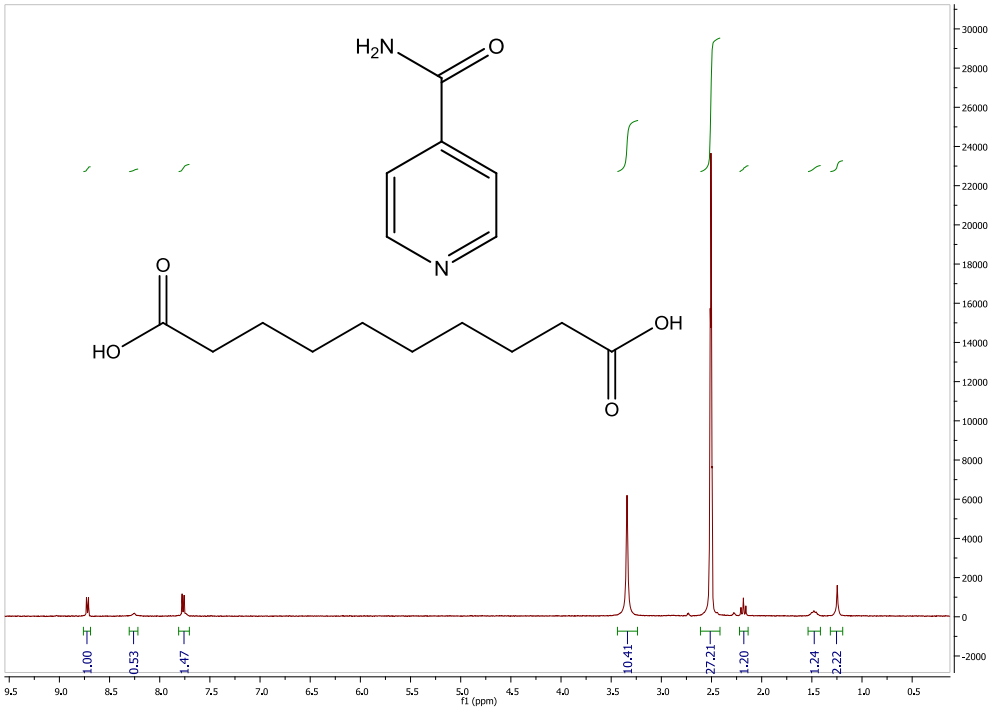

Isonicotinamide:	7.75 (3H,dd and s),	8.25 (1H,s),	8.72 (2H,dd)
Sebacic acid:	1.25 (8H, s),	1.47 (4H, t),	2.17 (4H,t),

Appendix 19:

19.1: ^{1}H NMR spectra of the isonicotinamide : undecanedioic acid adduct (solvent – DMSO)

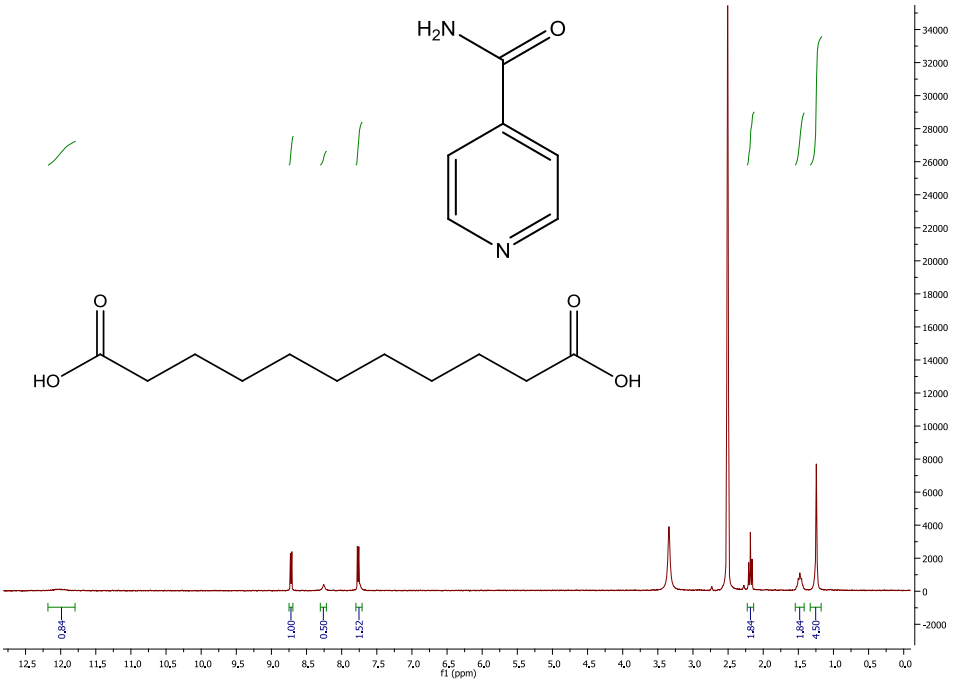

Isonicotinamide:	7.6 (3H,dd and s),	8.25 (1H,s),	8.70 (2H,dd)
Undecanedioic acid:	1.25 (10H, s),	1.47 (4H, t),	2.19 (4H,t), 12.0 (2H, s)

Appendix 20:

20.1: Table of values comparing density and packing fraction of the isonicotinamide : alkanediacid cocrystals and their respective pure acids

	Pure alkanediacid						1:1 isonicotinamide : alkanediacid cocrystal						2:1 isonicotinamide : alkanediacid cocrystal					
	Melting point ˚C	Density Mg/m^3	Packing fraction	No. H bonds	Total H..A Distance (& Average) Å	1/(Average Distance) * No. Hbonds	Melting point ˚C	Density Mg/m^3	Packing fraction	No. H bonds	Total H..A Distance (& Average) Å	1/(Average Distance) * No. Hbonds	Melting point ˚C	Density Mg/m^3	Packing fraction	No. H bonds	Total H..A Distance (& Average) Å	1/(Average Distance) * No. Hbonds
Oxalic	189.5	1.948	0.802										243	1.584	77.1	9	16.573	4.887
Malonic	135.6	1.669	0.749										170	1.490	73.1			
Succinic	188	1.624	0.777	4	6.924	2.311							206	1.480	74.1	9	(17.186	4.712
Glutaric	99	1.484	0.741	4	6.832	2.342	134	1.399	70.3				149	1.420	71.8			
Adipic	153	1.398	0.726	4	6.728	2.374	163	1.395	71.6	6	11.048	3.259	178	1.425	73.0	9	17.495	4.630
Pimelic	106	1.372	0.727	4	6.853	2.335	112	1.331	69	6	11.566	3.112						
Suberic	144	1.319	0.714	4	6.676	2.397	165	1.369	72	6	11.698	3.077						
Azelaic	106.5	1.303	0.720	4	6.816	2.347	142	1.283	68.3	6	11.483	3.134						
Sebacic	134.5	1.257	0.704	4	6.616	2.419							156					
Undecanedioic	109	1.181	0.254	2	4.15	0.964	123											

Appendix 21:

CrystEngComm

View Online
Dynamic Article Links

Cite this: DOI: 10.1039/c1ce05160a

www.rsc.org/crystengcomm

PAPER

The crystal structures and melting point properties of isonicotinamide cocrystals with alkanediacids $HO_2C(CH_2)_{n-2}CO_2H$ $n = 7$–9†

Laura J. Thompson, Raja S. Voguri, Louise Male and Maryjane Tremayne*

Received 2nd February 2011, Accepted 30th March 2011
DOI: 10.1039/c1ce05160a

The tunability of physiochemical properties of crystalline materials through controlled cocrystal formulation is an aim for both the pharmaceutical industry and crystal engineers. In this paper we report that the melting point alternation behaviour of odd and even alkanedicarboxylic acids is mimicked in a set of cocrystals in which isonicotinamide is combined in a 1 : 1 stoichiometry with pimelic acid, suberic acid and azelaic acid. All three structures contain hydrogen bonded chains of alternating acid and amide molecules between which acid–pyridine and acid–amide synthons are formed. Both isonicotinamide : pimelic acid and isonicotinamide : azelaic acid form structures in which the acid moiety adopts a twisted alkyl backbone conformation similar to that observed in the pure odd alkanediacid materials. The isonicotinamide : suberic acid cocrystal differs from the others reported here retaining both the elevated melting point and the planar acid conformation displayed by even alkanediacid materials in this series.

Introduction

Molecular cocrystals are becoming increasingly important within the pharmaceutical industry as an alternative source of new solid crystalline materials with the potential to provide optimal physical properties whilst retaining the chemical properties of the cocrystal components.[1–3] Physicochemical properties such as the melting point, stability and solubility of an active pharmaceutical ingredient can be tuned through cocrystal formulation.[4] Although there are many more advances to be made in this area, it has been shown that it is possible to exercise true control of these properties by consideration of the supramolecular assembly within a homologous set of cocrystal materials, as demonstrated by the structure–property relationship of the melting points of aliphatic dicarboxylic acids when cocrystallised with an anti-cancer drug.[5]

Useful application of this relationship between molecular structure and physical properties still depends on the predictable synthesis of cocrystal materials rather than the recrystallisation of starting compounds. Cocrystal synthesis relies on the preferential formation of heteromeric synthons rather than the formation of strong interactions between molecules of the individual components. One such robust heteromeric synthon is the acid–pyridine hydrogen bond (I) that is often formed in amide–acid cocrystals in combination with an amide–amide (II) or acid–amide (III) dimer, depending on the stoichiometry of the cocrystal (Scheme 1). The consistent preference for formation of synthon (I) is demonstrated by the propensity that both isonicotinamide and nicotinamide have shown for cocrystal formation with a range of alkanedicarboxylic acids.

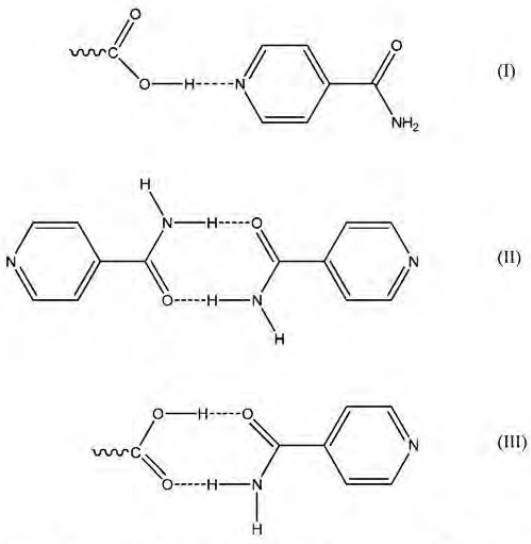

Scheme 1 Potential hydrogen bond synthons found in amide–acid cocrystals.

School of Chemistry, University of Birmingham, Edgbaston, Birmingham, B15 2TT, UK. E-mail: m.tremayne@bham.ac.uk

† Electronic supplementary information (ESI) available. CCDC reference numbers 810990–810992. For ESI and crystallographic data in CIF or other electronic format see DOI: 10.1039/c1ce05160a

Appendix 22:

22.1: Crystalline structure of nicotinamide : hydrogen oxalate 1:1

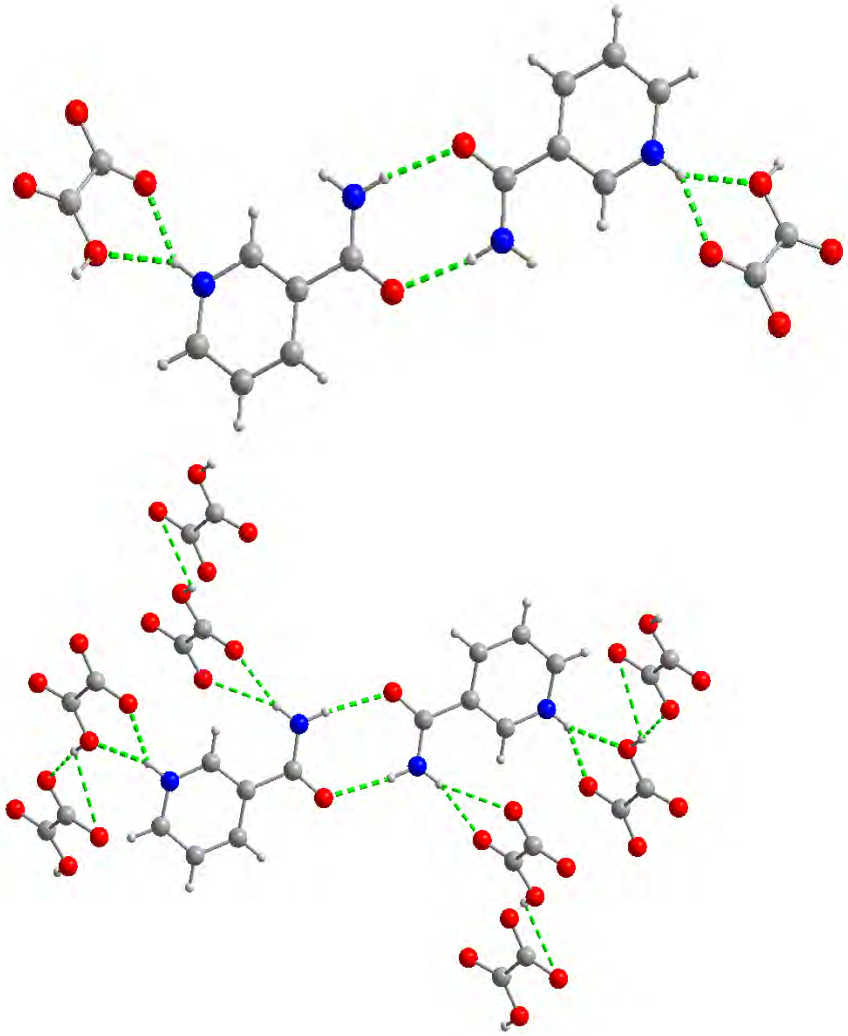

22.2: Crystalline structure of nicotinamide : malonic acid 2:1

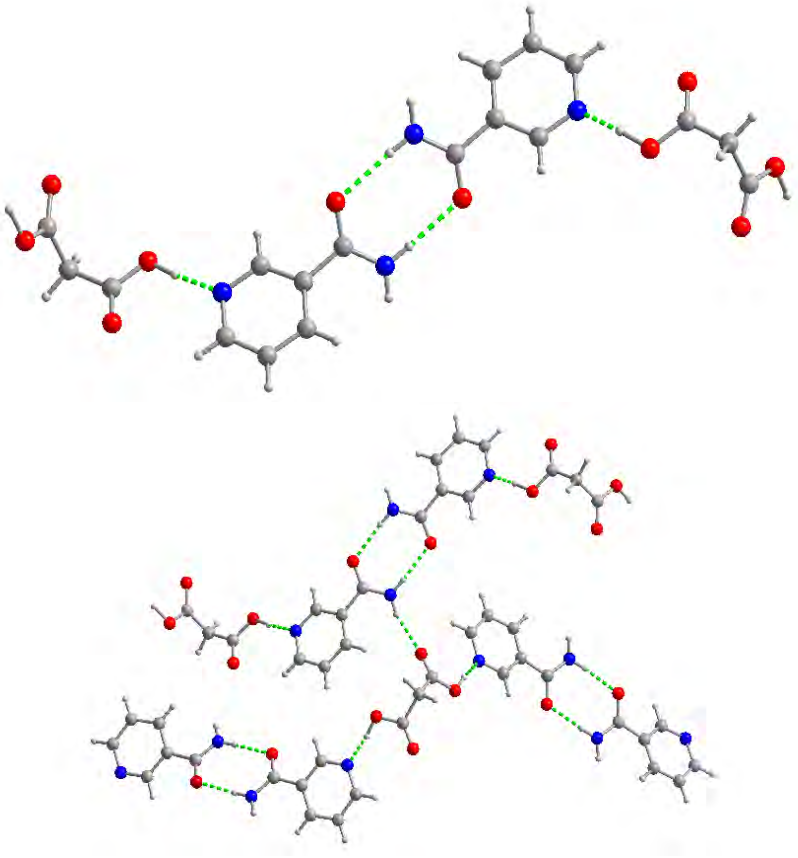

22.3: Crystalline structure of nicotinamide : hydrogen maleate 1:1

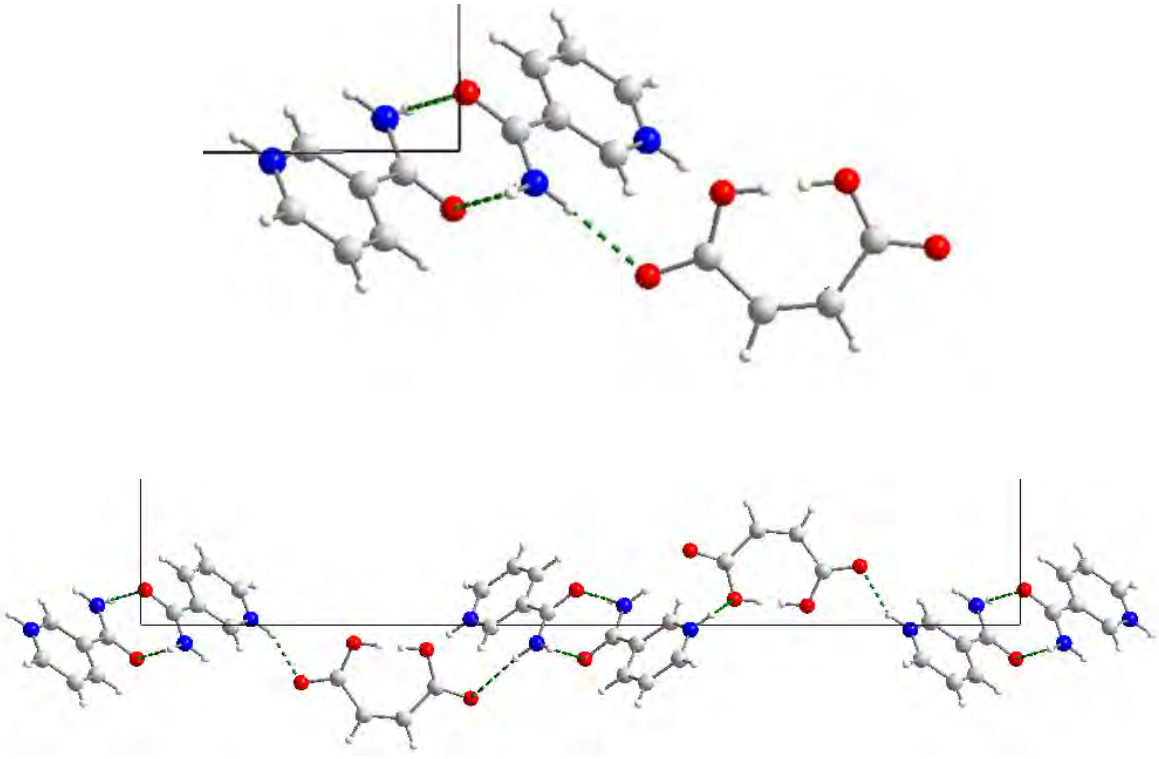

22.4: Crystalline structure of nicotinamide : fumaric acid 1:1

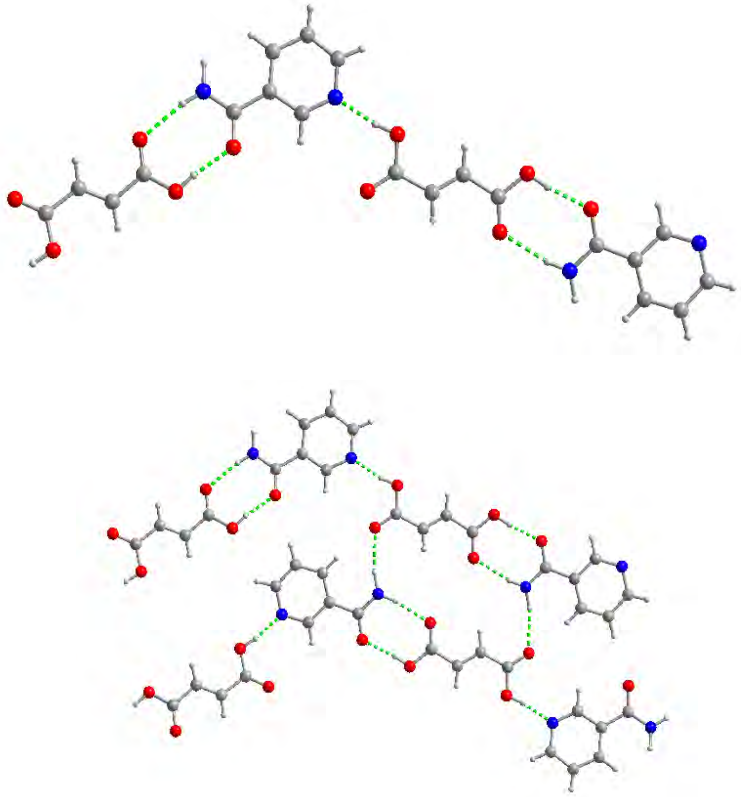

22.5: Crystalline structure of nicotinamide : fumaric acid 2:1

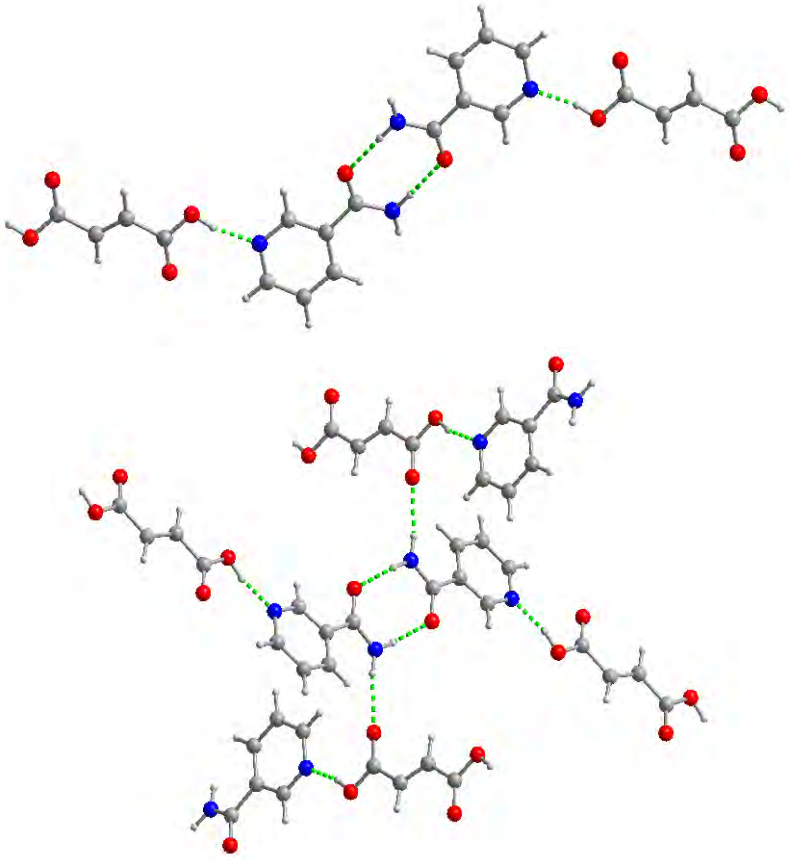

22.6: Crystalline structure of nicotinamide : glutaric acid 1:1

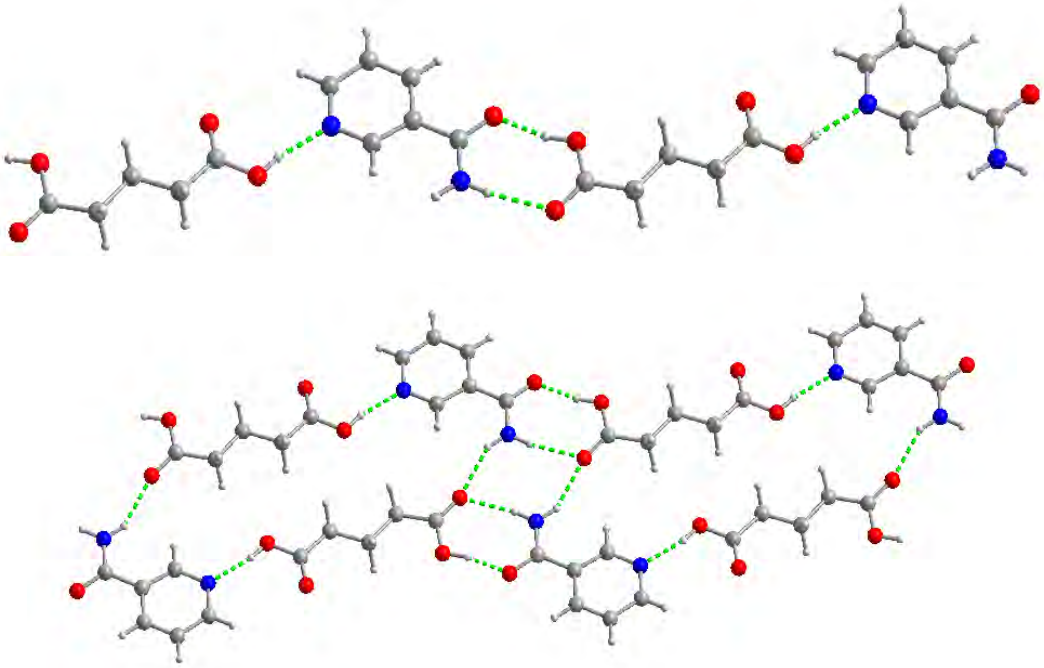

22.7: Crystalline structure of nicotinamide : adipic acid 1:1

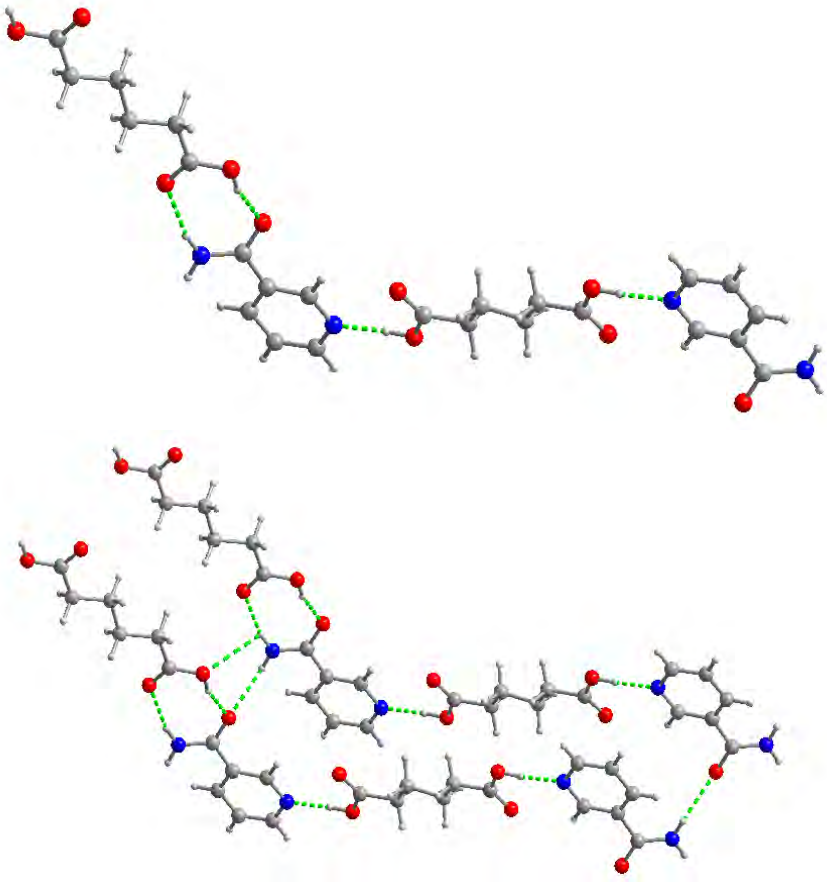

22.8: Crystalline structure of nicotinamide : adipic acid 2:1

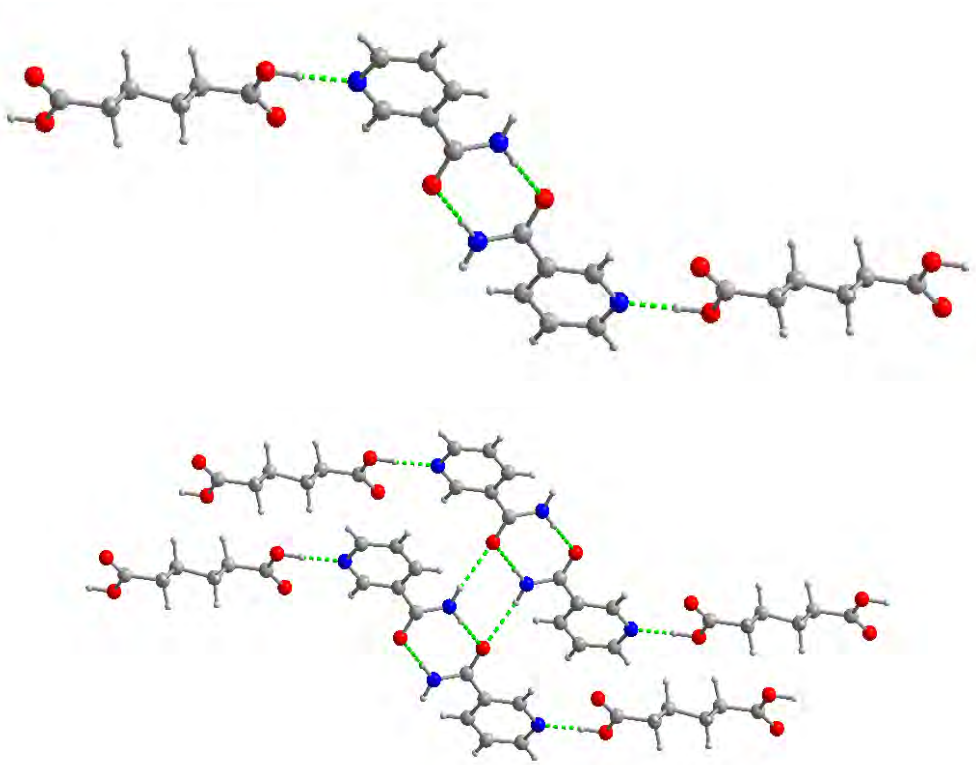

22.9: Crystalline structure of nicotinamide : pimelic acid 1:1

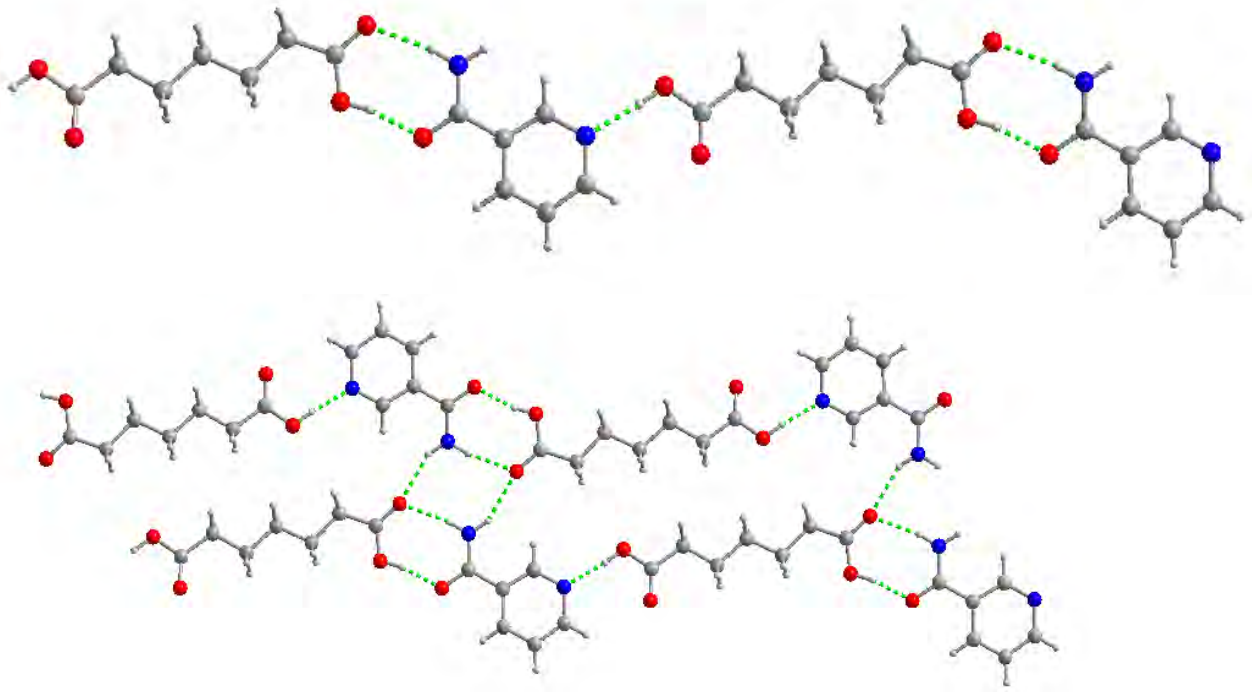

22.10: Crystalline structure of nicotinamide : suberic acid 1:1

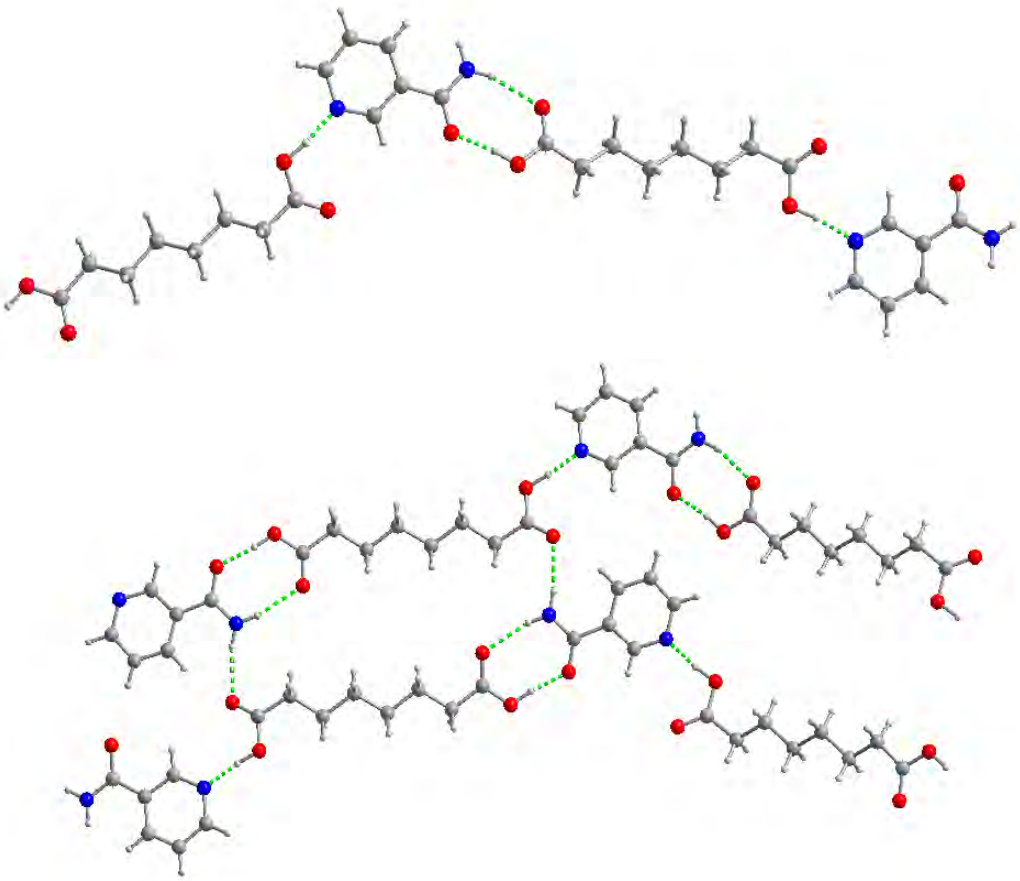

22.11: Crystalline structure of nicotinamide : suberic acid 2:1

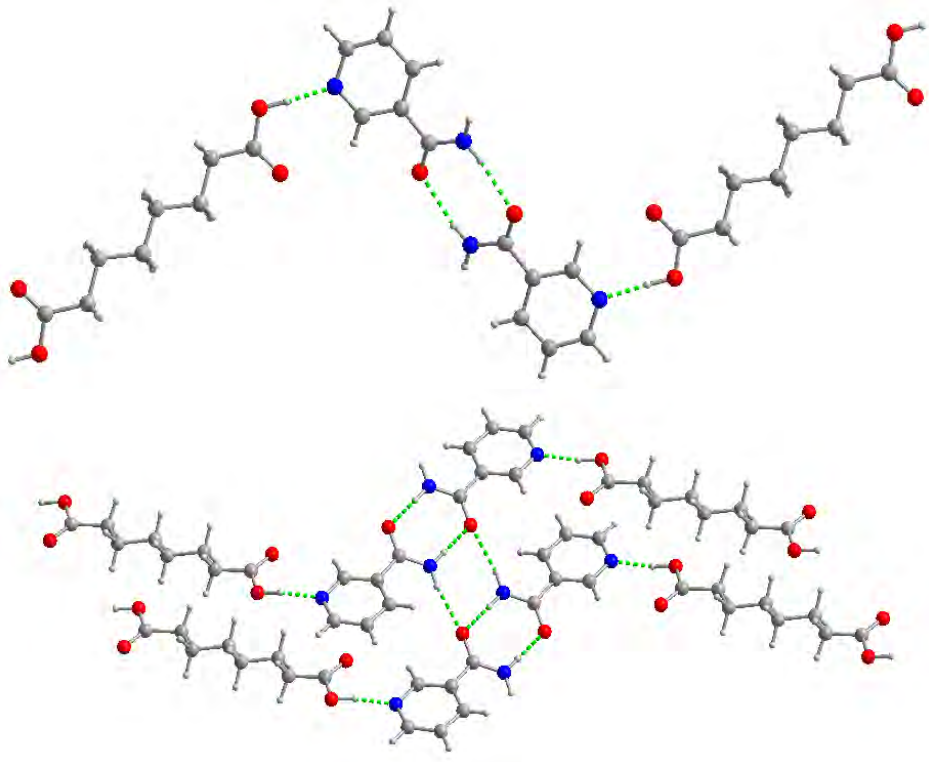

22.12: Crystalline structure of nicotinamide : azelaic acid 1:1

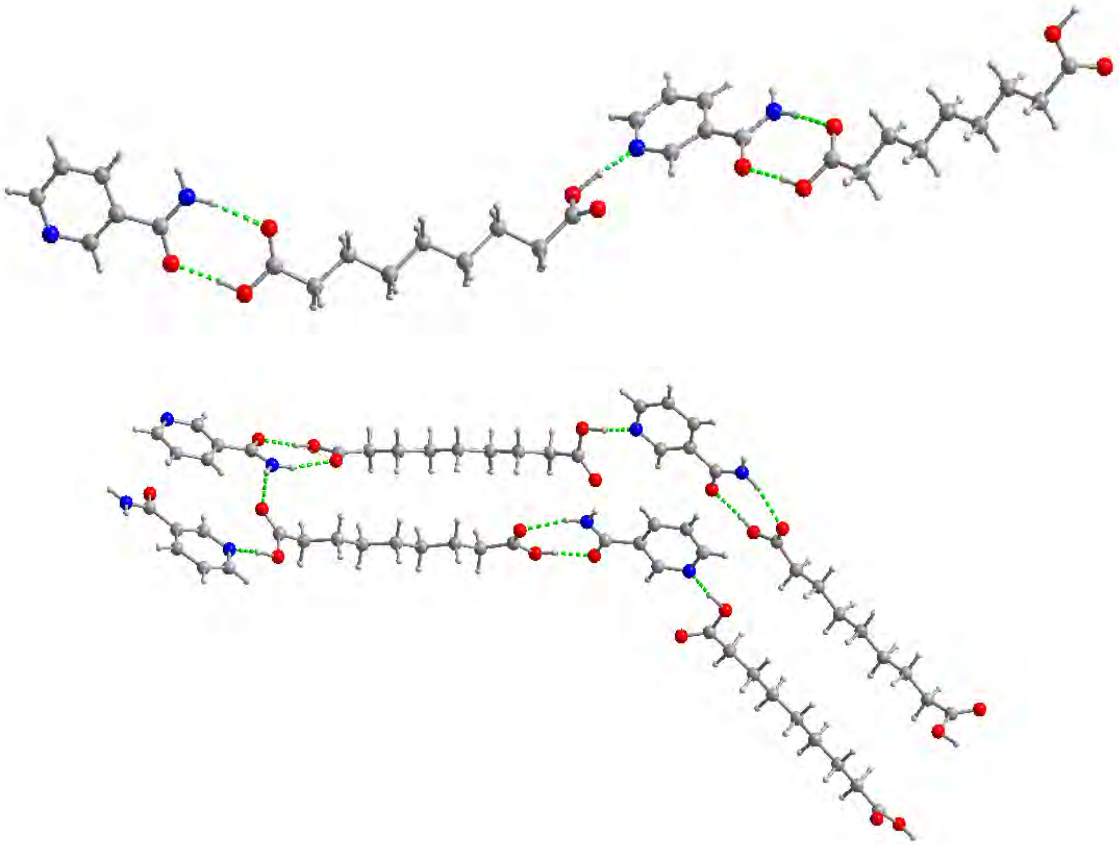

22.13: Crystalline structure of nicotinamide : sebacic acid 2:1

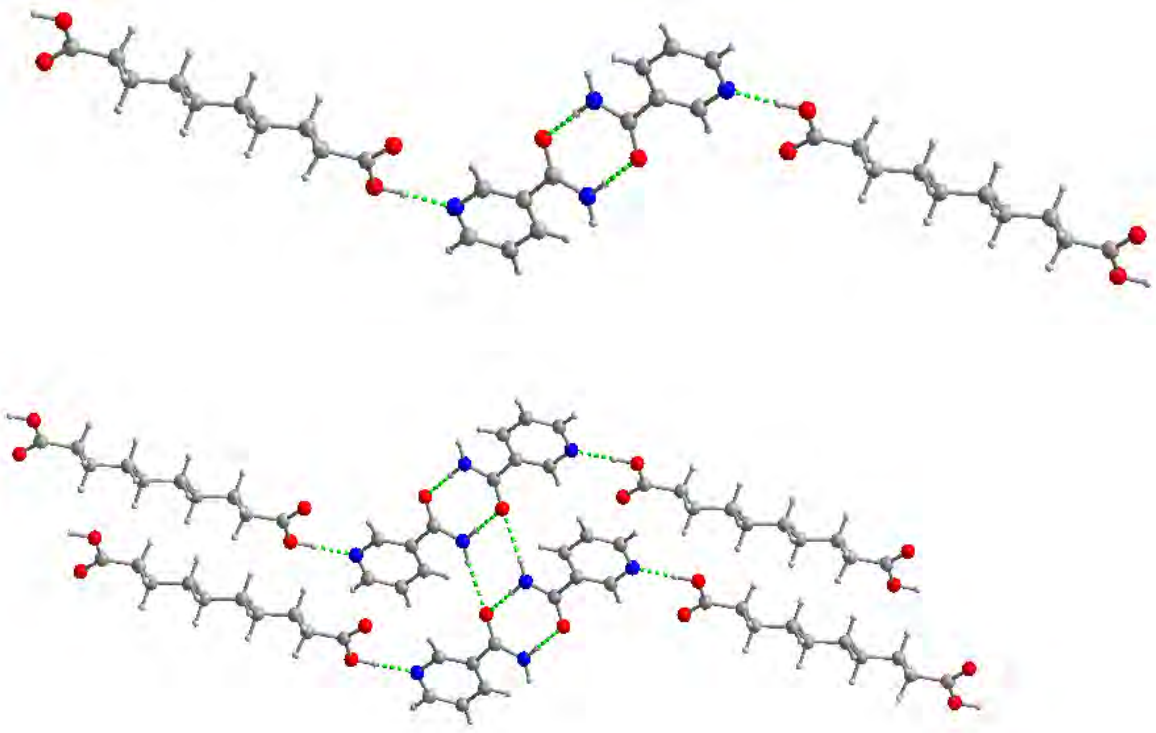

Appendix 23

23.1: ^{1}H NMR spectra of nicotinamide : succinic acid (experimental method 3.1) (solvent – DMSO)

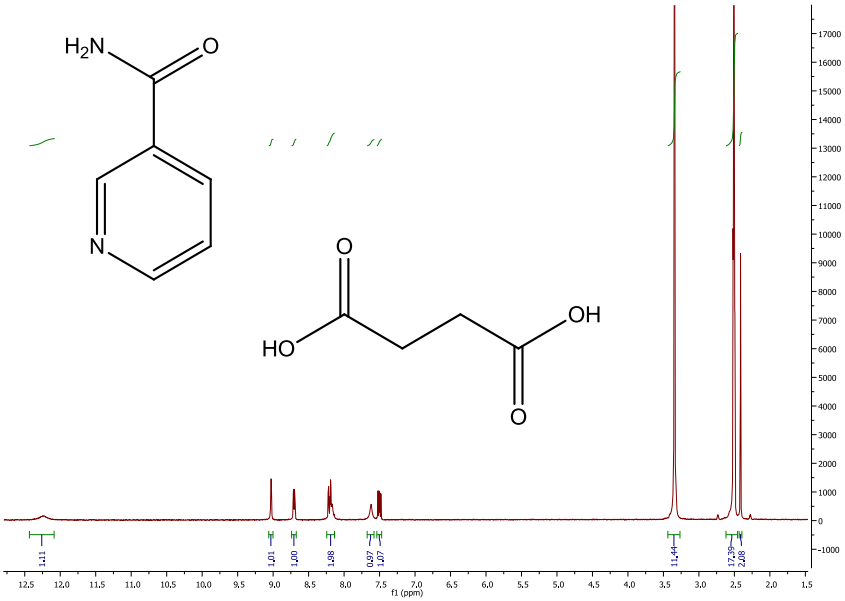

Nicotinamide: 7.50 (1H,q), 7.62 (1H,s), 8.20 (2H,dt), 8.71 (1H,dd), 9.30 (1H,d)
Succinic acid: 2.42 (2H, s), 12.20 (2H, s)

23.2: ^{1}H NMR spectra of nicotinamide : succinic acid (experimental method 3.2) (solvent – DMSO)

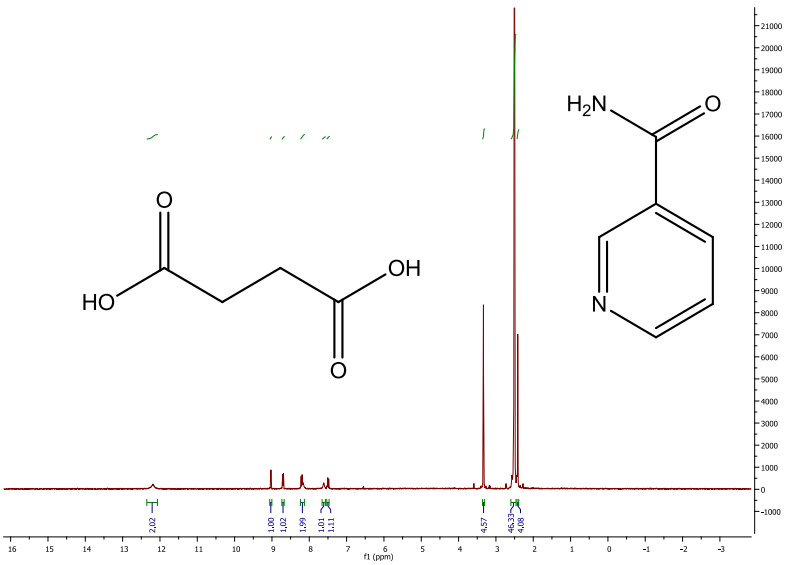

Nicotinamide: 7.50 (1H,q), 7.61 (1H,s), 8.20 (2H,dt), 8.71 (1H,dd), 9.40 (1H,d),
Succinic acid: 2.41 (2H, s), 12.19 (2H, s)

23.3: Ortep of nicotinamide : succinic acid, 2:1

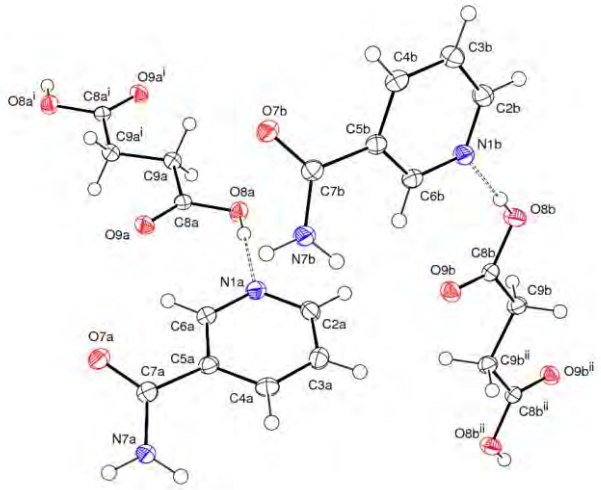

23.4: Crystallographic details of nicotinamide : succinic acid, 2:1

Empirical formula	$C_{16}H_{18}N_4O_6$	
Formula weight	362.34	
Temperature	120(2)K	
Wavelength	0.71073 Å	
Crystal system	Triclinic	
Space group	P -1	
Unit cell dimensions	a = 5.0872(2)Å b = 11.5569(5)Å c = 14.2784(5)Å	α = 77.433(2)° β = 86.726(2) ° γ = 89.418(2)°
Volume	818.01(6)Å^3	
Z	2	
Density (calculated)	1.471 Mg/m^3	
Absorption coefficient	0.115 mm^{-1}	
F(000)	380	
Crystal size	0.17 x 0.03 x 0.01 mm^3	
Theta range for data collection	3.59 to 26.02°	
Index ranges	-6<=h<=6, -14<=k<=14, -17<=l<=17	
Reflections collected	12664	
Independent reflections	3205 [R(int) = 0.0610]	
Completeness to theta = 26.02°	99.3%	
Max. and min. transmission	0.9989 and 0.9808	
Refinement method	Full-matrix least-squares on F^2	
Data / restraints / parameters	3205/0/237	
Goodness-of-fit on F^2	1.106	
Final R indices [I>2sigma(I)]	R_1 = 0.0555, wR_2 = 0.1162	
R indices (all data)	R_1 =0.0803, wR_2 = 0.1320	
Largest diff. peak and hole	0.244 and -0.267 e.Å^{-3}	

23.5: Intramolecular bond lengths (Å) and angles (°) in nicotinamide : succinic acid, 2:1

Bond length (Å)		Bond length (Å)		Bond length (Å)	
C2A-N1A	1.339(3)	C8A-O9A	1.213(3)	C5B-C7B	1.494(3)
C2A-C3A	1.384(4)	C8A-O8A	1.328(3)	C6B-N1B	1.338(3)
C2A-H2A	0.9500	C8A-C9A	1.500(3)	C6B-H6B	0.9500
C3A-C4A	1.382(3)	C9A-C9A^{i}	1.516(5)	C7B-O7B	1.242(3)
C3A-H3A	0.9500	C9A-H9AA	0.9900	C7B-N7B	1.331(3)
C4A-C5A	1.390(3)	C9A-H9AB	0.9900	N7B-H7BA	0.8800
C4A-H4A	0.9500	O8A-H8A	0.8400	N7B-H7BB	0.8800
C5A-C6A	1.391(3)	C2B-N1B	1.344(3)	C8B-O9B	1.212(3)
C5A-C7A	1.491(3)	C2B-C3B	1.379(3)	C8B-O8B	1.334(3)
C6A-N1A	1.341(3)	C2B-H2B	0.9500	C8B-C9B	1.498(3)
C6A-H6A	0.9500	C3B-C4B	1.382(4)	C9B-C9B^{ii}	1.528(5)
C7A-O7A	1.241(3)	C3B-H3B	0.9500	C9B-H9BA	0.9900
C7A-N7A	1.332(3)	C4B-C5B	1.392(3)	C9B-H9BB	0.9900
N7A-H7AA	0.8800	C4B-H4B	0.9500	O8B-H8B	0.8400
N7A-H7AB	0.8800	C5B-C6B	1.387(3)		

Bond angle (°)		Bond angle (°)		Bond angle (°)	
N1A-C2A-C3A	122.8(2)	O9A-C8A-O8A	123.6(2)	N1B-C6B-C5B	123.1(2)
N1A-C2A-H2A	118.6	O9A-C8A-C9A	124.2(2)	N1B-C6B-H6B	118.4
C3A-C2A-H2A	118.6	O8A-C8A-C9A	112.2(2)	C5B-C6B-H6B	118.4
C4A-C3A-C2A	119.0(2)	C8AC9A-C9A^{i}	112.7(2)	O7B-C7B-N7B	122.2(2)
C4A-C3A-H3A	120.5	C8A-C9A-H9AA	109.1	O7B-C7B-C5B	120.0(2)
C2A-C3A-H3A	120.5	C9A#1-C9A-H9AA	109.1	N7B-C7B-C5B	117.8(2)
C3A-C4A-C5A	119.0(2)	C8A-C9A-H9AB	109.1	C6B-N1B-C2B	117.7(2)
C3A-C4A-H4A	120.5	C9A#1-C9A-H9AB	109.1	C7B-N7B-H7BA	120.0
C5A-C4A-H4A	120.5	H9AA-C9A-H9AB	107.8	C7B-N7B-H7BB	120.0
C4A-C5A-C6A	118.2(2)	C8A-O8A-H8A	109.5	H7BA-N7B-H7BB	120.0
C4A-C5A-C7A	124.4(2)	N1B-C2B-C3B	123.1(2)	O9B-C8B-O8B	23.3(2)
C6A-C5A-C7A	117.4(2)	N1B-C2B-H2B	118.5	O9B-C8B-C9B	124.9(2)
N1A-C6A-C5A	123.0(2)	C3B-C2B-H2B	118.5	O8B-C8B-C9B	111.8(2)
N1A-C6A-H6A	118.5	C2B-C3B-C4B	118.8(2)	C8B-C9B-9B^{ii}	112.2(2)
C5A-C6A-H6A	118.5	C2B-C3B-H3B	120.6	C8B-C9B-H9BA	109.2
O7A-C7A-N7A	121.8(2)	C4B-C3B-H3B	120.6	C9B#2-C9B-H9BA	109.2
O7A-C7A-C5A	120.6(2)	C3B-C4B-C5B	119.0(2)	C8B-C9B-H9BB	109.2
N7A-C7A-C5A	117.6(2)	C3B-C4B-H4B	120.5	C9B#2-C9B-H9BB	109.2
C2A-N1A-C6A	118.0(2)	C5B-C4B-H4B	120.5	H9BA-C9B-H9BB	107.9
C7A-N7A-H7AA	120.0	C6B-C5B-C4B	118.2(2)	C8B-O8B-H8B	109.5
C7A-N7A-H7AB	120.0	C6B-C5B-C7B	122.3(2)		
H7AA-N7A-H7AB	120.0	C4B-C5B-C7B	119.4(2)		

Torsion angle (°)		Torsion angle (°)	
N1A-C2A-C3A-C4A	1.7(4)	N1B-C2B-C3B-C4B	-1.2(4)
C2A-C3A-C4A-C5A	-1.6(3)	C2B-C3B-C4B-C5B	0.8(4)
C3A-C4A-C5A-C6A	0.3(3)	C3B-C4B-C5B-C6B	0.4(3)
C3A-C4A-C5A-C7A	-180.0(2)	C3B-C4B-C5B-C7B	-175.7(2)
C4A-C5A-C6A-N1A	1.2(3)	C4B-C5B-C6B-N1B	-1.5(4)
C7A-C5A-C6A-N1A	-178.6(2)	C7B-C5B-C6B-N1B	174.4(2)
C4A-C5A-C7A-O7A	153.6(2)	C6B-C5B-C7B-O7B	-152.2(2)
C6A-C5A-C7A-O7A	-26.7(3)	C4B-C5B-C7B-O7B	23.7(3)
C4A-C5A-C7A-N7A	-27.8(3)	C6B-C5B-C7B-N7B	26.5(3)
C6A-C5A-C7A-N7A	151.9(2)	C4B-C5B-C7B-N7B	-157.6(2)
C3A-C2A-N1A-C6A	-0.3(3)	C5B-C6B-N1B-C2B	1.3(4)
C5A-C6A-N1A-C2A	-1.2(3)	C3B-C2B-N1B-C6B	0.1(4)
O9A-C8A-C9A-C9A^{iii}	-3.5(4)	O9B-C8B-C9B-C9B^{iv}	2.9(4)
O8A-C8A-C9A-C9A^{iii}	176.4(2)	O8B-C8B-C9B-C9B^{iv}	-176.6(2)

Symmetry transformations used to generate equivalent atoms:
i) -x+3,-y+2,-z+1 ii) -x,-y+1,-z+1 iii) -x+3,-y+2,-z+1 iv) -x,-y+1,-z+1

Appendix 24

24.1: ^{1}H NMR spectra of nicotinamide : undecanedioic acid (solvent – DMSO)

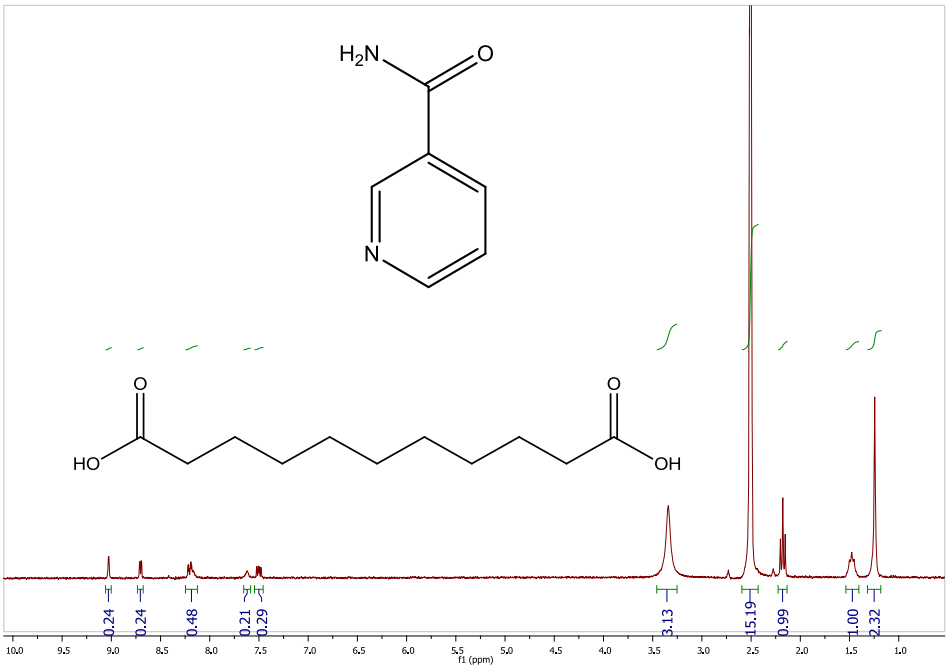

Nicotinamide: 7.50 (1H,q), 7.63 (1H,s), 8.19 (2H,dt), 8.71 (1H,dd), 9.20 (1H,d)
Undecanedioic acid: 1.25 (10H, s), 1.47 (4H, t), 2.18 (4H, t)

24.2: The diffraction pattern simulated from the single crystal structure compared to that of the laboratory experimental powder diffraction pattern of nicotinamide : undecanedioic acid

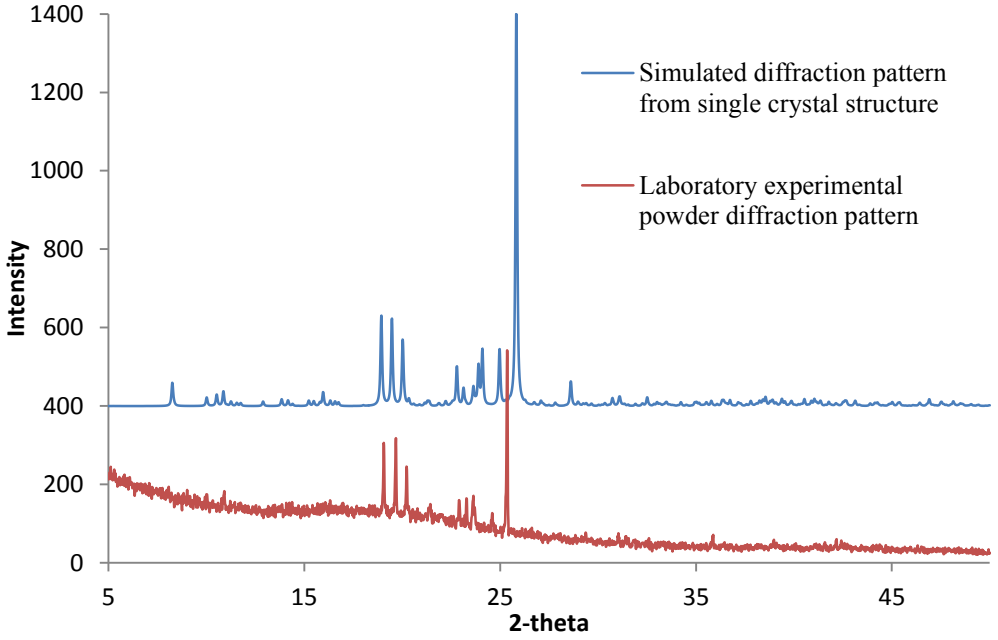

24.3: Ortep of nicotinamide : undecanedioic acid, 1:1

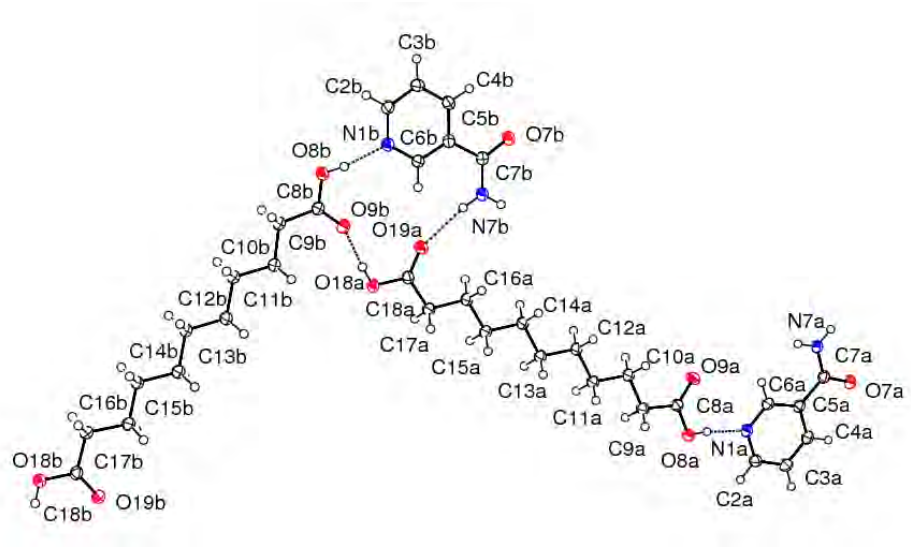

24.4: Crystallographic details of nicotinamide : undecanedioic acid, 1:1

Empirical formula	$C_{17}H_{26}N_2O_5$	
Formula weight	338.40	
Temperature	120(2)K	
Wavelength	1.54184 Å	
Crystal system	Triclinic	
Space group	P -1	
Unit cell dimensions	a = 9.1939(1)Å b = 11.6336(2)Å c = 17.6109(3)Å	α = 106.738(1)° β = 90.588(1) ° γ = 105.479(1)°
Volume	1730.63(5)$Å^3$	
Z	4	
Density (calculated)	1.299 Mg/m^3	
Absorption coefficient	0.788 mm^{-1}	
F(000)	728	
Crystal size	0.24 x 0.10 x 0.04 mm^3	
Theta range for data collection	6.45 to 66.60°	
Index ranges	-10<=h<=10, -13<=k<=13, -20<=l<=20	
Reflections collected	15786	
Independent reflections	5925 [R(int) = 0.0288]	
Completeness to theta = 66.60°	97.0%	
Max. and min. transmission	0.9691 and 0.8333	
Refinement method	Full-matrix least-squares on F^2	
Data / restraints / parameters	5925/0/437	
Goodness-of-fit on F^2	1.040	
Final R indices [I>2sigma(I)]	R_1 = 0.0373, wR_2 = 0.0985	
R indices (all data)	R_1 = 0.0442, wR_2 = 0.1047	
Largest diff. peak and hole	0.196 and -0.262 $e.Å^{-3}$	

24.5: Intramolecular bond lengths (Å) and angles (°) in nicotinamide : undecanedioic acid, 1:1

Bond length (Å)		Bond length (Å)		Bond length (Å)	
N1B-C2B	1.337(2)	C12A-H12C	0.9900	O9B-C8B	1.220(2)
N1B-C6B	1.344(2)	C13A-C14A	1.522(2)	O18B-C18B	1.334(2)
C2B-C3B	1.377(2)	C13A-H13A	0.9900	O18B-H18B	0.8400
C2B-H2B	0.9500	C13A-H13C	0.9900	O19B-C18B	1.209(2)
C3B-C4B	1.387(2)	C14A-C15A	1.524(2)	C8B-C9B	1.502(2)
C3B-H3B	0.9500	C14A-H14A	0.9900	C9B-C10B	1.515(2)
C4B-C5B	1.387(2)	C14A-H14C	0.9900	C9B-H9BA	0.9900
C4B-H4B	0.9500	C15A-C16A	1.525(2)	C9B-H9BB	0.9900
C5B-C6B	1.395(2)	C15A-H15C	0.9900	C10B-C11B	1.526(2)
C5B-C7B	1.514(2)	C15A-H15A	0.9900	C10B-H10D	0.9900
C6B-H6B	0.9500	C16A-C17A	1.521(2)	C10B-H10B	0.9900
C7B-O7B	1.237(2)	C16A-H16C	0.9900	C11B-C12B	1.521(2)
C7B-N7B	1.329(2)	C16A-H16A	0.9900	C11B-H11D	0.9900
N7B-H7BA	0.8800	C17A-C18A	1.500(2)	C11B-H11B	0.9900
N7B-H7BB	0.8800	C17A-H17A	0.9900	C12B-C13B	1.524(2)
O8A-C8A	1.316(2)	C17A-H17C	0.9900	C12B-H12D	0.9900
O8A-H8A	0.8400	N1A-C2A	1.336(2)	C12B-H12B	0.9900
O9A-C8A	1.214(2)	N1A-C6A	1.337(2)	C13B-C14B	1.522(2)
O18A-C18A	1.335(2)	C2A-C3A	1.381(2)	C13B-H13D	0.9900
O18A-H18A	0.8400	C2A-H2A	0.9500	C13B-H13B	0.9900
O19A-C18A	1.207(2)	C3A-C4A	1.385(2)	C14B-C15B	1.525(2)
C8A-C9A	1.504(2)	C3A-H3A	0.9500	C14B-H14D	0.9900
C9A-C10A	1.517(2)	C4A-C5A	1.391(2)	C14B-H14B	0.9900
C9A-H9AA	0.9900	C4A-H4A	0.9500	C15B-C16B	1.524(2)
C9A-H9AB	0.9900	C5A-C6A	1.395(2)	C15B-H15D	0.9900
C10A-C11A	1.526(2)	C5A-C7A	1.512(2)	C15B-H15B	0.9900
C10A-H10A	0.9900	C6A-H6A	0.9500	C16B-C17B	1.523(2)
C10A-H10C	0.9900	C7A-O7A	1.238(2)	C16B-H16B	0.9900
C11A-C12A	1.522(2)	C7A-N7A	1.329(2)	C16B-H16D	0.9900
C11A-H11A	0.9900	N7A-H7AA	0.8800	C17B-C18B	1.497(2)
C11A-H11C	0.9900	N7A-H7AB	0.8800	C17B-H17D	0.9900
C12A-C13A	1.525(2)	O8B-C8B	1.309(2)	C17B-H17B	0.9900
C12A-H12A	0.9900	O8B-H8B	0.8400		

Bond angle (°)		Bond angle (°)		Bond angle (°)	
C2B-N1B-C6B	118.7(1)	H13A-C13A-H13C	107.7	C8B-C9B-H9BA	108.4
N1B-C2B-C3B	122.9(1)	C13A-C14A-C15A	111.9(1)	C10B-C9B-H9BA	108.4
N1B-C2B-H2B	118.5	C13A-C14A-H14A	109.2	C8B-C9B-H9BB	108.4
C3B-C2B-H2B	118.5	C15A-C14A-H14A	109.2	C10B-C9B-H9BB	108.4
C2B-C3B-C4B	118.3(1)	C13A-C14A-H14C	109.2	H9BA-C9B-H9BB	107.4
C2B-C3B-H3B	120.8	C15A-C14A-H14C	109.2	C9B-C10B-C11B	111.1(1)
C4B-C3B-H3B	120.8	H14A-C14A-H14C	107.9	C9B-C10B-H10D	109.4
C5B-C4B-C3B	119.8(1)	C14A-C15A-C16A	114.1(1)	C11B-C10B-H10D	109.4
C5B-C4B-H4B	120.1	C14A-C15A-H15C	108.7	C9B-C10B-H10B	109.4
C3B-C4B-H4B	120.1	C16A-C15A-H15C	108.7	C11B-C10B-H10B	109.4
C4B-C5B-C6B	118.0(2)	C14A-C15A-H15A	108.7	H10D-C10B-H10B	108.0
C4B-C5B-C7B	117.8(1)	C16A-C15A-H15A	108.7	C12B-C11B-C10B	114.3(1)
C6B-C5B-C7B	124.2(1)	H15C-C15A-H15A	107.6	C12B-C11B-H11D	108.7
N1B-C6B-C5B	122.2(1)	C17A-C16A-C15A	111.56(1)	C10B-C11B-H11D	108.7
N1B-C6B-H6B	118.9	C17A-C16A-H16C	109.3	C12B-C11B-H11B	108.7
C5B-C6B-H6B	118.9	C15A-C16A-H16C	109.3	C10B-C11B-H11B	108.7
O7B-C7B-N7B	122.5(1)	C17A-C16A-H16A	109.3	H11D-C11B-H11B	107.6
O7B-C7B-C5B	118.8(1)	C15A-C16A-H16A	109.3	C11B-C12B-C13B	113.0(1)
N7B-C7B-C5B	118.9(1)	H16C-C16A-H16A	108.0	C11B-C12B-H12D	109.0
C7B-N7B-H7BA	120.0	C18A-C17A-C16A	113.8(1)	C13B-C12B-H12D	109.0
C7B-N7B-H7BB	120.0	C18A-C17A-H17A	108.8	C11B-C12B-H12B	109.0
H7BA-N7B-H7BB	120.0	C16A-C17A-H17A	108.8	C13B-C12B-H12B	109.0
C8A-O8A-H8A	109.5	C18A-C17A-H17C	108.8	H12D-C12B-H12B	107.8
C18A-O18A-H18A	109.5	C16A-C17A-H17C	108.8	C14B-C13B-C12B	113.9(1)
O9A-C8A-O8A	122.2(1)	H17A-C17A-H17C	107.7	C14B-C13B-H13D	108.8
O9A-C8A-C9A	125.1(1)	O19A-C18A-O18A	122.6(1)	C12B-C13B-H13D	108.8
O8A-C8A-C9A	112.7(1)	O19A-C18A-C17A	124.4(1)	C14B-C13B-H13B	108.8
C8A-C9A-C10A	115.6(1)	O18A-C18A-C17A	113.0(1)	C12B-C13B-H13B	108.8
C8A-C9A-H9AA	108.4	C2A-N1A-C6A	119.0(1)	H13D-C13B-H13B	107.7
C10A-C9A-H9AA	108.4	N1A-C2A-C3A	122.5(1)	C13B-C14B-C15B	112.5(1)
C8A-C9A-H9AB	108.4	N1A-C2A-H2A	118.8	C13B-C14B-H14D	109.1
C10A-C9A-H9AB	108.4	C3A-C2A-H2A	118.8	C15B-C14B-H14D	109.1
H9AA-C9A-H9AB	107.4	C2A-C3A-C4A	118.6(1)	C13B-C14B-H14B	109.1
C9A-C10A-C11A	110.7(1)	C2A-C3A-H3A	120.7	C15B-C14B-H14B	109.1
C9A-C10A-H10A	109.5	C4A-C3A-H3A	120.7	H14D-C14B-H14B	107.8
C11A-C10A-H10A	109.5	C3A-C4A-C5A	119.7(1)	C16B-C15B-C14B	114.0(1)
C9A-C10A)-H10C	109.5	C3A-C4A-H4A	120.1	C16B-C15B-H15D	108.8

C11A-C10A-H10C	109.5	C5A-C4A-H4A	120.1	C14B-C15B-H15D	108.8
H10A-C10A-H10C	108.1	C4A-C5A-C6A	117.7(1)	C16B-C15B-H15B	108.8
C12A-C11A-C10A	114.0(1)	C4A-C5A-C7A	117.7(1)	C14B-C15B-H15B	108.8
C12A-C11A-H11A	108.8	C6A-C5A-C7A	124.7(1)	H15D-C15B-H15B	107.7
C10A-C11A-H11A	108.8	N1A-C6A-C5A	122.6(1)	C17B-C16B-C15B	111.1(1)
C12A-C11A-H11C	108.8	N1A-C6A-H6A	118.7	C17B-C16B-H16B	109.4
C10A-C11A-H11C	108.8	C5A-C6A-H6A	118.7	C15B-C16B-H16B	109.4
H11A-C11A-H11C	107.7	O7A-C7A-N7A	122.8(1)	C17B-C16B-H16D	109.4
C11A-C12A-C13A	112.9(1)	O7A-C7A-C5A	118.5(1)	C15B-C16B-H16D	109.4
C11A-C12A-H12A	109.0	N7A-C7A-C5A	118.7(1)	H16B-C16B-H16D	108.0
C13A-C12A-H12A	109.0	C7A-N7A-H7AA	120.0	C18B-C17B-C16B	113.8(1)
C11A-C12A-H12C	109.0	C7A-N7A-H7AB	120.0	C18B-C17B-H17D	108.8
C13A-C12A-H12C	109.0	H7AA-N7A-H7AB	120.0	C16B-C17B-H17D	108.8
H12A-C12A-H12C	107.8	C8B-O8B-H8B	109.5	C18B-C17B-H17B	108.8
C14A-C13A-C12A	113.9(1)	C18B-O18B-H18B	109.5	C16B-C17B-H17B	108.8
C14A-C13A-H13A	108.8	O9B-C8B-O8B	122.4(1)	H17D-C17B-H17B	107.7
C12A-C13A-H13A	108.8	O9B-C8B-C9B	124.5(1)	O19B-C18B-O18B	122.6(1)
C14A-C13A-H13C	108.8	O8B-C8B-C9B	113.1(1)	O19B-C18B-C17B	124.8(1)
C12A-C13A-H13C	108.8	C8B-C9B-C10B	115.7(1)	O18B-C18B-C17B.	112.7(1)

Torsion angle (°)		Torsion angle (°)	
C6B-N1B-C2B-C3B	-0.1(2)	C6A-N1A-C2A-C3A	-0.3(2)
N1B-C2B-C3B-C4B	-0.3(2)	N1A-C2A-C3A-C4A	-0.2(2)
C2B-C3B-C4B-C5B	0.7(2)	C2A-C3A-C4A-C5A	0.6(2)
C3B-C4B-C5B-C6B	-0.7(2)	C3A-C4A-C5A-C6A	-0.5(2)
C3B-C4B-C5B-C7B	178.2(1)	C3A-C4A-C5A-C7A	179.9(1)
C2B-N1B-C6B-C5B	0.1(2)	C2A-N1A-C6A-C5A	0.28(2)
C4B-C5B-C6B-N1B	0.3(2)	C4A-C5A-C6A-N1A	0.1(2)
C7B-C5B-C6B-N1B	-178.6(1)	C7A-C5A-C6A-N1A	179.7(1)
C4B-C5B-C7B-O7B	3.5(2)	C4A-C5A-C7A-O7A	2.5 (2)
C6B-C5B-C7B-O7B	-177.7(1)	C6A-C5A-C7A-O7A	-177.0 (1)
C4B-C5B-C7B-N7B	-175.5(1)	C4A-C5A-C7A-N7A	-178.3(1)
C6B-C5B-C7B-N7B	3.4(2)	C6A-C5A-C7A-N7A	2.2(2)
O9A-C8A-C9A-C10A	-2.1(2)	O9B-C8B-C9B-C10B	11.2(2)
O8A-C8A-C9A-C10A	178.7(1)	O8B-C8B-C9B-C10B	-170.4(1)
C8A-C9A-C10A-C11A	-179.8(1)	C8B-C9B-C10B-C11B	-179.5(1)
C9A-C10A-C11A-C12A	179.4(1)	C9B-C10B-C11B-C12B	178.4(1)
C10A-C11A-C12A-C13A	179.8(1)	C10B-C11B-C12B-C13B	175.8(1)
C11A-C12A-C13A-C14A	-179.1(1)	C11B-C12B-C13B-C14B	-177.4(1)
C12A-C13A-C14A-C15A	179.0(1)	C12B-C13B-C14B-C15B	-176.6(1)
C13A-C14A-C15A-C16A	177.5(1)	C13B-C14B-C15B-C16B	179.7(1)
C14A-C15A-C16A-C17A	177.4(1)	C14B-C15B-C16B-C17B	-178.1(1)
C15A-C16A-C17A-C18A	-178.0(1)	C15B-C16B-C17B-C18B	-179.0(1)
C16A-C17A-C18A-O19A	-6.8(2)	C16B-C17B-C18B-O19B	-5.1(2)
C16A-C17A-C18A-O18A	174.1(1)	C16B-C17B-C18B-O18B	175.6(1)

Appendix 25:

Acta Crystallographica Section C
Crystal Structure Communications
ISSN 0108-2701

The cocrystal nicotinamide–succinic acid (2/1)

Laura J. Thompson, Raja S. Voguri, Adam Cowell, Louise Male and Maryjane Tremayne*

School of Chemistry, University of Birmingham, Edgbaston, Birmingham B15 2TT, England
Correspondence e-mail: m.tremayne@bham.ac.uk

Received 1 July 2010
Accepted 9 July 2010
Online 20 July 2010

In the asymmetric unit of the crystal structure of nicotinamide–succinic acid (2/1), $2C_6H_6N_2O{\cdot}C_4H_6O_4$, there are two independent nicotinamide molecules in general positions and two half succinic acid molecules which lie about inversion centres. The structure contains acid–pyridine and amide–amide synthons with nicotinamide molecules forming ladders of alternating $R_2^2(8)$ and $R_4^2(8)$ rings linked through succinic acid to generate a corrugated hydrogen-bonded sheet. This sheet is a common supramolecular unit found in other 2:1 nicotinamide–dicarboxylic acid cocrystals, but the presence of two crystallographically distinct nicotinamides with *anti* and *syn* conformations, forming two distinct sheets within the same structure, is a novel packing feature in this type of material.

Comment

Molecular cocrystals are becoming increasingly important within the pharmaceutical industry as they represent a new source of solid-state materials which have the potential to provide optimal physical properties while retaining the chemical properties of the individual components (Almarsson & Zaworotko, 2004; Vishweshwar *et al.*, 2006; Blagden *et al.*, 2008). However, successful synthesis of these multicomponent materials relies on the preferential formation of heteromeric synthons rather than the formation of strong interactions within the structures of the individual cocrystal formers. Both nicotinamide and isonicotinamide have demonstrated the propensity for cocrystal formation with a range of carboxylic acids (Aakeröy *et al.*, 2002; Vishweshwar *et al.*, 2003; Chakrabarty *et al.*, 2006; Amai *et al.*, 2006; Schmidtmann *et al.*, 2007; Karki *et al.*, 2009; Orola *et al.*, 2009), showing consistent preference for the formation of a heteromeric acid–pyridine hydrogen bond, (I) (Fig. 1). The formation of an amide–amide, (II), or acid–amide, (III), hydrogen bond (Fig. 1) is then dependent on the stoichiometry of the cocrystal; those formed with a monocarboxylic acid in a 1:1 ratio or with a dicarboxylic acid in a 2:1 ratio show a preference for the formation of synthon (II), whereas cocrystals with the dicarboxylic acid in a 1:1 ratio tend to form synthon (III). This is clearly illustrated in cases where both 1:1 and 2:1 cocrystal stoichiometries have been identified; for example, nicotinamide–adipic acid, nicotinamide–suberic acid (Karki *et al.*, 2009), nicotinamide–fumaric acid (Orola *et al.*, 2009), isonicotinamide–glutaric acid and isonicotinamide–adipic acid (Vishweshwar *et al.*, 2003).

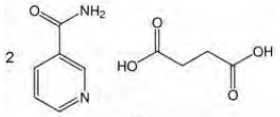

(1)

We report here the crystal structure of the nicotinamide–succinic acid 2:1 cocrystal, (1). Cocrystal (1) was prepared by slow evaporation from a 1:1 stoichiometric ratio of starting materials as described previously, although no crystal structure was reported in that case (Karki *et al.*, 2009).

The crystal structure of (1) displays an extended hydrogen-bond network generated by the acid–pyridine and amide–amide synthons expected in a cocrystal of this composition in a 2:1 stoichiometry, but unlike other nicotinamide–acid cocrystals, (1) contains two crystallographically distinct nicotinamide molecules with different conformations. Nicotinamide molecule *A* (denoted by atom labels 'a' in Fig. 2) adopts an *anti* conformation with the heterocyclic N and amide N on opposite sides of the molecule [torsion angle C6*A*—C5*A*—C7*A*—N7*A* = 151.9 (2)°; Table 1] whereas nicotinamide molecule *B* (denoted by atom labels 'b' in Fig. 2) adopts a *syn* conformation [torsion angle C6*B*—C5*B*—C7*B*—N7*B* = 26.5 (3)°; Table 1]. A search of the Cambridge Structural Database (Allen, 2002) revealed that in other nicotinamide adducts the nicotinamide molecule displays only one conformation in each structure (either the *anti* or *syn*), and there are more examples of structures adopting the *anti* rather than the *syn* conformation. An electron-density map was used to identify the posi-

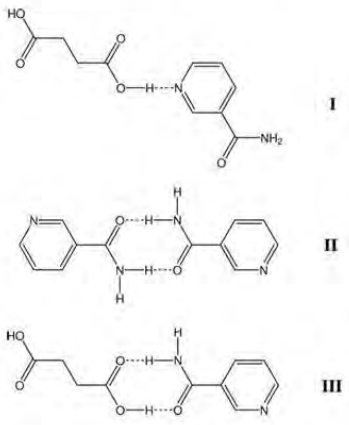

Figure 1
Potential hydrogen-bond synthons found in acid–amide cocrystals.

 doi:10.1107/S0108270110027319

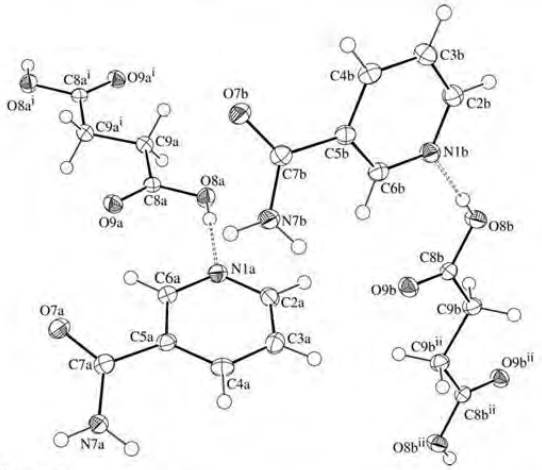

Figure 2
The independent molecules of (1), showing the atom-numbering scheme and the hard intermolecular hydrogen bonds (dashed lines). Displacement ellipsoids are drawn at the 50% probability level and H atoms are shown as small spheres of arbitrary radii. [Symmetry codes: (i) $-x+3, -y+2, -z+1$; (ii) $-x, -y+1, -z+1$.]

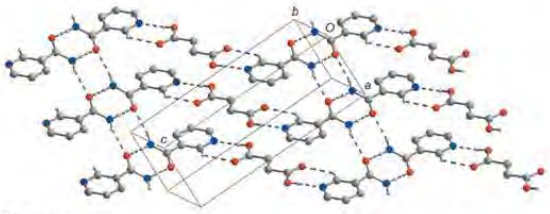

Figure 3
A view of the corrugated hydrogen-bonded sheet in the *ac* plane formed by nicotinamide *A* and succinic acid *A* molecules. Hydrogen bonds are shown as dashed lines. H atoms not involved in hydrogen bonding have been omitted for clarity.

tions of the carboxyl H atoms (H8*A* and H8*B*) in (1), confirming that this is a neutral cocrystal form rather than a salt (see *Experimental*).

Each nicotinamide molecule (*A* and *B*) is involved in four intermolecular hydrogen bonds with *A* and *B* molecules, respectively; one hard O—H···N(heterocyclic) interaction and one soft C—H···O=C hydrogen bond to a succinic acid molecule, and two hard N—H···O=C hydrogen bonds to other nicotinamide molecules of the same conformation (Table 2). More specifically, the carboxyl oxygen O8*A* acts as a hydrogen-bond donor, *via* H8*A*, to heterocyclic atom N1*A* of nicotinamide *A* at (*x*, *y*, *z*) with the acid–pyridine packing motif (I) reinforced by C6*A* in the nicotinamide acting as a soft hydrogen-bond donor through H6*A* to the other carboxyl oxygen O9*A* at (*x*, *y*, *z*). Propagation of this motif through inversion within the succinic acid molecule generates the 2:1 nicotinamide–succinic acid unit in which succinic acid *A* is capped at both ends by molecules of nicotinamide *A*. These units are then linked together through a complementary

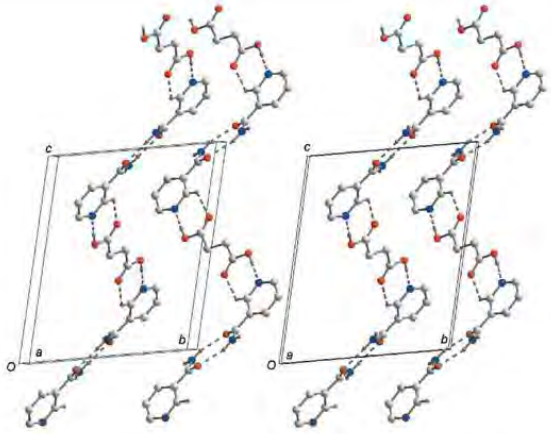

Figure 4
A stereoview of part of the crystal structure of (1), showing the chains formed by nicotinamide *A* and succinic acid *A* molecules running along [20$\bar{1}$] (right) and by nicotinamide *B* and succinic acid *B* molecules running along [201] (left). Hydrogen bonds are shown as dashed lines. H atoms not involved in hydrogen bonding have been omitted for clarity.

amide dimer $R_2^2(8)$ motif, (II) (Bernstein *et al.*, 1995), formed by N7*A* *via* H7*AA* to O7*A* at $(1-x, 2-y, 2-z)$ to generate a chain running in the [20$\bar{1}$] direction. The chains are linked through a second complementary N—H···O interaction formed by N7*A* through H7*AB* donation to O7*A* at $(-1+x, y, z)$, resulting in the formation of ladders of alternating $R_4^2(8)$ and $R_2^2(8)$ rings and the generation of an extended corrugated hydrogen-bonded sheet in the *ac* plane (Fig. 3).

Nicotinamide *B* is involved in a similar set of intermolecular interactions with succinic acid *B* and other nicotinamide *B* molecules, generating the same synthons and motifs as nicotinamide *A*. The formation of a dimer with nicotinamide *B* at $(2-x, 1-y, 2-z)$ generates a chain linking the 2:1 nicotinamide *B*–succinic acid *B* units, which in this case runs in the [201] direction. These chains are then linked to others to give a second corrugated hydrogen-bonded sheet also in the *ac* plane. Hence, the structure of (1) contains alternating sheets comprised purely of *A* molecules and then purely of *B* molecules in which the chains run in opposing directions (Fig. 4). There are no strong interactions between alternating sheets and all strong hydrogen-bond donors and acceptors are used in the hydrogen-bond network.

The corrugated hydrogen-bonded sheet formed by nicotinamide *A* in the *anti* conformation is a common supramolecular unit found in other 2:1 nicotinamide–dicarboxylic acid cocrystals in which the alkyl chain in the acid is longer, such as nicotinamide–adipic acid, nicotinamide–suberic acid and nicotinamide–sebacic acid (Karki *et al.*, 2009). Similar *anti* conformation chains are also formed by 2:1 cocrystals with malonic and fumaric acids, but in these cases the chains are linked through a further acid–amide interaction rather than through the formation of nicotinamide ladders. There are no other reports of the *syn* conformation in this series of cocrystals, although it is found in the synthon (III)-based acid–

amide chains formed in the 1:1 stoichiometry nicotinamide: glutaric acid and nicotinamide–pimelic acid cocrystals (Karki *et al.*, 2009).

In conclusion, the single-crystal structure of (1) highlights the formation of a supramolecular hydrogen-bonded sheet that is also seen in other nicotinamide–dicarboxylic acid cocrystals of this stoichiometry. However, the formation of two distinct sheets with *anti* and *syn* nicotinamide conformations is a novel packing feature in this type of material. This display of both typical and atypical structural behaviour within (1) may be (i) a result of the succinic acid being at the interface of two distinct preferred packing modes dependent on the size of the acid component, or (ii) an indication that other packing modes may be exhibited through potential polymorphic behaviour.

Experimental

All starting materials were purchased from Sigma Aldrich and used without purification. Nicotinamide (0.0138 g, 1.13×10^{-4} mmol) and succinic acid (0.0133 g, 1.13×10^{-4} mmol) were dissolved in warm methanol (5 ml) in a 1:1 stoichiometric ratio. The resulting solution was cooled to room temperature and, on slow evaporation of the solvent, crystals were formed. A colourless lath-shaped crystal of (1) was selected and used for single-crystal X-ray diffraction.

Crystal data

$2C_6H_6N_2O{\cdot}C_4H_6O_4$
M_r = 362.34
Triclinic, $P\overline{1}$
a = 5.0872 (2) Å
b = 11.5569 (5) Å
c = 14.2784 (5) Å
α = 77.433 (2)°
β = 86.726 (2)°
γ = 89.418 (2)°
V = 818.01 (6) Å^3
Z = 2
Mo $K\alpha$ radiation
μ = 0.12 mm^{-1}
T = 120 K
0.17 × 0.03 × 0.01 mm

Data collection

Bruker–Nonius APEXII CCD camera on κ-goniostat diffractometer
Absorption correction: multi-scan (*SADABS*; Sheldrick, 2007)
T_{min} = 0.981, T_{max} = 0.999
12664 measured reflections
3205 independent reflections
2455 reflections with $I > 2\sigma(I)$
R_{int} = 0.061

Refinement

$R[F^2 > 2\sigma(F^2)]$ = 0.056
$wR(F^2)$ = 0.132
S = 1.11
3205 reflections
237 parameters
H-atom parameters constrained
$\Delta\rho_{max}$ = 0.24 e Å^{-3}
$\Delta\rho_{min}$ = −0.27 e Å^{-3}

The presence of atoms H8*A* and H8*B* bonded to O8*A* and O8*B*, respectively [showing (1) is a cocrystal rather than a salt], was confirmed by the observation of peaks in those locations in an electron-density map, in addition to analysis of the C8*A*/*B*—O8*A*/*B* and C8*A*/*B*—O9*A*/*B* bond lengths (Table 1). All H atoms were then added at calculated positions and refined using a riding model, with C—H = 0.95 Å for aromatic H atoms, 0.99 Å for methylene H atoms, N—H = 0.88 Å and O—H = 0.84 Å and with U_{iso}(H) = 1.2U_{eq}(C), 1.2U_{eq}(N) and 1.5U_{eq}(O). In the case of the O8*A*—H8*A* and O8*B*—H8*B* groups, the riding model used (AFIX 147) allowed the chosen C—C—O—H torsion angle to maximize the electron density at the calculated H-atom position such that the final positions for H8*A* and H8*B* are very close to the peaks initially observed in the electron-density map.

Table 1
Selected geometric parameters (Å, °).

C7*A*—O7*A*	1.241 (3)	C7*B*—O7*B*	1.242 (3)
C7*A*—N7*A*	1.332 (3)	C7*B*—N7*B*	1.331 (3)
C8*A*—O9*A*	1.213 (3)	C8*B*—O9*B*	1.212 (3)
C8*A*—O8*A*	1.328 (3)	C8*B*—O8*B*	1.334 (3)
O7*A*—C7*A*—N7*A*	121.8 (2)	O7*B*—C7*B*—N7*B*	122.2 (2)
O9*A*—C8*A*—O8*A*	123.6 (2)	O9*B*—C8*B*—O8*B*	123.3 (2)
C6*A*—C5*A*—C7*A*—N7*A*	151.9 (2)	C6*B*—C5*B*—C7*B*—N7*B*	26.5 (3)
O8*A*—C8*A*—C9*A*—C9*A*^{i}	176.4 (2)	O8*B*—C8*B*—C9*B*—C9*B*^{ii}	−176.6 (2)

Symmetry codes: (i) $-x+3, -y+2, -z+1$; (ii) $-x, -y+1, -z+1$.

Table 2
Intermolecular hydrogen-bonding and weak interactions (Å, °) for (1).

D—H···*A*	*D*—H	H···*A*	*D*···*A*	*D*—H···*A*
O8*A*—H8*A*···N1*A*	0.84	1.85	2.691 (3)	174.1
C6*A*—H6*A*···O9*A*	0.95	2.52	3.206 (3)	129.5
N7*A*—H7*AA*···O7*A*^{iii}	0.88	2.10	2.953 (3)	164.1
N7*A*—H7*AB*···O7*A*^{iv}	0.88	2.15	2.899 (3)	142.2
O8*B*—H8*B*···N1*B*	0.84	1.84	2.682 (3)	176.0
C6*B*—H6*B*···O9*B*	0.95	2.61	3.268 (3)	126.9
N7*B*—H7*BA*···O7*B*^{v}	0.88	2.06	2.941 (3)	173.6
N7*B*—H7*BB*···O7*B*^{ii}	0.88	2.22	2.947 (3)	139.1

Symmetry codes: (iii) $-x+1, -y+2, -z+2$; (iv) $x-1, y, z$; (v) $-x+2, -y+1, -z+2$.

Data collection: *COLLECT* (Hooft, 1998); cell refinement: *DENZO* (Otwinowski & Minor, 1997) and *COLLECT*; data reduction: *DENZO* and *COLLECT*; program(s) used to solve structure: *SHELXS97* (Sheldrick, 2008); program(s) used to refine structure: *SHELXL97* (Sheldrick, 2008); molecular graphics: *ORTEP-3 for Windows* (Farrugia, 1997) and *DIAMOND* (Brandenburg & Putz, 1999); software used to prepare material for publication: *WinGX* (Farrugia, 1999).

We thank the University of Birmingham and the EPSRC for the support for LJT, RSV and AC. The EPSRC National Crystallography Service is thanked for collection of the single-crystal X-ray diffraction data. The powder diffraction facilities used in this research were obtained through the Science City Advanced Materials project with support from Advantage West Midlands (AWM) and part funded by the European Regional Development Fund (ERDF).

Supplementary data for this paper are available from the IUCr electronic archives (Reference: FG3180). Services for accessing these data are described at the back of the journal.

References

Aakeröy, C. B., Beatty, A. M. & Helfrich, B. A. (2002). *J. Am. Chem. Soc.* **124**, 14425–14432.
Allen, F. H. (2002). *Acta Cryst.* B**58**, 380–388.
Almarsson, O. & Zaworotko, M. J. (2004). *Chem. Commun.* pp. 1889–1896.
Amai, M., Kamijo, M., Nagase, H., Ogawa, N., Endo, T. & Ueda, H. (2006). *Anal. Sci.* **22**, x121–x122.
Bernstein, J., Davis, R. E., Shimoni, L. & Chang, N. L. (1995). *Angew. Chem. Int. Ed. Engl.* **34**, 1555–1573.

Blagden, N., Berry, D. J., Parkin, A., Javed, H., Ibrahim, A., Gavan, P. T., De Matos, L. L. & Seaton, C. C. (2008). *New J. Chem.* **32**, 1659–1672.
Brandenburg, K. & Putz, H. (1999). *DIAMOND*. Crystal Impact GbR, Bonn, Germany.
Chakrabarty, D., Nagase, H., Kamijo, M., Endo, T. & Ueda, H. (2006). *Anal. Sci.* **22**, x27–x28.
Farrugia, L. J. (1997). *J. Appl. Cryst.* **30**, 565.
Farrugia, L. J. (1999). *J. Appl. Cryst.* **32**, 837–838.
Hooft, R. W. W. (1998). *COLLECT*. Nonius BV, Delft, The Netherlands.
Karki, S., Friscic, T. & Jones, W. (2009). *CrystEngComm*, **11**, 470–481.
Orola, L. & Veidis, M. V. (2009). *CrystEngComm*, **11**, 415–417.
Otwinowski, Z. & Minor, W. (1997). *Methods in Enzymology*, Vol. 276, *Macromolecular Crystallography*, Part A, edited by C. W. Carter Jr & R. M. Sweet, pp. 307–326. New York: Academic Press.
Schmidtmann, M., Gutmann, M. J., Middlemiss, D. S. & Wilson, C. C. (2007). *CrystEngComm*, **9**, 743–745.
Sheldrick, G. M. (2007). *SADABS*. University of Göttingen, Germany.
Sheldrick, G. M. (2008). *Acta Cryst.* A**64**, 112–122.
Vishweshwar, P., McMahon, J. A., Bis, J. A. & Zaworotko, M. J. (2006). *J. Pharm. Sci.* **95**, 499–516.
Vishweshwar, P., Nangia, A. & Lynch, V. M. (2003). *Cryst. Growth Des.* **3**, 783–790.